Engineering Materials

Ram K. Gupta *Editor*

Pseudocapacitors

Fundamentals to High Performance Energy Storage Devices

Springer

Engineering Materials

This series provides topical information on innovative, structural and functional materials and composites with applications in optical, electrical, mechanical, civil, aeronautical, medical, bio- and nano-engineering. The individual volumes are complete, comprehensive monographs covering the structure, properties, manufacturing process and applications of these materials. This multidisciplinary series is devoted to professionals, students and all those interested in the latest developments in the Materials Science field, that look for a carefully selected collection of high quality review articles on their respective field of expertise.

Indexed at Compendex (2021) and Scopus (2022)

Ram K. Gupta
Editor

Pseudocapacitors

Fundamentals to High Performance Energy Storage Devices

Springer

Editor
Ram K. Gupta
Polymer Chemistry
Department of Chemistry
National Institute for Materials
Advancement
Pittsburg State University
Pittsburg, KS, USA

ISSN 1612-1317 ISSN 1868-1212 (electronic)
Engineering Materials
ISBN 978-3-031-45429-5 ISBN 978-3-031-45430-1 (eBook)
https://doi.org/10.1007/978-3-031-45430-1

© The Editor(s) (if applicable) and The Author(s), under exclusive license to Springer Nature Switzerland AG 2024

This work is subject to copyright. All rights are solely and exclusively licensed by the Publisher, whether the whole or part of the material is concerned, specifically the rights of translation, reprinting, reuse of illustrations, recitation, broadcasting, reproduction on microfilms or in any other physical way, and transmission or information storage and retrieval, electronic adaptation, computer software, or by similar or dissimilar methodology now known or hereafter developed.
The use of general descriptive names, registered names, trademarks, service marks, etc. in this publication does not imply, even in the absence of a specific statement, that such names are exempt from the relevant protective laws and regulations and therefore free for general use.
The publisher, the authors, and the editors are safe to assume that the advice and information in this book are believed to be true and accurate at the date of publication. Neither the publisher nor the authors or the editors give a warranty, expressed or implied, with respect to the material contained herein or for any errors or omissions that may have been made. The publisher remains neutral with regard to jurisdictional claims in published maps and institutional affiliations.

This Springer imprint is published by the registered company Springer Nature Switzerland AG
The registered company address is: Gewerbestrasse 11, 6330 Cham, Switzerland

Paper in this product is recyclable.

Preface

The demand for high-efficiency energy storage devices is growing to meet the current demand for growing technologies. The materials used in energy devices along with their architect are some of the most important factors in providing high-performance energy devices. Pseudocapacitive materials offer plenty of opportunity for scientists to tune their electrochemical properties and thus the performance of the devices. There are many strategies in pseudocapacitive materials that can be adapted to improve their performance such as morphology, doping, the introduction of multivalent ions, design approaches of the devices, and the use of emerging pseudocapacitive materials.

This book aims to provide fundamentals of pseudocapacitive materials, their synthetic approaches, and architectural aspects to improve their properties and emerging materials. Many fundamental approaches to tuning the properties of pseudocapacitive materials and their applications in energy storage devices are covered. All the chapters are covered by experts in this field, providing a unique opportunity for the readers to learn many important concepts of electrochemical energy storage devices under one title. The proposed book covers the fundamentals, synthetic approaches, and strategies to tune the properties of pseudocapacitive materials and emerging pseudocapacitive materials, their concepts, and their applications in energy storage devices.

Ram K. Gupta
Associate Professor of Polymer
Chemistry
Department of Chemistry
National Institute for Materials
Advancement
Pittsburg State University
Pittsburg, KS, USA

Contents

Pseudocapacitance: An Introduction 1
Anit Joseph and Tiju Thomas

Pseudocapacitance: Fundamentals to Advanced Applications 19
Shilpa Pande, Bidhan Pandit, Shoyebmohamad F. Shaikh, and Jahangeer Ahmed

Pseudocapacitance: Mechanism and Characteristics 39
G. Srividhya and N. Ponpandian

Emerging Pseudocapaciting Materials 57
Muhammad Abdullah, Wenrui Jiang, Xin Chen, and Shandiao Xu

Pseudocapacitance: Tuning Electrochemical Properties 75
Jinfeng Sun, Anning Zhang, Qian Zhang, and Changzhou Yuan

Pseudocapacitive Materials for Electrolytes 95
Lucia Díaz-Patiño, Lorena Álvarez Contreras, Minerva Guerra-Balcázar, and Noé Arjona

Electrochemical Properties of Metal Hydroxides 115
Hamideh Mohammadian Sarcheshmeh and Mohammad Mazloum Ardakani

Pseudocapacitance in Double Perovskite Material 133
Mostafa M. Omran, Ahmed I. Abdel-Salam, Delvin Aman, and Saad G. Mohamed

Conducting Polymers for Pseudocapacitors 157
Quoc Bao Le, Rudolf Kiefer, Phuong Nguyen Xuan Vo, Natalia E. Kazantseva, and Petr Saha

MXenes for Pseudocapacitors 177
Harishchandra S. Nishad, Rajesh R. Jaiswar, Sachin D. Tejam, and Pravin S. Walke

MXenes-Based Composites for Pseudocapacitors 195
Li Sun and Chunxu Pan

Hydrogel and Its Composites for Pseudocapacitors 217
Jeffery Horinek, Allen Davis, and Ram K. Gupta

Pseudocapacitive Materials for 3D Printed Supercapacitors 237
Arthi Gopalakrishnan, Vishnu Surendran, Venkataraman Thangadurai, and Benjamin Tutolo

Pseudocapacitive Materials for Flexible Supercapacitors 257
Fang Cheng, Xiaoping Yang, and Wen Lu

Redox-Active Polymers for Batteries 277
Aswathy Vijayakumar Kumar, Treesa Karangattuserriyil James, and Suresh Mathew

Carbon-Based Pseudocapacitive Materials for Next Generation Batteries 297
B. Jeevanantham and M. K. Shobana

Surfactant-Assisted Pseudocapacitive Materials for Li-Ion Batteries 315
Wan Mohd Abd Kalam, Hong Ngee Lim, Izwaharyanie Ibrahim, and Chuan Yi Foo

Pseudocapacitive Materials for Metal-Sulfur Batteries 333
Yogita Dahiya, Shivani Agarwal, Manoj Kumar, Debasish Sarkar, and Ankur Jain

Pseudocapacitive Materials for Metal-Air Batteries 353
Allen Davis and Ram K. Gupta

Pseudocapacitive Materials-Based Metal-Air Batteries 375
Sanjeev Verma, Vikas Kumar Pandey, Ram K. Gupta, Shivani Verma, and Bhawna Verma

Pseudocapacitive Materials for 3D Printed Batteries 389
Sagar Jariwala, Yash Desai, and Ram K. Gupta

Pseudocapacitance: An Introduction

Anit Joseph and Tiju Thomas

Abstract An electrochemical energy storage device that can deliver high power and energy density is needed globally. To accomplish this one method adopted involves the use of pseudocapacitive materials that use reversible surface or near-surface Faradaic processes to store charges. By doing so, they can overcome the mass transfer and capacity limits of batteries and electrical double-layer capacitors. Both chemical and electrostatic processes are used to store charges in pseudocapacitors. Pseudocapacitors have a charge transfer process that is comparable to that of a battery. There is a greater rate of transfer because of the use of a thinner redox material on the electrode or less ion penetration into the structure from the electrolyte. Technology is still in need of development in materials performance and device reliability. Research is still being done to determine the materials and electrochemical properties that can produce high energy density at quicker charge–discharge rates. In this context, transition metal oxides are attractive. With this as the background, the latest developments in pseudocapacitor materials and devices are discussed here.

Keywords Pseudocapacitor · History · Charging mechanism · Theories · Devices

1 Introduction

Energy has become an important concern for both governments and the scientific community. This is in response to the shifting global landscape. More effective energy storage device development has attracted a lot of attention. Electrochemical energy storage that can deliver high power and high energy density is needed globally. This is so since smart grids, e-mobility, and related segments require high power-density energy storage. One such device, the supercapacitor, has advanced significantly over

A. Joseph (✉) · T. Thomas (✉)
Department of Metallurgical and Materials Engineering, Indian Institute of Technology Madras (IITM), Chennai 600036, India
e-mail: anitjoseph3@gmail.com

T. Thomas
e-mail: tijuthomas@iitm.ac.in; tt332@cornell.edu

© The Author(s), under exclusive license to Springer Nature Switzerland AG 2024

R. K. Gupta (ed.), *Pseudocapacitors*, Engineering Materials,
https://doi.org/10.1007/978-3-031-45430-1_1

the past ten years and has the potential to enable considerable improvements in energy storage [1].

Supercapacitors, often called ultracapacitors or electrochemical capacitors, use thin electrolytic dielectrics and high surface area electrode materials to produce capacitances that are many orders of magnitude greater than those of regular capacitors. By doing this, supercapacitors can preserve the typical high-power density found in conventional capacitors while also achieving higher energy densities. The electrostatic capacitor with a dry separator is the most fundamental of the three types of capacitors. This conventional capacitor is primarily used for filtering and tuning radio frequencies because of its extremely low capacitance. The size varies from a few pico-farads (pf) to low microfarads (μF) [2]. The electrolytic capacitor is rated in microfarads, which is a million times greater than an electrostatic capacitor and offers a higher capacitance. These capacitors are employed for filtering, buffering, and signal coupling. The electrostatic capacity has a positive and negative that needs to be observed, just like a battery. The third type is a supercapacitor, which has a rating in farads and is thousands of times more powerful than an electrolytic capacitor.

A supercapacitor is a device for storing energy that is frequently subject to charge and discharge cycles at high currents and short duration. However, these devices have a low energy density, which limits their ability to be used in real-world situations. One of the crucial parts for enhancing the supercapacitor's performance is the electrode. A large specific surface area, thermal stability, an ideal pore size distribution, conductivity, and good corrosion resistance are only a few of its crucial characteristics. Choosing the right active components and raised electrodes is crucial to develop potentially active supercapacitors. At the electrode and electrolyte interface, the SC operation stores electrical energy through a Faradaic or non-Faradic mechanism [2].

2 Classification

Based on the energy storage mechanism, supercapacitors are mainly classified into three types (Fig. 1):

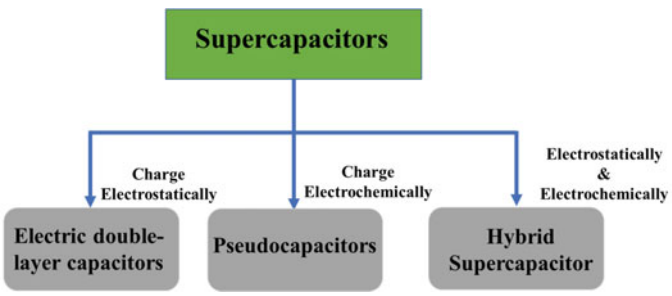

Fig. 1 Classification of supercapacitor

1. Electric double-layer capacitors
2. Pseudocapacitors
3. Hybrid supercapacitors

2.1 Electric Double-Layer Capacitors (EDLCs)

EDLCs use charge separation to store energy in a manner like that of a conventional capacitor. The critical distinction is in the greater capacitance values offered by EDLCs, which are made possible using high-surface-area porous materials (often activated carbon). instead of porous electrode materials, two-dimensional flat plates are commonly found in traditional capacitors. According to their name, EDLCs are known to store charge by creating electric double layers at the supercapacitors' electrode–electrolyte interface. In stationary and mobile systems where high power is required, EDLCs are used. EDLCs can provide quick energy harvesting, like car brakes, due to their low time constant (less than a minute). Through reversible ions (i.e., ions of electrolyte) adsorption onto the electrode, EDLCs are known to store charge electrostatically. Polarisation separates the charge at the electrolyte/electrode contact, resulting in double-layer capacitance.

Compared to a traditional capacitor, EDLCs can store several orders of magnitude more energy because of the following reasons:

(1) The improved capacity for charge storage on an electrode with a substantially extended surface area (made possible by the presence of numerous pores within an electrode material with an extensive surface area).
(2) The thin electrical double layer forms at an electrode and an electrolyte interface.

In that there are two electrodes positioned in an electrolyte and separated by an ion-permeable separator to avoid electrical contact, EDLC supercapacitors are constructed similarly to batteries (Fig. 2a). In the charged state, the anions and cations in the electrolyte flow in opposite directions towards the positive and negative electrodes, creating two double layers—one at each electrode–electrolyte interface. A difference in potential exists throughout the cell due to the ion separation. The entire cell can be viewed as two capacitors connected in series, as each electrode–electrolyte interaction acts as a capacitor.

2.2 Pseudocapacitors (PC)

Pseudocapacitors utilize a Faradaic reaction to store energy. The transfer of charge between an electrode and an electrolyte is stored electrostatically. In a pseudocapacitor, the electrode material undergoes both reduction and oxidation when a voltage is applied. It entails the movement of charge through the double layer, which causes Faradic current to flow through the electrode material of the supercapacitor (Fig. 2b).

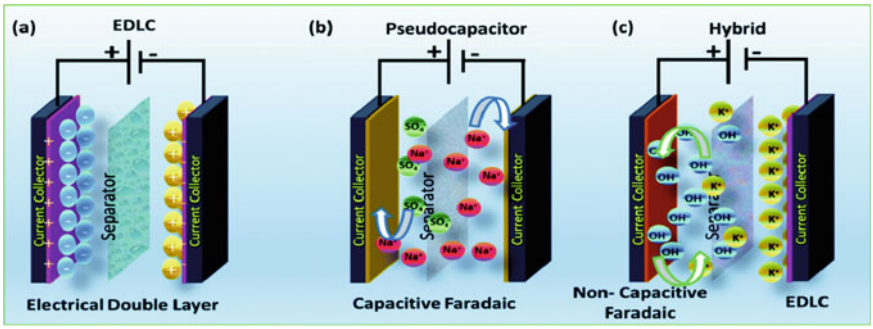

Fig. 2 Charge storage mechanism of supercapacitors: **a** EDLCs, **b** pseudocapacitors, and **c** hybrid supercapacitors. Adapted with permission [3], copyright (2021), Royal Society of Chemistry

Compared to EDLCs, the Faradic technique used in pseudocapacitors accelerates the electrochemical reactions that lead to higher specific capacitance and energy densities.

2.2.1 Historical Development of Pseudocapacitance

The term "pseudo-capacity," coined by David C. Grahame in 1941 to indicate surplus capacity not linked to the development of the electrical double-layer, is where the word "pseudocapacitance" comes from Grahame [4]. Then, in the early 1960s, Conway and Gileadi employed pseudocapacitance to investigate the electrochemical charge transfer mechanisms related to surface adsorption (Fig. 3) [5, 6]. Conway and Gileadi's theoretical framework for pseudocapacitance was proposed around the same time that experimental observations were identified. The distinctive characteristics of quick electrochemical charge transfer processes of surface-bound species include underpotential deposition (UPD), adsorbed electrolysis intermediates, and modified (thin-film) electrodes [7].

In 1971, Trasatti and colleagues published their initial findings on the charge storage behavior of a thin layer of ruthenium oxide in sulfuric acid, which led to the discovery of pseudocapacitance in transition metal oxides [8]. The thin film RuO_2 electrode, in contrast to a single crystal RuO_2 electrode, displayed a highly symmetric and reversible cyclic voltammogram, which was later attributed to reversible redox processes at the RuO_2 electrode surface. The specific capacitance can be substantially greater than what has been achieved with carbon materials that solely display EDL capacitance, reaching approximately 720 F/g in a voltage window of 1 V (which is equivalent to a specific capacity of 200 mAh/g) at a scan rate of 2 mV/s [9].

Amorphous, hydrated $MnO_2 \cdot xH_2O$ exhibited capacitor-like behavior in pH-neutral aqueous electrolytes, according to research by the Goodenough group in 1999. The specific capacitance, measured around 200 F/g in an electrolyte of aqueous KCl at 1.2 V, is thought to have resulted via surface redox reactions of MnO_2 with

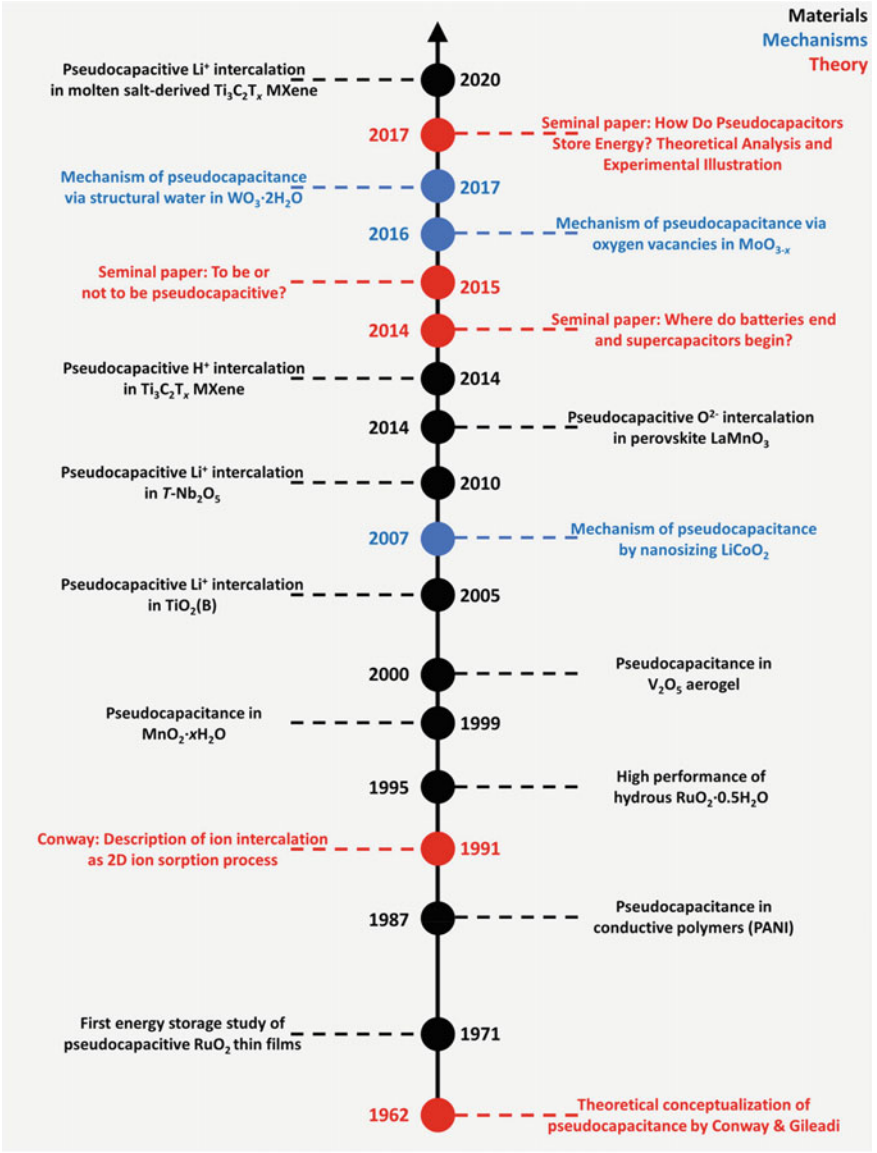

Fig. 3 Timeline of major developments in the field of pseudocapacitance: new pseudocapacitive materials, mechanisms, and theoretical concepts. Adapted with permission [10], copyright (2020), American Chemical Society

potassium cations. Despite having low electrical conductivity, MnO_2 is one of the most researched pseudocapacitive materials to date. This is because of the material's economic and ecological sustainability [11]. Pseudocapacitive charge storage in Li^+ intercalation materials using organic electrolytes first appeared in the 1980s. Conway suggested characterizing these processes in terms of pseudocapacitance in the early 1990s. He saw Li^+ intercalation as a 2D ion sorption process between transition metal oxides and sulfide layers [1, 12]. Levi and Aurbach, who modeled Li^+ intercalation in terms of a Frumkin intercalation isotherm, suggested a similar course of action [13].

The development of nanostructured and defect-rich electrochemical energy storage materials (EES), many of which have pseudocapacitive characteristics, has increased dramatically during the past ten years. Extrinsic pseudocapacitance, Come et al. [14] which distinguishes materials that appear to display capacitive behavior over a large range of particle size and dimensions has been coined when the pseudocapacitive behavior arises because of nanostructuring. The specific surface area is increased through nanostructuring, which also improves the area of contact between the electrode and the electrolyte. Figure 3 provides a timeline of significant advancements in the field of pseudocapacitance. These improvements, when combined, have made substantial advancements in the development of EES with simultaneous high power, energy density, and reliability.

2.2.2 Types of Pseudocapacitance

According to Faradaic mechanisms, there have primarily been three forms of pseudocapacitance, as depicted in Fig. 4 [15]. The first one is adsorption pseudocapacitance or underpotential deposition. Cations in the electrolyte produce a monolayer that is adsorbed and formed on the surface of a metal electrode with greater redox potential. For instance, pseudocapacitance can be produced by Pb^{2+} underpotential deposition processes that occur at a specific potential on the surface of an Au electrode [16]. Augustyn et al. [15] state that the first kind of pseudocapacitance, adsorption pseudocapacitance, is represented by Eqs. (1) and (2). The electrosorption of cation A^+ onto the surface of the conductive surface M is assumed to follow the Langmuir-type electrosorption isotherm [17]:

$$\mathrm{M} + \mathrm{A}^+ + \mathrm{e}^- \leftrightarrow \mathrm{MA}_{\mathrm{ads}} \tag{1}$$

$$\frac{\theta}{\theta - 1} = KC_A e^{\frac{VF}{RT}} \tag{2}$$

where C_A stands for the cation concentration, the surface coverage of MA_{ads} is θ, the surface coverage of M is $1 - \theta$, F stands for the Faraday constant, R for the ideal gas

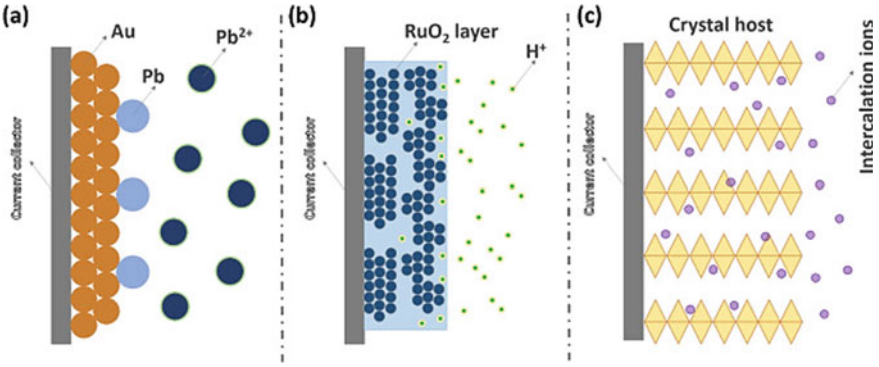

Fig. 4 Three different reversible pseudocapacitances: **a** underpotential deposition; **b** Faradaic redox pseudocapacitance, and **c** intercalation pseudocapacitance. Adapted with permission [19], copyright (2020), Elsevier

constant, V for the electrode voltage, and T for temperature. K stands for the ratio of the forward and reverse reaction rate constants.

The second one is the redox pseudocapacitance, which is more common. With an associated Faradaic charge transfer between the ions in the liquid electrolyte and the solid electrode, it typically occurs on the electrode surface or subsurface. For instance, the 2+, 3+, and 4+ oxidation states of RuO_2 were implicated in the redox reactions that were seen during potential cycling. This process predominates in the charging mechanism together with proton transfer giving rise to pseudocapacitance [18].

The third type is intercalation pseudocapacitance. It happens when ions are intercalated into the layers or tunnels of a redox-active material, and a quick Faradaic charge transfer occurs alongside it without changing the crystallographic phase. As a result, during an electrochemical reaction, it maintains an ultra-stable structure. As stated earlier, Faradaic redox pseudocapacitance only happens on the material's surface, and electrolyte ions never enter the electrode's interior. The ions will be able to inhabit the tunnels or empty positions inside most materials due to the intercalation process. Because of how quickly the intercalation process occurs, it behaves more like the electrode reaction of an SC than a battery. As a result, intercalation pseudocapacitive materials typically have substantially superior rate capabilities than battery materials [19]. Conway devised a method for creating a pseudocapacitor that stores charge due to the potential dependence. Most intrinsic type pseudocapacitors don't exhibit the Faradaic electrochemical response.

2.2.3 Material Selection and Electrode Architecture

Electrode materials for pseudocapacitors can be generally classified mainly into two groups, such as:

1. Transition metal-sulfides, hydroxides, carbides, oxides, nitrides, and oxynitrides
2. Conducting polymers

Materials that exhibit PC behavior include metal oxides (MOs), metal nitrides (MNs), metal oxynitrides (MONs), metal sulphides (MSs), metal carbides (MCs), metal hydroxides (MOHs) and conducting polymers (CPs). The Faradaic charge transfer that occurs at the electrode/electrolyte interface and is used by pseudocapacitors (PCs) to store charge can be recognized by redox peaks in the CV curve [15, 20]. For current technological advancements, the material performance of these distinct groups of materials is important. Despite these benefits, Faradaic behavior in electrode materials causes significant leakage currents (usually in the range of <1 μA to 5 mA) due to the charge transfer across the electrode/electrolyte interface [21, 22]. The self-discharge effect in SCs is primarily caused by the high leakage current, which restricts the practical applications. By applying an insulating layer as a blocking layer to an electron at the electrode/electrolyte interface, leakage currents have been attempted to be reduced.

Many new electrode materials, including transition metal (TM) oxides/hydroxides/sulfides/carbides/nitrides, MXenes, and conducting polymers-based materials, have electrochemical properties that are neither entirely capacitive nor Faradaic, according to Simon et al. [23], Brousse et al. [24], and Gogotsi and Penner [25]. Scientists are concerned about the anomaly between these materials' origin and two fundamentally different energy storage techniques. Due to their electrochemical characteristics, several are categorized as "battery mimic" or "battery-like" materials. Typical redox peaks and voltage plateaus may be seen in the CV and GCD curves, which indicate that charge storage typically occurs at a particular potential.

Transition Metal Oxides

Due to their high theoretical capacitances, low cost, and reversible Faradaic redox reactions that produce higher specific capacitances compared to carbonaceous materials based on an electrical double-layer charge storage mechanism, pseudocapacitive oxides of transition metals (Ni [26], Co [27], Fe [28], Mn [29], etc.) are extensively researched. Despite the intense electrochemical activity, transition metal oxides often have low conductivities, significantly reducing rate capability. As a result of their naturally low electronic and ionic conductivities, their actual practical capacitances are much below what is predicted by theory. Many methods have recently been investigated for modifying their nanostructures, including doping the metals to improve conductivity and redox activity, adding transition metal oxides to a conducting substrate, and combining oxide composites with different oxidation states [30].

Transition Metal Nitrides

Transition metal nitrides (TMNs) are interstitial metallic compounds with covalent and ionic characteristics due to the integration of the nitrogen atom into the parent metal's interstitial sites. These materials stand out due to their distinctive electrical structure, exceptional mechanical resilience, improved chemical stability, and intriguing electrocatalytic activity. Numerous applications of TMNs have attracted considerable scientific interest, primarily for energy storage and conversion [31]. TMNs typically undergo simultaneous metallic, ionic, and covalent bonding, with the M–N bonding expanding the parent metal's lattice and contracting its d-bands. The greater density of states (DOS) and shortage of the d-band in TMNs around the Fermi level allow them to behave like noble metals during electrocatalysis [32].

Transition Metal Oxynitrides

Due to their distinct physicochemical characteristics, a new class of prospective innovative electrode materials for SCs comprises MONs and MNs. Oxynitrides are created when nitrogen is introduced to the oxide lattice, drastically enhancing certain of the material's physical and chemical properties. For instance, when nitrogen is introduced, one frequently notices an increase in hydrophilic nature, an improvement in chemical inertness, and a decrease in the band gap. This increase in electronic conductivity enhances SCs' rate capability, a crucial component of SC technology. The charge storage mechanism of SCs varies depending on the metal content of the oxynitrides [33].

Transition Metal Sulfides

As a novel family of pseudo-capacitive materials, transition metal sulfides have received much attention due to their high energy density capacity. Bimetallic sulfides offer superior electrochemical properties than those of their oxide counterparts, including a two-orders-of-magnitude increase in electrical conductivity and a much-improved redox reaction. The hydrothermal method, followed by anion exchange, has been used to develop the majority of binary metal sulfide nanostructures from their corresponding metal oxide/hydroxide precursors.

This technique is based on the Kirkendall effect, a mechanism that allows for the possible formation of variable morphologies [34]. The Kirkendall effect, which highlights the differences in the atomic diffusion coefficients of chemical constituents, is a well-known phenomenon originating from the mutual diffusion process of chemical constituents over an interface. Due to the uneven diffusion speeds of the two chemical components, vacancies will be generated close to the interface of the chemical component that diffuses more quickly, changing the location of the initial interface during the diffusion process. Vacancies gradually merge into cavities, which then develop into a hollow structure [35].

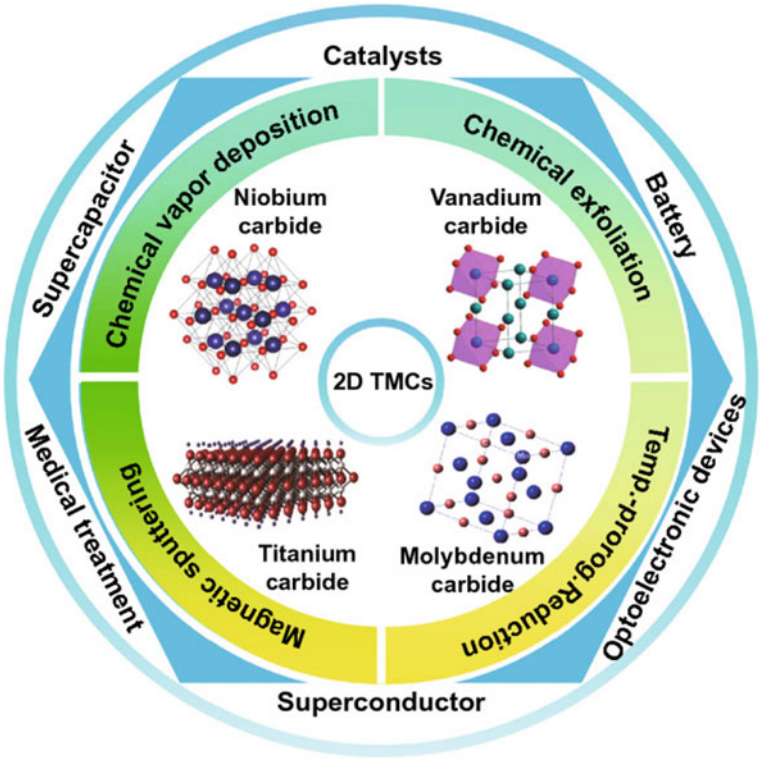

Fig. 5 Applications of 2D transition metal carbides [37]. This article is licensed under a Creative Commons Attribution 4.0 International License

Transition Metal Carbides

For energy storage and catalysis, transition metal carbides (TMCs) have distinctive properties like low resistivity (metallic), high melting temperature, and high electrochemical activities. Dimensional shrinking of bulk TMCs to 0, 1, or 2–dimensional nanostructures (thickness vs. lateral size <1%) has drawn attention to give more control over a variety of attributes and to add additional functionality [36]. Due to its many exceptional dimensionality and structure-dependent features, TMCs have become a hot topic in the development of layered materials since 2004. TMCs are primarily interstitial alloys made of carbon and transition metal atoms. However, only niobium carbide, vanadium carbide, molybdenum carbide, and titanium carbide have received sufficient investigation thus far because of the low chemical activity and complicated synthesis conditions of these TMCs (Fig. 5) [37].

Transition Metal Dichalcogenides (TMDC)

TMDCs are 2D monolayered materials with both "Faradaic" and "non-Faradaic" electrochemical properties, a large surface area, thin layers, high surface tenability, and the potential to improve performance in various fields. Similar to graphene, 2D TMDCs are a nearly 1 nm-thin material that is ideal for a narrow electron transport channel that might speed up ion diffusion. TMDCs are inorganic materials with the chemical formula X-M-X or MX_2, where X (chalcogens) is S, Se, or Te, and M is the transition metal element. Because of their 2D character, TMDCs are a promising electrode material with various rich physicochemical features that can improve energy storage performance.

A key element in determining charge storage performance is materials chemistry, which is concentrated on the strategic design and development of innovative electrode materials for energy storage applications. The energy density, power density, and safety of these devices, such as batteries and SCs, are principally attributed to electrode materials with high electroactivity, electron/ion conductivity, and structural/electrochemical stability. The energy density, power density, and safety of these devices, such as batteries and SCs, are principally attributed to electrode materials with high electroactivity, electron/ion conductivity, and structural/electrochemical stability. The right components, chemical bonds, electronic and atomic structures, crystal structures, and morphologies of those materials can be chosen to achieve high electrochemical performances in accordance with the function-directed materials design rule.

To tailor the qualities of the material and create high-electrode materials, several parameters can be used, including electronegativity, atom radius, chemical bonding, and oxidation state. General materials chemistry guidelines will make the rational design of electrode materials with improved electrochemical performance easier. As a result, there needs to be a connection between the synthesis processes and the material's structure, components, and size. Different elements, electrical structures, crystal structures, and macroscopic scale morphologies, sizes, and material architectures (hollow, core–shell, tubes, wires, flakes, etc.) can all be designed into materials at various scales [2].

2.2.4 Theories of Electrode–Electrolyte Interfaces in Pseudocapacitive Materials

Due to the intricate relationship between the terminal voltage of supercapacitors, they cannot be utilized or researched in the same ways as conventional capacitors. After quick charge–discharge cycles, there is a significant variation in the terminal voltage. A simple resistive, capacitive RC circuit could not describe a supercapacitor's behavior. Many modified RC circuits are proposed to represent a supercapacitor system based on physical reasoning. Still, none of them can account for all the parameters of SCs and can simultaneously analyze the effects of the interfacial electric field

and temperature variation. This is the cause of the mismatch between a supercapacitor system's theoretical and real outcomes. Capacitance dependence of polarisable electrodes on the potential, self-discharge process, and temperature variation should all be included when creating a more realistic model. Additionally, it is essential to investigate the electrolyte conductivity in the electrode's pores, pore resistance, ballistic transport, and electrode conductivity [38].

The theoretical pseudocapacitance of metal oxide can be calculated using Eq. (3):

$$C = \frac{nF}{MV} \tag{3}$$

where F is the Faraday constant, n is the average number of electrons exchanged during a redox reaction, M is the molar mass of metal oxide, and V is the operating voltage window. Supercapacitor ideal models are attainable using molecular dynamics and modern computing technologies. Theoretical modelling of pseudocapacitors is scarce compared to the amount of theoretical and computational work done on EDLCs. Developing a precise strategy for modelling pseudocapacitors is challenging because of the complexity of interfacial redox processes [39]. The behaviour of reactants, and surface redox kinetics, all affect pseudocapacitance. It is hard to address these difficulties in a single model. It is crucial to create a model for investigating pseudocapacitance since none exists.

Continuum Models

The Poisson-Nernst-Planck (PNP) concept of electrodiffusion is typically used in continuum models to analyse the electrolyte and electrode interface. Because of the strong interfacial electric field, modeling does not employ constant values for the physical and chemical parameters but treats them as their surroundings' functions. L Pilon and Harnan Wang created a continuum theory-based 3D model for simulations based on organized mesoporous electrode architectures [40]. Hainan Wang and Pilon's model accurately simulated the electrode architecture composed of CP204-S15 carbon with mesopores produced by Woo et al. [41] accounted for the ion's finite size and the diffuse layer, stern layer, and other layers.

In addition, the hybrid pseudocapacitor based on lithium intercalation and diffusion in metal oxide is described using a 1D continuum transport model [42]. A similar study was conducted to create a model that would describe a pseudocapacitor based on RuO_2 [43]. The main objective was to study the shifts in pseudocapacitance over the electrode's thickness. Thicker electrodes were discovered to cause losses, particularly toward the conclusion of the oxidation process. The electrolyte was considered to have a high ion concentration. Another study examined an electrochemical capacitor/battery hybrid system's performance using a one-dimensional model [44].

Quantum Models

The main components of quantum models are density functional theory DFT and ab initio quantum chemistry. Numerous investigations based on DFT have been conducted for the electrode materials utilized in pseudocapacitors [45]. RuO_2 (110)'s pseudocapacitive behaviour was simulated using joint density functional theory (JDFT) [46]. The resulting capacitive curve was comparable to the experimental cyclic voltammetry (CV) curve that showed the exact position of the redox peak. JDFT in the JDFTx package used the linear polarizable continuum model (linear PCM) to determine the electronic chemical potential and total energy. The ultrasoft pseudopotential described the interaction between nuclei and electrons. Total charge per unit chemical potential shift, or $Q_{tot}/\Delta\mu$, was used to quantify total capacitance.

Simplified Analytical Models

Mathematical equations in these models describe the flow of charged particles and the pace of reaction [47]. These models describe the electrical behavior of SC using partial differential equations. Li et al. [48] created another model for asymmetric supercapacitors. The energy capacity, charge–discharge cycle energy efficiency, electrode-specific capacitance, and electrolyte conductivity may all be calculated using this model. The experimental and theoretical values of the quantities for heterogeneous electrochemical supercapacitors of the $PbO_2|H_2SO_4|C$ system matched the voltage range of 0.8–2.2 V. However, there is a tiny discrepancy between the two above 2.2 V.

2.2.5 Device-Level Merits and Demerits Associated with Pseudocapacitors

Although EDLCs have quick charge–discharge rates, high power densities, and extended cycling lives, the amount of energy they can store is much less than that of batteries. Pseudocapacitors can produce substantially higher capacitance and energy density when compared to EDLCs since they incorporate reversible redox Faradaic processes during charge and discharge. Low power densities and unstable materials result from these materials' poor electrical conductivity and delayed responsiveness.

To solve this problem and obtain high capacitances, these materials are typically placed on highly conductive substrates [48]. Energy density must be raised without sacrificing power density or cycle life to use flexible SCs in real-world applications. High power density and extremely long cycle lives for well-developed EDLCs have been provided, whereas high capacitances are possible with pseudocapacitors. Therefore, combining the benefits of EDLCs with pseudocapacitors to create composite electrode materials is a workable method to achieve larger power and energy densities.

2.3 Hybrid Supercapacitor

In recent years, hybrid supercapacitors have become popular due to their enhanced energy density performance without affecting their power density. The hybrid supercapacitor offers higher specific capacitance than current electric double-layer capacitors and pseudocapacitors. In general, the hybrid supercapacitors' asymmetric behavior, which results from combining an EDLC and a pseudocapacitor, enhances the respective capacitance values (Fig. 2c). This asymmetrical strategy represents a fresh start on the path to the much-needed pollution-free, durable, and effective energy-storing performance. According to their use in hybrid electric vehicles, research into creating new sophisticated storage devices finds a huge and promising future. The most important component for energy-efficient applications requires the introduction of novel materials to achieve a noticeably greater surface-to-volume ratio.

The storage concepts for hybrid supercapacitors combine the EDLC and pseudocapacitor storage principles. The pseudocapacitor lacks the limiting property of EDLC, and vice versa. When these two components are combined, the constraints of the individual components are obscured, which has the benefit of improving the capacitance. Depending on the assembly setup, hybrid supercapacitors can be either symmetric or asymmetric.

3 Conclusion

Pseudocapacitive materials typically offer both fast rate and high capacitance, unlike EDLC and battery materials. This benefit has encouraged a lot of study into pseudocapacitive materials and associated energy storage technologies. As nanoscience and nanotechnology have advanced quickly in recent years, an increasing number of electrodes based on nanomaterials have been created for batteries and supercapacitors. As a result, a simple kinetics analysis cannot be used to distinguish between battery- and pseudocapacitive materials. Comparatively less theoretical and computational work has been done on pseudocapacitors compared to EDLCs. Despite the abundance of SC devices on the market, there are still several issues, including high leakage current, small surface areas, and instability. Asymmetric and symmetric electrode configurations were extensively researched to help with supercapacitor problems. Asymmetric supercapacitors frequently offer a larger operating voltage window and better energy storage capacities than symmetric supercapacitors. Supercapacitor technology needs to make significant improvements in both device performance (energy density) and market-relevant metrics (price, durability, and thermal stability) to compete with current battery technology.

References

1. B.E. Conway, Transition from "Supercapacitor" to "Battery" behavior in electrochemical energy storage. J. Electrochem. Soc. **138**, 1539 (1991)
2. P. Bhojane, Recent advances and fundamentals of pseudocapacitors: materials, mechanism, and its understanding. J. Energy Storage **45**, 103654 (2022)
3. N. Swain, B. Saravanakumar, M. Kundu, L. Schmidt-Mende, A. Ramadoss, Recent trends in template assisted 3D porous materials for electrochemical supercapacitors. J. Mater. Chem. A **9**, 25286–25324 (2021)
4. D.C. Grahame, Properties of the electrical double layer at a mercury surface. I. Methods of measurement and interpretation of results. J. Am. Chem. Soc. **63**, 1207–1215 (1941)
5. S. Srinivasan, E. Gileadi, The potential-sweep method: a theoretical analysis. Electrochim Acta **11**, 321–335 (1966)
6. B.E. Conway, E. Gileadi, Kinetic theory of pseudo-capacitance and electrode reactions at appreciable surface coverage. Trans. Faraday Soc. **58**, 2493–2509 (1962)
7. F. Scholz, E.P.M. Leiva, Moïse Haïssinsky: The discoverer of underpotential deposition. ChemElectroChem **5**, 849–854 (2018)
8. S. Trasatti, G. Buzzanca, Ruthenium dioxide: a new interesting electrode material. Solid state structure and electrochemical behaviour. J. Electroanal. Chem. Interfacial Electrochem. **29**, A1–A5 (1971)
9. J.P. Zheng, P.J. Cygan, T.R. Jow, Hydrous ruthenium oxide as an electrode material for electrochemical capacitors. J. Electrochem. Soc. **142**, 2699 (1995)
10. S. Fleischmann, J.B. Mitchell, R. Wang, C. Zhan, D. Jiang, V. Presser, V. Augustyn, Pseudocapacitance: from fundamental understanding to high power energy storage materials. Chem. Rev. **120**, 6738–6782 (2020)
11. H.Y. Lee, J.B. Goodenough, Supercapacitor behavior with KCl electrolyte. J. Solid State Chem. **144**, 220–223 (1999)
12. B.E. Conway, Two-dimensional and quasi-two-dimensional isotherms for Li intercalation and UPD processes at surfaces. Electrochim. Acta **38**, 1249–1258 (1993)
13. M.D. Levi, D. Aurbach, Frumkin intercalation isotherm—a tool for the description of lithium insertion into host materials: a review. Electrochim. Acta **45**, 167–185 (1999)
14. J. Come, V. Augustyn, J.W. Kim, P. Rozier, P.-L. Taberna, P. Gogotsi, J.W. Long, B. Dunn, P. Simon, Electrochemical kinetics of nanostructured Nb_2O_5 electrodes. J. Electrochem. Soc. **161**, A718 (2014)
15. V. Augustyn, P. Simon, B. Dunn, Pseudocapacitive oxide materials for high-rate electrochemical energy storage. Energy Environ. Sci. **7**, 1597–1614 (2014)
16. B.-Y. Chang, E. Ahn, S.-M. Park, Real-time staircase cyclic voltammetry fourier transform electrochemical impedance spectroscopic studies on underpotential deposition of lead on gold. J. Phys. Chem. C **112**, 16902–16909 (2008)
17. B.E. Conway, H. Angerstein-Kozlowska, The electrochemical study of multiple-state adsorption in monolayers. Acc. Chem. Res. **14**, 49–56 (1981)
18. D. Rochefort, A.-L. Pont, Pseudocapacitive behaviour of RuO_2 in a proton exchange ionic liquid. Electrochem. Commun. **8**, 1539–1543 (2006)
19. Y. Liu, S.P. Jiang, Z. Shao, Intercalation pseudocapacitance in electrochemical energy storage: recent advances in fundamental understanding and materials development. Mater. Today Adv. **7**, 100072 (2020)
20. W. Wei, X. Cui, W. Chen, D.G. Ivey, Manganese oxide-based materials as electrochemical supercapacitor electrodes. Chem. Soc. Rev. **40**, 1697–1721 (2011)
21. B.W. Ricketts, C. Ton-That, Self-discharge of carbon-based supercapacitors with organic electrolytes. J. Power Sourc. **89**, 64–69 (2000)
22. B.E. Conway, W.G. Pell, T.-C. Liu, Diagnostic analyses for mechanisms of self-discharge of electrochemical capacitors and batteries. J. Power Sourc. **65**, 53–59 (1997)
23. P. Simon, Y. Gogotsi, B. Dunn, Where do batteries end and supercapacitors begin? Science **343**, 1210–1211 (2014)

24. T. Brousse, D. Bélanger, J.W. Long, To be or not to be pseudocapacitive? J. Electrochem. Soc. **162**, A5185 (2015)
25. Y. Gogotsi, R.M. Penner, Energy storage in nanomaterials—capacitive, pseudocapacitive, or battery-like? ACS Nano **12**, 2081–2083 (2018)
26. R.A. Patil, C.-P. Chang, R.S. Devan, Y. Liou, Y.-R. Ma, Impact of nanosize on supercapacitance: study of 1D nanorods and 2D thin-films of nickel oxide. ACS Appl. Mater. Interfaces **8**, 9872–9880 (2016)
27. F. Ning, M. Shao, C. Zhang, S. Xu, M. Wei, X. Duan, Co_3O_4@layered double hydroxide core/shell hierarchical nanowire arrays for enhanced supercapacitance performance. Nano Energy **7**, 134–142 (2014)
28. Y. Ding, S. Tang, R. Han, S. Zhang, G. Pan, X. Meng, Iron oxides nanobelt arrays rooted in nanoporous surface of carbon tube textile as stretchable and robust electrodes for flexible supercapacitors with ultrahigh areal energy density and remarkable cycling-stability. Sci. Rep. **10**, 11023 (2020)
29. O. Ghodbane, J.-L. Pascal, F. Favier, Microstructural effects on charge-storage properties in MnO_2-based electrochemical supercapacitors. ACS Appl. Mater. Interfaces **1**, 1130–1139 (2009)
30. S.R. Ede, S. Anantharaj, K.T. Kumaran, S. Mishra, S. Kundu, One step synthesis of Ni/$Ni(OH)_2$ nano sheets (NSs) and their application in asymmetric supercapacitors. RSC Adv. **7**, 5898–5911 (2017)
31. B. Gao, X. Li, K. Ding, C. Huang, Q. Li, P.K. Chu, K. Huo, Recent progress in nanostructured transition metal nitrides for advanced electrochemical energy storage. J. Mater. Chem. A **7**, 14–37 (2019)
32. J.-L. Calais, Band structure of transition metal compounds. Adv. Phys. **26**, 847–885 (1977)
33. A. Joseph, T. Thomas, Recent advances and prospects of metal oxynitrides for supercapacitor. Progr. Solid State Chem. **68**, 100381 (2022)
34. W. Liu, H. Niu, J. Yang, K. Cheng, K. Ye, K. Zhu, G. Wang, D. Cao, J. Yan, Ternary transition metal sulfides embedded in graphene nanosheets as both the anode and cathode for high-performance asymmetric supercapacitors. Chem. Mater. **30**, 1055–1068 (2018)
35. Y. Yin, R.M. Rioux, C.K. Erdonmez, S. Hughes, G.A. Somorjai, A.P. Alivisatos, Formation of hollow nanocrystals through the nanoscale Kirkendall effect. Science **304**, 711–714 (2004)
36. X. Zhao, W. Sun, D. Geng, W. Fu, J. Dan, Y. Xie, P.R.C. Kent, W. Zhou, S.J. Pennycook, K.P. Loh, Edge segregated polymorphism in 2d molybdenum carbide. Adv. Mater. **31**, 1808343 (2019)
37. T. Qin, Z. Wang, Y. Wang, F. Besenbacher, M. Otyepka, M. Dong, Recent progress in emerging two-dimensional transition metal carbides. Nanomicro Lett. **13**, 183 (2021)
38. Kumar A. Bharti, G. Ahmed, M. Gupta, P. Bocchetta, R. Adalati, R. Chandra, Y. Kumar, Theories and models of supercapacitors with recent advancements: impact and interpretations. Nano Express **2**, 22004 (2021)
39. C. Zhan, C. Lian, Y. Zhang, M.W. Thompson, Y. Xie, J. Wu, P.R.C. Kent, P.T. Cummings, D. Jiang, D.J. Wesolowski, Computational insights into materials and interfaces for capacitive energy storage. Adv. Sci. **4**, 1700059 (2017)
40. H. Wang, L. Pilon, Mesoscale modeling of electric double layer capacitors with three-dimensional ordered structures. J Power Sourc. **221**, 252–260 (2013)
41. S.-W. Woo, K. Dokko, H. Nakano, K. Kanamura, Preparation of three dimensionally ordered macroporous carbon with mesoporous walls for electric double-layer capacitors. J. Mater. Chem. **18**, 1674–1680 (2008)
42. H.-L. Girard, H. Wang, A.L. d'Entremont, L. Pilon, Enhancing faradaic charge storage contribution in hybrid pseudocapacitors. Electrochim. Acta **182**, 639–651 (2015)
43. T. Kadyk, M. Eikerling, Charging mechanism and moving reaction fronts in a supercapacitor with pseudocapacitance. J. Electrochem. Soc. **161**, A239 (2013)
44. G. Sikha, R.E. White, B.N. Popov, A mathematical model for a lithium-ion battery/electrochemical capacitor hybrid system. J. Electrochem. Soc. **152**, A1682 (2005)

45. Y. Liu, F. Zhou, V. Ozolins, Ab Initio study of the charge-storage mechanisms in RuO_2-based electrochemical ultracapacitors. J. Phys. Chem. C **116**, 1450–1457 (2012)
46. C. Zhan, D. Jiang, Understanding the pseudocapacitance of RuO_2 from joint density functional theory. J. Phys.: Condens. Matter **28**, 464004 (2016)
47. S. Devan, V.R. Subramanian, R.E. White, Analytical solution for the impedance of a porous electrode. J. Electrochem. Soc. **151**, A905 (2004)
48. L. Li, Z. Wu, Y. Shuang, X.-B. Zhang, Advances and challenges for flexible energy storage and conversion devices and systems. Energy Environ. Sci. **7**, 2101 (2014)

Pseudocapacitance: Fundamentals to Advanced Applications

Shilpa Pande, Bidhan Pandit, Shoyebmohamad F. Shaikh, and Jahangeer Ahmed

Abstract The electrochemical energy storage advancement requires the use of either high-power density (like batteries) or high-energy density (like electrochemical capacitors) devices. For both current and upcoming applications, materials that can give high energy densities as well as high power densities in a single package are in increased demand. The faradaic process of power involves surface or near-surface redox processes. It provides a way for doing so by employing high charge–discharge rates and high-power densities. The focus of this chapter is on the pseudocapacitive characteristics of transition metal oxides. Pseudocapacitance will be explained in length in this chapter before going over its electrochemical properties. The following section of this chapter will be a review of the most prominent pseudocapacitive elements found in both aqueous & non-aqueous electrolytes. Near the end, there is a full discussion of the key problems with pseudocapacitive materials and a look into the future.

Keywords Electrochemical energy storage · Pseudocapacitive mechanisms · Aqueous pseudocapacitor materials · Non-aqueous electrolyte pseudocapacitor materials · Supercapacitors · Lithium-ion battery

S. Pande (✉)
Department of Applied Physics, Laxminarayan Innovation Technological University, Nagpur, Maharashtra 440033, India
e-mail: sap7001@gmail.com

B. Pandit
Department of Materials Science and Engineering and Chemical Engineering, Universidad Carlos III de Madrid, Avenida de la Universidad 30, 28911 Leganés, Madrid, Spain

S. F. Shaikh · J. Ahmed
Department of Chemistry, College of Science, King Saud University, P. O. Box 2455, Riyadh 11451, Saudi Arabia

© The Author(s), under exclusive license to Springer Nature Switzerland AG 2024

R. K. Gupta (ed.), *Pseudocapacitors*, Engineering Materials,
https://doi.org/10.1007/978-3-031-45430-1_2

1 Introduction

Batteries and electrochemical capacitors are two examples of electrochemical energy storage (EES), a technology that is widely used to power today's almost universally portable electronics and enable the electrification of the transportation sector. One more implementation for EES is the integration of such technologies into renewable energy sources (RESs) like solar and wind to supply electricity to the electricity grid [1, 2]. This application was created because of the need to modernize the power infrastructure in many industrialized nations and the anticipated rise in global energy demand over the following several decades (arising partially from the demand to electrify developing countries). Even though EES offers a wide range of possible uses, it also has several disadvantages, most of which are associated with the requirement for materials that are more effective for storing and transferring large energy. In a perfect world, these processes would be carried out using materials that are readily available and don't produce any harmful by-products. This would elevate the EES devices' safety while also lowering the cost of them in consumer goods and stationary electricity [3].

Transition metal oxides within one or both electrodes have an impact on EES's efficacy [4]. This chapter discusses pseudocapacitance and transition metal oxide pseudocapacitors. Pseudo capacity is brought on by reversible redox activities that happen at or close to the surface of a substance in contact with an electrolyte and are not impeded by solid-state ion transport. Both intrinsic and extrinsic behaviour, as well as aqueous or non-aqueous electrolytes, are possibilities [5]. Pseudocapacitive materials charge and discharge in seconds and minutes as opposed to batteries, which charge in milliseconds [6]. Hence, research and development into pseudocapacitance are driven by the enormous energy & power densities of a single material [7].

Figure 1 shows how a high-power lithium-ion battery's energy density holds steady across discharge times longer than 10 min. This energy is being lost more quickly because of resistive losses in battery cells. Slow electron and ion passage account for a considerable portion of resistive losses. Heat is produced through resistive losses, especially when they occur quickly, and this heat can lead to thermal runaway and other dangers. Yet, despite their tiny total stored energy, commercially available EDLCs maintain a constant energy density over all time periods. Pseudocapacitive materials appear to flourish in the time range between 10 s and 10 min when EDLCs and lithium-ion batteries function best.

It is beneficial to have such a high-rate EES for a range of applications since these applications demand either a huge amount of energy that is to be stored or a rapid delivery of that energy. As a result, having such a high-rate EES is favourable for these applications. One illustration of this would be the accumulation of kinetic energy in seaports [8] or using regenerative braking [9]. Additional examples include the implementation of power quality applications within the power grid and the usage of pulse power in communication devices [10]. In addition to this, it would be of great assistance if the amount of time needed to charge portable electronics, most notably electric vehicles, was reduced [11]. Background, development of pseudocapacitance,

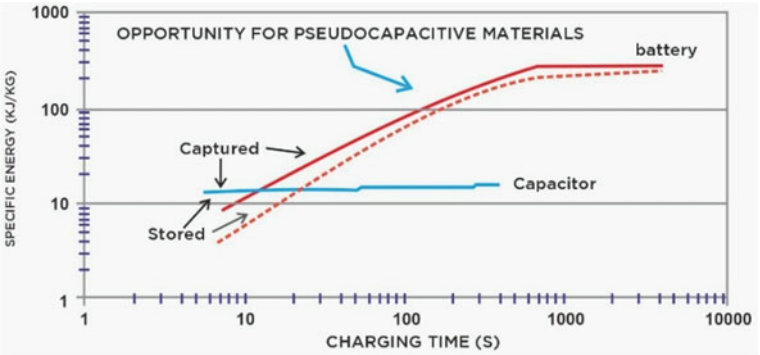

Fig. 1 The relationship between specific energy and recharge time for an electronic higher-rate lithium-ion battery & Electric double layer capacitor (EDLC)

the electrochemical characteristics of this behaviour, pseudocapacitance in aqueous electrolytes, and pseudocapacitance in non-aqueous electrolytes are covered in this chapter.

2 Background

Although known since the beginning that charges could collect on solids, General Electric got the first electrochemical capacitor patent in 1957 [12]. This was true even though charges may build up on solids from the beginning of time. Except for lithium-ion batteries, most energy storage technologies were invented in the late 19th and early twentieth centuries, making this a late entrant. This suggested a late field entrance. The patent states "it is not known with confidence what happens when the equipment is used as energy storage devices." A high-surface-area electrode is essential. Carbons are useful due to their high conductivity, large surface areas, and low density. These devices store charge by adhering electrolyte ions to electrified materials, and carbons are the best materials for this. Electrostatic charge storage does not require redox processes. EDLCs are these devices. Commercial devices store 3–6 Wh/kg [13].

EDLCs have been extensively reviewed. EDLC research focuses on how pore structure and electrode area affect capacitance. Double-layer capacitances of 150 F/g are ideal for carbon pore diameters in ionic liquid electrolytes [13, 14]. Functionalizing surface with nitrogen and oxygen groups, using pore widths that match electrolyte ion size, using redox-active species, or producing ionic liquid mixes to improve cell voltage and temperature can increase EDLC energy densities. Graphene-EDLCs are popular. Graphene has 100–250 F/g capacitance due to its large surface area. These materials' sheet-like nanoscale structure precludes

gravimetric-normalized capacitance. Graphene allows versatile EDLC device topologies [15]. Figure 2 depicts pseudocapacitance's evolution, including new materials, mechanisms, and ideas [16].

Fig. 2 Pseudocapacitance timeline: novel materials, processes, and theoretical notions

3 Types of Energy Storage Devices

Energy storage systems can range from alternatives that are quick to respond for near real-time and daily management of the networks to solutions that have a longer duration for the unpredictability of week-to-week variations as well as more predictable seasonal variations in supply and demand. Services such as managing power quality and balancing load, as well as providing backup power for outage management, are examples of important use cases. It is possible to classify the many forms of energy storage into the following five major groups of technology.

Battery Storage: Batteries are an electrochemical technology that can consist of one or more cells and have a positive terminal known as a cathode and a negative terminal known as an anode. Batteries are the oldest form of storage, the most prevalent form of storage, and the most commonly accessible form of storage. A wide variety of chemical compositions can be found in batteries. The lithium-ion and lead acid batteries are the most well-known and are used extensively in portable electronic gadgets and cars respectively. Nickel–cadmium, and sodium–sulfur are two more common forms of solid batteries; the zinc–air battery is a relatively new variety. Flow batteries using liquid electrolyte solutions are another type of battery. These batteries can use a variety of chemistries, such as vanadium redox, iron-chromium, and zinc-bromine. Although supercapacitors are not, strictly speaking, batteries, it is possible to classify them as an electrochemical technology due to their application, which is notable for a sub-minute level response.

Thermal Storage: The essence of thermal storage is the capturing and releasing of heat or cold in a solid, liquid, or air medium, with the possibility of involving changes in the state of the medium itself, such as moving from a gas to a liquid or from a solid to a liquid and vice versa. Cryogenic storage, which uses molten salt and liquid air, is one of the technologies that can be used to store energy. With the advent of concentrated solar power, molten salt has become a commercially feasible heat storage option. However, the requirement for massive subterranean storage caverns may limit this and other potential heat storage methods.

Mechanical Storage: The kinetic forces of rotation or gravitation can be used to store energy in mechanical storage devices, making these systems possibly the simplest type of energy storage. Yet, to achieve this level of feasibility in today's grid applications, the most recent technologies are required. The most common methods involve energy storage using flywheels and devices that use compressed air, although gravitational energy is a relatively new technology that is still being developed and has several different applications.

Pumbed Hydro: The storage of energy using pumped hydro systems that are based on big water reservoirs have been widely deployed during much of the course of the previous century to become the most frequent kind of utility-scale storage worldwide. These types of systems require the circulation of water between two reservoirs located at different levels, with the "energy storage" occurring in the water located in the

upper reservoir and the "energy release" occurring when the water is transferred to the lower reservoir.

Hydrogen: The new method of energy storage known as hydrogen would require the hydrogen to be converted from electricity through the process of electrolysis before being stored in tanks. It is possible for it to later go through the process of re-electrification or be supplied to new applications such as transportation, industrial, or residential use as a complement or alternative for gas.

4 Role of Pseudocapacitive Materials

To circumvent the kinetic constraints of lithium-ion batteries (LIBs) and reach energy densities greater than electrical double-layer capacitors, pseudocapacitive electrode materials are being researched. Any anion or cation can be employed with pseudocapacitance, giving it the best option for energy storage outside of Li^+. Early in the 1960s, pseudocapacitance was developed to describe surface Faradaic processes including hydrogen adsorption and underpotential deposition. Although single-crystal RuO_2 did not exhibit cyclic voltammograms, thin films for hydrous RuO_2 cycled within the acidic electrolyte did. Storage of energy was the result [17]. Jiang and others [18] connected the response for capacitive electrochemical to the electrochemical mechanism. Pseudocapacitive materials have a large charge storage capacity as compared to batteries while also undergoing reversible electrochemical processes in a lot less time than EDLCs. In comparison to LIBs and EDLCs, pseudo capacities have intermediate cycle stability. The atomic process is typically credited to highly reversible surface or intercalation charge transport responses that are uncontrolled by solid-state diffusion (Fig. 3).

Afterward, a description of the pseudocapacitive electrochemical behavior will be provided. Pseudocapacitive compounds link batteries and EDLCs. The distinction between these three categories of materials is being eroded by nanostructured materials and carbons having redox-active functional groups. Due to their high reversibility and lack of solid-state diffusion restrictions at minutes, pseudocapacitive electrochemical materials exhibit exceptional efficiency at the high density of current. To produce the pseudocapacitive materials, an atomic comprehension of kinetic & thermodynamic mechanisms that lead to particular electrochemical behavior is required.

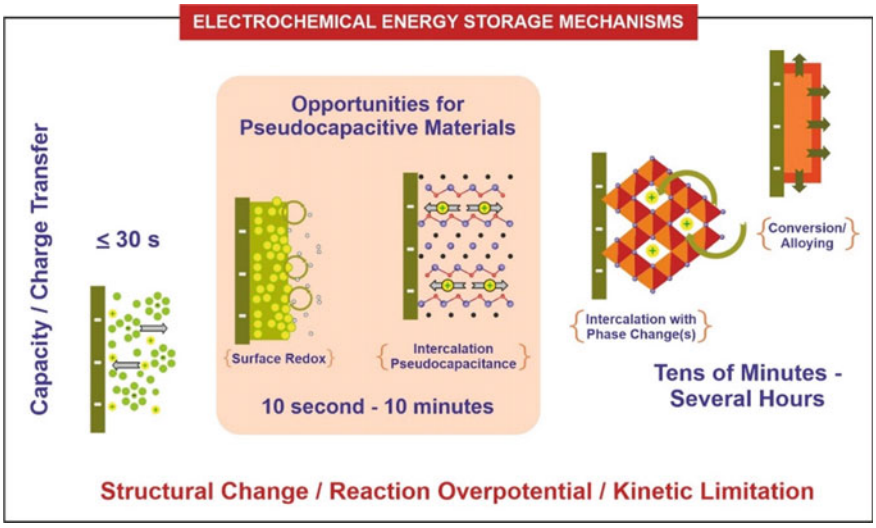

Fig. 3 Techniques for the electrochemical energy storage are categorised according to their capacity, changes in electrode structure, reaction over potential, and kinetic restrictions

5 Types of Pseudocapacitive Mechanisms

Conway discovered several different faradaic pathways that might result in capacitive electrochemical properties [19]. The following summarises each of these mechanisms: (i) underpotential deposition; (ii) the redox pseudocapacitance; & (iii) intercalation pseudocapacitance. Figure 4 provides a visual representation of these processes.

Under prospective deposition takes place when the metal ions establish adsorbed monolayer upon a different metal surface along a redox potential that is significantly greater than their overall redox potential. Lead deposition on a gold electrode illustrates under potential deposition. Once ions are electrochemically reabsorbed onto a material's surface and undertake faradaic charge transfer, redox pseudocapacitance results. When ions intercalate into the redox-active material layers or tunnels, faradaic charge transfer occurs, however, the crystallographic phase is unaffected [20]. Intercalation pseudocapacitance occurs. Electrochemical fingerprints share a link between potential and the amount of charge formed by adsorption and desorption at the interface of electrolyte/electrode or inside a material's inner surface. Physical processes and materials cause these three mechanisms:

$$E \sim E^0 - \frac{RT}{nF} \ln\left(\frac{X}{1-X}\right) \tag{1}$$

here, E represents the potential (V), T represents temperature (K), whereas, R depicts the ideal gas constant (8.314 J/mol · K), n represents the total electrons, F represents

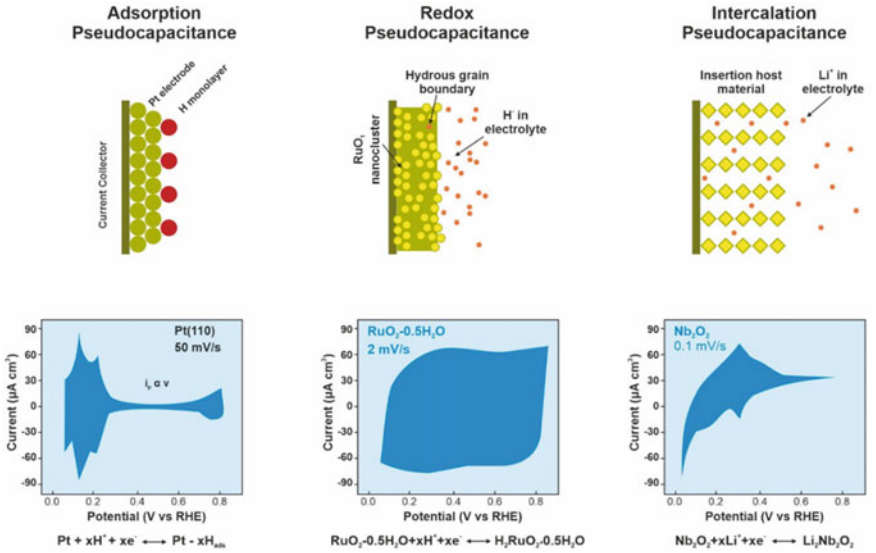

Fig. 4 Types of reversible redox mechanisms

Faraday's constant (96 485 C/mol), & X represents the fractional coverage extent of inner structure or the surface [21]. In the above equation, capacitance (C; F/g) might be expressed in the regions wherein plot of X versus X is linear:"

$$C = \left(\frac{nF}{m}\right)\frac{X}{E} \tag{2}$$

where m represents the active substance's overall molecular weight. Since the X versus E is not linear such as within a capacitor, and capacitance isn't constant. Hence, the capacitance is called pseudocapacitance [22, 23].

Despite the equation's thermodynamic basis for pseudocapacitance, these materials' kinetic behavior determines their energy storage potential. Reactions at the surface or just limited by the surface have a high-rate capability because they are not constrained by the diffusion of solid-state. Transition metal oxides with pseudocapacitive action have this crucial feature. These components are used in rechargeable batteries [23]. High energy densities are possible with rechargeable batteries because they store charge in bulk solid form. The cathode and anode active materials' solid-state diffusion restricts these devices' power capacity.

6 Electrochemical Features of Pseudocapacitance

The phenomenon known as pseudo capacity can be caused by a variety of causes, as was previously mentioned. In electrochemical terms, the appearance of some of the properties covered in this section is due to pseudocapacitance. This presents a description of pseudocapacitive energy storage [24], which is dependent on the response to (i) voltage sweep, as seen in the cyclic voltammetry; (ii) constant current, as seen in the galvanostatic cycling; & (iii) alternating current, as is seen in the impedance spectroscopy.

The sweep rate (v, mV/s) for the experiment of cyclic voltammetry is what determines how long the experiment will last. This same parameter also establishes the chronology of the experiment. Based on whether the reaction of redox is controlled by surface reactions or diffusion processes, the current approach to a given sweep rate will vary (capacitive) [25]. In the particular instance of the capacitive process, the overall reaction varies directly along v, whereas the current response differs indirect means with v by a factor of half in the case of a redox reaction confined by semi-infinite linear diffusion. Because of this, the fundamental connection described below may be utilized to characterise the current that is flowing through any material at a specific potential [26]:

$$i(V) = k_1 v^{1/2} + k_2 v \tag{3}$$

An analysis of the capacity and sweep rate relationship was first suggested by Fröhlich et al. [27] and was included in a similar study. Surface-related capacity will always exist, even at high sweep rates, because it will remain constant with the rate of sweep. Even when the sweep rate is quite high, this is true. When processes are restricted by infinitesimally slow linear diffusion, the capacity that results will vary with $v^{-1/2.}$ The infinite-sweep rate capacity, $Q_{v=\infty}$, is used in the equation below to describe the capacitive contribution. The last contribution is made up of the capacity that is regulated by diffusion. This capacity is restricted by a value of $v^{-1/2.}$

$$Q = Q_{v=\infty} + \text{ constant } \left(v^{-1/2}\right) \tag{4}$$

Peak potential and sweep rate both characterise quick energy storage. During slow charge–discharge intervals, capacitive systems have very minimal potential hysteresis between charging and discharging. When charge–discharge periods are short, this is true. At slow sweep rates, cyclic voltammetry reveals negligible or zero potential difference among the cathodic & anodic peak currents for just a layer of about 30 nm Nb_2O_5 nanocrystals.

Nernstian processes with a modest potential difference are also reversible. A reaction with n electrons has a maximum voltage differential of 59 mV [28]. This behaviour in transition metal oxides indicates either rapid energy storage without any phase shift or, in some incredibly uncommon circumstances, rapid energy storage with very little volume difference between the charged and discharged phases. It

is crucial to remember that, even when used in areas of an electrochemical system where polarization is minimal, polarisation processes in electrochemical systems will always lead to peak voltage separation. This means that for thin layers of the transition-type metal oxides, an experiment must be run at sweep rates of about 100 mV/s; the average range for these rates is between 1 and 10 mV/s [29].

Another technique to check for pseudocapacitive behaviour in a system is AC impedance; however, the interpretation of the impedance data depends on the equivalent circuit that is best suited for the system. Moreover, the outcomes of the measurements for the double-layer capacitance and the pseudocapacitance might be comparable. Ideal capacitors have a vertical Nyquist representation (imaginary vs. real impedance, Z) with a phase angle of 90°. A constant-phase equivalent circuit member represents pseudocapacitive behavior.

$$Z = 1/B\ (i\omega)^{p} \tag{5}$$

In this case, Z denotes the impedance, B represents the constant value, u denotes the frequency, & p denotes a variable constant.

It is controversial whether the capacitance values shall be utilized to characterize the electrochemical type of charge storage behavior of these materials because substances that do not exhibit any of these electrochemical properties do not have the property of being pseudocapacitive. In order to determine whether or not a material actually possesses pseudocapacitance, it is essential to carry out exhaustive research into the electrochemical behavior of the substance in question. This will allow one to determine definitively whether pseudocapacitance is present. Figure 5 provides a breakdown and summary of the electrochemical properties that are characteristic of pseudocapacitive materials in general [24]. Considering the primary considerations that have been presented up until this point, the electrochemical behavior of a variety of different pseudocapacitive materials will be investigated and addressed in the following sections.

Intrinsic Versus Extrinsic Pseudocapacitance

It is possible for a material's pseudocapacitance either to be intrinsic to the substance or extrinsic, i.e., to be created using suitable material engineering techniques. Despite whether the material is reviewed to be an extrinsic or intrinsic pseudo capacitor, it

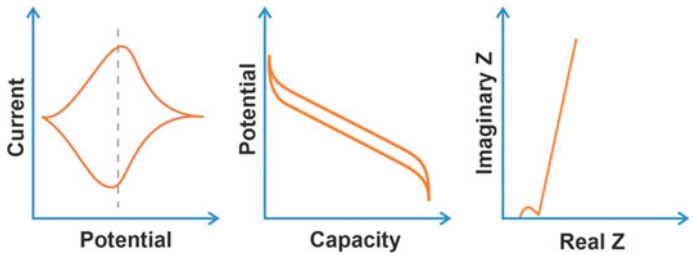

Fig. 5 The electrochemical characteristics that are typical of materials with pseudocapacitance

displays all of these characteristics, so its properties are identical in both cases. Despite the diverse particle sizes & morphologies existing in these components, intrinsic pseudocapacitive materials show capacitive charge storage characteristics. Examples of these materials include $RuO_2 \cdot nH_2O$, MnO_2, and Nb_2O_5 [30]. Extrinsic materials, in contrast, hand, do not possess pseudocapacitance within the standard state because of the phase transitions that occur during the ion storage. When used on such materials, elevating the surface area via nanostructuring results in better high-rate behavior because diffusion lengths are reduced and, in some situations, phase transformations are suppressed. These two things working together have led to this improvement. These two features are shared by a large amount of transition metal oxides [31].

7 Pseudocapacitive Electrode Architectures

Pseudocapacitance experiments are usually done on electrodes that minimize thickness effects (such electrolyte starvation or decreased particle-to-particle electron transmission) or are used for a specific operando characterization. These electrodes affect particle electron transport. Once a pseudocapacitive material shows enticing high-power behavior, the next step is to preserve the thin film responsiveness in an electrode architecture with a large volumetric or areal capacity. This usually requires areal loadings larger than 10 mg/cm^2. A continuous current and ionic network must span an electrode for high rates. Hence, electrode thickness alone doesn't always effective [32, 33].

Two methods can produce the electrode's electrical conductivity: (i) employing conductive additives like carbon black that are uniformly dissolved with an active material, or (ii) using hybridization to link the carbon and active material at the nanoscale. The electrode must maintain its networked and hierarchical porosity to properly access the electrolyte. Blending both phases is crucial when applying conductive additives. A calibrated mixing technique and an adequate particle amount and size of the conductive component are needed. Nanostructured active materials, which make up most pseudocapacitive materials, need this. Combining particles would make it hard to keep the nanoscale active material near the conductive additive across numerous cycles. That can be difficult. Hybridizing the active material along a conductive carbon network is advised [34, 35].

In conclusion, one may distinguish between covering active materials on carbon sources, forming conductive carbon shells to cover active material, and co-synthesizing carbon and active content by carefully analyzing these three approaches. Current applied research aims to create three-dimensional scaffolds or conductive networks with great areal performance at high speeds. Three-dimensional porous graphene networks containing Nb_2O_5 can be used. Connected gyroid structures with active material nanoparticles in a 3-D porous carbon framework are another example. These two examples demonstrate active materials [36, 37].

8 Various Materials of Energy Storage Devices

Pseudocapacitive materials are promising for ion adsorption and/or intercalation-based energy storage devices with high rates, energy densities, and efficiency. Hybrid capacitors and rechargeable batteries use them as electrodes. However, two variables must be understood to integrate pseudocapacitive materials into devices: (1) the electrolyte, which may differ for materials that function at pseudocapacitive time scales and require quick interfacial charge transfer, and (2) the influence of electrode coupling or cross talk. Pseudocapacitive and fast interfacial electron transport may require a specific electrolyte.

Novel pseudocapacitive materials and gadgets will become more common. Pseudocapacitive MXenes need the proper electrolyte solvent, as shown recently. Wang and colleagues used Ti_3C_2 instead of dimethyl sulfoxide or acetonitrile to show that propylene carbonate doubled the charge storage capacity of organic electrolytes containing Li^+ [38]. The carbonate electrolyte allowed complete Li^+ desolation and frequent pseudocapacitive intercalation. Hence, matching electrode materials and selecting an appropriate solvent, electrode material, and electrolyte salt can improve a tested system's pseudocapacitive performance.

Pseudocapacitive materials are attractive for applications other than electrochemical energy storage because their electrochemical charge transfer reactions are fast and reversible (EES). One of the most frequent ways for water deionization is capacitive deionization, which uses EDL to adsorb aqueous ions on carbon electrodes. This water ion removal process is one of the most effective. This method is frequently considered the best. Pseudocapacitive materials, like EES, could increase ion storage capacity and maintain fast storage timescales for water filtration. Like EES. Pseudocapacitive have been investigated for purposes other than energy storage [38–40]. The quick ion intercalation kinetics of these materials could enable fast actuation in actuators [41]. Actuators are just one example. Two types of pseudocapacitor components have been described in the following sections.

8.1 Aqueous Pseudocapacitor Materials

Numerous different transition metal oxides for pseudocapacitive energy storage throughout aqueous electrolytes have been investigated. The behavior of such materials is influenced by their structural characteristics, hydration state characteristics, and electrolyte composition. One of the most fundamental differences between aqueous & non-aqueous types of pseudocapacitive materials is the impact of the structure & the surface-bound water. When structural water is present, it can provide an enormous "inner surface" which is open to ion adsorption, like in $RuO_2 \cdot nH_2O$. Surface-bound water is absent from non-aqueous pseudocapacitive materials, though. It's probable that the structural water also aids in the migration of ions into the inner

surface. The following list of the most significant chemicals that can be found in aqueous electrolytes will be covered in this section.

8.1.1 MnO_2

While Lee and Goodenough were analysing the features of amorphous $MnO_2 \cdot nH_2O$ in an aqueous electrolyte containing KCl in 1999, they made the initial discovery of MnO_2's pseudocapacitive behavior. The formation of a rectangular voltammogram & storage of roughly 200 F/g (240 C/g, 4 min) demonstrated that this material stored charge through rapid faradaic reactions. This conclusion was made because of the material's ability to store charges. In most circumstances, the pseudocapacitive energy storage of the manganese dioxide (MnO_2) in the aqueous electrolyte is enabled by the redox process among the +4 & +3 oxidation states of manganese at the surface & in bulk:

$$MnO_2 + xA^+ + xe^- \leftrightarrow A_xMnO_2 \tag{6}$$

In this case, A stands for an alkali metal cation. Theoretically, given a 0.9 V potential window, 1-electron redox reaction (x = 1) equates to about 1233 F/g (1110 C/g). MnO_2 is particularly enticing when compared to RuO_2 because it is readily available and inexpensive. MnO_2 has been demonstrated through electrochemical research to have characteristics of intrinsic pseudocapacitive charge storage [42]. It is a highly desired material for use in electrochemical capacitors that are based on aqueous solutions due to its low cost, ample supply, and high theoretical capacitance. To reach its complete theoretical capacitance in the thick layers and at fast transfer rates, this material must first increase its low degree of electronic conductivity [24]. This is a major challenge.

8.1.2 $RuO_2 \cdot nH_2O$

The first pseudocapacitance material was hydrous RuO_2. Due to its exceptional qualities, improved electrodes have been made from its rarity and expensive cost. These works have sought to maximize theoretical capacitance and minimize RuO_2 use. The traditional slurry method achieves a capacitance value of about 720 F/g and charge–discharge period of approximately 8 min when the mass loading of $RuO_2 \cdot nH_2O$ is increased to a high level (30 mg/cm^2). The capacitance that can be theoretically expected from $RuO_2 \cdot nH_2O$ is half of this value. When RuO_2 nanoparticles are spread over activated carbon, the capacitances that are produced are 1340 F/g for the charging–discharging duration of 1 min. This value is close to what was projected. Because of the effective electrolyte exposure, capacitance, and rate rise exhibited by $RuO_2 \cdot nH_2O$. Areal capacitance is decreased thanks to this electrode architecture's lower mass loading of $RuO_2 \cdot nH_2O$/ area of footprint, which is, of course, referenced in Makino et al. [43].

8.1.3 Nanostructured Layered Metal Hydroxides

$M^{2+}(OH)_2$ lamellar structures are made up of MO_6 octahedra that are separated from one another by hydrogen atoms. Whenever some of the transition metals appear in the +3 state, the intercalation of anion species into the interlayer space can compensate for the slabs' higher positive charge, which results in layered dual hydroxide formation. The interlayer gap in hydroxides is on the order of several nanometres, which enables reversible ion intercalation. The hydroxides of transition metals like nickel and cobalt play an important role as electrodes within the rechargeable aqueous types of batteries. These materials undergo at least one phase shift, which allows them to maintain constant potential during the galvanostatic charging–discharging thereby simultaneously limiting their rate capabilities [44].

8.2 Emergence of Pseudocapacitance in RuO_2

RuO_2 was shown to contain a novel electrochemical capacitance known as pseudocapacitance, which incorporates faradaic charge-transfer reactions. This kind of capacitance was found in RuO_2. From electrolyte proton storage, a RuO_2 thin film type electrode established a faradaic charge carrier mechanism. Although being faradaic, the Cyclic Voltammogram (CV) was rectangular like a capacitor [16–18, 43]. The following formula describes how hydrated RuO2 stores protons:

$$RuO_x(OH)_y + \delta H^+ + \delta e^- \leftrightarrow RuO_{x-\delta}(OH)_{x+\delta} \tag{7}$$

Four RuO_2 $0.5H_2O$ properties enable fast faradaic reactions along with a higher capacitance: (i) the redox behavior of the Ru4+ cation, which permits a faradaic type energy storage; (ii) metallic conductivity exhibited by RuO_2, which facilitates rapid electron transfer; (iii) structural water, which allows rapid transport of proton inside the "inner surface"; & (iv) a large "outer" surface area, which reduces diffusivity. Four traits define the faradaic effect. Unfortunately, except for extremely small devices like micro-supercapacitors, the high price of ruthenium (which is now around US$2,000 per kilogram) makes it unfeasible for devices based on RuO_2 to be used widely. Nonetheless, the behavior of hydrous RuO_2 was the first to show that certain systems can produce electrochemical properties similar to those of a capacitor as a result of reversible faradaic processes. The examination of RuO_2 also helped scientists understand the qualities of a material that would be suitable for use as a pseudo capacitor in aqueous electrolytes.

8.3 Non-aqueous Electrolyte Pseudo Capacitor Materials

Nonaqueous lithium-ion and sodium-ion electrolytes can cause pseudocapacitive behavior in some materials. Pseudocapacitance occurs when an ion causes a redox reaction, neutralizing the charge. They may also have fast-ion-insertion structures. Structural water does not conduct ions like in aqueous pseudocapacitive materials since electrolytes are not aqueous. Unlike structural water in aqueous pseudocapacitive materials. Structural water may destroy the electrochemical cell. Non-aqueous electrolytes use pseudocapacitive materials with increased capacitance over higher potential ranges than aqueous electrolytes. Non-aqueous electrolytes lack water. This is one of several benefits of using these materials.

$$E = 1/2\left(CV^2\right) \tag{8}$$

E stands for energy density and is expressed in (J/g), C for capacitance and is expressed in (F/g) & V for potential range (V). With this, extending the potential range from the value of 1–4 V can increase energy density by almost an order of magnitude.

8.3.1 Amorphous Materials

The charge–discharge behavior of amorphous materials is characterized by a single-phase ion intercalation action. If they are repeatedly subjected to electrochemical cycling or if the intercalation of ions happens after a specific composition has been reached, certain crystalline materials can change into amorphous ones, as will be illustrated in more detail for V_2O_5 in the following section. Even though amorphous materials' chaotic structure can benefit EES, it's probable that these materials won't be as capable as their crystalline counterparts. Their high-rate capabilities determine if amorphous substances are appropriate for pseudocapacitive EES [45–48]. Amorphous Nb_2O_5 & MoO_3 depict lower capacitances as compared to the crystalline counterparts, even when charging for a brief period of time and also within the form of thin film. These results suggest that crystalline materials have better kinetics or charge storage, which increases specific capacitance.

8.3.2 V_2O_5

Vanadium oxide's layered structures improve EES greatly. Vanadium's numerous oxidation states make its chemistry quite complex. An article described several of these items. Vanadium's high oxidation state allows formula units to store more than one electron (+5, +4, +3, & +2 are all electrochemically accessible). This property makes V_2O_5 a very desirable material for use in EES [49].

8.3.3 TiO_2(B) and Hydrogen Titanates

Hydrogen titanates, particularly $H_2Ti_3O_7$ and TiO_2 (B), have been explored for pseudocapacitive electro electrochemical storage. Like other titanium oxides, these materials store charge via the Ti + 4/ + 3 redox pair; in addition, lithium-ion intercalation occurs at potentials lower than 2 V versus Li/Li^+. Heating these materials causes dehydration and thus the creation of the TiO_2(B) phase, which also comprises two edge-sharing TiO_6 octahedra with linked corners. The edge-sharing TiO_6 octahedra that make up the layered structures of the hydrogen titanates are spaced apart by protons [27, 36].

8.3.4 T-Nb_2O_5

At sweep speeds of up to a value of 50–60 mV/s, which correspond to charging-discharging times of one minute, the T-Nb_2O_5 material exhibits properties that are typical of pseudocapacitive charge storage. Large redox peaks may be seen in the cyclic voltammograms, or CVs, that appear below 2 V. In addition, the galvanostatic charging-discharging character trait is nearly linear. Throughout a wide range of sweep rates, peak current rises linearly with the sweep rate. Together with TiO_2(B) and the hydrogen titanates, T-Nb_2O_5 could be identified as a material with intrinsic intercalation pseudocapacitance throughout non-aqueous electrolytes. Given that T-Nb_2O_5 doesn't contain any water, this is the case. Unlike other kinds of intrinsic pseudo capacitors, including those based on V_2O_5, these don't need to have a lot of surface area [43].

9 Conclusions

The appealing combination of a high EES rate and a high EES energy density can be found in pseudocapacitive transition metal oxides. Because of their low energy density, such types of materials possess the potential to surpass the restrictions imposed by electrochemical capacitors. According to an analytical definition, pseudocapacitance exists anytime the potential is based on the charge level of the charged item. The numerous electrochemical properties displayed by a material showing pseudocapacitive behavior can all be rapidly and easily identified using a CV, AC impedance, or a charge–discharge plot of galvanostatic. Certain substances, including $RuO_2 \cdot 0.5H_2O$, TiO_2(B), MnO_2, and Nb_2O_5, naturally function as pseudo capacitors. This means that even with small surface areas and composite electrode designs, the pseudocapacitive behavior can be seen. The pseudocapacitive behavior of other materials can only be observed when utilizing electrodes with extremely high surface areas and complicated designs, which serve to reveal as much of the surface of a material as is reasonably possible to the electrolyte. These resources consist of the bulk forms of common battery components like $Ni(OH)_2$ and V_2O_5 are typically employed

in extrinsic pseudocapacitors. It is crucial to show pseudocapacitive electrochemical capabilities that go beyond only having a high capacitance over a brief period when working with materials of this kind.

Pseudocapacitor materials must overcome two major hurdles to be used in electronics. Devices need continual material and electrode measurements. As noted, charge–discharge operations on a material that lasts tens of minutes utilizing modest weight loadings or thin films may confuse the material as a high energy density pseudo capacitor. A pseudo capacitor's charge–discharge behavior must be less than one minute, its capacitance must be more than 300 F/g, and its active material mass loading must be >1 mg/cm^2.

The design of pseudocapacitive devices is the second significant challenge. Two pseudocapacitive transition metal oxide electrodes are uncommon in electronics. It can be challenging to locate pseudocapacitive material couplings with high-voltage devices & good rate capabilities. To attain greater power and energy densities within the same material, EES should switch from low mass loading, three-electrode studies to high mass loading, two-electrode cells with higher rate capabilities.

References

1. L. Hao, B. Luo, X. Li, M. Jin, Y. Fang, Z. Tang, Y. Jia, M. Liang, A. Thomas, J. Yang, L. Zhi, Terephthalonitrile-derived nitrogen-rich networks for high performance supercapacitors. Energy Environ. Sci. **5**, 9747–9751 (2012)
2. X. Hua, Z. Liu, M.G. Fischer, O. Borkiewicz, P.J. Chupas, K.W. Chapman, U. Steiner, P.G. Bruce, C.P. Grey, Lithiation thermodynamics and kinetics of the TiO_2 (B) nanoparticles. J. Am. Chem. Soc. **139**, 13330–13341 (2017)
3. I. Hanghofer, B. Gadermaier, H.M.R. Wilkening, Fast rotational dynamics in argyrodite-type Li6PS5X (X: Cl, Br, I) as seen by 31P nuclear magnetic relaxation—on cation-anion coupled transport in thiophosphates. Chem. Mater. **31**, 4591–4597 (2019)
4. H. Chen, T.N. Cong, W. Yang, C. Tan, Y. Li, Y. Ding, Progress in electrical energy storage system: a critical review. Prog. Nat. Sci. **19**, 291–312 (2009)
5. H.L. Ferreira, R. Garde, G. Fulli, W. Kling, J.P. Lopes, Characterisation of electrical energy storage technologies. Energy **53**, 288–298 (2013)
6. M. Zhu, J. Park, A.M. Sastry, Fracture analysis of the cathode in li-ion batteries: a simulation study,.ECS Meet. Abstr. MA2012-01, 972–972 (2012)
7. J.R. Miller, A.F. Burke, Electrochemical capacitors: challenges and opportunities for real-world applications. Electrochem. Soc. Interface **17**, 53–57 (2008)
8. P. Miller, John R., Simon, Electrochemical capacitors for energy management. Science (80–), **5889**, 651–652 (2008)
9. H. Gualous, H. Louahlia-Gualous, R. Gallay, A. Miraoui, Supercapacitor thermal modeling and characterization in transient state for industrial applications. IEEE Trans. Ind. Appl. **45**, 1035–1044 (2009)
10. H. Lv, Q. Pan, Y. Song, X.X. Liu, T. Liu, A review on nano-/microstructured materials constructed by electrochemical technologies for supercapacitors. Nano-Micro Lett. 12 (2020)
11. X. Fan, B. Liu, J. Liu, J. Ding, X. Han, Y. Deng, X. Lv, Y. Xie, B. Chen, W. Hu, C. Zhong, Battery technologies for grid-level large-scale electrical energy storage. Trans. Tianjin Univ. **26**, 92–103 (2020)

12. N. Zaman, R.A. Malik, H. Alrobei, J. Kim, M. Latif, A. Hussain, A. Maqbool, R.A. Karim, M. Saleem, M.A. Rafiq, Z. Abbas, Structural and electrochemical analysis of decarburized graphene electrodes for supercapacitor applications. Crystals **10**, 1–12 (2020)
13. T. Brousse, D. Bélanger, J.W. Long, To be or not to be pseudocapacitive? J. Electrochem. Soc. **162**, A5185–A5189 (2015)
14. M.E. Abdelhamid, A.P. O'Mullane, G.A. Snook, Storing energy in plastics: a review on conducting polymers & their role in electrochemical energy storage. RSC Adv. **5**, 11611–11626 (2015)
15. A.M. Bryan, L.M. Santino, Y. Lu, S. Acharya, J.M. D'Arcy, Conducting polymers for pseudocapacitive energy storage. Chem. Mater. **28**, 5989–5998 (2016)
16. F.Z. Amir, V.H. Pham, J.H. Dickerson, Facile synthesis of ultra-small ruthenium oxide nanoparticles anchored on reduced graphene oxide nanosheets for high-performance supercapacitors. RSC Adv. **5**, 67638–67645 (2015)
17. J.S. Seenath, D. Pech, D. Rochefort, Investigation of protic ionic liquid electrolytes for porous RuO_2 micro-supercapacitors. J. Power. Sources **548**, 232040 (2022)
18. Q. Jiang, N. Kurra, M. Alhabeb, Y. Gogotsi, H.N. Alshareef, All pseudocapacitive MXene-RuO_2 asymmetric supercapacitors. Adv. Energy Mater. **8** (2018)
19. Y. Jiang, J. Liu, Definitions of pseudocapacitive materials: a brief review. Energy Environ. Mater. **2**, 30–37 (2019)
20. Q. Gui, L. Wu, Y. Li, J. Liu, Scalable wire-type asymmetric pseudocapacitor achieving high volumetric energy/power densities and ultralong cycling stability of 100,000 times. Adv. Sci. **6**, 1802067 (2019)
21. Q. Wei, R.H. DeBlock, D.M. Butts, C. Choi, B. Dunn, Pseudocapacitive vanadium-based materials toward high-rate sodium-ion storage. Energy Environ. Mater. **3**, 221–234 (2020)
22. Y. Jiang, Y. Shen, J. Dong, S. Tan, Q. Wei, F. Xiong, Q. Li, X. Liao, Z. Liu, Q. An, L. Mai, Surface pseudocapacitive mechanism of molybdenum phosphide for high-energy and high-power sodium-ion capacitors. Adv. Energy Mater. **9** (2019)
23. M.R. Lukatskaya, S. Kota, Z. Lin, M.-Q. Zhao, N. Shpigel, M.D. Levi, J. Halim, P.-L. Taberna, M.W. Barsoum, P. Simon, Y. Gogotsi, Ultra-high-rate pseudocapacitive energy storage in two-dimensional transition metal carbides. Nat. Energy **2**, 17105 (2017)
24. V. Augustyn, P. Simon, B. Dunn, Pseudocapacitive oxide materials for high-rate electrochemical energy storage. Energy Environ. Sci. **7**, 1597 (2014)
25. B. Dunn, H.D. Abruña, P.-L. Taberna, J.W. Kim, S.H. Tolbert, M.A. Lowe, J. Come, P. Simon, V. Augustyn, High-rate electrochemical energy storage through Li^+ intercalation pseudocapacitance. Nat. Mater. **12**, 518–522 (2013)
26. T. Liu, Y. Li, Addressing the Achilles' heel of pseudocapacitive materials: long-term stability. InfoMat. **2**, 807–842 (2020)
27. K. Fröhlich, M. Ťapajna, A. Rosová, E. Dobročka, K. Hušeková, J. Aarik, A. Aidla, Growth of high-dielectric-constant TiO[sub 2] films in capacitors with RuO[sub 2] electrodes. Electrochem. Solid-State Lett. **11**, G19 (2008)
28. H.-S. Kim, J.B. Cook, S.H. Tolbert, B. Dunn, The development of pseudocapacitive properties in nanosized-MoO_2. J. Electrochem. Soc. **162**, A5083–A5090 (2015)
29. A. Jadon, S. Prabhudev, G. Buvat, S.G. Patnaik, M. Djafari-Rouhani, A. Estève, D. Guay, D. Pech, Rethinking pseudocapacitance: a way to harness charge storage of crystalline RuO_2. ACS Appl. Energy Mater. **3**, 4144–4148 (2020)
30. H.B. Li, M.H. Yu, F.X. Wang, P. Liu, Y. Liang, J. Xiao, C.X. Wang, Y.X. Tong, G.W. Yang, Amorphous nickel hydroxide nanospheres with ultrahigh capacitance and energy density as electrochemical pseudocapacitor materials. Nat. Commun. **4**, 1894 (2013)
31. X. Yu, S. Yun, J.S. Yeon, P. Bhattacharya, L. Wang, S.W. Lee, X. Hu, H.S. Park, Emergent pseudocapacitance of 2d nanomaterials. Adv. Energy Mater. **8**, 1702930 (2018)
32. Y. Gogots, P. Simon, True performance metrics in electrochemical energy storage. Science (80–), **334**, 917–918 (2011)
33. L. Yu, G.Z. Chen, Supercapatteries as high-performance electrochemical energy storage devices. Electrochem. Energy Rev. **3**, 271–285 (2020)

34. C. Wang, X. Wang, C. Lin, X.S. Zhao, Lithium titanate cuboid arrays grown on carbon fiber cloth for high-rate flexible lithium-ion batteries. Small **15**, 1902183 (2019)
35. Z. Chen, V. Augustyn, J. Wen, Y. Zhang, M. Shen, B. Dunn, Y. Lu, High-performance supercapacitors based on intertwined CNT/V_2O_5 nanowire nanocomposites. Adv. Mater. **23**, 791–795 (2011)
36. T.S. Dörr, S. Fleischmann, M. Zeiger, I. Grobelsek, P.W. de Oliveira, V. Presser, Ordered mesoporous titania/carbon hybrid monoliths for lithium-ion battery anodes with high areal and volumetric capacity. Chem.—A Eur. J. **24**, 6358–6363 (2018)
37. S. Fleischmann, T.S. Dörr, A. Frank, S.W. Hieke, D. Doblas-Jimenez, C. Scheu, P.W. de Oliveira, T. Kraus, V. Presser, Gyroidal niobium sulfide/carbon hybrid monoliths for electrochemical energy storage. Batter. Supercaps. **2**, 668–672 (2019)
38. X. Wang, T.S. Mathis, K. Li, Z. Lin, L. Vlcek, T. Torita, N.C. Osti, C. Hatter, P. Urbankowski, A. Sarycheva, M. Tyagi, E. Mamontov, P. Simon, Y. Gogotsi, Influences from solvents on charge storage in titanium carbide MXenes. Nat. Energy **4**, 241–248 (2019)
39. M.E. Suss, V. Presser, Water desalination with energy storage electrode materials. Joule **2**, 10–15 (2018)
40. P. Srimuk, X. Su, J. Yoon, D. Aurbach, V. Presser, Charge-transfer materials for electrochemical water desalination, ion separation and the recovery of elements. Nat. Rev. Mater. **5**, 517–538 (2020)
41. F. Zhu, Q. Xiao, Z. Hu, J. Ma, S. Komarneni, In situ formation of MnO_2/$Ni(OH)_2$@nickel foam with porous architecture for triggering persulfate-based advanced oxidation process. J. Porous Mater. **29**, 1629–1637 (2022)
42. D. Chen, D. Ding, X. Li, G.H. Waller, X. Xiong, M.A. El-Sayed, M. Liu, Probing the charge storage mechanism of a pseudocapacitive MnO_2 electrode using in operando Raman spectroscopy. Chem. Mater. **27**, 6608–6619 (2015)
43. S. Makino, T. Ban, W. Sugimoto, Towards implantable bio-supercapacitors: pseudocapacitance of ruthenium oxide nanoparticles and nanosheets in acids, buffered solutions, and bioelectrolytes. J. Electrochem. Soc. **162**, A5001–A5006 (2015)
44. S. Fleischmann, J.B. Mitchell, R. Wang, C. Zhan, D. Jiang, V. Presser, V. Augustyn, Pseudocapacitance: from fundamental understanding to high power energy storage materials. Chem. Rev. **120**, 6738–6782 (2020)
45. B. Pandit, S.A. Pande, B.R. Sankapal, Facile SILAR processed Bi_2S_3:PbS solid solution on MWCNTs for high-performance electrochemical supercapacitor. Chinese J. Chem. **37**, 1279–1286 (2019)
46. S.S. Karade, A. Agarwal, B. Pandit, R.V. Motghare, S.A. Pande, B.R. Sankapal, First report on solution processed α-Ce_2S_3 rectangular microrods: an efficient energy storage supercapacitive electrode. J. Colloid Interface Sci. **535**, 169–175 (2019)
47. S.A. Pande, B. Pandit, B.R. Sankapal, Electrochemical approach of chemically synthesized HgS nanoparticles as supercapacitor electrode. Mater. Lett. **209**, 97–101 (2017)
48. S. Patil, S. Raut, B. Pandit, S.N. Pandey, S.A. Pande, B. Sankapal, Web-analogues one-dimensional iron hydroxide@cadmium hydroxide nanostructure: electrochemical supercapacitor. J. Mater. Sci. Mater. Electron. **32**, 22472–22480 (2021)
49. S.A. Pande, B. Pandit, B.R. Sankapal, Vanadium oxide anchored MWCNTs nanostructure for superior symmetric electrochemical supercapacitors. Mater. Des. **182**, 107972 (2019)

Pseudocapacitance: Mechanism and Characteristics

G. Srividhya and N. Ponpandian

Abstract Pseudocapacitance is a mechanism of charge storage in electrochemical devices, which has the capability of delivering higher energy density than conventional electrochemical double-layer capacitance and higher power density than batteries. In contrast to electric double-layer capacitors (EDLC) where charge storage is mainly due to the electrostatic interaction of ions in the electrolyte with the electrode, in pseudocapacitors charge storage between the electrode–electrolyte interface is associated with a highly reversible redox reaction or intercalation. Though by definition pseudocapacitors involve faradic processes, they are largely different from faradic processes that occur in batteries. With extensive research and development of nanoscale materials, which give different electrochemical capacitive signatures for varying particle size, the definition of pseudocapacitance is highly misinterpreted and often a battery-type material is reported as pseudocapacitive material, misreporting the capacitance to exaggerated values. There is a lack of understanding among the electrochemical research community in differentiating the pseudocapacitive process from others. This chapter aims to provide a comprehensive note on understanding the fundamentals of pseudocapacitance, its origin, and different type of pseudocapacitive charge storage mechanisms. The electrochemical characteristics of pseudocapacitive along with that of EDLC and battery-type material are discussed to help the reader understand the differentiation.

Keywords Supercapacitors · Pseudocapacitance · Double layer capacitance · Charge storage mechanism · Specific capacitance

G. Srividhya · N. Ponpandian (✉)
Department of Nanoscience and Technology, Bharathiar University, CoimbatoreTamilnadu 641 046, India
e-mail: ponapandian@buc.edu.in

© The Author(s), under exclusive license to Springer Nature Switzerland AG 2024

R. K. Gupta (ed.), *Pseudocapacitors*, Engineering Materials,
https://doi.org/10.1007/978-3-031-45430-1_3

1 Introduction

Supercapacitors are electrochemical charge storage devices that have very high capacitance values when compared with conventional dielectric capacitors. The higher values of the capacitance of electrochemical supercapacitors, that use nanomaterials as electrodes, mainly arise from the following two features:

(i) the origin of the double layer of charges in the electrode–electrolyte interface, acting as a molecular dielectric of very small thickness
(ii) the usage of porous carbonaceous materials with high surface area as the electrode

$$\text{Capacitance, } C = \frac{\varepsilon A}{d} \tag{1}$$

where ε is the permittivity, A is the surface area of the electrode, and d is the thickness of the dielectric. With reduced d due to petite double layer thickness and increased A, supercapacitors show very high capacitance values. Hence, they can serve in numerous modern applications such as wearable and portable electronics, particularly power devices and electrical vehicles, where lithium-ion batteries (LIBs) could not deliver high power density. Conventionally, supercapacitors or ultra-capacitors are double-layer capacitors; even though they have high power density and rate capability, they have low energy storage capability (5–10 Wh/kg) [1], and hence are restricted to use in emerging electrical vehicles applications. However, there is another type of capacitance with high energy density, called pseudocapacitance, where the storage of charge is different from the electrochemical double-layer capacitors (EDLCs), with the accompanying of faradic processes. Thus, pseudocapacitance enables us to find a middle ground between high-energy–density LIBs and high-power-density EDLCs.

The term "pseudo" is a Greek word that means "appear like" or "pretend". Hence, pseudocapacitance is a mechanism that is not true to the original or traditional electrochemical capacitance which arises purely from the establishment of a double layer in the interface between a charged (polarized) electrode and electrolyte. Generally, two types of processes or reactions take place in an electrode–electrolyte interface.

(i) non-faradic electrosorption and desorption of opposite electrolyte ions onto the charged electrode surface, well within the electrode–electrolyte interface, with no chemical reaction or phase transformation taking place.
(ii) faradic redox reactions, where the electron transfer across the electrode–electrolyte interface takes place, ensuing the formation of new chemical species, involving phase transformation.

Since the faradic redox reactions involve phase transformation, they are mass transfer limited. Among the three processes that govern the mass transfer, convection does not play a significant role, considering the very thin (extending only up to a few nanometres) interfaces and the migration effect is made negligible with the use of

a heavily concentrated electrolyte. Hence, faradic processes across the interface are controlled mainly by diffusion, making them extend up to minutes.

The EDLCs are governed by the non-faradic process and hence occur within seconds, delivering high power. Though pseudocapacitors also involve faradic processes, they are highly reversible, extending from a few seconds to a few minutes, and not controlled by diffusion. This chapter discusses the charge storage mechanism, the origination of pseudocapacitance, and the characteristics of pseudocapacitive devices in the following sections.

2 Capacitance and Pseudocapacitance in the Electrode–Electrolyte Interface

Though the current chapter focuses on the pseudocapacitance charge storage mechanism, and detailed EDLC mechanism is out of scope, a brief discussion of EDLC and consequently electric double layer (EDL) is necessary for proper understanding of the subject.

Hermann Von Helmholtz proposed that when a conductive charged electrode is immersed into an electrolyte, counter-ions in the electrolyte are attracted towards the electrolyte, forming two layers of opposite charges next to each other as shown in Fig. 1a. This double layer of charges acts like a molecular dielectric where the charge is stored electrostatically. The physical separation of charges constitutes a capacitance C, which is a differential constant, dependent on dielectric permittivity and double-layer thickness (Eq. 1). Later, the Gouy-Chapman duo suggested a diffuse ionic layer, rather than a static ionic layer, considering the charge distribution of the electrolyte ions. The failure of Guoy-Chapman model to explain high capacitance was overcome by Otto Stern who proposed a combination of a Stern layer of immobile adsorbed ions, as proposed by Helmholtz, and a diffuse layer of ions, as suggested by Guoy-Chapman model. The potential at the interface varies in a linear fashion in the Stern layer and exponentially in the diffuse layer with respect to the distance. The formation and collapse of the double layer are almost instantaneous, occurring in the time scale of microseconds, resulting in rapid charging and discharging, which exceptional cycle-life.

On further development with the EDL, D. C. Grahame put forth that some charged or neutral species without the solvation shell, can penetrate the Stern layer and get "specifically adsorbed" to the electrode surface. Here, the solvation shell refers to electrolyte ions that are surrounded by solvent molecules. The specifically adsorbed ions can involve in charge transfer with the electrode, resulting in pesudocapacity, which refers to reversible ionic capacity under high potential (opposite to that of the ionic charge) at the electrode, which is not associated with the EDL. Later Bockris, Devanathan, and Muller (BDM) trio modified the Grahame model, where the solvent molecules show a preferred orientation at the electrode surface and align themselves according to the electric field in the interface, influencing the permittivity to a large extent. The distance between the surface of the electrode and the centre of the solvent

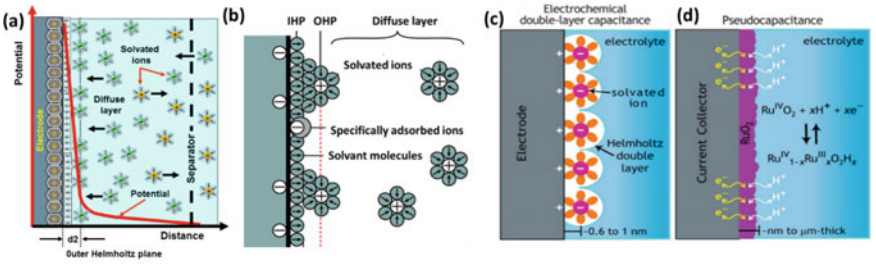

Fig. 1 Schematic illustration of EDL **a** Stern model and **b** BDM model. Schematic of charge storage through **c** double-layer capacitance and **d** pseudocapacitance. Adapted with permission [2], copyright (2011), Springer Nature

molecules forms the inner Helmholtz plane (IHP) as given in Fig. 1b. The specifically adsorbed ions present in the IHP contribute to pseudocapacitance.

The electrochemical investigation of Trassati and Buzzanca on ruthenium oxide thin films showed that at low voltages ruthenium oxide electrode show capacitor-like behaviour with specifically adsorbed ions. Though the specific adsorption of ions suggests a partial charge transfer between the electrode and the electrolyte, the cyclic voltammogram of these electrodes was near-rectangular like that of EDLCs [3]. The definition of pseudocapacitance was first given by B.E. Conway [4]. He explained that pseudocapacitance originates at the electrode surface, when there is a transfer of charges across the double layers, as in batteries, however, due to thermodynamic reasons, there is linear relation, between the charge acceptance (Δq) and the change in potential (ΔV), such that the derivative dQ/dV is equal to capacitance.

$$C = \frac{dQ}{dV} \tag{2}$$

Hence, pseudocapacitance, though faradic in origin, shows rectangular cyclic voltammetry (CV) signature and shows direct proportionality between the charge and the potential. It is to be noted that pseudocapacitance does not denote the absence of an EDL, rather that highly reversible charge transfer occurs across the EDL.

Fig. 1c, d gives an idea about the distance from the electrode surface at which EDLC and pseudocapacitance arise can be understood. In EDLCs, the charge storage mainly occurs in the Helmholtz double layer of nanometre thickness, whereas in pseudocapacitors, the H^+ ions from the electrolyte at micrometre distances are passed over to get specifically adsorbed to the electrode in IHP, resulting in a surface redox reaction. The surface or near-surface redox reactions that cause pseudocapacitance are significantly faster than those taking place in batteries, and hence the electrochemical signatures of pseudocapacitance are like that of EDLC, but with substantially increased capacitance. For instance, the theoretical specific capacitance value that can be attained with activated carbon with EDLC nature is 300 F/g, whereas that of hydrated ruthenium oxide is 3 times greater with a value of 1580 F/g [5]. It is to be noted that the charge is transferred only across the surface and there is no chemical reaction between the specifically adsorbed ions and the electrode's atoms, i.e.,

no chemical bonds are created, or no phase transformation occurs, as in batteries. Hence, pseudocapacitors have better energy density than EDLCs and have better power density than batteries

3 Pseudocapacitance Charge Transfer Mechanisms

Pseudocapacitance occurs via three identified faradic pathways, as follows.

(i) Under-potential deposition (UPD)
(ii) Surface redox pseudocapacitance
(iii) Intercalation pseudocapacitance

The three mechanisms of pseudocapacitance are depicted in Fig. 2.

3.1 Under-Potential Deposition

The general term, Under-potential deposition (UPD) is the deposition of atomic monolayers of a metal from its cationic solution, onto a different metal substrate (mostly a noble metal) at potentials that are less negative than the thermodynamic reduction potential that is usually required for the deposition of the metal as the substrate. The deposition of lead (Pb) monolayer into gold (Au) surface is a characteristic example of UPD [7]. During this process, a partial and highly reversible charge transfer occurs between the deposited metal and the substrate metal. The CV profile of such process shows strong redox peaks that are attributed to the formation of metal monolayer structures onto the noble metal substrate. At very low sweep rates of ~5 mV/s, the peak current shows a linear dependence of the scan rate, denoting

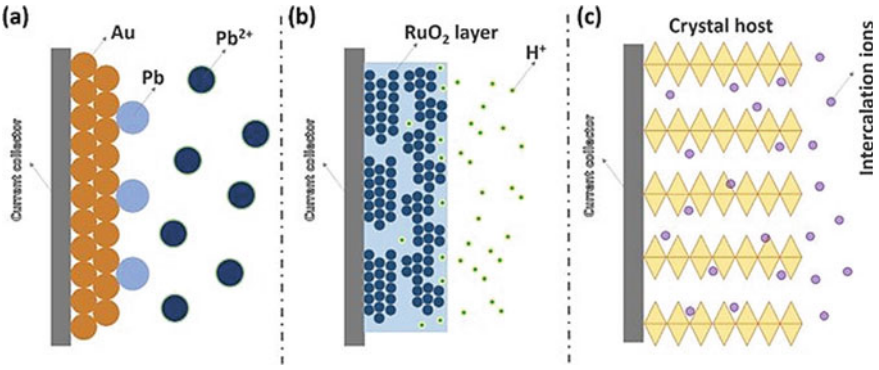

Fig. 2 Schematic of Pseudocapacitance mechanisms **a** UPD, **b** surface redox pseudocapacitance and **c** intercalation pseudocapacitance. Adapted with permission [6], copyright (2020), Elsevier

the foundation of a faradic capacitance. Different from electrodeposition, UPD is the adsorption of the metal atom onto the underlying metal substrate, along with a partial charge transfer between the metals. This process is not employed to develop high capacitive devices, as it works only in a limited potential window, thus leading to low capacitance. Moreover, the usage of noble metals like gold makes them economically unviable.

3.2 Surface Redox Pseudocapacitance

Redox pseudocapacitance originates from the kinetically fast redox reaction between an electrode and the electrolyte. Thin films of metal oxides such as RuO_2 exhibit redox pseudocapacitance, which is chiefly due to the fast kinetics of electron–proton transfer by RuO_2 due to high conductivity [3]. Metal oxides such as MnO_2 and Fe_2O_3 and conductive polymers show pseudo capacitive nature, due to their multiple oxidation states that enable fast redox reactions. In conducting polymers, the charge storage occurs via electrochemical doping of ions from the electrolyte to the electrode leading to the reduction of oxidation of the polymer backbone. Redox pseudocapacitors show near rectangular CV curves and linear variation of current with scan rate. It is to be noted that even in EDLCs, redox pseudocapacitance contributes to nearly 5 to 10% of the energy, due to the faradic reactivity of oxygen functional groups present at the edges of the EDLC electrode, due to the electrode preparation technique.

3.3 Intercalation Pseudocapacitance

The rapid intercalation of ions into the tunnels, layers, and crystal structure of redox-active electrodes, resulting in a faradic reaction without any phase transformation, give rise to intercalation pseudocapacitance, as demonstrated by Augstyn et al. [8]. In contrast to LIBs where the intercalation is a slow, diffusion-controlled process that results in a phase transformation, intercalation pseudocapacitors undergo rapid diffusion of ions and hence, there is no phase transformation [9]. Intercalation pseudocapacitance commonly occurs in non-aqueous electrolytes. In transition metal oxides like TiO_2, Nb_2O_5 and layered materials like nitrides (MXenes) and sulfides, there are certain crystallographic planes wherein the Li^+ can be inserted very rapidly, without inducing a phase change [10]. The non-diffusion limited intercalation pseudocapacitance shows power density that cannot be achieved with LIBs. The cyclic voltammograms of intercalation pseudocapacitors show redox peaks, owing to partial charge transfer with the insertion and removal of ions from the host crystal or electrode tunnel, with reversible redox peaks, separated by a very small voltage difference. Similar to redox capacitors, the current increases linearly with the sweep rate, denoting that the process is not diffusion limited (where current increases linearly with the square root of the sweep rate).

4 Origin of Pseudocapacitance

In EDLCs, the double layer is formed due to the addition or removal of the delocalized high-energy electrons in the conduction band from the electrode, from the conduction band. The polarization caused by this change in the conduction band electrons in the electrode is balanced by the transfer of positive or negative ionic charges in the electrolyte side of the electrode–electrolyte interface. The density of charges on the electrode surface is voltage-dependent, and hence the capacitance is also dependent on voltage in EDLCs [11].

In faradic redox batteries, the localized valence band electrons in the electrode and the ions of the electrolyte have widely separated energy levels. At particular or few potentials, the valence band electrons are transferred from electrode to electrolyte or vice-versa, resulting in a chemical reaction with redox peaks in CVs at those potentials.

In pseudocapacitance, however, the delocalized valence band electrons give rise to non-diffusion limited faradic charge transfer. In general, semiconductor transition metal oxide and conducting polymers have delocalized valence band electrons that have closely spaced energy levels, constituting a band that corresponds to a range of potentials, at which continuous and consecutive charge transfer occurs, resulting in a constant current over the range of potential. Hence, even though pseudocapacitance is faradic in origin, it shows a rectangular CV as that of EDLC [12].

Conway developed a theory for the origin of adsorption pseudocapacitance (UPD), which could be extended to the other two types of pseudocapacitance, namely, redox and intercalation pseudocapacitance. The electrosorption of a cation A^+ onto a conductive metal substrate M can be given as.

$$M + A^+ + e^- \leftrightarrow M_{ads} \tag{3}$$

According to Frumkin, the charge on the metal surface, q_m in an EDL can be given as

$$q_m = q_0(1-\theta) + q_1\theta \tag{4}$$

where θ is the surface coverage of M_{ads} on the electrode's surface, q_1 is the charge related to the surface adsorption and q_0 is the charge related to the bare surface (1-θ).

According to Frumkin isotherm,

$$\left(\frac{\theta}{1-\theta}\right)e^{-2g\theta} = KC_A \tag{5}$$

where K is the reaction rate constant that is dependent on the potential across the capacitor, V, C_A is the concentration of the cationic species, and g is the interaction parameter of the adsorbed species, which depends on the real gas constant R, temperature T, and Faraday's constant F and is given as.

$$g = \frac{RT}{VF} \tag{6}$$

Taking logarithm for (5), we get.

$$\ln\theta - \ln(1-\theta) - 2g\theta = \ln K + \ln C_A \tag{7}$$

On differentiating (6) with respect to V,

$$\left(\frac{1}{\theta} + \frac{1}{(1-\theta)} - 2g\right)\frac{d\theta}{dV} = \frac{dlnK}{dV} = \frac{q_1 - q_o}{RT\Gamma_m} \tag{8}$$

Now, capacitance C is given as [13],

$$C = \frac{dq_m}{dV} \tag{9}$$

From Eq. (4), we have,

$$C = (1-\theta)\frac{dq_0}{dV} - q_0\frac{d\theta}{dV} + \theta\frac{dq_1}{dV} + q_1\frac{d\theta}{dV} \tag{10}$$

$$C = C_1(1-\theta) + C_2\theta + (q_1 - q_0)\frac{d\theta}{dV} \tag{11}$$

where $dq_o/dV = C_1$ and $dq_1/dV = C_2$.

Substituting for $d\theta/dV$ from Eq. (8) in Eq. (11),

$$C = C_1(1-\theta) + C_2\theta + \frac{(q_1 - q_0)^2}{RT\Gamma_m}\left(\frac{\theta(1-\theta)}{1 - 2g\theta(1-\theta)}\right) \tag{12}$$

Equation 12 is referred to as Temkin's isotherm. When there is a repulsive interaction between the adsorbed species, $g > 0$; and when the interaction is attractive, $g < 0$. The first two terms in Eq. (12) correspond to the double layer capacitance C_{dl} and hence the pseudocapacitance, C_ϕ is given as.

$$C_\phi = \frac{(q_1 - q_0)^2}{RT\Gamma_m}\left(\frac{\theta(1-\theta)}{1 - 2g\theta(1-\theta)}\right) \tag{13}$$

Since the adsorbed species are of the same charge, the most common type of interaction among the adsorbed species will be that of lateral repulsion. When the repulsive interaction between the adsorbed species is negligibly small, $g = 0$. Therefore, Eq. (13) becomes.

$$C_\phi = \frac{(q_1 - q_0)^2}{RT\Gamma_m}(\theta(1-\theta)) \tag{14}$$

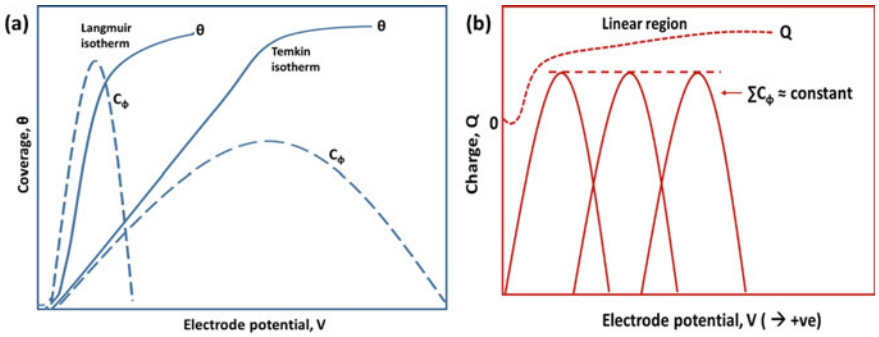

Fig. 3 **a** Variation of surface coverage, θ and pseudocapacitance, C_ϕ with electrode potential V for Langmuir and Temkin isotherms and **b** Illustration of overlapping of three consecutive redox process resulting in a constant capacitance C_ϕ over a broad range of potentials

Equation (14) is referred to as Langmuir isotherm and denotes that for a Langmuir type isotherm, the pseudocapacitance is linearly dependent on the applied voltage and the surface coverage. C_ϕ reaches the maximum value, when θ is equal to 0.5.

As can be seen from Fig. 3a, the pseudocapacitance is the maximum for the ideal Langmuir type isotherm; the surface coverage varies as a function of the applied potential. However, the pseudocapacitance depends on the potential only for a narrow potential window. The steepness of the isotherm and thus the dependence of pseudocapacitance on the potential can be increased to a broad range under two following conditions:

(i) when there a significant lateral repulsion between the adsorbed species ($g > 0$), with increasing surface coverage.
and/or.
(ii) deposition of adsorbed species in distinguishable consecutive steps of adsorption, with increasing surface coverage, as shown in Fig. 3b

Figure 3b illustrates the overlapping of three consecutive redox reactions, giving rise to the development of a constant capacitance (linear variation of charge with potential), as demonstrated by Conway in RuO_2 [14]. Conway extended the theory of origin of adsorption pseudocapacitance to redox and intercalation pseudocapacitance, by substituting the surface coverage θ, with the concentration of oxidant/reductant [Ox]/[Red] and lattice occupancy X, respectively.

5 Intrinsic and Extrinsic Pseudocapacitance

The terms intrinsic and extrinsic pseudocapacitance are conceptual annexes to redox and intercalation pesuedocapacitance, respectively. A material is called an intrinsically pseudocapacitive, when its pseudocapactive nature does not change with

change with the material's physical properties, particularly size. In an extrinsic pseudocapacitive material, the pseudocapacitive nature of the material can change into a battery-type faradic nature, depending on the particle size or other material properties. The term "extrinsic" means that the pseudocapacitance is not the true charge storage nature of the material, but an external feature that can influenced upon the material under certain physical condition.

Intercalation pseudocapacitance has been particularly proved to be "extrinsic" in nature. The study on the effect of nanosize on high-rate Li ion intercalation in $LiCoO_2$by Okubo et al. showed that $LiCoO_2$ which is battery-type material with diffusion controlled intercalation, started to show pseudocapacitive nature of high kinetics, when the size of $LiCoO_2$ was reduced to less than 10 nm [15]. With reducing the particle size, the diffusion length decreases resulting in high-rate capability. Moreover, since nanostructures have increased surface area, the phase transformation of $LiCoO_2$ is subdued. The increased number of active sites is also among the reasons for the charge storage type transformation [16]. The size-dependent charge storage behaviour transformation in thin and thick films is depicted in Fig. 4a–c. The galvanostatic charge–discharge curves of bulk $LiCoO_2$ shows pronounced plateaus, which are characteristic of Li ion batteries, showing that the relation between voltage and the charge is not linear. On reducing the size of $LiCoO_2$, the voltage dependency of charge commences, as the extent of plateau region is reduced, as can be seen in Fig. 4d. For 11 nm, the charge storage is in a transition stage, with combined effect of diffusion controlled and non-diffusion-controlled intercalation. However, for the particle size of 8.2 and 6 nm, the charge storage mechanism becomes completely pseudocapacitive, with linear voltage-charge relation.

Intercalation pseudocapacitance can also be the intrinsic charge storage nature of a material. Nb_2O_5 is a perfect example of intrinsic pseudocapacitive material, which retains its capacitive nature, even after size tuning. Certain crystallographic planes of Nb_2O_5 facilitates rapid intercalation of Li ions, for both bulk and thin films

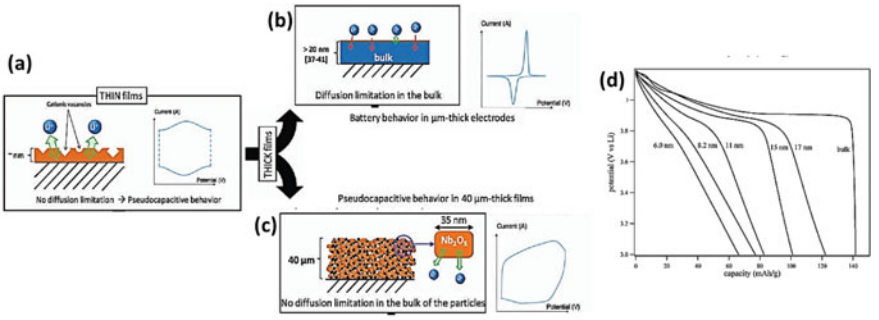

Fig. 4 **a–c** Schematic representation of extrinsic and intrinsic pseudocapacitance in materials due to size effect. Adapted with permission [17] © 1948, IOP Publishing and **d** Charge–Discharge studies of $LiCoO_2$ of various crystallite size, showing extrinsic pseudocapacitance nature. Adapted with permission [15], copyright (2007), American Chemical Society

[17]. Though it is usually deemed that with decreasing particle size, the diffusion limited battery-type intercalation transforms into non-diffusion limited pseudocapacitive intercalation, due to reduced diffusion length and higher surface area, it is not conclusive. Theoretical studies have reported that the contrary can also take place, where with decreasing particle size, the charge storage changes from pseudocapacitive intercalation to battery-type intercalation [18]. More number of comprehensive studies and theoretical elucidation are required in determining the size related pseudocapacitive nature of materials.

6 Electrochemical Features of Pseudocapacitance

6.1 CV and GCD Characteristics

As discussed, the extrinsic pseudocapacitance is dependent on the material properties, rather than the material itself. With advancement in material processing and nanotechnology, vast number of electrode materials for pseudocapacitive charge storage are reported. However, most researchers fail to understand the distinction between pseudocapacitive and battery type charge storage, often leading to misreporting of data with exaggerated or sometimes undermined capacitance values [19]–[21]. Specific capacitance, which is not applicable to battery-type materials, are calculated and reported due to misunderstanding of battery-type materials as pseudocapacitors. A comprehensive understanding of the electrochemical features of different charge storage mechanisms is necessary to avoid such misreports on pseudocapacitors with misleading capacitance values.

As discussed earlier, there are three mechanisms of pseudocapacitance, among which UPD is not quite used for charge storage device application. Redox pseudocapacitance is the most common form and intercalation pseudocapacitance came to the limelight of research in the recent times, with the development of different nanostructures. In all types of pseudocapacitance mechanisms, the following characteristics are common.

(i) There is a linear relation between the stored charge and the applied potential
(ii) The processes are rapid and kinetically controlled; diffusion has negligible effect on them
(iii) There is no phase transformation or chemical reaction taking place

The different charge storage mechanisms have unique electrochemical signatures, in CV and CD studies. The pseudocapacitance mechanisms, despite the difference in type, show similar electrochemical signatures. A proper understanding of these features can help identify the underlying charge storage technique. Figure 5 illustrates the electrochemical signatures of the different type of charge storage. The double layer capacitance shows rectangular CV and linear charge–discharge (CD) curves. Since the double layer formation is instantaneous, the current sharply increases

within a few millivolt and then remains almost constant with increased potential. The same is true of discharging of the EDLC, where current decreases sharply due to instant collapse of the EDL, when discharged (Fig. 5a). The galvanostatic charge discharge (GCD) curves under constant current, shows linear variation of charging and discharging time with respect to potential as shown in Fig. 5b.

Redox pseudocapacitance shows near rectangular CV and its GCD profile mildly deviates from linearity as represented in Fig. 5c, d. The constant charging or discharging current is not maintained due to the parasitic redox reaction that originates pseudocapacitance. The CV signature of intercalation pseudocapacitance has redox peaks, separated by small voltage difference (Fig. 5e), indicating the fast insertion and removal of Li^+ ions. In GCD profile, the change in the charge is slightly stagnant as depicted in Fig. 5f. In the case of battery-type charge storage, there are pronounced redox peaks in the CV profile, with larger peak-to-peak separation voltages, greater than 0.1 to 0.2 V. There are potential plateaus in the GCD profile, denoting that the charge does not change linearly with the potential.

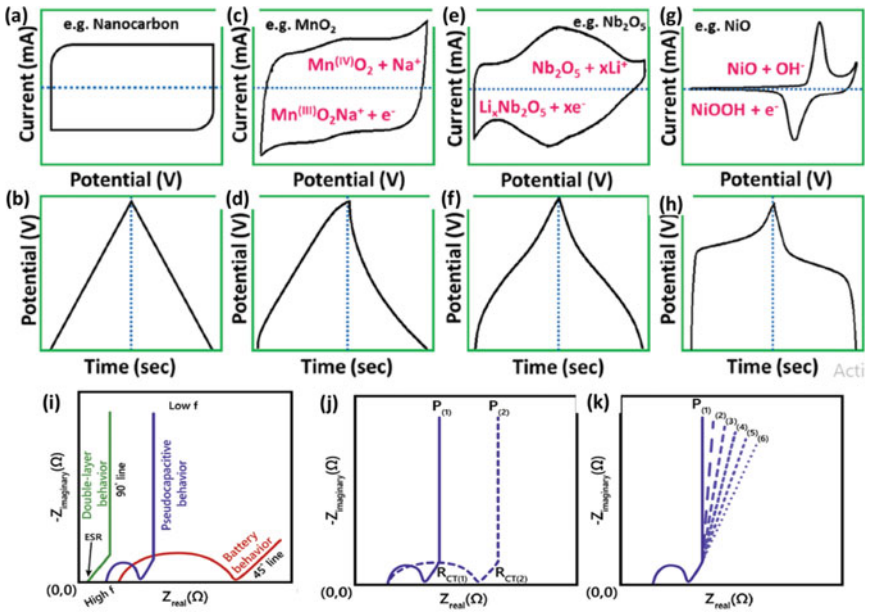

Fig. 5 Cyclic voltammetry and galvanostatic charge–discharge signatures of **a**, **b** double layer capacitance, **c**, **d** redox pseudocapacitance, **e**, **f** intercalation pseudocapacitance and **g**, **h** faradic battery type storage. Adapted with permission [1], copyright (2020), Springer Publishing Company. **i** Typical impedance spectra of EDLCs, pseudocapacitors and batteries; Identification of diffusion limited charge transfer from EIS **j** at two different potential giving different R_{CT} values and **k** at different potentials yielding the same R_{CT} value. Adapted with permission [23], copyright (2019), John Wiley and Sons

6.2 Electrochemical Impedance Spectroscopy Characteristics

The Electrochemical Impedance Spectroscopy (EIS) is an effective technique to characterize an electrochemical cell. Unlike dynamic methods like CV and GCD, EIS allow the analysis of electrochemical cell in a static condition. An AC voltage of small amplitude is imposed on the cell, along with the fixed DC potential, and the impedance response of the cell is analyzed, over a frequency range (typically 100 kHz to 10 MHz). Typically, EIS data is inferred in two forms, namely, (i) Nyquist plot, that plots real impedance against imaginary impedance and (ii) Bode plot, which represents the phase angle and modulus of impedance as a function of frequency. The values on the real axis (X-axis) of Nyquist plots account to pure resistance in the cell and a 90° line parallel to the imaginary axis (Y-axis) accounts to the pure capacitance.

Figure 5i shows the EIS signature of EDLCs, pseudocapacitive and battery-type materials. ESR is the equivalent series resistance that arises due to the resistance of the cell components. For a double layer capacitor, right after ESR, there is a 45° line, followed by the 90° line. The 45° line corresponds to the fast change in the imaginary impedance, as a corroboration to the immediately accessible charge sites. The impedance spectrum of pseudocapacitive materials have a semi-circle in the high frequency region, which corresponds to the parasitic charge transfer associated with redox or intercalation pseudocapacitance. The semi-circle is followed by the 45° line and 90° line, showing the capacitive behaviour of the pseudocapacitors, unlike in batteries, where the 90° line is absent and 45° line in the low frequency region corresponds to diffusion induced impedance.

The diffusive or capacitive nature of charge transfer can be identified using EIS for materials in transitional area, by measuring EIS at different potentials. For diffusion-controlled charge transfer, the charge transfer resistance (R_{CT}) changes for different potentials as shown in Fig. 5j, whereas for pseudocapacitive materials, even when measured at different potentials, the R_{CT} value does not change as shown in Fig. 5k.

Pseudocapacitance has electrochemical features that are very similar to EDLCs. Despite the type of pseudocapacitance (redox or intercalation), the following electrochemical features are prominently common to pseudocapacitors.

(i) The CV curve is not rectangular (as in EDLCs), but near rectangular. If there are any redox peaks in CV, they are separated by very small voltages, typically within the range of 0.1 to 0.2 V. Redox peaks separated by a larger voltage differences account to batter-type materials [9]

(ii) Under constant current (galvanostatic condition), the potential varies linearly with time, though not perfectly linear as in EDLCs. Parasitic redox reactions and kinetic intercalations lead to small changes in capacitance value, which is constant for EDLCs. There are no potential plateaus in the GCD profile. Potential plateaus are characteristics of batteries.

7 Evaluation Parameters: Specific Capacitance and Specific Capacity

The charge developed in a dielectric capacitor is proportional to the voltage applied across the parallel plates. From the traditional definition, the positive constant of proportionality between the charge and the voltage is called capacitance, which is the amount of charge Q, in coulombs stored in the capacitor to the applied potential V. Capacitance is a measure of charge storage capability in a given potential range and its unit is given in Farads.

$$Q \propto V \tag{15}$$

$$C = \frac{Q}{V} \tag{16}$$

Since, in double layer capacitors, the charge storage is analogous to that of a dielectric capacitor, the capability of EDLCs are measured in capacitance, most times with respect to the mass of the electrode material, called specific capacitance. The specific capacitance of EDLCs can be calculated from the GCD experiments, as follows:

$$C = \frac{i}{dV/dt} \tag{17}$$

where, i is the constant current, dV/dt is the slope of the discharge portion of GCD analysis.

The (mass) specific capacitance is given by the formula,

$$C = \frac{i}{m\left(dV/dt\right)} = \frac{i \times t}{m \times \Delta V} \tag{18}$$

where, m is the mass of the electrode material, t is the discharge time and ΔV is the potential window. The discharge time is taken in the notion that it renders the charge delivering capability.

The formula given in Eq. (18) is widely used by the research community to calculate the specific capacitance of pesudocapacitors. However, one should bear in mind that, pseudocapacitance does not show perfect linearity. Hence, in GCD profiles, pseudocapacitors do not have a single slope for the potential vs time plot. Hence, using the formula, given in Eq. (18) will not be a precise estimation of capability of the pseudocapacitor. A more appropriate or accurate method will be integrating the area under the discharge curve in GCD to account for the infinitesimal changes in the slope.

$$C = \frac{i \int dt}{m \times \Delta V} \tag{19}$$

The unit of specific capacitance is given in Farads/gram.

For pseudocapacitive materials, it is possible to calculate specific capacity and charge capacity, as the stored charge is not entirely constant in the maintained potential window. Capacity can be referred to as the amount of net charge stored at the capacitor. The specific capacity measures the number of ions or electrons that can be accepted by a certain mass of the electrode.

$$Charge\,capacity = \frac{i \int dt}{m}\left(Cg^{-1}\right) \tag{20}$$

$$Specific\,capacity = \frac{i \int dt}{m \times 3600}\left(Ahg^{-1}\right) \tag{21}$$

or

$$Specific\,capacity = \frac{i \int dt}{m \times 3600}\left(Ahg^{-1}\right) \tag{22}$$

It is a recommended practice to calculate both specific capacitance and specific capacity for pseudocapacitive materials to compare with the storage metrics of EDLCs and batteries [23].

8 Understanding the Transition Region, Capacitive and Diffusive Contribution in Pseudocapacitors

Modern development in nanomaterials and extrinsic pseudocapacitance has broadened the pseudocapacitive electrochemical energy storage as a better alternative to batteries and traditional EDLCs [22]. If there are multiple peaks in the CVs of pseudocapacitive material, then the possibility of diffusion limitation should not be neglected. In fact, in all EDLCs with carbon materials, there are surface parasitic redox reactions due to surface functionalities that lead to 5 to 10% diffusive contribution of charge. Similarly, even in batteries, the double layer capacitance could lead to a minimal charge contribution. Hence, for pseudocapacitors, especially extrinsic pseudocapacitors, which display combined charge storage mechanisms (capacitive as in EDLCs and diffusive as in batteries) with material properties, the assessment of charge storage kinetics is necessary to understand the overall charge storage contribution. Particularly with the recent advancements with fast kinetics LIBs and high energy intercalation psuedocapacitors, the distinguishing line should be drawn based on the contribution of charge storage kinetics for correct reporting of capacitance or capacity of the electrochemical energy storage device.

The capacitive and diffusive contribution can be quantified using different techniques. The power law given in Eq. (23) relates the peak current to the scan rate and is useful to number the capacitive (surface process) contribution and diffusive (bulk process) contribution.

$$i = av^b \tag{23}$$

where, i is the peak current, ν is the scan rate and a and b are constants. Based on the value of b, the type of charge storage kinetics can be determined. For diffusion limited, faradic, bulk redox reactions, the peak current varies as a function of square root of scan rate. For kinetically controlled surface processes like EDLC, the current varies as a linear function of scan rate. Hence, b = 0.5 for diffusive processes (batteries) and b = 1.0 for capacitive processes (EDLCs). For pseudocapacitors, particularly intercalation pseudocapacitors, there is a combination of both capacitive and diffusive processes, and the value of b ranges between 0.5 to 1.0. The computation of the value of b, will shed more information about the kinetics of the pseudocapacitive materials. The value of b can be obtained from the Dunn's method, by measuring CV at different scan rates [24].

The logarithmic interpretation of Eq. (23) can be given as follows:

$$\log i = \log a + b \log \upsilon \tag{24}$$

Hence, by plotting log of the peak current versus the log of the scan-rate, the value of b can be obtained from the slope, which is useful in identifying the dominating charge transfer process, as illustrated in Fig. 6a

The capacitive and diffusive current contribution an also be calculated from another interpretation of the power law as given in Eq. (25).

As we know, total current is the sum of capacitive and diffusion current.

$$i = i_{cap} + i_{diff} = k_1 \nu + k_2 \nu^{0.5} \tag{25}$$

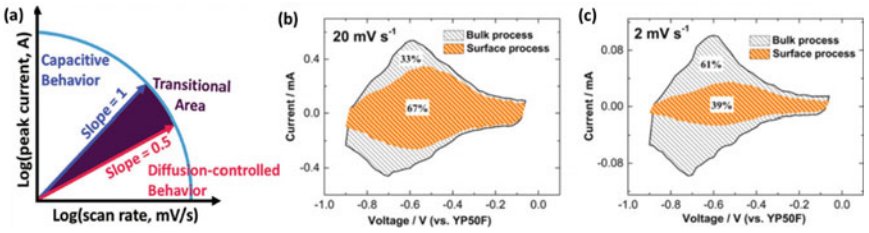

Fig. 6 **a** Illustration of the power law dependence of the peak current on scan rate for capacitive, diffusive and transitional behaviour. Adapted with permission from [1] © 2020, John Wiley and Sons and **b**, **c** Determination of current contribution by Dunn's methods for MXenes at different scan rate. Adapted with permission, copyright (2019), John Wiley and Sons

$$\frac{i}{\nu^{0.5}} = k_1 \nu^{0.5} + k_2 \tag{26}$$

Equation (26) is in the form of a line between i/ν and $\nu^{0.5}$, where k_1 and k_2 are the slope and intercept, respectively, By measuring CV at different scan rates and by plotting $i/\nu^{0.5}$ and the square root of the scan rate, the values of k_1 and k_2 can be obtained from the slope and intercept. By substituting k_1 and k_2 in Eq. (25) for a particular scan rate, the current contribution can be determined for the diverse potentials in CV.

This method can also be used to understand how the kinetics changes at different scan rates, where in general, for slower scan rates the diffusion takes control and at higher scan rates, the current is kinetically. Figure 6b shows that the charge storage in MXene is a surface dominated process in high scan rates, whereas in slower scan rates, the bulk process dominates the charge storage as shown in Fig. 6c.

9 Conclusion

Pseudocapacitance is a unique electrochemical charge storage mechanism that combines the features of both double layer capacitance and battery-type charge storage. Pseudocapacitors are fundamentally different from the batteries despite the fact that they both entail faradic phenomena by definition. The definition of pseudocapacitance is often misunderstood, leading to the reporting of battery-type materials as pseudocapacitive materials and reporting capacitance to inflated values. This is due to the extensive research and development of nanoscale materials, which give different electrochemical capacitive signatures for varying particle size. To distinguish the pseudocapacitive process from other electrochemical processes, a fundamental understanding of charge storage mechanisms is required. This chapter seeks to offer an in-depth explanation of the electrochemical charge storage mechanisms, foundations of pseudocapacitance, different pseudocapacitance types and the electrochemical characteristics of pseudocapacitance for the understanding of the viewer to distinguish the type of charge storage and pseudocapacitive mechanism.

References

1. N.R. Chodankar, H.D. Pham, A.K. Nanjundan, J.F.S. Fernando, K. Jayaramulu, D. Golberg, Y.K. Han, D.B. Dubal, True meaning of pseudocapacitors and their performance metrics: asymmetric versus hybrid supercapacitors. Small **16**(37), 2002806 (2020)
2. J.W. Long, D. Bélanger, T. Brousse, W. Sugimoto, M.B. Sassin, O. Crosnier, Asymmetric electrochemical capacitors-stretching the limits of aqueous electrolytes. MRS Bull. **36**(7), 513–522 (2011)

3. S. Trasatti, G. Buzzanca, Ruthenium dioxide: a new interesting electrode material. Solid state structure and electrochemical behaviour. J. Electroanal. Chem. Interfacial Electrochem. **29**(2), A1–A5 (1971)
4. B. E. Conway, *Electrochemical Supercapacitors* (Springer US, Boston, MA, 1999)
5. P. Simon, Y. Gogotsi, Materials for electrochemical capacitors. Nat. Mater. **7**(11), 845–854 (2008)
6. Y. Liu, S.P. Jiang, Z. Shao, Intercalation pseudocapacitance in electrochemical energy storage: recent advances in fundamental understanding and materials development. Mater. Today Adv. **7**, 100072 (2020)
7. U. Schmidt, S. Vinzelberg, G. Staikov, Pb UPD on Ag(100) and Au(100)—2D phase formation studied by in situ STM. Surf. Sci. **348**(3), 261–279 (1996)
8. V. Augustyn, J. Come, M.A. Lowe, J.W. Kim, P.L. Taberna, S.H. Torbet, H.D. Abruna, P. Simon, B. Dunn, High-rate electrochemical energy storage through Li+ intercalation pseudocapacitance. Nat. Mater. **12**(6), 518–522 (2013)
9. P. Simon, Y. Gogotsi, B. Dunn, Where do batteries end and supercapacitors begin? Science **343**(6176), 1210–1211(1979, 2014)
10. S. Fleischmann, J.B. Mitchell, R. Wang, C. Zhang, D. Jiang, V. Presser, V. Augustyn, Pseudocapacitance: from fundamental understanding to high power energy storage materials. Chem. Rev. **120**(14), 6738–6782 (2020)
11. A. Rajapriya, S. Keerthana, N. Ponpandian, C.M. Hussain, M.B. Ahamed, *Smart Supercapacitors—Fundamental Understanding of Charge Storage Mechanism* (Elsevier, 2023)
12. G.Z. Chen, Linear and non-linear pseudocapacitances with or without diffusion control. Prog. Nat. Sci.: Mater. Int. **31**(6), 792–800 (2021)
13. A.K. Shukla, S. Sampath, K. Vijayamohanan, Electrochemical supercapacitors: energy storage beyond batteries. Curr. Sci. **79**(12), 1656–1661 (2000)
14. B. E. Conway, The electrochemical behavior of ruthenium oxide (RuO_2) as a material for electrochemical capacitors, in *Electrochemical Supercapacitors* (Springer, Boston, MA, US, 1999)
15. M. Okubo, E. Hosono, J. Kim, M. Enomoto, N. Kojima, T. Kudo, H. Zhou, I. Honma, Nanosize effect on high-rate Li-ion intercalation in $LiCoO_2$ electrode. J. Am. Chem. Soc. **129**(23), 7444–7452 (2007)
16. Y. Jiang, J. Liu, Definitions of pseudocapacitive materials: a brief review. Energy Environ. Mater. **2**(1), 30–37 (2019)
17. J. Come et al., Electrochemical kinetics of nanostructured Nb_2O_5 electrodes. J. Electrochem. Soc. **161**(5), A718–A725 (2014)
18. E. M. Gavilán-Arriazu, M.P. Mercer, O.A. Pinto, O.A. Oviedo, D.E. Barraco, H.E. Hoster, E.P.M. Leiva, Numerical simulations of cyclic voltammetry for lithium-ion intercalation in nanosized systems: finiteness of diffusion versus electrode kinetics. J. Solid State Electrochem. **24**(11–12), 3279–3287 (2020)
19. M. Zhou, F. Lu, X. Shen, W. Xia, H. He, X. Zeng, One-pot construction of three dimensional $CoMoO_4/Co_3O_4$ hybrid nanostructures and their application in supercapacitors. J. Mater. Chem. A Mater. **3**(42), 21201–21210 (2015)
20. Y. Lan et al., Phosphorization boosts the capacitance of mixed metal nanosheet arrays for high performance supercapacitor electrodes. Nanoscale **10**(25), 11775–11781 (2018)
21. I. Shaheen, K.S. Ahmad, C. Zequine, R.K. Gupta, A.G. Thomas, M.A. Malik, Facile ZnO-based nanomaterial and its fabrication as a supercapacitor electrode: synthesis, characterization and electrochemical studies. RSC Adv. **11**(38), 23374–23384 (2021)
22. T.S. Mathis, N. Kurra, X. Wang, D. Pinto, P. Simon, Y. Gogotsi, Energy storage data reporting in perspective—guidelines for interpreting the performance of electrochemical energy storage systems. Adv. Energy Mater. **9**(39), 1902007 (2019)
23. J. Wang, J. Polleux, J. Lim, B. Dunn, Pseudocapacitive contributions to electrochemical energy storage in TiO_2 (Anatase) nanoparticles. J. Phys. Chem. C **111**(40), 14925–14931 (2007)
24. H. Shao, Z. Lin, K. Xu, P.-L. Taberna, P. Simon, Electrochemical study of pseudocapacitive behavior of Ti3C2Tx MXene material in aqueous electrolytes. Energy Storage Mater. **18**, 456–461 (2019)

Emerging Pseudocapaciting Materials

Muhammad Abdullah, Wenrui Jiang, Xin Chen, and Shandiao Xu

Abstract Current environmental problems are largely the consequence of the recent growing trends in global energy demand and its utilization, which ultimately resulted in the motivation to develop new routes to explore new energy materials. In response to this, supercapacitors have drawn much attention due to their relatively high power densities and long life cycles as compared to other energy devices. Supercapaciting materials are roughly divided into electric double-layer capaciting materials and pseudocapaciting materials. Between them, pseudocapacitor materials are attractive due to their high specific capacitance, which can lead to increased energy densities in the supercapacitors. In this chapter, we discuss the different types of pseudocapaciting materials, including pseudocapaciting nanoparticles developed based on the glycerate template method, composite pseudocapaciting materials consisting of nanosheets and/or nanoplates, negative electrode pseudocapaciting materials, and other emerging pseudocapaciting materials. In each category, the material selection, structural variations, and electrochemical performances of the pseudocapaciting materials will be addressed, respectively. Not only the state of art progress of the field is presented, but also the future development trends are discussed accordingly.

Keywords Pseudocapaciting materials · Glycerate template method · Nanosheets/nanoplates · Electrodes

1 Introduction

Unlike traditional electrical double-layer supercapacitor materials that store energy as a result of separating electric charges in a dielectric material, pseudo-capacitors use materials that undergo reversible faradaic redox reactions at the interface of electrode and electrolyte to store and release electrical energy. Pseudocapaciting

M. Abdullah · W. Jiang · X. Chen (✉) · S. Xu
Key Laboratory for Ultrafine Materials of Ministry of Education, and Shanghai Key Laboratory of Advanced Polymeric Materials, School of Materials Science and Engineering, East China University of Science and Technology, Shanghai 2002237, P.R. China
e-mail: xinchen73@ecust.edu.cn

© The Author(s), under exclusive license to Springer Nature Switzerland AG 2024

R. K. Gupta (ed.), *Pseudocapacitors*, Engineering Materials,
https://doi.org/10.1007/978-3-031-45430-1_4

materials are currently the subject of intense research as compared with electrical double-layer materials due to their higher capacitance, greater energy storage density, and outstanding energy conversion efficiency. Therefore, pseudocapacitive materials have become the hot spot and forefront of research [1]. The researchers are currently investigating innovative methodologies for fabricating pseudocapacitive materials with enhanced performance characteristics.

There are several common types of emerging pseudocapacitor materials. Conducting polymers such as polypyrrole (PPy), polythiophene (PTh), and polyaniline (PANI) have been investigated for their pseudocapacitive behavior due to their relatively high conductivity and reversible redox behavior [2]. Metal oxide materials such as tungsten oxide (WO_3), vanadium oxide (V_2O_5), and manganese oxide (MnO_2) have shown pseudocapacitive behavior due to the reversible redox reactions of their transition metal ions [3]. In addition to oxides, chalcogenides are also a subject of interest in the research area. As an example, Muhammad F. Ahmad et al. efficiently synthesized trimetallic Zn-Ni-Co-S/Se/Te through a hydrothermal approach followed by a solvothermal technique. The resulting material was utilized as electrodes, exhibiting outstanding supercapacitor performance. The research provides the energy storage mechanism of trimetallic chalcogenides through the utilization of a three-electrode supercapacitor in an aqueous KOH electrolyte. The electrode material comprising Zn, Ni, Co, and Se demonstrates outstanding specific capacitance of 1239.7 F/g at a current density of 1 A/g, thereby indicating its competitive superiority [4]. Two-Dimensional Materials such as graphene are attractive in the supercapacitor field due to their high surface area and fast electron transport, and they have been investigated for their pseudocapacitive behavior. MXenes represent another type of two-dimensional material that is composed of transition metals (M) and other elements such as carbon, nitrogen, and silicon (X). The most important features of these materials are their high electrical and thermal conductivity, excellent mechanical strength, and chemical stability. The electrical and thermal conductivities of MXenes are better than many traditional metals and semiconductor materials, with a wide range of application prospects. Metal–Organic Frameworks are a class of materials composed of metal ions and organic ligands with high porosity, which allows for high surface area and high capacitance. Details of these different types of pseudocapacitor materials will be reviewed in the other chapters of the book. In this chapter, we will address some fundamentals of the emerging pseudocapaciting materials.

2 Pseudocapaciting Materials Developed Based on the Glycerate Template Method

The research and development of nanomaterial morphology is one of the critical aspects of emerging pseudocapaciting materials. The most significant parameters of electrode materials are specific surface area and porosity, which can be controlled

through the size and morphology of the materials. In recent years, the majority of scholars have spent a great deal of time on the morphology of electrode materials to improve the specific capacitance, energy density, and stability of supercapacitors. Researchers are designing and synthesizing nanostructures with different compositions and geometric properties [5].

The most frequently employed methods consist of the in situ template method, the emulsion template method, the glycerate template method, etc. The glycerate template method can be utilized as a representative approach in which simple glycerate or its complex can be used as the template. Subsequently, a series of techniques such as the solvothermal method, etching technology, phosphating, and vulcanization technology can be employed to obtain various metal compounds that possess a counter-shape that is similar to the glycerate template. The nanomaterials synthesized through the glycerol template method usually have unique and complex detailed structures, a high specific surface area, and excellent porosity. Besides dense nanoparticles [6], hollow particles can also be prepared [7]. As a versatile tool, the glycerol template method is often used in the field of pseudo-capacitor materials to improve the electrochemical performance of supercapacitors, such as specific capacitance, cycle stability, capacitance retention, etc., which has great research potential and broad development prospects.

2.1 Glycerate Template Method

The key step in the glycerate template method is to build the template, which is first used to control the material morphology and then sacrificed when the actual material structure is formed. Liu et al. employed a straightforward approach to synthesize $MnCo_2O_4$ hollow spheres with exceptional uniformity. This involved the utilization of solvothermal synthesis to construct highly uniform MnCo-glycerate spheres, followed by thermal annealing in an oxygen-rich environment to yield the desired final material [8]. One trend in the field is to build materials/templates with more metal elements. Maryam Amiri et al. reported the synthesize of $CuCo_2V_2O_8$ hollow spheres, in which Cu-Co glycerate template spheres are firstly formed, and then an anion-exchange process is used for the formation of uniform spherical Cu-Co-V precursors, followed by a subsequent annealing to form uniform porous $CuCo_2V_2O_8$ hollow spheres, as shown in Fig. 1 [9]. In Wei's work, NiCoMn-glycerate spheres are first achieved in glycerol/isopropanol via a solvothermal method, and then the glycerate templates are chemically etched to form hierarchical Ni–Co–Mn hydroxide hollow architectures in 1-methyl-2-pyrrolidone (NMP)/H_2O [7]. The glycerol template method is currently undergoing refinement and enrichment through innovative efforts, leading to the understanding of numerous novel ideas.

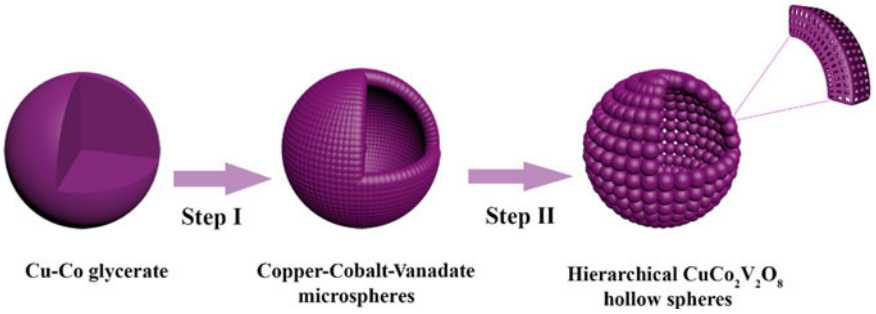

Fig. 1 Synthesis of hierarchical nanoporous quaternary $CuCo_2V_2O_8$ hollow spheres. Adapted with permission [9], Copyright (2020), Elsevier

2.2 Emerging Progress with the Glycerate Template Approach

The present progress in advanced supercapacitor development involves the production of composite materials and the enhancement of their material performance. This is because composites have the ability to keep the beneficial material properties of their individual components while also achieving comprehensive properties that are unattainable by a single component, which is called synergistic effect. Combining two compounds, one of which has high specific capacitance and the other has high conductivity, can produce a composite with both high specific capacitance and high conductivity. It may also be achieved by combining one component with high specific capacitance with another component with more nanochannels to help ion transportation, or by making a composite with aboundant active multiphase boundaries, etc. [10].

It is attractive to develop facile methods for composite material preparation. For example, our group used a self-template method to make unique bimetallic copper cobalt selenide (CCS) hollow nanosphere composites. The modified Cu_7Se_4-$Cu_xCo_{1-x}Se_2$ composite is achieved through a hydrothermal process with a comparatively short duration (2 h, denoted as CCS-2 h), rather than enhancing the reaction completion. Figure 2 describes the synthetic procedure for the copper selenide and copper cobalt selenide composites. First, the CuCo-glycerate nanospheres are made in a mixture of organic solvents. Consequently, a selenium supplier (Na_2SeO_3) and reducing agent ($N_2H_4{\cdot}H_2O$) are introduced for the hydrothermal treatment, which changes active SeO_3^{2-} into Se^{2-}. After that, the exchange of ions takes place across the glycerate template and Se^{2-}, resulting in the formation of nanostructured composite spheres made up of copper selenide/copper cobalt selenide. The composite demonstrates interesting characteristics, including a specific capacitance of 349.1 F/g at a current density of 1 A/g, excellent rate efficiency with 80.1% capacitance retention as the current density boosts to 20 A/g, and outstanding superior electrochemical stability with 106.4% capacitance retention beyond 5000 cycles. Additionally, the

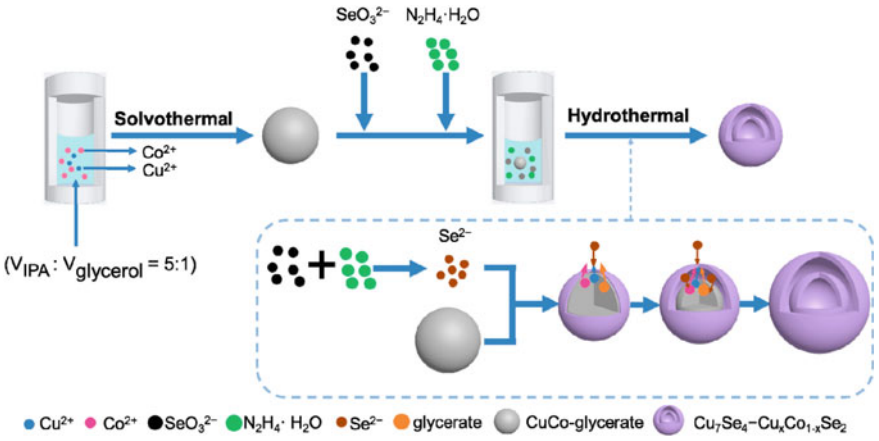

Fig. 2 A Schematic representation of the synthesis procedure for the double-shell hollow nanospheres of copper cobalt selenides. Adapted with permission [11], Copyright (2020), Elsevier

utilization of CCS-2 h and activated carbon electrodes in the creation of an asymmetric supercapacitor has led to favorable results with an energy density of 26.84 Wh/kg at 700 W/kg as well as an admirable cycling efficiency of 94.1% capacitance retention following 5000 cycles. The present study indicates the potential use of composites comprising transition metal selenides in supercapacitor applications. Furthermore, it proposes a novel approach to develope high-performance materials for supercapacitors [11].

In further research, Cheng et al. successfully synthesized hollow spheres of Ni-Mn hydroxide with a hierarchical structure through an etching methodology. Initially, solid spheres of NiMn-glycerate are obtained in the form of templates. Then, NiMn-glycerate templates undergo treatment in mixed solvents of 1-methyl-2-pyrrolidone and water, resulting in the formation of hierarchical Ni-Mn hydroxide hollow spheres through etching. The efficiency of electrical energy storage of the Ni-Mn hydroxide hollow spheres with a hierarchical structure was studied in a 3 M KOH solution through the utilization of a three-electrode system. Figure 3a displays the cyclic voltammogram (CV) profiles ranging from 5 to 30 mV/s. The presence of a visible redox peak is observed, demonstrating the characteristic pseudocapaciting properties of Ni-Mn hydroxide. The redox peaks observed in the experiment are a result of the faradaic reactions that occur between M–O/M–O-OH (where M represents the elements Ni and Mn) and hydroxide ions (OH^-). The Ni-Mn hydroxide exhibits pseudocapacitive characteristics, as evidenced by the curved potential peaks observed in galvanostatic charge–discharge (GCD) curves, as illustrated in Fig. 3b. The specific capacity values obtained from the GCD curves are presented in Fig. 3c as a function of various current densities. The Ni-Mn hydroxide hollow spheres exhibited a hierarchical structure and demonstrated excellent electrochemical performance, with a specific capacity of 1680 F/g at a current density of 2 A/g and 1104 F/g at 10 A/g. The extraordinary rate capability of Ni-Mn hydroxide is being observed. At a current

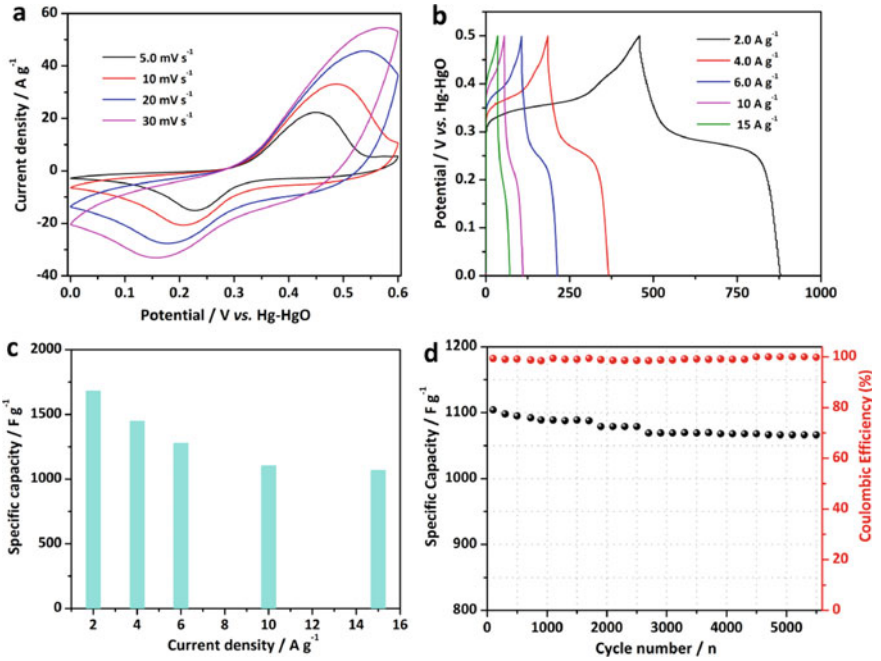

Fig. 3 Electrochemical performances of the hierarchical Ni-Mn hydroxide hollow spheres in three-electrode measurements: **a** CV and **b** GCD profiles, **c** specific capacity versus current density histograms, **d** cycles performance and coulombic efficiency at 10 A/g. Adapted with permission [12], Copyright (2021), Elsevier

density of 15 A/g, the capacitance remains at 1068 F/g, representing approximately 63.6% of the capacitance observed at a current density of 2 A/g. In addition, the results presented in Fig. 3d demonstrate that the Ni-Mn hydroxide electrode displays remarkable stability over a long cycle life. Particularly, it retains 96.6% of its initial value after undergoing 5500 cycles, with a coulombic efficiency exceeding 99%. These findings suggest that the Ni-Mn hydroxide electrode holds great potential as a material for outstanding-peformance supercapacitors [12].

3 Composite Pseudocapaciting Materials Consisting of Nanosheets and/or Nanoplates

Nanosheets and/or nanoplates can provide a very high specific area, which is very helpful for achieving a superior specific capacitance of the material. For example, Chai's team employed a simple single step potentiostatic deposition technique to fabricate a $NiCo_2S_4$ nanostructured electrode on F-doped SnO_2 (FTO) substrates

without the use of any binder. The optimization of the electrodepositing solution to control the Ni/Co mole ratio results in the fabrication of a nanosheet-like $NiCo_2S_4$ free-standing electrode. At a current density of 1 A/g, the electrode yields an outstanding specific capacitance of 1080 F/g. Even after 2000 cycles at 5 A/g, there is no decrease in the specific capacitance [13]. Although a nanosheet sample itself can achieve good supercapacitor performance, composing it with other components can further improve the materials properties through a synergistic effect. Composite pseudocapacitor materials consisting of nanosheets and/or nanoplates have achieved significant progress in recent years. These materials have the potential to revolutionize the field of energy storage by enabling the development of high-performance supercapacitors and batteries with improved energy and power densities. In these composites, if either the nanosheets/nanoplates or the other component is a pseuducapaciting material, then the composite would exhibit a Pseuducapaciting property.

Zhang et al. report regarding the NiCo-layered double hydroxide (LDH) hollow spheres synthesized with Co-glycerate as the substitute template and cobalt source. The assembly of hollow spheres involves the utilization of chaotic NiCo-LDH nanosheets. The hollow configuration of the spheres prevents the accumulation of LDH nanosheets, thereby facilitating the exposure of more active sites and reducing the diffusion path of electrolyte ions. The NiCo-LDH hollow spheres that were prepared exhibit a notable specific capacitance of 1962 F/g when measured at 1 A/g and an excellent capacitance retention rate of 66.4% at a current density of 30 A/g. The utilization of NiCo-LDH hollow spheres as positive electrodes in the production of asymmetric supercapacitors results in a significant energy density of 62.9 Wh/kg when subjected to a power density of 0.8 kW/kg. The present study aims to establish a simple method for synthesizing hollow spheres of layered double hydroxides (LDHs) that can be utilized in the production of supercapacitors. The use of transmission electron microscopy (TEM) has served as a tool for the observation of the NiCo-LDH hollow sphere's structural characteristics. The TEM images presented in Figs. 4a, b demonstrate the presence of void space within the hollow sphere as well as the existence of the outside nanosheet shells with a thickness of approximately 50 nm. The presence of void space facilitates the storage of electrolytes, thereby reducing the diffusion distance. Additionally, the nanosheet shells provide an extensive range of active sites that enhance the redox reaction. The homogeneous distribution of Ni, Co, and O elements in the associated elemental mapping, as illustrated in Fig. 4c, significantly verify the creation of nanosheet-assembled NiCo-LDH hollow spheres, demonstrating a clear dark-bright distinction between the shells and interiors [14]. Remarkable progress has been made in the research of many composite nanosheet materials, further revealing their huge potential.

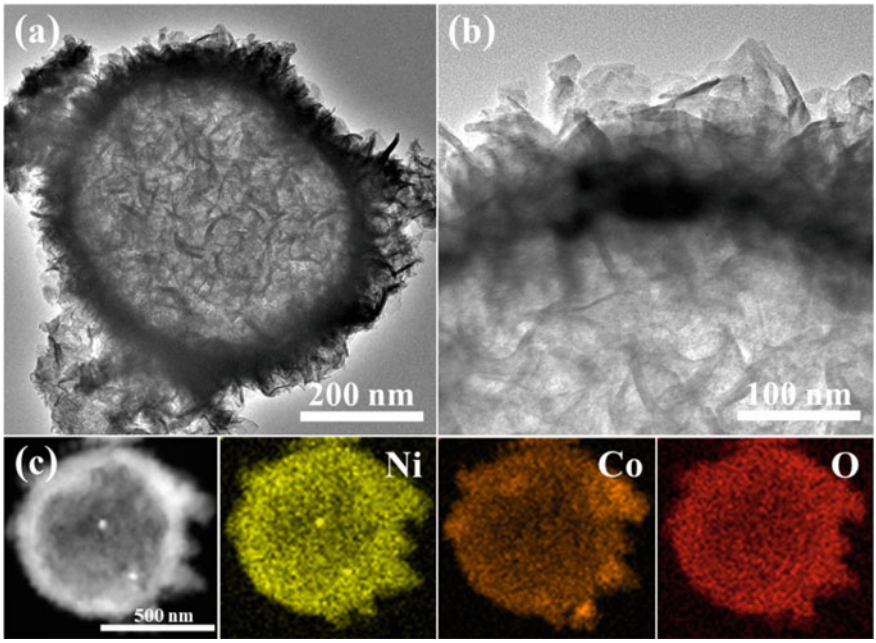

Fig. 4 **a**, **b** Transmission electron microscopy images of NiCo-LDH. **c** Scanning TEM picture of NiCo-LDH with elemental mapping of Ni, Co, and O. Adapted with permission [14], Copyright (2022), Elsevier

4 Negative Electrode Pseudocapaciting Materials

An electrochemical energy storage device comprises a positive electrode, an electrolyte, and a negative electrode. The majority of the research papers on pseudocapaciting materials appear to be about the positive electrode material; however, the research on the negative electrode surely has a vital role in the field. Negative electrode Pseudo-capacitive materials are a kind of material employed in energy-storing devices, such as a supercapacitor or hybrid supercapacitor, where the negative electrode undergoes a reversible redox reaction with the electrolyte to store energy. These materials offer high specific capacitances, good cycling stability, and fast charge–discharge rates, making them appealing for use in applications requiring considerable power [15].

Different kinds of materials used for negative electrodes exhibit a broad range of operational voltages, which has a significant impact on their efficiency in complete SC devices using an aqueous electrolyte. The working potential ranges of several materials used for negative electrodes using an electrolyte are summarized in Fig. 5. The literature review indicates that the operational potential range for three different activated carbon (AC) negative electrode materials is estimated to be 0 to −1 V and 0 to −1.1 V. The voltage window for three different graphene oxide negative

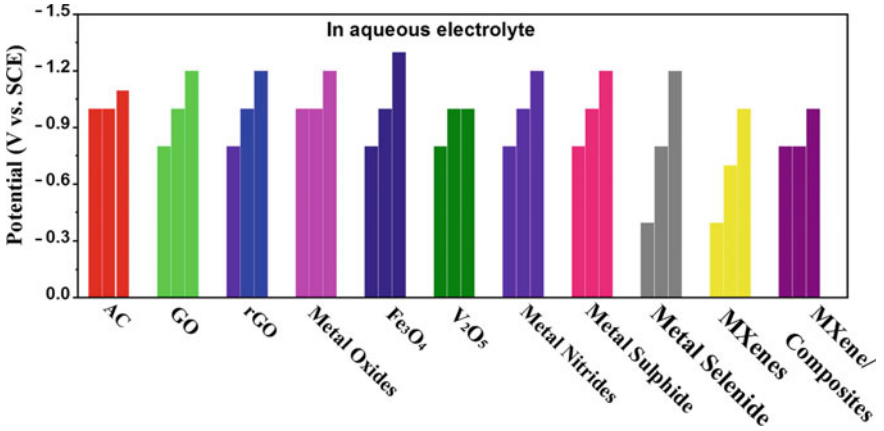

Fig. 5 The working voltage windows of several negative electrode materials with an aqueous electrolyte. Adapted with permission [16], Copyright (2023), Elsevier

electrode materials, is approximately from 0 to −0.8 V, 0 to −1 V, and 0 to −1.2 V, as illustrated. It is observed that among the various materials, the metal oxide (Fe_3O_4) exhibits the broadest potential window as compared to the other materials. This can help in the selection of suitable negative electrode materials. The operational potential range of electrode materials with aqueous electrolytes might be altered by changing their nanostructure, crystal configuration, and particle dimensions. With a deep understanding of this phenomenon, considerable study and improvement of negative electrodes to generate highly energetic SCs devices are now possible [16].

4.1 Metal Sulfides for Negative Electrode Pseudocapaciting Materials

Metal sulfides, as one type of metal chalcogene, have been extensively researched as negative electrodes for pseudo-capacitor applications based on their superior theoretical capacitances, high electrical conductivity, and chemical stability. In pseudocapacitors made of metal sulfide, electrochemical processes take place at the metal sulfide electrode's surface, where ions from the electrolyte are reduced or oxidized, resulting in charge storage. Metal ions and sulfide ions are created when metal sulfides go through reversible redox reactions during charging. The electrons from the redox process are moved to the electrode and stored there for further use. When an electrode is discharged, the electrons that have been stored are freed, and the metal ions and sulfide ions unite to create a metal sulfide electrode. Metal sulfides such as MoS_2, Bi_2S_3, and WS_2 are currently being investigated as promising possibilities for energy storage applications [17, 18].

Javed, Najam, et al. designed a unique negative electrode material for supercapacitors consisting of a binder-free linked composite nanosheet array of two-dimensional bimetallic ZnS/FeS on carbon cloth (2D-ZFS@CC). The 2D-ZFS@CC material exhibits superior capacitance of 1367.5 F/g/1641 C/g at a current density of 3 A/g, an operating voltage range of -1.4–0.0 V, 58.5% rate-capability, and 87% capacitance retention in comparison to the bimetallic oxide $ZnFe_2O_4$. This superior performance is accomplished by meticulously controlling the structure to create multiple pores with a wide available surface area and significant porosity, resulting in excellent capacitance. Moreover, quick charge transfer is made possible by the active material's lack of a binder. Additionally, the kinetic investigation showed that the 2D-ZFS@CC electrode stores energy via a hybrid charge storage method, having b-values for the anodic and cathodic peaks of 0.70 and 0.72, respectively. These results show 2D-ZFS@CC's tremendous potential as a negative electrode material for supercapacitors in the future [19].

The utilization of metal sulfides as negative electrode pseudocapacitors exhibit great potential owing to their interesting attributes such as high specific capacitance, excellent cycling stability, and economic feasibility. The present investigation focuses on enhancing the properties of materials and developing energy storage devices that are feasible for use in real life.

4.2 Metal Nitrides for Negative Electrode Pseudocapaciting Materials

Metal nitrides have gained significant attention as potential negative electrodes for pseudo-capacitors. These materials undergo reversible surface redox reactions when used as negative electrodes in pseudo-capacitors. During the charging process, metal ions present in the nitride oxidize and subsequently release electrons into the electrode, while nitrogen ions present in the electrolyte undergo reduction and acquire electrons from the electrode. The reverse occurs during discharging, with metal ions decreasing and nitrogen ions oxidizing. The redox processes that happen on the surface of metal nitride lead to the formation of an induced double layer at the interface of electrode and electrolyte, resulting in high capacitance and rapid charge/discharge rates. Therefore, metal nitrides are well-suited for applications as negative electrodes in pseudo-capacitors that demand high power density and extended cycling life [20]. Metal nitrides, namely titanium nitride (TiN), tungsten nitride (WN), and niobium nitride (NbN), exhibit favorable characteristics, including high conductivity, strong chemical stability, and quick charge transfer kinetics, therefore making them promising materials for negative electrode applications.

Ramadoss et al. employed a physical vapor deposition technique to fabricate titanium nitride on a flexible graphite substrate. The incorporation of nitrogen into the electrode material resulted in an enhancement of the surface's wettability and

improved its conductivity. Remarkably, the as-fabricated negative electrode exhibited pseudocapacitive behavior, demonstrating an impressive specific capacitance of about 86 mF/cm^2 under 1 mA/cm^2 over a broad operational voltage window of -1.1 to 0 V. It also displayed outstanding cycling stability, retaining 80% of its capacitance over 3000 cycles at a current density of 3 mA/cm^2 [21].

Metal nitrides exhibit high capacitance, remarkable cycling stability, and tunable properties, making them the future class of materials for negative electrode pseudocapacitive energy storage devices.

4.3 Hydroxide/LDH for Negative Electrode Pseudocapaciting Materials

Transitional metal oxides and hydroxides like MnO_2, NiO, $Ni(OH)_2$, CoO, and Co_3O_4 and their binary systems are among the traditional pseudocapacitive materials. The advancement of novel materials for electrodes with superior specific energy density and power density is essential for enhancing the overall efficiency of such SCs, since the efficiency of these SCs is heavily reliant upon the electrode materials. The remarkable electrochemical properties, device capabilities, and promising energy storage potential of LDHs and the corresponding derivatives make them a promising class of 2D nanomaterials [22]. LDHs have an anionic brucite structure and are two-dimensional in nature. These compounds are known to contain divalent and trivalent cations that are electrochemically active, such as Ni, Co, Al, and Fe. The strong pseudo-capacitive performance, high redox activity, and environmental friendliness of LDHs have made them particularly interesting materials for energy storage applications. In contrast, the majority of LDHs described for electrode materials have low electrical conductivity and cycle stability. Assembling LDHs with conductive materials will therefore be an effective means of improving the electrodes' electrical conductivity and cycle stability [23].

Liang & Zhitomirsky presented the synthesis of a novel material for energy storage in the negative electrodes of asymmetric supercapacitors. The material is a composite of Zn-Fe double hydroxide (Zn-Fe-DH) and multiwalled carbon nanotube (MWCNT), with the incorporation of celestine blue (CB) dye serving as a versatile additive. The electrodes demonstrated excellent cyclic stability and a capacitance of 5.2 F/cm^2 in a potential range of -1.0 to -0.2 V compared to a saturated calomel electrode. A novel asymmetric device has been developed, featuring negative electrodes composed of Zn-Fe-DH-MWCNT and positive electrodes coated with polypyrrole on MWCNT. A partially overlapping potential window allowed for the achievement of favorable capacitive behavior in both the cathode and anode materials at a high active mass of 40 mg/cm^2. A capacitance value of 2.2 F/cm^2 was determined at a scan rate of 2 mV/s [24]. Overall, research into hydroxide negative electrode pseudocapacitors continues to grow, with continued attempts to improve performance and broaden their applications.

4.4 Conducting Polymers, Metal Oxides, and MXenes for Negative Electrode Pseudocapaciting Materials

Conducting polymers. The optimal electrode material for supercapacitors is conductive polymers (CPs) because of their cost-effectiveness, excellent conductivity, high flexibility, and ease of manufacture. In addition, CPs have significant potential as both positive and negative electrodes due to their acceptable electrochemical characteristics in aqueous electrolytes with a broad operating voltage range from −1.0 to 1.0 V. Due to their exceptional stability, superior conductivity in the doped state, and quick redox operation capability, conducting polymers display a pseudo-capacitor type charge storage mechanism [25].

Metal oxides. Metal oxides are being widely investigated as negative electrodes in pseudocapacitors, which are electrochemical devices for storing energy that stores energy through reversible redox processes at the electrode–electrolyte interface. Metal oxides have great potential as negative electrodes in pseudocapacitors because of their large theoretical specific capacitance, which relies upon their redox activity, allowing reversible charge storage through faradaic processes. Additionally, metal oxides have high cycling stability, indicating that they can go through several charge/discharge cycles without significantly degrading or losing performance [26].

MXenes. MXenes have exhibited attractive efficiency and high specific capacitance when utilized as negative electrodes in pseudocapacitors. The redox activity exhibited by MXenes is responsible for their specific capacitance, as it facilitates the reversible storage of charge via faradaic reactions. Furthermore, MXene's strong electrical conductivity enables the fast mobility of ions and excellent power density. MXene has several advantages, including hydrophilicity, elemental structure flexibility, metallic nature, rapid charge transfer mobility, unique in-plane anisotropic structures, attractive physical and optical characteristics, and an adjustable band gap. In general, MXenes are materials with multiple layers that can be separated into large numbers of layers or individual flakes through the use of sonication and intercalation techniques [27].

More detailed discussions of conducting polymers, metal oxides, and MXenes can be found in the other chapters of the book.

5 Other Emerging Pseudocapaciting Materials

In addition to the pseudocapacitive materials discussed earlier, there are several other emerging materials that show promising potential for energy storage applications:

Hydroxide positive electrode materials. Hydroxides represent an exciting class of pseudocapacitive materials that exhibit higher specific capacitance, energy density, and superior cycle stability in comparison to traditional pseudocapacitive materials. These advantages have made hydroxides a research focus in multiple fields, including energy storage, water electrolysis, and supercapacitors.

As an example, Dipali et al. present the oriented attachment growth of innovative ZnCo and ZnCo@NiCo LDH on graphene-coated nickel foam (NF) by an all-hydrothermal route for enhanced supercapacitor studies. The oriented growth allows a route through which distinct nano-architectures are produced, which is highly beneficial for enhanced electrochemical performance owing to their high surface area and porous nature. High-performance electrodes consisting of ultrathin nanosheets of Zn-Co and nano-flakes of Ni-Co LDHs supported on highly porous and conducting 3D graphene foam were fabricated using a facile, one-pot hydrothermal synthesis route grown by an oriented growth mechanism without any additives or oxidants, as shown in Fig. 6. The hydrothermal process involves the hydrolysis of urea, resulting in the production of OH^- ions. These OH^- ions then interact with the separated Zn^{2+} and Co^{2+} ions, leading to the formation of ZnCo-hydroxide [$ZnCo_2(OH)_6$]. The ZnCo-hydroxide electrode underwent a 16-h reaction to form optimized nanoflowers, following which the samples were utilized for the subsequent deposition of NiCo hydroxide under hydrothermal conditions. The ultrathin nature of the nanosheets and the conducting nature of graphene foam, as well as the composite LDH structure, lead to superior supercapacitor performance of the studied electrode, which exhibits excellent values of areal capacitance of 2453 mF/cm^2, energy density of 1202 mWh/cm^2, and cycling stability of 108% after 5000 charge–discharge cycles within the working potential range of −0.2 to 0.6 V. The ultrathin nature of the nanosheets and the conducting nature of graphene foam, as well as the synergistic effect of the composite LDH structure, lead to superior supercapacitor performance [28].

He et al. prepared C/NiMn-LDH/Ni_3S_2 on a NF substrate through the integration of hydrothermal and electrodeposition techniques, resulting in remarkable electrochemical properties. The C/NiMn-LDH/Ni_3S_2/NF electrode exhibits a specific capacitance of 3490 mF/cm^2 when subjected to a current density of 2 mA/cm^2.

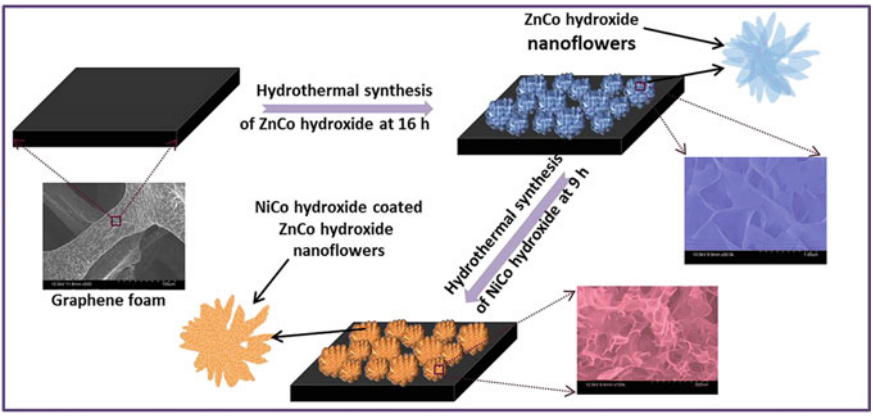

Fig. 6 Schematic illustration of ZnCo@NiCo hydroxide nanostructure synthesis. Adapted with permission [28], Copyright (2019), Elsevier

Further, it retains 84.25% of its initial energy even after undergoing 5000 continuous cycles and shows an exceptional specific energy value of 64.46 Wh/kg at a power density of 1279.96 W/kg. The outstanding electrochemical efficiency can be attributed to the synergistic effect resulting from the combined influence of the components. The physical characteristics and the microstructure of the obtained samples were studied using SEM. As illustrated in Figs. 7a–c, following the vulcanization process, a flocculent Ni_3S_2 film forms on the surface of the NF material. This film contributes to an increase in the roughness of the NF surface, thereby providing a larger area for the subsequent deposition of the hydroxide nanosheets. The Ni_3S_2/NF surface is observed to be fully coated by interlinked nanosheets of NiMn-LDHs, as depicted in Figs. 7d–f. The structural characteristics of the C/NiMn-LDH/Ni_3S_2/NF composite are displayed in Figs. 7g–i. The presence of the carbon coating on the surface of the nanosheets does not result in any apparent structural alterations when compared to NiMn-LDH/Ni_3S_2/NF [29].

Phosphate positive electrode material. Phosphates are mainly used as electrolytes in pseudo-capacitive materials to separate electrodes and promote ion transport. They can provide stable ion transport channels, allowing electrons to shuttle back and forth inside the capacitor. Phosphates are commonly used as solid-state electrolyte materials due to their excellent ion conductivity and chemical stability. In typical pseudo-capacitors, phosphates are concentrated between the electrodes of the capacitor, forming an electric field and a capacitance effect. By precisely controlling

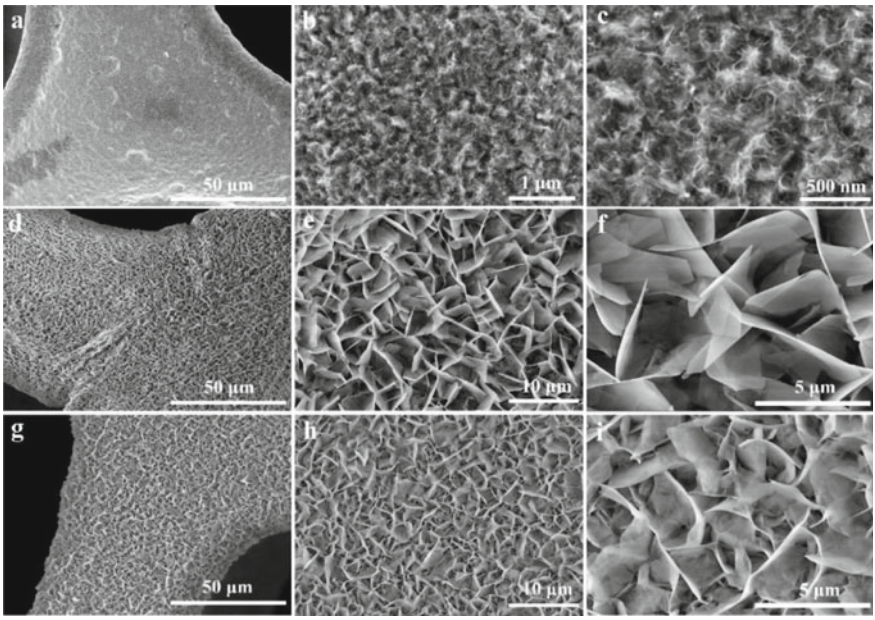

Fig. 7 SEM image of (**a–c**) Ni_3S_2 precursor arrays, (**d–f**) NiMn-LDH/Ni_3S_2 and (**g–i**) C/NiMn-LDH/Ni_3S_2 with various magnifications. Adapted with permission [29], Copyright (2021), Elsevier

the composition and structure of phosphates, the concentration of electric ions can be increased, and the capacitance performance of the capacitor can be improved [30].

For example, Zhang et al. discovered a simple surfactant-assisted self-assembly approach for synthesizing amorphous, hierarchically porous frameworks of NiCo phosphate at room temperature. The electrochemical capacitance performance of the prepared transition metal phosphate (SDBS-Ni_2CoPO_4) has been observed to be significantly enhanced, with a maximum value of 191.6 mAh/g at a current density of 0.5 A/g. This performance is due to the amorphous and mesopore structure of the material, which enables it to maintain a capacitance of 142.5 mAh/g even at a high current density of 10 A/g. In addition, the material had higher cyclic stability (77% retention after 2000 charge–discharge cycles at 10 A/g). Furthermore, an asymmetric supercapacitor consisting of SDBS-Ni_2CoPO_4//graphene was fabricated using an aqueous KOH electrolyte, exhibiting an impressive energy density of 36.5 Wh/kg at a power density of 150 W/kg over a working potential range from 0 to 1.5 V. The present study offers an easy and environmentally friendly approach for synthesizing cost-effective transition metal phosphates, which exhibit excellent efficiency as electrode materials in pseudocapacitive devices [31].

Lignin positive electrode material. In recent years, researchers have found that lignin-based carbon nanofibers are a new type of pseudocapacitive material with excellent capacitance performance. Lignin is a natural polymer compound that has high thermal stability and conductivity and can be prepared into carbon nanofibers by pyrolysis. Studies have shown that lignin-based carbon nanofibers have a high specific surface area and pore volume, which is conducive to electrolyte adsorption and ion transmission. In addition, the unique structure of lignin can improve the thermal stability and conductivity of carbon nanofibers, thereby enhancing their capacitance performance. The redox activity of the quinone structure present in lignin enables its direct utilization as a cathode material in rechargeable batteries. Quinones are considered electron carriers that exhibit mobility, and their six-membered ring structure, which contains a C = O functional group, allows for a facile and reversible two-electron redox reaction. The utilization of carbonized lignin as a sustainable conductor has been found to be effective in facilitating efficient electron transport. Additionally, the heterogeneous morphology of lignin has been observed to contribute to the diffusion of metal ions. The benefits of its potential as a cathode material, lignin's electron transfer capabilities are limited due to its insulating properties. In order to facilitate electrochemical reactions, it is necessary to enhance the electronic conductivity either intrinsically or extrinsically. Implementing systematic research into the impact of chemical functionality, conductive additives, and elemental doping can facilitate the development of effective cathode materials based on lignin [32, 33].

Besides the information discussed above, quantum dots and heterogeneous structures are also interesting. Research has demonstrated that the utilization of quantum dots as electrodes in supercapacitors can greatly improve their performance [34]. Heterostructural (HS) materials represent a novel category of materials that comprise heterogeneous domains characterized by mechanical or physical properties that differ

significantly. The interaction among these heterogeneous areas generates a synergistic effect wherein the synthetic characteristics exceed those estimated by mixing standards. Heterogeneous materials exhibit superior mechanical and physical characteristics that are unattainable by conventional homogenous materials. The generation of active sites along with defects within the grain boundaries of the heterostructure materials yields numerous redox activities, greater ionic conductivity, and reduced diffusion pathways, all of which may help improve the supercapacitors performance [35].

With continued development and optimization, emerging pseudocapacitive materials hold great potential for a wide range of energy storage and conversion applications, including portable electronics, electric vehicles, and grid-scale energy storage.

6 Conclusion

In conclusion, pseudocapacitors are a promising energy storage technology due to their high energy density and large capacitance. This chapter has reviewed the emerging pseudocapaciting materials that are being developed to improve the performance of these devices. One trend is the control of morphology through the template method, which has been used to create pseudocapaciting materials with high surface areas and excellent electrochemical performance. Other than nanospheres that can be readily prepared by a glycerate template method, composite materials consisting of nanosheets and/or nanoplates have also been synthesized and shown great potential due to their large surface area and unique properties. Moreover, negative electrode pseudocapaciting materials and other emerging positive electrode pseudocapaciting materials are discussed. Overall, the progress made so far is promising, and these materials have the potential to revolutionize the field of energy storage and conversion. On the other hand, the research on emerging pseudocapaciting materials still has much to be explored in terms of improving their performances. With further research and development, pseudocapacitors may become a viable alternative to traditional batteries and capacitors, offering a more efficient and sustainable means of storing and utilizing energy.

Acknowledgements The authors acknowledge the support of the National Natural Science Foundation of China (21875066); the Shanghai Leading Academic Discipline Project (B502), and the Shanghai Key Laboratory Project (08DZ2230500).

References

1. P. Bhojane, Recent advances and fundamentals of pseudocapacitors: materials, mechanism, and its understanding. J. Energy Storage **45**, 103654 (2022)

2. N.N. Loganathan, V. Perumal, B.R. Pandian, R. Atchudan, T.N.J.I. Edison, M. Ovinis, Recent studies on polymeric materials for supercapacitor development. J. Energy Storage **49**, 104149 (2022)
3. R. Zhao, L. Zhang, C. Wang, L. Yin, Tetramethyl ammonium cation intercalated layered birnessite manganese dioxide for high-performance intercalation pseudocapacitor. J. Power Sources **353**, 77–84 (2017)
4. M. Ahmad, I. Hussain, T. Nawaz, Y. Li, X. Chen, S. Ali, M. Imran, X. Ma, K. Zhang, Comparative study of ternary metal chalcogenides (MX; M= Zn–Co–Ni; X= S, Se, Te): formation process, charge storage mechanism and hybrid supercapacitor. J. Power Sources **534**, 231414 (2022)
5. J.Y. Wang, Y. Cui, D. Wang, Design of hollow nanostructures for energy storage, conversion and production. Adv. Mater. **31**(38), 1801993 (2019)
6. X. Chen, Y. Li, C. Li, H. Cao, C. Wang, S. Cheng, Q. Zhang, A novel strategy of multi-element nanocomposite synthesis for high performance ZnO-$CoSe_2$ supercapacitor material development. Chin. J. Chem. **39**(9), 2441–2450 (2021)
7. C. Wei, C. Cheng, K. Wang, X. Li, H. Xiao, Q. Yao, Hierarchical Ni–Co–Mn hydroxide hollow architectures as high-performance electrodes for electrochemical energy storage. RSC Adv. **11**(25), 15258–15263 (2021)
8. Z. Liu, F. Teng, C. Yuan, Z. Ul Abideen, W. Gu, Z. Liu, Highly uniform $MnCo_2O_4$ hollow spheres-based all-solid-state asymmetric micro-supercapacitor via a simple metal-glycerate precursor approach. Energ. Technol. **7**(9), 1900314 (2019)
9. M. Amiri, S.S.H. Davarani, S.K. Kaverlavani, S.E. Moosavifard, M. Shamsipur, Construction of hierarchical nanoporous $CuCo_2V_2O_8$ hollow spheres as a novel electrode material for high-performance asymmetric supercapacitors. Appl. Surf. Sci. **527**, 146855 (2020)
10. Q. Zhang, Q. Zang, Q. Shi, Z. Xiao, K.-P. Wang, L. Zong, L. Wang, Formation of V_6O_{11}@$Ni(OH)_2$/NiOOH hollow double-shell nanoflowers for the excellent cycle stability of supercapacitors. Dalton Trans. **50**(10), 3693–3700 (2021)
11. X. Yang, X. Chen, H. Cao, C. Li, L. Wang, Y. Wu, C. Wang, Y. Li, Rational synthesis of Cu_7Se_4-$CuxCo_{1-x}Se_2$ double-shell hollow nanospheres for high performance supercapacitors. J. Power Sources **480**, 228741 (2020)
12. C. Cheng, C. Wei, Y. He, L. Liu, J. Hu, W. Du, Etching strategy synthesis of hierarchical Ni-Mn hydroxide hollow spheres for supercapacitors. J. Energy Storage **33**, 102105 (2021)
13. Z. Chai, Z. Wang, J. Wang, X. Li, H. Guo, Potentiostatic deposition of nickel cobalt sulfide nanosheet arrays as binder-free electrode for high-performance pseudocapacitor. Ceram. Int. **44**(13), 15778–15784 (2018)
14. X. Zhang, W. Lu, Y. Tian, S. Yang, Q. Zhang, D. Lei, Y. Zhao, Nanosheet-assembled NiCo-LDH hollow spheres as high-performance electrodes for supercapacitors. J. Colloid Interface Sci. **606**, 1120–1127 (2022)
15. S. Islam, M.M. Mia, S.S. Shah, S. Naher, M.N. Shaikh, M.A. Aziz, A.J.S. Ahammad, Recent advancements in electrochemical deposition of metal-based electrode materials for electrochemical supercapacitors. Chem. Rec. **22**(7), e202200013 (2022)
16. M.S. Javed, A. Mateen, I. Hussain, S. Ali, S. Asim, A. Ahmad, E. Tag Eldin, M.A. Bajaber, T. Najam, W. Han, The quest for negative electrode materials for Supercapacitors: 2D materials as a promising family. Chem. Eng. J. **452**, 139455 (2023)
17. R. Barik, P.P. Ingole, Challenges and prospects of metal sulfide materials for supercapacitors. Curr. Opin. Electrochem. **21**, 327–334 (2020)
18. V. Sharma, S.J. Kim, N.H. Kim, J.H. Lee, All-solid-state asymmetric supercapacitor with MWCNT-based hollow $NiCo_2O_4$ positive electrode and porous Cu_2WS_4 negative electrode. Chem. Eng. J. **415**, 128188 (2021)
19. M.S. Javed, T. Najam, M. Sajjad, S.S.A. Shah, I. Hussain, M. Idrees, M. Imran, M.A. Assiri, S.H. Siyal, Design and fabrication of highly porous 2D bimetallic sulfide ZnS/FeS composite nanosheets as an advanced negative electrode material for supercapacitors. Energy Fuels **35**(18), 15185–15191 (2021)

20. Y. Tan, L. Meng, Y. Wang, W. Dong, L. Kong, L. Kang, F. Ran, Negative electrode materials of molybdenum nitride/N-doped carbon nano-fiber via electrospinning method for high-performance supercapacitors. Electrochim. Acta **277**, 41–49 (2018)
21. A. Ramadoss, A. Tripathy, A. Mohanty, N. Swain, G.S. Kaliaraj, S.Z. Noby, K. Kirubavathi, K. Selvaraju, Binder-free TiN/graphite based thin film negative electrode for flexible energy storage devices. Vacuum **211**, 111848 (2023)
22. X. Gao, P. Wang, Z. Pan, J.P. Claverie, J. Wang, Recent progress in two-dimensional layered double hydroxides and their derivatives for supercapacitors. Chemsuschem **13**(6), 1226–1254 (2020)
23. L. Li, J. Fu, K.S. Hui, K.N. Hui, Y.-R. Cho, Controllable preparation of 2D nickel aluminum layered double hydroxide nanoplates for high-performance supercapacitors. J. Mater. Sci.: Mater. Electron. **29**(20), 17493–17502 (2018)
24. W. Liang, I. Zhitomirsky, Zn-Fe double hydroxide-carbon nanotube anodes for asymmetric supercapacitors. Front. Mater. **7**, 137 (2020)
25. Q. Liu, J. Qiu, C. Yang, L. Zang, G. Zhang, E. Sakai, H. Wu, S. Guo, Robust quasi-solid-state integrated asymmetric flexible supercapacitors with interchangeable positive and negative electrode based on all-conducting-polymer electrodes. J. Alloy. Compd. **887**, 161362 (2021)
26. C. Rogier, G. Pognon, C. Galindo, G.T.M. Nguyen, C. Vancaeyzeele, P.-H. Aubert, MoO_3–carbon nanotube negative electrode designed for a fully hybrid asymmetric metal oxide-based pseudocapacitor operating in an organic electrolyte. ACS Appl. Energy Mater. **5**(8), 9361–9372 (2022)
27. M.M. Baig, I.H. Gul, S.M. Baig, F. Shahzad, 2D MXenes: synthesis, properties, and electrochemical energy storage for supercapacitors—a review. J. Electroanal. Chem. **904**, 115920 (2022)
28. D.S. Patil, S.A. Pawar, J.C. Shin, H.J. Kim, Layered double hydroxide based on ZnCo@NiCo-nano-architecture on 3D graphene scaffold as an efficient pseudocapacitor. J. Power Sources **435**, 226812 (2019)
29. Y. He, D. Liu, H. Zhao, J. Wang, Y. Sui, J. Qi, Z. Chen, P. Zhang, C. Chen, D. Zhuang, Carbon-coated NiMn layered double hydroxides/Ni_3S_2 nanocomposite for high performance supercapacitors. J. Energy Storage **41**, 103003 (2021)
30. S. Alam, M.I.K. Fizza Fiaz, M.Z. Iqbal, F. Alam, Z. Ahmad, H.H. Hegazy, Advancements in asymmetric supercapacitors: Material selection, mechanisms, and breakthroughs with metallic oxides, sulfides, and phosphates. J. Energy Storage **72**, 108208 (2023)
31. X. Zhang, N. Shang, S. Gao, C. Wang, Y. Gao, Z. Wang, Surfactant assisted self-assembly of NiCo phosphate with superior electrochemical performance for supercapacitor. Appl. Surf. Sci. **483**, 529–535 (2019)
32. R. Yadav, O. Zabihi, S. Fakhrhoseini, H.A. Nazarloo, A. Kiziltas, P. Blanchard, M. Naebe, Lignin derived carbon fiber and nanofiber: manufacturing and applications. Compos. B Eng. **255**, 110613 (2023)
33. H.Y. Jung, J.S. Lee, H.T. Han, J. Jung, K. Eom, J.T. Lee, Lignin-based materials for sustainable rechargeable batteries. Polymers **14**(4), 673 (2022)
34. S. Satpathy, N.K. Misra, V. Goyal, S. Das, V. Sharma, S. Ali, An AI-based newly developed analytical formulation for discharging behavior of supercapacitors with the integration of a review of supercapacitor challenges and advancement using quantum dots. Symmetry-Basel **15**, 844 (2023)
35. S. Saha, P. Samanta, N. Murmu, T. Kuila, A review on the heterostructure nanomaterials for supercapacitor application. J. Energy Storage **17**, 181–202 (2018)

Pseudocapacitance: Tuning Electrochemical Properties

Jinfeng Sun, Anning Zhang, Qian Zhang, and Changzhou Yuan

Abstract Recently, advanced electrochemical energy storage technology has come to require both high energy and power densities. Pseudocapacitance originates from the charge transfer reaction across the electrochemical interface and depicts higher capacitance than capacitors and faster electrochemical kinetics than traditional batteries, providing the opportunity to fulfill this goal. However, due to the intrinsic poor electrical conductivity, or inadequate structural stability, the rate performance and cycling stability of pseudocapacitive materials are still unsatisfactory. Thus, various strategies have been proposed to tune the electrochemical performance of pseudocapacitive materials for achieving both high energy and power. In this chapter, we highlight some recent works in developing pseudocapacitive materials for electrochemical energy storage systems. By introducing the research advances of both "intrinsic" and "extrinsic" pseudocapacitive materials, tune strategies such as nanostructure design, doping, introducing oxygen vacancies, interlayer engineering, heterostructure engineering, etc., have been carefully discussed. We hope this work will be of directive significance for the design and fabrication of high-performance electrode materials.

Keywords Pseudocapacitance · Fast kinetics · Electrochemical properties · Pseudocapacitive materials · Tuning strategies

1 Introduction

Batteries can exhibit high energy density (~200 Wh/kg), however, the diffusion-limited redox reactions always result in slow charging (tens of minutes-several hours) [1, 2]. Supercapacitors show much lower energy density (5–10 Wh/kg) but very fast charging (on the order of seconds) because of the surface-controlled ion adsorption mechanism [1]. Over the past few decades, plenty of research has been reported for the development of energy storage materials that can simultaneously possess

J. Sun · A. Zhang · Q. Zhang · C. Yuan (✉)
School of Materials Science & Engineering, University of Jinan, Jinan 250022, P. R. China
e-mail: mse_yuancz@ujn.edu.cn

© The Author(s), under exclusive license to Springer Nature Switzerland AG 2024

R. K. Gupta (ed.), *Pseudocapacitors*, Engineering Materials,
https://doi.org/10.1007/978-3-031-45430-1_5

high energy and high power density. Pseudocapacitance originates from the charge transfer reaction across the electrochemical interface and depicts electrochemical behaviors resembling capacitors, providing the opportunity to fulfill this goal.

Pseudocapacitance was first used to describe the absorption of hydrogen on metal surfaces by Conway and now was divided into three categories based on the storage mechanism: adsorption, surface redox, and intercalation pseudocapacitance [3, 4]. RuO_2 and MnO_2 are the most reported examples of surface redox pseudocapacitive materials. They store charges through fast and reversible redox reactions at/near the surface of the materials. Intercalation pseudocapacitive materials such as bronze-phase TiO_2 (i.e., TiO_2(B)) and orthorhombic Nb_2O_5 store charges through ions intercalating into/out of these materials, and no phase change can be observed during this process. These materials although exhibit different mechanisms, they all show pseudocapacitive properties inherently, i.e., their pseudocapacitive behavior is independent of their morphology or particle size. These materials are "intrinsic" pseudocapacitive materials. In recent years, the investigation of intrinsic pseudocapacitive materials has been focused on improving the electrochemical performance of the materials including the capacitance, rate capability, and cycling stability. In 2007, researchers found that some battery materials could depict pseudocapacitive properties when they were downsized into nanoscale, which were categorized as "extrinsic" pseudocapacitive materials. The most noted example of the extrinsic kind is $LiCoO_2$, in which a large fraction of Li^+ storage sites are on/near the surface when the particle size decreases below 20 nm [5]. After that, engineering materials such as V_2O_5, VO_2, Li_3VO_4, and so on into nanoscales to achieve pseudocapacitive Li^+ intercalation behavior have also been reported.

In this chapter, we highlight some recent works in developing pseudocapacitive materials for electrochemical energy storage systems, focusing on different kinds of methods to tune the electrochemical performance of pseudocapacitive materials for achieving both high energy and power densities. Strategies such as nanostructure design, doping, oxygen vacancies, interlayer engineering, heterostructure engineering, etc., have been discussed, which may have direct significance for the investigation of high-performance pseudocapacitive materials.

2 Tuning Strategies for Intrinsic Pseudocapacitive Materials

Typical examples of intrinsic pseudocapacitive materials like MnO_2, RuO_2, and iron oxides generally demonstrate faster reaction kinetics than the battery materials and larger capacitance than the EDLC materials. Regrettably, due to the intrinsic poor electrical conductivity and inadequate structural stability, the rate performance and cycling stability of these transition metal oxides are usually far from the level of EDLCs. If not optimized, they may suffer from obvious capacitance decay during long-term cycling.

MnO_2 have received considerable attention as pseudocapacitive materials thanks to their advantages such as high theoretical capacitance (1370 F/g), natural abundance, and low costs [6]. Till now, a variety of strategies have been reported for improving the electrochemical performance of MnO_2, including but not limited to introducing vacancies, expanding interlayer spacing, constructing nanoarchitectures, and compositing with conductive components. Choi and co-workers used a fluid dynamic-induced shear process to exfoliate layered birnessite-type MnO_2 into ultrathin 2D MnO_2 sheets and during which dopamine was also added to intercalated into the MnO_2 layers [6]. After calcination, the randomly stacked and interlayer-expanded MnO_2/nitrogen-doped carbon (MnO_2/C) composite was obtained, which can provide fast and efficient ions and electrons transport (Fig. 1a). Even at a high mass loading of 19.7 mg/cm^2, the MnO_2/C electrode exhibited high specific gravimetric (480.3 F/g) and areal capacitances (9.4 F/cm^2) at 0.5 mA/cm^2, as well as superior rate capability (Fig. 1b). Peng et al. reported the synthesis of oxygen defect-modulated sodium-intercalated manganese oxides ($Na_{0.55}Mn_2O_{4-x}\cdot 1.5H_2O$) for pseudocapacitors [7]. The crystal structure of $Na_{0.55}Mn_2O_{4-x}\cdot 1.5H_2O$ show that the [MnO_6] octahedron site consists of Mn^{3+} and Mn^{4+}, with Na^+ and H_2O residing in the tunnels (Fig. 1c). The monolayer thickness of $Na_{0.55}Mn_2O_{4-x}\cdot 1.5H_2O$ was evaluated as 0.732 nm which is benefit to ion transport and can withstand the stress related to the crystal deformation during charging/discharging. As a result, the $Na_{0.55}Mn_2O_{4-x}\cdot 1.5H_2O$ electrode depicted a rapid kinetics-dominated capacitive process with high capacitance of 475.5 F/g at 1 A/g (Fig. 1d). The faster Na^+ diffusion in $Na_{0.55}Mn_2O_{4-x}\cdot 1.5H_2O$ than pristine Mn_3O_4 electrode is also confirmed by the lower Warburg coefficient (Fig. 1e). By coupling the interfacial modulation and the Kirkendall effect, Wang and co-workers constructed the α-MnO_2/δ-MnO_2 hollow heterostructure that shows high aspect ratio with plenty of exposed active sites [8]. According to the theoretical calculation and electrochemical kinetic analysis, the improved the charge-transfer and electrolyte ion-adsorption/transport kinetics can be attributed to the existence of a potential built-in field within the heterostructure that enhanced the intrinsic reactivity of the electrode, consequently. The 30 mg/cm^2 electrode showed a high areal capacitance of 4762 mF/cm^2 (1 mA/cm^2), superior rate performance (79% capacitance retention when current increased from 1 to 100 mA/cm^2), as well as good cycling stability.

In 2005, Zukalova and co-workers first reported the pseudocapacitive charge storage behavior of TiO_2(B) fibers [9]. TiO_2(B) with parallel infinite channels can accommodate Li^+ with no significant structure distortion. In the following years, TiO_2 has been extensively investigated for Li^+ and Na^+ storage. A variety of efforts such as microstructure design, doping, and constructing composites have been attempted to tune the electrochemical properties of TiO_2(B) [10–12]. Lan et al. precisely designed and constructed mesoscale TiO_2 structures for high volumetric capacities [10]. The mesoporous TiO_2 presents a spherical morphology which was made up of aligned cylindrical TiO_2 bundles (Fig. 2a). This novel structure provided a high tap density of the active materials (1.1–1.7 g/cm^3) and a high accessible surface area for electrolyte ions to access, thus affording both high volumetric and gravimetric capacities. The nearly symmetric charge/discharge curves with slight aberration are the

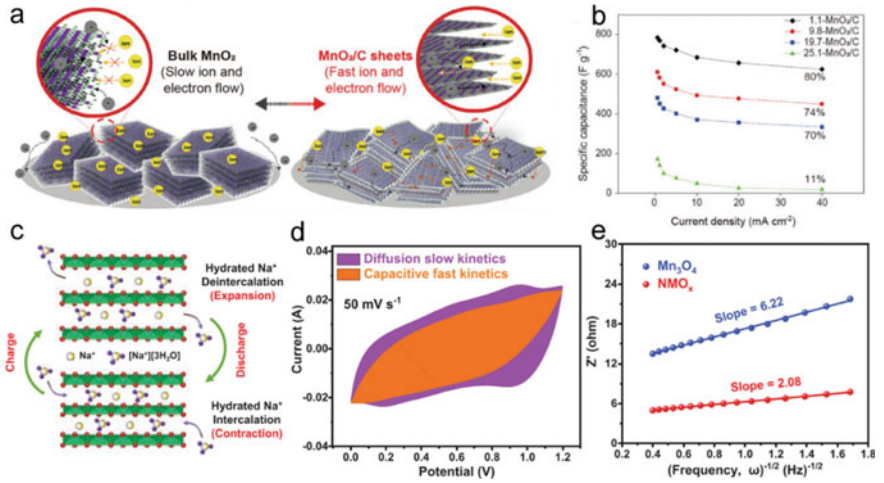

Fig. 1 **a** Schematic illustrations of ions and electrons transport on bulk MnO_2 and MnO_2/C electrodes. **b** Rate performance of MnO_2/C electrodes with different mass loading. Adapted with permission [6], Copyright (2021), Wiley–VCH GmbH. **c** The schematic diagram of the interplanar spacing evolution of the $Na_{0.55}Mn_2O_{4\text{-}x}{\cdot}1.5H_2O$. **d** Capacitive contribution of the $Na_{0.55}Mn_2O_{4\text{-}x}{\cdot}1.5H_2O$ electrode at 50 mV/s. **e** Z′ against $\omega^{-1/2}$ plots of the electrodes. Adapted with permission [7], Copyright (2022), Wiley–VCH GmbH

typical characteristic of pseudocapacitance (Fig. 2b). In addition, the rate capability of the ordered mesoporous TiO_2 samples are much superior to the hollow TiO_2 spheres and nanoparticles (Fig. 2c). Wang and co-workers constructed Nb-doped TiO_2 nanosheets that perpendicularly onto the substrate, endowing the TiO_2 nanostructure with an ion-conducting surface as well as expanded ions diffusion channels (Fig. 2d) [11]. The TEM images of Nb-TiO_2 show an expanded atomic spacing ($d_{(200)} = d_{(020)} = 0.21$ nm) compared with the pristine TiO_2 (Fig. 2e, f). The two crystal planes interlaced with each other with 90°, indicating that {001} lattice is the main exposed surface. As a result, the Nb-TiO_2 electrode delivered a high initial Coulombic efficiency of ~90% at 1 C and superior cycling stability even at a high rate of 60 C, indicating the fast insertion/extraction of Li^+ (Fig. 2g). The doping strategy is a generic approach to modulate the electric structure and kinetic behaviors of most host metal oxides for electrochemical energy storage. Although TiO_2 have received considerable interest for Li^+ and Na^+ batteries, the properties are still limited by their intrinsic low electric conductivity. Le and co-workers reported a microwave-assisted construction of mesoporous single-crystal-like TiO_2-graphene nanocomposite for pseudocapacitive sodium storage [12]. TiO_2 with spheroid shape and 100–350 nm diameters are uniformly anchored on the graphene sheets (Fig. 2h, i). The strong interaction of the TiO_2 and graphene ensures fast electron transfer within the hybrid nanostructure, resulting in pseudocapacitive charge storage behavior. The optimized nanocomposite depicted a high capacity of 268 mAh/g at 0.2 C with excellent rate

capabilities (Fig. 2j) and maintained 126 mAh/g even at a high current of 10 C for over 18,000 cycles.

Nb_2O_5 has been first researched for Li^+ storage in the 1980s by Reichman and Bard [13]. They found that Nb_2O_5 exhibited Li^+ and proton insertion and was also electrochromic. Kumagai et al. discovered that the insertion of Li^+ into Nb_2O_5 occurs under 2 V (*vs.* Li/Li^+), generating $Li_xNb_2O_5$ with $x \leq 2$ (theoretical capacity of 202 mAh/g) [14]. In 2010, mesoporous T-Nb_2O_5 films were reported to exhibit high levels of pseudocapacitive charge storage [15]. As shown in Fig. 3a, the CV curves delivered broad peaks, which are the typical features of pseudocapacitance. Due to the nanoscale porosity that provided a very short diffusion path length and the iso-oriented nature that could accommodate the volume change during charge/discharge, T-Nb_2O_5 depicted fast electrochemical kinetics comparable to the traditional redox

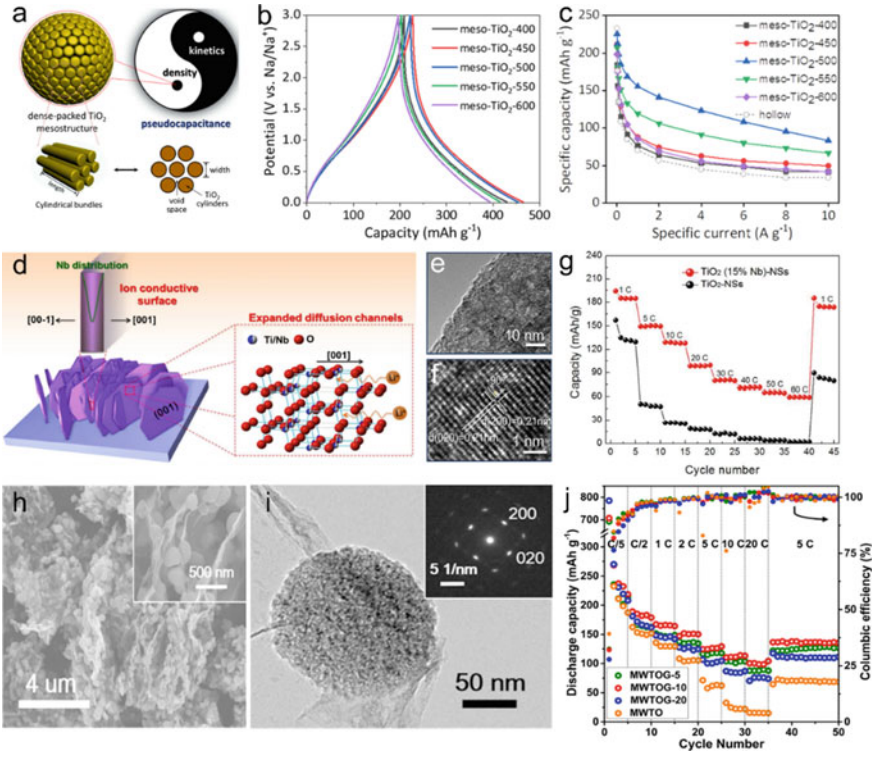

Fig. 2 **a** Schematic illustration of the 3D mesoscopic TiO_2. **b** Charge/discharge profiles and **c** Rate performance of the meso-TiO_2 anodes. Adapted with permission [10], Copyright (2021), American Chemical Society. **d** Structural design schematic of Nb-doped TiO_2 nanostructures. **e** TEM and **f** HRTEM images of Nb-TiO_2. **g** Comparison of rate performance for Nb-doped TiO_2 and pristine TiO_2 nanosheets. Adapted with permission [11], Copyright (2016), American Chemical Society. **h** SEM and **i** TEM images of TiO_2-graphene nanocomposite (inset of i is the SAED pattern). **j** Rate performance of TiO_2-graphene samples. Adapted with permission [12], Copyright (2017), American Chemical Society

pseudocapacitance of high surface area Nb_2O_5. These works have stimulated the investigations of Nb_2O_5 as electrochemical energy storage materials, and the crystal structure, nanostructure, particle size, and porosity have been finely tuned to realize the intercalation pseudocapacitance with fast kinetics. A series of Nb_2O_5 samples with constant pore size and precision-tailored wall thickness were synthesized and investigated for Li^+ storage [16]. With the wall thickness increased from 48.5 to 67.0 nm, the CV curves exhibited increased peak separation which is suggestive of the increased diffusion limitation process (Fig. 3b), indicating that the electrochemical properties were sensitively dependent upon the nanoarchitecture of Nb_2O_5. The calculated rate-dependent *b* value further described the transitions from surface-limited to diffusion-limited with the increasing wall thickness (Fig. 3c). Fu and co-workers developed yolk-shell Nb_2O_5 microspheres through a scalable spray drying method [17]. The obtained porous structure enabled Nb_2O_5 with a high intercalation capacity of 211 mAh/g and good rate performance. By a simple thermal treatment process, Liao et al. fabricated a series of nano-structured Nb_2O_5 with different phases and morphologies [18]. Electrochemical tests indicated that T-Nb_2O_5-700 nanoparticles with high surface area delivered the highest capacity and good rate performance. Except for nanostructuring, highly conductive materials such as carbon nanotubes (CNTs), graphene, etc. have been introduced to construct Nb_2O_5-based nanocomposites for improving the electron transport of the electrode. 3D porous carbon nanowebs incorporated with T-Nb_2O_5 nanoparticles have been synthesized and investigated for Li^+ storage [19]. Thanks to the improved conductivity of the composite, the electrode showed a high capacity of 125 mAh/g, fast Li^+ storage kinetics, and exceptional cycling stability over 70,000 cycles. Meng and co-workers developed an preintercalation strategy to improve the electronic conductivity of T-Nb_2O_5 and promote charge transfer [20]. After preintercalation of Li^+ into the T-Nb_2O_5 tunnels, the guest Li^+ leads to shallow donor levels that make the electrons easily donate from the donor level to the conduction band, thus considerably increasing the electronic conductivity. Moreover, the preintercalated Li^+ in the crystal structure can help electrolyte Li^+ ions to insert into the 4 g layer more easily during charging, leading to improved electrochemical properties (Fig. 3d). The pseudocapacitance contribution of the $Li_xNb_2O_5$/Graphene composite electrode can reach up to 80%, much superior to that of pristine T-Nb_2O_5 (Fig. 3e). Thereby, the composite delivered a high capacitance of 890 F/g at 1 mA/cm^2, good rate performance, and excellent cycling stability with 90% capacitance retention after 130,000 cycles. Moreover, the fabricated $Li_xNb_2O_5$/Graphene//MnO_2 asymmetric capacitor depicted a high energy density of 115 Wh/kg at 5500 W/kg.

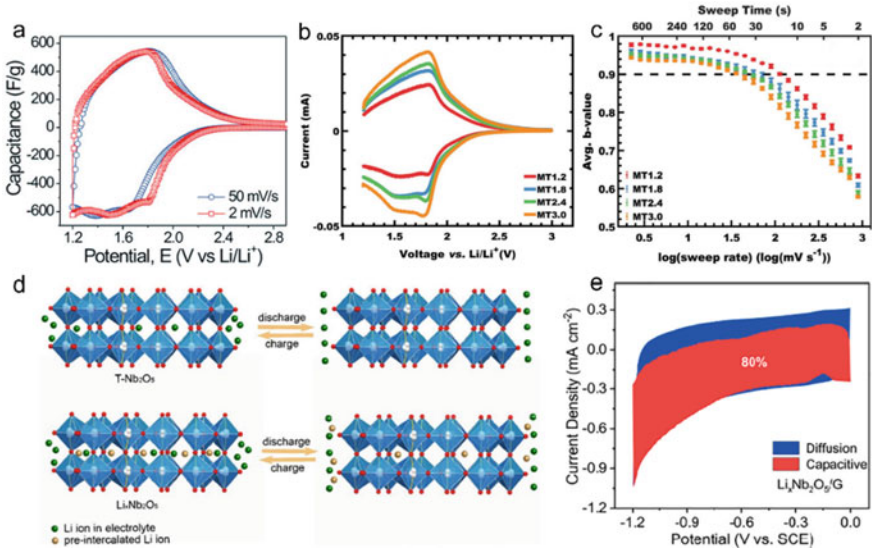

Fig. 3 **a** Potential-dependent capacitance calculated from CV responses at 2 and 50 mV/s, respectively. Adapted with permission [15], Copyright (2010), American Chemical Society. **b** CVs for the sample series at 2 mV/s and **c** *b*-value versus log plot of sweep rate. Adapted with permission [16], Copyright (2021), Wiley–VCH GmbH. **d** The schematic charge/discharge processes for T-Nb_2O_5 and $Li_xNb_2O_5$. **e** The pseudocapacitive contribution of $Li_xNb_2O_5$/Graphene electrode at 0.4 mV/s. Adapted with permission [20], Copyright (2022), Elsevier

3 Tuning Strategies for Extrinsic Pseudocapacitive Materials

In 2007, Okubo et al. reported the studies of nanosize effect on Li^+ intercalation behaviors in $LiCoO_2$ electrode [5]. The fluctuation in site energy caused by the lattice expansion near the surface layers resulted in the expected capacitive discharge curves. With the decrease in the crystallite size, the number of exposed surface layers increased, thus capacitive behavior became appreciable. These battery materials that could present pseudocapacitive properties when downsized into nanoscale were classified as "extrinsic" pseudocapacitive materials. Till now, plenty of works have been reported to arouse the pseudocapacitive response and optimize the kinetics of the battery materials. In this section, we will introduce the design strategies in detail including nanostructure design, doping, introducing vacancies, interlayer engineering, heterostructure engineering, etc., for the development of high-performance "extrinsic" pseudocapacitive materials.

3.1 Nanostructuring

Informed from the above, the contribution of near-surface Li^+ storage sites were increased through nanostructuring, hence presenting pseudocapacitive Li^+ intercalation behavior. Subsequently, downsizing battery materials such as V_2O_5, MoO_2, MoS_2, Li_3VO_4, etc. into nanoscale to achieve pseudocapacitive behavior have been reported. Kim et al. reported the development of pseudocapacitance properties in nanosized-MoO_2 [21]. They compared the Li^+ storage behavior of micro- and nanosized MoO_2 and found that nanostructuring could suppress the phase transformation caused by lithium insertion/deinsertion. The nanoscale MoO_2 delivered pseudocapacitive properties and much better electrochemical kinetics than the corresponding bulk material. *Ex-situ* XRD patterns verified that the lithium insertion/deinsertion induced phase transformation in the microsized MoO_2 has been obviously suppressed in the nanosized MoO_2 (Fig. 4a, b). In 2016, the same group reported the synthesis of MoS_2 nanocrystals which show high levels of pesudocapacitive contribution [22]. The MoS_2 nanocrystals were fabricated into carbon fiber-based composite electrodes which delivered fast electrochemical kinetics and excellent cycling performance. The *b*-values calculated for nanocrystalline MoS_2 were in the range of 0.94–0.98 (Fig. 4c), which are much higher than the bulk MoS_2 electrode (between 0.65 and 0.83). Quantitative kinetic analysis suggested that the capacitive charge storage in nanocrystal MoS_2 reached up to 83% (Fig. 4d). Asymmetric devices fabricated using the nanocrystal MoS_2-based electrode as anode exhibited a high energy density of 37 Wh/kg at 74 W/kg. Atomically thin 2D VO_2(B) nanoribbons have been constructed with dominant pseudocapacitive charge storage compared with the bulk counterparts [23]. HRTEM images showed that VO_2(B) with an interlayer spacing of ~0.62 nm was in a thickness of few layers (Fig. 4e). The ultrathin structure was beneficial to expose interlayers with fast migration channels and shorten the diffusion path of ions. Operando XRD measurement suggested that no noticeable evolution of crystal phase was observed during charge/discharge (Fig. 4f), revealing the successful conversion from battery type to pseudocapacitive charge storage mechanism. Consequently, the pseudocapacitance contribution of 2D VO_2(B) electrode reached up to 92% of the capacity at 0.3 mV/s. Even at a charge/discharge rate of 100 C, the 2D VO_2(B) still offered a high capacity of 140 mAh/g. SnS_2 has large interlayer spacing and alloying charge storage process with high capacity, thus receiving considerable interest as anode materials. Gao et al. fabricated 2D SnS_2 nanosheets on Zn-, N-, and S-doped carbon skeletons (SnS_2@ZnNS) and investigated the effect of calcination temperature on crystallinity and nanostructure [24]. The electrochemical test showed that the sample calcined at 350 °C exhibited the highest capacity and best rate capability (Fig. 4g), as well as good cycling performance. At 0.8 mV/s, the capacitive contribution of SnS_2@ZnNS-350 was calculated to 55.05% (Fig. 4h). The kinetic analysis further demonstrated the stronger pseudocapacitive response of SnS_2@ZnNS-350 than the other two samples, which can be ascribed to the good balance between the crystallinity and nanostructure. Dong and co-works synthesized $FeVO_4 \cdot nH_2O$ nanowires through a facile hydrothermal process [25]. Operando XRD and *ex-situ*

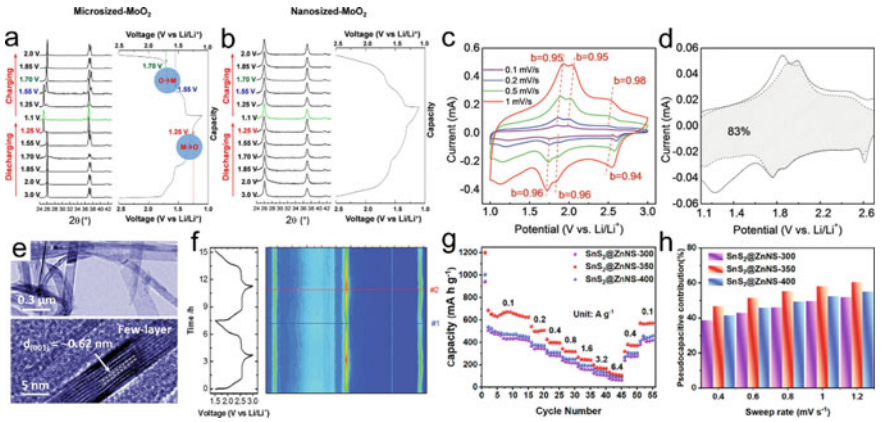

Fig. 4 *Ex-situ* XRD patterns of **a** microsized-MoO_2 and **b** nanosized-MoO_2 associated with the GCD curves. Adapted with permission [21], Copyright (2015), IOPscience. **c** CV curves and associated *b*-values for nanocrystal MoS_2. **d** Quantification of the capacitive contribution for nanocrystal MoS_2-based electrode. Adapted with permission [22], Copyright (2017), Wiley–VCH GmbH. **e** HRTEM images of 2D VO_2 (B) nanoribbons. **f** Operando XRD measurement for an atomically thin 2D electrode. Adapted with permission [23], Copyright (2018), Wiley–VCH GmbH. **g** Rate performance, and **h** Pseudocapacitive contributions at various sweep rates of the SnS_2@ZnNS samples. Adapted with permission [24], Copyright (2022), American Chemical Society

TEM characterizations verified that the $FeVO_4 \cdot nH_2O$ presented typical pseudocapacitive Na^+ intercalation behaviors with a 93% capacitive contribution of the capacity. In addition, the $FeVO_4 \cdot nH_2O$ anode depicted high capacity, excellent rate performance, and cycling stability.

Nanostructuring has been proven to be an effective strategy to tune the diffusion-controlled to surface-controlled pseudocapacitive behavior. The nanostructure shortens ion's diffusion path and exposes more interlayers with diffusion channels, minimizing the kinetic limitation and suppressing phase transition. The concern with extrinsic pseudocapacitive materials may be the scalable, low-cost synthesis method and how to maintain the electrochemical performance when constructed as thick electrodes for commercialization.

3.2 Defect Engineering

Besides nanostructuring, researchers have developed various strategies to tune the atomic structure or composition for improving the kinetics of the electron and ion transport of pseudocapacitive materials during the past few years. Introducing oxygen vacancies is a viable route to enhance the electrical conductivity of many transition metal oxides. Oxygen vacancies serving as shallow donors could increase the carrier concentration thereby promoting electrochemical kinetics [2].

Kim et al. investigated the effects of oxygen vacancies on the electrochemical properties of nanostructured MoO_{3-x} [26]. DFT calculation was carried out to definite stable oxygen vacancy sites and polaron configuration (Fig. 5a). The introduction of oxygen vacancies leads to an increase in electrical conductivity and a larger interlayer spacing that can provide faster kinetics and suppress the structure aberration during the insertion and deinsertion of Li^+. As a result, the MoO_{3-x} depicted improved capacity (Fig. 5b), pseudocapacitance contribution, rate capability, and cycling stability, as well as no solid-state diffusion limited kinetics (Fig. 5c). A similar approach has been reported to enhance pseudocapacitive charge storage in ultrathin CeO_{2-x} films [27]. CeO_{2-x} films (9–70 nm) were synthesized by electrodeposition with a high oxygen vacancy concentration of ~4–15 at%. The vacancies led to a decrease in the bandgap from 3.2 to 1.9 eV, enhancing the electron conduction and thus resulting in a high volumetric capacitance of 1873 F/cm^3. DFT calculation further illustrated the increased charge density around Ce ions in defective CeO_{2-x} compared to CeO_2. In addition, the intercrystallite water could promote proton conduction, leading to proton insertion/disinsertion pseudocapacitive behavior. VO_2 nanobelts with oxygen vacancies deposited on nitrogen-doped carbon nanosheets (VO_{2-x}/NC) were synthesized for pseudocapacitive Na^+ storage [28]. Experimental and DFT results illustrated that the oxygen vacancies were in favor of enhancing electronic conductivity and regulating the adsorption of Na^+, thereby resulted in a high reversible capacity of 270 mAh/g at 0.2 A/g and fast electrochemical kinetics. Moreover, the fabricated sodium-ion hybrid capacitors using VO_{2-x}/NC as anode displayed a high energy density of 122 Wh/kg. Du and co-workers developed a series of oxygen-rich vacancy MFe_2O_4/C (M = Ni, Mn, Co) materials (OV-MFO) for Li^+ storage via a simple solvothermal and subsequent calcination process [29]. The oxygen vacancies contributed to higher conductivity, additional active sites, and accelerated Li^+ diffusion, making for superior pseudocapacitive Li^+ storage than their counterpart electrodes. A hydrated VO_2 nanoribbon (HVO) with oxygen vacancies has been prepared for high-rate Zn^{2+} storage [30]. The defective crystalline structure provided suitable ambient spacing for rapidly accommodating and transporting of cations, exhibiting a fast Zn^{2+} diffusion coefficient, and a high reversible capacity of 396 mAh/g at 0.05 A/g [30].

This oxygen vacancy engineering strategy has been proven effective for tuning the electronic structure and reaction kinetics of transition metal-based electrode materials. On this basis, Zhu et al. reported the quantification of vanadium-defective clusters (i.e., up to 5.7%) in the V_2O_3 lattice and investigated its performance for Zn^{2+} storage [31]. The insertion of Zn^{2+} into the perfect V_2O_3 (P-V_2O_3) was blocked according to the positive Gibbs free energy (Fig. 5d). On the contrary, the vanadium-defective V_2O_3 (V_d-V_2O_3) accepted the insertion of Zn^{2+} and provided much higher capacity (Fig. 5e). In detail, part of the vanadium vacancies provided permanent sites for the preoccupation of a small amount of Zn^{2+}. Thus, the structure can maintain stability during the continuous insertion and extraction of Zn^{2+}. In addition, the other vanadium vacancies could weaken the strong interaction between Zn^{2+} and the host material, allowing free insertion/extraction of Zn^{2+} [31]. The capacitance

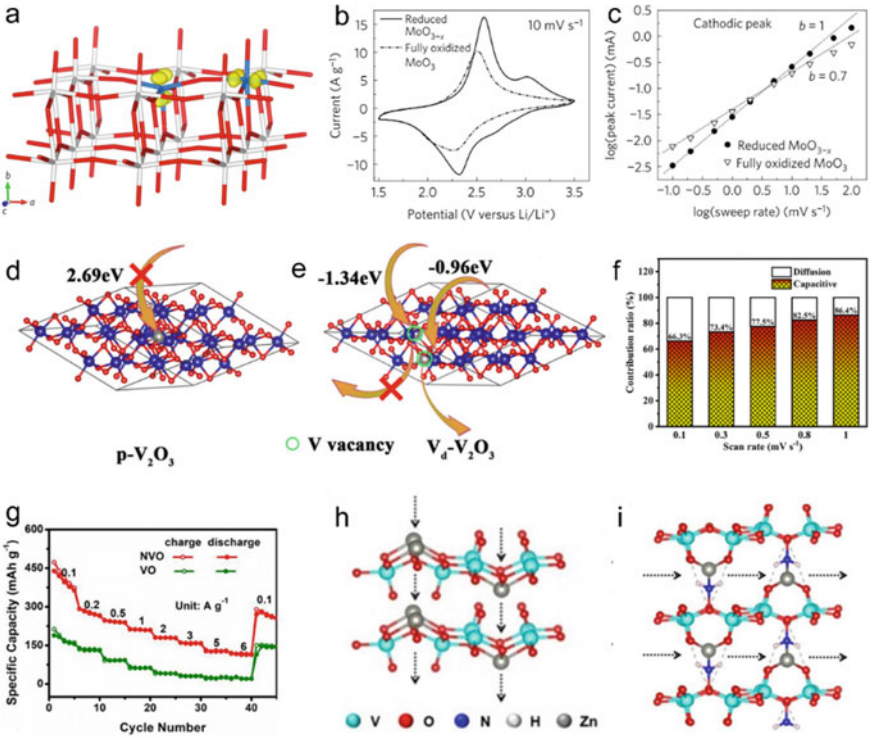

Fig. 5 **a** The most stable oxygen vacancy configuration and polaron formation in reduced MoO_{3-x}. **b** CVs of MoO_{3-x} and fully oxidized MoO_3 at 10 mV/s. **c** The calculated *b*-value for MoO_{3-x}. Adapted with permission [26], Copyright (2017), Nature. The Gibbs free energy of **d** P-V_2O_3 and **e** V_d-V_2O_3 for Zn^{2+} insertion. **f** Pseudocapacitance contribution of V_d-V_2O_3 at different scan rates. Adapted with permission [31], Copyright (2021), Nature. **g** Rate performances of NVO and pristine V_2O_5. The schematic diagrams of Zn^{2+} diffusion pathway in **h** V_2O_5 and **i** NVO. Adapted with permission [32], Copyright (2023), Elsevier

contribution was shown in Fig. 5f, indicating the capacitive dominant charge storage mechanism which can be attributed to the improved electrochemical kinetics of Zn^{2+}.

Atomic doping is also a widely used strategy to tune the electrochemical properties of pseudocapacitive materials. N-doped V_2O_5 (NVO) was synthesized to tune its Zn^{2+} storage properties [32]. N-doping decreased the bandgap energy of V_2O_5, thus increasing the electrical conductivity and weakening the strong electrostatic interaction between Zn^{2+} and V_2O_5. Besides, the existing form of N in NVO is -NH_2 connected to O-V. Different from the pristine V_2O_5 in which Zn^{2+} prefers to the vertical interlayer diffusion, Zn^{2+} ion diffusion pathway in NVO turns to the planner interlayer diffusion (Fig. 5h, i). As a result, the NVO exhibited much superior electrochemical properties than the pristine V_2O_5. The capacities at various current densities were higher than the undoped-V_2O_5 (Fig. 5g). Moreover, even after 3000 cycles at 10 A/g, NVO still maintained a high capacity of 111.1 mAh/g with only

slight capacity decay. Wang et al. reported the development of sulfur-doped yolk-shell $Na_2Ti_3O_7$ (s-NTO) spheres as anode materials for Na^+ storage [33]. By controlling the calcination condition (thiourea as a sulfur source), s-NTO can be successfully synthesized. Thanks to the synergistic effects of sulfur doping that improve the sluggish Na^+ insertion/deinsertion by narrowing the bandgap of NTO and the unique double-shell structures that provide enlarged surface area and ions diffusion channels, s-NTO exhibited improved electrochemical properties than the pristine NTO. Through a simple solvothermal method, a Mo-doped sodium titanate (MoNTO) was successfully synthesized as an anode for Na^+ storage [34]. The authors hold that Mo^{6+} with a comparable ionic radius to Ti^{4+} can partially replace Ti^{4+} in the lattice structure without structure damage. The highly charged Mo^{6+} in NTO crystal lattice not only improves the conductivity but also resulted in oxygen vacancies. The combined effect of these two features provided faster Na^+ storage kinetics, higher capacity, and prolonged cycling life. Wang and co-workers proposed an alternative strategy to tune the typical battery-type $Co(OH)_2$ to extrinsic pseudocapacitive materials by S^{2-} doping [35]. The electrostatic repulsion from S^{2-} ions increased the energy barrier for the insertion of OH^-, suppressing the bulk phase transformation. Besides, the surface absorbed H_2O molecules by S^{2-} decreased interaction between OH^- and $Co(OH)_2$. Consequently, after S^{2-} doped, the $Co(OH)_2$ delivered electrochemical characteristics, and surface-controlled kinetics of pseudocapacitance.

3.3 Interlayer Engineering

2D layered structure materials such as MoS_2, and V-based oxides have received considerable interest for electrochemical energy storage because of their merits of reversibly intercalating ions without structural destruction [36, 37]. However, they still suffer from sluggish ions diffusion and large internal strain during charge/discharge [36]. Modifying the interlayer structure of these materials has been verified as an effective way to improve the interfacial charge transfer and ions diffusion.

Zhao et al. fabricated MoS_2 nanoflowers with expanded interlayer spacing (more than 1.34 nm) deposited on carbon fibers (E-MoS_2/CF) for pseudocapacitive Na^+ storage (Fig. 6a) [36]. The enlarged interlayer spacing of MoS_2 nanoflowers not only decreased the ions diffusion pathways but also increased the available and accessible active surface area, enabling the fast Na^+ storage kinetics (Fig. 6b). Besides, the large interlayer spacing could accommodate the internal strain induced by ions insertion which is conducive to maintain the structure stability. E-MoS_2/CF electrode delivered a high capacity of 104 mAh/g at an ultrahigh rate of 20 A/g, as well as excellent cycling performance. The *b*-values were kept in the range of 0.9–1 at a large voltage range over 0.6 V, further illustrating its capacitive dominant charge storage process (Fig. 6c).

The interlayer distance of MoS_2 can also be modulated by inserting a guest species to form an intercalation compound [38, 39]. Li et al. fabricated poly(ethylene oxide)-intercalated MoS_2 composites (PEO-MoS_2) using PEO as an intercalating agent

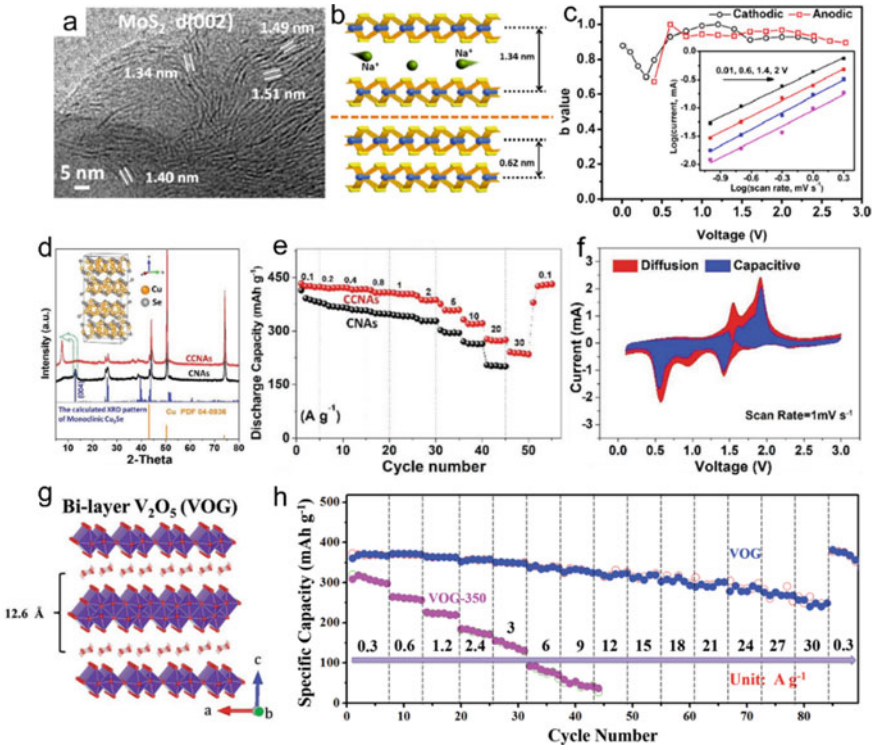

Fig. 6 **a** HRTEM image of the E-MoS_2/CF. **b** E-MoS_2/CF with enlarged interlayer spacing is in favor of rapid ions diffusion. **c** *b*-values versus voltage of the E-MoS_2/CF anode, insert: current versus scan rate plots. Adapted with permission [36], Copyright (2017), Elsevier. **d** XRD patterns of CTAB-Cu_2Se and pristine Cu_2Se, inset: the unit cell of α-phase Cu_2Se. **e** Rate performance. **f** Pseudocapacitance contribution of CTAB-Cu_2Se at 1 mV/s. Adapted with permission [41], Copyright (2020), Wiley–VCH GmbH. **g** The crystal structures of pristine $V_2O_5{\cdot}nH_2O$. **h** Rate capability of VOG and VOG-350. Adapted with permission [42], Copyright (2017), Wiley–VCH GmbH

through a facile exfoliation-restacking process [38]. By optimizing the amount of PEO, the interlayer spacing of MoS_2 could increase up to 1.45 nm. The optimized PEO-MoS_2 sample exhibited a high capacity of 210 mAh/g at 50 mA/g which is twice the commercial MoS_2 and showed improved rate performance. Similarly, an *in-situ* polyaniline (PANI) intercalation strategy to improve the Zn^{2+} storage properties of V_2O_5 has been reported [40]. The intercalated PANI not only expanded the interlayer spacing of V_2O_5 (1.39 nm) that favors the Zn^{2+} diffusion but also acted as interlayer pillars that maintains the structural stability during continuous charging/discharging. Additionally, the strong electrostatic interactions between the Zn^{2+} and the host O^{2-} can be effectively blocked by the unique π-conjugated structure of PANI. Benefitting from these advantages, the PANI-intercalated V_2O_5 exhibited an improved capacity of 197.1 mAh/g at 20 A/g, superior rate performance, and excellent cycling stability with a capacity retention of 97.6% over 2000 cycles. A nanosheet

array of Cu_2Se intercalated by cetyltrimethylammonium bromide (CTAB) has been developed (CCNAs) for Na^+ storage [41]. The CCNAs depicted expanded interlayer spacing of the (004) plane (Fig. 6d) which can increase the buffer space for volume expansion during charge/discharge and restrict the shutting of polyselenide intermediate [41]. Electrochemical tests suggested that the CCNAs exhibited a high capacity of 426.0 mAh/g at 0.1 A/g and can maintained at 238.1 mAh/g even at a high current of 30 A/g (Fig. 6e). Besides, the CCNAs exhibited typical pseudocapacitive behavior with a capacitive contribution of up to 77.8% at 1.0 mV/s (Fig. 6f).

Transition metal cations and crystal water can also be used as "pillars" to tune the interlayer structure of 2D materials. Xu et al. have investigated the role of crystal water on Zn^{2+} interaction into $V_2O_5{\cdot}nH_2O$ (Fig. 6g) [42]. The H_2O-solvated Zn^{2+} showed considerably decreased effective charge, reducing the electrostatic interactions with V_2O_5 framework. Thus, the Zn^{2+} diffusion kinetics has been effectively promoted. As a result, the fabricated $V_2O_5{\cdot}nH_2O$/graphene (VOG) based aqueous Zn ion battery delivered superior electrochemical properties. When the current density increases from 0.3 to 30 A/g, the specific capacity decreased from 372 to 248 mAh/g, indicating the outstanding rate performance (Fig. 6h). Mn^{2+} was preintercalated into the interlayer of V_2O_5 nanoribbons to enlarge the interlayer spacing, providing sufficient space and active sites for Zn^{2+} diffusion and accommodation [43]. Fe^{3+} preintercalated V_2O_5 xerogel was developed to inhibit interlayer changes during Na^+ insertion and deinsertion [44]. Note that, the electrochemical kinetics increased even though the Fe^{3+}-pillared V_2O_5 had a decreased interlayer spacing than the pristine material which can be attributed to the lower activation barriers of Fe-V_2O_5 for charge transfer.

Interlayer engineering has been proven a practical approach for tuning the interlayer structure and surface chemistries of the materials to achieve pseudocapacitive properties. However, during continuous electrochemical cycling, the structural water and preintercalated cations usually have problems with instability in the presence of chemical or electric potential gradients [2]. Controllable tuning of the interlayer structure of 2D materials with stable intercalant remains the focus of current research.

3.4 Heterostructure Engineering

Most of the extrinsic pseudocapacitive materials demonstrated unsatisfactory electrochemical properties due to the low electrical conductivity and large volume expansion during charging. Combining carbon materials like graphene, CNTs, carbon fibers, etc. can effectively enhance the conductivity, hence achieving optimized performance.

Sandwich-like SnS_2/Reduced graphene oxide/SnS_2 (SnS_2/rGO/SnS_2) was prepared through a simple hydrothermal process for high-rate Li^+/Na^+ storage [45]. SnS_2 nanosheets are covalently decorated on both sides of RGO sheets via C-S bonds. SnS_2 in the composite presented an expanded interlayer spacing of ~8.03 Å, which was benefit for the ion's insertion/extraction. High capacities of 844 and 765 mAh/

g for Li^+ and Na^+ ion batteries at a high rate of 10 A/g have been obtained, respectively, indicating excellent high-rate performance. Also, ultrathin SnS_2 nanosheets uniformly deposited on graphene enabled the pseudocapacitance dominant property of the composite, especially at large current density. To improve the gravimetric and areal capacities of transition metal dichalcogenides, Yousaf and co-workers developed a 3D trilayered CNT/$MoSe_2$/C heterostructure, in which $MoSe_2$ was sandwiched between an inner CNT core and an outer carbon layer (Fig. 7a,b) [46]. The CNT core with superior conductivity interconnected with each other to provide pathways for the electrons/Na^+ conduction. The outer carbon layer could protect $MoSe_2$ from direct exposure to the electrolyte. Moreover, the interlayer spaces of (002) plane of $MoSe_2$ were expanded during the annealing process, which facilitated the fast Na^+ diffusion. The obtained CNT/$MoSe_2$/C heterostructure was used as a freestanding electrode and exhibited a high capacity of 484 mAh/g at 100 mA/g. Due to the good conductivity of the heterostructure, CNT/$MoSe_2$/C provided a high areal capacity of 4.0 mAh/cm^2 (gravimetric capacity of 347 mAh/g) at 500 mA/g after 500 cycles even at a high mass loading of 13.9 mg/cm^2 (Fig. 7c). Yuan et al. constructed a freestanding anode for Na^+ storage with quantum-grade vanadium nitride (VN) nanodots anchored in 1D N/F co-doped carbon nanofiber cages (VNQDs@PCNFs-N/F) (Fig. 7d) [47]. The strong coupling between VNQDs and N/F co-doped 1D carbon cages effectively promoted ion/electron transport and facilitated the intercalation-conversion-deintercalation reaction of Na^+, ensuring fast electrochemical kinetics. After the first discharge/charge process, the curves almost overlapped, indicating the good reversibility of VNQDs@PCNFs-N/F (Fig. 7e). The cycling stability depicted in Fig. 7f shown that VNQDs@PCNFs-N/F electrode exhibited a higher reversible specific capacity (392.3 mAh/g) with good cycling stability than that of PCNFs (245.9 mAh/g) and VN@CNFs (234.3 mAh/g). Consequently, the hybrid capacitor assembled using VNQDs@PCNFs-N/F anode delivered a high energy density of 157.1 Wh/kg at 198.8 W/kg.

4 Conclusion and Perspectives

Pseudocapacitance bridges the fields of electrochemical capacitors and rechargeable batteries. During the past few decades, the studies in the field of pseudocapacitance included conceptual dispute, the emerging new pseudocapacitive materials, and tuning strategies for improving performance. In this chapter, we highlighted some recent works in developing pseudocapacitive materials for electrochemical energy storage systems. For intrinsic pseudocapacitive materials, we introduced the tuning strategies on MnO_2, TiO_2(B), and T-Nb_2O_5 for promoting the inherent pseudocapacitive responses. For extrinsic pseudocapacitive materials, design strategies such as nanostructuring, doping, oxygen vacancies, interlayer engineering, heterostructure engineering, etc., have been carefully discussed. Looking ahead, there are still substantial spaces for the development of new strategies aiming to further improve pseudocapacitance.

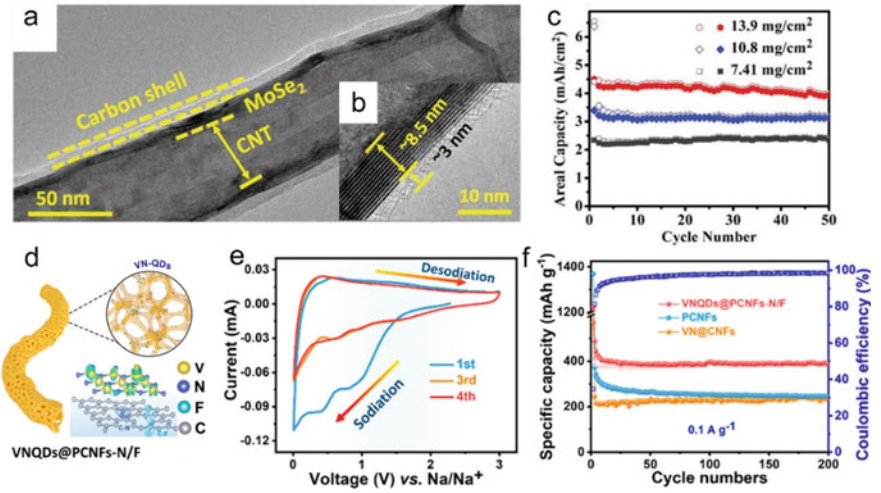

Fig. 7 **a** TEM and **b** HRTEM images of CNT/$MoSe_2$/C. **c** Areal capacity of CNT@$MoSe_2$/C with different mass loadings. Adapted with permission [46], Copyright (2019), Wiley–VCH GmbH. **d** Schematic illustration of VNQDs@PCNFs-N/F. **e** CV curves of VNQDs@PCNFs-N/F. **f** Cycling performance of the VNQDs@PCNFs-N/F, VN@CNFs, and PCNFs electrodes. Adapted with permission [47], Copyright (2022), American Chemical Society

1) Further investigation for energy storage mechanisms and new materials with structural moieties and compositions that enable intrinsic pseudocapacitance is still needed. Although extrinsic pseudocapacitance can be achieved through various modifications and nanosizing, this field is likely to continue to expand as researchers develop new methods for synthesizing nanomaterials. In addition, scalable, low-cost synthesis methods for nanosized extrinsic pseudocapacitive materials should be considered. For interlayer engineering to improve electrochemical performance, it is important to consider the stability of intercalants during continuous electrochemical cycling. Adjusting the interlayer structure should include stable intercalants that can withstand thousands of charging/discharging cycles at a high rate related to pseudocapacitive materials.

2) A deep understanding of charge storage principles of both intrinsic and extrinsic pseudocapacitance is still required which is of great significance for the exploitation of new electrode materials. The coupling of experimental and computational studies provides opportunities to qualitatively and quantitatively determine how the doping, vacancies, etc. affect the chemical, mechanical, and electronic properties of electrode materials.

3) The fundamental research of pseudocapacitive materials is generally performed on electrodes with relatively low mass loading to eliminate the mass transfer limitations. Integration of the lab-scale experience into commercial use still faces many challenges. Commercial use generally requires high mass loading of >10 mg/cm^2 to accommodate high-energy storage. With the increase in mass loading, electrochemical performances can rapidly decline, especially at a high rate. It is essential to

have a continuous electrical and ionic network across the entire electrode thickness. Construction of 3D conductive networks or scaffolds may be effective to address the low rate and cycling stability of the thick electrode materials, nevertheless, the accompanied issues arising from the decrease of packing density should be paid attention to.

References

1. C. Choi, D.S. Ashby, D.M. Butts, R.H. DeBlock, Q. Wei, J. Lau, B. Dunn, Achieving high energy density and high power density with pseudocapacitive materials. Nat. Rev. Mater. **5**, 5–19 (2020)
2. S. Fleischmann, J.B. Mitchell, R. Wang, C. Zhan, D. Jiang, V. Presser, V. Augustyn, Pseudocapacitance: From fundamental understanding to high power energy storage materials. Chem. Rev. **120**, 6738–6782 (2020)
3. B.E. Conway, E. Gileadi, Kinetic theory of pseudocapacitance and electrode reactions at appreciable surface coverage. Trans. Faraday Soc. **58**, 2493 (1962)
4. Z. Gan, J. Yin, X. Xu, Y. Cheng, T. Yu, Nanostructure and advanced energy storage: elaborate material designs lead to high-rate pseudocapacitive ion storage. ACS Nano **16**, 5131–5152 (2022)
5. M. Okubo, E. Hosono, J. Kim, M. Enomoto, N. Kojima, T. Kudo, H. Zhou, I. Honma, Nanosize effect on high-rate Li-ion intercalation in $LiCoO_2$ electrode. J. Am. Chem. Soc. **129**(23), 7444–7452 (2007)
6. J.-M. Jeong, S.H. Park, H.J. Park, S.B. Jin, S.G. Son, J.-M. Moon, H. Suh, B.G. Choi, Alternative-ultrathin assembling of exfoliated manganese dioxide and nitrogen-doped carbon layers for high-mass loading supercapacitors with outstanding capacitance and impressive rate capability. Adv. Funct. Mater. **31**, 2009632 (2021)
7. Z. Peng, S. Li, Y. Huang, J. Guo, L. Tan, Y. Chen, Sodium-intercalated manganese oxides for achieving ultra-stable and fast charge storage kinetics in wide-voltage aqueous supercapacitors. Adv. Funct. Mater. **32**, 2206539 (2022)
8. J. Wang, W. Guo, Z. Liu, Q. Zhang, Engineering of self-aggregation-resistant MnO_2 heterostructure with a built-in field for enhanced high-mass-loading energy storage. Adv. Energy Mater. **13**, 2300224 (2023)
9. M. Zukalova, M. Kalbac, L. Kavan, I. Exnar, M. Graetzel, Pseudocapacitive lithium storage in TiO_2(B). Chem. Mater. **17**, 1248–1255 (2005)
10. K. Lan, L. Liu, J.-Y. Zhang, R. Wang, L. Zu, Z. Lv, Q. Wei, D. Zhao, Precisely designed mesoscopic titania for high-volumetric-density pseudocapacitance. J. Am. Chem. Soc. **143**, 14097–14105 (2021)
11. H.-Y. Wang, H.-Y. Chen, Y.-Y. Hsu, U. Stimming, H.M. Chen, B. Liu, Modulation of crystal surface and lattice by doping: Achieving ultrafast metal-ion insertion in anatase TiO_2. ACS Appl. Mater. Interfaces **8**, 29186–29193 (2016)
12. Z. Le, F. Liu, P. Nie, X. Li, X. Liu, Z. Bian, G. Chen, H.B. Wu, Y. Lu, Pseudocapacitive sodium storage in mesoporous single-crystal-like TiO_2-graphene nanocomposite enables high-performance sodium-ion capacitors. ACS Nano **11**, 2952–2960 (2017)
13. B. Reichman, A.J. Bard, The application of Nb_2O_5 as a cathode in nonaqueous lithium cells. J. Electrochem. Soc. **128**, 344–346 (1981)
14. R. Kodama, Y. Terada, I. Nakai, S. Komaba, N. Kumagai, Electrochemical and in situ XAFS-XRD investigation of Nb_2O_5 for rechargeable lithium batteries. J. Electrochem. Soc. **153**, A583–A588 (2006)
15. K. Brezesinski, J. Wang, J. Haetge, C. Reitz, S.O. Steinmueller, S.H. Tolbert, B.M. Smarsly, B. Dunn, T. Brezesinski, Pseudocapacitive contributions to charge storage in highly ordered

mesoporous group V transition metal oxides with iso-oriented layered nanocrystalline domains. J. Am. Chem. Soc. **132**, 6982–6990 (2010)
16. W. Bergh, H.N. Lokupitiya, N.A. Vest, B. Reid, S. Guldin, M. Stefk, Nanostructure dependence of T-Nb_2O_5 intercalation pseudocapacitance probed using tunable isomorphic architectures. Adv. Funct. Mater. **31**, 2007826 (2021)
17. S. Fu, Q. Yu, Z. Liu, P. Hu, Q. Chen, S. Feng, L. Mai, L. Zhou, Yolk-shell Nb_2O_5 microspheres as intercalation pseudocapacitive anode materials for high-energy Li-ion capacitors. J. Mater. Chem. A **7**, 11234–11240 (2019)
18. J. Liao, R. Tan, Z. Kuang, C. Cui, Z. Wei, X. Deng, Z. Yan, Y. Feng, F. Li, C. Wang, J. Ma, Controlling the morphology, size and phase of Nb_2O_5 crystals for high electrochemical performance. Chin. Chem. Lett. **29**, 1785–1790 (2018)
19. M.Y. Song, N.R. Kim, H.J. Yoon, S.Y. Cho, H.-J. Jin, Y.S. Yun, Long-lasting Nb_2O_5-based nanocomposite materials for Li-ion storage. ACS Appl. Mater. Interfaces **9**, 2267–2274 (2017)
20. X. Meng, Z. Guan, J. Zhao, Z. Cai, S. Li, L. Bian, Y. Song, D. Guo, X. Liu, Lithium-pre-intercalated T-Nb_2O_5/graphene composite promoting pseudocapacitive performance for ultralong lifespan capacitors. Chem. Eng. J. **438**, 135492 (2022)
21. H.-S. Kim, J.B. Cook, S.H. Tolbert, B. Dunn, The development of pseudocapacitive properties in nanosized-MoO_2. J. Electrochem. Soc. **162**, A5083–A5090 (2015)
22. J.B. Cook, H.-S. Kim, T.C. Lin, C.-H. Lai, B. Dunn, S.H. Tolbert, Pseudocapacitive charge storage in thick composite MoS_2 nanocrystal-based electrodes. Adv. Energy Mater. **7**, 1601283 (2017)
23. C. Xia, Z. Lin, Y. Zhou, C. Zhao, H. Liang, P. Rozier, Z. Wang, H.N. Alshareef, Large intercalation pseudocapacitance in 2D VO_2(B): Breaking through the kinetic barrier. Adv. Mater. **30**, 1803594 (2018)
24. Y. Gao, P. Hai, L. Liu, J. Yin, Z. Gan, W. Ai, C. Wu, Y. Cheng, X. Xu, Balanced crystallinity and nanostructure for SnS_2 nanosheets through optimized calcination temperature toward enhanced pseudocapacitive Na^+ storage. ACS Nano **16**, 14745–14753 (2022)
25. J. Dong, Y. He, Y. Jiang, S. Tan, Q. Wei, F. Xiong, Z. Chu, Q. An, L. Mai, Intercalation pseudocapacitance of $FeVO_4 \cdot nH_2O$ nanowires anode for high-energy and high-power sodium-ion capacitor. Nano Energy **73**, 104838 (2020)
26. H.-S. Kim, J.B. Cook, H. Lin, J.S. Ko, S.H. Tolbert, V. Ozolins, B. Dunn, Oxygen vacancies enhance pseudocapacitive charge storage properties of MoO_{3-x}. Nat. Mater. **16**, 454–460 (2017)
27. S.S. Mofarah, E. Adabifiroozjaei, Y. Yao, P. Koshy, S. Lim, R. Webster, X. Liu, R.K. Nekouei, C. Cazorla, Z. Liu, Y. Wang, N. Lambropoulos, C.C. Sorrell, Proton-assisted creation of controllable volumetric oxygen vacancies in ultrathin CeO_{2-x} for pseudocapacitive energy storage applications. Nat. Commun. **10**, 2594 (2019)
28. B. Liu, H. Zhang, C. Yuan, Q. Geng, Y. Li, J. Hu, Z. Lu, J. Xie, A. Hao, Y. Cao, Construction of oxygen vacancies and heterostructure in VO_{2-x}/NC with enhanced reversible capacity, accelerated redox kinetics, and stable cycling life for sodium ion storage. J. Colloid. Interf. Sci. **646**, 34–43 (2023)
29. W. Du, Y. Zheng, X. Liu, J. Cheng, R.C.K. Reddy, A. Zeb, X. Lin, Y. Luo, Oxygen-enriched vacancy spinel MFe_2O_4/carbon (M = Ni, Mn, Co) derived from metal-organic frameworks toward boosting lithium storage. Chem. Eng. J. **451**, 138626 (2023)
30. N. Liu, X. Wu, L. Fan, S. Gong, Z. Guo, A. Chen, C. Zhao, Y. Mao, N. Zhang, K. Sun, Intercalation pseudocapacitive Zn^{2+} storage with hydrated vanadium dioxide toward ultrahigh rate performance. Adv. Mater. **32**, 1908420 (2020)
31. K. Zhu, S. Wei, H. Shou, F. Shen, S. Chen, P. Zhang, C. Wang, Y. Cao, X. Guo, M. Luo, H. Zhang, B. Ye, X. Wu, L. He, L. Song, Defect engineering on V_2O_3 cathode for long-cycling aqueous zinc metal batteries. Nat. Commun. **12**, 6878 (2021)
32. X. Xu, Y. Qian, C. Wang, Z. Bai, C. Wang, M. Song, Y. Du, X. Xu, N. Wang, J. Yang, Y. Qian, S. Dou, Enhanced charge transfer and reaction kinetics of vanadium pentoxide for zinc storage via nitrogen interstitial doping. Chem. Eng. J. **451**, 138770 (2023)
33. N. Wang, X. Xu, T. Liao, Y. Du, Z. Bai, S. Dou, Boosting sodium storage of double-shell sodium titanate microspheres constructed from 2D ultrathin nanosheets via sulfur doping. Adv. Mater. **30**, 1804157 (2018)

34. S. Chandel, C. Wang, S.P. Singh, N. Wang, A.K. Rai, Significant enhancement in the electrochemical performances of a nanostructured sodium titanate anode by molybdenum doping for applications as sodium-ion batteries. ACS Appl. Nano Mater. **5**, 18591–18602 (2022)
35. X. Wang, K. Liu, J. Li, Y. Liu, M. Wang, H. Cui, Creation of an extrinsic pseudocapacitive material presenting extraordinary cycling-life with the battery-type material $Co(OH)_2$ by S^{2-} doping for application in supercapacitors. Chem. Eng. J. **451**, 138969 (2023)
36. C. Zhao, C. Yu, M. Zhang, Q. Sun, S. Li, M.N. Banis, X. Han, Q. Dong, J. Yang, G. Wang, X. Sun, J. Qiu, Enhanced sodium storage capability enabled by super wide-interlayer-spacing MoS_2 integrated on carbon fibers. Nano Energy **41**, 66–74 (2017)
37. J. Lai, H. Zhu, X. Zhu, H. Koritala, Y. Wang, Interlayer-expanded $V_6O_{13}{\cdot}nH_2O$ architecture constructed for an advanced rechargeable aqueous zinc-ion battery. ACS Appl. Energy Mater. **2**, 1988–1996 (2019)
38. Y. Li, Y. Liang, F.C.R. Hernandez, H.D. Yoo, Q. An, Y. Yao, Enhancing sodium-ion battery performance with interlayer-expanded MoS_2-PEO nanocomposites. Nano Energy **15**, 453–461 (2015)
39. J. Chao, L. Yang, H. Zhang, J. Liu, R. Hu, M. Zhu, Engineering layer structure of MoS_2/polyaniline/graphene nanocomposites to achieve fast and reversible lithium storage for high energy density aqueous lithium-ion capacitors. J. Power. Sources **450**, 227680 (2020)
40. S. Liu, H. Zhu, B. Zhang, G. Li, H. Zhu, Y. Ren, H. Geng, Y. Yang, Q. Liu, C.C. Li, Tuning the kinetics of zinc-ion insertion/extraction in V_2O_5 by in situ polyaniline intercalation enables improved aqueous zinc-ion storage performance. Adv. Mater. **32**, 2001113 (2020)
41. Y. Xiao, X. Zhao, X. Wang, D. Su, S. Bai, W. Chen, S. Fang, L. Zhou, H.-M. Cheng, F. Li, A nanosheet array of Cu_2Se intercalation compound with expanded interlayer space for sodium ion storage. Adv. Energy Mater. **10**, 2000666 (2020)
42. M. Yan, P. He, Y. Chen, S. Wang, Q. Wei, K. Zhao, X. Xu, Q. An, Y. Shuang, Y. Shao, K.T. Mueller, L. Mai, J. Liu, J. Yan, Water-lubricated intercalation in $V_2O_5{\cdot}nH_2O$ for high-capacity and high-rate aqueous rechargeable zinc batteries. Adv. Mater. **29**, 1703725 (2017)
43. Y. Jiang, H. Xu, L. Ren, M. Ji, X. Shen, S. Li, $Mn_{0.26}V_2O_5{\cdot}nH_2O$ nanoribbons with fast ion diffusion channels and high electrical conductivity for intercalation pseudocapacitive Zn^{2+} storage, Energy Fuels **35**, 17948–17955 (2021)
44. Q. Wei, Z. Jiang, S. Tan, Q. Li, L. Huang, M. Yan, L. Zhou, Q. An, L. Mai, Lattice breathing inhibited layered vanadium oxide ultrathin nanobelts for enhanced sodium storage. ACS Appl. Mater. Interfaces **7**, 18211–18217 (2015)
45. Y. Jiang, D. Song, J. Wu, Z. Wang, S. Huang, Y. Xu, Z. Chen, B. Zhao, J. Zhang, Sandwich-like SnS_2/Graphene/SnS_2 with expanded interlayer distance as high-rate lithium/sodium-ion battery anode materials. ACS Nano **13**, 9100–9111 (2019)
46. M. Yousaf, Y. Wang, Y. Chen, Z. Wang, A. Firdous, Z. Ali, N. Mahmood, R. Zou, S. Guo, R.P. Han, A 3D trilayered CNT/$MoSe_2$/C heterostructure with an Eexpanded $MoSe_2$ interlayer spacing for an efficient sodium storage. Adv. Energy Mater. **9**, 1900567 (2019)
47. J. Yuan, M. Qiu, X. Hu, Y. Liu, G. Zhong, H. Zhan, Z. Wen, Pseudocapacitive vanadium nitride quantum dots modifed one-dimensional carbon cages enable highly kinetics-compatible sodium ion capacitors. ACS Nano **16**, 14807–14818 (2022)

Pseudocapacitive Materials for Electrolytes

Lucia Díaz-Patiño, Lorena Álvarez Contreras, Minerva Guerra-Balcázar, and Noé Arjona

Abstract The electrolyte plays a vital role in the performance and durability of electrochemical energy devices like supercapacitors, fuel cells, and batteries. The electrolyte is usually employed as an aqueous solution but is also found in non-aqueous forms like organic solvents, including protic and aprotic ionic liquids. It is used as a gel or solid polymer electrolyte (GPE/SPE) for flexible applications. The use of pseudocapacitive materials in electrolytes serves different purposes, including mechanical stability and ionic conductivity, to improve the electrode/electrolyte interface and water retention, among others. This chapter discusses the most outstanding achievements in this field, given the prospective improvement of electrochemical energy systems.

Keywords Pseudocapacitive materials · Electrolyte · Metal oxides · Gel polymer electrolyte · Graphene · Carbon nanotubes

1 Introduction to Pseudocapacitive Materials for Electrolytes

Solid-state electrochemical energy storage devices, such as supercapacitors and lithium-ion batteries, have acquired significant attention as the next-generation technology for addressing the limitations of conventional liquid-based devices, specifically low energy density, and safety concerns. However, despite their potential,

L. Díaz-Patiño · N. Arjona (✉)
Centro de Investigación y Desarrollo Tecnológico en Electroquímica S.C., Pedro Escobedo, Querétaro C.P. 76703, México
e-mail: wvelazquez@cideteq.mx

L. Á. Contreras
Centro de Investigación en Materiales Avanzados S.C., Complejo Industrial Chihuahua, Chihuahua C.P. 31136, México

M. Guerra-Balcázar
División de Investigación y Posgrado, Facultad de Ingeniería, Universidad Autónoma de Querétaro, Santiago de Querétaro, Querétaro C.P. 76010, México

© The Author(s), under exclusive license to Springer Nature Switzerland AG 2024

R. K. Gupta (ed.), *Pseudocapacitors*, Engineering Materials,
https://doi.org/10.1007/978-3-031-45430-1_6

electrochemical energy systems face limitations primarily associated with their electrode materials and electrolytes [1]. Over the past decade, remarkable advancements have been made in the understanding and design of advanced nanostructured materials, leading to notable improvements in electrochemical energy storage/conversion performance. The electrolyte is a crucial component in electrochemical energy systems, comprising solvents, electrolytes, and additives. The electrolyte serves as the essential ionic conductor connecting the two electrodes in electrochemical energy systems, enabling the flow of ionic current and influencing the electrochemical characteristics determining the voltage window, rate capability, cycling stability, determining performance, particularly in terms of capacitance (Cs) and energy density (E). The electrolyte facilitates the conduction of ions, acts as an ion source to supplement ions, and binds electrode particles together. To ensure proper charging and prevent depletion issues, it is key to maintain a high concentration of electrolytes, particularly organic electrolytes, to avoid the "electrolyte starvation effect" [2], ensuring proper charging and mitigating depletion problems.

The ionic conductivity, electrochemical window, working temperature range, stability, and safety are the fundamental properties that define the performance of the electrolyte. Additionally, for flexible energy systems, mechanical stability plays an important role. Thus, the rational modification of the electrolyte is fundamental to achieving higher performance and durability in electrochemical energy systems. Pseudocapacitive materials include carbon-based materials, conductive polymers, and metal-based materials like metal oxides, hydroxides, sulfides, and nitrides. In this regard, pseudocapacitive materials have been widely used as electrodes for applications like supercapacitors and batteries. However, they can also be used as dopants or modifiers in electrolytes to improve the before mentioned properties. In this chapter, the most outstanding electrolyte modifications for electrochemical energy systems are revised and discussed as a function of the pseudocapacitive material.

2 Types of Electrolytes for Energy Applications

It is worth noticing that different electrolytes are employed in electrochemical energy systems. They present exceptional characteristics for specific applications. However, these electrolytes must display high ionic conductivity for electrochemical energy applications to minimize internal resistance and enhance overall performance. Moreover, the electrolyte must demonstrate exceptional chemical and electrochemical stability to ensure long-term reliability. Furthermore, environmental friendliness is a significant consideration, prompting efforts to develop sustainable and non-toxic electrolyte options. Thus, various working electrolytes have been used, including water-based electrolytes, organic electrolytes, solid electrolytes, and ceramic electrolytes [3, 4]. Each class offers distinct advantages and features summarized in Fig. 1.

Nevertheless, electrolyte classification extends beyond a single category. In some instances, it is delineated based on the primary matrix of the electrolyte, resulting in

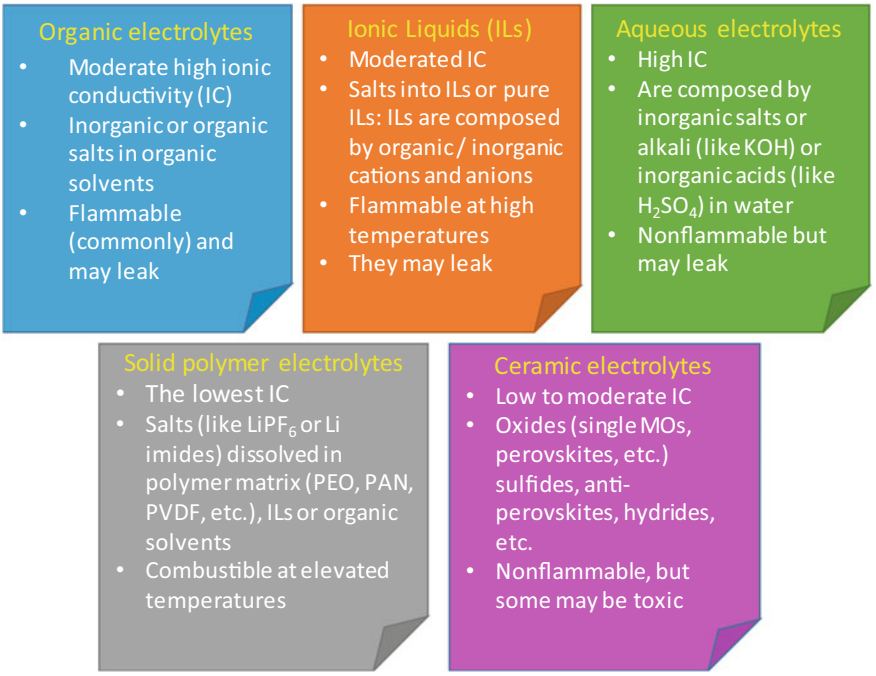

Fig. 1 Classification of electrolyte families, advantages, and limitations

the following types: (a) polymer-based solid-state electrolytes (including polymeric composite electrolytes and polymer gel electrolytes), (b) ceramic-based solid-state electrolytes (comprising oxide-based electrolytes and sulfide-based electrolytes), and (c) hybrid and composite electrolytes. In the following sub-sections, certain advantages and applications of electrolytes are provided for electrochemical energy systems.

2.1 Aqueous Electrolytes

In recent years, there has been significant interest in aqueous gel electrolytes owing to their notable features, including high ionic conductivity, low toxicity, easy processability, and cost-effectiveness. These electrolytes utilize water as the plasticizer. Within aqueous gel electrolytes, the electrolytic salts consist of strong acids such as H_2SO_4, HCl, H_3PO_4, strong bases like KOH, or neutral salts like Na_2SO_4 and LiCl. These salt compositions contribute to the conductivity and overall performance of the aqueous gel electrolytes. Utilizing aqueous gel electrolytes provides a promising avenue for developing safe, environmentally friendly, and economically viable energy storage systems [5]. However, aqueous electrolytes have a limited

working potential window, typically up to 1.23 V, due to the decomposition of water and the associated hydrogen and oxygen evolution reactions.

Consequently, they have yet to be widely used in conventional supercapacitors. However, aqueous electrolytes offer advantages such as high conductivity, low cost, easy preparation, and non-flammability. Neutral aqueous electrolytes have the added benefits of being environmentally friendly and easier to handle than acidic or basic electrolytes. The high conductivity of the electrolyte is crucial for improving the performance of supercapacitors, as it promotes better interaction between the electrolyte ions and the electrode materials, leading to enhanced power density and capacitance.

2.2 Non-aqueous Electrolytes (Organic, Ceramic, and Ionic Liquid-Based)

The conducting electrolytic salts and plasticizers also play crucial roles in solid-state electrolyte performance. These electrolytic salts and plasticizers can be categorized into three types: aqueous, organic, and ionic liquid electrolytes [4]. Despite the decent performance of supercapacitors (SCs) with aqueous electrolytes, they are limited by a small voltage window. Organic electrolytes have emerged as promising candidates to overcome this limitation and achieve high energy density in flexible SCs. Organic gel electrolytes typically consist of high molecular weight polymer matrices and organic conducting salts dissolved in aprotic solvents. In organic electrolytes, organic ammonium salts such as tetraethylammonium tetrafluoroborate ($TEABF_4$) [6], tetrabutylammonium hexafluorophosphate ($TBAPF_6$), and bis(trifluoromethyl sulfonyl) amine (TFSI-) played common roles as conducting salts [7]. To further enhance device performance, decamethylferrocenium (DmFc) was added to tetrabutylammonium perchlorate (TBAP)-tetrahydrofuran (THF) electrolytes. The redox reaction of DmFc provided additional pseudocapacitance, resulting in increased voltage windows, energy densities, and specific capacitances compared to SCs without DmFc. Mixed solvents have also been utilized to expand voltage windows. For example, a sodium bis(trifluoromethane sulfonyl)imide (NaTFSI):propylene carbonate (PC):ethylene carbonate (EC):dimethyl carbonate (DMC) system showed higher ionic conductivity compared to single-solvent gel electrolytes. Organic gel electrolytes enhance voltage windows and energy densities and offer broader working temperature ranges. Additionally, mixed solvent systems improve impedance performance and mitigate the flammability and toxicity of particular solvents. These advancements in organic electrolytes contribute to developing high-performance and versatile supercapacitor technologies [4].

Solvent-free ionic liquids (ILs) are considered promising solid-state innovative green electrolytes for high-performance supercapacitors (SCs) due to their ability to achieve large potential windows (up to 6.0 V). ILs are organic salts composed

of large cations and delocalized anions with low melting points, low vapor pressure, and negigible inflammability. The electrochemical performance of IL-based electrolytes depends on the chemical structures of the counter ions. Three fundamental parameters should be considered when selecting IL molecules for SCs: ionic conductivity, working voltage window, and melting point. Various cationic ILs have been developed, such as quaternary ammonium, sulfonium, imidazolium, pyrrolidinium, and piperidinium [8]. Common anionic ILs include tetrafluoroborate (BF_4^-), hexafluorophosphate (PF_6^-), bis(trifluoromethane sulfonyl)imide ($TFSI^-$), bis(fluoro sulfonyl)imide (FSI^-), and dicyanamide (DCA^-) as is shown in Fig. 2.

Compared to organic electrolytes, IL-based electrolytes can extend the voltage windows of SCs to 3.5–6 V, typically around 4 V, while maintaining high ionic conductivity in the range of 10^{-3} to 10 S/cm. This enables the development of SCs with improved performance and energy storage capabilities [4].

The ceramic-based solid-state electrolytes comprise the oxide-based and sulfide-based electrolytes widely used due to their high ionic conductivity and stability at high temperatures; some examples are oxides (garnets, NASICON/LISICON, perovskites, etc.), sulfides, LiPON, anti- perovskites, hydrides, etc. NASICON (Sodium Super Ion Conductor) is a family of ceramic materials with the general formula $Na_3Zr_2Si_2PO_{12}$. It exhibits high sodium ion conductivity, and potential applications in solid-state supercapacitors have been reported [9]. The hybrid and composite electrolytes combine organic and inorganic components, such as polyethylene oxide (PEO), with ceramic fillers like $Li_{1.3}Al_{0.3}Ti_{1.7}(PO_4)_3$, showing improved ionic conductivity and

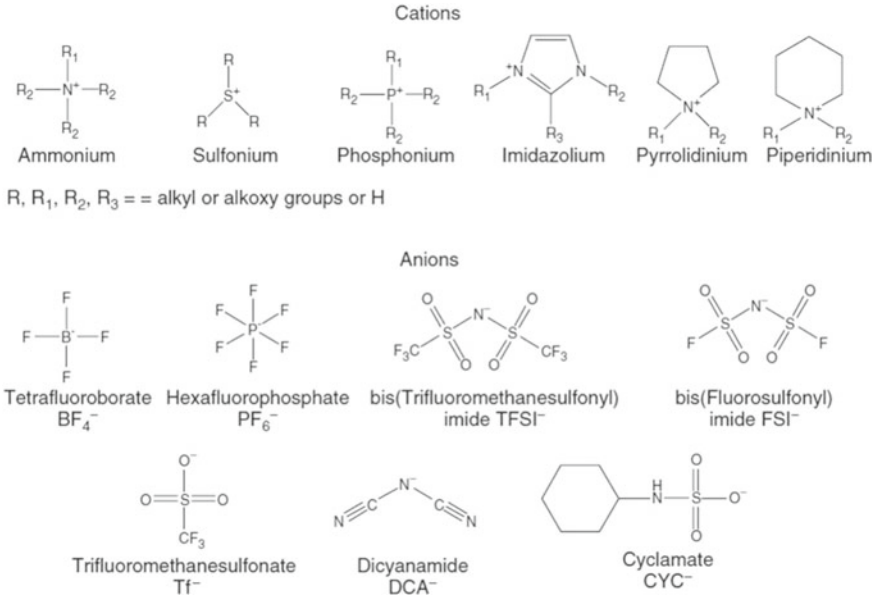

Fig. 2 The structures of typical ionic liquids. Adapted with permission [8], Copyright (2015) Springer

stability. These electrolytes are being extensively researched for their compatibility with different electrode materials [4]. Furthermore, hybrid and composite electrolytes that combine other materials are being explored, aiming to achieve a balance of desirable properties in solid-state electrolyte systems.

Overall, choosing electrolyte type in supercapacitors is crucial for optimizing performance parameters. Polymer-based solid-state electrolytes, such as polymeric composite and gel electrolytes, along with ceramic-based electrolytes like oxide-based and sulfide-based electrolytes, offer promising avenues for enhancing the efficiency and stability of supercapacitors.

2.3 Gel Polymer Electrolytes (GPEs)

In addition to single-component polymer-based electrolytes, there has been a growing focus on developing multicomponent polymer gel-based solid-state electrolytes to enhance electrochemical and mechanical performance. An example of such advancement is the creation of a multicomponent PVA-KOH gel electrolyte by grafting graphene oxide and amino groups onto the PVA backbone [10]. The grafted PVA-KOH gel electrolyte exhibits a significantly higher ionic conductivity of 108.7 mS/cm compared to the pure PVA-KOH gel electrolytes with 30.5 mS/cm conductivity. Notable improvements in mechanical properties accompany this enhancement in electrochemical performance. Furthermore, researchers have explored the synthesis of a multifunctional hydrogel polyelectrolyte through copolymerization of 2-acrylamido-2-methylpropane sulfonic acid (AMPS) and N,N-dimethylacrylamide (DMAAm). The resulting poly(AMPS-co-DMAAm)/laponite/GO hydrogel electrolytes demonstrate remarkable mechanical stretchability, stretching up to 1000% [4].

Additionally, these electrolytes exhibit excellent self-healing behavior under various conditions. Developing these multicomponent polymer gel-based solid-state electrolytes opens new possibilities for advanced energy storage systems. These electrolytes offer potential applications in flexible and durable energy storage devices by combining enhanced electrochemical performance and impressive mechanical properties. The polymeric composite electrolytes consist of a polymer matrix blended with inorganic fillers or salts. The presence of inorganic components enhances the ionic conductivity of the polymer matrix. One commonly used polymeric composite electrolyte is PEO combined with lithium salts, such as lithium perchlorate ($LiClO_4$) or lithium bis(trifluoromethane sulfonyl)imide (LiTFSI). Incorporating lithium salts enhances the ionic conductivity of the PEO matrix, making it suitable for various energy storage applications. The polymer gel electrolytes as polyacrylamide (PAA) gel electrolytes with liquid electrolytes like lithium salts dissolved in propylene carbonate (PC) are extensively studied. The gel structure provides mechanical stability, while the liquid electrolyte component enables high ionic conductivity, making them promising for flexible and solid-state energy storage devices.

2.4 Solid Polymer Electrolytes (SPEs)

Polymer-based solid-state electrolytes are composed of three primary constituents: polymer matrices, electrolytic salts, and plasticizers. These constituents synergistically prevent the leakage of liquid electrolytes. Commonly employed polymer matrices include polyvinyl alcohol (PVA), polyethylene oxide (PEO), polyacrylamide (PAM), poly-methyl methacrylate (PMMA), polyamine ester (PAE), and polyvinylidene fluoride (PVDF) [4]. Additionally, naturally occurring polymeric materials such as cellulose [11], chitin, and chitosan [12] have garnered significant attention as promising components in gel electrolytes due to their cost-effectiveness and wide availability. These materials hold immense potential for gel electrolyte applications, offering an affordable and easily accessible alternative. Their extensive use is observed in flexible devices. The incorporation of multicomponent polymeric hosts enhances the flexibility and stretchability of solid-state electrolytes, rendering them suitable for wearable and portable device applications.

3 Metal-Free Pseudocapacitive Materials for Electrolytes

3.1 Carbon-Derived Pseudocapacitive Materials

Carbonaceous materials are most used as electrode materials for energy storage and conversion devices, such as supercapacitors and batteries, due to their large surface area, high electrical conductivity, and excellent chemical stability. These materials are mainly characterized by the significant impact on their capacitance since this can be modulated through the pore size, pores' shape, and electrical conductivity [13]. On the other hand, electrolytes (aqueous, non-aqueous, SPEs, GPEs) are essential to developing electrochemical energy storage devices based on carbonaceous materials [14]. It should be noted that the interaction of the electrolytes with the electrodes directly affects the electrode–electrolyte interface and the structure of the active materials used to carry out the electrochemical processes; hence, the choice of electrolytes is a fundamental factor. To obtain safe and high-performance energy devices. To achieve this, it is necessary to investigate and understand the reaction mechanisms that take place at the carbonaceous materials-electrolyte interface, as well as the ionic conductivity, ionic solvation, and dielectric constant of the medium that can be used to know the capacity of the device, that is. That is, the amount of charge stored, as well as the operating voltage range, charge, and storage time. Likewise, it is necessary to consider different parameters when proposing an electrolyte to be used in the presence of carbon-based materials, such as the conductivity of the medium, the effects of the selected salt, the solvent, electrochemical and thermal stability, capacitance, specific capacitance, energy density, and power density [15]. For 2D materials, the advantages of porosity have been established before [16] and are summarized in Fig. 3.

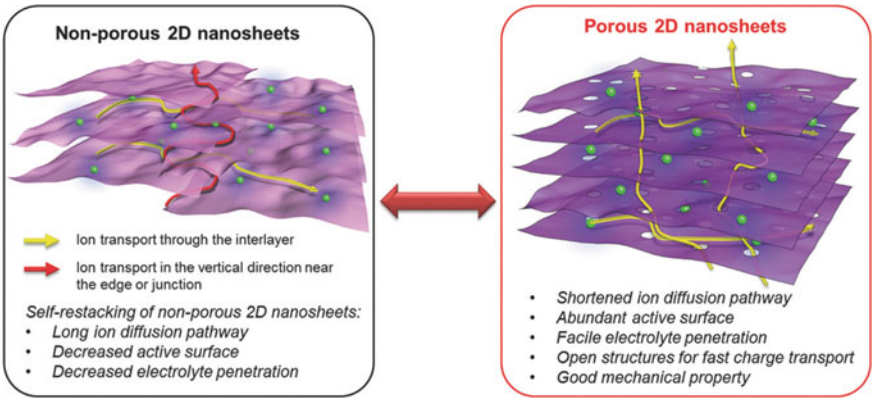

Fig. 3 Advantages of using porous carbonaceous materials in energy storage and conversion devices. Adapted with permission [16], Copyright (2017), Wiley

3.1.1 Carbon Nanotubes

Carbon nanotubes (CNTs) are a resistant material with high thermal conductivity and a large surface area, low resistance, low density, and good chemical stability. These intrinsic properties make this material a promising option for its application in energy storage and conversion devices.

Aqueous

The structure of carbon nanotubes can be assimilated to a porous structure; however, this carbon-based material especially possesses one-dimensional nano-spaces. When this material encounters an aqueous solution, the electrolyte is confined in these nano-spaces, and they tend to behave differently from other variants of carbonaceous materials. That is, the water acts as a mediator to drive the ions into the hydrophobic carbon nanotube, so the energy barrier for the penetration of the ions is eliminated. Likewise, this barrier is directly related to the solvation energies of the ions, as well as their hydration shell size within the carbon nanotubes by confinement, and they may become dehydrated [17].

Non-aqueous

For applications other than room temperature, aqueous electrolytes are no longer a possibility; this is since the solvated ions that are trapped in the nanoporous surface of the CNTs and can be affected by the cooling and heating behavior, which is of interest for the development of energy devices that operate at low temperatures. One of the most widely used non-aqueous electrolytes are ionic liquids and organic additives

with low melting point; these have shown excellent electrochemical results when operating at temperatures below −70 °C. However, it should not be forgotten that the material's porous structure is paramount in determining the device's performance [18].

3.1.2 Graphene

Graphene is composed of carbon atoms counted by sp2 hybridization, where it is tightly packed in the form of a single-layer, two-dimensional honeycomb structure. This material is one of the most used for its application in energy storage and conversion devices due to its large specific surface area and its high conductivity [13].

Aqueous

The electronic properties of graphene, such as the concentration of charge carriers, mobility, resistance, and work function, are susceptible to adsorbed molecules and environmental variations. Water-graphene interactions are highly dependent on their hydrophilicity. As the number of graphene layers increases, this material becomes more hydrophobic.

This, together with the concentration of charge carriers and the work function, influences its wetting properties and, in turn, water adsorption. Therefore, graphene is considered an excellent candidate for energy applications where it is required to have capillaries with nanometric dimensions for ionic transport [19].

Non-aqueous

Organic solvents usually have a larger solvated ion size compared to the use of aqueous electrolytes, so it is sought that the electrodes are porous materials such as graphene; likewise, the capacitance is directly affected by the porosity of the electrode, these solvents usually have good electrical performance, but they are not safe, and they are expensive [20].

SPE and GPE

It is common for energy storage and conversion devices to use liquid electrolytes, where they are encapsulated, which leads to obtaining a large volume and significant weight. Likewise, it is difficult to achieve the flexibility of the devices, for which there is already a lot of research for the replacement of liquid electrolytes by solid polymer electrolytes. It is necessary to involve flexible electrode materials, which must have excellent mechanical resistance due to stretching and bending conditions.

In addition, they must possess the characteristics offered by carbonaceous materials, such as large surface area and high electrical conductivity. On the other hand, devices that use CNTs and GPEs have excellent specific capacitance compared to devices that use aqueous H_2SO_4, and it is considered that the implementation of a GPE with a CNTs is more suitable for ionic transport of species by the size of the electrodes and their highly porous structure. Likewise, CNT can serve as an excellent template for other composite materials, such as PANI/N-CNT@CNT fiber [21]. In the case of graphene, which is a single or multilayer material, although it has beneficial characteristics for use in conjunction with SPEs and GPEs, it is not as suitable for flexible devices because electrolyte ions cannot access the stacked regions of the material, i.e., the electroactive sites of the material are not fully utilized. Its high cost and low performance compared to other electrolytes also represent a problem for its large-scale manufacturing [22].

3.2 Conductive Polymers Pseudocapacitive Materials

Conducting polymers are macromolecules with a conjugated structure, alternating the arrangement of C–C and C=C chains; In addition, these macromolecules are joined by Van der Waals forces, electrostatics, dipolar interactions, etc. [23] Electronic transport in this type of materials is usually affected by the transition between the same polymeric chains, this is because its high activation barriers. Likewise, it can be modulated by changing the doping level and the material's crystallinity.

Some of the most used polymeric materials are polyaniline (PANI) and polypyrrole (PPy); these are very interesting conducting polymers since they have a large capacitance for their application in various energy storage and conversion devices; however, they have low cyclic stability; this is caused by swelling of the material during operation. Despite this, it is possible to combine these conductive polymers and carbonaceous materials through different synthesis methods, as can be seen in Fig. 4, which are applied to overcome the limitations during stability. PANI has specific characteristics, such as its electrical and electrochemical activity, simple synthesis, and low cost, which makes it a good candidate for use as electrode material for energy storage and conversion devices. The capacitance of this material depends on the oxidation states of PANI, where it has been previously reported that the emeraldine semi-oxidized state of PANI has the highest conductivity and stability. Another important conductive polymeric material to consider is PPy, which is easy to synthesize, has large capacitance and high cyclic stability, etc., [24].

It has also been reported that PPy has balanced electrochemical properties for energy storage and conversion systems [25]. A disadvantage to consider of this material is its rigidity and, therefore, its poor mechanical ductility; another drawback is reduced to its low properties electrical in its amorphous phase, for which its structure, particle size, and morphology must be modulated continuously, so it is common to synthesize PPy composites that play a synergistic role, for example with carbonaceous materials [26].

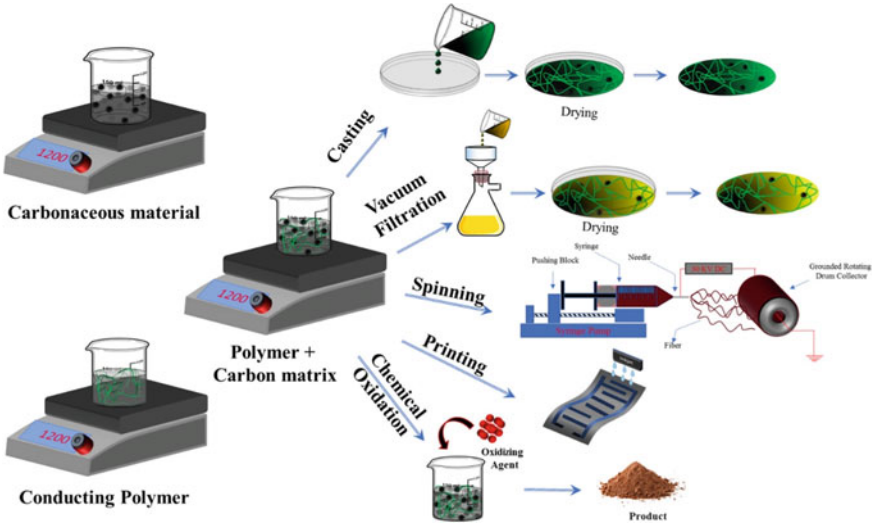

Fig. 4 Different methods of synthesis of composites based on polymer and carbon materials. Adapted with permission [24], Copyright (2022), Elsevier

4 Metal-Derived Pseudocapacitive Materials for Electrolytes

4.1 Metal Oxides (MOs) and Mixtures of Transition Metal Oxides (MTMOs)

Nanoparticulated single metal oxides have been used as nano-fillers for gel and solid polymer electrolytes. Al_2O_3 is one of the most used metal oxides for lithium batteries. This pseudocapacitive material has been used as a solid plasticizer during the polymer preparation, and it promotes the increase of the ionic conductivity of a series of polymers like poly(ethylene glycol), poly(vinylidene fluoride-co-hexafluoropropylene)[PVDF-HFP], polyvinyl alcohol, polyethylene oxide, among others [27–29]. It is worth noticing that the properties of the SPE have been modulated, changing the polymer and the filler mass loading, but also structural properties like size and shape are important to shift because these have a direct impact on the resulting SPE properties. Other metal oxides utilized as nano-fillers are TiO_2, MgO, and ZnO. Among them, ZnO has greatly influenced the ionic conductivity of PVDF-HFP polymers [30].

Mixtures of metal oxides/hydroxides can be divided mainly into those with a spinel crystalline structure, a perovskite crystalline structure, and layered double hydroxides (LDHs). The spinel structure (AB_2O_4) is composed of a *3d* metal with a 2+ valence (A), a second 3d metal with a 3+ valence (B_2), and oxygen (O_4). The perovskite structure has the formula ABX_3; A and B are cations, where often

A is a larger cation than B, being usually from group IIA, while B is typically a transition metal cation like Ti, while X is an anion (usually O). The LDHs are often the precursor to obtain spinel structures; the LDH is composed of two metallic cations like in the spinel structure, one with a 2+ valence and the other with a 3+ state. The anion and water molecules are found as interlayers, as observed in Fig. 5. The advantage of these structures are that multiple metallic cations can be found in the same crystalline structure, achieving a synergetic effect and, as a result, improving their functionality in applications like energy storage. For electrolytes, the $BaTiO_3$ perovskite as a nanocomposite in polymer electrolyte has been proposed for lithium batteries, achieving higher ionic conductivity in contrast with an unmodified membrane [31]. This perovskite was also used with PVDF and cellulose nanocrystals, enhancing the mechanical characteristics of stress (at 5% strain) and Young's module. The mechanical tensile and the viscoelastic response of SPEs with this perovskite, together with the experimental setup, is illustrated in Fig. 6 [32].

In the case of spinels, apart from the natural monometallic spinels (Co_3O_4, Fe_3O_4, Mn_3O_4), bimetallic spinels like $ZnAl_2O_4$ and $MgAl_2O_4$. This latter spinel has benefitted Mg-ion batteries, presenting higher ionic conductivity to those PVDF membranes modified with Al_2O_3. The electrochemical response by electrochemical impedance spectroscopy is shown in Fig. 6d, where the real impedance (z′) at high

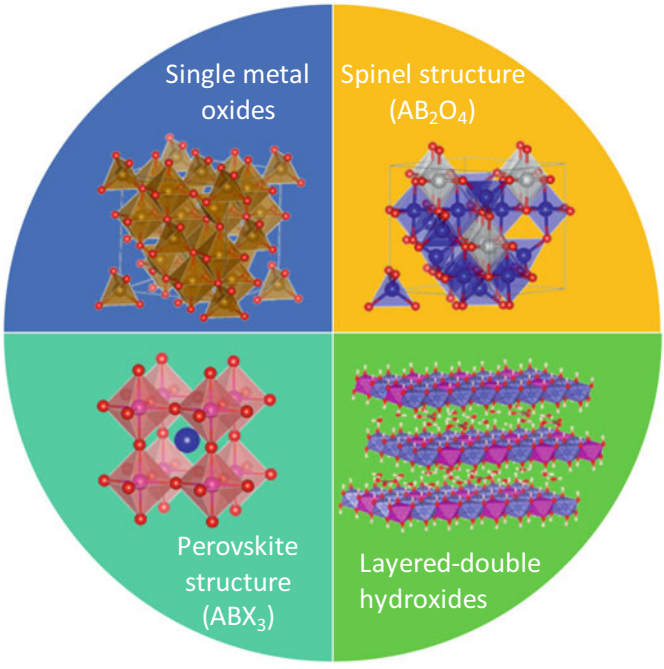

Fig. 5 Classification of single and mixtures of metal oxides/hydroxides as pseudocapacitive electrolyte materials

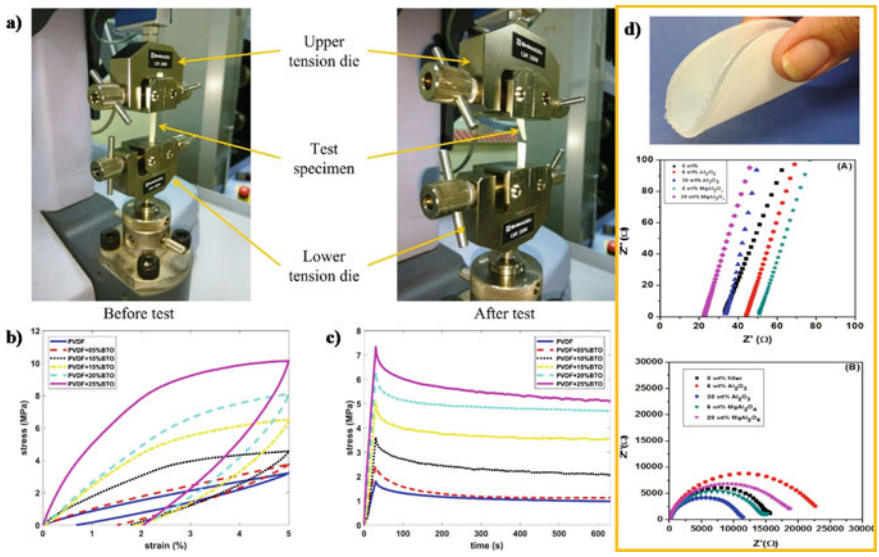

Fig. 6 **a** Setup for **b** the mechanical tensile and **c** viscoelastic response of PVDF electrolytes containing $BaTiO_3$ perovskites. Adapted with permission [32], Copyright (2020), Elsevier. **d** Photograph of a PVDF electrolyte modified with the $MgAl_2O_4$ spinel and the Electrochemical Impedance Spectroscopy response in contrast to Al_2O_3 as a function of mass loading. Adapted with permission [33], Copyright (2018), Wiley

frequencies is lower than those obtained with Al_2O_3, indicating higher conductivity [33]. Finally, LDHs play an essential role in electrolyte energy conversion/storage. For Li batteries, it has been well-established that LDHs like Mg–Al, and Co–Ni, can form hydrogen bonds with the polymer (PEO or PVA), restricting the movement of polymer's chains, inhibiting the migration of anions disfavoring the formation of Li dendrites [34, 35]. Vijayakumar et al. [36] recently reported an excellent review on 2D materials in electrolytes for Li batteries, where the exact mechanism to disfavor dendrite formation is discussed, as well as the interaction between the pseudocapacitive material as nano-filler, the polymer and the salt composing the GPE/SPE.

4.2 Chalcogenides and MXenes Pseudocapacitive Materials

LDHs, chalcogenides, and MXenes are another kind of 2D material, which are also crucial for polymer composite electrolytes [36]. Chalcogenides have been involved in the preparation of gel and solid polymer electrolytes (including ceramics) for energy purposes like Li batteries [37], PVDF-based Li batteries [38], solid-state Mg batteries [39], and rechargeable Mg-ion batteries [40]. It has been observed that chalcogenides provide high ionic conductivity to the electrolyte and high electronic conductivity in

solid-state Mg batteries (Fig. 7). The effect of different fillers on SPEs for solid-state Mg batteries is highlighted in Fig. 7, where it is possible to observe the impact of other non-pseudocapacitive materials on the intrinsic properties of these batteries, like Mg-ion conductivity, transference number, and mechanical stability. On the other hand, MXenes is a new class of 2D materials. Like LDHs, MXenes are 2D layered metal structures composed of transition metals in the form of carbides, nitrides, and carbonitrides. Because of their outstanding electrical conductivity, chemical properties like high hydrophilicity, and rich surface chemistry, MXenes are highly interesting materials for energy storage [41]. For instance, the $Ti_3C_2T_x$ MXene was incorporated into a PVDF-based SPE allowing efficient interfacial transport kinetics, while it participated in promoting the uniform deposition of Zn, enabling a higher performance of a Zn/VO_2 battery [42]. The deposition of uniform Zn metal has been shown essential to decrease the formation of Zn dendrites, while the proper combination with other polymers (some characteristics are presented in Fig. 7) can also allow for a decrease in the hydrogen evolution reaction and passivation [43], which are the typical anodic issues in rechargeable Zn batteries. Notably, the hydrophilic behavior of MXenes was used for developing PVA-based GPEs for rechargeable Zn-air batteries, where the MXene improved water retention as well as ionic conductivity, enhancing both performance and durability [44].

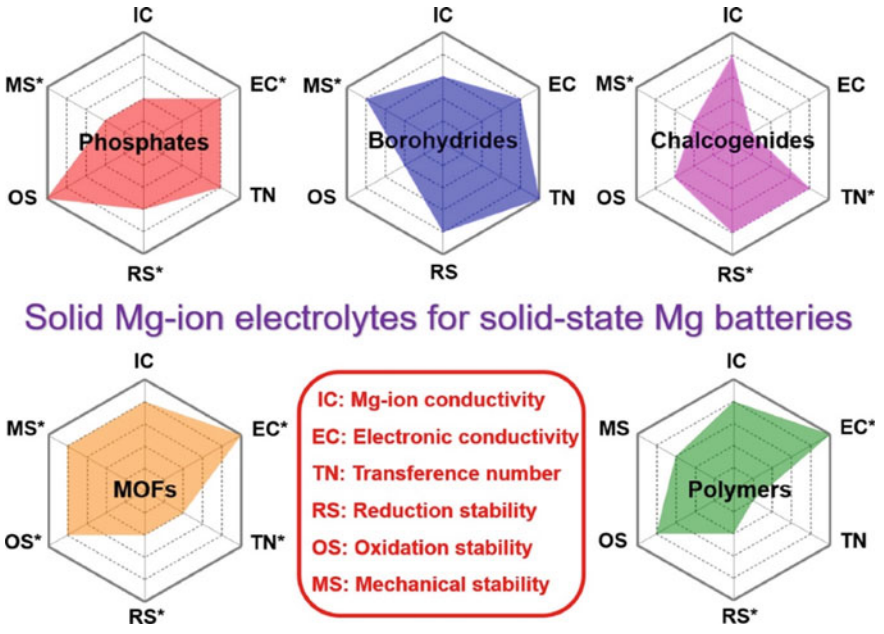

Fig. 7 The effect of the filler (phosphates, borohydrides, chalcogenides, MOFs, and polymers) on the resulting property of solid-state Mg batteries. Adapted with permission [39], Copyright (2023), Elsevier

4.3 Metal–Organic Frameworks Pseudocapacitive Materials

Metal–organic frameworks (MOFs) are an interesting group of materials; they are formed by metallic ions surrounded by organic ligands, resulting in a large amount of MOFs, and for electrochemical energy applications [45], MOFs can be used as obtained in composites and even, as MOF-derivate materials like heteroatom-doped carbon nanomaterials. In this way, the high surface area of MOFs, the high porosity and crystallinity, and tunable polarity make them ideal for improving the ion mobility in the electrolyte to boost the activity in applications like solid-state lithium batteries [46]. Notably, the open-metal sites provide to GPEs not only high ionic conductivity but also a high Li^+ transference number [47, 48]. There are at least 20,000 structures today reported, and because of the tunability of these materials [49] and their use as obtained in composites, derivatives, and defective forms. There is a world of possibilities in the field of energy conversion and storage systems where MOFs can be used in the electrodes or as fillers in electrolytes.

5 Conclusions

In conclusion, electrolyte significantly influences the performance and durability of electrochemical energy devices. The selection of the appropriate electrolyte type depends on the specific requirements of the application, including ionic conductivity, electrochemical window, working temperature range, stability, and safety. Extensive research has been conducted on pseudocapacitive materials, which encompass carbon-based materials, conductive polymers, and metal-based materials, as electrode materials for batteries and supercapacitors. However, these materials can also be electrolyte dopants or modifiers to enhance their properties. Aqueous electrolytes, such as aqueous gel electrolytes, possess several advantages, such as high ionic conductivity, low toxicity, ease of processing, and cost-effectiveness. Nonetheless, their utilization in conventional supercapacitors is limited due to their narrow working potential window. Non-aqueous electrolytes, comprising organic, ceramic, and ionic liquid-based electrolytes, have emerged as promising alternatives. Organic electrolytes, in particular, offer higher voltage windows, energy densities, and working temperature ranges compared to aqueous electrolytes. Ionic liquids provide innovative and environmentally friendly options for solid-state electrolytes due to their wide potential windows and high ionic conductivity. Gel polymer and solid polymer electrolytes have gained significant attention as multicomponent electrolyte systems. These electrolytes combine enhanced electrochemical performance with improved mechanical properties, making them suitable for flexible and durable energy storage devices. Polymer-based solid-state electrolytes, consisting of polymer matrices, electrolytic salts, and plasticizers, have demonstrated promising results in preventing the leakage of liquid electrolytes. In addition to electrolyte selection, incorporating pseudocapacitive materials into electrolytes has shown remarkable potential in enhancing

the performance of electrochemical energy systems. Carbon-derived pseudocapacitive materials, in particular, have been extensively investigated due to their large surface area, high electrical conductivity, and excellent chemical stability. Their performance can be further improved by modulating their capacitance through pore size and shape. The strategic modification of electrolytes using pseudocapacitive materials presents opportunities for achieving superior performance and durability in electrochemical energy systems. Ongoing research and development in this field will contribute to advancing electrochemical energy storage and conversion technologies, ultimately leading to more efficient and sustainable energy systems.

6 Challenges and Future Directions in Pseudocapacitive Materials for Energy Applications

The use of pseudocapacitive materials has been primarily as nano-fillers, enhancing the ionic conductivity, ion transference number, mechanical stability, and oxidation/reduction stability. Moreover, electrolyte selection greatly depends on the application. The use of aqueous solutions has the advantage of superior ionic conductivity, and thus, its substitution by gel, solid or ceramic electrolytes has presented different advantages and disadvantages like mechanical strength for flexible application or all-solid-state batteries/capacitors and restricted ion mobility. The composites formed by using pseudocapacitive materials into these non-aqueous electrolytes still present challenges to increasing the ionic conductivity at magnitudes like those in aqueous solutions. The fine integration should also allow for a decrease in certain issues. For instance, in rechargeable batteries, the anodic issues like passivation, shape changes, formation of dendrites during the charging process, and the hydrogen evolution reaction taking place as an undesired reaction decrease the durability and rechargeability of the battery. In this way, MOFs in all of their presentations (as prepared, as a precursor for doped carbon materials, etc.) have been visualized as efficient nano-fillers in GPEs and SPEs, and thus, its rational modification together with MXenes represent the most viable route to prepare efficient electrolytes. However, there is a long way to obtain efficient energy devices once these electrolytes become viable at industrial scales. Thus, the preparation method, interfacial phenomena, and decrease of anodic /cathodic issues assisted by the electrolyte formulation need further investigation for the success of this technology.

References

1. X. He, X. Zhang, A comprehensive review of supercapacitors: properties, electrodes, electrolytes and thermal management systems based on phase change materials. J. Energy Storage. **56**, 106023 (2022)

2. I. Voicu, H. Louahlia, H. Gualous, R. Gallay, Thermal management and forced air-cooling of supercapacitors stack. Appl. Therm. Eng. **85**, 89–99 (2015)
3. W. Fu, K. Turcheniuk, O. Naumov, R. Mysyk, F. Wang, M. Liu, D. Kim, X. Ren, A. Magasinski, M. Yu, X. Feng, Z.L. Wang, G. Yushin, Materials and technologies for multifunctional, flexible or integrated supercapacitors and batteries. Mater. Today **48**, 176–197 (2021)
4. Y. Yang, T. Zhu, L. Shen, Y. Liu, D. Zhang, B. Zheng, K. Gong, J. Zheng, X. Gong, Recent progress in the all-solid-state flexible supercapacitors. SmartMat **3**, 349–383 (2022)
5. A. Yu, V. Chabot, J. Zhang, *Electrochemical supercapacitors for energy storage and delivery: fundamentals and applications*, pp. 1–355 (2017)
6. G. Bahuguna, P. Ram, R.K. Sharma, R. Gupta, An organo-fluorine compound mixed electrolyte for ultrafast electric double layer supercapacitors. ChemElectroChem **5**, 2767–2773 (2018)
7. T. Lé, P. Gentile, G. Bidan, D. Aradilla, New electrolyte mixture of propylene carbonate and butyltrimethylammonium bis(trifluoromethylsulfonyl)imide (N_{1114} TFSI) for high performance silicon nanowire (SiNW)-based supercapacitor applications. Electrochim. Acta **254**, 368–374 (2017)
8. R. Holze, F. Béguin, E. Frąckowiak (eds), Supercapacitors—materials, systems, and applications. J. Solid State Electrochem. **19**, 1253 (2015)
9. G. Kaur, S.C. Sivasubramanian, A. Dalvi, Solid-state supercapacitors using ionic liquid dispersed Li^+-NASICONs as electrolytes. Electrochim. Acta **434**, 141311 (2022)
10. Z. Chen, Y. Yang, Z. Ma, T. Zhu, L. Liu, J. Zheng, X. Gong, Z. Chen, Y. Yang, Z. Ma, T. Zhu, L. Liu, X. Gong, J. Zheng, All-solid-state asymmetric supercapacitors with metal selenides electrodes and ionic conductive composites electrolytes. Adv. Funct. Mater. **29**, 1904182 (2019)
11. Y. Ji, N. Liang, J. Xu, D. Zuo, D. Chen, H. Zhang, Cellulose and poly(vinyl alcohol) composite gels as separators for quasi-solid-state electric double layer capacitors. Cellulose **26**, 1055–1065 (2019)
12. N.A. Choudhury, P.W.C. Northrop, A.C. Crothers, S. Jain, V.R. Subramanian, Chitosan hydrogel-based electrode binder and electrolyte membrane for EDLCs: experimental studies and model validation. J. Appl. Electrochem. **42**, 935–943 (2012)
13. Z. Zhai, L. Zhang, T. Du, B. Ren, Y. Xu, S. Wang, J. Miao, Z. Liu, A review of carbon materials for supercapacitors. Mater. Des. **221**, 111017 (2022)
14. K. Gajewska, A. Moyseowicz, D. Minta, G. Gryglewicz, Effect of electrolyte and carbon material on the electrochemical performance of high-voltage aqueous symmetric supercapacitors. J. Mater. Sci. **58**, 1721–1738 (2023)
15. M. Pershaanaa, S. Bashir, S. Ramesh, K. Ramesh, Every bite of Supercap: a brief review on construction and enhancement of supercapacitor. J. Energy Storage. **50**, 104599 (2022)
16. L. Peng, Z. Fang, Y. Zhu, C. Yan, G. Yu, Holey 2D nanomaterials for electrochemical energy storage. Adv. Energy Mater. **8**, 1702179 (2018)
17. T. Ohba, T. Ohba, Anomalously enhanced hydration of aqueous electrolyte solution in hydrophobic carbon nanotubes to maintain stability. ChemPhysChem **15**, 415–419 (2014)
18. Z. Supiyeva, X. Pan, Q. Abbas, The critical role of nanostructured carbon pores in supercapacitors. Curr. Opin. Electrochem. **39**, 101249 (2023)
19. C. Melios, C.E. Giusca, V. Panchal, O. Kazakova, Water on graphene: review of recent progress. 2D Mater. **5**, 22001 (2018)
20. A. Jangid, K.D. Verma, P. Sinha, K.K. Kar (ed.), *Handbook of Nanocomposite Supercapacitor Materials III*, vol. 6, 245 (Springer, Cham, 2021)
21. J. Tian, N. Cui, P. Chen, K. Guo, X. Chen, High-performance wearable supercapacitors based on PANI/N-CNT@CNT fiber with a designed hierarchical core-sheath structure. J. Mater. Chem. A. **9**, 20635–20644 (2021)
22. T. Lv, M. Liu, D. Zhu, L. Gan, T. Chen, T. Lv, M. Liu, D. Zhu, L. Gan, T. Chen, Shanghai key, nanocarbon-based materials for flexible all-solid-state supercapacitors. Adv. Mater. **30**, 1705489 (2018)
23. H. Zhang, X. Wang, H. Ma, M. Xue, Recent progresses on applications of conducting polymers for modifying electrode of rechargeable batteries. Adv. Energy Sustain. Res. **2**, 2100088 (2021)

24. E. Dhandapani, S. Thangarasu, S. Ramesh, K. Ramesh, R. Vasudevan, N. Duraisamy, Recent development and prospective of carbonaceous material, conducting polymer and their composite electrode materials for supercapacitor—a review. J. Energy Storage. **52**, 104937 (2022)
25. J. Wang, X. Li, X. Du, J. Wang, H. Ma, X. Jing, Polypyrrole composites with carbon materials for supercapacitors. Chem. Pap. **712**(71), 293–316 (2016)
26. L. Hao, D. Yu, Progress of conductive polypyrrole nanocomposites. Synth. Met. **290**, 117138 (2022)
27. S. Liu, W. Liu, D. Ba, Y. Zhao, Y. Ye, Y. Li, J. Liu, S. Liu, W. Liu, Y. Zhao, Y. Ye, J. Liu, D. Ba, Y. Li, Filler-integrated composite polymer electrolyte for solid-state lithium batteries. Adv. Mater. **35**, 2110423 (2023)
28. Nidhi, S. Patel, R. Kumar, Effect of Al_2O_3 on electrical properties of polymer electrolyte for electrochemical device application Mater. Today Proc. **46**, 2175–2178 (2021)
29. J. Wang, L. Fan, Q. Du, K. Jiao, Lithium ion transport in solid polymer electrolyte filled with alumina nanoparticles. Energy Adv. **1**, 269–276 (2022)
30. Nidhi, S. Patel, R. Kumar, PVDF-HFP based nanocomposite polymer electrolytes for energy storage devices dispersed with various nano-fillers. AIP Conf. Proc. **2220** (2020)
31. T. Sathyanathan, C.P. Sugumaran, Modeling and analysis of nano composite $BaTiO_3$ lithium polymer battery. IEEE Trans. Nanotechnol. **17**, 161–168 (2018)
32. F. Ram, P. Kaviraj, R. Pramanik, A. Krishnan, K. Shanmuganathan, A. Arockiarajan, PVDF/$BaTiO_3$ films with nanocellulose impregnation: Investigation of structural, morphological and mechanical properties. J. Alloys Compd. **823**, 153701 (2020)
33. J. Sharma, S. Hashmi, Magnesium ion-conducting gel polymer electrolyte nanocomposites: effect of active and passive nanofillers. Polym. Compos. **40**, 1295–1306 (2019)
34. X. Hui, P. Zhang, J. Li, D. Zhao, Z. Li, Z. Zhang, C. Wang, R. Wang, L. Yin, In situ integrating highly ionic conductive LDH-Array@PVA gel electrolyte and MXene/Zn anode for dendrite-free high-performance flexible Zn–Air batteries. Adv. Energy Mater. **12**, 2201393 (2022)
35. Q. Wang, J.F. Wu, Z.Y. Yu, X. Guo, Composite polymer electrolytes reinforced by two-dimensional layer-double-hydroxide nanosheets for dendrite-free lithium batteries. Solid State Ionics **347**, 115275 (2020)
36. V. Vijayakumar, M. Ghosh, K. Asokan, S. Babu Sukumaran, S. Kurungot, J. Mindemark, D. Brandell, M. Winter, J. Ravi Nair, V. Vijayakumar, J. Mindemark, D. Brandell, M. Ghosh, K. Asokan, S.B. Sukumaran, S. Kurungot, M. Winter, J.R. Nair, 2D Layered Nanomaterials as fillers in polymer composite electrolytes for lithium batteries. Adv. Energy Mater. **13**, 2203326 (2023)
37. X. Yu, A. Manthiram, A review of composite polymer-ceramic electrolytes for lithium batteries. Energy Storage Mater. **34**, 282–300 (2021)
38. Y. Zhang, C. Zhu, S. Bai, J. Mao, F. Cheng, Recent advances and future perspectives of PVDF-based composite polymer electrolytes for lithium metal batteries: a review. Energy Fuels (2023)
39. Y. Pang, Y. Zhu, F. Fang, D. Sun, S. Zheng, Advances in solid Mg-ion electrolytes for solid-state Mg batteries. J. Mater. Sci. Technol. **161**, 136–149 (2023)
40. M. Guo, C. Yuan, T. Zhang, X. Yu, M. Guo, C. Yuan, X. Yu, T. Zhang, Solid-state electrolytes for rechargeable magnesium-ion batteries: from structure to mechanism. Small **18**, 2106981 (2022)
41. M. Hu, H. Zhang, T. Hu, B. Fan, X. Wang, Z. Li, Emerging 2D MXenes for supercapacitors: status, challenges and prospects. Chem. Soc. Rev. **49**, 6666–6693 (2020)
42. J. Feng, D. Ma, K. Ouyang, M. Yang, Y. Wang, J. Qiu, T. Chen, J. Zhao, B. Yong, Y. Xie, H. Mi, L. Sun, C. He, P. Zhang, J. Feng, D. Ma, K. Ouyang, M. Yang, Y. Wang, T. Chen, B. Yong, Y. Xie, H. Mi, L. Sun, C. He, P. Zhang, J. Qiu, Multifunctional MXene-bonded transport network embedded in polymer electrolyte enables high-rate and stable solid-state zinc metal batteries. Adv. Funct. Mater. **32**, 2207909 (2022)
43. Z. Chen, X. Li, D. Wang, Q. Yang, L. Ma, Z. Huang, G. Liang, A. Chen, Y. Guo, B. Dong, X. Huang, C. Yang, C. Zhi, Grafted MXene/polymer electrolyte for high performance solid zinc batteries with enhanced shelf life at low/high temperatures. Energy Environ. Sci. **14**, 3492–3501 (2021)

44. Z. Chen, W. Li, X. Yang, C. Ke, H. Chen, Q. Li, J. Guo, Y. He, Z. Guo, X. Liang, Gel polymer electrolyte with MXene to extend cycle lifespan of flexible and rechargeable Zinc-Air batteries. J. Power. Sources **523**, 231020 (2022)
45. X. Li, X. Yang, H. Xue, H. Pang, Q. Xu, Metal–organic frameworks as a platform for clean energy applications. EnergyChem. **2**, 100027 (2020)
46. Z. Zhang, Y. Huang, H. Gao, C. Li, J. Hang, P. Liu, MOF-derived multifunctional filler reinforced polymer electrolyte for solid-state lithium batteries. J. Energy Chem. **60**, 259–271 (2021)
47. X. Lu, H. Wu, D. Kong, X. Li, L. Shen, Y. Lu, Facilitating lithium-ion conduction in gel polymer electrolyte by metal-organic frameworks. ACS Mater. Lett. **2**, 1435–1441 (2020)
48. Y. Xu, R. Zhao, J. Fang, Z. Liang, L. Gao, J. Bian, J. Zhu, Y. Zhao, Metal-organic framework (MOF)-incorporated polymeric electrolyte realizing fast lithium-ion transportation with high Li^+ transference number for solid-state batteries. Front. Chem. **10**, 1013965 (2022)
49. L. Jiao, J.Y.R. Seow, W.S. Skinner, Z.U. Wang, H.L. Jiang, Metal–organic frameworks: structures and functional applications. Mater. Today **27**, 43–68 (2019)

Electrochemical Properties of Metal Hydroxides

Hamideh Mohammadian Sarcheshmeh and Mohammad Mazloum Ardakani

Abstract The electrochemical capacitor has received remarkable attention due to its bridging performance for the power/energy interval between conventional capacitors and batteries/fuel cells. The electrochemical behavior of capacitors is mainly influenced by using electrode materials. One of the promising pseudocapacitive materials is metal hydroxide, whose electrochemical performances originated from reversible Faradaic reactions between the electrode and electrolyte interface. It is necessary to use advanced pseudocapacitive materials to manufacture supercapacitors to solve their problem of lower energy density (E) compared to lithium batteries. Different strategies, such as doping, various synthesis methods, fabrication of composites, and utilization of conductive substrates, have been introduced. This chapter represents investigations on pseudocapacitive electrode materials, essentially transition metal hydroxides. Some published reports about applications of metal hydroxides as pseudocapacitive electrode materials with their different structures and composites are summarized in this chapter. Some strategies to improve the electrochemical performance of transition metal hydroxides are mentioned.

Keywords Composite · Doping · Metal hydroxides · Pseudocapacitive electrode materials

1 Introduction

The most famous metal hydroxides as pseudocapacitive electrode materials are hydroxides based on transition metals including Ni, Co, and Mn with abundant redox states. They remarkably boost the E value in comparison with similar carbon-based materials. Nevertheless, their long-term stability and rate capability are generally low due to their approximately poor electrical conductivity. In order to practical utilizations, good stability, and high rate capability are essential to acquire acceptable power density (P) and E values [1]. Pseudocapacitive materials store electrical

H. Mohammadian Sarcheshmeh · M. Mazloum Ardakani (✉)
Faculty of Science, Department of Chemistry, Yazd University, 89195-741 Yazd, Iran
e-mail: mazloum@yazd.ac.ir

© The Author(s), under exclusive license to Springer Nature Switzerland AG 2024

R. K. Gupta (ed.), *Pseudocapacitors*, Engineering Materials,
https://doi.org/10.1007/978-3-031-45430-1_7

energy via reversible Faradaic reactions, which produce electrochemically active materials on the electrode surface and provide charge transfers between the electrode and electrolyte. It is necessary to mention that the specific capacitance (SC) values of pseudocapacitive electrodes are typically not significant owing to the poor charge transfer in bulk materials [2]. To acquire excellent capacitance, the size of electrode materials should be decreased to nano. Thus, most of the pseudocapacitive materials can operate to the charge storage. Among transition metals, Ni, Co and Mn have been extensively investigated as pseudocapacitive electrode materials due to their good capacitance values, and simple fabrication methods [3]. We will explain their applications in the following.

2 Nickel Hydroxides

They have been known as a noticeable pseudocapacitive electrode material owing to their significant electrochemical properties. Different techniques have been applied to prepare nickel (II) hydroxide ($Ni(OH)_2$) with higher capacitive performances. Some methods have been reported, e.g., chemical precipitation, sol–gel processes, and electrochemical deposition [4]. The range of SC values for nickel-based structures was 50–350 F/g. Nevertheless, the obtained SC values were much lower than their theoretical value (SC = 2082 F/g for $Ni(OH)_2$). This low obtained SC values reveals a limitation in the electrochemical practical of $Ni(OH)_2$ and, thus, a challenge to improve its specific capacitance. It is worth knowing that the performance of electrode materials can be improved by managing some of their characterizations such as morphologies and specific surface area. The materials involving a large surface area and a uniform porous structure in the nanometer sizes provide excellent performance. Among different synthetic methods, electrochemical techniques indicated significant ability in controlling nonporous materials morphologies [4]. The porous nickel film was prepared via the electrodeposition of an alloy of Ni–Cu [5]. The porous $Ni(OH)_2$ material electrode was produced using the electrodeposition of Ni $(OH)_2$ film on the mentioned prepared nonporous nickel substrate. This electrode indicated the SC value of 1434 F/g with E = 52.1 Wh/kg at a current density of 10 A/g. Shaikh et al. [6] introduced a procedure to synthesize β-$Ni(OH)_2$ using plating waste and change it into a valuable product. The hydroxide precipitation is a typical strategy for the treatment of waste electroless nickel plating baths, which produces a lot of $Ni(OH)_2$ waste with expensive handling and storage processes. Nickel plating is known as a plating technology that improves the strength, hardness, conductivity, corrosion resistance, and heat resistance of metallic substrates. The produced β-$Ni(OH)_2$ powder had a SC value of 332 F/g. Lokhande et al. [7] fabricated $Ni(OH)_2$ nanosheets on nickel foam via nickel foam oxidization in a solution, which led to a morphology conversion in the oxidative solution. Also, the thin $Ni(OH)_2$ nanosheet on nickel foam was synthesized with the SC = 2384.3 F/g, and 75% capability retention after 3000 contentious cycles [8].

3 Manganese Hydroxides

They have an acceptable theoretical SC = 1370 F/g, and high practical potential [9]. Some limitations, such as low cycle stability, and decreased electrical and ionic conductivities, restrict the utilization of manganese compounds in commercial applications. The utilization of 3D nickel foams in fabricating of Manganese (II) hydroxide ($Mn(OH)_2$) nanostructure electrodes indicated their capability in commercial applications [10]. Nickel foams, as 3D porous metallic templates, include large specific surface areas that can help to increase the metal hydroxide conductivity, boost their reaction kinetics, and absorb the stress induced by the swelling and contraction of the electrode materials.

4 Cobalt Hydroxides

Among transition metal hydroxides, cobalt compounds were extensively investigated as suitable materials with outstanding capacitive performance. Cobalt(II)hydroxide ($Co(OH)_2$) nanowires grown on nitrogen-modified microwave exfoliated graphite oxide (NMEG) indicated SC = 610 F/g with an E = 24.9 Wh/kg [3]. The $Co(OH)_2$ has received much consideration to examine the operation of crystalline nanomaterials with 3D structures as developed pseudocapacitive materials. However, amorphous phase materials were generally considered unacceptable for preparing capacitors due to their poor performance. It should be known that amorphous nanomaterials indicate relatively unique electrochemical performances. In this regard, the amorphous $Co(OH)_2$ nanostructures were prepared via an electrochemistry technique [11]. Amorphous $Co(OH)_2$ nanostructures (SEM and TEM images and XRD patterns for amorphous $Co(OH)_2$ can be seen in Fig. 1. These results verify the formation of amorphous structure) showed interestingly significant electrochemical behavior with a good SC value of 1094 F/g and remarkable cyclic stability during 8000 continuous cycles. Obtained results verified that the utilization of amorphous nanomaterials as developed pseudocapacitive electrode materials. The disordered $Co(OH)_2$ structures significantly enhanced the electrochemical performance. The proposed amorphous nanostructure indicated appropriate electrochemical properties due to these reasons: 1-The pure surface of the proposed electrodes can cause the effective interaction of $Co(OH)_2$ with electrolyte, 2-the 3D surfaces of prepared nanostructures have a larger specific surface to adsorb electrolytic ions on the electrode, 3-the amorphous structures. Also, a material involving low crystallinity or an amorphous phase can lead to more transportation channels than an extensively crystalline material [12].

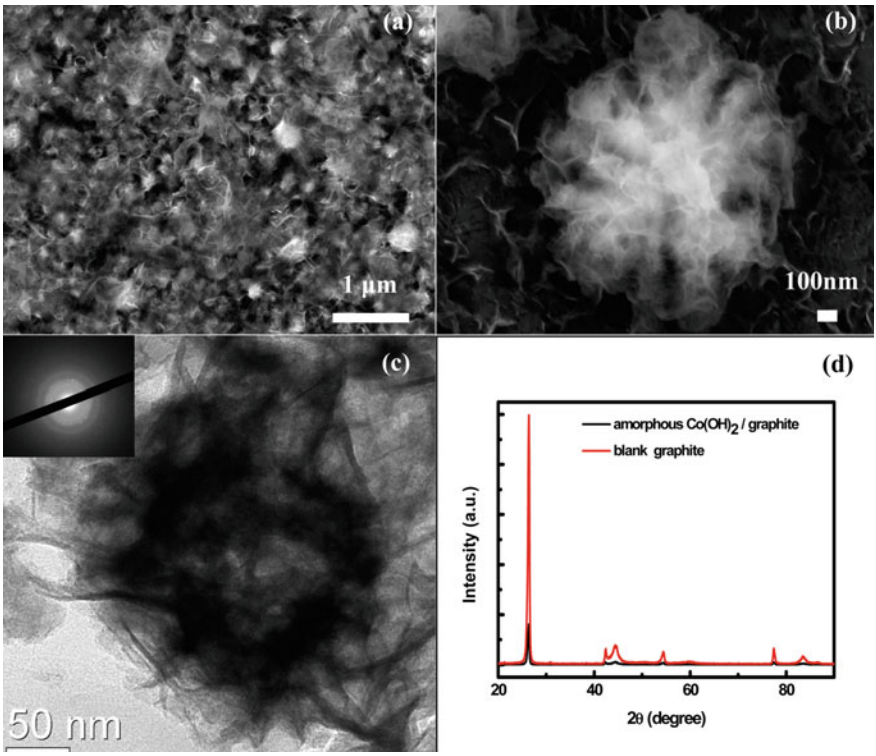

Fig. 1 **a**, **b** SEM images of the as-synthesized amorphous $Co(OH)_2$ nanostructures on graphite electrodes, **c** TEM images of the sample, and **d** XRD patterns of the products. Adapted with permission [11], Copyright (2014), American Chemical Society

5 Doped Metal Hydroxides

$Ni(OH)_2$ has been known as an acceptable electrode material. However, it is typically p-type with poor electrical conductivity and low stability, which restricts its acceptable electrochemical application. To solve these issues, different efforts have been made to enhance rate capability and electrical conductivity. A strategy was doping it with some elements. The similar ion radii sizes of Co and Ni allow Ni hydroxide to be doped with cobalt without causing severe lattice strain. Another strategy was increasing the specific surface area via the fabrication of mesoporous structures. It leads to enlarging the interface contacts effectively between active sites and electrolyte ions, creates spaces for volume increment in the duration of the cycling process, and enhances ion and electron transportation. A green method to produce novel nanostructured materials without employing surfactants or stabilizers is laser ablation in liquid (LAL) [13]. A nanosheet of Co-doped $Ni(OH)_2$ was prepared by a laser-induced cobalt colloid. This colloid operated as a doping

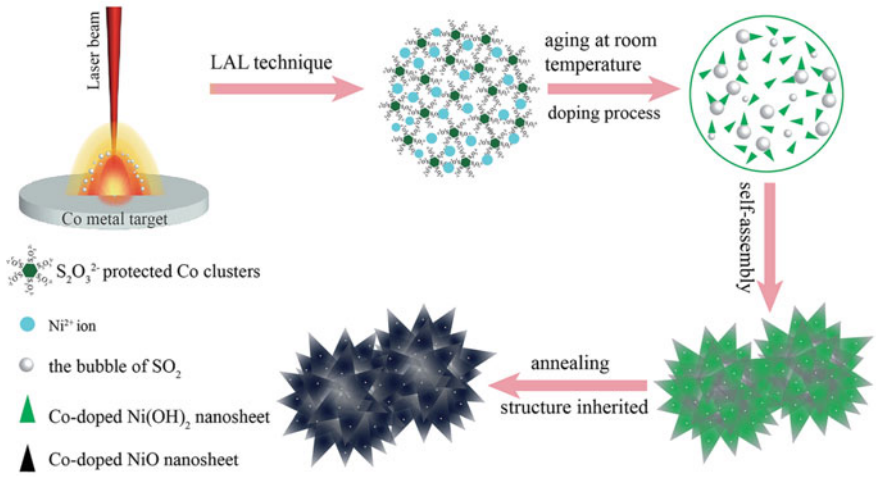

Fig. 2 Proposed formation process of Co-doped $Ni(OH)_2$ and oxide nanosheet network structures. Adapted with permission [14], Copyright (2016), Royal Society of Chemistry

solution [14]. Figure 2 shows all steps for fabrication process. The fabrication material involved two advantages: Co-doping and mesoporous structure preparation. The pseudocapacitive electrode based on Co-doped $Ni(OH)_2$ indicated a SC value equal to 1421 F/g at 6 A/g with a good stability (76% after 1000 consecutive cycles). The partial replacement of Co^{2+} instead of Ni^{2+} in the structure led to an increment in the number of holes in the valence bands, and, thus, provided high p-type conductivity [15]. Consequently, the increment of p-type conductivity for $Ni(OH)_2$ and mesoporous structure promotes contact area between electrode and electrolyte. Also it reduces the length of the channels for ion transportation.

6 The Competition Between Morphology and Chemical Doping

A wide range of research has been performed to boost the conductivity of active materials through their morphology controls and doping. Conductivity will increase using chemical doping. For example, nickel in the structure of $Ni(OH)_2$ was partially replaced by various cations such as (Al), (Zn), and (Co). Doping of $Ni(OH)_2$ electrode using Co increased its electrochemical performance via improvement of electrical conductivity. A $Co_{0.5}Ni_{0.5}(OH)_2$ composition, indicated SC = 1560 F/g [16]. Moreover, decreasing material size into nano-size increases the resistance because of reduced transportation distance for electronic and ionic species. Various $Ni(OH)_2$ nanostructures, e.g., nanoplates, nanoflowers, and hierarchical nanostructures, have been fabricated [17]. According to some investigations, $Ni(OH)_2$ material size can

be effectively changed by controlling the pH amount with some agents, for example, alkali metal hydroxides or hexamethylenetetramine. The size decreased-$Ni(OH)_2$ materials indicated higher electrochemical performances due to the increased mass transport. Therefore, it is obvious that morphology and doping influence the electrochemical behavior of $Ni(OH)_2$ when utilized independently [18]. Gyeonghee et al. [19] showed that the structural characterizations competed with chemical doping to affect the electrochemical behaviors of metal hydroxide electrodes. They changed the morphology and crystallinity characterization of $Ni(OH)_2$ using glucose in a solvothermal method. It significantly decreased metal hydroxide particle size. Modified metal hydroxides by glucose provided better ion transport because of more interlayer water. Ethyl glucosides were produced when glucose was used. They prevented the precursors diffusion in the time synthesis and, consequently limited the formation of larger crystals of $Ni(OH)_2$ particles. Significantly, the increment of SC value induced using glucose was less efficient at high Co amounts and more efficient at low Co amounts (high Ni) in the Co doped-$Ni(OH)_2$ materials, verifying a competitive effect between the morphology and doping. This competitive effect was attributed to the amount of continuity between particles and charge hopping. Amorphous materials have more metal vacancies on the surface which intensify inter-particle discontinuity. Therefore, charge hopping enhancement provided by chemical doping in greatly defective materials, may be less effective.

7 Metal Hydroxide Composites

Most pseudocapacitive materials are p-type semiconductors, which are kinetically unsuitable to provide fast electron transport and thus obtain a high (P) value. Thus, it is necessary to increase the ion and electron transport kinetics in the electrode and electrode–electrolyte surfaces. A suitable idea is the fabrication of composites with conductive matrixes. Pseudocapacitive materials can be incorporated into nonporous highly conductive substrates, for instance, carbon nanotube (CNT), carbon aerogel, mesoporous carbon, graphene, conducting polymers, and current collectors. These porous conductive substrates provide proper accessibility of ions and electrons to the active surfaces resulting in good performance [20]. It should be noted that improving electronic conductivities using conductive carbon substrates indicated some problems. The direct growth of metal hydroxides on substrates is complicated because their surfaces are incompatible. Thus, the oxidative treatment of carbon materials is necessary to enhance surface compatibility, which creates some structural defects and oxygen functional groups to facilitate the formation of metal hydroxides on these substrates. Metal hydroxides can simply grow on current collectors such as nickel foam and fluorine-doped tin oxide glass (FTO). Nevertheless, the number of active materials is extensively restricted owing to the coffined specific surface area and the low thickness of active material coating in the nickel foam or FTO.

Consequently, the obtained electrode capacitance is undesirable. Xiaowei [21] fabricated a conductive substrate via nickel-coated CNTs (Ni-CNTs) to vertically grow β-$Ni(OH)_2$ nanoplates on it. This Ni-CNTs@β-$Ni(OH)_2$ composite indicated SC = 1807 F/g.

7.1 Bimetallic Hydroxide Composites

The bimetallic hydroxides mainly reveal better electrochemical performances than unitary hydroxides. Improvement in performance is attributed to the complicated combination and synergistic effects of multiple metals. Newly, hydroxides based on nickel–cobalt (Ni–Co) have been investigated as significant electrode materials. In comparison with the unitary Ni or Co hydroxides, the bimetallic Ni–Co hydroxides exhibit more redox reactions and finally show an electrochemical performance related to the combination of the performance of Ni and Co ions. In addition, the Co ions can convert into the remarkably conductive CoOOH, which is proper to enhance the conductivity and, therefore, the fast electron transfer for electroactive materials [22]. A (Ni–Co) oxy-hydroxides with a mesoporous structure was acquired using the microwave-assisted hydrothermal annealing. Microwave irradiation can uniformly transfer heat to the substance resulting in higher homogeneous nucleation and lower crystallization time compared to usual heating processes, thus, improving the particle size distribution. The porosity of the Ni–Co oxy-hydroxide nanostructure was controlled by adding a surfactant agent. Ni–Co oxy-hydroxides showed SC = 636 F/g with the E, and P values equal to 17 Wh/kg and 1.6 kW/kg, respectively [23].

The nano-Ni/$Co(OH)_2$ nanoflake composite film exhibited a good SC value of 1920 F/g. This nano-Ni film was fabricated by a hydrogen bubble template and then $Co(OH)_2$ nanoflakes (~20 nm) were electrodeposited on it. Recently, the preparation of 3D porous nanometal films using the hydrogen bubble template has received much attraction because of their noticeable structural characterizations and attractive features. They exhibited greatly porous dendritic walls with a large surface area and open porous structures, which introduced them as appropriate materials for the fabrication of capacitors [21]. A chemical bath deposition (CBD) procedure was also reported to directly form nickel–cobalt hydroxide nanorod arrays onto a stainless-steel template. This proposed structure could decrease the electrolyte diffusion resistance in the electrode materials and increase their electrochemical charge–discharge. Significantly, this nanorod indicated SC = 456 F/g and a proper rate capability (90% retention after 1000 cycles) [24].

According to the crystal structures, the Ni and Co hydroxides generally include two phases: α-phase and β-phase. The α-phase hydroxides indicate superior electrochemical performance than their β-phase because they have disordered and weakly crystallized structures. Nevertheless, the α-phase can rapidly convert to β-form during the fabrication process, leading to a small fabrication yield. Some methods, for example, co-precipitation, hydrothermal, and microwave-assisted hydrothermal

methods, were utilized to fabricate the α-phase structures of Ni–Co hydroxides. The mentioned procedures significantly utilizes many surfactants and alkaline reagents [22]. Chen et al. [25] introduced a simple hydrothermal procedure to fabricate Ni–Co hydroxides with α-phase without using the alkali, and surfactant agents. They used 1-methyl-2-pyrrolidone (NMP) in the mixed solvent showing the principal function in the metal ions precipitation and α-phase hydroxides formation. The Ni–Co hydroxides as the electroactive materials indicated SC = 1337.4 F/g for $Ni_{0.67}Co_{0.33}$ hydroxide and a remarkably increased SC = 2286.7 F/g and 2248.9 for $Ni_{0.67}Co_{0.33}$ and $Ni_{0.5}Co_{0.5}$ hydroxides, respectively after growth on Ni foam. Xia and coworkers [22] reported a simple precursor conversion procedure to grow the α-phase Ni–Co hydroxides structure. This procedure is extensively used as a synthesis method. Using the precursors, it is possible to fabricate different specific morphologies and structures by precursors. These precursors will be converted into the corresponding form while keeping the morphology and structure. The SC value of bimetallic Ni–Co hydroxides (1600 F/g) was more significant than some α-phase hydroxides and their combinations, e.g., α-$Co(OH)_2$, α-$Ni(OH)_2$ and α-Ni $(OH)_2$/rGO, and also much better than different bimetallic Ni–Co materials e.g., Ni–Co hydroxides. The cyclic stability of the Ni–Co hydroxides was more significant than monometallic Ni hydroxides. The Ni–Co hydroxides exhibited much better stability and better rate capability due to adding Co ions. These ions helped to the stable presence of ethylene glycol molecules in the interlayer space of the α-phase Ni–Co hydroxides, leading to higher cycling stability. Metal hydroxides are not stable in the aqueous medium. When they are exposed to H_2O, they can quickly hydrolysis and decompose. Adding Co ion in the Ni–Co hydroxide could help keep ethylene glycol in the interlayer. The interlayer species are important for the α-phase hydroxide stability. They can efficiently inhibit the transformation of phases in hydroxides (α into β), and lead to good stability for bimetallic Ni–Co hydroxides compared to monometallic Ni hydroxides [22].

Hybridizing pseudocapacitive electrode materials using conductive materials to fabricate composites can be utilized for the improvement of electrical conductivity and electrochemical performance. A Ni–Co hydroxide growth on graphene petal foam was reported as a pseudocapacitive material, which indicated outstanding electrochemical performance. Composites are used to increase the resistance of complete electrodes and improve the utilization rate of active materials. A high conductive structure, $NiCo_2O_4$ nanowires array @ $NiCo(OH)_2$ nanosheets, was reported as an electrode material. The metallic $NiCo_2O_4$ increased composite conductivity and enhanced the electron transport in the prepared electrode. This electrode indicated the ultrahigh SC = 2890.6 F/g with 94.66% capacitive retention after 5000 continuous cycles [26].

7.2 Ternary Metal Hydroxide Composites

For improvement of charge storage and thus E value, numerous works have been reported to develop electrodes based on metal hydroxide composites to enhance redox activity or the electroactive sites density. However, there are various challenges with physically distributed components in heterogeneous composites: (i) the complex and expensive multi-step preparation process of the composites; (ii) reduced electron transfer efficiency due to the interface between heterogeneous components; (iii) The difficulty of using all electroactive sites of the composite. Therefore, multicomponent metal hydroxides (metal component number ≥ 3) with a homogeneous element distribution can overcome the mentioned problems. A triple hydroxide nanoneedles (Ni–Co–Mn) growth on plasma-grown graphitic petals (GPs) using a simple method was fabricated [27]. As explained earlier, to improve the charge transfer efficiency and decrease internal resistance, different templates have been used for metal hydroxides, e.g., Ni foam, stainless steel, and carbon-based nanomaterials. However, for fabricating active electrodes using these substrates with limited surface area, a binder is essential. Consequently, electrical conductivity, long-term stability, rate capability, and the E value of electrodes will be reduced. The GPs involving a low number of graphene layers are proper substrates for the pseudocapacitive electrodes because of their large surface area, good electrical conductivity, and binder-free utilization [28].

The porous Ni–Co–Mn triple hydroxide nanoneedles with a homogenous metal elements distribution, enhanced the redox state numbers and, therefore, electroactive sites. As a result, increased energy and power densities. 3D greatly conductive substrate involving a lot of sharp graphene edges, and the sharp nanoneedles could significantly improve electrolyte ions diffusion and therefore enhance the rate capability for the electrode. The electrode showed high charge storage efficiencies with SC = 1400 F/g and 117% performance retention after 3000 successive cycles. This significant long-term cyclic stability was attributed to the strong mechanical connection between the nanoneedles and GPs, continuous fiber-petal transition with crystalline continuity, and synergistic effect of three metals in the structure [27].

To fabricate flexible electrodes, carbon nanotube yarns (CNTY) can be used. They have good flexibility and high electrical and mechanical features. However, they typically exhibit poor SC and E values owing to the confined energy storage in the fabricated electric double-layer capacitive systems. Transition metal hydroxides as pseudocapacitive materials can be utilized to modify CNTYs to promote electrochemical performance [29]. Nevertheless, the cyclic stability and charge transport for functionalized CNTYs with transition metal hydroxides is unsuitable because of their poor structural stability and low electrical conductivity. The structural collapse of metal hydroxides is attributed to the swelling and shrinkage during consecutive cycling, thus reducing the cyclic long-term stability. Also, the poor interaction between metal hydroxides and CNTYs causes metal hydroxides easily separate from CNTY during continuous cycles, particularly at a large current density [30]. Recently, conducting 2D metal–organic frameworks (MOFs) have been known

as a good suggestion for active electrode materials owing to excellent porosity, good specific surface area, proper electrical conductivity, and adaptable functionalities. Nevertheless, they degrade due to the adsorption/desorption process of electrolyte ions during continuous cycling, and in the presence of acidic and alkaline environments [31]. Zhang et al. [32] introduced a simple but strong ship-in-a-bottle structure providing proper electrochemical behavior with improved kinetics and life cycling via growing $(Ni(OH)_2$ or $Co(OH)_2$ into MOF (Ni_3(2,3,6,7,10,11-hexaiminotriphenylene)$_2$, $Ni_3(HITP)_2$) nonporous and anchored them onto CNTY through π-π interactions. The physical nanoconfinement and hydrogen bonding between metal hydroxide and $Ni_3(HITP)_2$ interlock them to prevent structure collapse of the composite during charging/discharging. The $Ni(OH)_2$@$Ni_3(HITP)_2$@CNTY electrode exhibited a SC value of 496.0 mF/cm^2 at 0.4 mA/cm^2 with noticeable stability (92.3% capacitive retention after 10,000 successive cycles).

The Ni–Fe–Co hydroxides/N-doped carbon nanoplate (Ni Co Fe–NC) was fabricated by a simple method. N-doped carbon hydrogel with numerous hydrophilic groups such as COOH, OH, and C=O can react with H_2O molecules by hydrogen bonding and thus improve the material wettability and enhance the electrolyte accessibility. In addition, doping the carbon matrix by nitrogen will alter the charge density of carbon and therefore increase its pseudocapacitance property. The Ni Co Fe-NC showed SC = 1849 F/g and an E = 31.5 Wh/kg [33]. Table 1, shows a summary of the mentioned studies.

8 Layered Double Hydroxides (LDHs)

Newly, 2D nanosheet morphologies such as inorganic layered hydroxides have received remarkable attraction on electrochemical properties and energy applications. Much research has studied fabricating layered hydroxide electrodes that involve higher Faradaic reactions and larger capacities owing to an enhancement in pseudocapacitive performance. Bimetallic LDHs with the formula of $[M^{2+}{}_{1-x}M^{3+}{}_x(OH)_2]^{x+}[A^{n-}{}_{x/n} \cdot mH_2O]_{x-}$ (M^{2+} and M^{3+}, the bivalent and trivalent metal cations, respectively; A^{n-}, the charge-balancing anion of valence n; $x = M^{3+}/(M^{2+} + M^{3+})$) is a large category of the 2D inorganic materials. So far, most reported LDHs are Brucite or hydrotalcite structured compounds. By suitable controlling anionic species, lamellar LDHs can provide acceptable operations on energy storage resulting from the final 2D anisotropy, available large surface area, and a particular positively charged property [34]. Hwang et al. studied the pseudocapacitive performance of the Zn–Co LDH film prepared by the restacked Zn–Co LDHs nanosheets after exfoliation [35]. This film showed SC = 170 F/g. A simple formation of Ni–Co and Ni–Fe LDHs nanosheet arrays on the conductive substrate by a homogeneous precipitation method exhibited a proper E = 77.3 Wh/kg for Ni–Co LDH and E = 82.3Wh/kg for Ni–Fe LDHs [36, 37]. Pan et al. [38] introduced the growth of $ZnCo_{1.5}(OH)_{4.5}Cl_{0.5}.0.45H_2O$ (30 nm) on Ni foam and obtained a noticeable SC value of 3946.5 F/g. Nasir et al. reported a hybrid of Ni and Ni–Co LDH nanostructures wrapped in nitrogen-doped graphene

Table 1 Some pseudocapacitive electrode materials based on metal hydroxides

Electrode/(Substrate)	SC (F/g)	E (Wh/kg)	P (Kw/kg)	Cycle stability	References
Ni $(OH)_2$ film/(Porous Ni film)	1634 at 2 A g^{-1}	52.1	2500	59.3% after 500 cycles	[5]
β-Ni $(OH)_2$	330	11.5	207.5	–	[6]
Ni $(OH)_2$/(Ni foam)	2384.3 at 1 A g^{-1}	–	–	75% after 3000 cycles	[8]
$Co(OH)_2$ NW/(Nitrogen modified microwave exfoliated graphite oxide)	610	24.9	224	65% after 6000 cycles	[3]
Amorphous $Co(OH)_2$/(Graphite)	1094 at 1 mV · s^{-1}	–	–	95% after 8000 cycles	[11]
Co-doped Ni $(OH)_2$	1421 at 6 A g^{-1}	–	–	76% after 1000 cycles	[14]
β-Ni $(OH)_2$/(Ni-CNT)	1807 at 2 A g^{-1}	–	–	98% after 2000 cycles	[20]
Mesoporous Ni–Co oxy-hydroxide	636	17	1.6	–	[23]
3D porous nano-Ni/$Co(OH)_2$ nanoflake	1920 at 40 A g^{-1}	80	11	Good stability after 2000 cycles	[21]
Ni–Co hydroxide nanorod array	456	12.8	–	91% after 1000 cycles	[24]
α-phase Ni–Co hydroxides/(Ni foam)	2286.7 at 1 A g^{-1}	–	–	83.7% after 2000 cycles	[25]
α-phase Ni–Co hydroxides	1600 at 1 A g^{-1}	–	–	94% after 1000 cycles	[22]

(continued)

Table 1 (continued)

Electrode/(Substrate)	SC (F/g)	E (Wh/kg)	P (Kw/kg)	Cycle stability	References
$NiCo_2O_4$ NWA @$NiCo(OH)_2$/(Ni foam)	2890 at 0.625 A g^{-1}	45.83	2.5	94.66% after 5000 cycles	[26]
Ni–Co–Mn Hydroxide nanoneedles (Plasma-grown graphitic petals)	1400	30	39	95% after 3000 cycles	[27]
$Ni(OH)_2$ @$Ni_3(HITP)_2$@CNTY	496	49.8	340.0	90.9% after 10,000 cycles	[32]
Ni–Fe–Co hydroxides/N-doped carbon nanoplate/(Ni foam)	1849	31.5	–	92.2% after 5000 cycles	[33]

(Ni–Co LDH@NG) sheets. This hybrid had a particular composition involving considerably active positive, host ions, and charge-balancing counter anions (Cl^- and CO_3^{2-}) to stabilize the structure and solvation molecules that can boost the deep diffusion of electrolyte ions and provide the use of more redox sites. This hybrid had a single crystalline nature, and hence greatly orientated structure, improved the effective electron transport from the redox site to the current collector. Also, the excellent restriction of Ni–Co LDH nanostructures in NG sheets enhanced their final conductivity and structural stability. NG sheets effectively increased electronic and mass transport by creating a more excellent conductive template. Consequently, using Ni–Co LDH@NG promoted performance compared to some previously reported Ni–Co LDH. It indicated SC = 2925 F/g and a remarkable rate capability (90% capacitive retention during 10,000 successive cycles) [39].

8.1 Aluminum Based LDHs

Some LDHs, such as cobalt aluminum LDHs (Co–Al LDHs), nickel aluminum LDHs (Ni–Al LDHs), Ni–Co–Al LDHs, and their composites with greatly conductive matrixes such as graphene, CNT, and polymers were reported to indicate high capacitive performances. The morphology and phase transformation of Co–Al LDHs nanoplates were examined in the alkali solutions with high concentrations. The process depended on time, during which Co–Al LDHs were slowly transformed to β-$Co(OH)_2$ and CoOOH, and the structure changed to greatly porous. This phenomenon

could happen via the dissolution of the Al atoms of Co–Al LDHs, Co atom recrystallization, and further Co oxidation. It was revealed that the pseudocapacitive properties of the prepared materials changed with the soaking time (1–72 h), and a low soaking time resulted in a proper SC = 1123 F/g and good rate capability. Nevertheless, the formation of CoOOH (at a high immersion time) remarkably decreased the electrochemical performance [40].

8.2 Modification of LDHs

Previous research has exhibited that LDH materials with larger surface area and active sites indicate good theoretical capacitance. Nevertheless, their low conductivity and the random dopants dispersions, particularly with some conductive materials, intensively prevent their contractions with the active sites of electrolyte ions. Recently, nitrogen, oxygen, phosphorus, or cobalt vacancies were confirmed to significantly promote electrode redox activity via the enhanced electron distribution density, and electronic structure charge. Combination with heteroatom results in excellent redox activity and adjustment of electronic distribution configuration and thus indicate acceptable pseudocapacitive behaviors. Cobalt phosphide (CoP), known as an efficient dopant, is a kind of p-type semiconductor. The contact of the CoP with the transition metal LDH (as an n-type semiconductor) creates a p–n junction and shifts the energy levels to a thermal equilibrium state. In addition, transition metal LDH with positive charges is conducive to adsorbing charged electrolyte ions which enhances the subsequent redox reaction processes. According to mentioned explanation, an electrode based on a 3D structure hybrid containing CoP and Ni–Al LDH was synthesized on the carbon cloth (Ni–Al LDH/CoP/CC). It noticeably improved conductivity and included proper adsorption energy, which was effective in pseudocapacitive performances. Thus, the prepared electrode exhibited a proper SC = 1822.6 F/g, and excellent stability after 8000 cycles (95.3% capacitance retention). Also, it showed E = 182 Wh/kg, and P = 300 W/kg [41].

2D nanosheets of $Co(OH)_2$ and LDH have been known as proper pseudocapacitive electrode materials with a great E value in the aqueous medium. Cobalt-based LDHs compounds can be simply prepared. They provide fast guest ion insertion/desertion reactions due to high interlayer space. Nevertheless, these kinds of electrode materials can be simply dissolved and degraded in the high pH solutions during the cycling process, resulting in reducing cycle stability. Numerous researchers have reported synthesis and surface modification of the Co–Al LDH arrays on different conductive matrixes to develop the SC value and rate capability. However, the operation of Co–Al LDH was limited by the poor kinetics for charge distribution, leading to low stability at great current density. The most essential factor known for its high-rate capability is the chemical structure stability of electrode materials. According to this view, Cha et al. [42] introduced a composite of the core–shell nanostructure of metal sulfide and hydroxide using a wet-chemical surface modification procedure. Surface chemical reactions are used for complex nanostructures while preserving the

structure and nanometer size of the starting materials. The surface of the Co–Al LDH nanostructure was modified by cobalt sulfide (CoS) layers having a proper capacitive performance in alkaline electrolytes. The composition of Al^{2+} and Co^{3+} in the LDH hydroxide sheets inhibited phase conversion from α to β phase for $Co(OH)_2$ at the time of the charging/discharging process. In addition, a robust CoS shell prevented the collapse and decomposition of the Co–Al LDH in the alkali electrolyte. The prepared core–shell structured LDH electrode enhanced the cycle stability with SC = 2700 F/g for 4000 corneous cycles [42]. Some other researchers have investigated the surface modification of Co–Al LDHs nanostructure using inorganic materials, e.g., MnO_2, $Ni(OH)_2$, and platinum nanoparticles [42]. A composite of Co–Al LDH@MnO_2 nanowire was reported with the SC = 1837.8 F/g and proper stability (91.8% capacitive retention after 5000 continuous cycles) [43]. Table 2 summarizes the mentioned studies and some other examples [43–51].

Table 2 Some pseudocapacitive electrode materials based on LDHs

Electrode/(Substrate)	SC ($F \cdot g^{-1}$)	E (Wh kg^{-1})	P (Kw kg^{-1})	Cycle stability	Ref.
Zn–Co LDH nanosheets/(Ni foam)	3946.5 at 3 A g^{-1}	114.8	643.8	81% after 5000 cycles	[38]
Ni–Co LDH/(N-doped graphene)	2925 at 1 A g^{-1}	52	3191	90% after 10,000 cycles	[39]
Ni–Al LDH/CoP/(carbon cloth)	1822 at 0.5 A g^{-1}	182	300	95.3% after 8000 cycles	[41]
Core–shell CoS/Co–Al LDH/(Ni foam)	1503 at 2 A g^{-1}	–	–	–	[42]
Ni–Al LDH @MnO_2 NW	1837.8 at 1 A g^{-1}	–	–	91.8% after 5000 cycles	[43]
Hierarchical Ni–Al LDH/MWCNT/(Nickel foam)	1293 F cm^{-2} at 5 mA cm^{-2}	–	–	83% after 1000 cycles	[44]
Ni–Ti LDH films/(Nickel foam)	10.37 F cm^{-2} at 5 mA cm^{-2}	–	–	86% after 1000 cycles	[45]
Ni–Al LDH	2128 at 1 A g^{-1}	-	-	-	[46]

(continued)

Table 2 (continued)

Electrode/ (Substrate)	SC ($F \cdot g^{-1}$)	E ($Wh\ kg^{-1}$)	P ($Kw\ kg^{-1}$)	Cycle stability	Ref.
3D Mn-Ni LDH/ (graphene)	2219 at 0.73 A g − 1	47.29	7473	90% after 1400 cycles	[47]
Co–Fe LDH	456 at 2 A g − 1	–	–	–	[48]
Sandwich-like nanocomposite Co–Ni–Al LDH growth one both sides of RGO (RGO(X)@ Co–Ni–Al LDH,	1866 at 1 A/g	–	–	100% after 5000 cycles	[49]
PEDOT@ Ni–Co LDH/(Carbon cloth)	1508 at 1 A g^{-1}	77.1	750	90.1% after 10,000 cycles	[50]
Zn–Co@ Ni–Co LDH/(3D graphene foam)	7485 $mF \cdot cm^2$ at 5 mV s^{-1},	1202 $mWhcm^{-2}$	–	108% after 5000 cycles	[51]

References

1. G. Xiong, K. Hembram, R.G. Reifenberger, T.S. Fisher, MnO_2-coated graphitic petals for supercapacitor electrodes. J. Power Sourc. **227**, 254–259 (2013)
2. H.Y. Lee, S.W. Kim, H.Y. Lee, Expansion of active site area and improvement of kinetic reversibility in electrochemical pseudocapacitor electrode. Electrochem. Solid-State Lett. **4**, A19 (2001)
3. X. Cai, S.H. Lim, C.K. Poh, L. Lai, J. Lin, Z. Shen, High-performance asymmetric pseudocapacitor cell based on cobalt hydroxide/graphene and polypyrrole/graphene electrodes. J. Power Sourc. **275**, 298–304 (2015)
4. D.-D. Zhao, S.-J. Bao, W.-J. Zhou, H.-L. Li, Preparation of hexagonal nanoporous nickel hydroxide film and its application for electrochemical capacitor. Electrochem. Commun. **9**, 869–874 (2007)
5. D.-S. Kong, J.-M. Wang, H.-B. Shao, J.-Q. Zhang, C. Cao, Electrochemical fabrication of a porous nanostructured nickel hydroxide film electrode with superior pseudocapacitive performance. J. Alloy. Compd. **509**, 5611–5616 (2011)
6. A. Shaikh, B.K. Singh, K. Purnendu, P. Kumari, P.R. Sankar, G. Mundra, S. Bohm, Utilization of the nickel hydroxide derived from a spent electroless nickel plating bath for energy storage applications. RSC Sustain. (2023)
7. P.E. Lokhande, K. Pawar, U.S. Chavan, Chemically deposited ultrathin α-$Ni(OH)_2$ nanosheet using surfactant on Ni foam for high performance supercapacitor application. Mater. Sci. Energy Technol. **1**, 166–170 (2018)
8. X. Xiong, D. Ding, D. Chen, G. Waller, Y. Bu, Z. Wang, M. Liu, Three-dimensional ultrathin $Ni(OH)_2$ nanosheets grown on nickel foam for high-performance supercapacitors. Nano Energy **11**, 154–161 (2015)
9. A.V. Radhamani, M.K. Surendra, M.S.R. Rao, Tailoring the supercapacitance of Mn_2O_3 nanofibers by nanocompositing with spinel-$ZnMn_2O_4$. Mater. Des. **139**, 162–171 (2018)
10. R.M. Obodo, N.M. Shinde, U.K. Chime, S. Ezugwu, A.C. Nwanya, I. Ahmad, M. Maaza, P.M. Ejikeme, F.I. Ezema, Recent advances in metal oxide/hydroxide on three-dimensional nickel

foam substrate for high performance pseudocapacitive electrodes. Curr. Opin. Electrochem. **21**, 242–249 (2020)
11. H.B. Li, M.H. Yu, X.H. Lu, P. Liu, Y. Liang, J. Xiao, Y.X. Tong, G.W. Yang, Amorphous cobalt hydroxide with superior pseudocapacitive performance. ACS Appl. Mater. Interfaces **6**, 745–749 (2014)
12. M.C. Bernard, R. Cortes, M. Keddam, H. Takenouti, P. Bernard, S. Senyarich, Structural defects and electrochemical reactivity of β-$Ni(OH)_2$. J. Power Sourc. **63**, 247–254 (1996)
13. Z. Tian, C. Liang, J. Liu, H. Zhang, L. Zhang, Reactive and photocatalytic degradation of various water contaminants by laser ablation-derived SnO_x nanoparticles in liquid. J. Mater. Chem. **21**, 18242–18247 (2011)
14. D. Liang, S. Wu, J. Liu, Z. Tian, C. Liang, Co-doped Ni hydroxide and oxide nanosheet networks: laser-assisted synthesis, effective doping, and ultrahigh pseudocapacitor performance. J. Mater. Chem. A **4**, 10609–10617 (2016)
15. Y.J. Mai, J.P. Tu, X.H. Xia, C.D. Gu, X.L. Wang, Co-doped NiO nanoflake arrays toward superior anode materials for lithium ion batteries. J. Power Sourc. **196**, 6388–6393 (2011)
16. X. Liu, R. Ma, Y. Bando, T. Sasaki, A general strategy to layered transition-metal hydroxide nanocones: tuning the composition for high electrochemical performance. Adv. Mater. **24**, 2148–2153 (2012)
17. X. Ma, J. Liu, C. Liang, X. Gong, R. Che, A facile phase transformation method for the preparation of 3D flower-like β-$Ni(OH)_2$/GO/CNTs composite with excellent supercapacitor performance. J. Mater. Chem. A **2**, 12692–12696 (2014)
18. Z. Lu, Z. Chang, W. Zhu, X. Sun, Beta-phased $Ni(OH)_2$ nanowall film with reversible capacitance higher than theoretical Faradic capacitance. Chem. Commun. **47**, 9651–9653 (2011)
19. G. Lee, C.V. Varanasi, J. Liu, Effects of morphology and chemical doping on electrochemical properties of metal hydroxides in pseudocapacitors. Nanoscale **7**, 3181–3188 (2015)
20. X. Ma, Y. Li, Z. Wen, F. Gao, C. Liang, R. Che, Ultrathin β-$Ni(OH)_2$ nanoplates vertically grown on nickel-coated carbon nanotubes as high-performance pseudocapacitor electrode materials. ACS Appl. Mater. Interfaces. **7**, 974–979 (2015)
21. X.H. Xia, J.P. Tu, Y.Q. Zhang, Y.J. Mai, X.L. Wang, C.D. Gu, X.B. Zhao, Three-dimentional porous nano-Ni/$Co(OH)_2$ nanoflake composite film: a pseudocapacitive material with superior performance. J. Phys. Chem. C **115**, 22662–22668 (2011)
22. D. Xia, H. Chen, J. Jiang, L. Zhang, Y. Zhao, D. Guo, J. Yu, Facilely synthesized α phase nickel–cobalt bimetallic hydroxides: Tuning the composition for high pseudocapacitance. Electrochim. Acta **156**, 108–114 (2015)
23. H.-Y. Hsu, K.-H. Chang, R.R. Salunkhe, C.-T. Hsu, C.-C. Hu, Synthesis and characterization of mesoporous Ni–Co oxy-hydroxides for pseudocapacitor application. Electrochim. Acta **94**, 104–112 (2013)
24. R.R. Salunkhe, K. Jang, S. Lee, H. Ahn, Aligned nickel-cobalt hydroxide nanorod arrays for electrochemical pseudocapacitor applications. RSC Adv. **2**, 3190–3193 (2012)
25. H. Chen, J. Jiang, L. Zhang, Y. Zhao, D. Guo, Y. Ruan, D. Xia, One-pot fabrication of layered α-phase nickel-cobalt hydroxides as advanced electrode materials for pseudocapacitors. ChemPlusChem. **80**, 181–187 (2015)
26. Y. Zhang, Z. Shi, L. Liu, Y. Gao, J. Liu, High conductive architecture: bimetal oxide with metallic properties@ bimetal hydroxide for high-performance pseudocapacitor. Electrochim. Acta **231**, 487–494 (2017)
27. G. Xiong, P. He, L. Liu, T. Chen, T.S. Fisher, Plasma-grown graphene petals templating Ni–Co–Mn hydroxide nanoneedles for high-rate and long-cycle-life pseudocapacitive electrodes. J. Mater. Chem. A **3**, 22940–22948 (2015)
28. G. Xiong, K. Hembram, D.N. Zakharov, R.G. Reifenberger, T.S. Fisher, Controlled thin graphitic petal growth on oxidized silicon. Diam. Relat. Mater. **27**, 1–9 (2012)
29. C. Choi, H.J. Sim, G.M. Spinks, X. Lepró, R.H. Baughman, S.J. Kim, Elastomeric and dynamic MnO_2/CNT core–shell structure coiled yarn supercapacitor. Adv. Energy Mater. **6**, 1502119 (2016)

30. M. Zhi, C. Xiang, J. Li, M. Li, N. Wu, Nanostructured carbon–metal oxide composite electrodes for supercapacitors: a review. Nanoscale **5**, 72–88 (2013)
31. D.Y. Lee, S.J. Yoon, N.K. Shrestha, S.-H. Lee, H. Ahn, S.-H. Han, Unusual energy storage and charge retention in Co-based metal–organic-frameworks. Microporous Mesoporous Mater. **153**, 163–165 (2012)
32. K. Zhang, Q. Xu, X. Liu, J. Zhang, Y. Xu, M. Zhou, J. Li, M. Du, X. Qian, B. Xu, A ship-in-a-bottle architecture transmission metal hydroxides@ conducting MOF on carbon nanotube yarn for ultra-stable quasi-solid-state supercapacitors. J. Mater. Chem. A (2023)
33. W. Liu, X. Hu, H. Li, H. Yu, Pseudocapacitive Ni–Co–Fe Hydroxides/N-doped carbon nanoplates-based electrocatalyst for efficient oxygen evolution. Small **14**, 1801878 (2018)
34. P. Sun, R. Ma, X. Bai, K. Wang, H. Zhu, T. Sasaki, Single-layer nanosheets with exceptionally high and anisotropic hydroxyl ion conductivity. Sci. Adv. **3**, e1602629 (2017)
35. M.A. Woo, M.-S. Song, T.W. Kim, I.Y. Kim, J.-Y. Ju, Y.S. Lee, S.J. Kim, J.-H. Choy, S.-J. Hwang, Mixed valence Zn–Co-layered double hydroxides and their exfoliated nanosheets with electrode functionality. J. Mater. Chem. **21**, 4286–4292 (2011)
36. J. Yingchang, S. Yun, L. Yanmei, T. Wenchao, P. Zhichang, Y. Peiyu, L. Yuesheng, G. Qinfen, H. Linfeng, Charge transfer in ultrafine LDH nanosheets/graphene interface with superior capacitive energy storage performance (2017)
37. H. Chen, L. Hu, M. Chen, Y. Yan, L. Wu, Nickel–cobalt layered double hydroxide nanosheets for high-performance supercapacitor electrode materials. Adv. Func. Mater. **24**, 934–942 (2014)
38. Z. Pan, Y. Jiang, P. Yang, Z. Wu, W. Tian, L. Liu, Y. Song, Q. Gu, D. Sun, L. Hu, In situ growth of layered bimetallic ZnCo hydroxide nanosheets for high-performance all-solid-state pseudocapacitor. ACS Nano **12**, 2968–2979 (2018)
39. N. Mahmood, M. Tahir, A. Mahmood, W. Yang, X. Gu, C. Cao, Y. Zhang, Y. Hou, Role of anions on structure and pseudocapacitive performance of metal double hydroxides decorated with nitrogen-doped graphene. Sci. China Mater. **58**, 114–125 (2015)
40. T. Xu, X. Wu, Y. Li, W. Xu, Z. Lu, Y. Li, X. Lei, X. Sun, Morphology and phase evolution of CoAl layered double hydroxides in an alkaline environment with enhanced pseudocapacitive performance. ChemElectroChem. **2**, 679–683 (2015)
41. X. Wu, Z. Zhao, B. Huang, 0CoP-Doped nickel aluminum double hydroxide as superior electrode for boosting pseudocapacitive storage. Electrochim. Acta **361**, 137092 (2020)
42. J. Cha, E.B. Park, S.W. Han, Y.D. Kim, D. Jung, Core-shell structured cobalt sulfide/cobalt aluminum hydroxide nanosheet arrays for pseudocapacitor application. Chem.—Asian J. 14 (2019) 446–453.
43. X. Hao, Y. Zhang, Z. Diao, H. Chen, A. Zhang, Z. Wang, Engineering one-dimensional and two-dimensional birnessite manganese dioxides on nickel foam-supported cobalt–aluminum layered double hydroxides for advanced binder-free supercapacitors. RSC Adv. **4**, 63901–63908 (2014)
44. B. Wang, G.R. Williams, Z. Chang, M. Jiang, J. Liu, X. Lei, X. Sun, Hierarchical NiAl layered double hydroxide/multiwalled carbon nanotube/nickel foam electrodes with excellent pseudocapacitive properties. ACS Appl. Mater. Interfaces. **6**, 16304–16311 (2014)
45. Y. Gu, Z. Lu, Z. Chang, J. Liu, X. Lei, Y. Li, X. Sun, NiTi layered double hydroxide thin films for advanced pseudocapacitor electrodes. J. Mater. Chem. A **1**, 10655–10661 (2013)
46. G. Li, X. Zhang, D. Qiu, Z. Liu, C. Yang, C.B. Cockreham, B. Wang, L. Fu, J. Zhang, B. Sudduth, Tuning Ni/Al ratio to enhance pseudocapacitive charge storage properties of nickel–aluminum layered double hydroxide. Adv. Electron. Mater. **5**, 1900215 (2019)
47. I. Lee, G.H. Jeong, S. An, S.-W. Kim, S. Yoon, Facile synthesis of 3D MnNi-layered double hydroxides (LDH)/graphene composites from directly graphites for pseudocapacitor and their electrochemical analysis. Appl. Surf. Sci. **429**, 196–202 (2018)
48. X. Ge, C.D. Gu, X.L. Wang, J.P. Tu, Ionothermal synthesis of cobalt iron layered double hydroxides (LDHs) with expanded interlayer spacing as advanced electrochemical materials. J. Mater. Chem. A **2**, 17066–17076 (2014)
49. P. Huang, C. Cao, Y. Sun, S. Yang, F. Wei, W. Song, One-pot synthesis of sandwich-like reduced graphene oxide@ CoNiAl layered double hydroxide with excellent pseudocapacitive properties. J. Mater. Chem. A **3**, 10858–10863 (2015)

50. J. Zou, J. Zou, W. Zhong, Q. Liu, X. Huang, Y. Gao, L. Lu, S. Liu, PEDOT coating boosted NiCo-LDH nanocage on CC enable high-rate and durable pseudocapacitance reaction. J. Electroanal. Chem. **928**, 117069 (2023)
51. D.S. Patil, S.A. Pawar, J.C. Shin, H.J. Kim, Layered double hydroxide based on ZnCo@ NiCo-nano-architecture on 3D graphene scaffold as an efficient pseudocapacitor. J. Power Sourc. **435**, 226812 (2019)

Pseudocapacitance in Double Perovskite Material

Mostafa M. Omran, Ahmed I. Abdel-Salam, Delvin Aman, and Saad G. Mohamed

Abstract Double perovskite materials (DPMs) with the formula of $A_2BB'O_6$ have gained much attention as supercapacitor materials due to their compositional characteristics that improve the properties of conventional perovskite structure ABO_3 to gain higher electroactivity, conductivity, and faradic redox activity, in addition to their conventional structural stability. These advanced properties recently made DPMs promising materials for supercapacitor application, and they could show relatively high specific capacitance and specific energy density (E_d) at high specific power density (P_d). At the beginning of this chapter, the DPMs will be introduced in detail from a chemical perspective to address their chemical composition, common morphology, electrochemical characteristics, and the effect of oxygen intercalation on their electrochemical properties. Then, the electrochemical energy storage mechanism in DPMs will be discussed from the electrochemical interactions point of view, and the pseudocapacitive behavior will be explained through simple kinetics and thermodynamics concepts. After that, the recent developments in DPMs design and the correlation between the structural improvements and the change in the pseudocapacitance performance will be addressed. Finally, the pros and cons of using double perovskite as pseudocapacitive material will be discussed alongside future developments and directions in this type of pseudocapacitive material.

Keywords Double perovskite · Pseudocapacitance · Charge-storage mechanism · Cation leaching · Supercapacitor

M. M. Omran
Chemistry Department, Faculty of Science, Cairo University, Giza 12613, Egypt

A. I. Abdel-Salam
Nanotechnology Research Centre (NTRC), The British University in Egypt (BUE), El-Shorouk City, Suez Desert Road, Cairo 11837, Egypt

D. Aman
Catalysis Laboratory, Refining Department, Egyptian Petroleum Research Institute (EPRI), Nasr City, Cairo 11727, Egypt

S. G. Mohamed (✉)
Mining and Metallurgy Engineering Department, Tabbin Institute for Metallurgical Studies (TIMS), Tabbin, Helwan 11421, Egypt
e-mail: saadmohamed@tims.gov.eg

© The Author(s), under exclusive license to Springer Nature Switzerland AG 2024

R. K. Gupta (ed.), *Pseudocapacitors*, Engineering Materials,
https://doi.org/10.1007/978-3-031-45430-1_8

1 Introduction

After tens of years of research and investigating new materials for supercapacitors to fill the gap of the low specific power of batteries without losing their advantage as a high energy density (E_d) charge storage system, it is still unclear if this gap is fulfilled successfully [1]. Naturally, the supercapacitor is the most promising candidate to achieve such a goal; however, more efforts and new material investigations are still required, despite the huge efforts that have been paid to improve the specific energy of supercapacitors at the high specific power values [2]. Pseudocapacitive material moved the supercapacitor an extra mile toward increasing the specific energy of supercapacitors at moderated specific power values by combining both characteristics of regular electrical double-layer capacity (EDLC) supercapacitor as a high-power materials and redox batteries as an energy-dense material; however, a further improvement is needed to further increase the E_d of supercapacitors at the high-power density (P_d) [3].

Among the wide variety of newly designed materials for supercapacitor applications (especially pseudocapacitive materials) to acquire higher energy-density supercapacitors, perovskite oxides showed themselves as an exceptionally promising material as an open research area that can open horizons to new strategies and directions which can bring our needs of high energy-dense supercapacitors with the required high power-density. Perovskite oxides with the structure of ABO_3 are a great family of chemical structures, where A and B are different cations with relative atomic radios that allow for highly ordered crystal structure formations. These perovskite oxides are well known for their high conductivity, chemical stability, and relatively thermal stability. Perovskite oxides were intensively investigated as pseudocapacitive electrode material for several years and recorded exceptional capacitive properties; however, the relatively limited stability was a challenge due to cation leaching in the aqueous electrolytes, which prevented perovskite oxides from being further used as the future electrode material for supercapacitors [2, 4]. Several improvements have been made to perovskite oxides to improve their stability by composite formation with carbon-based materials, structural defects or oxygen vacancies creation, or oxygen substitution with halides, which successfully improved perovskite stability; however, another improvement opportunity of perovskite oxides has been explored by discovering new crystal structures of perovskite oxide like layered and columnar double perovskite, triple perovskite, quadruple perovskite, which seemed to be promising investigation area for improving the stability properties of single perovskite oxides [5, 6].

DPMs can be considered as an updated branch of the single perovskite materials with a different chemical structure of $ABB'O_6$, where A, B, and B′s are different cations, where A and both B and B′ have a relative atomic radius, while B and B′ should have a close atomic radius. This variation in B-site atoms initiates a variation in the internal interactions that leads to different properties [2]. A study has been made to found that in mixed cation perovskite $Pb(ZnNb)O_3$, the highly ordered B-site tends to be a slightly covalent structure, which is expected to enhance the cationic leaching

assessment and increase the electrochemical stability [7]. DPMs showed themselves as high E_d materials due to the variety of available charge storage pathways; a slight improvement in DPMs stability has been achieved through a controlled synthetic approach that keeps the high ordering of the mixed A-site and B-site cations; however, a further improvement could be made in this area due to the limitation of the intensive investigation of this kind of materials.

To understand exactly the right way to further discover more promising pseudocapacitive DPMs, these materials' chemical, and physical nature should be addressed alongside the state-of-the-art. In this chapter, the chemistry of DPMs, including the synthetic methodologies and their structural and electrochemical properties, will be clearly stated with useful refers to the previous work that has been made in this research area, the latest improvement methodologies and their outputs will be covered, and finally, the current challenges and future recommendations are addressed to ensure that this chapter is covering this research area from all aspects the of importance to researchers who are interested in pseudocapacitive materials in general.

1.1 Advances in Double Perovskite Materials

1.1.1 DPMs Characteristics and Properties

Single perovskites have been widely recognized as cost-effective pseudocapacitive materials. Their chemical composition is characterized by a nominal formula of ABO_3, where B site cations and O anions form share-corner BO_6 octahedral structures, while A cations occupy the 12-fold coordinated sites within the cavity formed by eight BO_6 octahedrons. The chemical composition of single perovskites can be easily adjusted using a wide variety of elements, which makes them highly customizable and easily doped perovskite structures [8]. In 1951, Steward and Rooksby discovered DPMs, which can be represented by the general formula $AA'BB'O_6$. These oxides are derived from the doped ABO_3 perovskite structure ($A_{1-x}A'_xB_{1-y}B'_yO_3$) and exhibit an extended super-lattice framework [9].

Over the years, extensive research has been conducted on DPMs due to their favorable characteristics, including high oxygen surface exchange kinetics, fast oxygen ion diffusion rates, and excellent mixed ionic and electronic conductivity at high temperatures. For illustration, if x (or y) in single doped perovskite is approximately 0.5 and A′ and A (or B′ and B) are differing significantly in size and/or charge, ordering of A-site (or B-site) cations can occur in different configurations (Fig. 1). This leads to the formation of a double perovskite, which is more accurately represented by the formula $AA'B_2O_6$ (or $A_2BB'O_6$) [4].

Comparing single-doped disordered perovskite oxide structures, represented by $A_{1-x}A'_xBO_3$ (or $AB_{1-y}B'_yO_3$), with the highly ordered double perovskite oxides structures of the form $AA'BB'O_6$, it was observed that the double perovskite structure minimizes lattice distortion and improves cycling stability. Additionally, the A/A′

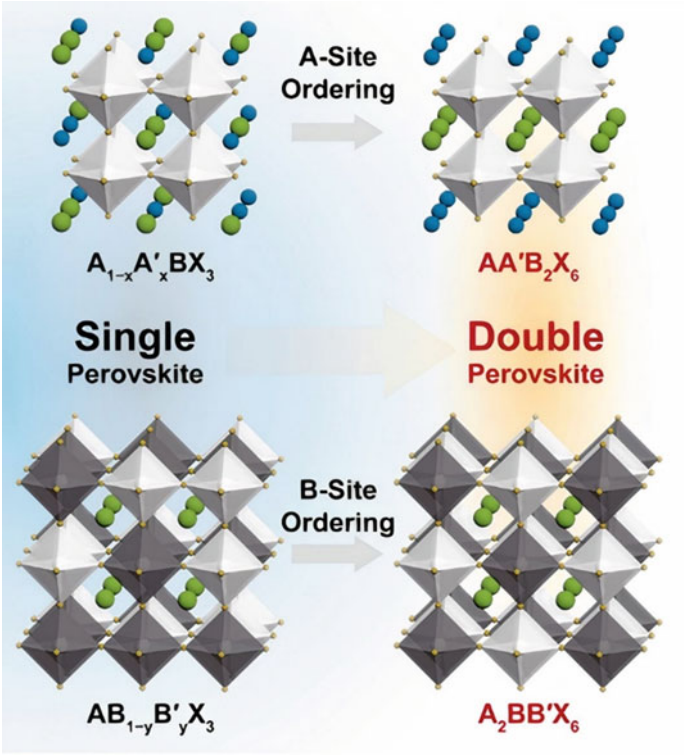

Fig. 1 A diagram illustrating the process of double perovskite formation. Adapted with permission [8], Copyright (2019), Elsevier

ions are bonded to oxygen atoms in a 12-fold coordination, while the B and B′ ions are bonded to oxygen atoms in a sixfold coordination in the layered ordering [10]. In general, the A-site metal plays a crucial role in enhancing thermodynamic stability, while the B-site metal controls the electrochemical reactions. In the context of electrode materials used in supercapacitors (SCs), alkaline-earth metals (such as Sr and Ba) and rare-earth metals (such as La and Sm) are commonly utilized as the primary A-site cations, whereas the B-site cation is typically a transition metal (such as Mn, Co, and Ni) [1].

Four main types of order observed in A-site and B-site ordered DPMs are layered, columnar, and rock-salt (Fig. 2). The resulting ordering pattern has alternating B and B′ patterns that interleave in 3D through the structure. The formula for this perovskite is $A_2BB'X_6$. The valence difference (ΔV) between B and B′ governs the driving force to generate the rock salt pattern, where a random pattern develops when $\Delta V \leq 3$ and the rock salt pattern results when $3 < \Delta V \leq 6$; the layered pattern occurs when $\Delta V = 2$. It has been proposed that the layered pattern is favored by Jahn–Teller distortion of either the BO_6 or $B'O_6$ octahedron. Because of the significant strain

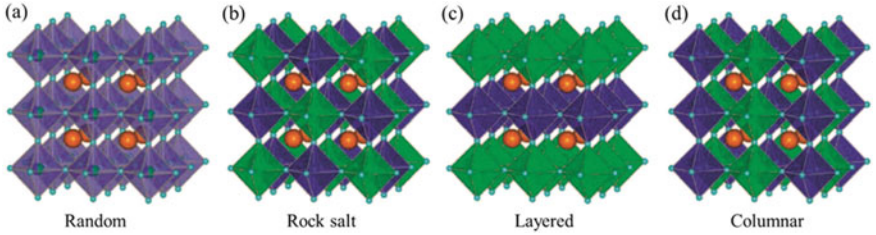

Fig. 2 The potential ordering patterns of BO_6 and $B'O_6$ octahedra in $A_2BB'O_6$ DPMs. The four possible ordering types depicted are **a** random, **b** rock-salt, **c** layered, and **d** columnar Adapted with permission [11], Copyright (2021), the Royal Scocity of Chemistry

between surrounding A cations in the very typical rock salt pattern, ordered B site replacement is more likely than A site ordering [11].

1.1.2 Crystal Structure Stability and Electronic Properties of DPMs

To evaluate the structural stability of $A_2BB'O_6$ double perovskite oxide, similar to a simple perovskite oxide ABO_3, Birch–Murnaghan's equation of state and calculating tolerance factor (τ) by using effective ionic radii, which is based on Goldschmidt's tolerance factor which is defined as

$$\tau = \frac{r_A + r_O}{\sqrt{2}\left[\frac{(r_B + (r_{B'})}{2} + r_O\right]} \tag{1}$$

where a τ tolerance factor, r_A, r_B, and $r_{B'}$ are the average ionic radii of A, B, and B′ ions, respectively, and r_O is the ionic radius of the oxygen anion [12]. The structural changes occurring in the entire $A_2BB'O_6$ family, depending on the value of τ, can be described as follows [6]:

- When t is less than 1.05, a hexagonal structure is preferred.
- In the range of $1.00 < \tau < 1.05$, it is likely that a cubic crystal structure with the *Fm3m* space group is formed.
- For values between $0.97 < \tau < 1.00$, the most probable crystal structure transforms a tetragonal structure with the space group *I4/m*.
- Finally, for τ less than 0.97, the compound tends to adopt either an orthorhombic structure (*Pbnm*) or a monoclinic structure (*P21/n*).

In the case of an ordered $A_2BB'O_6$ oxide with a rock salt-type arrangement of B/B′ cations and a τ value of 1.0, the crystal superstructure can be visualized as two separate perovskite layers, namely ABO_3 and $AB'O_3$, alternating along the [111] direction. Consequently, the lattice constant (a_{DP}) of the super unit cell is twice the size of a single perovskite (a_p), which is why it is referred to as a double perovskite [13]. Also, high stability ($\tau = 1$) depends on the bond nature in perovskite which

is not completely ionic but is partially covalent due to the resistance of π (B–O) bond with σ (A–O) bond and σ (B–O) with σ (B′–O) bond. Increasing the covalent bonding nature can serve as a protective mechanism against the leaching of metals [14]. The variety and unique crystal structure of DPMs can significantly enhance the electrochemical performance of electrodes. The electrical properties of electrodes are crucial for achieving fast kinetics in supercapacitors. DPMs exhibit a wide range of electronic structures, ranging from insulating to half-metallic and, in some cases, fully metallic. This versatility in electronic structures is made possible by the flexible composition framework of perovskite oxides.

For instance, the layered double perovskite structure with A-site ordering facilitates the diffusion of oxygen ions under electrochemical conditions. The stable crystalline structure of perovskite in alkaline electrolyte solutions is advantageous for long-term cycling stability. Therefore, to develop highly capacitive perovskite-based electrodes for oxygen anion intercalation-type supercapacitors, effective strategies encompassing detailed structural and electrochemical characterizations, calculation methods, and fabrication techniques of practical supercapacitors need to be realized. These strategies aim to increase specific capacitance, ensure long-term operational stability, and enhance energy and power densities. Furthermore, expanding the potential windows and specific capacitance will enhance the supercapacitors' E_d [15].

A study by Liu et al. investigated a DPM called $PrBaMn_2O_{6-\gamma}$, which exhibited a cubic phase with a layered structure. This unique structure facilitated the diffusion of oxygen ions and increased the concentration of oxygen vacancies. As a result, the electrode made from this oxide showed exceptional capacitance in supercapacitors [5]. Similarly, in another study by Wang et al., they examined an A site cation-ordered double perovskite oxide called $PrBaCo_2O_{6-\gamma}$. This oxide was utilized as an electrode material for anion intercalation supercapacitors. The perovskite structure of this oxide contained oxygen atoms situated in the Pr^{3+} planes. By removing some or even all of these oxygen atoms, numerous oxygen vacancies were created, significantly enhancing the diffusivity of ions during the electrochemical reaction [16].

1.2 Synthesis Approaches of DPMs

The flexibility of the double perovskite crystal structure gives it exceptional physical and chemical properties. However, there is no consensus on how the synthesis method, ion type and size, and resulting crystalline phases are interrelated. Regarding energy storage applications, the choice of synthesis method depends on the composition of the perovskite, as it affects the dielectric and conductive properties of DPMs [17]. The dielectric properties of materials, such as the orthorhombic Sr_2CeSbO_6 (SCS), are determined by the interplay between cations with varying oxidation states and the oxygen content within the structure [18]. Ba_2LaSbO_6 is a notable example of a perovskite compound that exhibits both chemical stability and a high

dielectric constant, making it suitable for applications as a superconductor in High-Temperature Superconducting (HTS) devices [19]. The discovery of superconductivity in copper-layered perovskites, which were annealed at high temperatures, was first reported by Bednorz and Muller in 1986 [20]. The synthesis methods employed can impact the crystal's superconductivity, as various factors such as structural defects, doping processes, dielectric properties, and ferroelectric characteristics may undergo changes that can influence the overall superconducting behavior [21].

1.2.1 Solid-State Reaction (SSR) Method

The SSR method is commonly used to synthesize DPMs. It involves mixing and high-temperature calcination of oxides or carbonate precursors to form polycrystalline bulk samples. For example, re-based DPM ceramics such as Sr_2FeReO_6 were synthesized by the solid-state method [22]. Rietveld analysis of the XRD data confirms a tetragonal I4/m crystal structure for the SFRO ceramic sample, with an average crystallite size of approximately 50 nm. Superstructural reflections, including the (011) diffraction peak, indicate the presence of long-range Fe/Reordering at the B-site of the SFRO crystal.

Although the solid-state reaction method can produce final products with particles at the nanometer scale, controlling the morphology and crystallite size of the final products becomes challenging, especially using high calcination temperatures [23]. In general, higher temperatures during the synthesis of perovskites result in the formation of a pure phase. However, this also leads to a decrease in surface area [24]. The ionic conductivity of perovskite oxides is affected by the calcination temperature, which in turn influences the densification of atomic packaging and the presence of different crystal coordination phases (such as rhombohedral, tetragonal, and cubic) [21]. Polycrystalline La_2CuMnO_6 double perovskite was synthesized through SSR at 1523 K. X-ray diffraction analysis confirmed orthorhombic symmetry using the *P21/n* space group. The La-O_1 bond length was larger than La-O_2, and Cu-O_2 had a larger bond length than Cu-O_1. Additionally, particle sizes have a known impact on the catalytic behavior in electrochemical reactions. Achieving a balance between specific surface areas, phase structure purity, and low-temperature calcination poses a significant challenge, as these three factors are closely interconnected [25].

1.2.2 Combustion Method

The combustion method is a highly attractive approach for synthesizing nanomaterials due to its self-propagating high-temperature synthesis process. It is favored for its flexibility and cost-effectiveness [26]. La_2CoMnO_6 double perovskite was successfully synthesized using a modified combustion route. X-ray diffraction (XRD) analysis with Rietveld refinement confirms the formation of a monoclinic crystal

structure with the space group P21/n. The Raman active modes of the MnO_6 octahedra correspond to the Jahn–Teller stretching mode (antisymmetric stretching vibrations) and symmetric stretching vibrations, while the breathing mode represents the symmetric stretching vibrations. The electrochemical performance of La_2CoMnO_6 as an electrode material for supercapacitors shows excellent cyclic stability, with 84% capacitance retention after 500 cycles [27].

1.2.3 Hydrothermal Method

The hydrothermal method is a prominent and well-established approach for synthesizing DPMs on the nanoscale. It offers advantages like lower working temperatures compared to the melting point of the reactants, a variety of autoclave options, and adjustable reaction parameters. An innovative Y_2MnCoO_6 double perovskite was synthesized through the hydrothermal process for the first time. In this study, we report on the structural, morphological, and energy-storage properties of Y_2MnCoO_6 double perovskite synthesized through the hydrothermal process. An innovative aspect of our work is the electrochemical investigation of Y_2MnCoO_6, as this composition is being synthesized for the first time using the hydrothermal technique. Powder X-ray diffraction analysis reveals the formation of a cubic crystal phase with Ia (206) symmetry, and the lattice parameters are determined to be $a = b = c = 10.60$ Å in the form of microspheres. The microsphere shape enhances charge movement at the nanoscale, providing a larger surface area for electrochemical reactions to occur. The specific capacitance value was calculated to be approximately 148.0 F/g at a current density of 0.5 A/g, with an impressive retention rate of approximately 85% after 10,000 cycles [28]. Y_2NiMnO_6 nanowires double perovskite, as an active material for the positive electrode in electrochemical supercapacitors prepared by a simple and low-temperature hydrothermal, which offers the advantages of a large active surface area at the nanoscale, thereby enhancing the electrochemical properties of the material. Y_2NiMnO_6 nanowire-based electrodes exhibited higher specific capacitance and cyclability (>1800 cycles), along with a good retention rate of 70.17% [29].

1.2.4 Sol–Gel Method

The sol–gel method finds extensive application in material science for producing solid materials from precursor molecules. This versatile approach enables the straightforward synthesis of various metal oxides, serving as active materials in diverse energy storage devices [30]. A sol–gel method was employed to prepare double perovskite Sr_2CoMoO_6 δ (DP-SCM), which exhibits a desirable rock salt structure with a 0-D arrangement. The presence of both Co and Mo elements in DP-SCM enhances its redox capability, leading to enhanced oxygen mobility. It has a high oxygen vacancy

content which enhances the oxygen anion diffusion rate (2.03×10^{-11} cm^2/s). DP-SCM demonstrates a remarkable capacitance of 747 F/g at 1 A/g accompanied by a notable rate capability of 56% up to 10 A/g [31].

$La_2B(II)MnO_6$ (where B = Cu, Co, Ni) was prepared as an electrode material using the sol–gel method and calcined at a moderate temperature [26]. The bonding force of the units B^{2+}–O–Mn^{4+} was found to weaken in the order of Cu > Ni > Co, as evidenced by the displacement of the stretching vibration Mn–O towards lower frequencies. In the case of LaCuMn, it exhibited a larger particle size and specific surface area, which suggests a favorable influence on the capacitive properties of LaCuMn oxide, which reached 781.25 F/g.

A novel electrode material for supercapacitor applications was developed based on a single-phase double perovskite oxide, Pr_2CrMnO_6. Structural analysis revealed a monoclinic structure with space group P21/n. The sample exhibited bond angle distortion in the form of octahedral tilt. At a current density of 2 A/g, the specific capacitance of the developed single-phase double perovskite oxide (Pr_2CrMnO_6) reached a noteworthy value of 177.4 F/g. This specific capacitance was found to be superior to that of Ni-Mn-based double perovskite oxides [32].

1.2.5 Other Methods

A supercapacitor electrode material consisting of La_2CoNiO_6 inorganic nanofibers was successfully synthesized using a polyvinylpyrrolidone/lanthanum nitrate-cobalt acetate-nickel acetate (PVP/LCN) precursor via electrostatic spinning. They found that the fibers were connected through rhombohedral La_2CoNiO_6 nanoparticles resulting in a linear spatial network structure. The three-electrode and two-electrode systems demonstrated a respectable specific capacitance of 335 and 129.1 F/g, respectively [33]. Enhancing the electrochemical performance of supercapacitor electrodes using the unique structures of double perovskite oxides remains a challenge. In this study, we developed hollow spherical porous La_2CoMnO_6 (HS-LCMO) materials prepared by impregnating carbon spheres as templates, followed by annealing to remove the template, as illustrated in Fig. 3. This method offers advantages such as low cost, simplicity, scalability, and improved electrochemical performance of La_2CoMnO_6. The electrochemical testing of HS-LCMO was compared to a reference sample (SG-LCMO) prepared through the sol–gel method. To broaden the application potential of supercapacitors, HS-LCMO and activated carbon (AC) were assembled into asymmetric supercapacitors, which showed a wide potential window of 2 V and achieved a high E_d. Furthermore, the supercapacitor devices maintained approximately 89.2% of the initial capacitance after 3000 cycles, indicating good cycling stability. This method offers the potential to simplify the synthesis of perovskite oxides and enhance the electrochemical performance of perovskite hollow spheres [34].

Fig. 3 Preparation flowchart of hollow spherical porous La_2CoMnO_6. Adapted with permission [34], Copyright (2020), Elsevier

2 Electrochemistry of DPMs

DPMs are considered one of the cheapest electrochemically active materials thanks to their highly ordered crystal structure, high conductivity, and electrochemical stability, like most perovskite materials. This electrochemical activity made DPM good candidates for various electrochemical applications like supercapacitors, lithium-ion batteries, and solar water splitting. In this section, the electrochemical activity of DPMs will be discussed and clarified from the pseudocapacitance point of view; this section aims to understand the mechanism of charge storage based on thermodynamic and kinetic aspects.

2.1 Charge Storage Mechanism

The highly ordered hierarchically structured DPM allows for the EDLC to occur, and the electrolytic anions (i.e., OH^-) can easily diffuse into the internal crystal structure to be accumulated electrostatically on the internal crystal surface of DPM. However, the specific surface area of DPMs is not high enough. It is rare to find DPM with

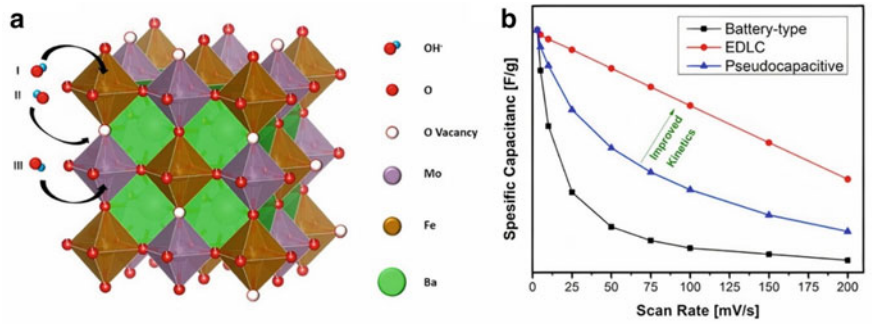

Fig. 4 **a** Demonstrates the probable charge storage mechanism in DPMs and **b** illustrates the different kinetics of different electrode material types

a specific surface area exceeding a few tens or hundreds of m^2/g, which leads to a low gravimetric EDLC in comparison to carbonaceous materials. Faradic current is the other form in which the charge can be stored in DPMs, which can be a result of several electrode/electrolyte chemical interactions. Transition metals in the DPM chemical structure are well known for their redox ability.

Pseudocapacitance is the common behavior of DPMs, especially in redox-active electrolytes (i.e., Potassium Hydroxide) due to a large number of vacancies for oxygen intercalation and transition metals redox interactions alongside the EDLC behavior (Fig. 4). The presence of oxygen vacancies is well known with the dramatic enhancement of charge storage capacity; however, the high degree of lattice distortion can lead to the cationic leaching effect, especially in aqueous electrolytes. Again, thanks to the mixed ionic structure of DPM, that enhances their electrochemical stability and subsequently provide a wider stable potential widow. In general, perovskite materials suffer from low specific surface area and low EDLC contribution in the charge storage cycle; however, the cationic leaching effect in aqueous electrolytes enhances the capacity of perovskite material during the early cycling, which is known to most researchers as an activation process, in which the surface cations are leached in electrolyte and increase the surface distortion leading for a higher exposed surface to the electrolyte. In DPMs, the cationic leaching is quite controlled by the mixed ionic lattice structure, allowing for the activation process to be carried out without further destruction of the crystal structure.

2.2 Electrochemical Stability and Reversibility

The electrochemical stability of DPMs can be the main reason for considering them as an upgrade of single perovskite materials that suffer from electrochemical instability due to cationic leaching. However, the electrochemical stability of DPMs will be discussed in this section from the thermodynamics point of view. The electrode

material can be described as thermodynamically stable and reversible when the reactions (faradic) that occur on the electrode surface or inside the electrode bulk are defined as reversible redox reactions, which in this case, the redox reaction is running smoothly in the two reversed direction with the same kinetics and quantities. Thermodynamic stability could be achieved in simple reversible redox reaction couple, but it is rarely found as 100% reversible in complicated systems such as perovskite materials that involve several reactions with different dynamics at the same time. However, the more enhanced thermodynamic stability of the electrode material in an electrochemical system is highly desired, which practically means longer life cycle stability for the electrochemical system.

Anuj Kumar Tomar et al. prepared $Sr_2CoMoO_{6-\delta}$ double perovskite electrode material which exhibited about 70 mV redox peak separation in KOH electrolyte at 10 mV/s scan rate, which can be considered a high degree of thermodynamic stability, which led to higher cycling stability for the fabricated device. The capacitance retention started to increase from 100% to about 150% as a result of activation through the cationic surface distortion (mentioned in the previous section) during the first 4,000 cycles and then exhibited a relatively high degree of electrochemical stability at about 150% of capacitance retention during the following 6,000 cycles [2].

The degree of thermodynamic reversibility of any redox reaction couple can be determined through the coulombic efficiency of the current combined in both oxidation and reduction reaction phases. However, in pseudocapacitive material, coulombic efficiency cannot express the thermodynamic stability and reversibility of the electrochemical system due to the EDLC current existence. The coulombic efficiency of the EDLC current is affected by the IR drop and the cumulative resistance in the electrochemical system, which means the redox reaction couple may exhibit a high degree of thermodynamic reversibility, but the overall coulombic efficiency is affected by the EDLC cumulative resistance. So, high coulombic efficiency means a high degree of thermodynamic reversibility, but low coulombic efficiency does not necessarily mean low electrochemical stability of the redox reaction couple in pseudocapacitive material like DPMs. The degree of thermodynamic reversibility of the redox couple in pseudocapacitive material can be determined either by the redox couple peak separation value, which should not exceed 100 mV at a low scan rate for an acceptable degree of reversibility or by narrowing the potential window so the redox reaction couple is completed with the minimum of EDLC current.

2.3 Electrochemical Kinetics

In any electrochemical charge storage system that involves a redox reaction, the reaction kinetics is a critical factor that affects the operation characteristics of that system. For instance, one of the major reasons why supercapacitors got intensively investigated during the past few decades is to enhance the low specific power of batteries, which leads the researchers to combine the characteristics of both battery

(high E_d) and conventional capacitors (high P_d). In a conventional capacitor, there are no chemical reactions, and the only factor that inhibits the flow of current is the material charge transfer resistance, and as the used material in conventional capacitors is metals, the internal resistance is very limited, and the current can flow through the connections freely resulting a high power. Batteries are usually based on reversible electrochemical systems; a redox reaction couple is involved, and the current flow is limited by the electrochemical reaction rate, which is controlled by the chemical reaction kinetics. The faster the kinetic reaction is achieved, the higher P_d can be afforded. EDLC supercapacitors involve no redox reaction, it is only the charge accumulation on the electrode surface, so the specific power of the EDLC-based charge storage system is controlled only by the ionic mobility of the electrolyte and the electrical resistance of the electrode material. Single perovskite and DPMs as pseudocapacitive materials have their power ability limited by both redox reactions' kinetics and EDLC cumulative resistance, which finally determine whether the DPMs have high P_d or not.

For pseudocapacitive materials, it is very complicated to study their reaction kinetics, especially when several types of interactions are involved; however, an easy way to have an idea about the kinetics of the electrode material is to study its capacitive performance at different scan rates of cyclic voltammetry (CV) and current density of galvanic charge and discharge (GCD) between the extremely high and extremely low values. For instance, in Fig. 4b, the CV technique distinguishes the capacitive performance of the kinetics-controlled material and resistance-controlled material. It is quite obvious that in kinetic-controlled materials such as battery-like materials, the quantity of stored charge via redox reactions is increased as much as the reaction time has been prolonged in slow scan rates and vice versa.

In resistance-controlled materials such as EDLC materials, the capacitive performance is affected only by the system resistance, which is constant for the single system, so that the drop in the capacitive performance is almost linear with the scan rate increasing (i.e., faster charge storage and higher currents). In pseudocapacitive materials like DPMs which combine both the kinetic-controlled and resistance-controlled processes, the capacitive performance in CV became in a case between kinetic-controlled and resistance-controlled behaviors and the faster reaction kinetics is achieved for the faradic current in pseudocapacitive material, the more the capacitive performance to be resistance-controlled like, which means a higher P_d could be afforded without a dramatic E_d drop.

2.4 Cation Leaching Assessing

Cationic leaching is a common effect in perovskite materials with the structure of ABO_3 due to its ionic chemical bonding nature. Thus the cations in perovskite materials tend to be leached especially in aqueous alkaline electrolytes, causing surface distortion in the early stage and crystalline dissociation in the late stage. The positive side of the cation leaching of perovskite materials is to increase the reactive surface

area, especially because perovskite materials have a very limited specific surface area, and by increasing the reactive surface area, the capacitive activity gets increased as some kind of activation. However, with the continued cation leaching during charging and discharging cycling, the perovskite material starts to get deactivated due to destroying the perovskite internal crystal structure.

DPMs are considered to be ionic-covalent mixed chemical bonding structures or partially covalent materials due to σ (B-O) bond resistance with σ (B′-O) bond, which prevents the continued leaching of the DPM crystal structure. Another mechanism of cation leaching assessment in DPMs was illustrated by Yagi et al. when they introduced the late transition metal (Cu) as a high valance metal to the earth alkali metal (Ca) to increase the covalency of the crystal structure and assessed the cation leaching effectively [35]. Cation leaching at a very fast rate can be detected using techniques like XRD and XPS, but it is quite difficult to detect cation leaching at slow leaching rates relying on the above-mentioned techniques, especially for DPMs that afford the cation leaching assessment. However, electrochemical techniques could indicate the leaching rate (the total irreversible electrochemical reaction, to be more specific) by comparing the anodic and cathodic currents at a specified narrow potential window. This technique could be effective for stable potential window determination to allow for longer lifetime stability.

3 DPMs as Pseudocapacitive Electrodes

3.1 Double Perovskite Material as Electrode Materials

Several research studies have investigated perovskite oxides as a class of metal oxides because of their high conductivities and rich oxygen vacancies [16]. Due to their unique structures, in which ions are arranged at either the A-site or B-site, DPMs have also piqued the attention of numerous researchers. Generally, Inside the perovskite lattice, cations are typically disorganized and uniformly scattered. However, in other instances, the cations could be arranged in the perovskite lattice as $AA'B_2O_6$ or $A_2BB'O_6$, which could improve the material's physical and chemical properties [1]. For instance, when a simple cubic perovskite with randomly occupied A-sites transfers into a layered crystal structure, the oxygen ion diffusivity increases by orders of magnitude [16]. This section provides a thorough discussion of the numerous DPMs that have been identified as excellent high-rate pseudocapacitive electrode materials.

3.1.1 A-Site Substitution in Double Perovskite

Generally, the B-site transition metal element strongly influences the SC performance of perovskite oxides. The redox process does not directly affect the A-site element,

such as lanthanide and alkaline earth. However, the electronic structure and coordination may be impacted by the A-site cation. When a low-valence cation, such as Sr^{2+} or Ca^{2+}, partially replaces the A-site, additional oxygen vacancies are created, and a significant portion of the transition-metal ions in the B-site is shifted into unstable oxidation states ($B^{m+}/B^{(m+1)}$ + redox pair). As a result, electronic conductivity is increased, and electrochemical performance is enhanced [1, 36].

Liu et al. prepared layered double perovskite structure-based manganite with an equimolar ratio of Pr and Ba elements in the A-site of the structure of $PrBaMn_2O_{6-\delta}$ (r-PBM) using the sol–gel method [5]. The electrochemical performance of the r-PBM structure was investigated in a 3-electrode system using Pt and Hg/HgO as counter and reference electrodes in the presence of 6 M KOH. It revealed a specific capacitance (C_s) value of about 1034.8 F/g at 1 A/g and 791 F/g at 10 A/g with a capacitance retention of about 76.5%, confirming the high-rate capability. Furthermore, it reveals cyclic stability with capacitance retention of about 92.8% after 5000 charge/discharge cycles. Wang et al. replaced the double perovskite manganite structure with a double perovskite cobaltite structure using the same ratio of the Pr and Ba elements in the A-site.

Using the sol–gel approach, they prepared $PrBaCo_2O_{5+\delta}$ (PBCO) double perovskite structure [16]. The electrochemical behavior of the PBCO was investigated in a 3-electrode system through CV, GCD, and cyclic stability. The electrode revealed a high specific capacity (C) value of about 301.6 C/g at 1 A/g, as well as high cyclic stability with capacity retention of about 93.3% after 2000 charge/discharge cycles. They mentioned that the PBCO has outstanding electrochemical behavior due to the excess oxygen vacancies that result from the partial or total removal of oxygen atoms from the Pr^{3+}, which improves the diffusion of oxygen ions and enables the formation of ion channels [37]. Zhong et al. tried to improve the electrochemical behavior of the $PrBaCo_2O_{5+\delta}$ through partial substitution of the Co ion in the B site with the Ni ion by using the sol–gel method [38]. The fabricated electrode from the Ni-doped $PrBaCo_2O_{5+\delta}$ with a doping ratio of 0.4 (PBCN04) revealed outstanding electrochemical characteristics with a C value of about 513.1 C/g at 1 A/g. The assembled device of structure PBCN04//AC includes the positive electrode of PBCN04 and negative electrode of AC, showed an E_d of about 48.3 Wh/kg at a P_d of 20,011.8 W/kg; the CV, GCD, and Ragone plots of the device are shown in Fig. 5 [38].

3.1.2 B-Site Substitution in Double Perovskite

Incorporating oxygen ions into the vacancies necessitates a corresponding change in the oxidation state of the B cation since the charge storage mechanism involves electrochemical processes. Another helpful technique to improve electrochemical performance is B-site doping, which can create oxygen vacancies and increase the stability of the crystal structure [1, 39].

The barium-based DPMs are the best category of double perovskite materials that show high pseudocapacitive performance. Xu et al. synthesized a barium-based

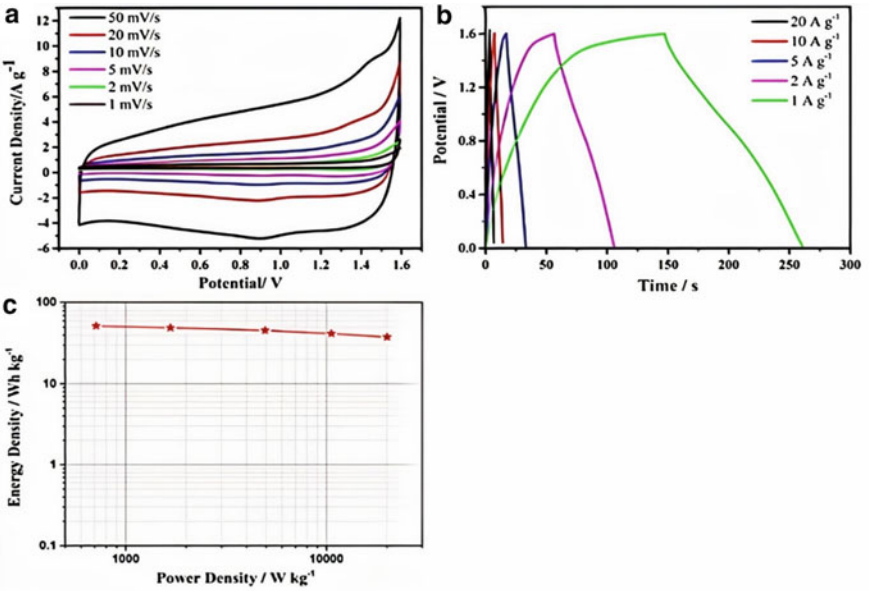

Fig. 5 **a** CV curves of PBCN04//AC, **b** GCD curves of PBCN04//AC at different current densities, **c** Ragone plots of PBCN04//AC. Adapted with permission [38], Copyright (2021), Elsevier

double perovskite structure using Bi, Sc, and Co elements in the B-site with ratios of 0.1:0.2:1.7 to obtain a B-site cation-ordered structure with a composition of $Ba_2Bi_{0.1}Sc_{0.2}Co_{1.7}O_{6-\delta}$ by the sol–gel method [40]. The electrochemical characteristics of the fabricated electrode from the material were evaluated by measuring the CV and GCD; see Fig. 6. It exhibited an outstanding value of C_s of about 1050 F/g at 1 A/g with high cyclic stability and capacity retention of about 74.2% after 3000 charge and discharge cycles. The fabricated device of structure $Ba_2Bi_{0.1}Sc_{0.2}Co_{1.7}O_{6-\delta}$//AC that includes a positive electrode of $Ba_2Bi_{0.1}Sc_{0.2}Co_{1.7}O_{6-\delta}$ and negative electrode of AC showed an E_d of about 70 Wh/kg at a P_d of 787 W/kg, as well as cycling stability of about 70% retention after 2000 charge/discharge cycles. Kumar A. and A. Kumar also synthesized a barium-based double perovskite structure by replacing the Bi and Sc elements in the B-site with Fe elements to obtain a perovskite structure with a composition of $Ba_2FeCoO_{6-\delta}$ [41]. While the fabricated electrode from the $Ba_2FeCoO_{6-\delta}$ revealed a C_s value of about 820 F/g at 3 A/g which is lower than that of the $Ba_2Bi_{0.1}Sc_{0.2}Co_{1.7}O_{6-\delta}$ in the previous study [40].

Multiple research studies have been carried out on the strontium-based double perovskite. Tomar et al. prepared strontium-based double perovskite with a composition of $Sr_2CoMoO_{6-\delta}$ using the sol–gel method [31]. This structure reveals amazing electrochemical behavior with a C_s of 474 F/g at 1 A/g indicating high capacitive performance. Furthermore, the electrode revealed fast kinetics ($\Delta EP \approx 0.013$ V@ 1 mV/s) of charge storage, confirming that there is no phase transition. Figure 7 exhibited the CV and GCD of the fabricated electrode. Moreover, a symmetric device was

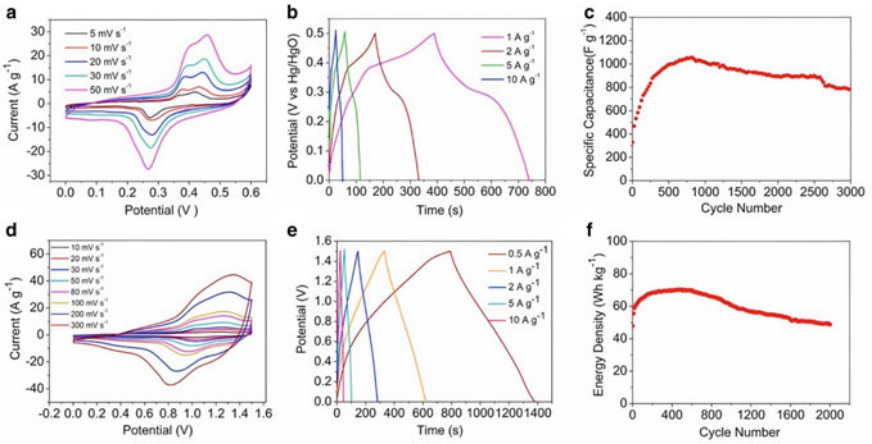

Fig. 6 **a** CV curves of $Ba_2Bi_{0.1}Sc_{0.2}Co_{1.7}O_{6-\delta}$ at different scan rates. **b** GCD curves at various current densities. **c** Cycling performance at 1 A g^{-1}. **d** CV curves of $Ba_2Bi_{0.1}Sc_{0.2}Co_{1.7}O_{6-\delta}$// AC. **e** GCD curves at different current densities of $Ba_2Bi_{0.1}Sc_{0.2}Co_{1.7}O_{6-\delta}$, and **f** Cycling stability of $Ba_2Bi_{0.1}Sc_{0.2}Co_{1.7}O_{6-\delta}$//AC at a current of 1 A/g. Adapted with permission [40], Copyright (2018), American Chemical Society

fabricated of $Sr_2CoMoO_{6-\delta}$ and showed a high Ed value of 64 Wh/kg at Pd of 855 W/kg. Figure 7 shows the Ragone plot and cyclic stability of the device.

Liu et al. also synthesized strontium-based double perovskite with partial substitution of molybdenum (Mo) with nickel in the B-site to obtain a perovskite structure with a composition of $Sr_2CoMo_{1-x}Ni_xO_{6-\delta}$ to improve the electrochemical behavior of the $Sr_2CoMoO_{6-\delta}$ double perovskite through oxygen anion-intercalation and faradaic surface redox pseudocapacitance [42]. The $Sr_2CoMo_{1-x}Ni_xO_{6-\delta}$ electrode material has been examined in a 3-electrode system to evaluate their electrochemical behavior; it reveals a high C_s of 930 F/g which is greater than that of the $Sr_2CoMoO_{6-\delta}$ in the previous study. While replacing the Mo metal in the $Sr_2CoMoO_{6-\delta}$ by Fe metal to obtain $Sr_2FeCoO_{6-\delta}$ double perovskite led to decreasing the C_s value to about 263 F/g at 1 A/g, this study was performed by Vats et al. [43]. This means that the partial substitution of Mo and Ni elements with Co element in the B-site gives outstanding electrochemical performance compared to the partial substitution with Fe element alone.

Several research studies have been performed on the lanthanum-based DPMs by varying the B-site element by using different transition metals to improve its electrochemical performance. Bavio et al. prepared $La_2B(II)MnO_6$ double perovskite using the B-site elements as Cu, Ni, and Co elements by the sol–gel method [26]. All prepared compositions were investigated in 3-electrode systems to evaluate their electrochemical performance; it was found that the La_2CuMnO_6 showed the highest C_s value, which was 781.25 F/g compared to the La_2NiMnO_6 and La_2CoMnO_6 which have C_s values of about 394.45 and 347.22 F/g, respectively. While the electrochemical impedance spectroscopy (EIS) confirms that all compositions have

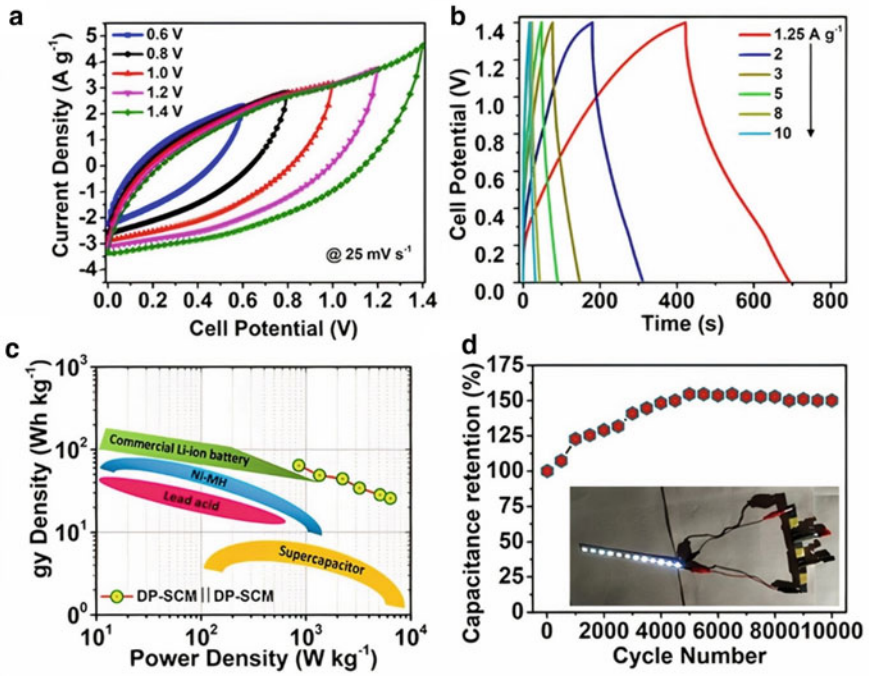

Fig. 7 **a** CV curves of $Sr_2CoMoO_{6-\delta}$, **b** GCD curves at different current densities, **c** Ragone plots of symmetric device, **d** cyclic stability of the device. Adapted with permission [31], Copyright (2020), American Chemical Society

good electrical conductivity and ion diffusion, which promotes perovskites as electrode materials for supercapacitors. Another lanthanum-based DPM of composition La_2ZnMnO_6 has been synthesized hydrothermally by Singh et al. [44], The electrochemical performance of the fabricated electrode was better than the La_2NiMnO_6 and La_2CoMnO_6 perovskite structures, but it was lower than the La_2CuMnO_6 since it has a C_s value of 515.5 F/g at 1 A/g, in addition to good cycling stability of about 86% retention after 1000 charge/discharge cycles.

Singh et al. also replaced the Zn element with the Ni element in the La_2ZnMnO_6 to obtain the DPM of the La_2NiMnO_6 composition. The La_2NiMnO_6 electrode revealed a C_s value of 478.2 5 F/g at 2 mV/s. Using the sol–gel method, Meng et al. prepared porous hollow spheres of lanthanum-based double perovskite structures of La_2CoMnO_6 composition [34]. The fabricated electrode showed a C_s value of 376 F/g at 1 A/g. Furthermore, a supercapacitor device of the structure La_2CoMnO_6//Ac was assembled using the positive electrode of La_2CoMnO_6 and the negative electrode of AC. The device exhibited an E_d of 65.8 Wh/kg at 1000 W/kg and good cycling stability of about 89.2% retention after 3000 charge/discharge cycles.

A research study has been performed on gadolinium-based DPMs to obtain promising materials for supercapacitor applications. Amit Kumar et al. prepared

Gd_2NiMnO_6 DPM using the wet chemical method. The pseudocapacitance performance of the as-prepared materials has been evaluated using a 3-electrode system; it revealed a C_s value of about 400.46 F/g at 1 A/g which is better than the C_s values of La_2NiMnO_6 [44] and La_2CoMnO_6 [34], confirming the role of the Gd element in enhancing the electrochemical performance of the DPMs for energy storage systems.

Another category of DPMs based on praseodymium has been studied as an active electrode material for supercapacitors. Rudra et al. prepared the Pr_2ZnMnO_6 double perovskite using a solid-state reaction approach [45]. It revealed the intercalated pseudocapacitive behavior with a C_s value of 69.14 F/g at 2 A/g when investigated in a 3-electrode system to evaluate their electrochemical performance. Muddelwar et al. replaced the Zn element with the Cr element in the Pr_2ZnMnO_6 structure by preparing the Pr_2CrMnO_6 DPM using the sol–gel method [32]. It revealed a C_s value of 177.4 F/g at 2 A/g, which is better than the C_s value of the Pr_2ZnMnO_6 structure, confirming the role of the Cr element in improving the pseudocapacitance performance of the praseodymium-based double perovskite.

Also, some research studies have been performed on the yttrium-based DPMs to improve the pseudocapacitance performance of the double perovskite materials. Mansoorie et al. synthesized the Y_2CuMnO_6 double perovskite using the wet chemical method [46]. The fabricated electrode revealed a C_s value of 15.6 F/g at 0.2 A/g when investigated in a 3-electrode system to evaluate their electrochemical performance. While the nanowires Y_2NiMnO_6 DPM that have been prepared hydrothermally by Alam et al. exhibited a C_s value of 77.76 F/g at 30 mA/g which is greater than that of the Y_2CuMnO_6 [29]. Devi et al. recently prepared the microsphere-like structure of Y_2MnCoO_6 double perovskite using hydrothermal [28]. By investigating the electrochemical performance of the as-prepared double perovskite structure in a 3-electrode system, it revealed a C_s value of about 148 F/g at 0.5 A/g, in addition to the high cycling stability of about 856% retention after 10,000 charge/discharge cycles. This result means that the electrochemical performance of the Y_2MnCoO_6 double perovskite is better than that of Y_2CuMnO_6 and Y_2NiMnO_6.

3.2 Challenges and Future Perspectives

The scientific community has been focusing on designing novel materials to help with the construction of cutting-edge electrode systems for effective energy harvesting and storage. Investigating these new materials is crucial for improving performance metrics, including power conversion efficiency, specific capacity, cycle life, and energy/power densities. The multidimensional (0D, 1D, 2D, and 3D) perovskites are a subset of these materials that have demonstrated significant potential for energy storage and harvesting devices [3]. The perovskites have a wide range of uses, as seen by the quick rise in articles published between 1980 and 2002. Even with doping A, B, or A and B sites, the rhombohedral, orthorhombic, and cubic phases of perovskites have been the most widely reported structures [21]. However, the currently available reports are insufficient for commercial applications and cannot be compared to other

supercapacitors that use well-known electrode materials. These materials' stability and toxicity are additional barriers to their usage in a variety of applications [47].

Perovskite materials have been used in energy devices since 2003; there hasn't been much research on their utilization in this field due to their use as electrocatalysts mostly focused on the ORR, OER, and HER reactions [21]. Additionally, the inappropriate performance of these materials is also caused by improper optimization of their properties. Therefore, the improvement and optimization of the perovskite materials' properties could be achieved by engineering their morphology and crystal structure as well as by doping new elements in the A and B sites, which results in enhancing their electrochemical behavior. Perovskites can exhibit a wide range of electrical, electronic, optical, and chemical properties because of the variety of their structure. Since 90% of the elements in the periodic table can fit into their crystal lattices, their chemical and physical properties can also be modified by doping or replacing their anions or cations with foreign metal ions of the same valence. Furthermore, their morphology could be tuned by changing the size of the doped ions, for instance, to create a 3D perovskite material, a small-size cation on the A-site can simply enter inside the BX_6 octahedra. In contrast, when a large-size cation is used on the A-site, 2D, 1D, or 0D structures frequently develop [2, 3].

In comparison to single perovskites, double perovskite structures are superior because they exhibit more oxygen vacancies; however, the doping in these materials may alter the perovskite structure, which occasionally results in subpar performance. Another obstacle to understanding the charge storage mechanisms is the shortage of theoretical studies about the structure and storage characteristics of various perovskite materials. To improve the electrochemical performance of the perovskite materials for the forthcoming applications, there is still much work to be done. The discovery of novel perovskite materials is the first and most crucial one [47, 48]. According to research studies, the supercapacitor behavior could be influenced by tuning the morphology and the particle size of the electrode materials; they could reveal rich active sites, which improve the charging kinetics and enhance supercapacitor performances. However, aggregation is the main problem that would decrease the active surface area.

There are numerous available synthesis techniques for the development of perovskite materials, but they are all currently poorly investigated and difficult to replicate. Therefore, it's critical to customize the synthesis techniques and ensure that the selected approach is scalable, repeatable, and economical for use at the commercial level as well as to achieve the proper design that preserves stability, structural coordination, and material neutrality. Despite these challenges, perovskite materials have several benefits, including good conductivity, low cost, and simple preparation. If the aforementioned problems can be solved, perovskite will be a promising and cutting-edge material for storage applications [21, 48].

4 Conclusions

DPMs are promising candidates for high energy density supercapacitor applications due to their pseudocapacitive behavior. The discussed variety of charge storage mechanisms allows for high charge/anion accumulation over the DPM, which offers longer discharge time at high current densities with suppressing the fast potential drop. The mixed B-site cations of highly ordered DPMs could enhance the cation-leaching assessment, which is increased the stability of DPMs. Several synthesis methodologies have been employed to obtain DPMs, which allowed for a more controlled material designing process. Several research investigations have demonstrated promising results regarding the improved stability and reaction kinetics of DPMs. Finally, the research area of employing DPMs as pseudocapacitive materials has to be more deeply investigated as it observes very promising results for future ultra-energy supercapacitors.

References

1. Y. Cao, J. Liang, X. Li, L. Yue, Q. Liu, S. Lu, A.M. Asiri, J. Hu, Y. Luo, X. Sun, Recent advances in perovskite oxides as electrode materials for supercapacitors. Chem. Commun. **57**, 2343–2355 (2021)
2. A.K. Tomar, A. Joshi, G. Singh, R.K. Sharma, Perovskite oxides as supercapacitive electrode: properties, design and recent advances. Coord. Chem. Rev. **431**, 213680 (2021)
3. P. Goel, S. Sundriyal, V. Shrivastav, S. Mishra, D.P. Dubal, K.H. Kim, A. Deep, Perovskite materials as superior and powerful platforms for energy conversion and storage applications. Nano Energy **80**, 105552 (2021)
4. C. Sun, J.A. Alonso, J. Bian, C.W. Sun, J.J. Bian, J.A. Alonso, Recent advances in perovskite-type oxides for energy conversion and storage applications. Adv. Energy Mater. **11** (2021)
5. Y. Liu, Z. Wang, J.P.M. Veder, Z. Xu, Y. Zhong, W. Zhou, M.O. Tade, S. Wang, Z. Shao, Highly defective layered double perovskite oxide for efficient energy storage via reversible pseudocapacitive oxygen-anion intercalation. Adv. Energy Mater. **8**, 1702604 (2018)
6. C.J. Bartel, C. Sutton, B.R. Goldsmith, R. Ouyang, C.B. Musgrave, L.M. Ghiringhelli, M. Scheffler, New tolerance factor to predict the stability of perovskite oxides and halides. Sci. Adv. **5** (2019)
7. N. Setter, L.E. Cross, The contribution of structural disorder to diffuse phase transitions in ferroelectrics. J. Mater. Sci. **15**, 2478–2482 (1980)
8. X. Xu, Y. Zhong, Z. Shao, Double perovskites in catalysis, electrocatalysis, and photo(electro)catalysis. Trends Chem. **1**, 410–424 (2019)
9. E.G. Steward, H.P. Rooksby, IUCr Pseudo-cubic alkaline-earth tungstates and molybdates of the R3MX6 type. urn:issn:0365-110X **4**, 503–507 (1951)
10. Q. Tang, X. Zhu, Half-metallic double perovskite oxides: recent developments and future perspectives. J. Mater. Chem. C **10**, 15301–15338 (2022)
11. H. Arandiyan, S.S. Mofarah, C.C. Sorrell, E. Doustkhah, B. Sajjadi, D. Hao, Y. Wang, H. Sun, B.J. Ni, M. Rezaei et al., Defect engineering of oxide perovskites for catalysis and energy storage: synthesis of chemistry and materials science. Chem. Soc. Rev. **50**, 10116–10211 (2021)
12. T. Sato, S. Takagi, S. Deledda, B.C. Hauback, S.I. Orimo, Extending the applicability of the Goldschmidt tolerance factor to arbitrary ionic compounds. Sci. Rep. **6**, 1–10 (2016)
13. S. Vasala, M. Karppinen, A2B′B″O6 perovskites: a review. Prog. Solid State Chem. **43**, 1–36 (2015)

14. A. Muñoz, J.A. Alonso, M.T. Casais, M.J. Martínez-Lope, M.T. Fernández-Díaz, Crystal and magnetic structure of the complex oxides Sr2MnMoO6, Sr2MnWO6and Ca2MnWO6: a neutron diffraction study. J. Phys. Condens. Matter **14**, 8817 (2002)
15. Y. Liu, S.P. Jiang, Z. Shao, Intercalation pseudocapacitance in electrochemical energy storage: recent advances in fundamental understanding and materials development. Mater. Today Adv. **7**, 100072 (2020)
16. Z. Wang, Y. Liu, Y. Chen, L. Yang, Y. Wang, M. Wei, A-site cation-ordered double perovskite PrBaCo2O5+δ oxide as an anion-inserted pseudocapacitor electrode with outstanding stability. J. Alloys Compd. **810**, 151830 (2019)
17. L. Zeng, L. Cui, C. Wang, W. Guo, C. Gong, In-situ modified the surface of Pt-doped perovskite catalyst for soot oxidation. J. Hazard. Mater. **383**, 121210 (2020)
18. C. Bharti, T.P. Sinha, Dielectric properties of rare earth double perovskite oxide Sr2CeSbO 6. Solid State Sci. **12**, 498–502 (2010)
19. R. Jose, J. Konopka, X. Yang, A. Konopka, M. Ishikawa, J. Koshy, Crystal structure and dielectric properties of a new complex perovskite oxide Ba2LaSbO6. Appl. Phys. A Mater. Sci. Process. **79**, 2041–2047 (2004)
20. J.G. Bednor, K.A. Muller, Possible high T superconductivity in the Ba-La-Cu-O system. Z. Phys. B Condens. Matter **64**, 189–193 (1986)
21. L.C.C.B. Oliveira, R. Venâncio, P.V.F. de Azevedo, C.G. Anchieta, T.C.M. Nepel, C.B. Rodella, H. Zanin, G. Doubek, Reviewing perovskite oxide sites influence on electrocatalytic reactions for high energy density devices. J. Energy Chem. **81**, 1–19 (2023)
22. H. Kato, T. Okuda, Y. Okimoto, Y. Tomioka, K. Oikawa, T. Kamiyama, Y. Tokura, Structural and electronic properties of the ordered double perovskites A2MReO6 (A = Sr, Ca; M = Mg, Sc, Cr, Mn, Fe, Co, Ni, Zn). Phys. Rev. B Condens. Matter Mater. Phys. **69** (2004)
23. Q. Tang, X. Zhu, Half-metallic double perovskite oxides: recent developments and future perspectives. J. Mater. Chem. C (2022)
24. C. Li, Z. Yu, H. Liu, K. Chen, High surface area LaMnO3 nanoparticles enhancing electrochemical catalytic activity for rechargeable lithium-air batteries. J. Phys. Chem. Solids **113**, 151–156 (2018)
25. D. Liu, M. Chen, X. Du, H. Ai, K. Ho Lo, S. Wang, S. Chen, G. Xing, X. Wang, H. Pan et al., Development of electrocatalysts for efficient nitrogen reduction reaction under ambient conditions. Adv. Funct. Mater. **31**, 2008983 (2021)
26. M.A. Bavio, J.E. Tasca, G.G. Acosta, M.F. Ponce, R.O. Fuentes, A. Visintin, Study of double perovskite La2B(II)MnO6 (B: Ni Co, Cu) as electrode materials for energy storage. J. Solid State Electrochem. **24**, 699–710 (2020)
27. A. Shereef, P.A. Aleena, J. Kunjumon, A.K. Jose, S.A. Thomas, M. Tomy, T.S. Xavier, S. Hussain, D. Sajan, Third-order nonlinear optical properties and electrochemical performance of La2CoMnO6 double perovskite. Mater. Sci. Eng. B **289**, 116262 (2023)
28. M. Devi, D. Nagpal, A. Vasishth, A. Kumar, A. Kumar, Structural and energy storage properties of hydrothermally synthesized Y2MnCoO6 double perovskite. Phys. Status Solidi **220**, 2200444 (2023)
29. M. Alam, K. Karmakar, M. Pal, K. Mandal, Electrochemical supercapacitor based on double perovskite Y2NiMnO6 nanowires. RSC Adv. **6**, 114722–114726 (2016)
30. M.B. Hanif, S. Rauf, M. Motola, Z.U.D. Babar, C.J. Li, C.X. Li, Recent progress of perovskite-based electrolyte materials for solid oxide fuel cells and performance optimizing strategies for energy storage applications. Mater. Res. Bull. **146**, 111612 (2022)
31. A.K. Tomar, A. Joshi, S. Atri, G. Singh, R.K. Sharma, Zero-dimensional ordered Sr2CoMoO6-δ double perovskite as high-rate anion intercalation pseudocapacitance. ACS Appl. Mater. Interfaces **12**, 15128–15137 (2020)
32. R.K. Muddelwar, J. Pani, A.B. Lad, K.U. Kumar, V.M. Gaikwad, H. Borkar, Pr2CrMnO6 double perovskite as new electrode material for electrochemical energy storage. Mater. Chem. Phys. **302**, 127726 (2023)
33. Y.-B. Wu, B. Jun, W. Bin-Bin, Preparation and supercapacitor properties of double-perovskite La2CoNiO6 inorganic nanofibers. Acta Phys. Chim. Sin. **31**, 315–321 (2015)

34. Z. Meng, J. Xu, P. Yu, X. Hu, Y. Wu, Q. Zhang, Y. Li, L. Qiao, Y. Zeng, H. Tian, Double perovskite La2CoMnO6 hollow spheres prepared by template impregnation for high-performance supercapacitors. Chem. Eng. J. **400**, 125966 (2020)
35. S. Yagi, I. Yamada, H. Tsukasaki, A. Seno, M. Murakami, H. Fujii, H. Chen, N. Umezawa, H. Abe, N. Nishiyama et al., Covalency-reinforced oxygen evolution reaction catalyst. Nat. Commun. **6** (2015)
36. J.T. Mefford, X. Rong, A.M. Abakumov, W.G. Hardin, S. Dai, A.M. Kolpak, K.P. Johnston, K.J. Stevenson, Water electrolysis on La1−xSrxCoO3−δ perovskite electrocatalysts. Nat. Commun. **7**, 1–11 (2016)
37. G. Kim, S. Wang, A.J. Jacobson, L. Reimus, P. Brodersen, C.A. Mims, Rapid oxygen ion diffusion and surface exchange kinetics in PrBaCo2O5+x with a perovskite related structure and ordered A cations. J. Mater. Chem. **17**, 2500–2505 (2007)
38. S. Zhong, Y. Chen, L. Yang, Y. Liu, X. Chen, C. Wang, Ni-doped perovskite PrBaCo2O5+δ as supercapacitor electrode with enhanced electrochemical performance. Mater. Lett. **297**, 130013 (2021)
39. A. Aguadero, D. Pérez-Coll, J.A. Alonso, S.J. Skinner, J. Kilner, A new family of mo-doped school 3-delta; Perovskites for application in reversible solid-state electrochemical cells. Chem. Mater. **24**, 2655–2663 (2012)
40. Z. Xu, Y. Liu, W. Zhou, M.O. Tade, Z. Shao, B-site cation-ordered double-perovskite oxide as an outstanding electrode material for supercapacitive energy storage based on the anion intercalation mechanism. ACS Appl. Mater. Interfaces **10**, 9415–9423 (2018)
41. A. Kumar, A. Kumar, Electrochemical behavior of oxygen-deficient double perovskite, Ba2FeCoO6-δ, synthesized by facile wet chemical process. Ceram. Int. **45**, 14105–14110 (2019)
42. Y. Liu, Z. Wang, Y. Zhong, X. Xu, J.P.M. Veder, M.R. Rowles, M. Saunders, R. Ran, Z. Shao, Activation-free supercapacitor electrode based on surface-modified Sr2CoMo1-xNixO6-δ perovskite. Chem. Eng. J. **390**, 124645 (2020)
43. A.K. Vats, N. Sangwan, J. Singh, A. Kumar, A. Kumar, Anion intercalation pseudocapacitance performance of oxygen-deficient double perovskite prepared via facile wet chemical route. Mater. Sci. Semicond. Process. **138**, 106300 (2022)
44. J. Singh, A. Kumar, U.K. Gautam, A. Kumar, Microstructure and electrochemical performance of La2ZnMnO6 nanoflakes synthesized by facile hydrothermal route. Appl. Phys. A Mater. Sci. Process. **126**, 1–9 (2020)
45. M. Rudra, H.S. Tripathi, A. Dutta, T.P. Sinha, Existence of nearest-neighbor and variable range hopping in Pr2ZnMnO6 oxygen-intercalated pseudocapacitor electrode. Mater. Chem. Phys. **258**, 123907 (2021)
46. F.N. Mansoorie, J. Singh, A. Kumar, Wet chemical synthesis and electrochemical performance of novel double perovskite Y2CuMnO6 nanocrystallites. Mater. Sci. Semicond. Process. **107**, 104826 (2020)
47. M. Mohan, N.P. Shetti, T.M. Aminabhavi, Perovskites: a new generation electrode materials for storage applications. J. Power. Sources **574**, 233166 (2023)
48. G.R. Monama, K.E. Ramohlola, E.I. Iwuoha, K.D. Modibane, Progress on perovskite materials for energy application. Results Chem. **4**, 100321 (2022)

Conducting Polymers for Pseudocapacitors

Quoc Bao Le, Rudolf Kiefer, Phuong Nguyen Xuan Vo, Natalia E. Kazantseva, and Petr Saha

Abstract The energy crisis has increased the need for energy storage materials with high power and energy density. To solve the problem, scientists have investigated the possibilities of pseudocapacitive materials, which may overcome the capacitive constraints of electrical double-layer capacitors and the mass transfer limitations of batteries, making them better energy storage applications. Conducting polymers, which offer unique qualities such as low cost, good electrochemical properties, and high conductivity, have garnered substantial interest in energy storage devices. Because of their high potential to increase working performance, conducting polymers have been studied in numerous energy storage devices such as supercapacitors, batteries, and fuel cells, making them intriguing alternative materials. This chapter comprehensively overviews conducting polymers' contributions to energy storage. We address the theoretical foundation of conductivity in conjugated polymers, multiple methods of producing conducting polymers, their uses in supercapacitors, and the distinctions between electrochemical supercapacitor technologies. Furthermore, we highlight recent breakthroughs in conducting polymers for energy storage, providing an overview of the field's current condition and future direction.

Keywords Electrochemical supercapacitors · Conducting polymers · Energy materials · Charge storage mechanisms

Q. B. Le (✉) · N. E. Kazantseva · P. Saha
University Institute, Tomas Bata University in Zlín, Nad Ovčírnou 3685, 760 01 Zlín, Czech Republic
e-mail: le@utb.cz

R. Kiefer
Conducting Polymers in Composites and Applications Research Group, Faculty of Applied Sciences, Ton Duc Thang University, Ho Chi Minh City 700000, Vietnam

P. N. X. Vo
Faculty of Applied Sciences, Ton Duc Thang University, Ho Chi Minh City 700000, Vietnam

© The Author(s), under exclusive license to Springer Nature Switzerland AG 2024

R. K. Gupta (ed.), *Pseudocapacitors*, Engineering Materials,
https://doi.org/10.1007/978-3-031-45430-1_9

1 Introduction

The Earth has recently faced a rising energy crisis and environmental pollution. Due to population growth leading to economic development, the energy demand rapidly increased, causing terrific environmental matters for our generations and children in the future. Especially since the great conflict in Europe in 2022, the energy crisis has become more momentous [1]. Scientists worldwide have concentrated on environmentally friendly alternative energy technologies, including supercapacitors and batteries built of sustainable materials and renewable energy resources. One area of interest is conducting polymer (CP) research. CP can exhibit electrical conductivity and quickly be processed into various shapes and sizes, making them ideal for electrodes in energy storage devices [2].

Supercapacitors (SC), or electrochemical double-layer capacitors (EDLCs), store energy by separating charge at the electrode/electrolyte interface. They have high energy density and fast charge/discharge times, which make them deserve hybrid electric vehicles, grid-scale energy storage, and portable electronics. However, the capacitance of supercapacitors needs improvement to meet the developing requirements of human activities. Notably, the materials used in their construction can be expensive and environmentally harmful [3].

Pseudocapacitors (PSCs) are a type of supercapacitor that stores energy via redox reactions of ions at the electrode/electrolyte interface [4]. This type of energy storage offers a much higher capacity than traditional capacitors, which store energy by accumulating electrical charge on two metal plates separated by an insulating material. The high energy storage capacity and fast charge/discharge times make PSCs ideal for hybrid electric vehicles, grid-scale energy storage, and portable electronics [4]. Compared to EDLCs, PSCs have high power densities, fast charge/discharge times, and a higher energy storage capacity [4].

Due to their electrical conductivity and versatility in processing, conducting polymers have become a viable material for supercapacitors. Including conductive polymers in the design may improve SCs' energy density, stability, and overall performance. These polymers may also be created from eco-friendly and sustainable ingredients, giving them a more environmentally sound option than conventional energy storage systems [5].

This chapter overviews recent developments in CPs for pseudocapacitors, including their synthesis, characterization, and performance of their composites. The fundamental principles of pseudocapacitance, different types of conducting polymers and their properties, and the directions for developing these polymers for PSCs are also covered.

2 Types of Pseudocapacitance

In the 1990s, Conway et al. proposed the concept of pseudocapacitance to describe the reversible capacitance associated with the electrochemical adsorption of species on the electrode surface (Fig. 1). Generally, pseudocapacitance can be classified into three types: (i) monolayer adsorption pseudocapacitance, (ii) surface redox pseudocapacitance (Faradaic pseudocapacitance), and (iii) intercalation pseudocapacitance [6].

2.1 Adsorption Pseudocapacitance

Adsorption pseudocapacitance results from the adsorption of ions or molecules onto the surface of an electrode (Fig. 1a). Unlike EDLC, which involves the accumulation of ions in the diffuse layer, adsorption pseudocapacitance occurs when ions or molecules are adsorbed onto the surface of the electrode. Electrodes made from porous materials, such as carbon-based or metal oxides, have large surface areas,

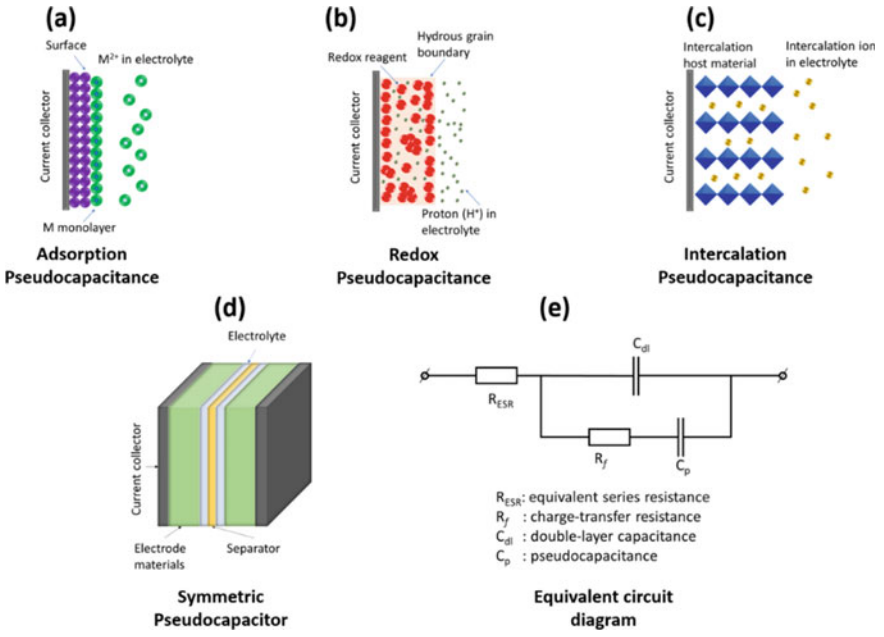

Fig. 1 Illustration of three types of reversible redox mechanisms that give rise to pseudocapacitance defined by Conway: **a** monolayer adsorption pseudocapacitance (underpotential deposition), **b** surface redox pseudocapacitance, **c** intercalation pseudocapacitance [7]; the **d** schematic of a pseudocapacitance, and **e** its corresponding equivalent circuit diagram modeling the cell electrical behavior [8]

which allow for increased ion adsorption. Hence, they are often used to observe this capacitance type [7].

While adsorption pseudocapacitance can improve the capacitance of electrochemical systems, it is not as reversible or stable as redox pseudocapacitance, which means the number of charge/discharge cycles before losing its capacitance is limited. Thus, it is essential to consider these limitations in designing electrochemical systems for energy storage applications. Overall, adsorption pseudocapacitance is a valuable mechanism for energy storage [7].

2.2 Redox Pseudocapacitance

The redox reactions occurring on the surface of an electrode cause redox pseudocapacitance (Fig. 1b). This type of Faradaic pseudocapacitance is formed as electrons transport between the electrode and the electrolyte. The redox processes on the electrode surface provide additional sites for charge storage, increasing the system's total capacitance. Because of their capacity to perform redox reactions, metal oxides or conducting polymers are commonly used as electrodes to drive this capacitance mechanism [7].

Because of enormous amounts of capacitance, this capacitance is particularly useful for energy storage devices. Furthermore, redox pseudocapacitance is frequently more reversible and stable than adsorption pseudocapacitance, allowing it to go through more charge/discharge cycles with no loss of capacitance [7].

2.3 Intercalation Pseudocapactiance

Intercalation pseudocapacitance, like redox pseudocapacitance, refers to the capacitance caused by the intercalation of ions or molecules into the lattice structure of electrode material (Fig. 1c). The transfer of electrons between the electrode and the electrolyte causes both forms of pseudocapacitance. However, the ions/molecules are injected into the electrode material's lattice structure in this mechanism [7].

Intercalation pseudocapacitance employs layered electrodes such as transition metal oxides or graphite. The layered structure of these materials provides a wide surface area for the ion intercalation, increasing overall capacitance. Furthermore, intercalation pseudocapacitance is frequently more reversible and persistent than the adsorption pseudocapacitance. As a result, the pseudocapacitors may endure longer charge/discharge cycles without losing capacitance. It is a valuable energy storage mechanism intensively explored and used in developing supercapacitors and other electrochemical energy storage devices [7].

2.4 Electrochemical Capacitors

Electrochemical SCs are commonly constructed with two electrodes separated by an electrical insulator, also known as a separator, in an electrolyte. These SCs, modeled as parallel plate capacitors, store energy as a polarized electric field between the electrodes, separated by a dielectric material. Electrochemical SCs are known for their high cycling times and efficiency, although they have a lower energy density than batteries. They have a higher power density than conventional capacitors, which allows them to be useful for applications that require rapidly distributing a large amount of charge. Figure 1d and e show the device configuration of an electrochemical SC made of nanostructured conducting polymer electrodes and its equivalent circuit diagram [8].

PSCs are a promising solution for filling the electrochemical energy storage technology gap. They offer a combination of battery-level energy density and EDLCs' cycling stability and power density [9]. It is worth noting that there is no material or device perform solely either a pseudocapacitive or EDLC mechanism [8]. A Helmholtz layer may form in pseudocapacitive electrodes with a large surface area, contributing to double-layer capacitance to some extent [9]. On the other hand, depending on synthesis process, the functional groups in EDLC electrodes can affect their capacitance by participating in faradaic charge storage [10].

PSCs have high capacitance, but their faradaic processes slow ion transport compared to electrostatic adsorption in EDLCs, resulting in low power [7]. A pseudocapacitive material should have high conductivity to improve charge transfer kinetics at the electrode. A conducting polymer must possess charge carriers, good charge mobility, efficient kinetics, and readily available solvated counterions to achieve high conductivity and electrochemical capacitance [11]. The concentration of charge carriers can be increased by n-doping (reducing) to insert electrons into the conduction band or p-doping (oxidizing) to remove electrons from the valence band. Equations 1 and 2 represent the general reactions of n-doping and p-doping using an undoped conducting polymer (CP) chain, oxidant (Ox), reductant (Red), counteranion (A–), and a countercation (C +), respectively [8].

$$\mathrm{CP} + \mathrm{nRed} \rightarrow \left(\mathrm{C}^{+}\right)\mathrm{nCP}^{\mathrm{n}-} + \mathrm{nRed}^{+} \tag{1}$$

$$\mathrm{CP} + \mathrm{nOx} \rightarrow \mathrm{CP}^{\mathrm{n}+}\left(\mathrm{A}^{-}\right)\mathrm{n} + \mathrm{nOx}^{-} \tag{2}$$

The equilibrium geometry of a polymer refers to its spatial arrangement of atoms or molecular units in the minimum energy state. This arrangement characterizes the balanced pull-and-push forces within the three-dimensional oriented networks of the polymer chains, and thus significantly impacts its physical and chemical properties, such as solubility, reactivity, and conductivity. The ionization of a polymer involves introducing positive or negative charges into the polymer chain, which changes the equilibrium geometry [12]. It leads to a shift in the highest occupied molecular orbital (HOMO) energy to increase and the lowest unoccupied molecular orbital

(LUMO) energy to decrease, creating new delocalized energy bands within the band gap of the polymer chain and forming charge "islands." The extent of ionization, or "doping," determines the degree of overlap and delocalization of these islands, thereby increasing the polymer's conductivity. Generally, higher ionization results in higher conductivity [12].

3 Polymeric Materials

Polymers are a common material with wide applications based on their advantages. Recently, the application of both biopolymers and synthetic polymers acquired significant attention from scientists. Biopolymers are derived from natural sources such as biological materials or living organisms and are considered renewable resources, while synthetic polymers are artificially fabricated compounds and are typically non-renewable. Among various types of polymers, conducting polymers (CPs) have gained significant attention, leading to their wide range of applications in material science and electronics. The presence of conjugated π-electrons in CPs is responsible for their extensive electronic properties, including low energy optical transitions, electrical conductivity, high electron affinity, and low ionization potential.

In 2022, Moon et al. conducted a study to explore the potential use of methyl 1H-pyrrole-3-carboxylate (MPC) polymer as a conducting electrode for SCs in various applications, including transient electronics, biomedical devices and biodegradable energy storage (Fig. 2a) [13]. The MPC polymer was synthesized using electrochemical and chemical polymerization methods and compared with polyprole (PPy) regarding capacitance, charge–discharge characteristics, impedance, and cycle life performance. They also combined MPC polymer with a biodegradable high-surface-area substrate made of poly (l-lactic acid) (PLLA), which showed similar capacitance values to PPy-PLLA composites and higher current per gram measurements than pure PLLA. The discharging current of MPC polymer followed a faradaic-current model, suggesting that the polymer reduction–oxidation mechanism plays a significant role in the charge storage mechanism. During the charging process, the current deviated from the faradaic model, likely due to side reactions or irreversibilities, which increased with each successive cycle. The MPC polymer and PPy electrodes showed appropriate retention when tested after 2000 cycles. Their results showed that PPy exhibited better stability than MPC during the longer working times. Despite the expectation of MPC polymer having higher capacitance loss due to its solubility in an aqueous environment, the results are promising for its use as an SC electrode material, and the team suggests depositing MPC polymer on a flexible nanomaterial substrate, such as carbon nanotubes, to extend its cycle life [13].

Energy storage devices rely on different material structures, each with unique advantages and disadvantages [9]. The selection of a material structure for a particular application depends on the desired properties and specific requirements. Researchers

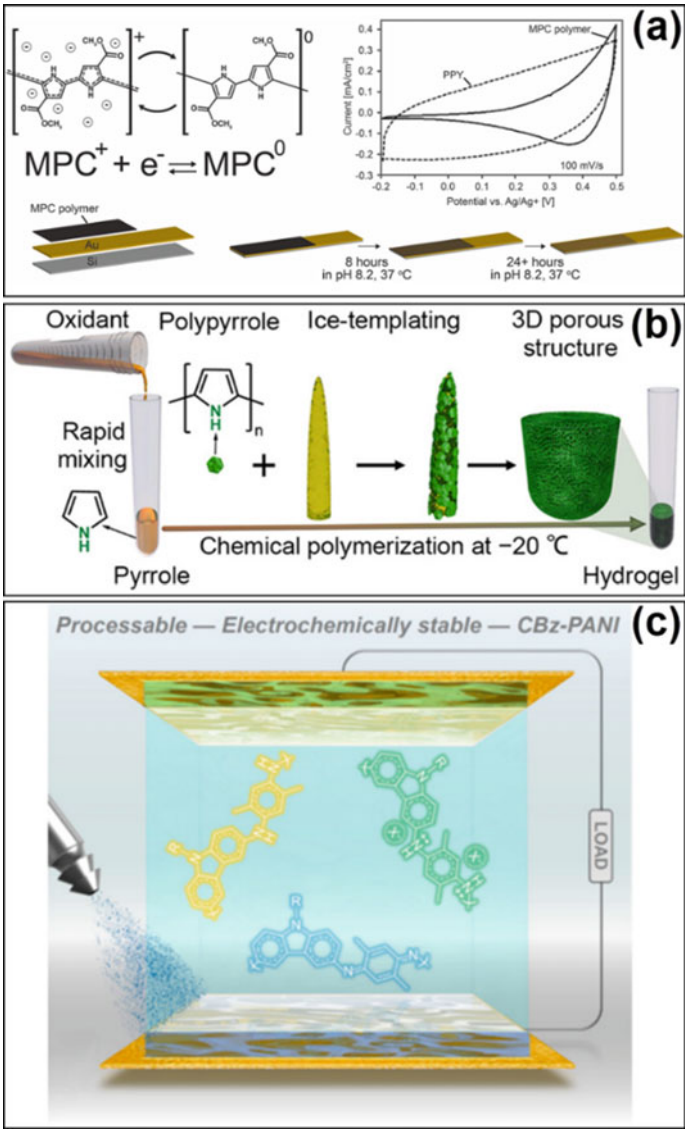

Fig. 2 **a** Structure and pseudocapacitive charge storage mechanism of MPC polymer via reversible oxidation–reduction reactions, the Planar electrodes of 1H-pyrrole-3-carboxylate (MPC) polymer (solid line) and Polypyrrole (PPy) (dashed line), schematic of planar MPC polymer electrodes tested and MPC polymer electrodeposited on an Au-coated Si wafer for planar electrode characterization. Adapted with permission [13], Copyright 2023, Elsevier; **b** schematic illustration of the fabrication route to polypyrrole hydrogel (PPH). Adapted with permission [14], Copyright 2023, American Chemical Society; **c** schematic preparation of PANI-derivatives from carbazole and 1,4-aryldiamines (Cbz-PANI), poly(9-(2-ethylhexyl)-carbazole-3,6-diyl-alt-2,5-dimethyl-p-phenylenediamine) (Cbz-PANI-1), and poly(9-(2-hexyldecyl)-carbazole-3,6-diyl-alt-p-phenylenediamine) (Cbz-PANI-2) for SC devices. Adapted with permission [15], Copyright 2023, American Chemical Society

are seeking alternative materials and fabrication techniques to enhance the sustainability and performance of these devices. Hydrogel is also an interesting material for energy conversion and storage applications, such as water electrolysis, fuel cells, rechargeable batteries, and SCs. Conducting polymer hydrogels (CPHs), including polyaniline, poly(3,4-ethylenedioxythiophene) (PEDOT), and polypyrrole (PPy), have gained attention for electrochemical applications. They have excellent features, such as ease of synthesis, low cost, lightness, environmental stability, and good electrochemical performance [7]. CPHs possess remarkable potential as electrode materials for future energy storage devices. However, conventional methods of synthesizing CPHs using cross-linkers, adhesives, or supporting frameworks lead to low porosity, unsatisfactory electrical conductivity, and harsh synthesis conditions. Researchers are currently exploring straightforward strategies to fabricate CPHs with desired porous nanostructures that can help address these challenges.

Gao and his colleagues introduced a new one-step ice-templating method to fabricate porous polypyrrole hydrogel (PPH) with interconnected PPy nanoparticles [14]. They conducted the polymerization of pyrrole using $FeCl_3.6H_2O$ as the oxidizing agent. The ice crystals formed in ethanol and water were used as the template to guide the formation of a three-dimensional (3D) porous structure at low temperatures (Fig. 2b). The PPy nanoparticles were designed to disperse on the surface of the ice crystals and form a 3D conductive structure. PPy is a widely studied and promising CPH electrode material due to its high conductivity, excellent pseudocapacitive performance, and nontoxicity. However, its low porosity has limited its practical application in the past. Efforts to improve the porosity of PPy-based electrode materials have involved integrating PPy into porous substrates or using other porous materials as sacrifice templates. By comparing the rate capability of ice-templated and conventional electrodes, they demonstrated that the ice-templated nanostructure of the PPH electrode significantly improved its rate capability by enabling the diffusion of electrolytes. This led to a high specific capacitance (226 F/g at a current density of 67.6 A/g), excellent rate performance (85% capacitance retention when current density increases from 1.35 to 67.6 A/g), and long cycling life (80% capacitance retention after 5000 cycles) [14].

Polyaniline (PANI), along with PPy, is one of the most extensively studied CPs. PANI has various beneficial characteristics, including ease of synthesis and low cost, non-redox doping, environmental stability in the doped state, reversible oxidative states, and high electrical conductivity [16]. As a result, PANI has a wide range of applications, such as sensors, energy storage devices, corrosion inhibitors, photovoltaic cells, microwave safeguards, and electromagnetic shielding materials. However, PANI faces two significant challenges: electrochemical aging, which results in electrochemical instability [17], and insolubility in common organic solvents [18]. Several approaches have been reported to address PANI's insolubility, such as incorporating solubilizing counterions and blending with solubilizing polymers. However, fewer reports address its electrochemical instability. The most common approach to address the latter is to dope the polymer with large counterions or prepare nanostructures [18].

Scott and colleagues [15] reported a PANI-derivative containing carbazole (Cbz-PANI) (Fig. 2c) with low cost, easy side-chain alteration at the nitrogen-containing 9H-position for improved dissolution, and ease of functionalization at the 3- and 6-positions for additional reactivity. Because carbazoles create relatively stable cations with high charge carrier mobility, they are also employed as charge transport materials. They explored different kinds of homopolymers prepared from carbazoles for their electrochromic and photoreactive properties named poly(9-(2-ethylhexyl)-carbazole-3,6-diyl-alt-2,5-dimethyl-p-phenylenediamine) (Cbz-PANI-1), and poly(9-(2-hexyldecyl)-carbazole-3,6-diyl-alt-p-phenylene-diamine) (Cbz-PANI-2). Both polymers were soluble in common organic solvents, making them easy to characterize and process. Cbz-PANI-1 was more conductive (2.8 S/cm) than Cbz-PANI-2 (0.70 S/cm) and had better film formation and a higher Mn. Additionally, it exhibited electrochromic properties, good electrochemical stability, and processability, making it a promising material for use in all-polymer symmetric supercapacitors [15].

PEDOT has received significant interest in various applications due to its relatively high chemical and thermal stability and high conductivity. In particular, PEDOT has shown promise in improving the performance of metallic neural microelectrodes by lowering impedance and increasing charge-injection capacity [19]. However, one major challenge in using PEDOT coatings on inorganic substrates is the relatively low adhesion, which can result in coating detachment under chronic neural recording or stimulation conditions, leading to a loss of device performance. Efforts have improved PEDOT adhesion and other conjugated polymers on metallic substrates. For instance, thiol-modified phenyl monolayers were found to enhance the adhesion of polythiophene to platinum [20], while surface-initiated Kumada catalyst-transfer polycondensation was used to increase the stability of poly(3-methyl-thiophene) films on indium-tin-oxide surfaces [21]. However, only a few studies have investigated PEDOT coatings' adhesion and mechanical stability. Researchers have explored various methods to improve the mechanical stability of PEDOT coatings, including polymerizing PEDOT with carbon nanotubes (CNTs) or using an EDOT-substituted silane (APTES-EDOT) as an adhesion promoter [22]. While these methods have provided valuable insights for optimizing PEDOT adhesion and mechanical stability, a better protocol is still under investigation. Strong bonding between the organic polymer and the inorganic glass substrate is necessary for improved performance in transparent energy storage devices. The phenyl functional groups on the silane monolayer can influence the molecular configuration of polymer chains, resulting in better performance of PEDOT-coated silanized glass electrodes [20]. Strong adhesion between the polymer coating and glass also leads to high cycle stability of the planar PEDOT SC. Improving PEDOT coatings' adhesion and mechanical stability on inorganic substrates remains an ongoing topic of interest in transparent devices. While several approaches have been developed, more research is still needed to create a perfect protocol to optimize PEDOT coatings' adhesion and mechanical stability [19–23].

4 Polymeric Carbon-Based Materials

One of the common materials applied for supercapacitors is carbon-based ones such as carbon black (CB) and activated carbon (AC). There are various ways to receive the AC, such as biomass pyrolyzes, which create a porous material with a large specific surface area, resulting in a high double-layer capacitance when operated in electrolytes [3, 24]. However, due to its poor electrical conductivity, CB particles are usually added to increase electron transportation. Conversely, CB has low specific capacitance, so adding this conductive filler lowers the overall specific capacitance in resulting devices. The materials need additional components to improve the specific capacitance and associate them with electrode films [3, 24].

Organic compounds provide an exciting alternative to inorganic alternatives for the active components in energy storage systems due to their excellent availability, safety, and sustainability when used as binders. However, binders like PTFE, PVDF, or Nafion have drawbacks such as limited hydrophilicity, high cost, and environmental issues because they are not biodegradable and release poisonous gases [25]. Conducting polymers can be used as binders for supercapacitors that have lately received increased attention. For example, poly(3,4-ethylenedioxythiophene) polystyrene sulfonate (PEDOT:PSS) is known for its excellent mixed ionic and electronic charge transport, with the electronic transport in the PEDOT phase and the ionic transport through the PSS phase. PEDOT:PSS can easily interface and composite with other organic and inorganic materials [26]. Composites of cellulose and PEDOT:PSS combines the mechanical strength and large specific surface area of cellulose with the electronic and electrochemical properties of PEDOT:PSS and carbon-based materials. Belaineh et al. reported PEDOT:PSS-cellulose electrode composites resulted in exceptional capacitance values and discharge performances. They successfully incorporated the materials into printing process protocols [27].

Du et al. have established a simple and cost-effective method for producing durable and conductive PEDOT:PSS bulk films using cellulose nanofibrils (CNF) as the building blocks (Fig. 3a) [28]. They used an in situ polymerization technique to create a PEDOT:PSS/CNF suspension, which was vacuum-filtered and treated with Dimethyl sulfoxide to create flexible and conductive PEDOT:PSS/CNF nano paper. The optimized PEDOT:PSS/CNP demonstrated outstanding flexibility, high tensile strength (72 MPa), and high electrical conductivity (66.67 S/cm). The assembled symmetrical supercapacitor using PEDOT:PSS/CNP electrodes showed an areal specific capacitance of 854.4 mF/cm^2 (equivalent to 122.1 F/cm^3) at 5 mV/s and the highest energy density at 30.86 μWh/cm^2 (equivalent to 4.41 mWhcm^3), excellent cycling stability retention of 95.8% after 10,000 charge/discharge cycles. PEDOT:PSS/CNP has the potential to be a viable electrode material for flexible supercapacitors due to its remarkable mechanical qualities and excellent electrochemical performance [28]. However, PEDOT:PSS is still one of the most expensive components in any such composite, so using small quantities of PEDOT:PSS as an electronic and mechanical adhesive within other active low-cost materials is an exciting strategy to achieve superior electrode properties while keeping the final cost

low. Hence, developing methods to utilize the common conducting polymers for PSC applications is always in focus.

One interesting material applied in energy storage devices is nitrogen doping carbon-based materials. Nitrogen doping can improve carbon materials' wettability and conductivity while providing additional pseudocapacitance for supercapacitors. There are two common ways of creating nitrogen-doped carbon materials. The first approach is the pyrolysis of nitrogen-containing precursors such as biomass, synthetic polymers, small molecules, and ionic liquids. The second method is the alteration (via chemical or thermal processes) of carbon materials with reagents or gases containing nitrogen atoms [29]. Selecting precursors is critical to both pore structure modulation and surface chemical modification. Precursor design is crucial to nitrogen-doped porous carbon compounds' physical and chemical characteristics. Precursors have been reported to manufacture nitrogen-doped porous carbon materials, including renewable biomass, polymers, and MOFs. Polymers containing N atoms can form different morphologies and pore structures designed in carbon-based materials. For the electrochemical applications, the N-containing polymers can be modified in their structures and compositions to enhance the chemical properties at the molecular level [31].

Organic cross-linked polymers are formed primarily of carbon, nitrogen, oxygen, and hydrogen components and have a network structure. Porous carbon materials with such polymers have a high heteroatom content, specific surface area, and excellent electrochemical characteristics. In particular, their design can be easily modified by varying the raw material ratio during synthesis [29]. Zou et al. produced a novel heteroatom-doped porous carbon material with a high specific surface area by carbonizing and activating polyphosphazene [32]. To make N/O-doped porous COCLPs, the researchers employed a network-structured organic cross-linked polymer as a carbon source. Their novel materials were obtained by optimizing the raw materials ratios exhibiting an excellent electrochemical performance of a specific capacitance of 438 F/g at a current density of 0.5 A/g tested in the three-electrode system.

In 2022, Lao et al. developed nitrogen/oxygen(N/O)-doped carbon-based porous materials via carbonization and activating an organic cross-linked polymer with a network structure (Fig. 3b) [29]. They used polyethylene glycol (PEG 6000), hydroxypropyl methylcellulose (HPMC), and 4,4-diphenylmethane diisocyanate (MDI) to make the organic cross-linked polymer. After fabrication, they acquired a large specific surface area (1589 m^2/g) and a high specific capacitance of 522 F/g at a current density of 0.5 A/g. Furthermore, the symmetric capacitor achieved an energy density of 18.04 Wh/kg at a power density of 200.0 W/kg. The material benefitted from the network structure of organic cross-linked polymers to form hierarchical porous carbon and the pseudocapacitance introduced by heteroatoms. Therefore, the proposed method for fabricating carbon materials provides a new strategy for developing electrode materials with high electrochemical performance [29].

SCs' energy and power density are influenced by the choice of electrolyte, with various options available, including organic and ionic liquids and aqueous electrolytes. Aqueous electrolytes are considered more environmentally friendly and

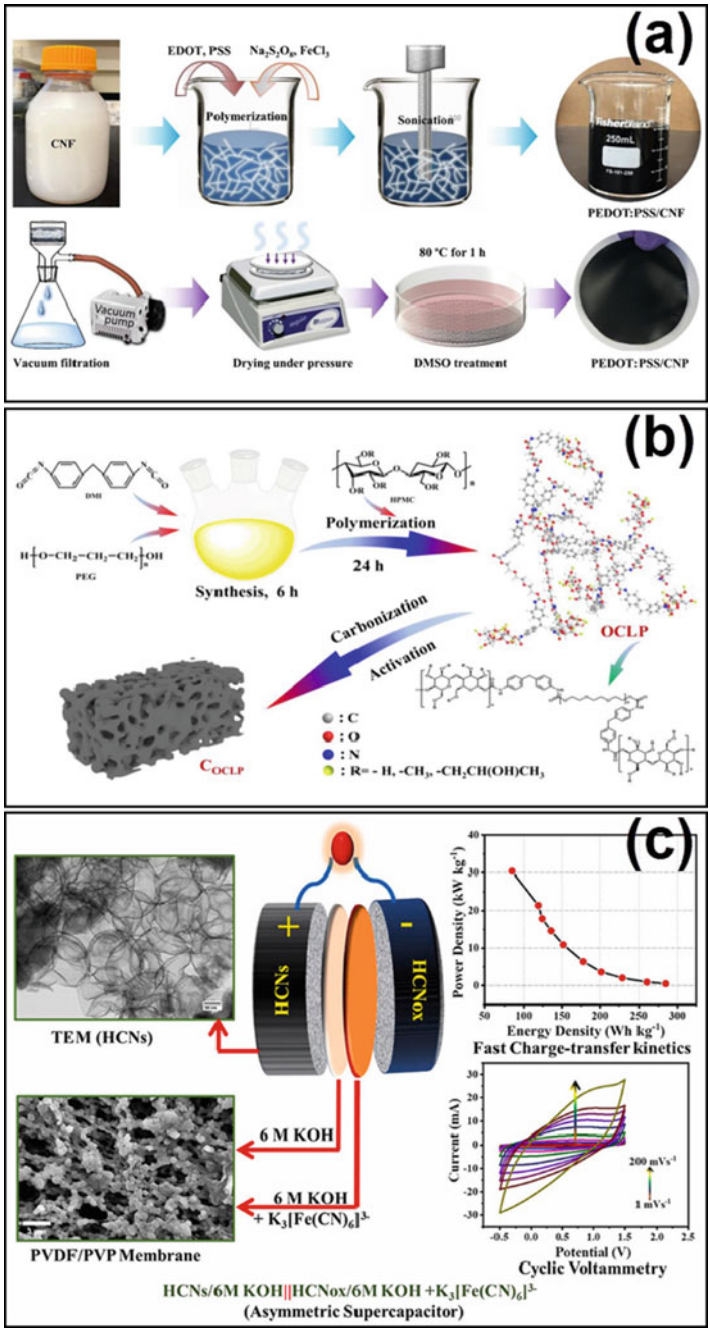
(a)
CNF
EDOT, PSS
$Na_2S_2O_8$, $FeCl_3$
Polymerization
Sonication
PEDOT:PSS/CNF
Vacuum pump
Vacuum filtration
Drying under pressure
80 °C for 1 h
DMSO treatment
PEDOT:PSS/CNP
(b)
DMI
PEG
HPMC
Polymerization
24 h
Synthesis, 6 h
OCLP
Carbonization
Activation
C_{OCLP}
: C
: O
: N
: R= - H, -CH_3, -$CH_2CH(OH)CH_3$
(c)
TEM (HCNs)
HCNs
HCNox
6 M KOH
6 M KOH
+ $K_3[Fe(CN)_6]^{3-}$
PVDF/PVP Membrane
Power Density (kW kg^{-1})
Energy Density (Wh kg^{-1})
Fast Charge-transfer kinetics
Current (mA)
200 mVs^{-1}
1 mVs^{-1}
Potential (V)
Cyclic Voltammetry
HCNs/6M KOH||HCNox/6M KOH +$K_3[Fe(CN)_6]^{3-}$
(Asymmetric Supercapacitor)

◀**Fig. 3** **a** Schematic illustration of the preparation of PEDOT:PSS/CNF and the fabrication of PEDOT:PSS/CNP. Adapted with permission [28], Copyright 2023, Elsevier. **b** Organic cross-linked polymer-derived porous carbon production technique in one pot. Adapted with permission [29], Copyright 2023, MDPI; **c** Scrupulously designed porous carbon nanostructures with high pore volumes and surface area with prepared polymer-derived honeycomb-like carbon nanostructures (HCNs), taking nano-spherical silica as a template, PVDF as a carbon source, and PMMA as a pore-forming agent. The cells used the electrolytes of 6 M KOH and 0.1 M $K_3(Fe(CN)_6)^{3-}$ solutions. A PVDF/PVP composite membrane has been developed as a separator to fabricate a coin-cell device. Adapted with permission [30], Copyright 2023, Elsevier

safer, with excellent ionic conductivity allowing greater charge storage in a shorter time [4]. Hence, SCs based on aqueous electrolytes are promising for grid-scale power storage. However, the ions in aqueous electrolytes do not contribute to the capacitance value as they form an electric double layer on the electrode surfaces. Redox-active species can be added to the electrolyte to enhance the ionic conductivity and increase the capacitance [33].

Porous carbon nanostructures, such as those with macro-, meso-, and micropores, have a high specific surface area and can store a significant amount of charge via the electrochemical double-layer capacitance mechanism. The macro pores serve as an electrolyte reservoir, while the mesopores mitigate ion diffusion paths, and the micropores store the charge by their appropriate pore dimensions [34]. Since EDLC materials retain charge on their surfaces, these structures enable higher power density. Furthermore, when the surface area increases, energy density also increases. Nevertheless, gaps between porous carbon structures can cause electrolyte flooding and increase total electrode weight, which does not give additional capacitance value and reduces electrical conductivity. Hence, building porous carbon structures with no cavities is difficult [34].

The porous structures offer two advantages. Firstly, the solid matrix linking the porous structures works as a single substrate, limiting electrolyte flooding and enhancing electrical conductivity due to the continuous phase. Secondly, the micropores in the solid matrix give additional surface area and a specified capacitance value. Heteroatom doping can improve electronic conductivity and wettability, but it can also increase chemical consumption or need extra post-synthesis operations, increasing material prices. High-temperature annealing can improve crystallinity and conductivity but uses more energy than lower-temperature calcination [34].

Zou et al. introduced a non-solvent induced phase separation (NIPS) method to synthesize honeycomb-like carbon nanostructures (HCNs) to make highly porous carbon structure, with nano-spherical silica as a template, PVDF as a carbon source, and PMMA as a pore-forming agent (Fig. 3c) [30]. In this method, a slurry of PVDF/PMMA/DMF was prepared, and cotton/SiO_2 nanosphere templates were added to it, followed by the addition of non-solvent water. It separated polymer-rich and polymer-lean phases, which generated gaps and pores, and a uniform coating of PVDF/PMMA mixture on the SiO_2 nanosphere. After annealing and washing away the template, a honeycomb structure with numerous micro and mesopores was obtained. The resulting material exhibited a high specific capacitance of 578.80 F/g in a 6 M KOH

solution. To construct a supercapacitor device, PVDF/PVP composite membrane was used as a separator, and the addition of redox-active species [0.1 M $K_3(Fe(CN)_6)^{3-}$] with the electrolyte substantially enhanced the super capacitance properties. The improved performance was attributed to the concerted effect of HCNs, HCNox, redox-active added electrolytes, and the PVDF/PVP composite separator [30].

5 Polymeric Composite Materials

PANI exhibits excellent properties in electrochemical working devices using different structures, such as nanowire arrays [35], spheres [17], or films [36]. According to electrochemical impedance studies, PANI films produced by the potentiodynamic technique of electrodeposition display high specific conductance and resistance [37]. However, PANI is prone to flaking off the deposited surface during the charge–discharge cycle. PANI-prepared composites were fabricated to address this issue and demonstrated greater capacitance and stability than their equivalents [38]. Those composites comprise a physical combination of conducting polymer, metal nanoparticles, carbon powder, graphite fibers, metal-embedded glass fibers, and other polymers [39]. The percolation hypothesis explains the electrical conductivity in these composites, which assigns electrons flowing between metallic phases. Via using composites containing metal nanoparticles such as PANI/Pd-Sn [40], PANI/Au [41], and PANI/Pt [36], scientists can design novel physicomechanical characteristics of the composites aiming at a higher working performance of PSCs.

However, the studies on supercapacitors using the synchronized concept of PANI/Pt are limited. Pt thin films are widely used in high-performance circuits due to their long-term stability, although alternative materials are being developed in microelectronics. Sumana et al. reported a new mechanism where Pt nanoparticles were potentiostatically electrodeposited onto a porous PANI layer on stainless steel (SS) (Fig. 4a) [36]. Ionic conductivity and supercapacitor performance were improved in PANI/Pt nanoflowers compared to the PANI/SS electrode in charge–discharge experiments. The layer of electrodeposited Pt nanoflowers increased the hardness of PANI on the electrode. The supercapacitor made from Pt-PANI hybrid electrodes has a quasi-rectangular form and a specific capacitance of 926 F/g. Pt nanoflowers increased ion transport across the bulk of the supercapacitor, reducing the abrupt reduction in specific capacitance during charge–discharge. The layer of electrodeposited Pt nanoflowers increased the hardness of PANI on the electrode. The supercapacitor has a large potential window, charge–discharge stability, and coulombic efficiency of 98% [36].

Due to its advantages, polypyrrole (PPy) is another commonly used polymer material for SC electrodes. However, its poor cycling stability, resulting from volumetric swelling and shrinking during charge/discharge cycles, leads to structural breakdown and the rapid decay of conductive polymer properties [42]. One of the effective methods to overcome the drawback is making the composite of PPy with

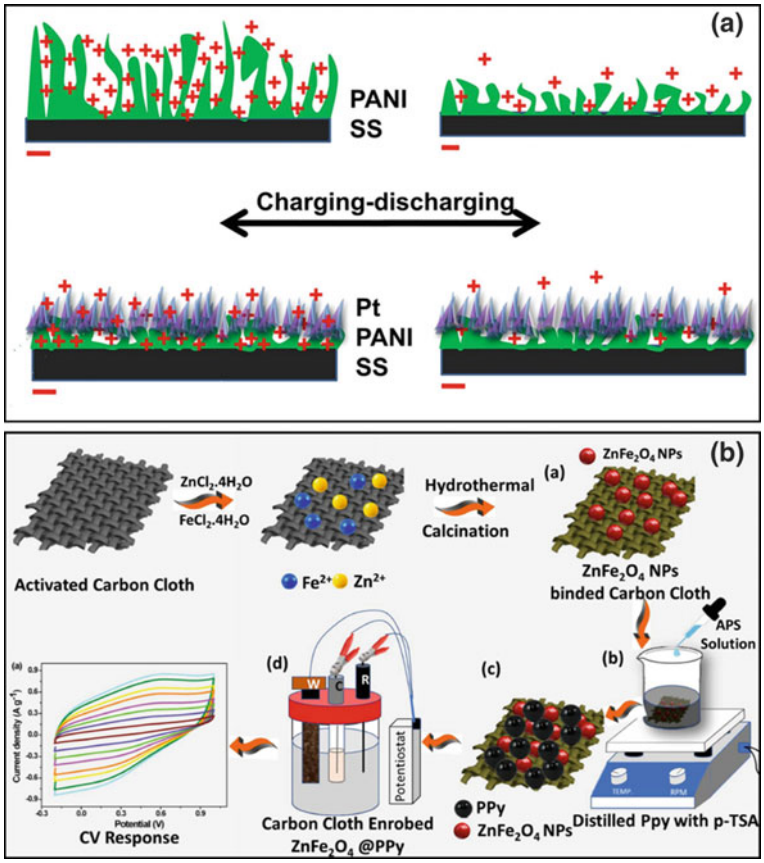

Fig. 4 **a** The probable mechanism for ion mobility at the electrode–electrolyte interface on PANI and PANI-Pt deposited electrodes during charge/discharge. Adapted with permission [36], Copyright 2023, Elsevier; **b** Schematic representation of: $ZnFe_2O_4$ NP formation on carbon cloth substrate, PPy creation on carbon cloth enrobed $ZnFe_2O_4$, CC-$ZnFe_2O_4$@PPy electrode, and electrochemical performance of CC-$ZnFe_2O_4$@PPy electrode. Adapted with permission [42], Copyright 2023, Elsevier

the ternary transition metal oxide (AB_2O_4), such as iron-based MFe_2O_4 ternary transition metal oxide. For example, $ZnFe_2O_4$ has shown great potential for SC applications due to its excellent electrochemical efficiency, spinal arrangement producing various active sites and ion diffusion pathways, and increasing electrochemical behavior and conductivity relative to binary metal oxides. However, it has poor electrical conductivity, and tends to agglomerate during charge/discharge cycles limit its SC implementations. Besides it, Carbon cloth (CC) is suitable for energy storage systems due to its 3D texture architectures, good electrical conductivity (1–10 S/cm), and outstanding mechanical stability. CC is a flexible biomaterial that provides extensive surface area for loading active materials. Devi et al. proposed a

general method for fabricating mesoporous $ZnFe_2O_4$@PPy nanocomposites on CC (Fig. 4b) [42]. In their study, $ZnFe_2O_4$@PPy nanocomposite was synthesized via simple hydrothermal and organic oxidative polymerization methods. Due to their respective design features, $ZnFe_2O_4$ nanoparticles that grow on CC have numerous chemical reaction active sites. Meanwhile, the PPy that forms on the $ZnFe_2O_4$ nanoparticle acts as a transverse conduit for electron transmission, lowering internal resistance. The perfect synthesis of these two materials offers good chemical and physical conditions for ion diffusion and rapid electron transmission, resulting in composites consisting of conducting polymer and ternary transition metal oxides with high working performance [42].

6 Conclusion and Future Perspective

Among various kinds of electrochemical energy materials, CPs exhibited excellent pseudocapacitance and flexibility in application. They can combine with different materials to increase the overall capacitance of PSC. Additionally, CP's flexibility allows them to transform into other materials structures, such as aerogel, via a simple reaction method. CPs, with their advantages, have much potential in the application of SCs. However, CPs also have hindrances, and the most significant one is their weak retention during long-time working performance. As mentioned, during the working process of SC, the organic molecules of CPs have to react with the ions from the electrolyte leading to their degradation. The strategy to overcome these problems is the combination of different materials to form the new composite materials, which can utilize the capacitance of each component to increase the overall working performance of SC.

Besides the mentioned advantages of CPs, choosing an electrolyte for the operation of SC also plays a vital role in their performance. Due to their organic structure, CPs are not dissolved but interact well with various organic solvents and aqueous electrolytes. Even though the common electrolyte used in SC studies now is aqueous electrolyte due to its safety and environmental friendliness, organic electrolytes also acquire significant interest from scientists. The research reports published in 2022 and 2023 related to CP materials applied for SC are described in Table 1. Optimizing electrolytes involved in SCs based on CPs materials can improve working performance. Consequently, CPs are potential materials for energy storage device studies and deserve further study to develop electrodes and devices with high specific capacitance and aim for industrial mass production.

Table 1 SC's working performance reports based on CP materials in 2022 and 2023

Materials	Specific capacitance (Scan rate)	Electrolyte	Retention rate (Cycles)	Ref.
PANI-Co_3O_4	593 F/g (0.5 A/g)	6 M KOH	89% (5000 cycles)	[43]
AC-PVA/rGO/PVP	223 F/g (1 A/g)	2.5 M KNO_3	99.3% (5000 cycles)	[44]
GO/PANI/$CoFe_2O_4$	781.27 F/g (1 mV/s)	1 M KOH	79.03% (5000 cycles)	[45]
Py-OXD-CMP/CNT	504 F/g (0.7 A/g)	1 M KOH	91.1% (2000 cycles)	[46]
TPU/CNT/PPyNF	712 mF/cm^2 5 mV/s	1 M H_2SO_4	85% (10,000 cycles)	[47]

Py: Pyrene
OXD-CMP: 1,3,4-oxadiazole-linked conjugated microporous polymers
TPU: thermoplastic polyurethane

Acknowledgements This work was supported by the Horizon Europe project TwinVECTOR of the European Union (Grant Agreement No. 101078935).

References

1. B. Luo, D. Ye, L. Wang, Recent progress on integrated energy conversion and storage systems. Adv. Sci. **4**, 1–15 (2017)
2. M.E. Yibowei, J.G. Adekoya, A.A. Adediran, O. Adekomaya, Carbon-based nano-filler in polymeric composites for supercapacitor electrode materials: a review. Environ. Sci. Pollut. Res. **28**, 26269–26279 (2021)
3. A. González, E. Goikolea, J.A. Barrena, R. Mysyk, Review on supercapacitors: technologies and materials. Renew. Sustain. Energy Rev. **58**, 1189–1206 (2016)
4. P. Bhojane, Recent advances and fundamentals of Pseudocapacitors: materials, mechanism, and its understanding. J. Energy Storage. **45**, 103654 (2022)
5. G.P. Hao, F. Hippauf, M. Oschatz, F.M. Wisser, A. Leifert, W. Nickel, N. Mohamed-Noriega, Z. Zheng, S. Kaskel, Stretchable and semitransparent conductive hybrid hydrogels for flexible supercapacitors. ACS Nano **8**, 7138–7146 (2014)
6. H. Huang, M. Niederberger, Towards fast-charging technologies in Li+/Na+ storage: From the perspectives of pseudocapacitive materials and non-aqueous hybrid capacitors. Nanoscale **11**, 19225–19240 (2019)
7. S. Fleischmann, J.B. Mitchell, R. Wang, C. Zhan, D.E. Jiang, V. Presser, V. Augustyn, Pseudocapacitance: from fundamental understanding to high power energy storage materials. Chem. Rev. **120**, 6738–6782 (2020)
8. A.M. Bryan, L.M. Santino, Y. Lu, S. Acharya, J.M. D'Arcy, Conducting polymers for pseudocapacitive energy storage. Chem. Mater. **28**, 5989–5998 (2016)
9. Q. B. Le, R. Kiefer, T. T. Dao, N. E. Kazantseva, P. Saha, Recent and future research related to the use of conducting polymers for supercapacitors, in: R. K. Gupta (Ed.), Springer International Publishing, Cham, pp. 289–309 (2022)

10. W. Gu, G. Yushin, Review of nanostructured carbon materials for electrochemical capacitor applications: advantages and limitations of activated carbon, carbide-derived carbon, zeolite-templated carbon, carbon aerogels, carbon nanotubes, onion-like carbon, and graphene, Wiley Interdiscip. Rev. Energy Environ. **3**, 424–473 (2014)
11. M.E. Abdelhamid, A.P. O'Mullane, G.A. Snook, Storing energy in plastics: a review on conducting polymers & their role in electrochemical energy storage. RSC Adv. **5**, 11611–11626 (2015)
12. M. C. Scharber, N. S. Sariciftci, Low band gap conjugated semiconducting polymers. Adv. Mater. Technol. **6** (2021)
13. J. Moon, V. Diaz, D. Patel, R. Underwood, R. Warren, Dissolvable conducting polymer supercapacitor for transient electronics. Org. Electron. **101**, 106412 (2022)
14. M. Huang, L. Li, Z. Ai, X. Gao, J. Qian, H. Xu, X. Su, J. Wu, Y. Gao, One-step fabrication of ice-templated pure Polypyrrole nanoparticle hydrogels for high-rate supercapacitors. ACS Appl. Nano Mater. **5**, 11940–11947 (2022)
15. M. Almtiri, T.J. Dowell, H. Giri, D.O. Wipf, C.N. Scott, Electrochemically stable carbazole-derived polyaniline for Pseudocapacitors. ACS Appl. Polym. Mater. **4**, 3088–3097 (2022)
16. Q.B. Le, T.-H. Nguyen, H. Fei, C. Bubulinca, L. Munster, N. Bugarova, M. Micusik, R. Kiefer, T.T. Dao, M. Omastova, N.E. Kazantseva, P. Saha, Electrochemical performance of composite electrodes based on rGO, Mn/Cu metal–organic frameworks, and PANI. Sci. Rep. **12**, 1–13 (2022)
17. L. Quoc Bao, T. -H. Nguyen, H. Fei, I. Sapurina, F. A. Ngwabebhoh, C. Bubulinca, L. Munster, E. D. Bergerová, A. Lengalova, H. Jiang, T. Trong Dao, N. Bugarova, M. Omastova, N. E. Kazantseva, P. Saha, Electrochemical performance of composites made of rGO with Zn-MOF and PANI as electrodes for supercapacitors. Electrochim. Acta. **367**, 137563 (2021)
18. V. Babel, B.L. Hiran, A review on polyaniline composites: synthesis, characterization, and applications. Polym. Compos. **42**, 3142–3157 (2021)
19. B. Wei, J. Liu, L. Ouyang, C.-C. Kuo, D.C. Martin, Significant enhancement of PEDOT thin film adhesion to inorganic solid substrates with EDOT-Acid. ACS Appl. Mater. Interfaces **7**, 15388–15394 (2015)
20. Z. Mekhalif, P. Lang, F. Garnier, Chemical pretreatment of platinum by aromatic and aliphatic thiols. Effect on polybithiophene electrodeposition and properties. J. Electroanal. Chem. **399**, 61–70 (1995)
21. L. Yang, S.K. Sontag, T.W. LaJoie, W. Li, N.E. Huddleston, J. Locklin, W. You, Surface-initiated Poly(3-methylthiophene) as a hole-transport layer for polymer solar cells with high performance. ACS Appl. Mater. Interfaces **4**, 5069–5073 (2012)
22. X. Luo, C.L. Weaver, D.D. Zhou, R. Greenberg, X.T. Cui, Highly stable carbon nanotube doped poly(3,4-ethylenedioxythiophene) for chronic neural stimulation. Biomaterials **32**, 5551–5557 (2011)
23. Q. Huang, J. Chen, S. Yan, X. Shao, Y. Dong, J. Liu, W. Li, C. Zhang, New donor–acceptor–donor conjugated polymer with twisted donor-acceptor configuration for high-capacitance electrochromic supercapacitor application. ACS Sustain. Chem. Eng. **9**, 13807–13817 (2021)
24. R. Jain, D. K. Sharma, S. Mishra, High-performance supercapacitor electrode of HNO 3 doped polyaniline/reduced graphene oxide nanocomposites. J. Electron. Mater. (2019)
25. Z. Zhu, Effects of various binders on supercapacitor performances. Int. J. Electrochem. Sci. **11**, 8270–8279 (2016). https://doi.org/10.20964/2016.10.04
26. H. Zhou, Z. Yan, X. Yang, J. Lv, L. Kang, Z.H. Liu, RGO/MnO2/polypyrrole ternary film electrode for supercapacitor. Mater. Chem. Phys. **177**, 40–47 (2016)
27. D. Belaineh, R. Brooke, N. Sani, M.G. Say, K.M.O. Håkansson, I. Engquist, M. Berggren, J. Edberg, Printable carbon-based supercapacitors reinforced with cellulose and conductive polymers. J. Energy Storage. **50**, 104224 (2022)
28. H. Du, M. Zhang, K. Liu, M. Parit, Z. Jiang, X. Zhang, B. Li, C. Si, Conductive PEDOT: PSS/cellulose nanofibril paper electrodes for flexible supercapacitors with superior areal capacitance and cycling stability. Chem. Eng. J. **428**, 131994 (2022)

29. J. Lao, Y. Lu, S. Fang, F. Xu, L. Sun, Y. Wang, T. Zhou, L. Liao, Y. Guan, X. Wei, C. Zhang, Y. Yang, Y. Xia, Y. Luo, Y. Zou, H. Chu, H. Zhang, Y. Luo, Y. Zhu, Organic cross-linked polymer-derived N/O-doped porous carbons for high-performance supercapacitor. Nanomaterials **12**, 2186 (2022)
30. S.K. Das, L. Pradhan, B.K. Jena, S. Basu, Polymer derived honeycomb-like carbon nanostructures for high capacitive supercapacitor application. Carbon N. Y. **201**, 49–59 (2023)
31. J. Kou, L.B. Sun, Nitrogen-doped porous carbons derived from carbonization of a nitrogen-containing polymer: efficient adsorbents for selective CO2 capture. Ind. Eng. Chem. Res. **55**, 10916–10925 (2016)
32. W. Zou, S. Zhang, Y. Abbas, W. Liu, Y. Zhang, Z. Wu, B. Xu, Structurally designed heterochain polymer derived porous carbons with high surface area for high-performance supercapacitors. Appl. Surf. Sci. **530**, 147296 (2020)
33. I.E. Rauda, V. Augustyn, B. Dunn, S.H. Tolbert, Enhancing pseudocapacitive charge storage in polymer templated mesoporous materials. Acc. Chem. Res. **46**, 1113–1124 (2013)
34. R. Mendoza, J. Oliva, V. Rodriguez-Gonzalez, Effect of the micro-, meso- and macropores on the electrochemical performance of supercapacitors: a review. Int. J. Energy Res. **46**, 6989–7020 (2022)
35. T. Zhang, H. Yue, X. Gao, F. Yao, H. Chen, X. Lu, Y. Wang, X. Guo, High-performance supercapacitors based on polyaniline nanowire arrays grown on three-dimensional graphene with small pore sizes. Dalt. Trans. **49**, 3304–3311 (2020)
36. V.S. Sumana, Y.N. Sudhakar, A. Varghese, G.K. Nagaraja, Pt nanoflower-poly(aniline) electrode material with the synchronized concept of energy storage in supercapacitor. Appl. Surf. Sci. **589**, 152994 (2022)
37. S.K. Mondal, K.R. Prasad, N. Munichandraiah, Analysis of electrochemical impedance of polyaniline films prepared by galvanostatic, potentiostatic and potentiodynamic methods. Synth. Met. **148**, 275–286 (2005)
38. N.Q. Khuyen, R. Kiefer, Q.B. Le, RGO/Ni-MOF composite modified with PANI applied as electrode materials for supercapacitor. Chem. Lett. **52**, 17–21 (2023)
39. Q. Meng, K. Cai, Y. Chen, L. Chen, Research progress on conducting polymer based supercapacitor electrode materials. Nano Energy **36**, 268–285 (2017)
40. H. Kebiche, F. Poncin-Epaillard, N. Haddaoui, D. Debarnot, A route for the synthesis of polyaniline-based hybrid nanocomposites. J. Mater. Sci. **55**, 5782–5794 (2020)
41. Z. Peng, L. Guo, Z. Zhang, B. Tesche, T. Wilke, D. Ogermann, S. Hu, K. Kleinermanns, Micelle-assisted one-pot synthesis of water-soluble polyaniline - gold composite particles. Langmuir **22**, 10915–10918 (2006)
42. R. Devi, J. Patra, K. Tapadia, J.-K. Chang, T. Maharana, Arrangement of ZnFe2O4@PPy nanoparticles on carbon cloth for highly efficient symmetric supercapacitor. J. Taiwan Inst. Chem. Eng. **138**, 104474 (2022)
43. I. I. Misnon, K. Manickavasakam, N. Nordin, R. Jose, Fabrication and electrochemical evaluation of polyhedral PANI-coated Co 3 O 4 electrode for supercapacitor application. Int. J. Appl. Ceram. Technol., 1–13 (2023)
44. D.T. Bakhoum, K.O. Oyedotun, S. Sarr, N.F. Sylla, V.M. Maphiri, N.M. Ndiaye, B.D. Ngom, N. Manyala, A study of porous carbon structures derived from composite of cross-linked polymers and reduced graphene oxide for supercapacitor applications. J. Energy Storage. **51**, 104476 (2022)
45. S. Verma, T. Das, V.K. Pandey, B. Verma, Nanoarchitectonics of GO/PANI/CoFe2O4 (Graphene Oxide/polyaniline/Cobalt Ferrite) based hybrid composite and its use in fabricating symmetric supercapacitor devices. J. Mol. Struct. **1266**, 133515 (2022)
46. M.G. Mohamed, M.M. Samy, T.H. Mansoure, S.U. Sharma, M.-S. Tsai, J.-H. Chen, J.-T. Lee, S.-W. Kuo, Dispersions of 1,3,4-oxadiazole-linked conjugated microporous polymers with carbon nanotubes as a high-performance electrode for supercapacitors. ACS Appl. Energy Mater. **5**, 3677–3688 (2022)
47. S.H. Hong, H.H. Shi, H.E. Naguib, Polypyrrole nanofoam/carbon nanotube multilayered electrode for flexible electrochemical capacitors. ACS Appl. Energy Mater. **5**, 4059–4069 (2022)

MXenes for Pseudocapacitors

Harishchandra S. Nishad, Rajesh R. Jaiswar, Sachin D. Tejam, and Pravin S. Walke

Abstract The emergence of transition metal carbides/nitrides (MXene) in 2011 has sparked significant interest in the development of 2D materials for energy storage applications. MXene's layered structure offers several advantages, such as increased active sites, rapid ionic diffusion, hydrophilicity, and a larger surface area. Moreover, the surface chemistry of MXene exhibits high-rate pseudocapacitance characteristics. This chapter aims to discuss various methods to alter the interlayer distance of MXenes and also discuss how these interlayers affect the electrochemical properties of the materials. Furthermore, the chapter explores various composites and hybrid structures involving MXene for pseudocapacitors. The storage capacity and kinetics of MXene are described in the context of pseudocapacitors. Finally, the challenges and prospects of MXene for supercapacitor applications are discussed.

Keywords MXene · Interlayer distance · Layered property · Composites MXene

1 Introduction

Clean and sustainable electric grid development is a global requirement to combat climate change. Electrochemical energy storage (EES) can play a key role in grid applications and enable seamless integration of green and carbon free energy. However, EES should meet the essential desires of high energy and power density [1–3]. For example, EES with high energy density provide long time power to the electric vehicles (EV), and high-power density provides intermittent power to the EV. EES devices for instance lithium ion batteries can store charge in the form of Li^+ ion intercalation/deintercalation, due to low ionic diffusion, it possesses lower power density [4]. Whereas, supercapacitor follow electric double layer charge storage, which is limited by surface mechanism, hence it cannot store large amount of energy

H. S. Nishad · R. R. Jaiswar · S. D. Tejam · P. S. Walke (✉)
National Centre for Nanosciences and Nanotechnology, University of Mumbai, Vidyanagari, Kalina, Mumbai, Santacruz (E) 400098, India
e-mail: shivshripsw@gmail.com

© The Author(s), under exclusive license to Springer Nature Switzerland AG 2024

R. K. Gupta (ed.), *Pseudocapacitors*, Engineering Materials,
https://doi.org/10.1007/978-3-031-45430-1_10

at a time and possess low energy density [5]. Therefore, research on the advancement of EES needs to enhance energy as well as power density. The alternative to the current technological advancement is the development of pseudocapacitive materials with enhanced surface redox reaction to store large amount of charge in the EES. Nanomaterials with large surface area would favor the irreversible surface redox reaction, but the electrolyte decomposition may led to low volumetric energy density.

In past two decades, after the discovery of 2D material like graphene, many materials have been developed through different exfoliation of various materials like black phosphorous (BP), boron nitride (BN), graphitic carbon nitride (g-C_3N_4), Transition metal dichalcogenides (TMD's), Transition metal oxides (TMO's) and layered double hydroxides (LDH's) but graphene got more attention due to its applications in energy storage [6–9]. The weak van der Waals bonding between the layers of graphene made limitation for uses in future research. Other Nobel metals like Ru, Pt, and Ir and other elements were also good candidates for grid scale but the natural abundance of these elements made it very costly for the practical application.

Generally, electrochemical charge storage devices such as batteries and supercapacitors follow various charge storage mechanisms. These mechanisms namely electric double layer capacitor, (EDLC), battery type and pseudocapacitor are governed by non-faradic, faradic process and combination of both process respectively [10]. Especially pseudocapacitors are dominated either by redox activities or by intercalation [11]. The materials following pseudocapacitive charge storage mechanism are known as pseudocapacitive materials. MXene is an emerging novel material that was developed by Yuri Gogotsi in the year 2011 [12]. These are basically transition metal carbides and nitrides with surface termination groups. MXenes are pseudocapacitive material electrode that possess high electronic conductivity and fast ionic diffusion this favors more suitable candidate for energy storage and grid scale [13]. MXenes are layered stacked structure of nanosheets and their composites have fascinated significant amount of interest in the development of pseudocapacitive property attributed to layered structure. The chemical formula of MXene is $M_{n+1}X_nT_x$ (n = 1–4) where M = Ti, V, Mo, Cr, Zr, Nb etc.; X represents C, N and the surface termination groups T = F, OH, Cl, O, etc.). The improved electrochemical properties and mechanical properties of 2D MXenes have gained prominent attention. Removal of Aluminum layer by suitable etching agent to form layered MXene $M_{n+1}X_nT_x$. [14].

MXene is derived from the layered hexagonal structure of MAX phase with space group $P6_3/mmc$. The first MAX phase was discovered by prof. Michel W. Barsoum, it has a laminated structure with anisotropic properties. Ti_3SiC_2 was the first MAX phase, which was a popular candidate for pseudocapacitive property. Further Prof Gogotsi et. al. derived MXene from MAX by etching with suitable etching agent (HF) [15]. The common layered structure of MXene is $Ti_3C_2T_X$. Hydrophobic nature of the MXenes is imparted due to the presence of surface termination groups (-OH, -F, O). This kind of material possesses more electrochemical active sites with high electrical conductivity for high energy, power density and fast charge storage. These fascinating properties made MXene promising candidate for EES like batteries and

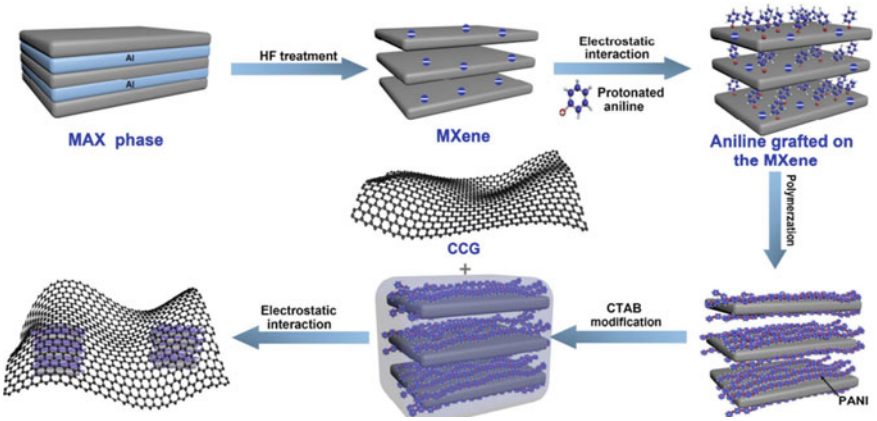

Fig. 1 Schematic illustration of Aluminum etching and aniline functionalization. Adapted with permission [14], Copyright (2018), American Chemical Society

supercapacitors [16]. Titanium and vanadium based MXenes and their composites ae mostly studied for the supercapacitors (Fig. 1).

2 Charge Storage and Kinematics in MXene

The EES devices possess charge storage mechanisms such as formation of electrical double layer in supercapacitors and ionic intercalation and deintercalation in batteries (e.g., Li^+ ion battery, Zn^{2+} ion battery). For grid scale application of EES, this mechanism provides insufficient performance as well as efficiency. The pseudocapacitive mechanism offers fast diffusion with redox reaction is alternative of this charge storage mechanism chemistry and emerged as potential application in grid scale. The sheet like structure of MXene (e.g., Ti_2CT_x, $Ti_3C_2T_X$, Mo_2CT_X and V_2CT_X) makes it promising material of class that uses intercalation pseudocapacitor mechanism [17–19]. The interlayer distance and stacked structure of MXene helps to enhance the electrochemical performance. After the complete etching of 'A' layer from MAX phase only, the stacks of MXene with 2D slits remain in the structure. Electrolytes with water molecules can easily confine into these slits that further boosts the capacitance. The reason for the enhancement is the negative dielectric constant, the dipolar nature of the water molecule can screen electric field and increases the capacitance for EDLC. The lateral layered structure improves the ionic diffusion and capacitance. $Ti_3C_2T_x$ fabricated using flash oxidation process resulted reversible capacity of 220 mAh g^{-1} at a C/18 after 30 cycles [20, 21]. 2D layered structure of MXene allows fast ion transport within 2D channels causes formation of redox active sites that add a pseudocapacitive part to the EDL mode of charge storage. It balances the flexibility of the layered nanosheets to accommodate large

ions for metal ion batteries and other EES. So, one of the effective ways to obtain the desired capacity is tuning of oxidation process. Incorporating water molecules to the 2D MXene lateral dimension can enhance the specific capacitance with better EDLC owing to dipolar polarization of water molecules. Stacked nanosheets of MXene minimize the exposures to electrolytes on the surfaces and fasten the ion intercalation leads to improved charge storage. Several researchers have examined the use of MXenes nanocomposite-based electrode material for EES. The electrode materials based on MXene show favorable properties such as large specific capacity and high rate of charge/ discharge. The partially delaminated layered structure of MXene allows ionic intercalation as well as electrical double layer formation for the charge storage contribution. Ultra -sonication method is more frequently used for the delamination of MXene nanosheets. Electrochemical properties of MXene electrode by delamination and without delamination process in aqueous as well as non-aqueous electrolytes are presented in this chapter [22].

3 Pseudocapacitive Asymmetric Devices

For better understanding of pseudocapacitive charge storage mechanism in supercapacitor, comparison of Cyclic Voltamogram (CV) curves of 2, 5-dihydroxy-1,4-benzoquinone (DBQ) and composite shown in Fig. 2a attributed to pseudocapacitive nature indicating semi-rectangular curve broaden by redox peaks [23].

The CV curves of an asymmetric device shown in Fig. 2b assembled, as DBQ@RGO//$TI_3C_2T_X$ in 3 M H_2SO_4 electrolyte at different scan rates (2–100 mV s^{-1}) [17]. CV curves show a combined double layer (flat ends) and Faradic (redox peaks) charge storage nature. No sign of electrolytic decomposition observed from the asymmetric devices even after reaching water-splitting potential. This pseudocapacitive phenomenon of asymmetric devices confirms the possibility to extend the potential window of the devices in protic electrolytes. At the higher scan rate of 100 mV s^{-1}, asymmetric devices exhibited good stability, better pseudocapacitive character, high rate performance and fast redox reaction kinetics. The charge storage mechanism in asymmetric capacitor was determined by CV curves with the following current (I) and scan rate (v) relation [17, 24, 25].

$$I = av^b \tag{1}$$

where a and b are two adjustable parameters. Plot of log (v) vs log (I) provides quantitative information regarding charge storage. The diffusion-controlled process consists of capacitance from battery type Faradaic intercalation and the response of current is directly proportional to the square root of the scan rate (i.e. b = 0.5). Capacitance for non-diffusion-controlled processes includes EDLC and due to the fast Faradaic charge transfer process with active atoms surface pseudocapacitance take place where the current response is directly proportional to scan rate (i.e. b = 1). In Fig. 2c, the b value obtained from anodic and cathodic peak currents are in

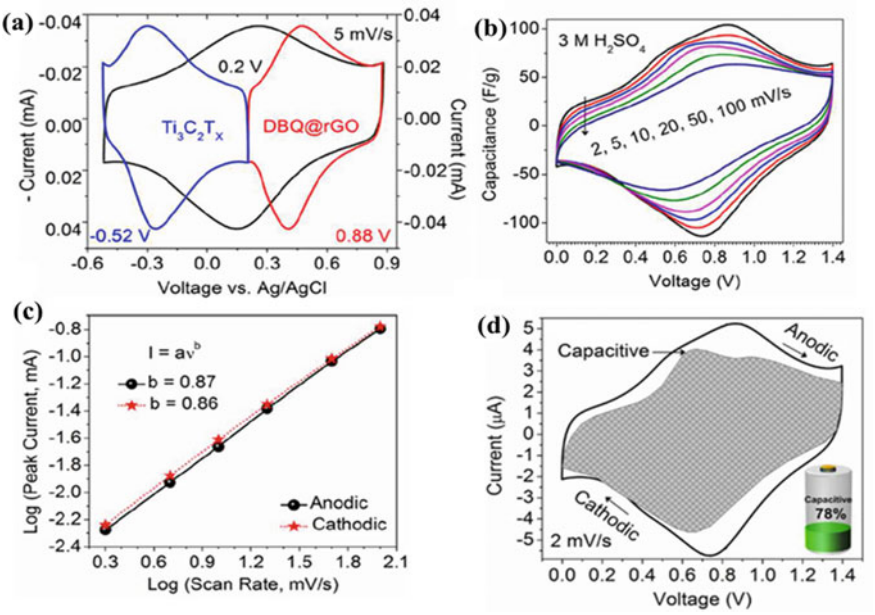

Fig. 2 **a** CV curves of an asymmetric cell at 5 mV s^{-1}, **b** CV curves at different scan rates of DBQ@rGO//$Ti_3C_2T_x$ **c** Corresponding b-value obtained using log (san rates) vs log (peak current) **d** Capacitive and diffusive contributions CV curve at 2 mV s^{-1}. Adapted with permission [17], Copyright (2019), Elsevier

0.86–0.87 range at 2–100 mV s^{-1}. From the b values, it is confirmed that the charge storage mechanism in all-pseudocapacitive asymmetric devices is battery type with no diffusion. Thus, the surface process limited redox and double-layer contributions of the DBQ@rGO and MXene qualify it as pseudocapacitive storage. Furthermore the asymmetric device enumerated the capacitive and diffusive contribution to the total current using following relationship.

$$I\,(V) = k_1(v) + k_2(v)^{0.5} \tag{2}$$

This relationship between current (I) at fixed potential is sum of the two processes, capacitive ($k_1\ v$) and diffusion-controlled process ($k_2\ v^{0.5}$). From the values of k_1 and k_2, it is possible to quantify the fraction of the current initiating from the capacitive and diffusion-controlled processes. The selected lower scan rate of 2 mV s^{-1} would permit precise estimation of the largest contribution to the diffusion-controlled process, which is 89% of the total current as shown in Fig. 2d. However, the high b-Value with high capacitive contribution at lowest scan rate confirmed the pseudocapacitive nature of DBQ@rGO electrodes [17, 25].

4 Intercalated Pseudocapacitor

MXene based electrodes exhibits intercalation of ions in the interlayer spacing from aqueous electrolyte to form EDL to narrow potential window of aqueous electrolyte promote pseudocapacitive performance [26]. While non aqueous electrolytes, the solvated ions intercalate into the interlayer spacing of the MXene in initial stage of charging process, narrowed solvation shell slowly collapse due to large potential difference in the interlayer spacing. Further charging initiate intercalation of desolvated ions and the atomic orbital of the MXene overlaps with the atomic orbital of desolvated ions for the formation of donor band. This gives rise to the intercalated pseudocapacitance through charge transfer between MXene nanosheets [27]. The differences in the charge storage mechanism between aqueous and non-aqueous electrolyte highlights dissimilarity of the electrochemical responses of MXenes. MXene possess better charge storage kinetics compared to the traditional 2D materials for EES devices, asymmetric capacitors using MXene electrode in aqueous and non-aqueous systems are capable of effectual operation at high charge and discharge rates.

4.1 Aqueous System

In aqueous electrolyte, ionic intercalation of hydrated cations (Li^+, Zn^{2+}, Na^+, K^+ etc.) without dehydration originated due to atomic orbitals of cation in hydration shell cannot hybridize with the atomic orbitals of MXene. Therefore, the separation of charge generates an inner potential difference ($\Delta\varphi = \varphi\_e^E - \varphi\_i^E$), where interlayer spacing is denoted by E; results in the formation of EDL. As a result of the small number of stored ions, electrochemical potential of the electron and ion should be always constant during the charge and discharge process. Hence, the potential difference governs the electrode potential during charging/discharging process. MXene has an insignificant pseudocapacitance nature to EDLC within the small potential window of aqueous electrolytes [28]. In acidic medium of electrolytes (e.g., H_2SO_4) distorted rectangular CV curves contributed to faradic reaction ($Mn^+ {}^-O + H^+ + e^- \rightarrow M\ (n - 1) + {}^-OH$). The in-situ X-ray absorption spectroscopy confirmed the reduction of M. Seemingly because of Faradaic reaction; acidic electrolytes provide the highest capacitance in aqueous electrolytes.

4.2 Non-Aqueous System

In the case of non-aqueous electrolytes, the salivation energy is very weaker than hydration energy. On the MXene electrode–electrolyte interface partial desolvation occurs, and hybridization of orbitals of surface termination group with atomic orbital

of cations occurs. The charge transfer between MXene and intercalated cations occurs with the hybridization of orbital. Organic electrolytes allow the large amount of electrons and cations for the storage results in large potential window, leading to significant changes in μ_e^E and μ_i^E due to the band-filling effect. Therefore, the enhancement in capacitance of MXene electrode from pseudocapacitive nature dominated by chemical potential, which is larger in organic (non-aqueous) than that of aqueous electrolytes. Modification of surface termination group and selection of proper intercalant can maximize the capacitance value. For example, Zn^{2+}, Na^+, K^+, Li^+ is intercalated into the matrix of MXene, 2 s orbital of ions interact with surface termination group to persuade large amount of charge transfer δ ($Mm^+ - Tn^- + Na^+ + e^- \rightarrow M(m^{-1} + \eta) + - T(n + \delta + \eta) - - X(1 - \delta) +$) where $X = Zn^{2+}$, Na^+, K^+, Li^+ [29, 30]. However, it should be accentuated that the change in chemical potentials, i.e., the redox reaction of 2D MXene electrode, plays a leading role in determining the pseudocapacitance.

5 Strategies to Tune the Interlayer Spacing

The controlling or tuning the interlayer spacing is a unique feature of Mxenes to enhance the electrochemical performance.

The modification of interlayer spacing in MXene through ion intercalation is a widely studied phenomenon. It involves the spontaneous insertion of cations, such as Na^+, Li^+, NH_4^+, K^+, and Mg^{2+}, from aqueous solutions into the interlayer regions of MXene [31]. Consider the example of ion intercalation in MXene interlayer spacing, the K^+ ion intercalation takes place via potassium hydroxide (KOH) treatment to interchange of -F with hydroxyl groups (OH^-) instantaneously. When $Ti_3C_2T_x$ was treated by KOH, the lattice parameter in the c-direction was enhanced from 25.0 Å to 19.2 Å, that suggesting the tuning interlayer distance via KOH treatment. Moreover, the introduction of organic molecule such as EDA (ethylene diamine), dicarboxylic acid Fig. 3a between the interlayer spacing of MXene enhances the performance of supercapacitor [16, 32, 33]. Because intercalating organic molecules into the MXene layers, EDA were able to increase the interlayer spacing. This enlargement facilitates better accessibility of electrolyte ions, which improves the energy storage capacity. Further, the introduction of polypyrrole (PPy), 0%, 24.2%, 39%, and 51.6% in the $Ti_3C_2T_x$, the 'd' spacing increases to 13 nm, 14.31 nm, 15.43 nm, and 17.76 nm respectively (Fig. 3b) [34]. However, the increase in interlayer spacing of MXene is not solely limited to ions or molecules. Other factors, such as heteroatom doping and structural geometry adjustments in MXene, also play significant roles in altering the interlayer properties. Doping candidates such as Nitrogen (N) and Sulphur (S) heteroatoms doped or Cobalt (Co)-doped MXenes have appeared as capable materials for supercapacitor application owing to their unique properties. These heteroatoms provide the significant advantage of enlarging the interlayer spacing between the MXene layers. Heteroatoms doped MXenes not only increase the interlayer spacing

to provide more space for ion intercalation, but also introduce numerous electrochemical active sites that promotes efficient ion adsorption and eventually enhance the electrochemical performance of the material [35]. The enlarged interlayer spacing of Mxene has various advantages; primarily the lower resistance to transport faster ionic and electronic movement. Moreover, it relieves strain within the material and facilitates volume expansion during the insertion/deinsertion mechanism. These combined effects contribute to improved performance and durability of the electrode material. More interestingly, the wrinkling and crumpling structures of MXene also tune the interlayer spacing. So, while designing electrode materials for the supercapacitor application, this parameter should be considered. The wrinkling or crumpling the MXene structures provides the lower resistance across the area that allows the fast ion transport (Fig. 4a, b) [36]. The restacking-free wrinkled MXene (TiC_2T_x) single layer along with sulfonic group with nitrogen decorated were achieved the specific capacitance of 260 F g^{-1} at 0.8 A g^{-1} along with 90% cycle stability even after 5000 cycles [37]. More interestingly due the wrinkling of MXene, the specific capacitance was three times higher than pristine MXene. Moreover, the crumbled MXene nanosheets in to the 3D architecture along with the porous structure demonstrated excellent pesudocapacitve property and exhibits the specific capacitance of 333 F g^{-1} at 1 A g^{-1} [38]. However, these crumbled MXenes are also stable at very higher current density, it showing specific capacitance of 132 F g^{-1} at 1000 A g^{-1}. So overall, the alteration of interlayer spacing of MXene materials can be done by various methods such as spontaneous intercalation of ions, insertion of molecules, hetero-atom doping, and crumbling or wrinkling of MXenes. These strategies play a very essential role in their design and optimization of interlayer spacing of MXene. Through this manipulation of the interlayer spacing, researchers can enhance the properties and performance of MXene materials, opening up new possibilities for their use in energy storage, electronics, and beyond.

6 Interlayer Spacing of MXene in Pesudocapacitor

For the preparation of MXenes, initial elimination of ‘A’ layers from MAX phase compounds, create the interlayer space between each MXene. The interlayer space offers the large active sites, fast ion transport, lower diffusion barrier and able to accommodate large umber ion between the layer. During the electrochemical reaction, intercalation involves the reversible insertion and extraction of cations (positively charged ions) into and out of the material’s layered structure (Fig. 4c). During intercalation, the host material undergoes structural changes to incorporate the cations between its layers. The cations are typically smaller in size compared to the spacing between the atomic layers, enabling them to fit into the interlayer spaces without disrupting the overall crystal structure. Especially, intercalated pseudocapacitor offers quick current response and larger surface functional groups during the electrochemical reaction. Moreover, in aqueous electrolyte, metal ions can interact with water molecules, forming an electric double-layer structure on the surface of

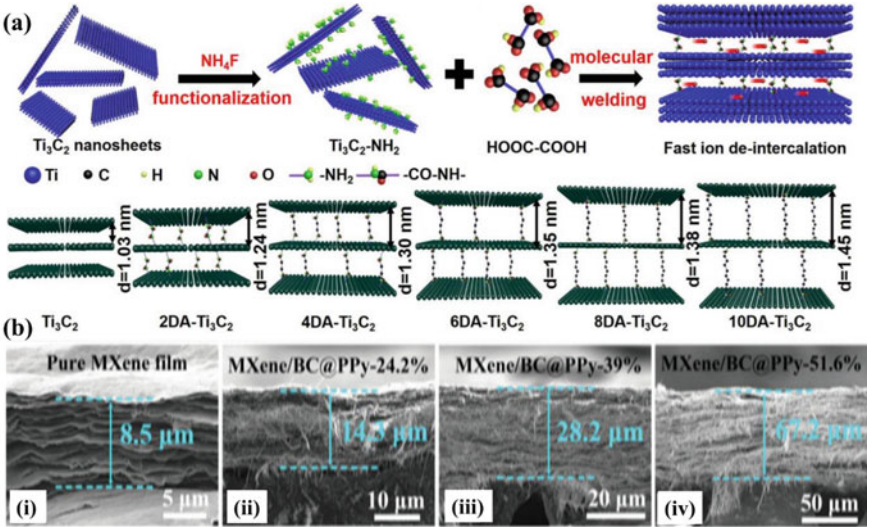

Fig. 3 Schematic illustration of intercalation of dicarboxylic acid between interlayer spaces of MXene along with structural representation. Adapted with permission [33], Copyright (2021), Elsevier. (**b–i**) FESEM image of MXene film, (**ii**, **iii**, and **iv**) FESEM image various composites of MXene respectively. Adapted with permission [34], Copyright (2021), Wiley

MXenes. Simultaneously, redox reactions take place between the surface functional groups of MXenes and the electrolyte. While in organic electrolyte at higher potential window can breakdown the electrical double layer structure.

7 Composites and Hybrid Structures of MXene

As graphene, TMOs, TMDs, and MOFs have shown a good conductivity and electrochemical properties but many efforts of their composites and hybrid materials proved enhance performance via synergetic effect. Hence systematic development of composites and/or hybrid.

MXene materials with complementary physical and electrochemical properties is excellent way to achieve giant pseudocapacitive storage [39]. Furthermore, pseudocapacitive materials have potential electrochemical properties, stability, long working life, high power, and energy density. In this context, two-dimensional layered structure is highly beneficial attributed to electrolytes more likely exposed to the electrode surface due to the greater surface-to-volume ratio. While these materials had good conductivity, they exhibited poor van der Waals bonding and hydrophobic nature. MXene is a class of two-dimensional material with a large surface-to-volume ratio, abundant electrochemical activity, and a high surface-to-volume ratio. In recent years, MXene-based composites have been gaining a lot of attention because of their 2D

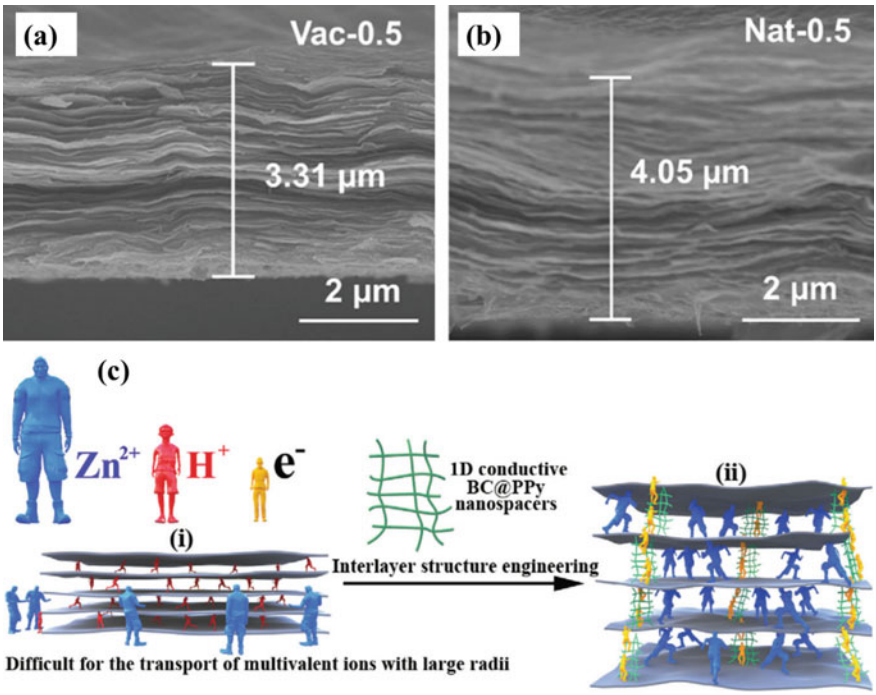

Fig. 4 **a**, **b** FESEM image of Ti3C3 vacuum drying, and natural drying, Adapted with permission [36], Copyright (2021), Springer. **c**–**i** schematic representation of different ions for MXene insertion, (ii) schematic illustration of ion inserted polypyrole between the interlayer space of MXene. Adapted with permission [34], Copyright (2021), Wiley

morphology, layered structures, and good flexibility. The combination of MXene with polymers, metal oxides, and carbon nanotubes has so far led to the development of several novel composite sites. MXene can improve polymer mechanical and thermal properties during composite formation because they have excellent mechanical properties, hydrophilic surfaces, and metallic conductivity. The surface hydrophilicity of single-layer MXene is higher than that of multi-layered MXene, and it is better compatible with polymers than that of multi-layered MXene [40]. Polymers are usually combined with MXene after they have been delaminated. The electrochemical actuator developed using a 3D structure of MXene/polystyrene-MXene demonstrated a significant bending strain (1.18%), a wide frequency bandwidth, excellent durability (90 percent of its performance is retained after 10,000 cycles), and an extremely high Young's modulus (about 246 MPa).

The MXene's outstanding actuation performance is because of its 3D structure along with high electrical conductivity and mechanical strength, MXene enables strong interaction between electrodes and rapid electron transfer [41]. Supercapacitors could benefit from MXene–oxide composite electrode materials as they are high in electrical conductivity and possess good electrochemical stability. By

combining metal oxides and sulphides, the theoretical capacity for a deposit can greatly increase MXene-based materials' energy storage capacity. Additionally, MXene can prevent metallic oxides and sulphides from collapsing. Additionally, the insertion can prevent MXene layers from re-stacking. For this reason, MXene-based composites are composed predominantly of metal oxides and sulphides. In addition to providing a large surface area for electrochemical reactions, MXene serves as a conductive framework that helps metal oxides to enhance its capacitance, stability, and overall performance. It is noteworthy that MXene composites are quite stable than other nanomaterials. Electrochemical performance of a composite is greatly influenced by its morphology, since pore size distribution, intercalation, and ion diffusion [42]. As one of the most promising transition metal oxides, MnO_2 features ultrahigh theoretical specific capacitance, excellent cycle stability, and ideal charge storage properties [43]. Guo et al. employed a wet spinning and electrochemical deposition method to grow MnO_2@MXene/CNT nanofibers, whose capacitance was 371.1 F cm^{-3}. This specific capacitance is much higher than MnO_2 electrodes and 1800% greater than CNT fiber electrodes. Overall 86.3% of the capacitance is retained after 10,000 cycles [44]. Zheng et al. prepared TiC_2T_x and $MoO_3/Ti_3C_2T_x$ composites (Fig. 5a–f) and between pristine $Ti_3C_2T_x$ and MoO_3 exhibit low electrochemical performance as comparison with $MoO_3/Ti_3C_2T_x$ (Fig. 5g, h). Further, the GCD curves of $MoO_3/Ti_3C_2T_x$ composites showed higher discharge time than other two materials (Fig. 4i). Thus $MoO_3/Ti_3C_2T_x$ anode containing $Ti_3C_2T_x$ bridging the molecular belts of MoO_3 generated 31.2 W h kg^{-1} gravimetric energy density and 39.2 Wh L^{-1} volumetric energy density [45]. As transition metal oxide contributes most of the weight to MXene, it has a high energy density. Cyclic stability was 94.2% after 10,000 cycles. The $CoFe_2O_4$ nanorods were prepared using MOFs attached to MXene nanosheets by Xie et al. In this case, Co-Fe oxide acts as a spacer between MXene layers, which increases the interlayer spacing and prevents restacking.

In addition to improving flexibility, Co-Fe enhances charge transfer with MXene. In LiCl electrolyte, the composite demonstrates a volumetric capacitance of 2467.6 F cm^{-3}. In addition to its electrochemical storage stability, this device has 88.2% capacitance retention after 10,000 charges and discharges, making it a better candidate for flexible and portable energy storage devices in the future [46]. Freestanding composite films comprising of $Ti_3C_2T_x$ nanosheets decorated with gold nanoparticles (AuNPs) were successfully synthesized via a self-reduction reaction between $Ti_3C_2T_x$ and an aqueous solution of $HAuCl_4$. The mixture solution was subjected to vacuum filtration to obtain the composite films. Subsequently, the MXene/AuNPs composite was employed as an electrode material for supercapacitors, marking the first utilization of MXene/AuNPs in this context (Fig. 6a–c). Remarkably, the electrochemical properties of the MXene/AuNPs electrodes were significantly enhanced in comparison to the pure $Ti_3C_2T_x$ electrodes [39]. Another composite material of MXene with NiFe-LDH materials were prepared via hydrothermal method. MXene

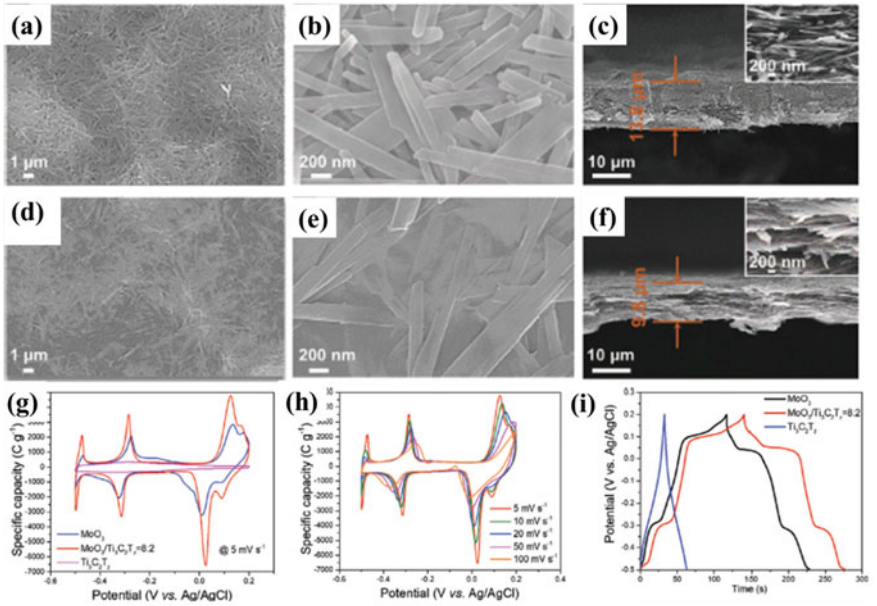

Fig. 5 **a** SEM images of MoO_3 in plan-view, **b** and cross-section view **c** $MoO_3/Ti_3C_2T_z$ composite in plan-view, **d**, **e** and cross-section view, **f** $Ti_3C_2T_z$ film in plan-view, **g** CV curves of MoO_3, MoO_3/TiC_2T_2, TiC_2T_x at 5 mV s^{-1}, **h** CV curves of MoO_3/TiC_2T_2 at different scan rates, **i** GCD curves of MoO_3, MoO_3/TiC_2T_2, TiC_2T_x at 5 A g^{-1}. Adapted with permission [45], Copyright (2021), Wiley

shows the nanoplate like morphology (Fig. 6d) while the composite of MXene/NiFe-LDH showing the Nanoflake like morphology (Fig. 6e). The electrochemical performance NiFe/MXene have higher specific capacitance value of 720.2 F g^{-1} than NiFe-LDH having 465 F g^{-1} [47]. Better performance and excellent electrical conductivity, high porosity, and mechanical stability of carbon nanotubes make them ideal conductive spacers for two-dimensional nanomaterials. MXene/CNT aerogels were fabricated by using easy directional freezing and freeze-drying methods to layer one-dimensional CNTs with MXene nanosheets. MXene nanosheets showed improved interactions because of the strong π-π interactions, whereas CNTs enhanced the network's interconnection. The resultant MXene/CNT composite aerogel shows high conductivity of 1600 S m^{-1} and an ultralow density of 7.0 mg cm^{-3}. Over 1000 cycles of compression and release, the MXene/carbon nanotube aerogel can retain approximately 85% of its initial strain. MXene/carbon nanotube aerogel possesses a specific capacitance of 142.5 F g^{-1} at 0.3 A g^{-1}. It concludes that MXene/carbon nanotubes are the most suitable material for flexible supercapacitors [48].

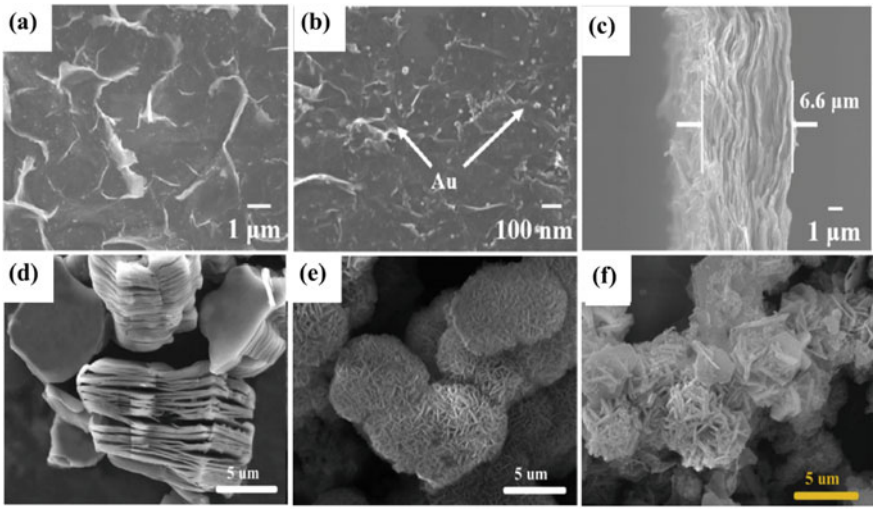

Fig. 6 **a**, **b** SEM images of MXene/AuNPs composite film at various magnification, **c** Cross-sectional view of MXene/AuNPs. Adapted with permission [40], Copyright (2021), Springer Nature. **d** SEM image of m-MXene, **e**, **f** SEM images of NiFe-LDH/MXene. Adapted with permission [47], Copyright (2020), Elsevier

8 Summery and Future Prospective

In summary, MXene materials exhibit exceptional charge storage capabilities and unique kinematics, making them promising candidates for pseudocapacitor electrodes. Further, different strategies can be utilized to tune the interlayer spacing of MXene such as spontaneous interaction of ions, molecules, crumping etc. whereas, the electrochemical property of MXene were investigated in both in aqueous and non-aqueous systems. Additionally, the integration of MXene into composites and hybrid structures further improved the overall performance of MXene-based pseudocapacitors. Currently, an emerging printing technology like continuous centrifugal coating are used for the fabrication of MXene based composites for microelectrode preparation. This printing method would be used to fabricate highly compact microelectrode. Pore engineering is one of the physical methods to emphasize the surface area of the MXene but due to the brittle nature of the MXene nanosheets, it is difficult to achieve by physical method. Chemical method used to modify the surface termination groups results in crumpling of MXene nanosheets. To achieve better electrochemical performance, modification of electrolyte to salvage charge storage ability for pseudocapacitor is necessary. EES devices like Li air batteries and current trending devices like Zn ion, Zn air batteries have experienced a resurrection due to progress in the technology for preparation of stable 2D materials. 2D MXene is an attractive material used as cathode preparation in Zn ion battery with improves specific capacity and stability and electrode material in supercapacitor with enhanced

cyclic stability, lifetime. A large number of theoretical study on ion batteries revealed electrochemical performance is not good as predicated, this is due to less fundamental understanding of mechanisms. Gap between fundamental understandings can be filled by operando characterization techniques to identify the errors and pursued suitable solution. Operando X-ray study for stabilizing effect on aqueous Zn capacitor with MXene based nanocomposite electrode advancing the path of research. MXenes worth as a consistent 2D electrode for EES devices, has been recognized by attempting various obstacles and this trend is expected to remain continue in the future for other materials. Therefore, MXene will grasp its true potential by fetching 2D materials to the large industrial-scale application.

References

1. M. Li, J. Lu, Z. Chen, K. Amine, 30 Years of Lithium-Ion Batteries. Adv. Mater. **30**, 1800561 (2018). https://doi.org/10.1002/ADMA.201800561
2. M. Fichtner, K. Edström, E. Ayerbe, M. Berecibar, A. Bhowmik, I.E. Castelli, S. Clark, R. Dominko, M. Erakca, A.A. Franco, A. Grimaud, B. Horstmann, A. Latz, H. Lorrmann, M. Meeus, R. Narayan, F. Pammer, J. Ruhland, H. Stein, T. Vegge, M. Weil, Rechargeable Batteries of the Future—The State of the Art from a BATTERY 2030+ Perspective. Adv. Energy Mater. **12**, 2102904 (2022). https://doi.org/10.1002/AENM.202102904
3. P. S. Walke, S. P. Gupta, H. Nishad, B. R. Sathe, D. J. Late, Engineering two-dimensional materials for high-performance supercapacitor devices. Fundam. Supercapacitor Appl. 2D Mater. 359–387. (2021). https://doi.org/10.1016/B978-0-12-821993-5.00001-7
4. J. Xie, Lu YC (2020) A retrospective on lithium-ion batteries. Nat. Commun. **111**(11), 1–4 (2020). https://doi.org/10.1038/s41467-020-16259-9
5. S.P. Gupta, P.S. Walke, Scalable multifunctional ultralight mesoporous micro yarn carbon for excellent durable supercapacitor and tremendous oils sorbent. Chem. Eng. J. **456**, 141011 (2023). https://doi.org/10.1016/J.CEJ.2022.141011
6. H.S. Nishad, S.P. Gupta, N.S. Khan, A.V. Biradar, J. Lee, S.M. Mane, P.S. Walke, Structural Transformation of Hydrated WO_3 into SnWO4 via Sn incorporation enables a superior pseudocapacitor and aqueous Zinc-Ion Battery. Energy Fuels (2023). https://doi.org/10.1021/ACS.ENERGYFUELS.3C00556/SUPPL_FILE/EF3C00556_SI_001.PDF
7. E.P. Asiwal, H.H. Nishad, C.S. Gujja, P.S. Walke, S.D. Pawar, Fabrication of anhydride core-based conductive layered Ni-MOF nanoflakes for high performance supercapacitors. New J. Chem. (2023). https://doi.org/10.1039/D2NJ06120A
8. H.S. Nishad, S.P. Gupta, V. Kotha, B.M. Patil, S.D. Chakane, M.G. Bute, S.W. Gosavi, D.J. Late, P.S. Walke, Enhanced van-der Waals separation in hydrated tungsten oxide nanoplates enables superior pseudocapacitive charge storage. J. Alloys Compd. **914**, 165227 (2022). https://doi.org/10.1016/J.JALLCOM.2022.165227
9. S.P. Gupta, H.H. Nishad, V.B. Patil, S.D. Chakane, M.A. More, D.J. Late, P.S. Walke, Morphology and crystal structure dependent pseudocapacitor performance of hydrated WO_3 nanostructures. Mater. Adv. **1**, 2492–2500 (2020). https://doi.org/10.1039/d0ma00518e
10. Y. Wang, L. Zhang, H. Hou, W. Xu, G. Duan, S. He, K. Liu, Jiang S (2020) Recent progress in carbon-based materials for supercapacitor electrodes: a review. J. Mater. Sci. **561**(56), 173–200 (2020). https://doi.org/10.1007/S10853-020-05157-6
11. H.T.H. Shi, S. Jang, A. Reza-Ugalde, H.E. Naguib, Hierarchically structured nitrogen-doped multilayer reduced graphene oxide for flexible intercalated supercapacitor electrodes. ACS Appl. Energy. Mater. **3**, 987–997 (2020). https://doi.org/10.1021/ACSAEM.9B02038/ASSET/IMAGES/MEDIUM/AE9B02038_0010.GIF

12. M. Naguib, M. Kurtoglu, V. Presser, J. Lu, J. Niu, M. Heon, L. Hultman, Y. Gogotsi, M.W. Barsoum, Two-Dimensional nanocrystals: Two-Dimensional nanocrystals produced by exfoliation of Ti3AlC2 (Adv. Mater. 37/2011). Adv. Mater. **23**, 4207–4207 (2011). https://doi.org/10.1002/ADMA.201190147
13. N.K. Chaudhari, H. Jin, B. Kim, D. San Baek, S.H. Joo, K. Lee, MXene: an emerging two-dimensional material for future energy conversion and storage applications. J Mater Chem A **5**, 24564–24579 (2017). https://doi.org/10.1039/C7TA09094C
14. J. Fu, J. Yun, S. Wu, L. Li, L. Yu, K.H. Kim, Architecturally robust Graphene-Encapsulated MXene Ti2CTx@Polyaniline composite for High-Performance Pouch-Type asymmetric supercapacitor. ACS Appl. Mater. Interfaces **10**, 34212–34221 (2018). https://doi.org/10.1021/ACSAMI.8B10195/SUPPL_FILE/AM8B10195_SI_001.PDF
15. K.R.G. Lim, M. Shekhirev, B.C. Wyatt, B. Anasori, Y. Gogotsi, Seh ZW (2022) fundamentals of MXene synthesis. Nat Synth **18**(1), 601–614 (2022). https://doi.org/10.1038/s44160-022-00104-6
16. M. Hu, H. Zhang, T. Hu, B. Fan, X. Wang, Z. Li, Emerging 2D MXenes for supercapacitors: Status, challenges and prospects. Chem. Soc. Rev. **49**, 6666–6693 (2020). https://doi.org/10.1039/d0cs00175a
17. M. Boota, C. Chen, K.L. Van Aken, J. Jiang, Y. Gogotsi, Organic-inorganic all-pseudocapacitive asymmetric energy storage devices. Nano Energy **65**, 104022 (2019). https://doi.org/10.1016/J.NANOEN.2019.104022
18. H. Tang, Q. Hu, M. Zheng, Y. Chi, X. Qin, H. Pang, Q. Xu, MXene–2D layered electrode materials for energy storage. Prog Nat Sci Mater Int **28**, 133–147 (2018). https://doi.org/10.1016/J.PNSC.2018.03.003
19. Q. Tang, Z. Zhou, P. Shen, Are MXenes promising anode materials for Li ion batteries? Computational studies on electronic properties and Li storage capability of Ti 3C 2 and Ti 3C 2X 2 (X = F, OH) monolayer. J. Am. Chem. Soc. **134**, 16909–16916 (2012). https://doi.org/10.1021/JA308463R/SUPPL_FILE/JA308463R_SI_001.PDF
20. S.A. Thomas, A. Patra, B.M. Al-Shehri, M. Selvaraj, A. Aravind, C.S. Rout, MXene based hybrid materials for supercapacitors: Recent developments and future perspectives. J Energy Storage **55**, 105765 (2022). https://doi.org/10.1016/J.EST.2022.105765
21. S. Yadav, A. Sharma, Importance and challenges of hydrothermal technique for synthesis of transition metal oxides and composites as supercapacitor electrode materials. J Energy Storage **44**, 103295 (2021). https://doi.org/10.1016/J.EST.2021.103295
22. M.R. Lukatskaya, S.M. Bak, X. Yu, X.Q. Yang, M.W. Barsoum, Y. Gogotsi, Probing the mechanism of high capacitance in 2D Titanium Carbide Using in Situ X-Ray absorption spectroscopy. Adv. Energy Mater. **5**, 2–5 (2015). https://doi.org/10.1002/aenm.201500589
23. Z. Wang, Z. Xu, H. Huang, X. Chu, Y. Xie, D. Xiong, C. Yan, H. Zhao, H. Zhang, W. Yang, Unraveling and regulating self-discharge behavior of Ti3C2Tx MXene-based supercapacitors. ACS Nano **14**, 4916–4924 (2020). https://doi.org/10.1021/ACSNANO.0C01056/SUPPL_FILE/NN0C01056_SI_001.PDF
24. M. Boota, Y. Gogotsi, MXene—Conducting polymer asymmetric pseudocapacitors. Adv. Energy Mater. **9**, 1802917 (2019). https://doi.org/10.1002/AENM.201802917
25. J. Wu, Q. Li, C.E. Shuck, K. Maleski, H.N. Alshareef, J. Zhou, Y. Gogotsi, L. Huang, An aqueous 2.1 V pseudocapacitor with MXene and V-MnO2 electrodes. Nano Res. **15**, 535–541 (2022). https://doi.org/10.1007/S12274-021-3513-X/METRICS
26. P. Zhang, J. Li, D. Yang, A. Soomro, B. Xu, P. Zhang, J. Li, D. Yang, R.A. Soomro, B. Xu, Flexible Carbon Dots-Intercalated MXene film electrode with outstanding volumetric performance for supercapacitors. Adv. Funct. Mater. **33**, 2209918 (2023). https://doi.org/10.1002/ADFM.202209918
27. J. Xu, T. Peng, Q. Zhang, H. Zheng, H. Yu, S. Shi, Intercalation effects on the electrochemical properties of Ti3C2TxMXene nanosheets for High-Performance supercapacitors. ACS Appl Nano Mater **5**, 8794–8803 (2022). https://doi.org/10.1021/ACSANM.2C00632/SUPPL_FILE/AN2C00632_SI_001.PDF

28. S. Zheng, C. Zhang, F. Zhou, Y. Dong, X. Shi, V. Nicolosi, Z.S. Wu, X. Bao, Ionic liquid pre-intercalated MXene films for ionogel-based flexible micro-supercapacitors with high volumetric energy density. J. Mater. Chem. A. **7**, 9478–9485 (2019). https://doi.org/10.1039/C9TA02190F
29. M. Okubo, A. Sugahara, S. Kajiyama, A. Yamada, MXene as a Charge Storage Host. Acc. Chem. Res. **51**, 591–599 (2018). https://doi.org/10.1021/ACS.ACCOUNTS.7B00481/SUPPL_FILE/AR7B00481_SI_001.PDF
30. J. Pang, R.G. Mendes, A. Bachmatiuk, L. Zhao, H.Q. Ta, T. Gemming, H. Liu, Z. Liu, M.H. Rummeli, Applications of 2D MXenes in energy conversion and storage systems. Chem. Soc. Rev. **48**, 72–133 (2019). https://doi.org/10.1039/C8CS00324F
31. R. Fang, C. Lu, A. Chen, K. Wang, H. Huang, Y. Gan, C. Liang, J. Zhang, X. Tao, Y. Xia, W. Zhang, 2 D MXene-based energy storage materials: interfacial structure design and functionalization. Chemsuschem **13**, 1409–1419 (2020). https://doi.org/10.1002/CSSC.201902537
32. K. Nasrin, V. Sudharshan, K. Subramani, M. Sathish, Insights into 2D/2D MXene Heterostructures for Improved Synergy in Structure toward Next-Generation Supercapacitors: A Review. Adv. Funct. Mater. **32**, 1–42 (2022). https://doi.org/10.1002/adfm.202110267
33. M.C. Liu, B.M. Zhang, Y.S. Zhang, B.N. Gu, C.Y. Tian, D.T. Zhang, Y.Q. Wang, B. Zhao, Y.Y. Wang, M.J. Liu, Y.J. Yu, K. Zhao, K.L. Bin, Y.L. Chueh, Regulating interlayer spacing with pillar and strain structures in Ti3C2 MXene layers by molecular welding for superior alkali metal ion storage. Mater Today Energy **22**, 100832 (2021). https://doi.org/10.1016/j.mtener.2021.100832
34. W. Cheng, J. Fu, H. Hu, D. Ho, Interlayer structure engineering of MXene-Based Capacitor-Type electrode for Hybrid Micro-Supercapacitor toward Battery-Level energy density. Adv. Sci. **8**, 1–13 (2021). https://doi.org/10.1002/advs.202100775
35. Y. Tang, J. Zhu, W. Wu, C. Yang, W. Lv, F. Wang, Synthesis of Nitrogen-Doped Two-Dimensional Ti 3 C 2 with enhanced electrochemical performance. J. Electrochem. Soc. **164**, A923–A929 (2017). https://doi.org/10.1149/2.0041706jes
36. N. Sun, Z. Guan, Q. Zhu, B. Anasori, Y. Gogotsi, B. Xu, Enhanced ionic accessibility of flexible MXene electrodes produced by natural sedimentation. Nano-Micro Lett **12**, 1–11 (2020). https://doi.org/10.1007/s40820-020-00426-0
37. Y. Li, Y. Deng, J. Zhang, Y. Shen, X. Yang, W. Zhang, Synthesis of restacking-free wrinkled Ti3C2Tx monolayers by sulfonic acid group grafting and N-doped carbon decoration for enhanced supercapacitor performance. J. Alloys Compd. **842**, 155985 (2020). https://doi.org/10.1016/j.jallcom.2020.155985
38. X. Zhang, J. Miao, P. Zhang, Q. Zhu, M. Jiang, B. Xu, 3D crumbled MXene for high-performance supercapacitors. Chinese Chem Lett **31**, 2305–2308 (2020). https://doi.org/10.1016/j.cclet.2020.03.040
39. Z.M. Qiu, Y. Bai, Y.D. Gao, C.L. Liu, Y. Ru, Y.C. Pi, Y.Z. Zhang, Y.S. Luo, Pang H (2021) MXenes nanocomposites for energy storage and conversion. Rare Met. **414**(41), 1101–1128 (2021). https://doi.org/10.1007/S12598-021-01876-0
40. X. Zhan, C. Si, J. Zhou, Z. Sun, MXene and MXene-based composites: synthesis, properties and environment-related applications. Nanoscale Horizons **5**, 235–258 (2020). https://doi.org/10.1039/C9NH00571D
41. T. Wang, T. Wang, C. Weng, L. Liu, J. Zhao, Z. Zhang, Engineering electrochemical actuators with large bending strain based on 3D-structure titanium carbide MXene composites. Nano Res. **14**, 2277–2284 (2021). https://doi.org/10.1007/S12274-020-3222-X/METRICS
42. C. Peng, Z. Kuai, T. Zeng, Y. Yu, Z. Li, J. Zuo, S. Chen, S. Pan, L. Li, WO3 Nanorods/MXene composite as high performance electrode for supercapacitors. J. Alloys Compd. **810**, 151928 (2019). https://doi.org/10.1016/J.JALLCOM.2019.151928
43. Y. Wei, W. Luo, Z. Zhuang, B. Dai, J. Ding, T. Li, M. Ma, X. Yin, Fabrication of ternary MXene / MnO 2 / polyaniline nanostructure with good electrochemical performances. Adv. Compos. Hybrid. Mater. **1082–1091** (2021). https://doi.org/10.1007/s42114-021-00323-z

44. Z. Guo, Y. Li, Z. Lu, Materials High-performance MnO_2 @ MXene/carbon nanotube fiber electrodes with internal and external construction for supercapacitors. J. Mater. Sci. **57**, 3613–3628 (2022). https://doi.org/10.1007/s10853-021-06840-y
45. Z. Zheng, W. Wu, T. Yang, E. Wang, Z. Du, W. Zheng, J. Halim, A. El Ghazaly, A.S. Etman, E.N. Tseng, P.O.Å. Persson, J. Rosen, M.W. Barsoum, Flexible Free-Standing MoO_3/Ti_3C_2Tz MXene composite films with high gravimetric and volumetric capacities. Adv. Sci. **8**, 1–9 (2021). https://doi.org/10.1002/advs.202003656
46. W. Xie, Y. Wang, J. Zhou, M. Zhang, J. Yu, C. Zhu, J. Xu, MOF-derived CoFe2O4 nanorods anchored in MXene nanosheets for all pseudocapacitive flexible supercapacitors with superior energy storage. Appl. Surf. Sci. **534**, 147584 (2020). https://doi.org/10.1016/J.APSUSC.2020.147584
47. H. Zhou, F. Wu, L. Fang, J. Hu, H. Luo, T. Guan, B.S. Hu, M. Zhou, Layered NiFe-LDH/MXene nanocomposite electrode for high-performance supercapacitor. Int. J. Hydrogen Energy **45**, 13080–13089 (2020). https://doi.org/10.1016/j.ijhydene.2020.03.001
48. T. Xu, Y. Wang, K. Liu, Q. Zhao, Q. Liang, M. Zhang, C. Si, Ultralight MXene/carbon nanotube composite aerogel for high—performance flexible supercapacitor. Adv. Compos. Hybrid. Mater. **8**, 1–9 (2023). https://doi.org/10.1007/s42114-023-00675-8

MXenes-Based Composites for Pseudocapacitors

Li Sun and Chunxu Pan

Abstract MXenes, a family of two-dimensional (2D) transition metal carbides/nitrides with a general formula of $M_{n+1}X_nT_x$ (n = 1–3), are demonstrated to act as a suitable electrode for high-performance energy storage devices owing to 2D lamellar structure, impressive density, metallic-like conductivity, availability of abundant active edge sites and tunable electrochemical properties, especially in supercapacitors. Nevertheless, MXenes have some demerits due to the aggregation and restacking of nanosheets, which hinder their further exploration. MXenes with the unique 2D layered surface and rich surface functional groups are easy to combine with other functional materials (transition metal oxides, transition metal disulfide compounds, conductive polymers, etc.) to construct composites, which can prevent MXenes aggregation, thereby promoting the formation of stable dispersions. Furthermore, owing to synergistic effects, the electrochemical performance of MXenes-based composites is superior to that of two precursors. In this chapter, the latest research progress of MXenes-based composites is elaborated and discussed. This chapter reviews various methods for preparing MXenes-based composites, introduces their applications in supercapacitors, and analyzes their excellent electrochemical properties. Similarly, we mainly focus on the current development, challenges, and prospects of MXenes-based composites for pseudocapacitors application.

Keywords 2D materials · MXenes-based composites · Electrochemical performance · Pseudocapacitors · Metal carbides/nitrides

L. Sun
Northwest Institute for Non-ferrous Metal Research, Xi'an 710016, People's Republic of China

C. Pan (✉)
School of Physics and Technology, MOE Key Laboratory of Artificial Micro- and Nano-Structures, Wuhan University, Wuhan 430072, China
e-mail: cxpan@whu.edu.cn

© The Author(s), under exclusive license to Springer Nature Switzerland AG 2024

R. K. Gupta (ed.), *Pseudocapacitors*, Engineering Materials,
https://doi.org/10.1007/978-3-031-45430-1_11

1 Introduction

Among various energy storage devices in modern electronic devices, supercapacitors as a new, green, safe, and efficient energy storage device have received widespread attention [1, 2]. How to achieve the advantages of fast charging/discharging, high power density, ultra-long cycle life, and excellent mechanical properties of supercapacitors under the premise of improving energy density has always been the focus of researchers in the field of new energy storage technology [3]. As an important component of supercapacitors, electrode materials are essential for their performance improvement [3]. At present, traditional electric double-layer capacitor materials (low energy density) and pseudocapacitor materials (poor stability or conductivity) have their own limitations [4]. Therefore, to realize the development and application of high-performance supercapacitors, there is an urgent need to build new high-efficiency electrode materials with reasonable morphology and structure, high electrochemical performance, high energy, and power density, and long cycle life.

The ways to improve the performance of supercapacitors mainly include active material selection and structure control. In 2011, Professor Michel W. Barsoum and Professor Yury Gogotsi first reported the successful synthesis of $Ti_3C_2T_x$ (MXenes) by selectively etching the original Ti_3AlC_2 (MAX phase), which sparked research on MXenes [5]. The MXenes can be expressed as $M_{n+1}X_nT_x$ or $M_{n+1}X_n$ (M and X are as in the MAX phase and T is O, OH, H, or F) [6]. MXenes can be semiconductive or metal-conductive with conductivity up to 6500 S/cm [4]. The conductivity depends on the atomic species of M and X, as well as the -T group. In addition, MXenes exhibit much higher pseudocapacitance than other capacitive materials. The MXenes solution has clay-like properties and therefore has a specific ability to form binder-free electrodes that reach high capacities (up to 900 F/m^3) at 2 mV/s [4]. Moreover, due to unique atomic layer thickness and lateral size, MXenes can withstand various deformations and has broad application prospects in the fields of new energy vehicles, portable electronic devices, flexible and wearable devices [7]. High capacitance (especially volumetric capacitance) and similar metallic conductivity make MXenes a promising active material for designing supercapacitors with high-energy and high-power density. However, pure MXenes typically exhibit unsatisfactory supercapacitors performance (low specific capacitance of 245 F/g in H_2SO_4 electrolyte), hindering its application as a commercial electrode material [4]. Therefore, various attempts have been made to overcome the problem of MXenes as electrodes, resulting in the idea of hybridization with pseudocapacitive materials to achieve effective performance improvement. In addition, the introduction of pseudocapacitive materials into the two-dimensional (2D) MXenes structure will effectively suppress the restacking and aggregation of nanosheets. So far, MXenes have successfully combined metals, metal sulfides, metal oxides, polypyrrole, etc., and applied in various fields, such as batteries, supercapacitors, electromagnetic wave absorption, water purification, etc. [7–10].

To understand the research progress of MXenes composites quickly and conveniently in pseudocapacitors, this chapter elaborates and discusses the latest research

progress of Mxenes-based composites, reviews various methods for preparing Mxenes-based composites, introduces their applications in supercapacitors, and analyzes their excellent electrochemical properties. Similarly, we mainly focus on the current development, challenges, and future prospects of Mxenes-based composites for pseudocapacitors application.

2 MXenes Based Composites for Pseudocapacitors

With the unique 2D layered structure, rich surface functional groups, and high electronic conductivity, MXenes are considered a promising material for preparing composites in energy storage applications [11]. At present, various active materials (metal oxides, metal sulfides, conductive polymers, etc.) have been combined with MXenes to achieve synergistic effects [11–13]. In composites, MXenes will provide high electron conductivity to promote rapid electron transfer, increase the achievable surface area, and stabilize the structure of the active material [8]. On the other hand, the active component serves as a spacer to increase interlayer spacing and reduce the reaccumulation of MXenes, thereby achieving rapid ion transport and improving ion accessibility [7]. In addition, active materials such as metal oxides, metal sulfides, and conductive polymers undergo reversible redox reactions to provide high pseudocapacitance for high energy storage [11]. Therefore, MXenes-based composites typically exhibit enhanced electrochemical performance, which represents an important and promising direction for MXenes in supercapacitor applications.

2.1 MXenes/Metal Compound Composites

Metal compounds have received widespread attention due to their low cost, natural abundance, environmental friendliness, and high theoretical capacitance, making them ideal materials for high-performance electrode materials in supercapacitors [7]. However, low conductivity significantly hinders their electrochemical performance. The strategy to further improve the performance of metal compound-based supercapacitors is to combine them with other high-conductivity materials to construct nanocomposites for assisting in rapid electron transfer [14]. Compared with metal compounds, MXenes have excellent conductivity but relatively low capacitance. Integrating MXenes with transition metal compounds into supercapacitor electrodes can combine their respective advantages while compensating for their respective shortcomings.

2.1.1 MXenes/Metal Oxide Composites

Metal oxides such as MnO_2, RuO_2, Co_3O_4, NiO, TiO_2, WO_3, Fe_2O_3, ZnO, etc. have been widely used to combine with MXenes to construct composites to achieve excellent capacitive performance [7, 11, 14]. MnO_2 is considered one of the most attractive electrode materials for supercapacitors in the metal oxides family due to extraordinary characteristics, such as pseudocapacitance behavior and high theoretical specific capacitance (1370 F/g) [7]. Recently, researchers have studied the application of different structures MnO_2 combined with MXenes to construct nanocomposites for optimizing the electrochemical performance of electrodes in supercapacitors. Yu et al. prepared a conductive, highly deformable, independent, fully pseudopaccapacitive electrode ($Ti_3C_2T_x$/MnO_2 NWs) using solution treatment in Fig. 1a [15]. MnO_2 NWs with a diameter of 10–30 nm and a length of 50 μm have excellent flexibility, which serve as intermediate layers and additional electrochemical active materials between $Ti_3C_2T_x$ nanosheets in Fig. 1b. This structure prevents MXene from restacking, improves pseudocapacitance, and maintains the excellent flexibility of the composite paper. The volume capacitance of the nanocomposites as an electrode for supercapacitors can reach up to 1025 F/cm^3 at 0.2 mA/cm^2 in Fig. 1c. In addition, the MnO_2/$Ti_3C_2T_x$ electrode exhibits excellent cycling stability (with a capacitance retention of 98.38% after 10,000 cycles). Yang et al. prepared a flexible MnO_2/$Ti_3C_2T_x$ hybrid film composed of porous $Ti_3C_2T_x$ nanosheets and MnO_2 nanoshells, which can be directly used as electrodes for pseudocapacitors [16]. The unique porous structure of the film promotes the vertical and planar transport of ions through the nanopores within and between $Ti_3C_2T_x$ nanosheets. Compared with MnO_2 nanoshells and porous $Ti_3C_2T_x$ nanosheets, the specific surface area, specific capacitance, and cycling stability of the hybrid film were significantly improved. The nanocomposites, as an electrode for supercapacitors, have a mass-specific capacitance of 452 F/g and a volume capacitance of 1273 F/cm^3 at a current density of 1 A/g, respectively. In addition, the MnO_2/$Ti_3C_2T_x$ electrode has high capacitance retention (90% after 5000 cycles).

In addition to MnO_2, researchers have explored many other active materials, such as Fe_2O_3, NiO, Co_3O_4 and Fe_3O_4, which can improve electrochemical performance by combining with highly conductive MXenes. Due to the high theoretical capacitance (3625 F/g) and large volume scalability in the process of charge and discharge, Fe_2O_3 combined with MXenes to construct nanocomposites can effectively improve the performance of electrodes [9]. Lan et al. reported a flexible hybrid paper composed of Fe_2O_3 nanoparticles fixed on $Ti_3C_2T_x$ (Fe_2O_3 NPs@MX) through electrostatic self-assembly and annealing treatment method in Fig. 1d [17].

Fe_2O_3 nanoparticles effectively expanded the layer spacing of $Ti_3C_2T_x$ nanosheets, allowing more electrochemical active sites to store charges. At the same time, $Ti_3C_2T_x$ nanosheets form a continuous metal skeleton (Fig. 1e), which suppresses the volume expansion of Fe_2O_3 nanoparticles during charging and discharging process, and enhances cycling stability. The nanocomposites have an ultra-high volume capacitance of 2607 F/cm^3 (584 F/g) in Fig. 1f and highly cycling stability (121% capacitance retention after 13,000 cycles). In addition, the assembled

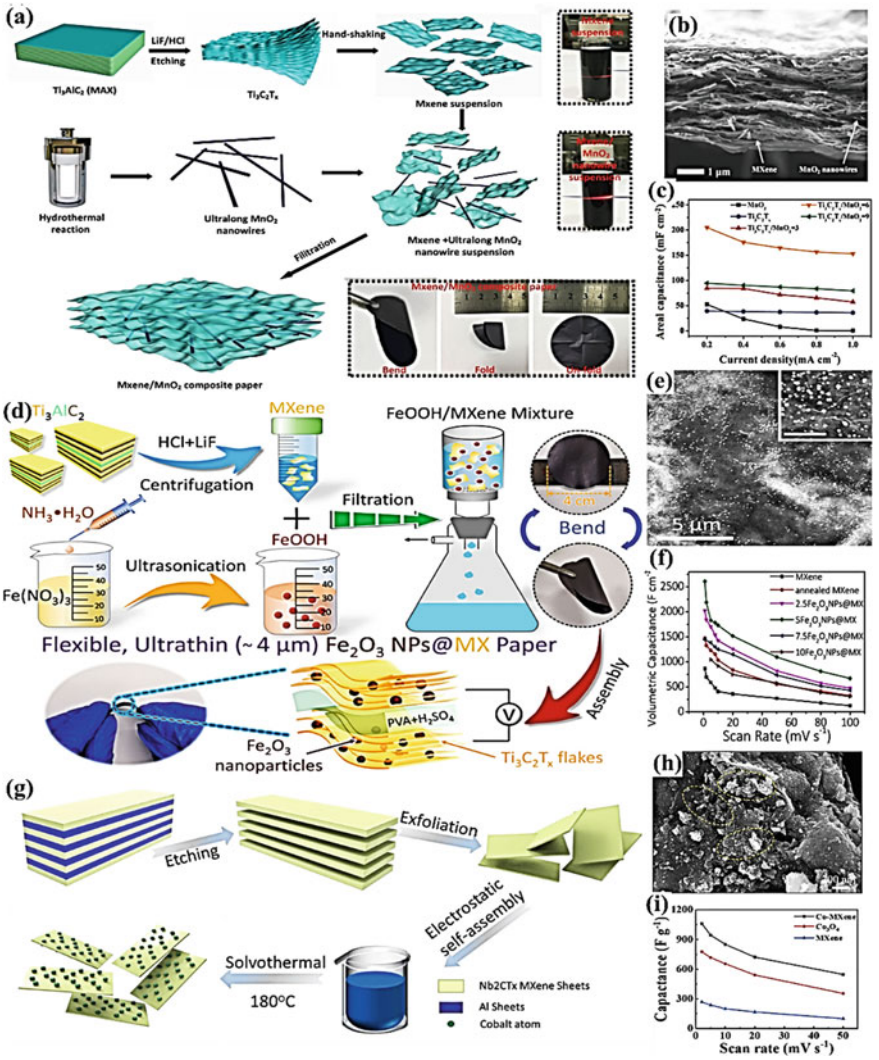

Fig. 1 $Ti_3C_2T_x/MnO_2$ NWs: **a** Preparation process; **b** SEM images and **c** Capacitance value. Adapted with permission [15], Copyright (2018), Wiley Online Library. Fe_2O_3 NPs@MX: **d** Preparation process; **e** SEM images and **f** Capacitance value. Adapted with permission [17], Copyright (2020), American Chemical Society. Co-MXene: **g** Preparation process; **h** SEM images and **i** Capacitance value. Adapted with permission [19], Copyright (2022), Elsevier

symmetrical solid-state supercapacitors show an energy density of 29.7 Wh/L and excellent mechanical flexibility. Ghule et al. synthesized NiO@MXene nanocomposites (NO@MX) in a controlled manner [18]. Firstly, 2D multi-layer MXene endows nanocomposite with excellent conductivity. The introduction of NiO inhibits the restacking of nanosheets, achieving a large surface area and providing more active

sites. Secondly, MXene enhances the electrical conductivity of NO@MX electrodes to improve electrochemical performance. The nanocomposite, as an electrode for supercapacitors, has an ultra-high specific capacitance of 1542 F/g. In addition, the all-solid-state asymmetric supercapacitors have an energy density of 10.7 Wh/kg and excellent stability (90.6% capacitance retention after 5000 cycles). Lou et al. successfully prepared Co-MXene composites by growing Co_3O_4 on the surface of Nb_2C-MXene using a hydrothermal method in Fig. 1g [19]. The composites have a high conductivity, 2D layered morphology, and an open structure. The self-assembly of Co_3O_4 between Nb_2C MXene layers (Fig. 1h) can effectively prevent the self-stacking of nanosheets. The high electrical conductivity and abundant active groups on the surface of MXene provide a large number of active sites for the uniform distribution of Co_3O_4. Nb_2C-MXene with a large specific surface area can be used as a substrate for growing Co_3O_4 nanoparticles to establish three-dimensional (3D) cross-linked structures, which provide an efficient electron transfer channel between Co_3O_4 nanoparticles and Nb_2C-MXene. In addition, the synergistic effect of MXene and Co_3O_4 makes the Co-MXene electrode has excellent electrochemical stability. The nanocomposites, as electrodes for supercapacitors, have a high specific capacitance of 1061 F/g at a current density of 2 A/g in Fig. 1i. In addition, the assembled asymmetric supercapacitors show an energy density of 60.3 Wh/kg and 93% capacity retention after 1000 cycles.

In addition to the above-mentioned metal oxides, other metal oxides (V_2O_5, MoO_3, WO_3, etc.) with high electrochemical properties have also been used to combine with MXenes to construct high-performance supercapacitors electrode materials. V_2O_5 shows the advantages of high voltage windows, good theoretical capacitance, low toxicity, and low cost, and has been widely used in energy storage devices, such as lithium-ion batteries and supercapacitors [5]. Ma et al. prepared $Ti_3C_2T_x$ MXene/V_2O_5 (MV) films by vacuum-assisted filtration of a mixture of MXene nanosheets and V_2O_5 nanofibers [20]. The introduction of V_2O_5 nanofibers effectively inhibits the self-stacking of MXene nanosheets, and the thickness of MV film can be adjusted by controlling the dosage of V_2O_5 nanoparticles. The MV films show excellent capacitive properties (319.1 F/g, 0.5 A/g) and cyclic stability (70.4%, 5000 cycles, 3 A g^{-1}), thanks to the efficient intercalation of V_2O_5 nanofibers. In addition, the asymmetric supercapacitors have a capacitance retention rate of 83.9% after 8,000 cycles and an energy density of 20.83 Wh/kg, indicating good energy storage capacity. Yuan et al. prepared MXene/MoO_3 hybrid membranes by vacuum-assisted filtration of MXene nanosheet suspension and MoO3 nanoribbon dispersion in Fig. 2a [21]. In composites, the ultra-thin MoO_3 nanoribbons (~16 nm) are easily in full contact with the conductive MXene substrate to reduce the inherent resistance and expose more electrochemically active sites for high capacitance behavior. At the same time, MoO_3 nanoribbons act as an effective intermediate layer between MXene nanosheets in Fig. 2b, preventing MXene from restacking, and enabling full expression of MXene capacitance. The composites as electrodes show ultra-high volume capacitance of 1817 F/cm^3 (545 F/g) at a scanning rate of 3 mV/s in Fig. 2c, exceedingly most previously reported MXene electrode materials. The composites

also maintain a good rate performance (773 F/cm^3 at 200 mV/s) and excellent electrochemical stability (100% capacitance retention after 5000 cycles). In addition, the symmetric supercapacitors can produce a volume energy density of 44.6 Wh/L (13.4 Wh/kg). Han et al. synthesized WO_3-Ti_3C_2-MXene composites by hydrothermal electrostatic adsorption and achieved in-situ synergy without additives or catalysts in Fig. 2d [22]. In the Hexa-WO_3-Ti_3C_2 hybrid, WO_3 nanoparticles are uniformly distributed on MXene nanosheets in Fig. 2e. This synergistic growth in WO_3-Ti_3C_2 hybridization eventually leads to a tight interaction between WO_3 and Ti_3C_2. In addition, the large specific surface area provides a larger channel for ion movement. The Hexa-WO_3-Ti_3C_2 hybrid anode exhibits excellent specific capacitance (566 F/g) in Fig. 2f and excellent stability (92.33% capacitance retention after 5000 cycles) at 2 mV/s due to rigid tunnel, high surface area, enhanced conductivity, and greater electrostatic interaction. The energy density of the supercapacitor assembled by the composites reaches 35.9 Wh/kg.

Currently, nanocomposites made by combining metal oxides with high-conductivity MXenes have been widely discussed due to their excellent performance. However, the electrochemical performance of MXenes can also be further improved by binding with bimetallic oxides, as their coupling enhances the REDOX reaction [7]. Yang et al. successfully prepared $Ti_3C_2T_x$ MXene composites loaded with Co–Ni bimetallic oxides by atomic layer deposition technology [23]. The uniform distribution of metal oxide nanoparticles on MXene nanosheets provides more active sites for pseudocapacitance generation, and the synergistic effect between CoO_x and NiO greatly improves the electrochemical performance. Compared with pure $Ti_3C_2T_x$ MXene, the electrochemical performance of $xCoO_x$–NiO/$Ti_3C_2T_x$ nanocomposites has been greatly improved. CoO_x–NiO/$Ti_3C_2T_x$ shows a high specific capacitance of 1960 F/g at 1 A/g, a rate performance of 87.3% at 1–18 A/g, and a capacitor retention of 90.2% after 8,000 cycles. Esfandiar et al. electrodeposited $Ti_3C_2T_x$ MXene on the surface of nickel foam and then constructed $RuCo_2O_4$/$Ti_3C_2T_x$-MXene hybrid materials by growing $RuCo_2O_4$ nanostructures in Fig. 2g–h [24]. $RuCo_2O_4$/$Ti_3C_2T_x$ MXene@NF has a high specific capacitance of 450 F/g at a current density of 3 A/g in Fig. 2i and 94% capacitor retention after 4000 cycles. In addition, the assembled symmetric supercapacitors have an energy density of 20.4 Wh/kg.

2.1.2 MXenes/metal Sulfide Composites

Metal sulfides are also very promising electrode materials for supercapacitors due to their high theoretical capacitance [13]. Metal sulfides generally have higher electron conductivity than metal oxides. In order to further improve the electrical conductivity of MXenes and buffer the volume changes during REDOX, the composite electrode materials for pseudocapacitors by combining various metal sulfides with MXenes have been reported recently [14]. Zhao et al. constructed multidimensional CoS_2 on the surface of MXene using cobalt chloride hexahydrate as the cobalt source by one-step solvothermal method in Fig. 3a [25]. The structure of MXene/CoS_2 composites not only inhibits the aggregation and stacking of MXene nanosheets, but

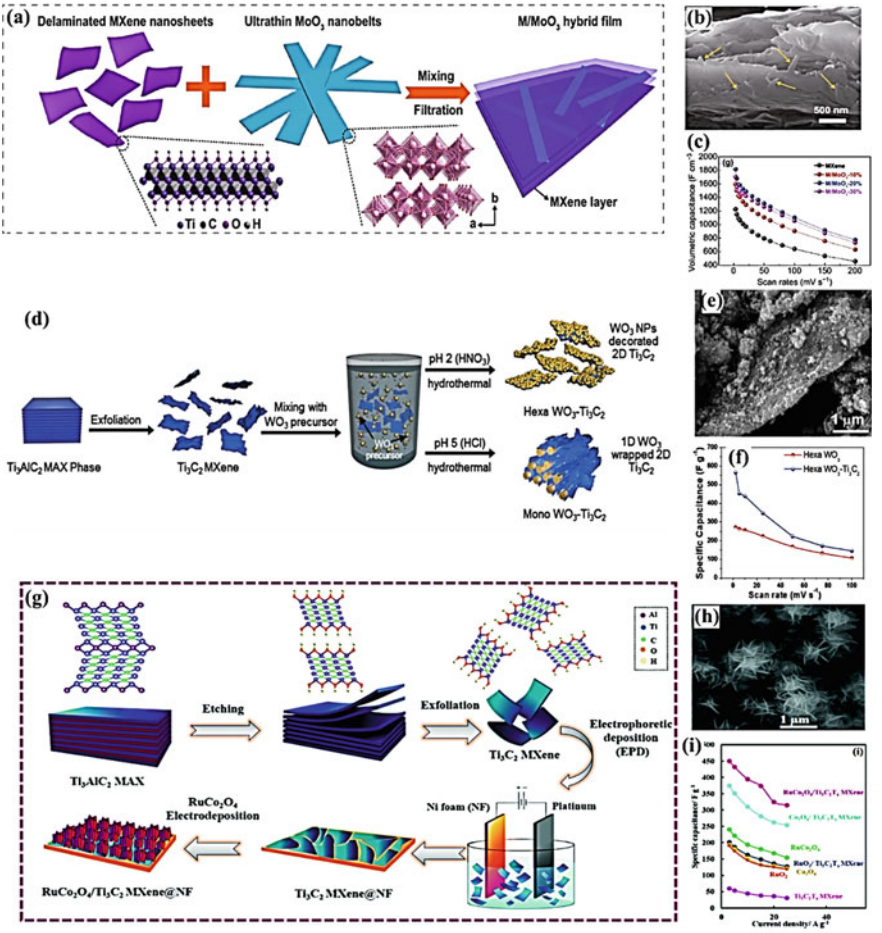

Fig. 2 MXene/MoO_3 hybrid membranes: **a** Preparation process; **b** SEM images and **c** Capacitance value. Adapted with permission [21], Copyright (2020), Springer. Hexa-WO_3-Ti_3C_2 hybrid: **d** Preparation process; **e** SEM images and **f** Capacitance value. Adapted with permission [22], Copyright (2018), Wiley Online Library. $RuCo_2O_4/Ti_3C_2T_x$ MXene@NF: **g** Preparation process; **h** SEM images and **i** Capacitance value. Adapted with permission [24], Copyright (2022), Royal Society of Chemistry

also increases the specific surface area of composites in Fig. 3b. Simultaneously, with the addition of cobalt ions, the active site of metal ions on the MXene surface increases, which also promotes the transfer efficiency between metal ions, improving electrochemical performance. The specific capacitance of the composites can reach 1320 F/g at a current density of 1 A/g in Fig. 3c. In addition, the asymmetric supercapacitors based on the composites show a wide potential window of 1.6 V and a high energy density of 28.8 Wh/kg, maintaining an initial specific capacitance of 98% after 5000 cycles. Qi et al. cultured flower-like 3D NiS on MXene ($Ti_3C_2T_x$)

by one-step hydrothermal method in Fig. 3d [26]. The nanosheets in the composite are interconnected to form a macroporous network structure, which facilitates the transfer of ions and charges. The 3D flower-like NiS prevents the aggregation of MXene and increases the metal ion sites in Fig. 3e. Compared with pure MXene, MXene/NiS composites achieve a specific capacity of 857.8 F/g at 1 A/g, about four times that of MXene in Fig. 3f. After 3,000 cycles, the composites still maintain 99.49% capacitance value. The asymmetric supercapacitors have an energy density of 17.688 Wh/kg. A small light bulb (12 V, 2W) can light up by the supercapacitor's device for more than 100 s. Zhong et al. synthesized the heterogeneous structure of MoS_2 deposited in multilayer $Ti_3C_2T_x$ nanosheets by a simple hydrothermal method [27]. MoS_2 is vertically arranged on the surface of $Ti_3C_2T_x$ nanosheets, forming an interconnected network structure, which increases the specific surface area of the electrode materials and improves the accessibility of the electrolyte. Meanwhile, the $Ti_3C_2T_x$ nanosheets provide a highly conductive and stable substrate for the growth of MoS_2. This structure greatly accelerates electron transfer, reduces the aggregation of 2H-MoS_2, and thus improves electrochemical performance. The MoS_2–$Ti_3C_2T_x$ heterostructure greatly improves the performance of supercapacitors. The specific capacitance reaches 303.8 F/g at a current density of 1 A/g, which is five times that of 2H phase MoS_2 (62.8 F/g) and three times that of $Ti_3C_2T_x$ (105.8 F/g). Meanwhile, the MoS_2–$Ti_3C_2T_x$ electrode exhibits excellent cycling stability (with capacitance retention of 82% after 10,000 cycles). The symmetrical supercapacitors based on MoS_2–$Ti_3C_2T_x$ show a specific capacitance of 115.2 F/g at 0.5 A/g, a good coulombic efficiency (over 90%), and cycling stability (capacitance retention of 72.3% after 10,000 cycles).

In addition to single metal sulfides, multiple metal sulfides ($NiCo_2S_4$, $CuCo_2S_4$, $ZnCo_2S_4$, etc.)/MXenes composites have also been reported. Javed et al. prepared a heterogeneous nickel cobalt sulfide nanoflower, which is embedded in the exfoliated $Ti_3C_2T_x$-MXene layer (HS-NCS@MXene) [28]. NCS nanoflowers are evenly dispersed in the MXene layer, forming a sandwich structure. HS-NCS@MXene exhibits excellent pseudocapacitive performance in a three-electrode system. The capacitance can reach 2637 F/g at 2.5 A/g, and a stable cycle life of 96% capacitance retention after 10,000 cycles. The asymmetric solid-state supercapacitors based on the composites can operate in a potential range of 1.6 V, providing a high capacitance of 226 F/g, a stable cycle life (92%) of 20,000 cycles, and a high energy density of 80 Wh/kg. Chen et al. reported a simple two-step strategy for designing layered 3D porous $CuCo_2S_4$/MXene composite electrodes to enhance storage performance [29]. This structure in $CuCo_2S_4$/MXene composites not only provides an abundant active site for the Faraday reaction, but also supplies a more effective way for rapid electron/ion transfer, and limits the volume expansion during the charging and discharging process. The $CuCo_2S_4$/MXene-3 electrode shows a specific capacity of 1351.6 C/g at 1 A/g and maintains excellent cycling stability (capacity retention of 95.2% after 1000 cycles). In addition, the energy density of the solid-state asymmetric supercapacitor device based on the composites reaches 78.1 Wh/kg. Qi et al. fabricated MXene/$ZnCo_2S_4$ composites by fixing $ZnCo_2S_4$ on MXene nanosheets surface using an electrostatic self-assembly method in Fig. 3g [30]. Due to the synergistic effect

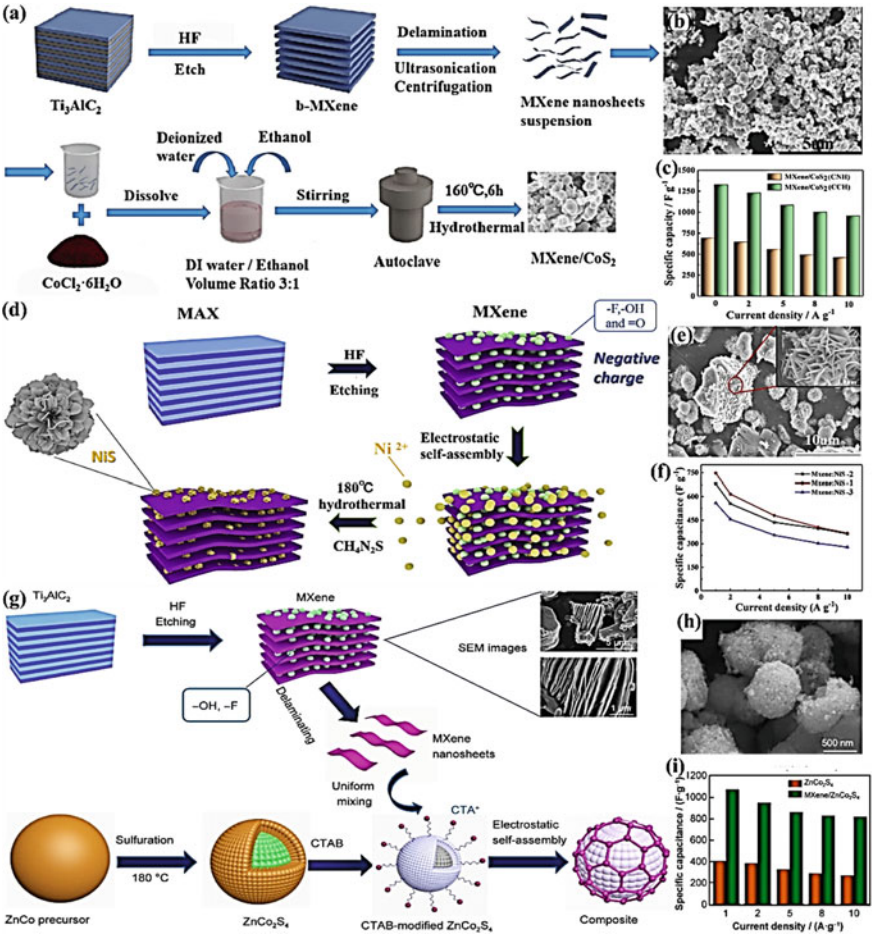

Fig. 3 MXene/CoS_2 composites: **a** Preparation process; **b** SEM images and **c** Capacitance value. Adapted with permission [25], Copyright (2020), Wiley Online Library. MXene/NiS composites: **d** Preparation process; **e** SEM images and **f** Capacitance value. Adapted with permission [26], Copyright (2020), Elsevier. MXene/$ZnCo_2S_4$ composites: **g** Preparation process; **h** SEM images and **i** Capacitance value. Adapted with permission [30], Copyright (2022), Springer

between MXene nanosheets and $ZnCo_2S_4$ core–shell nanospheres in Fig. 3h, the prepared composites exhibit a fast ion transfer rate and charge–discharge process. The capacity of MXene/$ZnCo_2S_4$ composites can reach 1072 F/g, which is much larger than that of $ZnCo_2S_4$ (407 F/g) in Fig. 3i. The asymmetric supercapacitors device based on the composites provides a 1.7 V potential window, superior cyclic stability (95.41% capacitor retention), and a high energy density of 30.46 Wh/kg. Fan et al. prepared a composite composed of 2D layered Ti_3C_2 and NiCoMn-S nanoparticles by a simple one-step hydrothermal method [31]. Many NiCoMn-S nanoparticles are distributed on the surface of Ti_3C_2, and even inserted into the Ti_3C_2 layer, providing

rich electrochemical active site for redox reaction, and enhancing the mechanical stability of the composites. In addition, the charge transfer resistance of NiCoMn–S/Ti_3C_2 composites is lower than that of pure NiCoMn-S, indicating that the 2D layered structure of Ti_3C_2 improves conductivity and enhances additional electron channels for ion transport. The specific capacity of NiCoMn-S/Ti_3C_2-3.4% reaches 347.1 C/g at a current density of 1 A/g, which is higher than that of pure NiCoMn-S (270.2 C/g). The asymmetric supercapacitors device based on this composite material achieves an energy density of 16.2 Wh/kg.

2.1.3 MXenes/metal Hydroxide Composites

Metal hydroxides are also considered a promising electrode material for energy storage devices due to their large surface area, abundant exposed sites, high theoretical capacitance, and infinite ion diffusion channels between layers [32]. However, the low conductivity and aggregation in electrochemical ion storage processes lead to a sharp decrease in capacity, resulting in poor stability and rate performance during long cycles, which hinders their commercial application [33]. Therefore, the combination of metal hydroxides and highly conductive MXenes can exert the synergistic effect between them to overcome the agglomeration problem in energy storage applications, and effectively improve the electrochemical performance. α-$Ni(OH)_2$ has unique physical and chemical properties, such as multivalent, precise electrochemical redox behavior, high theoretical capacitance value (2358 F/g, 0–0.44 voltage window), cost-effectiveness, and environmental friendliness. Ghosh et al. prepared a composite (MXene-$Ni(OH)_2$) in Fig. 4a, that α-Ni(OH)2 slides within the MXene layer in Fig. 4b, thereby preventing their reaccumulation [32]. In nanocomposites, MXene has larger layer spacing, accessible active site, and rapid ion/electron transfer, and α-$Ni(OH)_2$ exhibits faster redox reactions. Due to the synergistic effect between MXene and α-$Ni(OH)_2$, MXene-$Ni(OH)_2$ nanocomposites exhibit excellent specific capacitance of 1046.4 F/g at 5 A/g in Fig. 4c. The flexible all-solid-state asymmetric supercapacitors device based on the nanocomposites provides a high energy density of 29.3 Wh/kg and maintains 90% capacitance even after ~5000 cycles. Yu et al. prepared the cobalt hydroxide coupled $Ti_3C_2T_x$ MXene layers on nickel foam ($Co(OH)_2$–$Ti_3C_2T_x$@NF) by hydrothermal method [33]. The porous structure of nickel foam can ensure the rapid diffusion of electrolytes, and the heterogeneous structure prevents the agglomeration of layered materials. The 2D/2D heterostructure formed by the coupling of layered hydroxides and MXene can expose a larger specific surface area, increase the REDOX active site, and improve electrochemical performance. $Co(OH)_2$–$Ti_3C_2T_x$@NF has a high specific capacitance of 1400 F/g and a cycle stability of 98.2% after 10,000 cycles.

In addition to single metal hydroxides, double metal hydroxides are also considered an attractive alternative electrode for supercapacitors. Yang et al. prepared NiCo hydroxides/$Ti_3C_2T_x$ nanosheet composites with strong contact using $Ti_3C_2T_x$ MXene as the substrate [34]. It is found that NiCo hydroxides can replicate the MXene structure, generate enough contacts, accelerate electron transfer, and expose

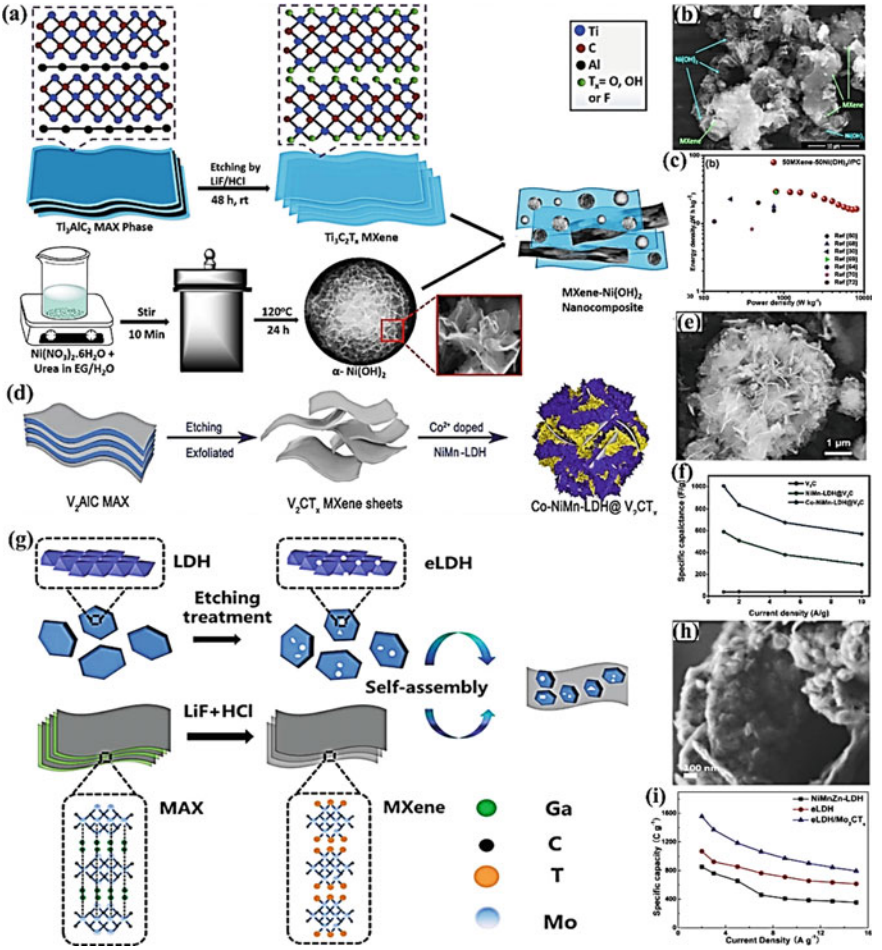

Fig. 4 MXene-$Ni(OH)_2$ nanocomposites: **a** Preparation process; **b** SEM images and **c** Ragone plot. Adapted with permission [32], Copyright (2022), American Chemical Society. CNMV composites: **d** Preparation process; **e** SEM images and **f** Capacitance value. Adapted with permission [35], Copyright (2022), Elsevier. NiMnZn hydroxide/Mo_2CT_x: **g** Preparation process; **h** SEM images and **i** Capacitance value. Adapted with permission [36], Copyright (2022), American Chemical Society

abundant electric active sites, thus improving the electrochemical kinetics. $Ti_3C_2T_x$ MXene can enhance the redox reaction kinetics of NiCo hydroxides nanosheets. The complete contact between $Ti_3C_2T_x$ MXene and NiCo hydroxides can significantly enhance conductivity, provide abundant reaction sites, increase the contact area of electrolyte ions, and improve charge storage capacity. The prepared NiCo hydroxides/$Ti_3C_2T_x$ electrode has a specific capacitance of 1030 F/g at 1 A/g, and the maximum energy density of the asymmetric supercapacitors based on the materials

can reach 59 Wh/kg. Han et al. successfully synthesized 2D/2D co-doped NiMn-layered hydroxide/V_2CT_x MXene (CNMV) electrode materials through a co-doping and electrostatic co-assembly method in Fig. 4d [35]. 2D V_2CT_x MXene as substrate has high conductivity, while NiMn-layered hydroxide has abundant electrochemical activity. The two components are closely combined to form 2D/2D nanoflower-like CNMV electrodes in Fig. 4e. The nano-flower-like composites not only overcome the poor specific capacitance of the original V2CTx MXene, but also the low conductivity and cycling performance of metal hydroxides. The CNMV electrode has a high specific capacitance of 1005 F/g at 1 A/g in Fig. 4f, and the asymmetric supercapacitors assembled based on CNMV have a high energy density of 30.16 Wh/kg. Dai et al. prepared 2D-on-2D nanohybrids of NiMnZn hydroxide/Mo_2CT_x with oxygen-rich vacancy by electrostatic assembly in Fig. 4g–h [36]. Mo_2CT_x MXene can provide conductive channels during rapid Faraday reactions, inhibit the reaccumulation of NiMnZn hydroxide nanosheets, and facilitate maximum exposure of their surface or edge active sites. The strategy of etching Zn atoms can effectively regulate the valence states of active Ni/Mn atoms and generate abundant oxygen defects in NiMnZn hydroxide, which is beneficial for electrochemical applications. The strong coupling between NiMnZn hydroxide and Mo_2CT_x can further regulate the surface electronic structure and oxygen vacancy content of NiMnZn hydroxide. Compared with pure NiMnZn hydroxide, Mo_2CT_x, and initial NiMnZn hydroxide, the specific capacity (1577 C/g at 2 A/g) in Fig. 4i, cyclic stability and good abundance of NiMnZn hydroxide/Mo_2CT_x nanohybrids obtained were greatly improved. In addition, the maximum energy density of the asymmetric all-solid supercapacitors based on the materials reached 92.6 Wh/kg.

2.2 MXenes/polymer Composites

Compared with other pseudocapacitive materials, conductive polymers exhibit additional advantages in supercapacitors due to simple synthesis, good conductivity, good flexibility, and high redox activity [12]. Many conductive polymers can achieve high capacitance in acidic electrolytes, as can MXenes/conductive polymer composites. At present, many conductive polymers, such as polyaniline (PANI), poly (3,4-ethylenedioxythiophene) (PEDOT), polypyridine (PPy), and polydopamine (PDA), combine with MXenes to prepare composites with excellent electrochemical performance [12]. Gogotsi et al. prepared a high-performance 3D PANI@M-$Ti_3C_2T_x$ composites by casting homogeneous polyaniline layer on 3D porous $Ti_3C_2T_x$ MXene in Fig. 5a–b [37]. The compact and highly integrated PANI@MXene heterostructure possesses a larger work function, so they have high anodic oxidation electrochemical stability and can be used as stable positive terminals. This electrode synergistically utilizes the high capacitance of PANI at a positive potential and the high-speed capability of MXene, which allows the PANI@M-$Ti_3C_2T_x$ electrode to have a high specific capacitance of 1632 F/cm^3, and a high-capacity retention of 827 F/cm^3 at a scanning rate of up to 5000 mV/s in Fig. 5c. The asymmetric supercapacitors

device assembled based on this material achieves a volumetric energy density of 50.6Wh/L. Yuan et al. proposed high conductivity PANI nanoparticles (PANI-NPs, ~10 nm) as intercalation agents, and adjusted MXene nanoflake interlayer by self-assembly method [38]. PANI-NPs not only inhibit the self-stacking of MXene, but also provides more ion transfer pathways. In addition, conductive PANI-NPs filled between MXene layers can construct interconnected conductive channels in the form of nanoparticles. Meanwhile, PANI-NPs will slightly change the thickness of the MX/PANI-NPs mixed film, resulting in higher volumetric capacitance. The capacitance of the MX/PANI NPs-10% electrode is 1885 mF/cm^2 (377 F/g), which can maintain a high capacitance of 873 F/cm^3 even when the MXene load reaches 5 mg/cm^2. In addition, the symmetrical supercapacitors assembled based on MX/PANI NPs hybrid films have a bulk energy density (20.9 Wh/L). Zhang et al. established a simple and effective method for preparing $Ti_3C_2T_x$/PEDOT: PSS hybrid membranes, which involves filtering $Ti_3C_2T_x$/Levios PH1000 composite ink, and then treating by H_2SO_4 in Fig. 5d–e [39]. The process of H_2SO_4 treatment can remove some insulating PSS on the $Ti_3C_2T_x$/PEDOT: PSS hybrid film, thereby significantly improving the conductivity of the composites. In addition, conductive PEDOT can not only serve as a pillar between $Ti_3C_2T_x$ sheets, exposing more electroactive surfaces and reducing ion diffusion pathways but also serve as a conductive bridge to form multidimensional electron transfer channels for accelerating the electrochemical reaction process. The specific surface area of $Ti_3C_2T_x$/PEDOT: PSS ($Ti_3C_2T_x$/P-100-H) hybrid film treated with H_2SO_4 increased by 4.5 times, and the capacity reached 1065 F/cm^3 at 2 mV/s, demonstrating excellent rate performance in 1 M H_2SO_4 electrolyte in Fig. 5f. The asymmetric supercapacitors based on the materials show an energy density of 23mWh/cm^3 and a power density of 7659 mW/cm^3. Ma et al. prepared MXene/PPy (M-PPy) composite films using MXene nanosheets and PPy nanofibers as raw materials by vacuum-assisted filtration in Fig. 5g [40]. By introducing PPy nanofibers, the layer spacing of MXene nanosheets is expanded in Fig. 5h, providing more transport channels and ion reachability sites. The introduction of PPy nanofibers effectively prevents the self-accumulation of MXene nanosheets, while the interlayer gap of MXene nanosheets effectively overcomes the expansion of PPy during the charging and discharging process. M-PPy3 shows high capacitance (563.8 F/g) in Fig. 5i and excellent cycling performance (79.5%, 6000 cycles). The asymmetric supercapacitors assembled based on the materials have a capacitance retention rate of 86.8% after 6000 charging/discharging tests at 2 A/g, and an energy density of 35.3 Wh/kg, demonstrating excellent energy storage capacity. Zhang et al. successfully synthesized $Ti_3C_2T_x$/PDA composite membrane electrodes by one-step in-situ polymerization of dopamine on the surface of $Ti_3C_2T_x$ nanosheets [41]. The introduction of PDA effectively prevents the restacking of $Ti_3C_2T_x$ nanosheets, which is conducive to exposing more active sites, increasing interlayer spacing, and promoting electron transfer and ion diffusion. Compared with pure $Ti_3C_2T_x$, this structure is advantageous for fast Faraday reactions. In addition, the strong bonds are formed between the O–H groups and/or N–H groups of the PDA ring and the –O and/or –F terminal groups on the surface of the $Ti_3C_2T_x$ nanosheets. Titanium ion in the $Ti_3C_2T_x$ nanosheets and the –O group originated from catechol structure can form a

strong chelation, leading to a stable electrode structure. The $Ti_3C_2T_x$/PDA composite electrode shows a capacitance of 715 mF/cm^2 at a scanning rate of 2 mV/s and maintains an initial capacitance of 95.5% after 10,000 cycles, demonstrating long cycle stability. When the mass load increases to 13.6 mg/cm^2, the capacitance can increase to 3440 mF/cm^2.

2.3 MXenes Based Other Composites

In addition to metal oxides, metal sulfides, metal hydroxides and polymers, many other materials have been combined with MXenes for pseudocapacitors, such as metal organic frameworks, metal phosphides, black phosphorus, selenide, antimony alkenes, MXene, etc. [7, 11]. Li et al. utilized 2D aminated $Ti_3C_2T_x$ to in-situ stabilize a bimetallic Ni/Co metal organic framework (Ni/Co MOF) with high redox activity, and constructed a layered heterostructure composites with excellent wettability in Fig. 6a [42]. Due to the high conductivity and good wettability of aminated MXene, bimetallic Ni/Co MOF can be uniformly in-situ stabilized on the surface of aminated MXene in Fig. 6b, ensuring excellent electron and ion transport from redox active centers, good interface compatibility, and large contact area. The modified MXene is beneficial for slowing down van der Waals interactions between functional groups, and leading to separation of sheet-like structures. The synergistic effect of high redox activity Ni/Co in bimetallic Ni/Co MOF provides a rapid redox effect for Faraday capacitors. Therefore, Ni/Co-MOF@TCT-NH_2 has an ultra-high specific capacitance of 1924 F/g at 0.5 A/g, and an ultra-long cycle stability of 10,000 times at 10A/g. In addition, the asymmetric supercapacitors device assembled based on the materials exhibits a maximum specific energy density of 98.1 Wh/kg at 600 W/kg and excellent rate stability. Sun et al. demonstrated the in-situ coupling of NiCoP bimetallic phosphides and Ti_3C_2 MXene to establish a heavy-duty NiCoP/MXene (NCPM) electrode in Fig. 6c–d [43]. The 3D printed NCPM electrode with layered pores and adjustable mass load shows easy charge transfer and electrolyte permeation, enhancing rate ability and cycling stability. Therefore, the printed electrode has a sturdy and open frame, while combines the good capacitance of NiCoP and the excellent conductivity of MXene. The electrode respectively achieves a high area and volume capacitance of 20 F/cm^2 and 137 F/cm^3 even under a high-quality load of approximately 46.3 mg/cm^2. The asymmetric supercapacitors assembled based on the materials can easily achieve ultra-high area and volume energy densities of 0.89 mWh/cm^2 and 2.2 mWh/cm^3, respectively.

Yang et al. reported a black phosphorus (BP)@MXene compact film in Fig. 6e [44]. 3D porous network structure is successfully made by in-situ growth of BP nanoparticles on crumbled MXene flakes. The strong interfacial interaction (Ti–O-P bonds) formed at the BP-MXene interfaces not only enhances the atomic charge polarization in the BP-MXene heterostructures, leading to efficient interfacial electron transport, but also stabilizes the 3D porous dense architecture with much improved mechanical robustness. The introduction of BP nanoparticles effectively

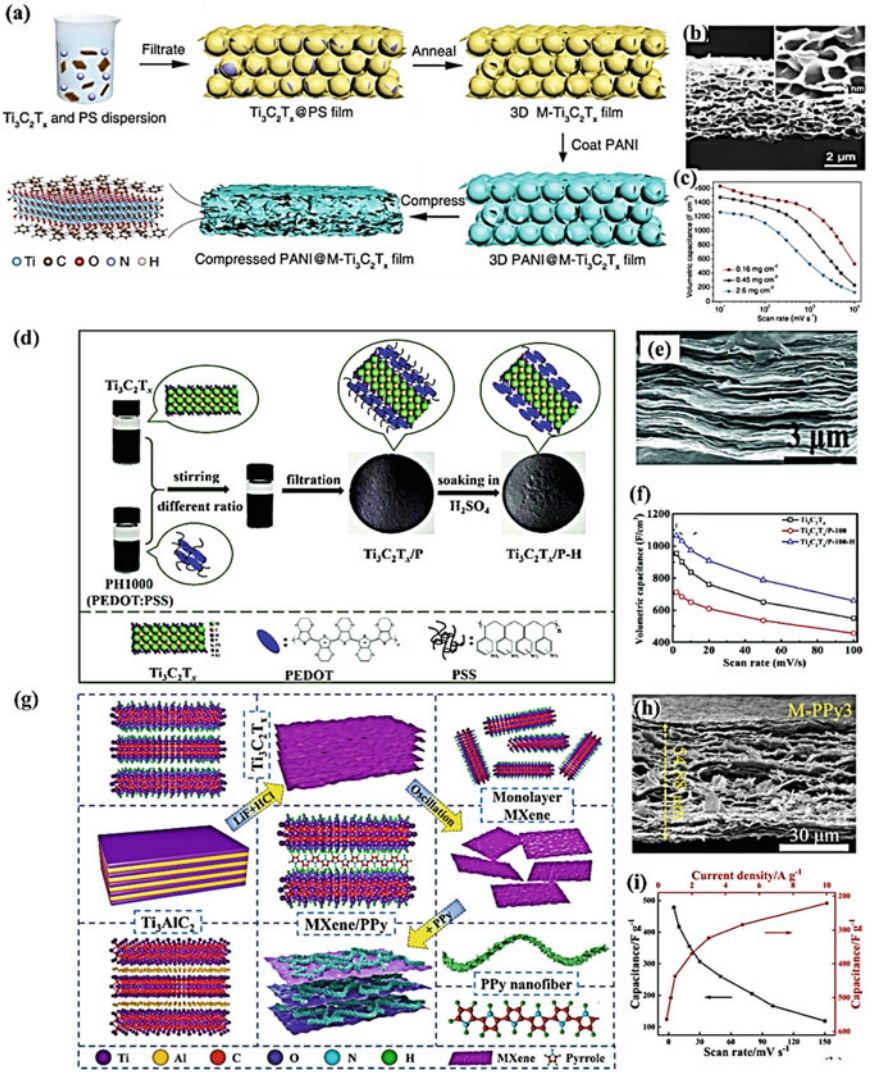

Fig. 5 3D PANI@M-$Ti_3C_2T_x$ composites: **a** Preparation process; **b** SEM images and **c** Capacitance value. Adapted with permission [37], Copyright (2020), Wiley Online Library. $Ti_3C_2T_x$/P-100-H: **d** Preparation process; **e** SEM images and **f** Capacitance value. Adapted with permission [39], Copyright (2019), Royal Society of Chemistry. M-PPy composite films: **g** Preparation process; **h** SEM images and **i** Capacitance value. Adapted with permission [40], Copyright (2023), Elsevier

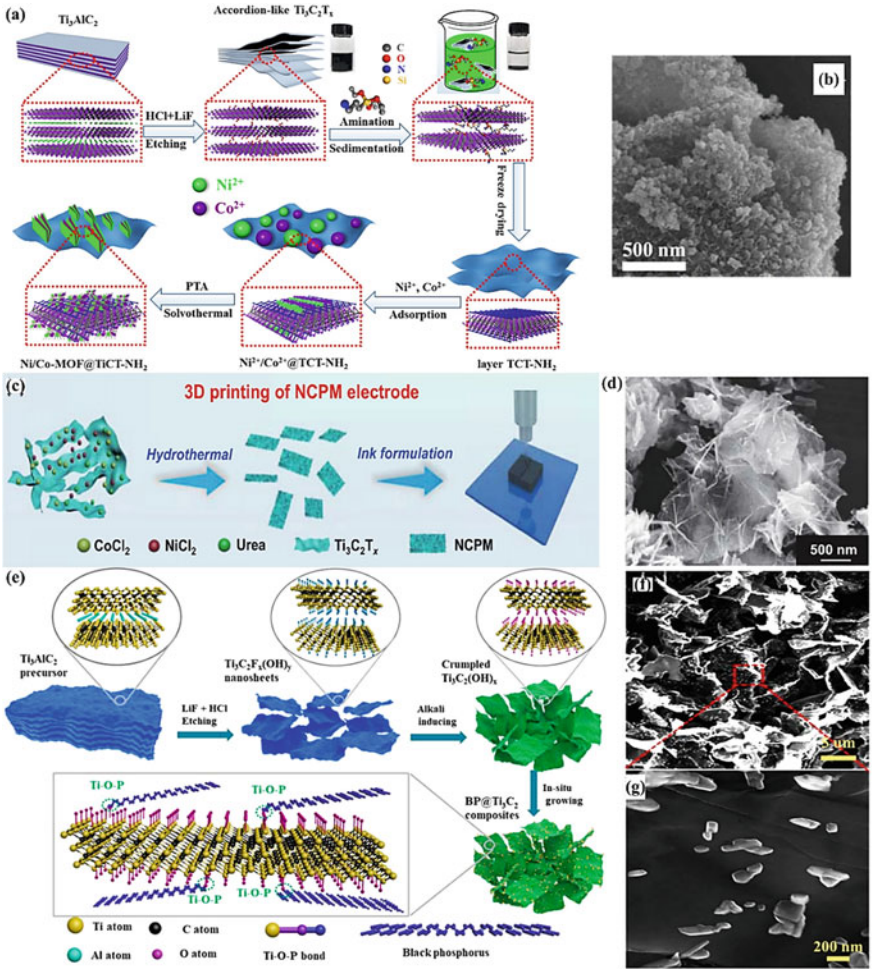

Fig. 6 Ni/Co-MOF@TCT-NH_2: **a** Preparation process; **b** SEM image. Adapted with permission [42], Copyright (2023), Elsevier. NCPM: **c** Preparation process; **d** SEM image. Adapted with permission [43], Copyright (2020), Springer. BP-MXene composites: **e** Preparation process; **f** and **g** SEM image. Adapted with permission [44], Copyright (2021), American Chemical Society

prevents the self-stacking of MXene nanosheets in Fig. 6f–g. BP@MXene film electrode provides an impressive volume capacitance of 781.6 F/cm^3 (at 2.0 mV/s) in a neutral Na_2SO_4 electrolyte and exhibits high-rate capacity (91.2% capacitance retention, 718.4 F/cm^3 at 1000 mV/s). BP@MXene based supercapacitors with commercial grade mass load (~15 mg/cm^2) exhibit a high stacking volume energy density of 72.6 Wh/L, which is close to the performance of lead-acid batteries (50–90 Wh/L), and has long-term stability (a capacitance retention rate of 90.58% after 50,000 cycles).

Wang et al. prepared ZIF-67 nanoboxes on the surface of MXene nanosheets using in-situ growth methods, and successfully constructed a unique honeycomb-like 2D layered nanocomposite (MXene@$CoSe_2$/Ni_3Se_4) in Fig. 7a [45]. The vertical anchoring of $CoSe_2$/Ni_3Se_4 nanosheets derived from ZIF-67 on MXene nanosheets can effectively inhibit the self-polymerization of MOF derivatives in Fig. 7b and improve the conductivity of the composites. In addition, the strong chemical interaction between $CoSe_2$/Ni_3Se_4 nanosheets and MXene nanosheets promotes the charge transfer kinetics of the structure, thereby improving the cyclic stability of the composites. When the current density is 1 A/g, the specific capacitance of MXene@$CoSe_2$/Ni_3Se_4 can reach 1019 C/g. The asymmetric supercapacitors assembled based on the materials can achieve an energy density of 41.2 Wh/kg at a power density of 3.1 kW/kg.

Zhu et al. introduced antimonene into MXene films, and achieved the preparation of high electrochemical performance composite films with excellent deformability and editing properties in Fig. 7c [46]. Antimonene nanosheets have excellent electrochemical activity, ultra-thin/foldable performance, and a large aspect ratio, making them an ideal choice for hybridization with MXene to form uniform and dense thin films in Fig. 7d. The presence of antimonene effectively improves the stability and

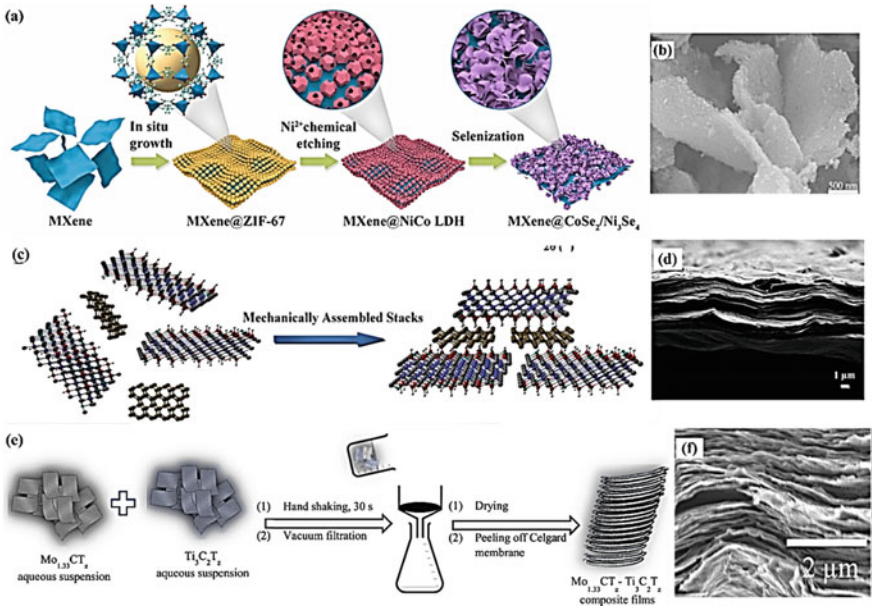

Fig. 7 MXene@$CoSe_2$/Ni_3Se_4: **a** Preparation process; **b** SEM image. Adapted with permission [45], Copyright (2022), Elsevier. Antimonene/MXene: **c** Preparation process; **d** SEM image. Adapted with permission [46], Copyright (2019), Wiley Online Library. $Mo_{1.33}CT_z$–$Ti_3C_2T_z$. composite films: **e** Preparation process; **f** SEM image. Adapted with permission [47], Copyright (2021), Elsevier

energy storage capacity of antimonene/MXene electrodes in acidic and neutral electrolytes. The films have a significant area capacitance of 3403 mF/cm^2 in 1 M H_2SO_4, corresponding to an ultra-high specific volume capacitance of 4255 F/cm^3. The flexible electrode can also achieve excellent values of 2192 F/cm^3 (1754 mF/cm^2) and a wider potential window in LiCl.

Etman et al. introduced a one-step method for preparing MXene composite films using $Mo_{1.33}CT_z$ and $Ti_3C_2T_z$ in Fig. 7e [47]. The composite films exhibit extremely high flexibility and good electronic conductivity (140 S/cm). The composite films show stronger porosity and more curved layered morphology in Fig. 7f, which can enhance the transport of ions in the plane, and increase the number of active sites that can be reached by the electrochemical reaction. The composite films exhibit a high capacitance of 1380 F/cm^3 (460 F/g) in 1 M H_2SO_4, and a capacitance retention rate of 96% after 17,000 cycles.

3 Summary

The development of new materials for electrochemical energy conversion and storage plays an important role in the development of a sustainable society. New 2D carbides, carbonitrides, and nitride MXenes with unique intrinsic properties have been successfully prepared through selective etching of the MAX phase in various materials [1]. MXenes material has the characteristics of 2D layered structure, metal-like conductivity, high density, variable surface termination, and embedded pseudocapacitance, being an ideal material for designing advanced supercapacitors with high energy and power density [48]. However, there are still some issues that need to be addressed with pure MXenes, such as poor mechanical properties, easy stacking, relatively small lateral dimensions, and poor stability in oxidizing atmospheres. Due to the stable layered structure, high conductivity, and abundant surface functional groups, MXenes allow for various modifications to form composites for electrodes in supercapacitors [10]. Therefore, various modification strategies have been developed to improve the performance of MXenes. This chapter summarizes the latest methods and progress that MXenes combine with various functional materials (such as metal oxides, metal sulfides, metal hydroxides, conductive polymers, etc.) to build composites for the application of supercapacitors. MXenes composites are considered an important way to improve the performance of Mxenes-based electrodes for supercapacitors. The addition of functional materials also expands the interlayer spacing to reduce the stacking of 2D MXenes nanosheets, enhances the accessible surface area of ions, and enables rapid electron transfer in the material. Synergies are also introduced, effectively improving capacitance performance. Despite significant progress in the past few years, MXenes composites still face significant challenges that need to be addressed in order to promote their practical applications: (1) Preparation strategies, reasonable structural design, and functionalization methods for Mxenes-based electrode materials. (2) In terms of electrode structure, the optimal porous and layered structure design can reduce the waste of gap space and improve packaging density.

(3) The influence of functional groups on conductivity and electrochemical performance requires in-depth understanding. (4) By improving the oxidation stability of MXenes, the cycling stability of the electrode is improved. Always, in the near future, MXenes may develop into an excellent sturdy electrode material for energy storage devices, and many fields still need to be studied.

References

1. R. Ma, Z. Chen, D. Zhao, X. Zhang, J. Zhuo, Y. Yin, X. Wang, G. Yang, F. Yi, $Ti_3C_2T_x$ MXene for electrode materials of supercapacitors. J. Mater. Chem. A **9**, 11501–11529 (2021)
2. Y. Wang, Y. Wang, Recent progress in MXene layers materials for supercapacitors: high-performance electrodes. SmartMat. **4**, e1130 (2022)
3. S. Sahoo, R. Kumar, E. Joanni, R.K. Singh, J.-J. Shim, Advances in pseudocapacitive and battery-like electrode materials for high performance supercapacitors. J. Mater. Chem. A **10**, 13190–13240 (2022)
4. Q. Zhu, J. Li, P. Simon, B. Xu, Two-dimensional MXenes for electrochemical capacitor applications: progress, challenges and perspectives. Energy Storage Mater. **35**, 630–660 (2021)
5. V.M. Hong Ng, H. Huang, K. Zhou, P.S. Lee, W. Que, J.Z. Xu, L.B. Kong, Recent progress in layered transition metal carbides and/or nitrides (MXenes) and their composites: synthesis and applications. J. Mater. Chem. A **5**, 3039–3068 (2017)
6. Y. Cui, J. Zhu, H. Tong, R. Zou, Advanced perspectives on MXene composite nanomaterials: Types synthetic methods, thermal energy utilization and 3D-printed techniques. iScience **26**, 105824 (2023)
7. S.A. Thomas, A. Patra, B.M. Al-Shehri, M. Selvaraj, A. Aravind, C.S. Rout, MXene based hybrid materials for supercapacitors: Recent developments and future perspectives. J. Energy Storage **55** (2022)
8. J. Yang, W. Bao, P. Jaumaux, S. Zhang, C. Wang, G. Wang, MXene-based composites: synthesis and applications in rechargeable batteries and supercapacitors. Adv. Mater. Interfaces **6**, 1802004 (2019)
9. M.S. Javed, A. Mateen, I. Hussain, A. Ahmad, M. Mubashir, S. Khan, M.A. Assiri, S.M. Eldin, S.S.A. Shah, W. Han, Recent progress in the design of advanced MXene/metal oxides-hybrid materials for energy storage devices. Energy Storage Mater. **53**, 827–872 (2022)
10. M. Ramezani Farani, B. Nourmohammadi Khiarak, R. Tao, Z. Wang, S. Ahmadi, M. Hassanpour, M. Rabiee, M.R. Saeb, E.C. Lima, N. Rabiee, 2D MXene nanocomposites: Electrochemical and biomedical applications. Environ. Sci.-Nano **9**, 4038–4068 (2022)
11. L. Li, D. Zhang, J. Deng, Y. Gou, J. Fang, H. Cui, C. Zhang, M. Cao, Application of MXene-based materials in hybrid capacitors. Sustain Energ. Fuels **5**, 3278–3291 (2021)
12. W. Luo, Y. Ma, T. Li, H.K. Thabet, C. Hou, M.M. Ibrahim, S.M. El-Bahy, B.B. Xu, Z. Guo, Overview of MXene/conducting polymer composites for supercapacitors. J. Energy Storage **52**, 105008 (2022)
13. N.R. Hemanth, T. Kim, B. Kim, A.H. Jadhav, K. Lee, N.K. Chaudhari, Transition metal dichalcogenide-decorated MXenes: promising hybrid electrodes for energy storage and conversion applications. Mater. Chem. Front. **5**, 3298–3321 (2021)
14. Y. Luo, W. Que, X. Bin, C. Xia, B. Kong, B. Gao, L.B. Kong, Flexible MXene-based composite films: Synthesis, modification, and applications as electrodes of supercapacitors. Small **18**, e2201290 (2022)
15. J. Zhou, J. Yu, L. Shi, Z. Wang, H. Liu, B. Yang, C. Li, C. Zhu, J. Xu, A conductive and highly deformable all-pseudocapacitive composite paper as supercapacitor electrode with improved areal and volumetric capacitance. Small **14**, e1803786 (2018)

16. X. Zhang, B. Shao, A. Guo, Z. Sun, J. Zhao, F. Cui, X. Yang, MnO_2 nanoshells/$Ti_3C_2T_x$ MXene hybrid film as supercapacitor electrode. Appl. Surf. Sci. **560**, 150040 (2021)
17. Y. Ma, H. Sheng, W. Dou, Q. Su, J. Zhou, E. Xie, W. Lan, Fe_2O_3 nanoparticles anchored on the $Ti_3C_2T_x$ MXene paper for flexible supercapacitors with ultrahigh volumetric capacitance. ACS Appl. Mater. Interf. **12**, 41410–41418 (2020)
18. R.A. Chavan, G.P. Kamble, S.B. Dhavale, A.S. Rasal, S.S. Kolekar, J.-Y. Chang, A.V. Ghule, NiO@MXene nanocomposite as an anode with enhanced energy density for asymmetric supercapacitors. Energy Fuels **37**, 4658–4670 (2023)
19. B. Shen, X. Liao, X. Zhang, H.-T. Ren, J.-H. Lin, C.-W. Lou, T.-T. Li, Synthesis of Nb_2C MXene-based 2D layered structure electrode material for high-performance battery-type supercapacitors. Electrochim. Acta **413**, 140144 (2022)
20. W. Luo, Y. Sun, Z. Lin, X. Li, Y. Han, J. Ding, T. Li, C. Hou, Y. Ma, Flexible $Ti_3C_2T_x$ MXene/V_2O_5 composite films for high-performance all-solid supercapacitors. J. Energy Storage **62**, 106807 (2023)
21. Y. Wang, X. Wang, X. Li, R. Liu, Y. Bai, H. Xiao, Y. Liu, G. Yuan, Intercalating ultrathin MoO_3 nanobelts into MXene film with ultrahigh volumetric capacitance and excellent deformation for high-energy-density devices. Nanomicro Lett. **12**, 115 (2020)
22. S.B. Ambade, R.B. Ambade, W. Eom, S.H. Noh, S.H. Kim, T.H. Han, 2D Ti_3C_2 MXene/WO_3 hybrid architectures for high-rate supercapacitors. Adv. Mater. Interfaces **5**, 1801361 (2018)
23. X. Zhang, B. Shao, A. Guo, Z. Gao, Y. Qin, C. Zhang, F. Cui, X. Yang, Improved electrochemical performance of CoO_x–NiO/$Ti_3C_2T_x$ MXene nanocomposites by atomic layer deposition towards high capacitance supercapacitors. J. Alloy. Compd. **862**, 158546 (2021)
24. P. Asen, A. Esfandiar, H. Mehdipour, Urchin-like hierarchical ruthenium cobalt oxide nanosheets on $Ti_3C_2T_x$ MXene as a binder-free bifunctional electrode for overall water splitting and supercapacitors. Nanoscale **14**, 1347–1362 (2022)
25. H. Liu, R. Hu, J. Qi, Y. Sui, Y. He, Q. Meng, F. Wei, Y. Ren, Y. Zhao, W. Wei, One-step synthesis of nanostructured CoS_2 grown on titanium carbide MXene for high-performance asymmetrical supercapacitors. Adv. Mater. Interfaces **7**, 1901659 (2020)
26. H. Liu, R. Hu, J. Qi, Y. Sui, Y. He, Q. Meng, F. Wei, Y. Ren, Y. Zhao, A facile method for synthesizing NiS nanoflower grown on MXene ($Ti_3C_2T_x$) as positive electrodes for "supercapattery." Electrochim. Acta **353**, 136526 (2020)
27. W. Hou, Y. Sun, Y. Zhang, T. Wang, L. Wu, Y. Du, W. Zhong, Mixed-dimensional heterostructure of few-layer MXene based vertical aligned MoS_2 nanosheets for enhanced supercapacitor performance. J. Alloy. Compd. **859**, 157797 (2021)
28. M.S. Javed, X. Zhang, S. Ali, A. Mateen, M. Idrees, M. Sajjad, S. Batool, A. Ahmad, M. Imran, T. Najam, W. Han, Heterostructured bimetallic-sulfide@layered Ti_3C_2T-MXene as a synergistic electrode to realize high-energy-density aqueous hybrid-supercapacitor. Nano Energy **101**, 107624 (2022)
29. X. Chen, H. Ge, W. Yang, P. Yang, Construction of $Ti_3C_2T_x$ MXene wrapped urchin-like $CuCo_2S_4$ microspheres for high-performance asymmetric supercapacitors. Dalton Trans. **52**, 3746–3754 (2023)
30. J.-Q. Qi, C.-C. Zhang, H. Liu, L. Zhu, Y.-W. Sui, X.-J. Feng, W.-Q. Wei, H. Zhang, P. Cao, MXene-wrapped $ZnCo_2S_4$ core-shell nanospheres via electrostatic self-assembly as positive electrode materials for asymmetric supercapacitors. Rare Met. **41**, 2633–2644 (2022)
31. J. Zhang, Z. Yao, W. Zou, Q. Shen, M. Fan, T. Ma, Trimetal NiCoMn sulfides cooperated with two-dimensional Ti_3C_2 for high performance hybrid supercapacitor. J. Solid State Chem. **308**, 122909 (2022)
32. R.S. Karmur, D. Gogoi, M.R. Das, N.N. Ghosh, High-performance flexible supercapacitor device composed of a hierarchical 2D MXene-Ni$(OH)_2$ nanocomposite and biomass-derived porous carbon electrodes. Energy Fuels **36**, 8488–8499 (2022)
33. C. Zhu, C. Pei, H.S. Park, X. Yu, Design of 2D/2D heterostructure by coupling cobalt hydroxides with MXene on nickel foam for high energy density supercapacitors. J. Alloy. Compd. **948**, 169809 (2023)

34. X. Zhang, S. Yang, S. Liu, X. Che, W. Lu, Y. Tian, Z. Liu, Y. Zhao, J. Yang, $Ti_3C_2T_x$ MXene-coupled NiCo-layered double hydroxide nanosheets with entire contact for high-performance supercapacitors. ACS Appl. Energy Mater. **6**, 636–643 (2022)
35. Y. Zhang, J. Cao, J. Li, Z. Yuan, D. Li, L. Wang, W. Han, Self-assembled Cobalt-doped NiMn-layered double hydroxide (LDH)/V_2CT MXene hybrids for advanced aqueous electrochemical energy storage properties. Chem. Eng. J. **430**, 132992 (2022)
36. F. Liu, C. Wang, L. Wang, F. Huang, J. Fan, N. Shi, M. Han, Z. Dai, Oxygen-vacancy-rich NiMnZn-layered double hydroxide nanosheets married with Mo_2CT_x MXene for high-efficiency all-solid-state hybrid supercapacitors. ACS Appl. Energy Mater. **5**, 3346–3358 (2022)
37. K. Li, X. Wang, S. Li, P. Urbankowski, J. Li, Y. Xu, Y. Gogotsi, An ultrafast conducting polymer@MXene positive electrode with high volumetric capacitance for advanced asymmetric supercapacitors. Small **16**, e1906851 (2020)
38. X. Wang, Y. Wang, D. Liu, X. Li, H. Xiao, Y. Ma, M. Xu, G. Yuan, G. Chen, Opening MXene ion transport channels by intercalating PANI nanoparticles from the self-assembly approach for high volumetric and areal energy density supercapacitors. ACS Appl. Mater. Interf. **13**, 30633–30642 (2021)
39. L. Li, N. Zhang, M. Zhang, X. Zhang, Z. Zhang, Flexible $Ti_3C_2T_x$/PEDOT:PSS films with outstanding volumetric capacitance for asymmetric supercapacitors. Dalton Trans. **48**, 1747–1756 (2019)
40. W. Luo, Y. Sun, Y. Han, J. Ding, T. Li, C. Hou, Y. Ma, Flexible $Ti_3C_2T_x$ MXene/polypyrrole composite films for high-performance all-solid asymmetric supercapacitors. Electrochim. Acta **441**, 141818 (2023)
41. H. Wang, L. Li, C. Zhu, S. Lin, J. Wen, Q. Jin, X. Zhang, In situ polymerized $Ti_3C_2T_x$/PDA electrode with superior areal capacitance for supercapacitors. J. Alloy. Compd. **778**, 858–865 (2019)
42. L. Yue, L. Chen, X. Wang, D. Lu, W. Zhou, D. Shen, Q. Yang, S. Xiao, Y. Li, Ni/Co-MOF@aminated MXene hierarchical electrodes for high-stability supercapacitors. Chem. Eng. J. **451**, 138687 (2023)
43. L. Yu, W. Li, C. Wei, Q. Yang, Y. Shao, J. Sun, 3D printing of NiCoP/Ti_3C_2 MXene architectures for energy storage devices with high areal and volumetric energy density. Nanomicro Lett. **12**, 143 (2020)
44. Z. Pan, L. Kang, T. Li, M. Waqar, J. Yang, Q. Gu, X. Liu, Z. Kou, Z. Wang, L. Zheng, J. Wang, Black phosphorus@$Ti_3C_2T_x$ MXene composites with engineered chemical bonds for commercial-level capacitive energy storage. ACS Nano **15**, 12975–12987 (2021)
45. Y. Yang, X. Huang, C. Sheng, Y. Pan, Y. Huang, X. Wang, In-situ formation of MOFs derivatives $CoSe_2$/Ni_3Se_4 nanosheets on MXene nanosheets for hybrid supercapacitor with enhanced electrochemical performance. J. Alloy. Compd. **920**, 165908 (2022)
46. J. Yu, J. Zhou, P. Yao, H. Xie, M. Zhang, M. Ji, H. Liu, Q. Liu, C. Zhu, J. Xu, Antimonene engineered highly deformable freestanding electrode with extraordinarily improved energy storage performance. Adv. Energy Mater. **9**, 1902462 (2019)
47. A.S. Etman, J. Halim, J. Rosen, Mixed MXenes: $Mo_{1.33}CT_z$ and $Ti_3C_2T_z$ freestanding composite films for energy storage. Nano Energy **88**, 106271 (2021)
48. M.Q. Long, K.K. Tang, J. Xiao, J.Y. Li, J. Chen, H. Gao, W.H. Chen, C.T. Liu, H. Liu, Recent advances on MXene based materials for energy storage applications. Mater. Today Sustain. **19**, 100163 (2022)

Hydrogel and Its Composites for Pseudocapacitors

Jeffery Horinek, Allen Davis, and Ram K. Gupta

Abstract As the need for energy rises congruently with the global population, renewable alternatives are becoming a necessity. Traditional fossil-burning energy sources create large volumes of emissions. Meanwhile, common options for energy storage are non-recyclable and pollutive. In response to these failings, certain avenues of research are being performed. Material such as metal oxides, metal sulfides, and conductive polymers are promising candidates for electrocatalytic applications. This is due to the pseudocapacitive nature of these compounds, which allows for unique energy storage opportunities. Without a substrate, however, many of these materials would fail to operate as intended. Hydrogels, when used as either the precursor or the substrate, provide ample properties that improve electrocatalytic activities. The high porosity native to hydrogels and their analogs allow ions to interact with the electrocatalyst properly and more easily. Furthermore, the mechanical properties unique to hydrogels allow for flexible energy storage devices to be made.

Keywords Hydrogels · Composites · Pseudocapacitors · Energy storage · Electrochemistry

1 Introduction

In the year 2022, CO_2 projections reached a new high of more than 36.8 billion tons. Further projections for the year 2050 reveal emission numbers that could surpass 40 million tons [1, 2]. The energy industry is responsible for the largest single share of these emissions at about 35% [2]. With emissions from the energy sector being so high it is more important than ever to find clean sustainable forms of energy storage. In the realm of energy storage, there are two main types: utility-scale and grid-scale.

J. Horinek · A. Davis · R. K. Gupta (✉)
National Institute for Materials Advancement, Pittsburg State University, 1204 Research Road, Pittsburg, KS 66762, USA
e-mail: ramguptamsu@gmail.com

Department of Chemistry, Pittsburg State University, 1701 South Broadway Street, Pittsburg, KS 66762, USA

© The Author(s), under exclusive license to Springer Nature Switzerland AG 2024

R. K. Gupta (ed.), *Pseudocapacitors*, Engineering Materials,
https://doi.org/10.1007/978-3-031-45430-1_12

Utility-scale is the type of energy storage most people are familiar with. This form of energy storage can take on the form of devices like batteries and supercapacitors. However, with improvement, these materials could potentially be used for grid-scale energy storage. These types of energy storage are used in smaller applications such as the automotive industry and portable electronics [1]. Grid-scale energy storage, this type of storage involves the collection and conversion of electrical energy into a stored form. This most commonly takes on the form of pumped stored hydropower, flywheels, or thermal energy. When looking at the current materials used in these forms of energy storage the most common material used is lithium. This is mainly due to its use in lithium-ion batteries which are the most common energy storage device for electronics and automotive applications. The main reason lithium is so often used for these batteries is because of the excellent results it produces. These results include high energy density, cyclic stability, and rechargeability. However, due to several glaring issues such as high cost, detrimental environmental impact, and waning supply, many are trying to replace lithium with sustainable alternatives [2, 3].

As the push for sustainability gains increasing support, the renewability of the material has become a major factor for consideration. One such material that combines promising qualities and extreme sustainability is metal oxides [4–6]. Aside from applications in energy storage metal oxides can be found in applications such as catalysis, radar wave absorption, and hydrogen production [7]. This is due to several desirable properties including various valence states, low cost, and potential for redox reaction [7]. In the application of energy storage, these metal oxides are typically used as a component in the electrodes for various types of capacitors. However, metal oxides cannot meet the high demands for energy storage as they suffer from low initial coulombic efficiencies and relatively poor cycling performances. To combat these issues researchers are currently trying to enhance the lacking properties by combining the oxides with other materials to make hybrid structures [8]. Continuing with the trend of sustainable materials, metal organic frameworks (MOFs) have become quintessential in the quest for sustainability. MOFs are a 3D framework that consists of functional organic ligands that link to inorganic material clusters. These ligands then act as a form of scaffolding to create a porous 3D structure unique to the MOF [9]. As a material, MOFs have several unique properties such as high specific surface areas, substantial pore volumes, high concentrations of active sites, and tunable pore diameters [10]. A more in depth look at MOFs physical structure can be seen in Fig. 1 [11, 12]. Despite MOFs having several properties that give them an advantage as a material for energy storage, they have many glaring disadvantages. These include low electrical conductivity, poor cycle stability, and low specific capacitance. However, there has been great progress in attempting to fix these issues with a promising option being the introduction of metal oxides to the structure of the MOF [13].

While the above materials are typically used for electrodes, these are but one facet of an energy storage device. Hydrogels are a popular material for energy storage devices due to their ability to act as an electrolyte and/or separator. Hydrogels are popular for these applications due to their incredible flexibility and high porosity.

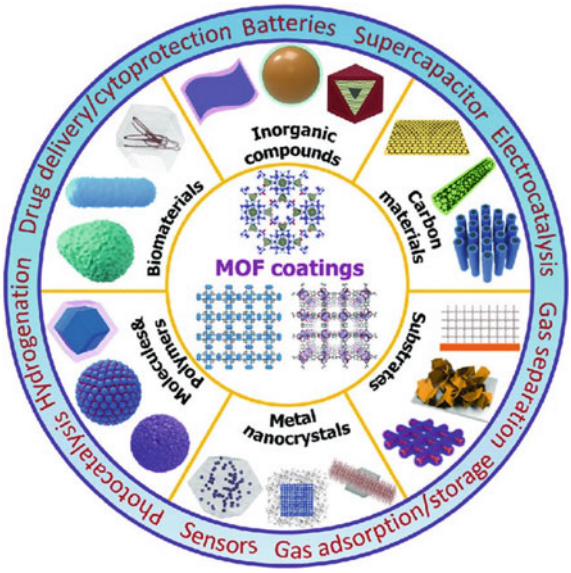

Fig. 1 Different MOF structures and their applications. Reproduced with permission [12], Copyright (2020), The Royal Society of Chemistry

Aside from these abilities, hydrogels also have several other desirable properties including excellent mechanical properties, high conductivity, biocompatibility, and generally low cost. Due to these unique properties, it comes of little surprise that hydrogels are used in many other applications outside of energy storage. Many of the popular applications for hydrogels can be seen in Fig. 2 [14]. When it comes to why hydrogels should be used in energy storage there is one reason that stands out from the rest and that is the sustainability of hydrogels. As material bio-based hydrogels are extremely sustainable. This is due to hydrogels being able to be synthesized from many different natural sources. These sources include, but are not limited to pectin, cellulose, chitosan, and carboxymethyl cellulose [15, 16].

Looking at the importance of composites for energy storage, composites have one key characteristic that other materials do not and that is adaptability. A material composite can be created for specific applications giving them a greater adaptability than other materials. This allows composites to have a role in energy storage not only now, but in the future as well.

2 Fundamentals of Pseudocapacitors

When selecting a device for energy storage, at least three aspects must be considered. These aspects are energy density, power density, and overall lifespan. To define these terms, energy density pertains to the total amount of energy maintained in the storage device. Power density relates to the rate at which said energy is delivered from the device, with different applications requiring varying power output. Finally,

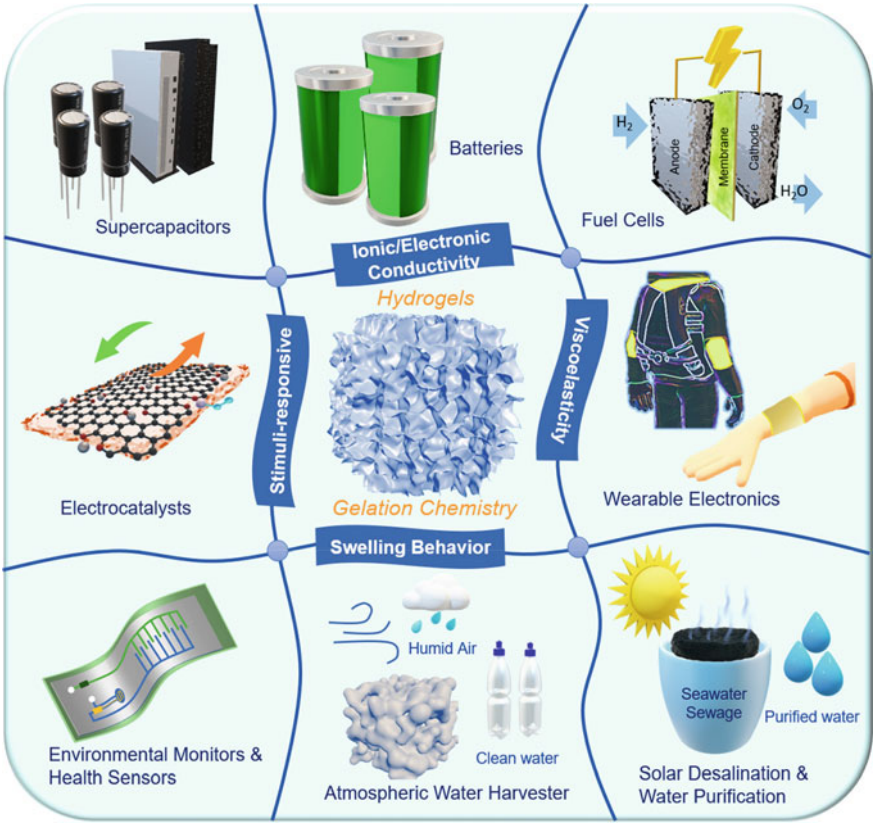

Fig. 2 Various applications of hydrogels. Reproduced with permission [14], Copyright (2020), American Chemical Society

while storage lifespan sounds straight forward, it is a complicated characteristic that relies on many aspects of the device in question. While these traits are common amongst different energy storage devices, they are not distributed equally. Fuel cells often demonstrate a high energy density and low power density [17], while batteries are generally moderate in both regards. Capacitors, meanwhile, often boast a high power density alongside a low energy density [18]. The high-power density seen in capacitors is attributed to the charge storage mechanism of the capacitor itself. The most basic form of a capacitor is the parallel plate capacitor. This device consists of two separate conducting plates separated by a dielectric material. The nature of these plates can vary, with tubular and circular capacitors also being common. Meanwhile, the dielectric is responsible for reducing the voltage needed per unit of charge stored. Electrolytic capacitors involve an electrolyte that acts as the cathodic end of the device, with a thin metal oxide layer acting as a dielectric. Both standard capacitor designs suffer from a lack of high-capacity energy storage, which is where supercapacitors come into play.

Supercapacitors maintain a much higher capacitance value as compared to traditional capacitors. The increase in capacitance is attributable to the different mechanisms employed by the different supercapacitor types. Electrostatic double-layer capacitors (EDLCs) were the first type of supercapacitor developed, taking advantage of the double layer effect to drastically increase capacitance. As opposed to the more traditional capacitors, EDLCs have highly porous carbon material for an electrode. The high surface area of this material allows for the formation of a Helmholtz layer on the electrode, which massively increases overall capacitance. On the opposite end of the spectrum exist pseudocapacitors, which use a vastly different mechanism of charge storage. Pseudocapacitors use faradaic electrochemical reactions to store charge chemically within the electrode in addition to surface charge storage. This process is very similar to the storage mechanisms seen in batteries, as such, pseudocapacitors trend towards higher energy densities [19]. Similarly, the overall sluggishness native to faradaic reactions means that power density tends to decline in these devices. Pseudocapacitive behavior in a device is generally defined over three separate mechanisms [20]. The most basic of these mechanisms is pseudocapacitive adsorption. Adsorption entails the formation of an ionic monolayer on the surface of the electrode. This property is relevant to all electrochemical capacitors and is even seen in hybrid EDLCs. Redox electrochemistry is the most widely researched subject for pseudocapacitance. A wide range of materials are available for redox pseudocapacitor design. These selections vary from simple transition metal oxides, sulfides, and phosphides to more complex metal organic frameworks and perovskites. The last mechanism for pseudocapacitance is intercalation, which involves the insertion of ions between planes of the host material. This process is commonly seen in lithium-ion batteries and is partially responsible for their widespread implementation. Schematics of these different types of pseudocapacitors can be seen in Fig. 3 [21].

While the above reactions host different mechanisms, each operate with reversibility in mind. The term redox stands for oxidation–reduction, a reaction

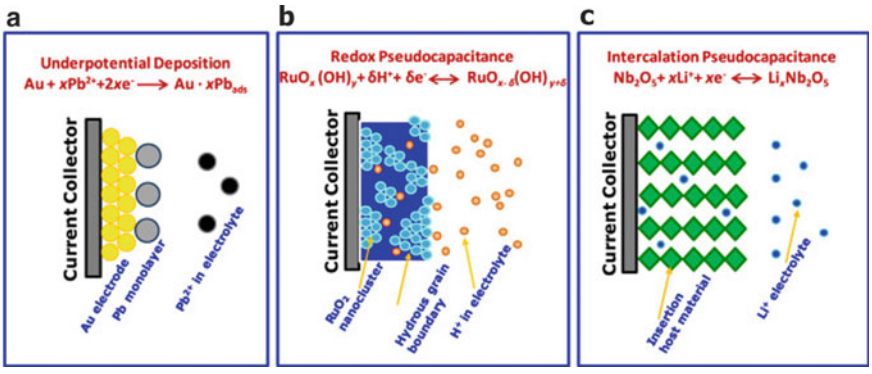

Fig. 3 This figure depicts the three different types of pseudocapacitance on the surface of the electrode. Reproduced with permission [21], Copyright (2020), Elsevier

wherein one chemical species donates an electron to another [22]. In the reaction, the oxidative species acts as an electron donator while the reductive agent acts as a receiver. A common example of this reaction is observed in transition metals, such as the rusting of iron, tarnishing of silver, and the formation of patina on copper. In terms of electrocatalytic application, the electron storage that occurs during oxidation allows for the sequestering of charge within the sample in addition to electrostatic storage. As such, the primary goal when creating a redox active pseudocapacitor is to benefit from the improved energy density without sacrificing power density. As mentioned, faradaic reactions struggle with slow rates, and redox reactions are no exception. This sluggishness is due to a variety of factors; however, active site availability is of note. Knowledge of the principles and electrochemical processes of pseudocapacitors is for naught if they cannot be characterized. Cyclic voltammetry (CV) is a form of analysis that ramps and reduces an electrode's potential versus time. Electrical current is then potted against this to reveal the electrochemical properties of the electrode in question [23]. To supplement this, galvanostatic charge discharge (GCD) can be performed to observe the storage capability of the device. In GCD, electric potential is plotted over time at a set current density (commonly at 1 A/g) [24]. From these two tests, other electrochemical capabilities can be derived. Specific capacitance is often derived from CV, while columbic efficiency can be gathered from GCD. GCD can also be used to observe energy density and power density, making it a power tool of analysis. Meanwhile, electrode stability and capacitance retention can be gathered from long-term charge–discharge over many cycles. Electrochemical impedance spectroscopy (EIS) allows for the observation of reaction at the interface of the electrode and can be useful for observing different electrochemical phenomena [25]. An example of some of these tests can be observed in Fig. 4 [26].

3 Hydrogel and Composites

Hydrogels are hydrophilic three-dimensional cross-linked and branched polymeric networks. The high degree of cross-linking native to hydrogels allows them to absorb and retain water (about 70–99% of their structure) without the threat of being dissolved [27]. Hydrogels have been used by humans for thousands of years with a common example being that of gelatin. The first instance of man-made hydrogel was discovered by Otto Wichterle in 1960 for use as soft contact lenses [28]. Since then, researchers have developed new methods to synthesize wholly synthetic, bio-based, or hybrid hydrogels. Each of these gels features their own unique properties and characteristics. While these unique properties are useful for a variety of applications, these properties can be enhanced by making a composite. Composites are a material class that consists of a matrix and a reinforcement. The matrix is typically the main material of the composite, while the reinforcement is a different material that is enveloped in the matrix. An example of the would be the addition of carbon fiber to epoxy resin. In this scenario, your carbon fiber acts as the matrix of the composite while the epoxy acts as the reinforcement. The combination of these two materials

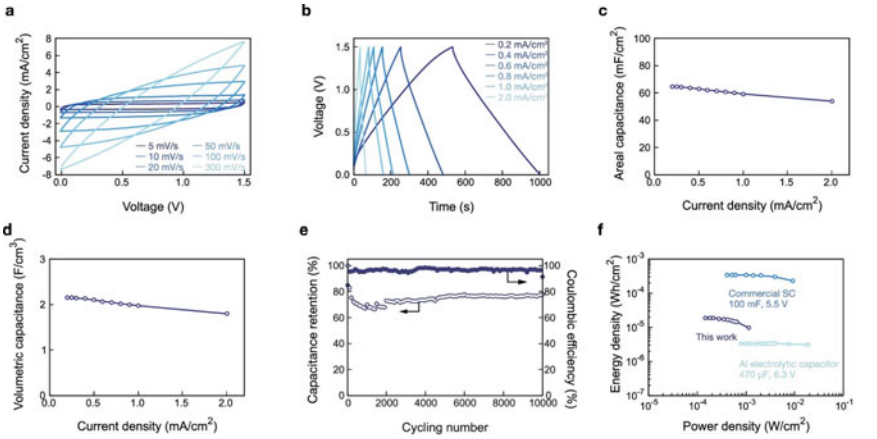

Fig. 4 **a** Example of CV curves over varying scan rates. **b** Example of GCD over different current densities. **c** Graph of areal capacitance over current density. **d** Graph of volumetric capacitance over current density. **e** Comparison of capacitance retention and coulombic efficiency over high cycle numbers. **f** Graph of energy density over power density. Reproduced with permission [26], Copyright (2022), American Chemical Society

then serves to enhance the properties of the overall material. Even though hydrogels are an extremely capable material they are still often used as the matrix for composites since some hydrogel applications require the characteristics to be adapted to fit the application.

When looking at the characteristics of hydrogels the degree of cross-linking is one of the most integral properties a hydrogel can have. This is because the degree of cross-linking influences almost all the other characteristics of a hydrogel. The characteristic that is most affected by the degree of cross-linking is the porosity of the gel. Typical hydrogels feature a volume that is >5% pores, and with hydrogels featuring a high percentage of pores the pore sizes are often used to help classify the gel. The classifications are shown in Table 1 [29].

For a gel to be synthesized to a certain pore size, the degree of cross-linking can be adjusted. A higher degree can be being used to produce gels with smaller pore sizes and vice versa [29]. The pore size of the hydrogel also influences the swelling and mechanical properties of the gel. Essentially, swelling is the ability of a hydrogel to absorb large amounts of liquid without dissolving. Gels that feature larger pore sizes

Table 1 Classifications of hydrogels based on their pore size

Hydrogel classification	Pore size
Nonporous hydrogels	1–10 nm
Microporous hydrogels	10–100 nm
Macroporous hydrogels	100 nm–1 μm
Superporous hydrogels	100 μm

absorb more liquid leading to increased swelling [18]. When it comes to mechanical properties, gels that are synthesized with a high degree of cross-linking are stiffer and more brittle. Whereas gels synthesized with a lower degree of cross-linking are more flexible and have more elastic properties [30].

When synthesizing hydrogels there are many routes that can be taken. The method chosen for synthesis can determine the properties of the gel. Meanwhile, there are many different methods to synthesize a gel, with the method chosen depending on the materials needed. One of the most common synthesis methods for these gels is the sol–gel method. The IUPAC Gold Book defines this process as, "Process through which a network is formed from solution by a progressive change of liquid precursor(s) into a sol, to a gel [31]". The process of sol–gel synthesis relies on two initial reactions; the first part is hydrolysis followed by polycondensation. In hydrolysis the initial compounds are reacted with water, forming a multifunctional monomer. Once the monomers are formed, polycondensation begins. In polycondensation, the cross-linking of the polymer begins, creating clustered sites of polymer. These particles constitute the "sol" of the sol–gel method. Once the formation of sol is complete the gelation process can begin. This is the reaction where sol solution transitions from a liquid to a solid material. Once the gelation process reaches its end the aging process of the gel can commence. Throughout this stage there are a handful of processes that happen, and these processes include: the formation of additional crosslinks, a transformation in the size of the gel's pores, and an overall decrease in the size of the gel. The end of the aging process constitutes the end of the sol–gel method. An illustration of this process can be seen in Fig. 5 [32].

When trying to synthesize hydrogels from graphene oxide often the best route for synthesis is the hydrothermal method. Hydrothermal synthesis involves the heterogenous reactions of materials with three crucial factors. These factors being an aqueous environment, higher than standard temperature, and pressure. An illustration of a study using this synthesis method can be seen in Fig. 6 [33]. In a study by Hu et al., graphene oxide hydrogels were synthesized via the hydrothermal method [33]. This was accomplished by taking a single layer graphene oxide dispersed in a liquid media

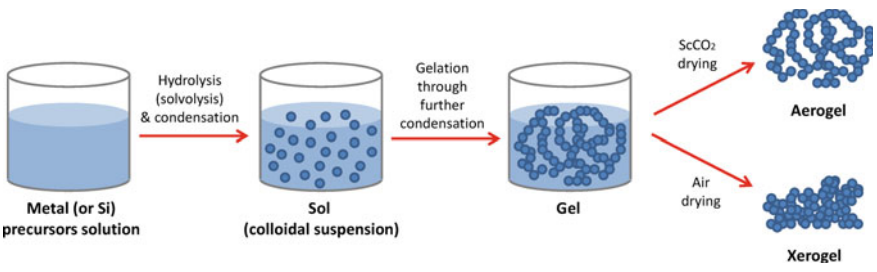

Fig. 5 Image showing the different phases of the sol–gel method of synthesis. Reproduced with permission [32], Copyright (2018) by the authors. Licensee MDPI, Basel, Switzerland. This article is an open access article distributed under the terms and conditions of the Creative Commons Attribution (CC BY) license

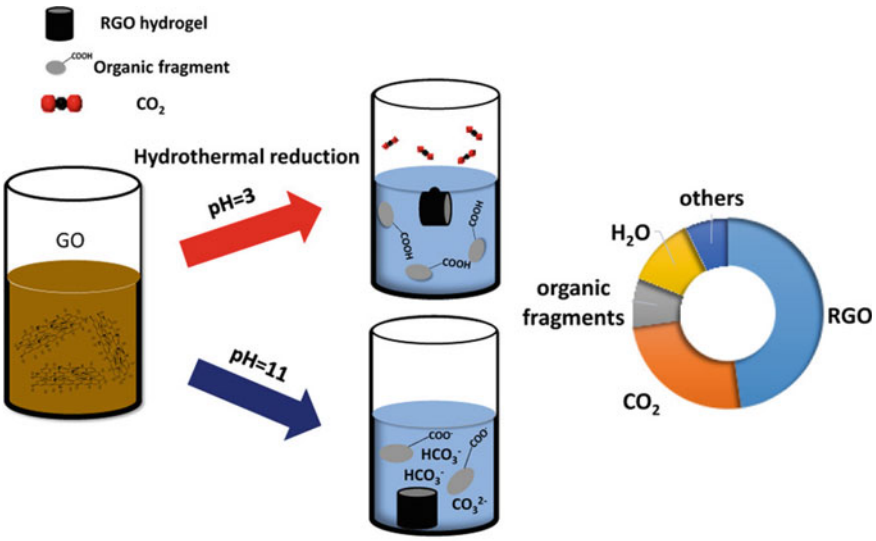

Fig. 6 Graphic showing the process of synthesizing a graphene oxide hydrogel. Reproduced with permission [33], Copyright (2016), American Chemical Society

and placing it into a Teflon lined autoclave. The completion of this synthesis yielded a graphene oxide-based hydrogel with a water content of >98%.

A more recent method of hydrogel synthesis is rapidly rising in popularity due to the increasing prevalence of additive manufacturing (3D printing) technology. Much study has been done to allow for the ability to 3D print hydrogels. There are several ways to complete this process, but the most common is direct ink writing. This type of printing involves taking ink (Ink is a liquid phase polymer that is extruded during the direct ink writing) and depositing it layer by layer to form. This is illustrated by Fig. 7 [34]. In a study by Zhang et al. chitosan based ink was used to 3D print a bio based hydrogel [34]. This process occurred by immersing chitosan microspheres with an into a pre-polymerization solution which contained the monomer and the cross-linker (N, N′-methylenediacrylamide). Then to catalyze the printing ink, acetic acid was introduced into the solution, inducing the swelling of the microspheres, and allowing them to absorb the pre-polymerization solution. These microspheres were then run through vacuum filtration and centrifugation to remove the aqueous medium from the microspheres allowing for a printable ink. This ink was then transferred to an extrusion nozzle. The nozzle threatens layer by layer to successfully create a hydrogel monolith.

One of the biggest advantages of a hydrogel material is that they can have their rheological properties tuned. This means that depending on their application they can have specific properties tuned to better fit that specific application [35]. Another advantage of hydrogels is that they can be self-healing. This means that when synthesized for self-healing it gives the gel the ability to autonomously repair damage. Thus, allowing them to maintain their integrity during long term applications [36]. Another

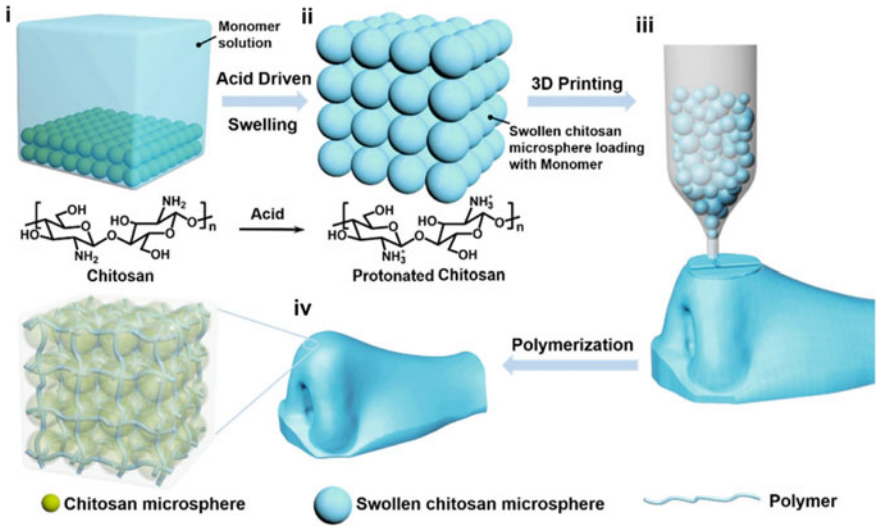

Fig. 7 Image detailing the process of 3D printing a hydrogel. Reproduced with permission [34], Copyright (2023), American Chemical Society

incredible advantage of hydrogels is their ability to act as a precursor for aerogels, xerogels, and other derivatives. To create aerogels, supercritical drying, or lyophilization can be used, while ambient pressure drying forms xerogels [37, 38]. Hydrogels do face some issues, however, with one major issue being the potential for a rapid decrease in the properties of the gel. This typically happens when the gel suffers some form of damage to its structure. Once the structure of a gel is damaged a rapid decrease in the properties of the gel can be noted since the structure of a gel is so integral to the gel's characteristics [39].

Another challenge that inhibits hydrogels is the randomness of the pore size. Certain studies have produced models that can help to predict pore size [30], but these studies only provide an average of the pore size. As of now there has been one way to reliably control the size of hydrogel pores [40]. In terms of electrochemistry, hydrogels have been found to suffer from rather low energy densities. These lower energy densities are caused by altering the structure of the gel to enhance the mechanical properties [41]. As stated, earlier gels that are stiffer feature smaller pore sizes. In terms of electrochemistry, when the pore size of a gel is decreased a decrease in the electrochemical properties can be seen. More specifically speaking a decrease in the energy density of the gel [41].

4 Hydrogel and Composites for Pseudocapacitors

When considering hydrogels for pseudocapacitor applications, there are multiple roles that must be considered. Generally, hydrogels can find use in three different parts of a pseudocapacitor. The first and most substantive option is as an electrocatalyst. Due to their porous framework, hydrogel precursors make for an excellent substrate for electrocatalyst synthesis. Hydrogel based films meanwhile, serve as a popular option as an electrolyte separator. Finally, hydrogels, either in their native state or modified, are a popular option as an electrolyte for electrolytic pseudocapacitors. Hydrogels are also a popular selection when designing a flexible pseudocapacitor, due to their inherent strength and flexibility. By themselves, hydrogels are generally non pseudocapacitive, which is where the inclusion of composite materials is needed.

Carbon is an extremely pervasive element that is responsible for our very lives. Additionally, materials like carbon black, polyaniline, and graphite are but a few examples of carbon's conductivity. Due to these factors, many hydrogels used for energy storage are organic in nature. One exception to this standard is reduced graphene oxide (rGO) hydrogel. These hydrogels are synthesized hydrothermally from graphene oxide, after which they can be used for further synthesis into an electrocatalyst. In one experiment, Gong et al. synthesized a resveratrol (Res)/rGO composite that demonstrated excellent energy storage capability. Res is a highly substituted phenolic compound that is produced by many species of plants. In this context, Res was used to help separate the different layers of rGO to improve the fantastic qualities of graphene. Graphene by itself is prone to agglomerations, when oxidized, these agglomerations become exfoliated, massively increasing surface area. Regrettably, graphene oxide is an insulator, requiring reduction to regain conductivity. Thus begets the need for a molecular separator with conductive properties such as Res. To create the electrodes, the Res/rGO hydrogels were first sliced and lyophilized, then pressed onto nickel foam and epoxy coated at the nonactive portions. The synthesis of the hydrogel, alongside a diagram of Res function in the composite, can be seen in Fig. 8 [42].

For testing, the Res/rGO composites electrodes were differentiated based on their mass ratios. The 3:1 (m_{GO}/m_{Res}) ratio sample resulted in the most promising data out of all the samples tested. CV scans of the Res/rGO samples demonstrated traditional redox behavior at 10 mV/s. Meanwhile, Res/rGO3 demonstrated a GCD time around 1400 s at 1A/g and 1800s at 0.5 A/g in the negative range. Furthermore, the Res/rGO3 electrodes presented a high specific capacitance of 588 F/g at 1 A/g. In terms of stability, the Res/rGO3 electrodes had a low charge-transfer resistance alongside a capacitance retention of 88.8% after 10,000 cycles at 2 A/g.

Metal oxides are commonly seen as the final chemical state for a variety of metals. From the metal oxides formed during battery operation to the corrosion of iron and steel, these compounds are everywhere. While they might be the natural end state for metals, their reversibility makes them a perfect candidate for pseudocapacitor application. In the energy field, metal oxides are commonly divided between noble metal oxides and transition metal oxides. Noble metals such as ruthenium oxide and iridium

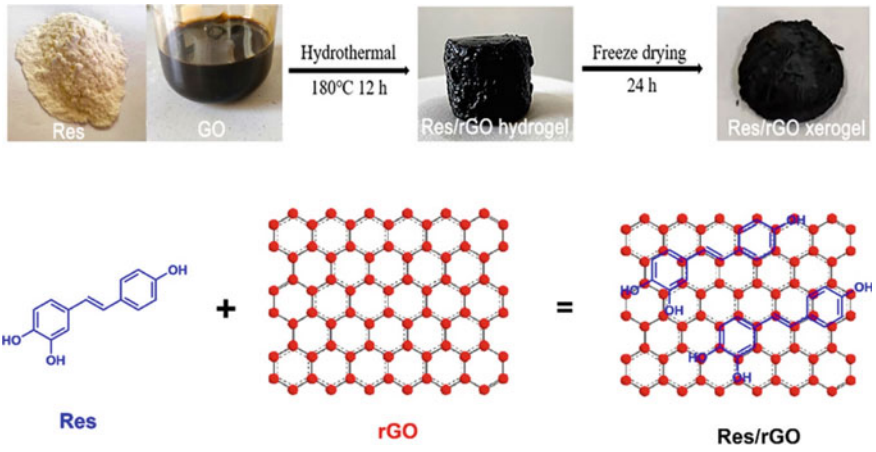

Fig. 8 Images of Res/rGO composite at different stages of synthesis alongside a graphic depicting the stacking of Res on rGO sheets. Reproduced with permission [42], Copyright (2023), American Chemical Society

oxide act as powerful electrocatalysts, but their scarcity makes them prohibitively expensive for widespread application. Conversely, transition metal oxides can vary in electrocatalytic effect, but are widespread and low cost. Iron oxide is perhaps the most widespread metal oxide, making it especially interesting for development. Gupta et al. explored a polyaniline/graphene/iron oxide hydrogel composite for pseudocapacitor development [43]. Synthesis of the composite material occurred in three distinct steps. The graphene was synthesized from flaked graphite via a modified Hummer's method. To create the intermediate binary composite, graphene oxide was placed into an ethylene glycol solution and sonicated. After this, varying amounts of ferric chloride was added to the solutions alongside hydrazine hydrate and stirred. The solutions were then microwave treated to form the composite. To incorporate polyaniline into the mix, aniline, phytic acid, carbon cloth, and the graphene intermediate were added to deionized water, sonicated, and cooled. This solution was then added to a pre-cooled ammonium persulfate and stirred, creating the hydrogel. To make the electrodes, the hydrogel coated carbon cloths were dried, lyophilized, and placed into a Swagelok assembly for testing, as seen in Fig. 9 [43]. Of all the composites created for testing, the sample denoted PGF_5@cc performed the best for testing. The CV plot demonstrated good pseudocapacitive behavior at scan rates up to 100 mV/s, alongside a good GCD time just above 1800 at 0.5 A/g. The specific capacitance calculated from GCD was 1115 F/g. The stability of PGF5@cc was maintained at 82% at 1 A/g after 10,000 cycles.

Like metal oxides, metal sulfides are immensely common in nature. Materials like iron pyrite and lead galena are ores of their respective metals that are mined worldwide. Also like metal oxides, metal sulfides are commonly researched for their electrocatalytic capabilities [44]. One advantage of metal sulfides is that they are often more conductive than metal oxides. Solid state metal oxides are generally considered

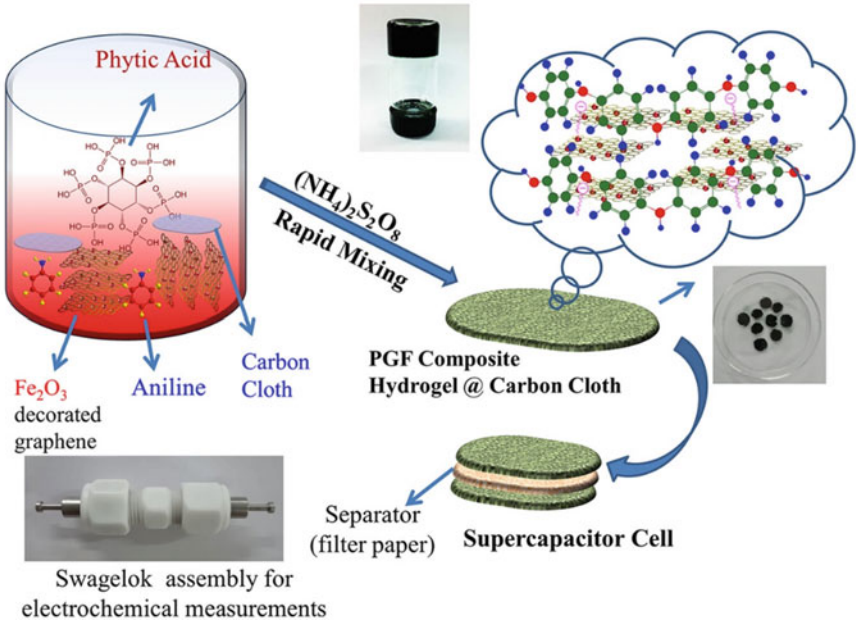

Fig. 9 Graphic depicting the synthesis of PGF@cc and the resulting device made for characterization. Reproduced with permission [43], Copyright (2020), American Chemical Society

to be nonconductors, meanwhile many metal sulfides fall well within the range of semi-conduction. Taking advantage of metal sulfide conductivity, Niu et al. devised a Ni_3S_2 carbon composite sourced from alginate hydrogels [45]. Alginate is unique when compared to other hydrogels thus far as it is easily sourced as a renewable biomaterial. Sodium alginate (SA) is a naturally derived hydrogel precursor that can be extracted and refined from brown algae. In terms of synthesizing the composite, SA and thiourea were stirred into an aqueous solution and added dropwise into a rapidly stirring nickel chloride solution. This process created hydrogel beads which were lyophilized into aerogels, carbonized, washed, and made into Ni/Ni_3S_2@CNS pseudocapacitor electrodes. Preliminary electrochemical testing observed that an electrode made from gels consisting of a 2:1 SA-thiourea ratio calcined at 800 °C (Ni/Ni_3S_2@CNS-2-800) performed the best for supercapacitor application. GCD demonstrated a charge–discharge time of 1200 s at 0.5 A/g, with CV demonstrating pseudocapacitive behavior even at 100 mV/s scan rate. Specific capacitance at 0.5 A/g was observed at 720 F/g, with specific capacitance maintained at 500 F/g at 10 A/g. This material also demonstrated a capacitance retention of 85% after 5000 cycles at 10 A/g, indicating potential for higher amperage applications.

Conducting polymers are a class of material that has proved useful in energy storage. First explored in the early to mid-1900s, conducting polymers have expanded to fill a variety of niches in supercapacitor applications. Polyvinylidene fluoride (PVDF) is often used as a binder, improving the adhesion of electrocatalysts to

an electrode [46]. Polyaniline, meanwhile, has seen use in electronics applications, specifically circuitry. Another advantage of conducting polymers is their flexibility. Flexible energy storage is a hot topic in the scientific community, especially in the field of wearable electronics. Wearable electronics are often hampered by bulkiness and weight. The bulkiness of a worn electronic device can reduce maneuverability and ergonomics, potentially causing damage to the user or device. Weight, meanwhile, can cause strain to the user, leading to discomfort. To combat this, many designs have been made that incorporate flexible hydrogel supercapacitors, often with the inclusion of equally flexible conductive polymers.

When designing flexible supercapacitors, there are a few factors that need to be kept in mind. Flexibility is the most obvious factor, as devices that can twist and bend are valuable for application. Stretchability is important for devices that need to fold, extend, or retract. To this effect, Wang et al. designed a highly stretchable polypyrrole (PPy) hydrogel film for supercapacitor construction [47]. The high degree of flexibility was obtained through a unique hydrogel composite synthesis procedure. The first hydrogel used in this composite was made from polyacrylic acid (PAA). PAA is a unique polymer due to its ability to link via ionic bonds. Ionomers such as PAA tend to demonstrate self-healing ability, alongside a higher degree of flexibility due to the transient nature of its bonds. PPy, meanwhile, is a conducting polymer with the ability to interact with the ionic groups of PAA. In this synthesis, PAA-Fe substrates were developed and placed into PTFE molds. The resulting gels were then stretched to certain degrees and immersed in liquid nitrogen until entirely frozen. After the gels were frozen, they were immersed in a 1:1 ethanol–water solution alongside an equimolar amount of APS and pyrrole. Polymerization on the surface of the frozen gels were allowed to occur over set times, after which they were allowed to thaw in water. The composite gels were finally washed multiple times and made into a supercapacitor. A schematic of the composite hydrogel synthesis is visible in Fig. 10 [47].

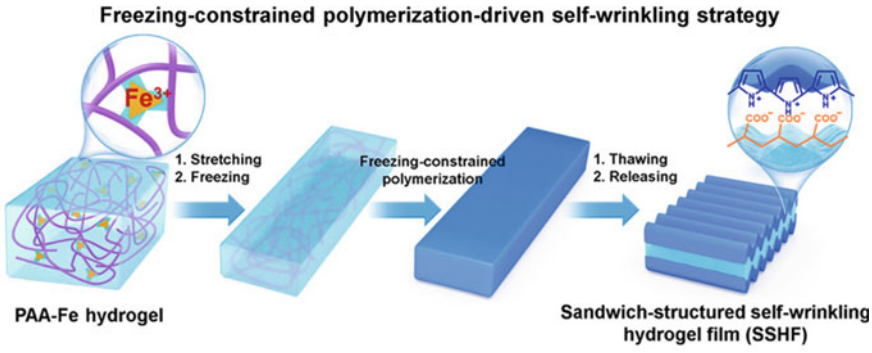

Fig. 10 Image depicting the synthesis of SSHF hydrogels, as well as the accordion like structure of the final product. Reproduced with permission [47], Copyright (2022), American Chemical Society

The hydrogel composite's electrochemical measurements were tested under multiple conditions. The most optimal sample, SSHF-2, was measured in its native state, during stretching at up to 500%, and after repeated cut heal processes. In each of the states, good pseudocapacitive behavior was observed at a 10 mV/s scan rate in CV testing. At baseline, GCD trials demonstrated a charge–discharge time just under 200 s at 1 A/g. When comparing the original with 500% stretch, charge discharge time dropped to just above 120 s. Finally, the 500% sample was cut and rejoined, where it was observed that minimal time was lost, even after 7 cut and rejoin cycles. Specific capacitance was observed to be 79.5 F/g at 0.5 A/g, while GCD held relatively stable out to 5000 cycles. It was noted that while this device was near the lower end of the supercapacitor spectrum, its enhanced physical properties, all in one design, and ability to stack both in series and parallel made it an excellent candidate for flexible device fabrication.

Low capacitance values are not uncommon when designing flexible supercapacitors. The material properties required for flexural ability often prove antithetical to capacitor materials. Metals like to maintain their shape once bent, while other materials are liable to snap when significant force is applied. One method to improve the energy storage of flexible supercapacitors was explored by Wu et al. [48]. In this study, the team created a quasi-solid-state zinc-ion hybrid supercapacitor. Hybrid supercapacitors are a subset of supercapacitors that implement battery-like operation in their design. This is achieved by creating separate electrodes, one that operates via EDLC behavior, and one the operates like ion batteries. Additionally, the device created takes advantage of an eutectogel electrolyte for ion transport. Eutectogels are a cousin of hydrogels that use ionic liquids as their solvent. The eutectic solvents used in this experiment not only improve the electrochemistry of the device but endow antifreeze properties to the gel. Synthesis of this material occurred over 3 steps. First, graphene oxide hydrogel was synthesized and purified for later use. Meanwhile, the eutectogel was made from a 1:5 molar ratio solution of acrylamide and zinc perchlorate hexahydrate. This solution was stirred until transparent then cured in a 60 °C oil bath. With the gels obtained, they were made into a protodevice where the graphene gel was pressed into a titanium mesh, pressed to the eutectogel, with zinc foil layered onto the other side. The protodevice was then further cross-linked in a 50 °C oil bath, after which it was made into the hybrid supercapacitor device. Pseudocapacitance was confirmed via CV at 10 mV/s over all trials. GCD was tested in its ambient state, at cryogenic temperatures, and at varying degrees of flexing. In its ambient state, charge–discharge times reached around 1100 s at 0.8 A/g, with times between −20 and 70 °C ranging from 550 to 800 s at 1 A/g, respectively. Flexural charge discharge was observed to barely change between bends from 0 to 180°. The hybrid capacitor also demonstrated a high energy density of 117.5 Wh/kg alongside a power density of 833.8 W/kg. The device operating at different angles can be observed in Fig. 11 [48].

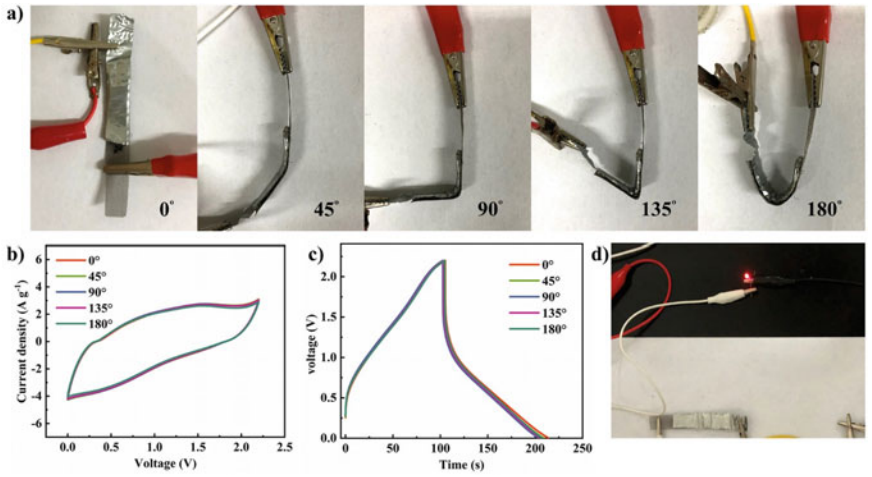

Fig. 11 **a** Photographs of an assembled flexible ZHSC at various bending angles. **b** CV curves at different bending angles. **c** GCD curves at different bending angles. **d** Optical images of a green LED lit up by assembled ZHSC. Reproduced with permission [48], Copyright (2022), American Chemical Society

5 Conclusion

Given the ever-growing need for clean renewable energy, new solutions have arisen to match. Hydrogel composites are an up-and-coming solution to the mounting energy concerns faced globally. Electrochemically involved hydrogels that bend, stretch, and twist can be used for the development of flexible electronics. Such applications are important for medical devices or ergonomically compatible consumer products. These medical devices can include blood monitors, portable sensors, and other necessary apparatuses. In the realm of consumer electronics, flexible power sources can be used in watches, clothing, and cybernetics. Meanwhile, pseudocapacitive composites help to improve the energy density of super capacitors. By improving the energy density, their application falls in line with more traditional storage methods. The additional power density afforded by supercapacitors, in conjunction with their rechargeability, make for a potential alternative to batteries. Redox active materials have been demonstrated to increase many of the properties conducive to energy storage. This is due to the chemical reactions that allow further energy storage within the chemical structure of the electrocatalyst. When considering these devices for practical applications, it is well to consider the drawbacks. While often improved when compared to batteries, pseudocapactivie supercapacitors suffer from a lower net power density compared to EDL capacitors. This again is due to the time required to facilitate a chemical reaction, as opposed to the near instantaneous energy transfer of capacitance. However, this limitation is only a drawback in high power applications and is less of an issue for more general use products. The more glaring issue is the generally weak electrical properties seen in flexible devices. This limitation is the regrettable

tradeoff for the enhanced flexural properties. For practical application, this compromise needs to be amended, either through expanding the amount of devices used, or by engineering a better material. Nevertheless, pseudocapacitive hydrogel composites represent an emerging class of material that holds promise for energy applications.

References

1. D. Zheng, C. Sun, W. Pan, G. Guo, Y. Zheng, C. Liu, J. Zhu, Nanostructured Fe_2O_3@C negative electrodes for stable asymmetric supercapacitors with high-performance. Energy Fuels **35**, 16915–16924 (2021)
2. Z. Yuan, L. Wang, D. Li, J. Cao, W. Han, Carbon-reinforced Nb_2CTx MXene/MoS_2 nanosheets as a superior rate and high-capacity anode for sodium-ion batteries. ACS Nano **15**, 7439–7450 (2021)
3. S. Nishimura, Y. Suzuki, J. Lu, S. Torii, T. Kamiyama, A. Yamada, High-temperature neutron and X-ray diffraction study of fast sodium transport in alluaudite-type sodium iron sulfate. Chem. Mater. **28**, 2393–2399 (2016)
4. J. Choi, A. Nkhama, A. Kumar, S.R. Mishra, F. Perez, R.K. Gupta, A facile preparation of sulfur doped nickel–iron nanostructures with improved HER and supercapacitor performance. Int. J. Hydrogen Energy **47**, 7511–7521 (2022)
5. I. Shaheen, K.S. Ahmad, C. Zequine, R.K. Gupta, A.G. Thomas, M.A. Malik, Modified sol-gel synthesis of Co_3O_4 nanoparticles using organic template for electrochemical energy storage. Energy **218**, 119502 (2021)
6. S. Aloqayli, C.K. Ranaweera, Z. Wang, K. Siam, P.K. Kahol, P. Tripathi, O.N. Srivastava, B.K. Gupta, S.R. Mishra, F. Perez, Nanostructured cobalt oxide and cobalt sulfide for flexible, high performance and durable supercapacitors. Energy Storage Mater. **8**, 68–76 (2017)
7. M. Fu, W. Chen, H. Yu, M. Gao, Q. Liu, General synthesis of two-dimensional porous metal oxides/hydroxides for microwave absorbing applications. Inorg. Chem. **61**, 678–687 (2022)
8. R. Packiaraj, K. Mahendraprabhu, P. Devendran, N. Nallamuthu, B. Palanivel, K.S. Venkatesh, R. Karuppannan, Electrochemical performances of ZnO–NiO–CuO mixed metal oxides as smart electrode material for solid-state asymmetric device fabrication. Energy Fuels **36**, 603–617 (2022)
9. D.L. Singh, T.K. Ghosh, V. Mishra, S. Ramasamy, M.K. Sahoo, R.R. Gangavarapu, Three-dimensional lanthanide-based nanoporous metal-organic frameworks for high-performance supercapacitors. ACS Appl. Nano Mater. **5**, 15237–15249 (2022)
10. A. Gupta, C.A. Allison, M.E. Ellis, J. Choi, A. Davis, R. Srivastava, F.M. de Souza, D. Neupane, S.R. Mishra, F. Perez, A. Kumar, R.K. Gupta, T. Dawsey, Cobalt metal–organic framework derived cobalt–nitrogen–carbon material for overall water splitting and supercapacitor. Int. J. Hydrogen Energy **48**, 9551–9564 (2023)
11. X.F. Lu, Y. Fang, D. Luan, X.W.D. Lou, Metal-organic frameworks derived functional materials for electrochemical energy storage and conversion: a mini review. Nano Lett. **21**, 1555–1565 (2021)
12. J. Meng, X. Liu, C. Niu, Q. Pang, J. Li, F. Liu, Z. Liu, L. Mai, Advances in metal–organic framework coatings: versatile synthesis and broad applications. Chem. Soc. Rev. **49**, 3142–3186 (2020)
13. K. Jayaramulu, S. Mukherjee, D.M. Morales, D.P. Dubal, A.K. Nanjundan, A. Schneemann, J. Masa, S. Kment, W. Schuhmann, M. Otyepka, R. Zbořil, R.A. Fischer, Graphene-based metal-organic framework hybrids for applications in catalysis, environmental, and energy technologies. Chem. Rev. **122**, 17241–17338 (2022)
14. Y. Guo, J. Bae, Z. Fang, P. Li, F. Zhao, G. Yu, Hydrogels and hydrogel-derived materials for energy and water sustainability. Chem. Rev. **120**, 7642–7707 (2020)

15. N. Chelfouh, G. Coquil, S. Rousselot, G. Foran, E. Briqueleur, F. Shoghi, L. Caradant, M. Dollé, Apple pectin-based hydrogel electrolyte for energy storage applications. ACS Sustain. Chem. Eng. **10**, 15802–15812 (2022)
16. E. Cevik, S.T. Gunday, A. Bozkurt, A. Iqbal, S.M. Asiri, A.N. Alqarni, A. Almofleh, Scalable, quasi-solid-state bio-polymer hydrogel electrolytes for high-performance supercapacitor applications. ACS Sustain. Chem. Eng. **10**, 10839–10848 (2022)
17. S. Tominaka, S. Ohta, H. Obata, T. Momma, T. Osaka, On-chip fuel cell: micro direct methanol fuel cell of an air-breathing, membraneless, and monolithic design. J. Am. Chem. Soc. **130**, 10456–10457 (2008)
18. Z. Liang, M. Liu, L. Shen, L. Lu, C. Ma, X. Lu, X. Lou, C.-L. Jia, All-inorganic flexible embedded thin-film capacitors for dielectric energy storage with high performance. ACS Appl. Mater. Interfaces **11**, 5247–5255 (2019)
19. W. Raza, F. Ali, N. Raza, Y. Luo, K.H. Kim, J. Yang, S. Kumar, A. Mehmood, E.E. Kwon, Recent advancements in supercapacitor technology. Nano Energy **52**, 441–473 (2018)
20. S. Fleischmann, J.B. Mitchell, R. Wang, C. Zhan, D. Jiang, V. Presser, V. Augustyn, Pseudocapacitance: from fundamental understanding to high power energy storage materials. Chem. Rev. **120**, 6738–6782 (2020)
21. M. Sarno, Chapter 22—Nanotechnology in energy storage: the supercapacitors, in *Catalysis, Green Chemistry and Sustainable Energy*, ed. by A. Basile, G. Centi, M. De Falco, G. Iaquaniello (Elsevier, 2020), pp. 431–458
22. J. Li, Z. Wang, L. Yang, Y. Liu, Y. Xing, S. Zhang, H. Xu, A flexible Li–air battery workable under harsh conditions based on an integrated structure: a composite lithium anode encased in a gel electrolyte. ACS Appl. Mater. Interfaces **13**, 18627–18637 (2021)
23. N. Elgrishi, K.J. Rountree, B.D. McCarthy, E.S. Rountree, T.T. Eisenhart, J.L. Dempsey, A practical beginner's guide to cyclic voltammetry. J. Chem. Educ. **95**, 197–206 (2018)
24. L. Zeng, T. Wu, T. Ye, T. Mo, R. Qiao, G. Feng, Modeling galvanostatic charge–discharge of nanoporous supercapacitors. Nat. Comput. Sci. **1**, 725–731 (2021)
25. A.C. Lazanas, M.I. Prodromidis, Electrochemical impedance spectroscopy–a tutorial. ACS Meas. Sci. Au. **3**, 162–193 (2023)
26. S. Yamada, A transient supercapacitor with a water-dissolvable ionic gel for sustainable electronics. ACS Appl. Mater. Interfaces **14**, 26595–26603 (2022)
27. E. Axpe, D. Chan, G.S. Offeddu, Y. Chang, D. Merida, H.L. Hernandez, E.A. Appel, A multiscale model for solute diffusion in hydrogels. Macromolecules **52**, 6889–6897 (2019)
28. O. Wichterle, D. Lím, Hydrophilic gels for biological use. Nature **185**, 117–118 (1960)
29. R. Foudazi, R. Zowada, I. Manas-Zloczower, D.L. Feke, Porous hydrogels: present challenges and future opportunities. Langmuir **39**, 2092–2111 (2023)
30. T. Kopač, A. Ručigaj, M. Krajnc, The mutual effect of the crosslinker and biopolymer concentration on the desired hydrogel properties. Int. J. Biol. Macromol. **159**, 557–569 (2020)
31. J.V Alemán, A.V Chadwick, J. He, M. Hess, K. Horie, R.G. Jones, P. Kratochvíl, I. Meisel, I. Mita, G. Moad, S. Penczek, R.F.T. Stepto, Definitions of terms relating to the structure and processing of sols, gels, networks, and inorganic-organic hybrid materials (IUPAC Recommendations 2007), vol. 79 (2007), pp. 1801–1829
32. Y. Tao, P.P. Pescarmona, Nanostructured oxides synthesised via $scCO_2$-assisted sol-gel methods and their application in catalysis. Catalysts **8**, 212 (2018)
33. K. Hu, X. Xie, T. Szkopek, M. Cerruti, Understanding hydrothermally reduced graphene oxide hydrogels: from reaction products to hydrogel properties. Chem. Mater. **28**, 1756–1768 (2016)
34. R. Zhang, J. Guo, X. Yang, X. Jiang, L. Zhang, J. Zhou, X. Cao, B. Duan, Ink based on the tunable swollen microsphere for a 3d printing hydrogel with broad-range mechanical properties. ACS Appl. Mater. Interfaces **15**, 15917–15927 (2023)
35. D. Skoulas, G. Mangiapia, D. Parisi, M. Kasimatis, E. Glynos, E. Stratikos, D. Vlassopoulos, H. Frielinghaus, H. Iatrou, Tunable hydrogels with improved viscoelastic properties from hybrid polypeptides. Macromolecules **54**, 10786–10800 (2021)
36. J. Lei, X. Li, S. Wang, L. Yuan, L. Ge, D. Li, C. Mu, Facile fabrication of biocompatible gelatin-based self-healing hydrogels. ACS Appl. Polym. Mater. **1**, 1350–1358 (2019)

37. X. Gao, R.J. Esteves, T.T.H. Luong, R. Jaini, I.U. Arachchige, Oxidation-induced self-assembly of Ag nanoshells into transparent and opaque Ag hydrogels and aerogels. J. Am. Chem. Soc. **136**, 7993–8002 (2014)
38. X. Li, S. Liu, Recovery and reutilization of the solvents and catalyst used in the sol-gel synthesis of silica xerogel. ACS Sustain. Chem. Eng. **7**, 7094–7101 (2019)
39. W. Wang, S. Liu, L. Liu, S. Alfarhan, K. Jin, X. Chen, High-speed and high-resolution 3d printing of self-healing and ion-conductive hydrogels via μCLIP. ACS Mater. Lett. **5**, 1727–1737 (2023)
40. C. Xue, Y. Huang, X. Zheng, G. Hu, Hopping behavior mediates the anomalous confined diffusion of nanoparticles in porous hydrogels. J. Phys. Chem. Lett. **13**, 10612–10620 (2022)
41. C. Gao, Z. Gao, Y. Wei, N. Luo, Y. Liu, P. Huo, Flexible wood enhanced poly(acrylic acid-co-acrylamide)/quaternized gelatin hydrogel electrolytes for high-energy-density supercapacitors. ACS Appl. Mater. Interfaces **15**, 2951–2960 (2023)
42. X. Gong, Y. Wang, K. Yao, J. Yang, Y. Li, X. Ge, H. Xie, G. Pan, R. Xing, Supercapacitors based on resveratrol/reduced graphene oxide composites. ACS Appl. Nano Mater. **6**, 4162–4169 (2023)
43. A. Gupta, S. Sardana, J. Dalal, S. Lather, A.S. Maan, R. Tripathi, R. Punia, K. Singh, A. Ohlan, Nanostructured polyaniline/graphene/Fe_2O_3 composites hydrogel as a high-performance flexible supercapacitor electrode material. ACS Appl. Energy Mater. **3**, 6434–6446 (2020)
44. Y.-S. Cheng, Y.-T. Wu, S. Aulia, C.-C. Chang, M. Rinawati, T.-Y. Lee, J.-Y. Chang, N.L.W. Septiani, B. Yuliarto, M.-H. Yeh, Robust cobalt manganese sulfide thin film as an electrocatalytic layer for quantum dot-sensitized solar cells with the polysulfide electrolyte. ACS Sustain. Chem. Eng. **11**, 6903–6913 (2023)
45. W. Niu, Z. Xiao, Z. Zhao, S. Zhai, N. Liu, C. Qin, High-performance asymmetric supercapacitor based on Ni_3S_2 nanoparticles immobilized on carbon nanosheets from sodium alginate. J. Alloys Compd. **885**, 161194 (2021)
46. M. Wang, Q. Tan, L. Liu, J. Li, A. Facile, Environmentally friendly, and low-temperature approach for decomposition of polyvinylidene fluoride from the cathode electrode of spent lithium-ion batteries. ACS Sustain. Chem. Eng. **7**, 12799–12806 (2019)
47. Y. Wang, Y. Liu, Z. Wang, D.H. Nguyen, C. Zhang, T. Liu, Polymerization-driven self-wrinkling on a frozen hydrogel surface toward ultra-stretchable polypyrrole-based supercapacitors. ACS Appl. Mater. Interfaces **14**, 45910–45920 (2022)
48. Y. Wu, Y. Deng, K. Zhang, J. Qiu, J. Wu, L. Yan, Ultrahigh conductive and stretchable eutectogel electrolyte for high-voltage flexible antifreeze quasi-solid-state zinc-ion hybrid supercapacitor. ACS Appl. Energy Mater. **5**, 3013–3021 (2022)

Pseudocapacitive Materials for 3D Printed Supercapacitors

Arthi Gopalakrishnan, Vishnu Surendran, Venkataraman Thangadurai, and Benjamin Tutolo

Abstract Recent advancements in wearable, flexible, and portable electronics have stimulated a swift increase in demand for compatible energy storage devices with promising performance. Supercapacitors offer the potential to satisfy the demands for complicated design and integrated functionality due to their highly adaptable manufacturing process. This chapter provides a review of recent advancements in 3D-printed supercapacitors using pseudocapacitive materials. A brief introduction on the subject is addressed with the main concepts of ink formulations and their constraints, optimization steps, and printing technologies. Moreover, we review various pseudocapacitive electrode materials, e.g., metal oxides, conducting polymers, chalcogenides, metal–organic frameworks, and MXenes, and their conversion into printable inks used for 3D printing supercapacitors. We conclude by discussing major limitations and the future perspectives in 3D printable supercapacitors.

Keywords Pseudocapacitors · 3D printing electrodes · Supercapacitors · Solid-state · Ink writing

1 Introduction

Pseudocapacitive materials have drawn significant attention in the effort to create advanced energy storage systems due to their high specific capacitance and outstanding rate capability. In addition, pseudocapacitive materials, which undergo fast and reversible redox reactions, have shown great promise in improving the energy

A. Gopalakrishnan (✉) · B. Tutolo
Department of Geoscience, University of Calgary, Calgary, AB T2N 1N4, Canada
e-mail: arthi.gopalakrishnan@ucalgary.ca

V. Surendran · V. Thangadurai
Department of Chemistry, University of Calgary, Calgary, AB T2N 1N4, Canada

© The Author(s), under exclusive license to Springer Nature Switzerland AG 2024

R. K. Gupta (ed.), *Pseudocapacitors*, Engineering Materials,
https://doi.org/10.1007/978-3-031-45430-1_13

density and power delivery of supercapacitors. A new method for creating supercapacitors with improved performance and design flexibility has just surfaced: additive manufacturing, more commonly known as 3D printing. Incorporating pseudocapacitive materials into 3D-printed supercapacitors offers the potential for higher energy storage and improved device performance [1]. The advent of 3D printing has revolutionized the manufacturing landscape, enabling the production of complex and customized structures with precise control over their geometry. By leveraging computer-aided design (CAD) models, 3D printing facilitates the layer-by-layer deposition of materials, eliminating the need for traditional fabrication methods such as casting or lithography. This additive manufacturing approach offers numerous advantages, including reduced material waste, enhanced integration capabilities, and the ability to tailor electrode architectures for optimal electrochemical performance [2].

In this chapter, we explore recent advancements in the field of pseudocapacitive materials for 3D-printed supercapacitors. We examine the different classes of pseudocapacitive materials, such as transition metal oxides, conducting polymers, and metal–organic frameworks, and highlight their unique properties and electrochemical performance. We build on this foundation by delving into the fabrication techniques and strategies employed for integrating these materials into 3D-printed electrode architectures, ensuring enhanced mass loading, efficient charge transfer, and improved overall device performance. Furthermore, this chapter discusses the challenges and opportunities associated with the use of pseudocapacitive materials in 3D-printed supercapacitors. It addresses issues such as material selection, electrode design optimization, and post-processing treatments, aiming to provide insights into the development of high-performance energy storage devices. We conclude by exploring potential applications and future research directions for 3D-printed supercapacitors utilizing pseudocapacitive materials, ranging from wearable electronics and portable energy systems to large-scale energy storage. By combining the unique capabilities of pseudocapacitive materials and 3D printing technology, novel energy storage solutions can be developed, paving the way for the next generation of high-performance supercapacitors with tailored architectures and improved electrochemical performance.

2 3D Printing Technologies

The emerging 3D printing technologies offer different types of printing techniques, which control the electrode architecture and geometry, thus enhancing the energy/power density of the supercapacitor devices. Overall, 3D printing follows a series of operations from model design to printing and to the post-treatment process, following the basic operational procedure given in Fig. 1a [3]. First, the ink composition is prepared according to the printable conditions. Then, using computer-aided design, a 3D model is prepared and converted to layer data to be printed. Finally, the printed material is post-treated by various processes to acquire desired 3D objects. Different

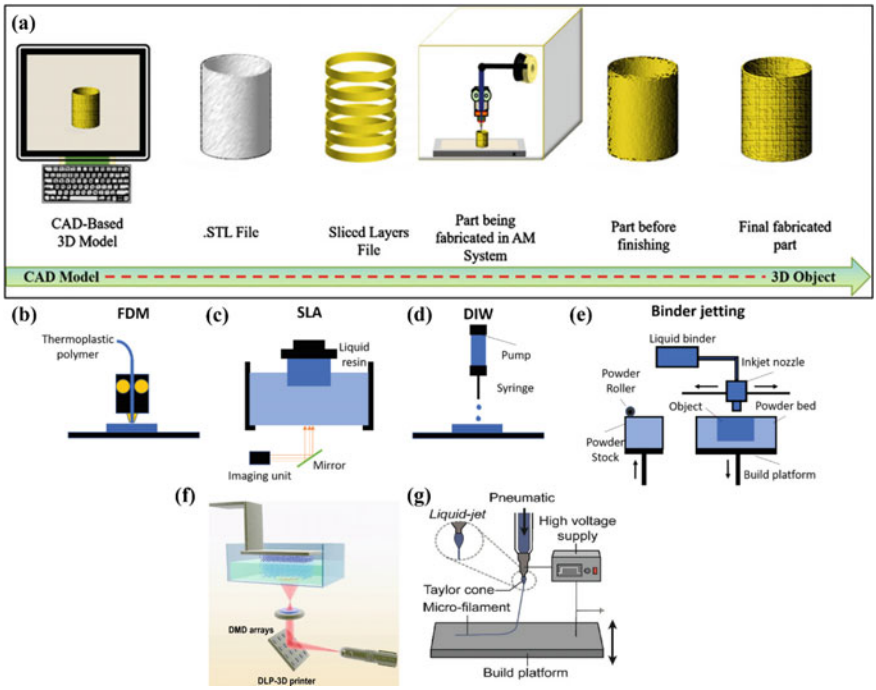

Fig. 1 **a** Overview of basic additive manufacturing procedure in preparation of 3D objects; **b** fused deposition modeling (FDM); **c** stereolithography (SLA); **d** direct ink writing (DIW); and **e** binder jetting. Adapted with permission [3], Copyrights (2021), Distributed under a Creative Commons Attribution Non-commercial License 4.0 (CC BY-NC). **f** digital light signal (DLP) 3D printer based on digital mirror device (DMD) arrays; **g** inkjet printing process. Adapted and reproduced with permission [1], Copyright (2022), John Wiley and Sons

types of 3D printing methods (Fig. 1b–g) have been used to fabricate 3D electrodes and devices [1–4].

2.1 Fused Deposition Modeling

Fused deposition modeling (FDM) is a widely used 3D printing technique that involves layer-by-layer extrusion of a thermoplastic filament through a heated nozzle to construct objects. This method offers advantages such as low cost, ease of use, and a wide range of compatible materials, including acrylonitrile butadiene styrene (ABS), polylactic acid (PLA), and nylon. However, it should be noted that FDM exhibits some limitations, including limited resolution and the visibility of layer lines on the final prints. Despite these limitations, FDM is widely used among researchers to manufacture complex objects with ease. The electrochemically active materials mix with the thermoplastic materials and form the filament for the deposition.

2.2 Stereolithography

Stereolithography (SLA) is an additive manufacturing technique known for its high precision and ability to produce intricate designs. In SLA, a liquid photopolymer resin is selectively cured using an ultraviolet (UV) light source, solidifying each layer. SLA is commonly used in applications such as jewelry, dental models, and prototypes requiring fine details. While SLA delivers excellent resolution and smooth surface finishes, it requires expensive equipment and provides limited choices in terms of available materials.

2.3 Selective Laser Sintering

Selective laser sintering (SLS) is a 3D printing method that employs a high-powered laser to selectively fuse powdered materials, layer by layer. This technique enables the use of various materials, including nylon, polyamide, metals, and ceramics, making it suitable for applications such as functional prototypes, end-use parts, and objects with complex geometries. It offers advantages such as versatility and good strength and durability. The drawbacks of SLS include the need for costly equipment and the possibility of yielding a rough surface finish.

2.4 Digital Light Processing

Digital light processing (DLP) is a 3D printing process that employs a digital projector to expose an entire layer of liquid resin to UV light, solidifying it in one pass. DLP is known for its fast-printing speeds and high accuracy, making it valuable for applications such as dental models, jewelry, and small functional parts. DLP utilizes a spatial light modulating element to project a specifically patterned light, allowing for the printing of planar figures in a single step, significantly reducing printing time while achieving high-resolution patterns and smooth surfaces. Nonetheless, it should be noted that DLP has limitations in terms of material choices compared to other techniques and may offer a rough surface compared to SLA.

2.5 Binder Jetting

Binder jetting is a 3D printing technique that selectively deposits a liquid binding agent onto thin layers of powdered material, which are then fused together [5]. This method finds applications in the production of large-scale objects, architectural

models, and sand-casting molds due to its high-speed printing capabilities and cost-effectiveness for larger objects. However, it is important to consider that binder jetting does have limitations in terms of material properties and may result in low-resolution prints.

2.6 Direct Ink Writing

Direct ink writing (DIW) is one of the most popular additive manufacturing techniques employed for fabricating energy storage devices, utilizing an extrusion-based approach. The successful implementation of this technique relies on ink rheological properties that ensure optimal ink fluidity and filament shape retention throughout the three essential processes: internal flow within the syringe and nozzle, extrusion from the nozzle, and deposition onto substrates. The fabrication of energy storage devices using the direct ink writing technique has certain limitations, including the need for ink with specific properties, compromised mechanical strength, and the necessity for additional post-treatment procedures. For the successful construction of desired patterns, the ink or slurry must possess high viscosity and shear-thinning characteristics, ensuring that the extruded filament or line maintains its shape without distortion. DIW has been successfully employed to print various materials such as carbon-based substances, conductive polymers, and metal oxide-based active components [6].

2.7 Inkjet Printing

While primarily a 2D method, layer-by-layer printing can also be utilized to enhance pattern thickness, offering several benefits such as precise control over material deposition, efficient pattern design, and waste reduction. The inkjet printing (IJP) technique is particularly noteworthy for its cost-effectiveness and adaptability to the mass production of personalized items. Notably, various metal oxides and graphene-based inks have demonstrated success in printing pseudocapacitive energy storage devices [7].

3 Electrode Design and Architectures

Designing the architecture of electrodes is a viable approach to enhancing the energy density and power density of energy storage devices like batteries and supercapacitors. While traditional fabrication methods have limitations in controlling the geometry and architecture of electrodes and electrolytes, 3D printing offers promising possibilities to precisely manipulate material architecture (e.g., dimension, porosity, morphology) and improve energy storage device performance. By utilizing specific

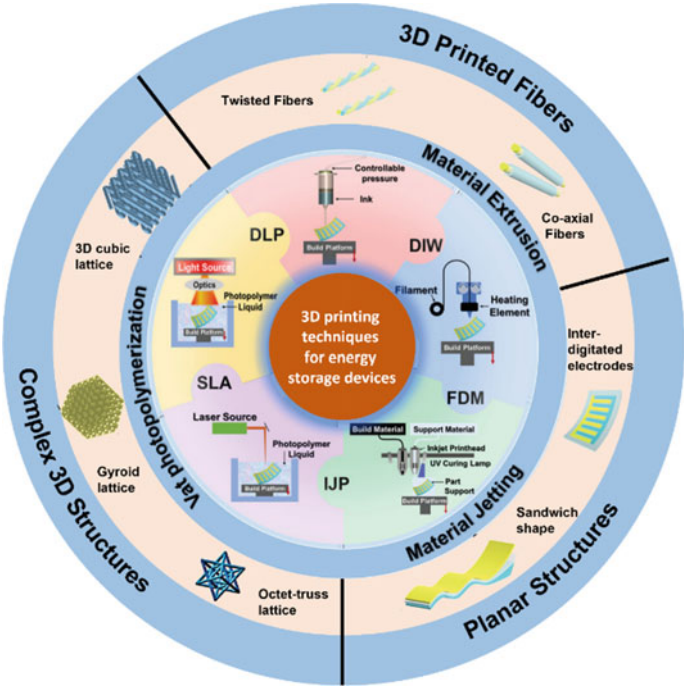

Fig. 2 Overview of 3D printing techniques and their electrode architectures. Adapted with permission [1], Copyright (2022), John Wiley and Sons

3D printing techniques like DIW, FDM, and SLA, complex capacitor structures can be produced with high precision (Fig. 2), enabling the efficient storage and discharge of electrical energy [3]. These techniques offer the flexibility to create intricate electrode designs and optimize the capacitor's performance, leading to enhanced energy storage capabilities. The flexibility of the 3D printing techniques allows for designing complex structures.

3.1 Interdigitated Structures

The interdigitated electrode structure refers to a configuration where the cathode and anode "fingers" of energy storage devices are closely interconnected in an interleaved manner. This interdigitated approach increases the contact area between the electrodes and electrolyte, reducing ion transfer distances between the electrodes. Unlike planar electrodes, the interdigitated structure requires 3D printing techniques for fabrication, such as DIW, FDM, and SLA [8]. Among these methods, DIW is frequently employed due to its simplicity and the ability to use different active materials for ink printing.

3.2 Vertically Aligned Structures

High energy density and high-power density in batteries and supercapacitors are made possible through the design of vertically aligned structures. The vertically aligned array with low tortuosity facilitates ion transport, withstands volume changes, and enhances cycling stability. Various 3D printing methods such as FDM and SLA can be utilized to create vertically aligned structures by precisely extruding or curing electrode materials along a single axis, enabling the fabrication of thick electrodes with aligned structures [9, 10].

3.3 Complex 3D Structures

Sophisticated hierarchical porous structures, characterized by a significant surface-to-volume ratio, can be readily manufactured using 3D printing methods like DIW and FDM [11]. Wearable energy storage devices with flexibility and breathability can be achieved through fiber or fabric electrode design, overcoming the limitations of conventional electrodes. 3D printing enables the fabrication of flexible fibers woven into fabric structure electrodes, offering porosity, stretchability, and high electrochemical performance [12]. This integration of 3D-printed fiber structure electrodes into textile fabrics holds promise for future wearable electronic applications, ensuring functionality and breathability [7].

4 Pseudocapacitive Materials-Based 3D Printed Supercapacitors

The focus on supercapacitor research is significantly towards the development of high-performance electrode materials. The supercapacitor electrode materials ideally should hold a high specific surface area, large electroactive sites, tunable porosity, high electronic conductivity, and stability [13]. Pseudocapacitive materials offer higher specific capacitance but lower rate performance in comparison to carbon-based electrode materials [1].

4.1 Transition Metal Oxides

Transition metal oxides (TMOs) offer large pseudocapacitance that leads to a higher energy density for 3D-printed capacitors. However, their low electrical conductivity reduces the energy density of the device and affects the electrochemical stability. These limitations can be overcome by using combinations of conductive materials

for printable inks. The most widely used pseudocapacitive metal oxide material is manganese oxide (MnO_2), due to its low cost, facile synthesis, and high theoretical capacitance. Wang et al. developed highly concentrated 2D δ-MnO_2 nanosheet-based ink formulations that could be inkjet printed onto oxygen plasma-treated glass and polyimide substrates without the formation of a coffee-ring effect [12]. The fabricated all-solid-state flexible micro-supercapacitors (MSCs) using polyvinyl alcohol/lithium chloride (PVA/LiCl) electrolyte, attained a volumetric energy density of 1.8 $\times$ 10^{-4} Wh cm^{-3} at 0.018 W cm^{-3} with 88% retention over 3600 cycles. Zhao et al. prepared α-MnO_2 nanorods with reduced graphene oxide (rGO) and ethylene-propylene oxide symmetrical triblock copolymer (pluronic F127) as composite ink material for electrodes (Fig. 3a) [14]. The addition of rGO to the MnO_2 nanorods increases the overall conductivity of the electrodes and F127 with amphiphilic functional groups and rheological properties, helps in forming a stable dispersion ink. The extrusion-based 3D printed one-layer electrode delivered a high specific capacitance of 422 F g^{-1} at the current density of 0.1 A g^{-1} and reached a high energy density of 19.35 Wh kg^{-1} at a power density of 50 W kg^{-1}. These 3D-printed supercapacitor electrodes demonstrated their practical applications like charging a mobile phone and powering LEDs. Yao et al. developed a high-level loading of MnO_2 material (182.2 mg cm^{-2}) to the 3D-printed graphene aerogel, which exhibited a high areal capacitance of 44.13 F cm^{-2} [15]. The fabricated symmetric supercapacitor device with 3D printed Graphene/MnO_2 electrodes (4 mm thickness), delivered an energy density of 1.56 mWh cm^{-2}. To avoid manufacturing difficulties, Seol et al. reported end-to-end printing of all units of supercapacitors including electrodes, electrolytes, substrates, and current collectors [16]. Here, the graphene-Mn_3O_4 nanocomposite ink was used as electrodes with gel polymer electrolyte and Ag-based current collector. All printed pseudocapacitors exhibited a high energy and power density of 14.74 Wh kg^{-1} and 400.8 W kg^{-1}, respectively. Khomami group developed a unique laser ablation synthesis in solution (LASiS) method to prepare hybrid nanocomposites of MnOx/Mn_3O_4 and rGO [17]. The LASiS-printed interdigitated hybrid electrodes showed an outstanding specific capacitance of 325 F g^{-1} compared to the commercial MnO_2-graphene composite of 189 F g^{-1}.

Another, promising printable pseudo-material is ruthenium dioxide (RuO_2) with a high theoretical capacitance of 1450 F g^{-1} was used along with a single-walled carbon nanotube (SWCNT) by Chen et al. [18]. The SWCNT/RuO_2 nanowire hybrid thin film electrode prepared via ink-jet printing improved specific energy density to 18.8 Wh kg^{-1} at a specific power of 96 kW kg^{-1} using PVA/phosphoric acid (H_3PO_4) solid electrolyte. Another typical TMO is Fe_2O_3 with high theoretical capacitance, but low electronic conductivity during the electrochemical process. Tang et al. developed a novel Fe_2O_3/graphene/silver ink for 3D printing solid-state MSCs via extrusion printing [19]. The 3D-printed pseudocapacitor device exhibited a high areal energy density of 65.4 μWh cm^{-2} and remarkable capacitance retention of 90.2% over 500 bending cycles. Nickel oxide (NiO) possesses a high theoretical capacity of 1292 C g^{-1}. Giannakou et al. demonstrated inkjet printing of NiO-based interdigitated co-planar symmetrical MSCs [20]. This device achieved a maximum areal capacitance of 155 mF cm^{-2} and operates until 1.5 V delivering state-of-art

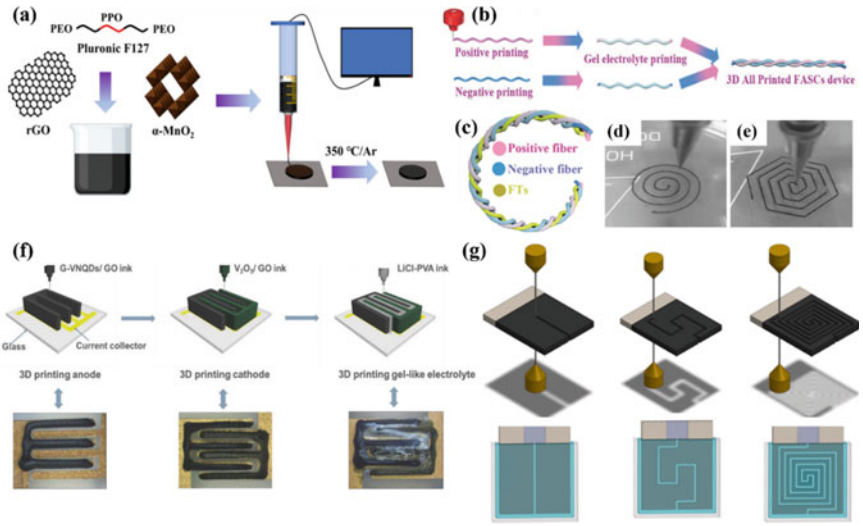

Fig. 3 **a** Schematic illustration of α-MnO_2/rGO ink preparation and 3D printing of electrode. Adapted with permission [14], Copyright (2018), Springer Nature; **b**, **c** Schematic of the fabrication of FASC device using 3D-printed electrodes, FASC device/FTS-integrated configuration; **d**, **e** Optical images of the printed wet fiber during the process. Adapted with permission [21], Copyright (2018), John Wiley and Sons; **f** Schematic of 3D printed asymmetric MSCs on the current collectors with layer-by-layer interdigitated electrodes consisting of G–VNQDs/GO ink as an anode (1st step) and V_2O_5/GO ink as a cathode (2nd step). Adapted with permission [22], Copyright (2018), John Wiley and Sons; **g** Fabrication Mo-MoOx MSC devices with different patterns using EDDW onto Mo metal sheet. Adapted with permission [23], Copyright (2023), Elsevier

high energy-power density. Vanadium oxides (V_2O_5) and nitrides (VN) emerged as pseudocapacitive materials due to the multiple valence states of vanadium, wide potential window, active redox reversibility, high theoretical capacitance, and robust stability during the charge–discharge process. Zhao et al. fabricated fiber-shaped 3D printed electrodes for wearable integrated electronics applications along with printed temperature sensors. The fiber-shaped printed asymmetric pseudocapacitor device was assembled using SWCNT/V_2O_5 as cathode and SWCNT/VN as anode with PVA/potassium hydroxide (KOH) as printed gel electrolyte (Fig. 3b–e) [21]. The twisted fiber-shaped device exhibited outstanding mechanical flexibility, high areal capacitance (116 mF cm^{-2}), high areal energy/power density of 41.28 μWh cm^{-2} /480 μW cm^{-2}, and temperature sensitivity of the integrated device is 1.95% $°C^{-1}$. Shen et al. developed quasi-solid-state 3D printed asymmetric MSCs using V_2O_5 ink as cathode and graphene-vanadium nitride quantum dots (G-VNQDs) ink as an anode in highly concentrated graphene-oxide (GO) dispersions (Fig. 3f) [22]. The 3D printed MSCs via layer-by-layer interdigitated electrodes with PVA/LiCl gel electrolyte achieved ultrahigh areal specific capacitance of 207.9 mF cm^{-2} and superior areal energy density of 73.9 μWh cm^{-2}. Tung et al. prepared graphene-cobalt ferrite (G-CoFe) ink for the 3D printing of electrodes on graphite paper using

the DIW technique [6]. The assembled supercapacitor device with 5 × 5 cm^2 electrodes exhibited a specific capacitance of 304 F g^{-1} with 94.7% retention over 16,000 cycles. Moreover, the device was used to demonstrate powering of a 5 V LED lamp for 15 min with a booster circuit. In addition to TMOs, metal hydroxides were also studied for their feasibility towards printed supercapacitors. Xu et al. developed 3D ceramic interdigitated pseudocapacitive MSCs (pMSCs) using the one-step electric discharge direct writing (EDDW) method with computer-aided design patterns as shown in Fig. 3g [23]. The fabricated binder and additive-free 3D pMSCs using a 3D patterned Mo-MoOx device delivered a high areal capacitance of 49.1 mF cm^{-2} with capacitance retention of 96% over 5000 cycles using 1 M KOH as electrolyte.

4.2 Conducting Polymers

The conducting polymers with high electrical conductivity, flexibility, active redox states, and lightweight are amongst the most ideal and economic pseudocapacitive electrode materials. One among them is polyaniline (PANI). Dou et al. used 3D printing to pattern rapidly formed PANI hydrogel as electrodes for supercapacitors [24]. The PANI hydrogel electrodes in three-electrode cells exhibited a capacitance of 422 F g^{-1} at 0.2 A g^{-1} and high-rate performance. The drawbacks of polymers as electrodes are their poor cyclic stability and moderate conductivity. Thus, these polymers are always combined with carbon to increase their stability and conductivity. Xu et al. formulated nano-graphene platelets (NGP)/PANI composite inks for the fabrication of electrodes using inkjet printing [25]. The demonstrated two-electrode NGP/PANI films on carbon fabric substrates with 1 M H_2SO_4 as an electrolyte, exhibited a maximum capacitance of 70 F g^{-1} and energy density of 2.4 Wh kg^{-1} at a high-power density of 124 kW kg^{-1} with good cycling stability. Wang et al. used PANI/GO gel as composite ink for 3D printing via the direct ink writing method (Fig. 4a, b) [8]. The 3D-printed interdigitated PANI/rGO electrodes after reduction were constructed to form a planar solid-state pseudocapacitor device. The device exhibited an impressive areal capacitance of 1329 mF cm^{-2} with PVA-H_2SO_4 gel electrolyte. Liu et al., developed highly concentrated water-dispersible GO/PANI composite inks for all-solid-state supercapacitors using extrusion printing [26]. The fabricated interdigitated flexible asymmetric MSCs with a wide operating voltage of up to 1.2 V delivered specific energy of 4.83 mWh cm^{-3} at 25.3 W cm^{-3} and cyclic stability of ~100% retention over 5000 cycles.

Zhang et al. prepared a new-type polypyrrole (PPy)/PANI co-axis nanotube ink which is adaptable and 3D printed directly onto various substrates [27]. The all-printed MSCs device with PVA gel as electrolyte delivered a high capacitance of 151.2 mF cm^{-3} with volumetric energy of 19.6 mWh cm^{-3} and flexibility for wearable electronics. Lu et al. prepared a porous iron-nickel/PANI nanocages ink for 3D printing multiscale supercapacitor device using powder bed technologies, which delivered a high specific capacitance of 540.68 F g^{-1} [28]. Other than PANI and PPy polymers, researchers have used aqueous poly(3,4-ethylene dioxythiophene)

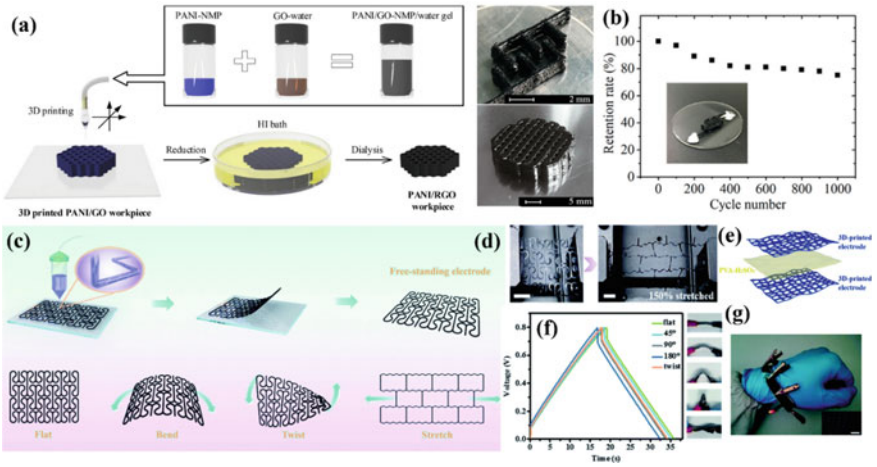

Fig. 4 **a** Preparation of PANI/GO inks and 3D printing process of PANI/RGO workpiece & planar structure, **b** Capacitance retention rate for the planar device over 1000 cycles at 50 mA cm^{-2}. Adapted with permission [8], Copyrights (2018), Elsevier; **c** Fabrication of highly deformable 3D-printed electrodes with NPR structures and under different deformation conditions, **d** re-entrant structure electrodes with the maximum stretch state, **e** construction of symmetric full SC device, **f** GCD curves of the stretchable symmetric SC under different conditions, **g** Photograph of the wearable PEDOT:PSS/CNT SSC. Scale bars: 6 mm. Adapted with permission [29], Copyrights (2013), Royal Society of Chemistry

(PEDOT) and poly(4-styrene sulfonic acid) (PSS) in combination with metal oxides and carbon as composite ink for printing electrodes. Yang et al. fabricated highly stretchable self-standing 3D printed additive-free electrodes using PEDOT: PSS/CNT hybrid ink, as shown in Fig. 4c–g [29]. The fabricated quasi-solid-state printed supercapacitor using PVA-H_2SO_4 electrolyte achieved an areal capacitance of 990 mF cm^{-2} and areal energy density of 0.065 mWh cm^{-2} at a power of 0.4 mW cm^{-2} with ultra-long cycling stability of 74.7% retention over 14,000 cycles.

4.3 Metal Dichalcogenides

Another important class of pseudocapacitive material is the metal dichalcogenides (TMDs), which possess various oxidation states, large active sites for adequate electrochemical performance, and large surface areas with both faradaic and non-faradaic surface behaviors [30]. Moreover, the 2D TMDs have a unique structure of a single sheet has a metal atomic layer sandwiched between the chalcogenide layers through covalent bonding. Among the TMDs, the most used electrode material is the molybdenum disulfide (MoS_2) nanosheets. Shao et al. reported electro-hydro-dynamic-assisted preparation of the 3D 1 T-phase crumpled MoS_2 stable ink formulation for inkjet printing [31]. The inkjet printed asymmetric MSCs, with rGO as cathode

onto flexible photo paper with a wide voltage of 1.75 V in 1 M magnesium sulfate ($MgSO_4$) as an electrolyte, delivered a maximum areal energy of 3.85 μWh cm^{-2} at 12.6 μW cm^{-2} and an outstanding stability of 96% retention over 20,000 cycles. Yang et al. demonstrated 3D core-sheath extrusion-based printing of CNT-MoS_2-CNT/graphene ink with high mass loading of 55% (Fig. 5a–c) [10]. The assembled symmetric supercapacitor device with polyvinylidene fluoride (PVDF) nanofibers as separator and PVA-based gel polymer as an electrolyte, delivered an areal energy density of 49 μWh cm^{-2} with an areal capacitance of 558 mF cm^{-2}. Ghosh et al. electrodeposited the MoS_x layer onto a 3D-printed nanocarbon electrode surface to form a MoS_x-coated free-standing 3D electrode [32]. The fabricated symmetric solid-state-supercapacitor device with PVA-H_2SO_4 electrolyte delivered a maximum areal energy density of 0.2 μWh cm^{-2} at 16.26 μW cm^{-2} without any use of the current collector. Odnevall group used the SLM technique to fabricate pseudocapacitor devices using MoS_2/Mo_2S_3 nanocomposite ink [9]. The electrode performance of the SLM printed electrode in a three-electrode cell offered a specific capacitance of 83.1 mF cm^{-2} and areal energy of 1.66 mWh cm^{-2}. Zhao et al. used copper sulfate KCu_7S_4/rGO composite ink for MSCs using the direct ink writing method [33]. The assembled symmetric capacitor with 3D printed electrodes with 8 layers with PVA-KOH gel electrolyte delivered remarkable areal and gravimetric capacitance of 7.33 F cm^{-2} and 815.8 F g^{-1}, respectively, and high areal energy of 286 μWh cm^{-2} at 2.16 μW cm^{-2}. Later, the KCu_7S_4/rGO composite ink was incorporated with MWCNT to form a 3D-printed rGO/MWCNT/ KCu_7S_4 electrode with 8 layers [34]. The assembled device exhibited enhanced areal and gravimetric capacitance of 27.8 F cm^{-2} and 1674.3 F g^{-1}, respectively compared to the electrode without MWCNT.

4.4 Transition Metal Carbides/carbonitrides (MXenes)

In addition to the above-mentioned materials, a novel printable material that includes MXene has attracted significant attention in recent years for printable energy storage devices. These MXenes possess negatively charged surfaces for better hydrophilicity, high metallic conductivity due to alternate layers of metal and carbon atoms, and excellent redox activity. Zhang et al. developed MXene- based additive-free inks for 3D printing MSCs by extrusion and inkjet printing methods [35]. The all-printed flexible MSCs with PVA-H_2SO_4 as gel electrolyte delivered volumetric capacitance of 562 F cm^{-3} and areal energy of 0.32 μWh cm^{-2} with 97% capacitance retention after 14,000 cycles. Yu et al. reported N-doped MXene (Ti_3C_2) ink used for screen and extrusion-printed supercapacitors [36]. The 3-layered electrode SC exhibited high areal and volumetric energy densities of 0.42 mWh cm^{-2} and 0.83 mWh cm^{-3}, respectively. Yang et al. formulated aqueous $Ti_3C_2T_x$ inks for extrusion-based free-standing 3D printed interdigitated supercapacitors free-of current collector by freeze-drying as shown in Fig. 5d–f [37]. The 3D printed MSCs in PVA-H_2SO_4 solid

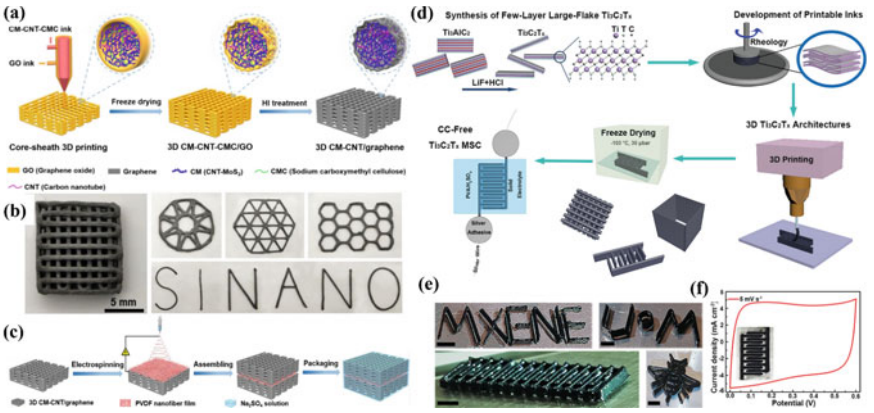

Fig. 5 **a** Schematic artwork of the 3D-printed CM-CNT/graphene electrode process, **b** photographs of 3D-printed CM-CNT/graphene electrode from a top view and in different 2D geometric patterns, **c** Fabrication process of symmetric CM-CNT/graphene//PVDF nanofiber//CM-CNT/graphene pseudocapacitor. Adapted with permission [10], Copyrights (2021), Elsevier. **d** Illustration of the manufacturing of 3D printing of freestanding MXene architectures strategy that includes synthesis, ink preparation, 3D printing of inks, freeze-drying to retain the shapes, and probing of the final device, **e** 3D printed architectures- MXene (4 layers), University of Manchester (UoM) (5 layers), interdigitated (4 layers) and bee (3 layers) designs all printed through a 330 μm nozzle with a printing speed of 6–10 mm s^{-1}. All scale bars in 3 mm, **f** CV curves of interdigitated MSCs at a scan rate of 5 mV s^{-1}. Adapted with permission [37], Copyrights (2019), John Wiley and Sons

electrolyte delivered 0.0244 mWh cm^{-2} at 0.64 mW cm^{-2} with unique rheological properties. Interestingly, Huang et al. developed multi-scale MXene ($Ti_3C_2T_x$) hydrogel electrodes by unidirectional freeze-drying for fabricating all-MXene 3D printed MSCs devices [11]. The 3D printed interdigitated all-MXene electrode with PVA-H_2SO_4 gel polymer delivered a high areal capacitance of 2004 mF cm^{-2} with high rate capability and outstanding areal energy of 100 mWh cm^{-2} at a power density of 0.38 mW cm^{-2}. Orangi et al. reported water-based additive-free MXene ($Ti_3C_2T_x$) ink for all-solid-state MSCs [38]. The fabricated interdigitated 3D printed electrodes on polymer substrates with PVA-H_2SO_4 gel polymer electrolyte exhibited impressive areal capacitance of 1035 mF cm^{-2} for 10 layers of electrode and areal energy of 51.7 μWh cm^{-2} at 5.7 mW cm^{-2}. Gogotsi group introduced 4D printing technology for fabricating a family of MXene hydrogels ($Ti_3C_2T_x$, Nb_2CT_x, and $Mo_2Ti_2C_3T_x$) with low-temperature tolerance for MSCs using polymer composition and additives [39]. The 4D printed MSCs using $Ti_3C_2T_x$ as hydrogel electrode and PVA-ethylene glycol-H_2SO_4 as gel electrolyte, delivered high areal energy of 92.88 μWh cm^{-2} at 6.96 mW cm^{-2} with ultrahigh capacitances of 2.31 F cm^{-2}.

4.5 Metal–organic Frameworks

Metal–organic frameworks (MOFs) are a new class of coordination polymers used as supercapacitor electrodes due to their highly porous nature, tunable porosity, various structures, and tunable chemical properties [40]. The preparation of MOFs-based inks mostly depends on additives that lead to low rheological properties. Zhang et al. reported MOF-derived carbon via laser scribing to fabricate 12-interdigitated MSCs using MOF-199 with copper and zeolitic imidazolate framework (ZIF-67) with cobalt [40]. The laser-scribed asymmetric MSCs in 1 M H_2SO_4 electrolyte delivered maximum areal energy of 0.7 mWh cm^{-2} at 1 mW cm^{-2} and areal capacitance of 8.1 F cm^{-2} with good cyclic stability of 94% over 10,000 cycles. Wu et al. developed a heterostructure using MOF (ZIF-67) with covalent 2D black phosphorus (BP) – BP/ZIF-67 ink with CNT and polymer binder for fabricating wearable and flexible supercapacitor (FSCs), as shown in Fig. 6a, b [41]. The 3D printed FSCs by extrusion process with PVDF-hexafluoropropylene (HFP)/1-eutyl-3-methylimidazoliumtetrafluoroborate ($EMIBF_4$) electrolyte ink exhibited volumetric capacitance of 506 F cm^{-3}, areal energy/power densities of 109.8 mWh cm^{-2} at 0.675 mW cm^{-2} and maintains 89.3% capacitance retention after 12,000 cycles.

4.6 Hybrid Electrode Combination

To mitigate the limitations of individual pseudocapacitive materials and to overcome the challenges faced during ink formulations, hybrid composite-based ink was proposed by the combination of two or three different materials. Li et al. prepared hybrid ink using the pseudoplastic nanocomposites comprised of $Ti_3C_2T_x$ MXene, manganese dioxide (MnO_2) nanowires, Ag NWs, and fullerene (C60) for extrusion-based 3D printing of electrodes (Fig. 6c–g) [42]. The 3D-printed interdigitated MSCs with unidirectional freezing of electrodes infused with PVA-KOH gel polymer electrolyte exhibited areal capacitance of 216.2 mF cm^{-2} and energy density of 19.2 μWh cm^{-2} with long-term cyclic stability. Yu et al. demonstrated a hybrid electrode consisting of bimetallic phosphide (NiCoP) and Ti_3C_2 MXene ink (NCPM) using layer-by-layer 3D printing [43]. The assembled asymmetric supercapacitor cell with 3D-printed NCPM as positive and activated carbon as negative electrode in 2 M KOH as electrolyte, delivered a volumetric energy density of 2.2 mWh cm^{-3} with improved rate capability. Similarly, a solid-state asymmetric supercapacitor (SS-ASC) was fabricated by the Pumera group using a 3D-printed nanocarbon framework coated with MoS_{3-x} (MoS_{3-x}@3DnCF) as positive and exfoliated $Ti_3C_2T_x$ MXene as a negative electrode using PVA-H_2SO_4 gel electrolyte [44]. The 3D-printed interdigitated SS-ASC exhibited a high volumetric capacitance of 556.09 mF cm^{-3} that can work in a potential of up to 1.6 V and robust cyclic life over 25,000 cycles.

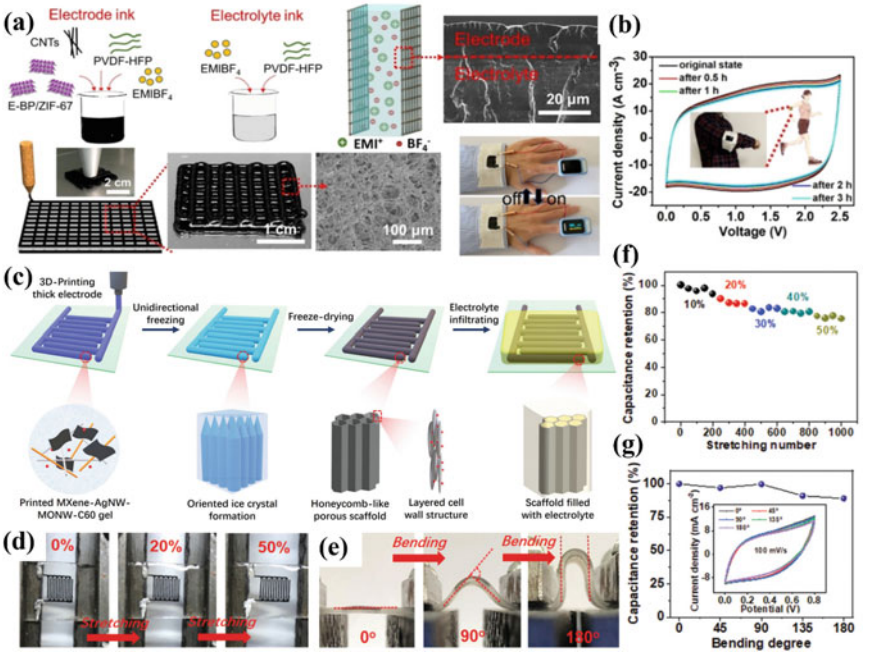

Fig. 6 **a** Representation of the all-integrated solid-state FSC by 3D printing and its cross-sectional morphology of assembled supercapacitor with photographs of a health care device powered by FSC woven into cloth on the right side, **b** CV curves of E-BP/ZIF-67 FSC under at a scan rate of 50 mV s^{-1} under consecutive motions. Adapted with permissions [41], Copyrights (2021), John Wiley and Sons; **c** Schematic of the fabrication process of stretchable interdigitated MSCs through 3D printing and unidirectional freezing, **d** Optical images under 0% to 50% stretch, **e** under 0° to 180° bending, **f** capacitance retention as a function of stretching over 1000 cycles, **g** capacitance retention at different bending degrees (inset: CV curves at 100 mV s^{-1} under bending condition). Adapted with permission [42], Copyrights (2020), John Wiley and Sons

Furthermore, the SS-ASC in series combination was demonstrated to power a 1.8 V green LED for 2 min.

Recently, integrating energy storage devices with multifunctional wearable and portable electronics or devices is of utmost demand. Ma et al. prepared an aqueous printable MXene/PEDOT: PSS (MP) hybrid ink to print MSCs using inkjet printing [7]. The printed interdigitated planar MSCs delivered a maximum volumetric capacitance of 754 F cm^{-3} and comparative specific energy of 9.4 mWh cm^{-3}. Moreover, MP-MSC when integrated with the printed temperature sensor and solar cell, delivered a remarkable response of 2% and high flexibility under various bending stages. Lin et al. integrated a printed supercapacitor device into a self-powered sensor system onto a single flexible substrate including a solar cell demonstrated in a wristband model as shown in Fig. 7a [45]. The inkjet-printed interdigitated planar supercapacitor electrodes consist of MnO_2/rGO/PEDOT:PSS hybrid ink onto a flexible Ni-coated polyethylene terephthalate (PET) substrate delivering areal capacitance of

12.9 mF cm^{-2} and specific energy of 4.5 mWh cm^{-2}. The fully printed device consists of supercapacitors to store photovoltaic energy, power functional LED devices, and simultaneously function without charging modules, which was demonstrated for wearable practical wristband electronics shown in Fig. 6b. Zhao et al. reported coaxial fiber-shaped asymmetric supercapacitors (FASC) using the direct coherent multi-ink writing (DCMW) technique as shown in Fig. 7c–f [46]. The fiber-shaped printed V_2O_5 nanowires (NWs) with MWCNT were used as positive and VN nanowires with MWCNT were used as negative electrodes for fabricating FASC using PVA-KOH as electrolyte ink. The FASC device delivered a high areal capacitance of 152.7 mF cm^{-2} with a wide operating voltage of 1.6 V and gravimetric energy density of 21.2 Wh kg^{-1} at high material loading of 16.4 mg cm^{-2}. This FASC device was then integrated into solar cells and an electric motor to demonstrate a self-powered system converting solar to electrical energy and into mechanical energy (Fig. 7g).

5 Implications and Future Perspectives

Advancements in 3D printing technology offer unique advantages for pseudocapacitors and other electrochemical energy storage devices that can enable the creation of high-energy density devices with complex structures and design freedom. To advance the future of 3D-printed electrochemical energy storage systems, it is vital to enhance the intrinsic conductivity of 3D-printed electrodes. This can be accomplished through techniques like active material composites or separate current collectors coated with energy storage materials. Furthermore, addressing the obstacles associated with high-performance feedstock materials and optimizing ink formulations plays a critical role in improving the printing process and achieving high-performance 3D-printed supercapacitors. Enhancing the mechanical properties of printed electrodes through innovative approaches and simulation methods is essential for durability and stability. While commercialization is still in progress, the potential market for 3D-printed pseudocapacitors, batteries, and integrated systems is promising. However, overcoming limitations and optimizing manufacturing processes will be necessary for successful large-scale production and cost competitiveness. With continued research and development, it is expected that 3D-printed energy storage devices will find widespread applications, contributing to the advancement of energy storage technologies.

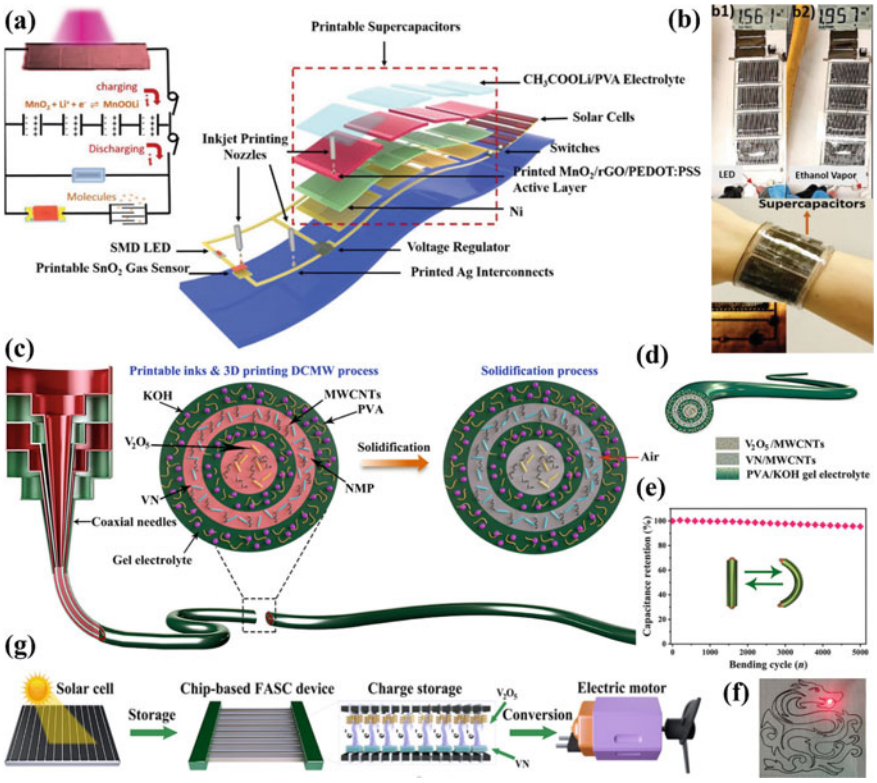

Fig. 7 **a** Schematic representation of printable supercapacitors integrated wearable monolithically self-powered smart sensor system, **b** Voltage drop on LED (b1) without and (b2) with detection of ethanol in ambient. Inset: multimeter readings and photos of a wearable wristband. Adapted with permission [45], Copyrights (2018), John Wiley and Sons. **c** 3D printing extrusion process of the printable coaxial FASC device and its subsequent solidification process, **d** assembled FASC device, **e** capacitance retention under several bending cycles, **f** Photo of a fully charged 3D printed coaxial FASC device powering a red 1.5-V LED, **g** Schematic of the self-powered system where the solar energy is converted into electrical energy and then into mechanical energy. Adapted with permission [46], Copyrights (2021), Distributed under a Creative Commons Attribution Non-commercial License 4.0 (CC BY-NC)

Acknowledgements Authors thank in part to funding from the University of Calgary- Eyes High Postdoc fund and the Natural Sciences and Engineering Research Council of Canada (NSERC) Collaborative Research and Development (CRD) grants.

References

1. M. Li, S. Zhou, L. Cheng, F. Mo, L. Chen, S. Yu, J. Wei, 3D printed supercapacitor: techniques, materials, designs, and applications. Adv. Funct. Mater **33**(1) (2023)
2. D.M. Soares, Z. Ren, S.B. Mujib, S. Mukherjee, C.G. Martins Real, M. Anstine, H. Zanin, G. Singh, Additive manufacturing of electrochemical energy storage systems electrodes. Adv. Energy Sustain. Res. **2**(5), 2000111 (2021)
3. T. Chu, S. Park, K. Fu, 3D printing-enabled advanced electrode architecture design. Carbon Energy **3**(3), 424–439 (2021)
4. W. Zong, Y. Ouyang, Y.E. Miao, T. Liu, F. Lai, Recent advances and perspectives of 3D printed micro-supercapacitors: from design to smart integrated devices. Chem. Commun. **58**(13), 2075–2095 (2022)
5. B. Rezaei, T.W. Hansen, S.S. Keller, Stereolithography-derived three-dimensional pyrolytic carbon/mn3o4nanostructures for free-standing hybrid supercapacitor electrodes. ACS Appl. Nano Mater. **5**(2), 1808–1819 (2022)
6. D.T. Tung, L.T.T. Tam, H.T. Dung, N.T. Dung, H.T. Ha, N.T. Dung, T. Hoang, T.D. Lam, T.V. Thu, D.T. Chien, P.N. Hong, P.N. Minh, N.V. Quynh, L.T. Lu, Direct ink writing of graphene-cobalt ferrite hybrid nanomaterial for supercapacitor electrodes. J. Electron. Mater. **49**(8), 4671–4679 (2020)
7. J. Ma, S. Zheng, Y. Cao, Y. Zhu, P. Das, H. Wang, Y. Liu, J. Wang, L. Chi, S. Liu, Z. S. Wu, Aqueous MXene/PH1000 hybrid inks for inkjet-printing micro-supercapacitors with unprecedented volumetric capacitance and modular self-powered microelectronics. Adv. Energy Mater. **11**(23) (2021)
8. Z. Wang, Q. Zhang, S. Long, Y. Luo, P. Yu, Z. Tan, J. Bai, B. Qu, Y. Yang, J. Shi, H. Zhou, Z.Y. Xiao, W. Hong, H. Bai, Three-dimensional printing of polyaniline/reduced graphene oxide composite for high-performance planar supercapacitor. ACS Appl. Mater. Interf. **10**(12), 10437–10444 (2018)
9. N. Alinejadian, S. H. Kazemi, I. Odnevall, SLM-processed MoS2/Mo2S3 nanocomposite for energy conversion/storage applications. Sci. Rep. **12**(1) (2022)
10. Z. Yang, X. Lv, C. Zhang, Y. Zhang, S. Jia, Y. Niu, Y. Zhang, B. Wang, T. Zhao, H. Fu, Q. Li, Core-sheath 3D printing of highly conductive and MoS2-loaded electrode with pseudocapacitive behavior. Chem. Eng. J. **423** (2021)
11. X. Huang, J. Huang, D. Yang, P. Wu, A multi-scale structural engineering strategy for high-performance MXene hydrogel supercapacitor electrode. Adv. Sci. **8**(18) (2021)
12. Y. Wang, Y.Z. Zhang, D. Dubbink, J.E. ten Elshof, Inkjet printing of δ-MnO2 nanosheets for flexible solid-state micro-supercapacitor. Nano Energy **49**, 481–488 (2018)
13. A. Gopalakrishnan, S. Badhulika, Hierarchical architectured Dahlia flower-like NiCo<inf>2</inf>O<inf>4</inf>/NiCoSe<inf>2</inf>as a bifunctional electrode for high-energy supercapacitor and methanol fuel cell application. Ener. Fuels **35**(11) (2021)
14. X. Zhao, B. Liu, P. Pan, Z. Yang, J. He, H. Li, J. Wei, Z. Cao, H. Zhang, J. Chang, Q. Bao, X. Yang, Fabrication of reduced graphene oxide/manganese oxide ink for 3D-printing technology on the application of high-performance supercapacitors. J. Mater. Sci. **56**(13), 8102–8114 (2021)
15. B. Yao, S. Chandrasekaran, J. Zhang, W. Xiao, F. Qian, C. Zhu, E.B. Duoss, C.M. Spadaccini, M.A. Worsley, Y. Li, Efficient 3D printed pseudocapacitive electrodes with ultrahigh MnO 2 loading. Joule **3**(2), 459–470 (2019)
16. M.L. Seol, I. Nam, E.L. Ribeiro, B. Segel, D. Lee, T. Palma, H. Wu, D. Mukherjee, B. Khomami, C. Hill, J.W. Han, M. Meyyappan, All-printed in-plane supercapacitors by sequential additive manufacturing process. ACS Appl. Energy Mater **3**(5), 4965–4973 (2020)
17. M. Mokhtarnejad, E.L. Ribeiro, D. Mukherjee, B. Khomami, 3D printed interdigitated supercapacitor using reduced graphene oxide-MnOx/Mn3O4 based electrodes. RSC Adv. **12**(27), 17321–17329 (2022)

18. P. Chen, H. Chen, J. Qiu, C. Zhou, Inkjet printing of single-walled carbon nanotube/RuO2 nanowire supercapacitors on cloth fabrics and flexible substrates. Nano Res. **3**(8), 594–603 (2010)
19. K. Tang, H. Ma, Y. Tian, Z. Liu, H. Jin, S. Hou, K. Zhou, X. Tian, 3D printed hybrid-dimensional electrodes for flexible micro-supercapacitors with superior electrochemical behaviours. Virtual Phys. Prototyp. **15**(S1), 511–519 (2020)
20. P. Giannakou, M.G. Masteghin, R.C.T. Slade, S.J. Hinder, M. Shkunov, Energy storage on demand: Ultra-high-rate and high-energy-density inkjet-printed NiO micro-supercapacitors. J. Mater. Chem. A Mater. **7**(37), 21496–21506 (2019)
21. J. Zhao, Y. Zhang, Y. Huang, J. Xie, X. Zhao, C. Li, J. Qu, Q. Zhang, J. Sun, B. He, Q. Li, C. Lu, X. Xu, W. Lu, L. Li, Y. Yao, 3D printing fiber electrodes for an all-fiber integrated electronic device via hybridization of an asymmetric supercapacitor and a temperature sensor. Adv. Sci. **5**(11) (2018)
22. K. Shen, J. Ding, S. Yang, 3D printing quasi-solid-state asymmetric micro-supercapacitors with ultrahigh areal energy density. Adv. Energy Mater **8**(20) (2018)
23. Y. Xu, P. Deng, R. Chen, W. Xie, Z. Xu, Y. Yang, D. Liu, F. Huang, Z. Zhuang, I. Zhitomirsky, K. Shi, Electric discharge direct writing of 3D Mo-MoOx pseudocapacitive micro-supercapacitors with designable patterns. Ceram Int. (2023)
24. P. Dou, Z. Liu, Z. Cao, J. Zheng, C. Wang, X. Xu, Rapid synthesis of hierarchical nanostructured Polyaniline hydrogel for high power density energy storage application and three-dimensional multilayers printing. J. Mater. Sci. **51**(9), 4274–4282 (2016)
25. Y. Xu, I. Hennig, D. Freyberg, A. James Strudwick, M. Georg Schwab, T. Weitz, K. Chih-Pei Cha, Inkjet-printed energy storage device using graphene/polyaniline inks. J. Power. Sources **248**, 483–488 (2014)
26. Y. Liu, B. Zhang, Q. Xu, Y. Hou, S. Seyedin, S. Qin, G. G. Wallace, S. Beirne, J. M. Razal, J. Chen, Development of graphene oxide/polyaniline inks for high performance flexible microsupercapacitors via extrusion printing. Adv. Funct. Mater **28**(21) (2018)
27. Y. Zhang, T. Ji, S. Hou, L. Zhang, Y. Shi, J. Zhao, X. Xu, All-printed solid-state substrate-versatile and high-performance micro-supercapacitors for in situ fabricated transferable and wearable energy storage via multi-material 3D printing. J. Power. Sources **403**, 109–117 (2018)
28. X. Lu, T. Zhao, X. Ji, J. Hu, T. Li, X. Lin, W. Huang, 3D printing well organized porous iron-nickel/polyaniline nanocages multiscale supercapacitor. J. Alloys Compd. **760**, 78–83 (2018)
29. J. Yang, Q. Cao, X. Tang, J. Du, T. Yu, X. Xu, D. Cai, C. Guan, W. Huang, 3D-Printed highly stretchable conducting polymer electrodes for flexible supercapacitors. J. Mater. Chem. A. Mater. **9**(35), 19649–19658 (2021)
30. N. Alinejadian, L. Kollo, I. Odnevall, Progress in additive manufacturing of MoS2-based structures for energy storage applications – a review. Mater. Sci. Semicond. Process **139** (2022)
31. Y. Shao, J.H. Fu, Z. Cao, K. Song, R. Sun, Y. Wan, A. Shamim, L. Cavallo, Y. Han, R.B. Kaner, V.C. Tung, 3D crumpled ultrathin 1T MoS2for Inkjet printing of Mg-Ion asymmetric micro-supercapacitors. ACS Nano **14**(6), 7308–7318 (2020)
32. K. Ghosh, M. Pumera, Free-standing electrochemically coated MoSx based 3D-printed nanocarbon electrode_Nanoscale. Nanoscale **13**, 5744–5756 (2021)
33. Y. Zhao, F. Liu, Z. Zhao, P. Bai, Y. Ma, A. Alhadhrami, G.A.M. Mersal, Z. Lin, M.M. Ibrahim, Z.M. El-Bahy, Direct ink printing reduced graphene oxide/KCu7S4 electrodes for high-performance supercapacitors. Adv. Compos. Hybrid Mater **5**(2), 1516–1526 (2022)
34. Y. Zhao, F. Liu, K. Zhu, S. Maganti, Z. Zhao, P. Bai, Three-dimensional printing of the copper sulfate hybrid composites for supercapacitor electrodes with ultra-high areal and volumetric capacitances. Adv. Compos. Hybrid Mater **5**(2), 1537–1547 (2022)
35. C. Zhang, (John), L. McKeon, M. P. Kremer, S. H. Park, O. Ronan, A. Seral-Ascaso, S. Barwich, C. Coileáin, N. McEvoy, H. C. Nerl, B. Anasori, J. N. Coleman, Y. Gogotsi, V. Nicolosi, Additive-free MXene inks and direct printing of micro-supercapacitors. Nat. Commun. **10**(1) (2019)

36. L. Yu, Z. Fan, Y. Shao, Z. Tian, J. Sun, Z. Liu, Versatile N-Doped MXene ink for printed electrochemical energy storage application. Adv. Energy Mater, **9**(34) (2019)
37. W. Yang, J. Yang, J. J. Byun, F. P. Moissinac, J. Xu, S. J. Haigh, M. Domingos, M. A. Bissett, R. A. W. Dryfe, S. Barg, 3D printing of freestanding MXene architectures for current-collector-free supercapacitors. Adv. Mater. **31**(37) (2019)
38. J. Orangi, F. Hamade, V.A. Davis, M. Beidaghi, 3D printing of additive-free 2D Ti3C2Tx (MXene) Ink for fabrication of micro-supercapacitors with ultra-high energy densities. ACS Nano **14**(1), 640–650 (2020)
39. K. Li, J. Zhao, A. Zhussupbekova, C. E. Shuck, L. Hughes, Y. Dong, S. Barwich, S. Vaesen, I. V. Shvets, M. Möbius, W. Schmitt, Y. Gogotsi, V. Nicolosi, 4D printing of MXene hydrogels for high-efficiency pseudocapacitive energy storage. Nat. Commun. **13**(1) (2022)
40. W. Zhang, R. Li, H. Zheng, J. Bao, Y. Tang, K. Zhou, Laser-assisted printing of electrodes using metal–organic frameworks for micro-supercapacitors. Adv. Funct. Mater **31**(14) (2021)
41. T. Wu, Z. Ma, Y. He, X. Wu, B. Tang, Z. Yu, G. Wu, S. Chen, N. Bao, A covalent black phosphorus/metal–organic framework hetero-nanostructure for high-performance flexible supercapacitors. Angewandte Chemie Intern. Edition **60**(18), 10366–10374 (2021)
42. X. Li, H. Li, X. Fan, X. Shi, J. Liang, 3D-printed stretchable micro-supercapacitor with remarkable areal performance. Adv. Energy Mater **10**(14) (2020)
43. L. Yu, W. Li, C. Wei, Q. Yang, Y. Shao, J. Sun, 3D printing of NiCoP/Ti3C2 MXene architectures for energy storage devices with high areal and volumetric energy density. Nanomicro. Lett. **12**(1) (2020)
44. K. Ghosh, M. Pumera, MXene and MoS3−x Coated 3D-printed hybrid electrode for solid-state asymmetric supercapacitor. Small Methods **5**(8) (2021)
45. Y. Lin, J. Chen, M. M. Tavakoli, Y. Gao, Y. Zhu, D. Zhang, M. Kam, Z. He, Z. Fan, Printable fabrication of a fully integrated and self-powered sensor system on plastic substrates. Adv. Mater. **31**(5) (2019)
46. J. Zhao, H. Lu, Y. Zhang, S. Yu, O. I. Malyi, X. Zhao, L. Wang, H. Wang, J. Peng, X. Li, Y. Zhang, S. Chen, H. Pan, G. Xing, C. Lu, Y. Tang, X. Chen, Direct coherent multi-ink printing of fabric supercapacitors. Sci. Adv. **7**(3) (2021)

Pseudocapacitive Materials for Flexible Supercapacitors

Fang Cheng, Xiaoping Yang, and Wen Lu

Abstract Along with the rapid development of flexible and wearable electronics, there has been a strong need for flexible energy storage devices to power these devices. Flexible supercapacitors (FSCs), having the unique characteristics of high-power density, long lifetime, wide operating temperature range, and remarkable safety in a flexible fashion, have been extensively studied for this emerging technology. An ideal FSC would have both superior electrochemical performances and excellent mechanical deformabilities, which require thorough research on the electrode materials and device configurations of FSCs. This chapter reviews the recent progress on these aspects of FSCs. Electrode materials, specifically pseudocapacitive materials (including metal oxides, conducting polymers, and Mxenes) and their composites, of FSCs are firstly elucidated. This is followed by the discussion about the device configurations of pseudocapacitive material-incorporated FSCs, ranging from one-dimensional fiber-shaped to two-dimensional film-shaped and three-dimensional structural. Finally, the practical applications of pseudocapacitive material incorporated FSCs are summarized. In conclusion, the current challenges and future prospects for pseudocapacitive material-incorporated FSCs are discussed.

Keywords Flexible supercapacitors · Electrochemical performances · Mechanical deformabilities · Electrode materials · Pseudocapacitive materials · Device configurations

F. Cheng · W. Lu (✉)
College of Chemical Science and Engineering, Yunnan University, Kunming 650091, China
e-mail: wenlu@ynu.edu.cn

Institute of Energy Storage Technologies, Yunnan University, Kunming 650091, China

X. Yang
School of Metallurgy and Energy, Kunming University of Science and Technology, Kunming 650091, China

W. Lu
School of Materials and Energy, Yunnan University, Kunming 650091, China

© The Author(s), under exclusive license to Springer Nature Switzerland AG 2024

R. K. Gupta (ed.), *Pseudocapacitors*, Engineering Materials,
https://doi.org/10.1007/978-3-031-45430-1_14

1 Introduction

In recent years, the rapid applications of flexible and wearable electronic devices, such as flexible touch screens, artificial electronic skins, wearable electronic suits and smart sensors, miniature biomedical devices, and health monitoring and management, have dramatically influenced our daily lives [1, 2]. This has triggered the extensive research and development of flexible power sources [3], mainly including flexible batteries (FBs) and flexible supercapacitors (FSCs) [4–6]. Compared to FBs, FSCs possess the advantages of higher power density, wider operating temperature range, longer cycle life, and better safety but a distinct disadvantage of lower energy density. In this regard, owing to their higher capacitances than those of traditional electric-double-layer-capacitor (EDLC) materials, pseudocapacitive materials have been studied to enhance the energy density for FSCs, resulting in a family of pseudocapacitive material-incorporated FSCs [7–9] in the community of flexible power sources.

An ideal FSC would have not only superior electrochemical performances (including high energy/power densities, long lifetime, and high safety) but also the excellent mechanical deformabilities (such as flexibility, stretchability, bendability, foldability, and twistability) [5, 6], with the former largely determined by the properties of the electrode materials [10] and the latter by the configuration designs of the devices [3]. Herein, this chapter systematically discusses the recent progress in the research of pseudocapacitive electrode materials (including metal oxides (MOs), conducting polymers (CPs), and Mxenes (MXs) as well as their composites) for FSCs and the device configurations (from one-dimensional (1D) fiber-shaped to two-dimensional (2D) film-shaped and three-dimensional (3D) structural) of the resultant FSCs. This is followed by a discussion about the practical applications of pseudocapacitive material incorporated FSCs. Towards the conclusion, the current challenges and future prospects of pseudocapacitive material incorporated FSCs are spotlighted.

2 Pseudocapacitive Materials for FSCs

Different from the energy storage mechanism of a so-called electric double layer for an EDLC material, that of a pseudocapacitive material is characterized by its fast and reversible redox reactions at or near the electrode surface [11, 12]. This results in higher capacitances for pseudocapacitive materials and thus higher energy densities for pseudocapacitors over those of their EDLC counterparts [7, 8]. In the past decades, considerable efforts have been made to utilize a large variety of pseudocapacitive materials including, for example, MOs [3, 8], CPs [7, 13, 14], and MXs [9, 11], for developing FSCs. It is straightforward to directly fabricate pseudocapacitive materials into electrodes for FSCs. By doing so, however, some shortcomings exist in, for example, capacitance, rate capability, mechanical deformability, and cycling

stability (especially under repeated deformation conditions), for the resultant electrodes [3, 9, 11]. In this regard, processing pseudocapacitive materials into composite electrodes has been demonstrated to be efficient to address these limitations towards high-performance FSCs [14].

On the one hand, multiple pseudocapacitive materials can be incorporated to fabricate composite electrodes. By integrating the superiorities from different types of pseudocapacitive materials (such as high theoretical capacitances of MOs, excellent intrinsic flexibility of CPs, and high density and metallic-like conductivity of MXs), the resultant multi-component-pseudocapacitive-material composite electrodes can achieve enhanced properties over their original individual ingredients [3, 7–9, 14].

On the other hand, compositing pseudocapacitive materials with carbon nanomaterials has attracted considerable research efforts to develop flexible composite electrodes for FSCs. It is known that carbon nanomaterials (*e.g.*, graphene, carbon nanotube (CNT), and carbon nanofiber (CNF)) possess the excellent properties of large specific surface area (SSA), high electrical and thermal conductivities, outstanding flexibility, light weight, high Young's modulus, and high tensile strength [1, 5, 15]. By combing these unique advantages of carbon nanomaterials with the high capacitance of pseudocapacitive materials, the resultant composite electrodes exhibit significantly enhanced properties over their original pseudocapacitive-material counterparts [3, 7–9, 14].

2.1 Metal Oxides and Their Composites for FSCs

Owing to their high theoretical capacitances [5], MOs are an attractive group of pseudocapacitive materials for FSCs [3, 8]. However, the inherent brittleness and stiffness, low electrical conductivity, and poor stability and durability of MOs [10] inevitably limit their practical FSC applications. To address these issues, MOs have been composited with carbon nanomaterials and/or other pseudocapacitive materials.

The integration of MOs with carbon nanomaterials can not only reinforce the mechanical properties but also enhance the conductivity and capacitance for the resultant composites. Among various MOs, MnO_2 has been investigated the most intensively mainly because of its high theoretical capacitance (~1370 F g^{-1}), environmental friendliness, low cost, and abundant resources [8]. For example, Lv et al. [16] developed a stirring hydrothermal method to synthesize a ultralong MnO_2 nanowire/CNT (MNWs/CNT) composite, followed by sandwiching the resultant composite between two thin layers of nanocellulose fibers (NCFs) to achieve a mechanically strengthened MNW-NCF electrode (Fig. 1a). With a polyvinyl alcohol (PVA) gel electrolyte, this composite electrode was assembled into a honeycomb-like symmetric FSC, showing a high capacitance of 227.2 mF cm^{-2}. Mechanically, the FSC thus constructed presented excellent stretchability (Fig. 1b) and superior cycling stability upon varied deformations (Fig. 1c). Moreover, this FSC retained nearly 98% of its initial capacitance even subjected to stretch-release cycling under a 400% tensile

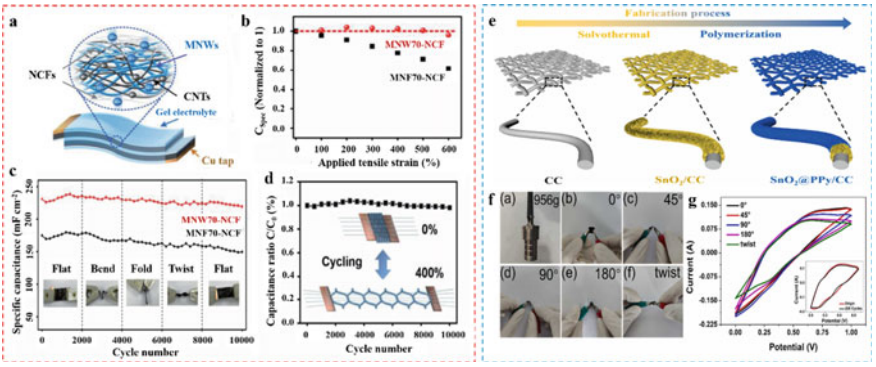

Fig. 1 **a** Schematic illustration of the construction of a MNWs/CNT-NCF based FSC (side view). **b** Normalized specific capacitances of different FSCs tested at 1.6 mA cm^{-2} under different strains. **c** Electrochemical performance comparison between different FSCs upon cycling at 1.6 mA cm^{-2} under various mechanical deformations. Insets are the photographs of FSCs under various mechanical deformations. **d** Capacitance retention ratio of the FSC at 1.6 mA cm^{-2} under a recycling tensile strain of 400%. Adapted with permission [16], Copyright (2018), Wiley–VCH. **e** Schematic illustration of the synthesis of a SnO_2@PPy/CC composite. **f** (a) photograph of a stainless steel autoclave hanged by the SnO_2@PPy/CC composite; (b–f) photographs of a SnO_2@PPy/CC based symmetric FSC under different bending angles and twisting state; **g**. cyclic voltammetry (CV) curves of the FSC at 50 mV s^{-1} under various bending and twisting conditions (inset is CV curves of the FSC before and after 200 bending cycles). Adapted with permission [17], Copyright (2022), Elsevier

strain for 10,000 cycles (Fig. 1d). Compared with a MnO_2 nanoflowers (MNFs)/CNT-NCF electrode (Figs. 1b, c), these achievements can be understood by the interconnected fabric-like microstructure of the MNWs/CNT enabled by the intact contact between the ultralong MnO_2 nanowire and CNT. Therefore, the enhanced electrochemical and mechanical performances of such carbon-MO composites indicate a good strategy for introducing carbon nanomaterials to process MOs into realistically useful electrodes for FSCs.

Alternatively, another strategy to overcome the shortcomings of MOs is to composite them with inherently conductive and flexible pseudocapacitive materials, *i.e.,* CPs. This way, the simultaneous utilization of the high capacitance of MOs and the intrinsic conductivity and flexibility of CPs makes the resultant composites superior over not only their MO but also the CP components. With this concept, for example, Zhuang et al. [17] developed a carbon cloth (CC) flexible scaffold supported SnO_2@polypyrrole (PPy) composite electrode (SnO_2@PPy/CC). The SnO_2 nanosheets were in-situ grown on CC fibers by a simple solvothermal method, followed by polymerizing PPy on the SnO_2 nanosheets thus prepared (Fig. 1e). Benefiting from the combination of SnO_2 and PPy, the as-obtained SnO_2@PPy/CC composite electrode showed significant improvements in both electrochemical and mechanical performances compared to its single-component counterpart without PPy. In particular, the conductivity and flexibility of PPy made the SnO_2-incorporated composite electrode conductive and flexible (inset (a) in Fig. 1f), while its electroactivity provided SnO_2 with additional pseudocapacitance. Consequently, a symmetric

FSC constructed from this composite electrode with a PVA-KOH gel electrolyte realized a high capacitance of 265.9 mF cm^{-2}, a maximum energy and power densities of 0.7 mWh cm^{-3} and 94.7 mW cm^{-3}, respectively, and a superior cycling stability. Moreover, this FSC exhibited excellent mechanical deformabilities without an apparent capacity decay under various bending and twisting conditions (Fig. 1f, g). The above results reveal the effectiveness of incorporating other pseudocapacitive materials to make MOs more suitable for practically useful FSCs.

2.2 Conducting Polymers and Their Composites for FSCs

CPs, mainly represented by polyaniline (PANi), PPy, polythiophene (PTh), and their derivatives, are another type of pseudocapacitive materials for FSCs, thanks to their high theoretical capacitance (*e.g.*, 750 F g^{-1} for PANi and 620 F g^{-1} for PPy). Compared to MOs, CPs possess the distinctive advantages of ease of production, environmental friendliness, and especially inherently high flexibility. However, CPs usually encounter with an inferior rate capability determined by their relatively low conductivity [10] and poor cycling stability by their volume change during the doping-dedoping process [7, 14]. Compositing CPs with carbon nanomaterials and/or other pseudocapacitive materials has been demonstrated to be simple yet effective to address such shortcomings.

The integration of the high capacitance from CPs and the excellent conductivity and stability from carbon nanomaterials endows the resultant carbon-CP composite electrodes with enhanced capacitance, rate capability, and cycling stability over their original CP and carbon counterparts. Among various CPs, PPy is a frequently studied candidate [7, 13]. For example, Li et al. [18] firstly painted reduced graphene oxides (rGO) layers on the surface of $SnCl_2$ modified polyester fibers (M-PEF) via a repeated "dyeing and drying" strategy, followed by in-situ polymerization of PPy onto the resultant rGO/M-PEF substrate to fabricate a PPy/rGO/M-PEF composite electrode (Fig. 2a). While the highly flexible and conductive rGO/M-PEF scaffolds served as a continuous conductive skeleton, the hierarchical PPy/rGO/M-PEF textile structures permitted a large loading of PPy, synergistically enabling excellent mechanical deformabilities with a high capacitance and rate capability for the resultant composite. When combined with a PVA/H_2SO_4 gel electrolyte, the PPy/rGO/M-PEF based symmetric FSC thus assembled showed an excellent rate capability with a high capacitance of 350 mF cm^{-2} at 50 mA cm^{-2} versus that of 474 mF cm^{-2} at 1 mA cm^{-2}, corresponding to a high energy and power densities of 0.0658 mWh cm^{-2} and 0.5 mW cm^{-2}, respectively. This FSC exhibited a remarkable cycling stability with its 100% capacitance retention after being charged/discharged for 10,000 cycles. Furthermore, it showed an outstanding bendability, maintaining its initial capacitance at 97.6% and 99.2% after being bend-cycled for 1000 cycles (Fig. 2b) and bent to an angle up to 180° (Fig. 2c), respectively.

As an important derivative of PTh, poly (3,4-ethylenedioxythiphoenes) (PEDOT) is attractive for FSCs, due to its easier processability, higher conductivity, and

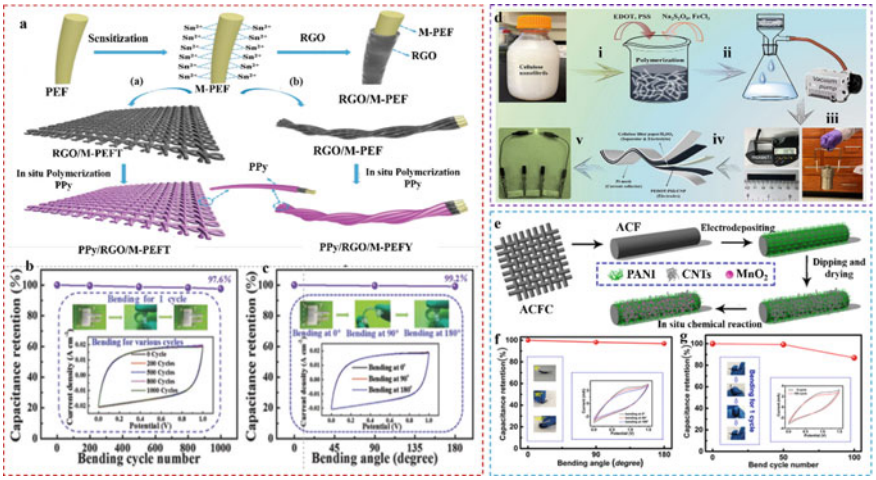

Fig. 2 **a** Schematic illustration of the synthesis route toward (a) a textile electrode (PPy/RGO/M-PEFT) and (b) a yarn electrode (PPy/RGO/M-PEFY). **b**. Capacitance retention and CV curves of the device after repeated bending. **c** Capacitance retention and CV curves of the device at different bending states. Adapted with permission [18], Copyright (2018), Wiley–VCH. **d** (i–ii) schematic illustration of the preparation of a PEDOT:PSS/CNP; (iii) digital photos of the PEDOT:PSS/CNP lifting an 2 kg autoclave; (iv) illustration of a PEDOT:PSS/CNP based FSC device; (v) digital photo of a green-light LED powered by three FSC devices in series. Adapted with permission [19], Copyright (2022), Elsevier. **e** Schematic illustration of the fabrication of an ACPM composite. **f**–**g** Capacitance retention, digital photographs, and CV curves of a solid-state ACPM//ACFC asymmetric SC under different bending angles and after bending for various cycles. Adapted with permission [20], Copyright (2018), American Chemical Society

better stability than other CPs such as PANi and PPy [19]. For example, Du et al. [19] developed a facile strategy to fabricate mechanically strong and conductive PEDOT: poly(styrenesulfonate) (PSS) bulk films (Fig. 2d). By using CNFs as building blocks to reinforce the mechanical strength, PEDOT:PSS/CNF suspension was firstly prepared via a simple in-situ polymerization process. Afterwards, a flexible and conductive PEDOT:PSS/CNF nanopaper (PEDOT:PSS/CNP) was obtained through vacuum filtration and dimethyl sulfoxide (DMSO) post-treatment (inset i-ii in Fig. 2d). The as-prepared PEDOT:PSS/CNP exhibited outstanding flexibility, electrical conductivity, and tensile strength and can lift up a heavy autoclave (inset iii in Fig. 2d). With a 1 M H_2SO_4 electrolyte, the PEDOT:PSS/CNP-based symmetric FSC (inset iv in Fig. 2d) delivered a capacitance of as high as 854.4 mF cm^{-2} (~122.1 F cm^{-3}) and realized a high energy density of 30.86 μWh cm^{-2} and power density of 28.27 mW cm^{-2}. It presented a high capacitance retention of 95.8% after being charged/discharged for 10,000 cycles and maintained its original capacitance even under severe deformations.

Moreover, another pseudocapacitive material can be introduced into the carbon-CP binary system as elaborated above, resulting in multi-component pseudocapacitive material-carbon nanomaterial composites with further enhanced properties [17,

20, 21]. For instance, Wang et al. [20] reported a layer-by-layer method to develop 3D activated carbon fiber cloth/CNT/PANi/MnO_2 (ACFC/CNT/PANi/MnO_2) (denoted as ACPM) composite textile electrodes. Specifically, PANi was firstly deposited on ACFC via an electropolymerization process, followed by the deposition of CNT and MnO_2 through a dipping-drying procedure and an in-situ chemical reaction, respectively (Fig. 2e). In the resultant multi-component composite electrode, the ACFC/CNT hybrid framework served as a porous and conductive 3D network to facilitate the transport of electrons and electrolyte ions, while PANi and MnO_2 synergistically ensured a high capacitance. As a consequence, the ACPM electrode thus prepared realized an ultra-high capacitance up to 4615 mF cm^{-2}. Coupling the ACPM electrode (as anode) with an ACFC cathode and a PVA/H_2SO_4 gel electrolyte, the as-assembled ACPM//ACFC asymmetric FSC presented excellent electrochemical and mechanical performances, delivering an energy and power densities of 413 μWh cm^{-2} and 16,120 μW cm^{-2}, respectively, and retaining its capacitance under different bending conditions (Fig. 2f, g). This work demonstrates the significance of incorporating multiple pseudocapacitive materials with carbon nanomaterials to fabricate composite electrodes with further enhanced properties for FSCs.

2.3 Mxenes and Their Composites for FSCs

With respect to MOs and CPs, MXs, *i.e.*, the 2D transition metal carbides and nitrides, are a relatively new member in the pseudocapacitive materials community. MXs have been intensively investigated for electrochemical energy storage due to their remarkable physical and chemical characteristics, including unique 2D layered structure, good processability, metallic conductivity, large SSA, excellent mechanical strength, hydrophilic nature, and ability to accommodate intercalants [9, 22]. These superior properties of MXs, along with their high theoretical capacity of 615 C g^{-1} [23], make them especially suitable for FSCs.

However, MXs may suffer from a undesirable capacitance because of their restacking of 2D nanosheets caused by the strong interplanar van der Waals interactions (leading to reduced ion-accessible SSA and blocked electrolyte ion diffusion) and an inferior rate capability because of their anisotropic behavior (leading to poor interlayer and interparticle conductivity) [24–26]. In order to address these shortcomings, MXs have been composited with carbon nanomaterials and/or other pseudocapacitive materials (*e.g.*, MOs or CPs), resulting in various composites, such as carbon-MX [24, 25, 27–29], MX/CP [30], and carbon-MX/MO [26]. In the resultant composites, carbon nanomaterials, MOs, and CPs can not only serve as special spacers to mitigate the restacking of MX nanosheets but also further boost the overall electrochemical and mechanical properties of the composites (owing to the synergistic effects from all constituents of these composites) [26, 31].

In the carbon-MX system, for example, Chen et al. [29] utilized vacuum filtration to incorporate CNF, porous carbon (PC), and $Ti_3C_2T_X$ to fabricate a free-standing $Ti_3C_2T_X$/CNF/PC composite electrode, in which CNF and PC formed a flexible

scaffold (Fig. 3a). In addition to constructing the flexible scaffold, CNF and PC can also serve as spacers to suppress the self-restacking of the $Ti_3C_2T_X$ nanosheets, thereby increasing the interlayer distance and creating open gaps for facilitating ion transport. Synergistically, owing to the porous structure of PC, abundant porosity and good mechanical properties of CNF, excellent conductivity of $Ti_3C_2T_X$, and the well-established 3D interconnected hierarchical structure of the composite, the $Ti_3C_2T_X$/CNF/PC electrode possessed a high SSA of 574.5 $m^2\ g^{-1}$ and a high conductivity up to 83.1 S cm^{-1}. Coupling this composite electrode with a PVA/KOH gel electrolyte, the resultant symmetrical FSC displayed a high capacitance of 143 mF cm^{-2}, an excellent rate capability (a capacitance retention of 50.9% at 10 mA cm^{-2}), a high energy and power densities of 2.4 uWh cm^{-2} and 2000 uW cm^{-2}, respectively, and especially superior mechanical deformabilities under various bending angles. These results highlight the significance of compositing MXs with multiple carbons (including carbon nanomaterials) in constructing a 3D conductive scaffold to enhance both the electrochemical and mechanical properties for the resultant carbon-MX composite electrodes.

Into the carbon-MX system as discussed above, moreover, the introduction of another pseudocapacitive material has been demonstrated to be efficient to further enhance the properties of the resultant multi-component composite electrodes. For example, Huang et al. [26] developed a vacuum-filtration assisted layer-by-layer strategy to synthesize a carbon-MX/MO-based multi-component composite for FSCs. Specifically, a CNT@MnO_2 composite was firstly prepared via a hydrothermal process, followed by embedding the as-synthesized CNT@MnO_2 into the MX

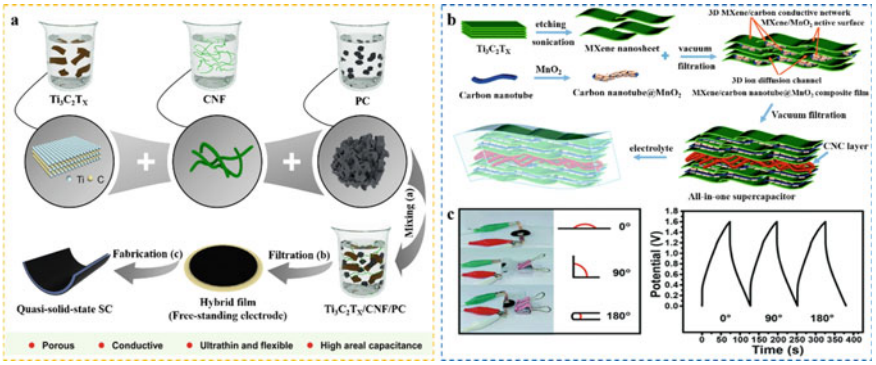

Fig. 3 **a** Schematic illustration of the preparation of a $Ti_3C_2T_X$/CNF/PC hybrid film and a quasi-solid-state SC: (a) mixing of a dispersion containing $Ti_3C_2T_X$, CNF, and PC; (b) vacuum assisted filtration of the dispersion into a $Ti_3C_2T_X$/CNF/PC hybrid film; (c) fabrication of a SC using two hybrid films as free-standing electrodes with a PVA/KOH gel electrolyte. Adapted with permission [29], Copyright (2020), Elsevier. **b** Schematic illustration of the preparation of a MXene/CNT@MnO_2 film and its corresponding all-in-one FSC device. **c** Digital photographs of the FSC under different bending conditions and its corresponding galvanostatic charge/discharge (GCD) curves at 0.5 A g^{-1}. Adapted with permission [26], Copyright (2021), The Royal Society of Chemistry

nanosheet interlayers to obtain the MX/CNT@MnO_2 composite film electrode (Fig. 3b). In this electrode, while the CNT@MnO_2 composites can suppress the restacking of MX nanosheets, the MX nanosheets and CNTs can form a 3D conductive network for MnO_2 loading, jointly facilitating the electron transport and electrolyte ion diffusion for the entire system. As a result of these unique features, the MX/CNT@MnO_2 composite electrode showed a high capacitance of 221 F g^{-1}. Incorporating this composite electrode with a PVA/Na_2SO_4 gel electrolyte, the resultant all-in-one FSC exhibited a high energy and power densities of 24.5 mWh cm^{-3} and 2.5 W cm^{-3}, respectively, as well as a good cycling stability (no apparent capacitance decay after 1800 cycles) and bendability (negligible change in capacitive behavior upon mechanical bending) (Fig. 3c). These promising results spotlight the excellence of combining multiple pseudocapacitive materials with carbon nanomaterials to fabricate superior multi-component composites for high-performance FSCs.

As discussed above, due to the shortcomings of their direct use, pseudocapacitive materials are usually processed into composites to fulfill their FSC applications. Specifically, pseudocapacitive materials can be incorporated each other or combined with carbon nanomaterials to fabricate composites with superior electrochemical and mechanical properties for FSCs. Therefore, with appropriate electrode and device design, these composites can be fabricated into FSCs in varied configurations to satisfy the application requirements for various wearable and flexible electronic devices, to be discussed as follows.

3 Device Configurations of Pseudocapacitive Material-Incorporated FSCs

Apart from the electrode properties, the device design is also essential in determining the performances of FSCs [32]. Pseudocapacitive material-incorporated FSCs have been fabricated in 1D fiber-shaped, 2D film-shaped, and 3D structural configurations to meet the application demands for varied mechanical deformation conditions [32, 33].

3.1 One-Dimensional Fiber-Shaped FSCs

1D FSCs are characterized by a fiber-shaped (or wire-like, cable-type) configuration possessing the advantages of lightweight and good stretchability and knittability [32, 33]. 1D fiber-shaped FSCs have been fabricated in three configurations, *i.e.*, parallel, twisted, and coaxial (or core–shell) [4, 32], with various pseudocapacitive materials [25, 34–41].

A parallel 1D fiber-shaped FSC consists of two fiber electrodes in parallel that are separated by an electrolyte. For instance, Li et al. [35] designed a prestraining-then-buckling method to develop a stretchable fiber-shaped FSC composed of two MnO_2/oxidized CNT fiber electrodes and a LiCl-PVA gel electrolyte on a poly(dimethylsiloxane) (PDMS) film in a continuously buckled pattern (Fig. 4a). The FSC thus fabricated displayed a remarkable capacitance of 409.4 F cm^{-3}, a superior energy and power densities of 14.2 mWh cm^{-3} and 6250 mW cm^{-3}, respectively, and an excellent cycling stability (98% of capacitance retention after 5000 cycles). Moreover, it showed negligible change in electrochemical properties under various stretching and folding conditions (Fig. 4b).

In a parallel 1D fiber-shaped FSC, the electric field formed in the radial direction (across the diameters) of its two parallel electrodes is not uniform, limiting its electrochemical performances [4]. This drawback can be addressed by arranging the two fiber electrodes in a more efficient configuration, such as with a twisted or coaxial structure.

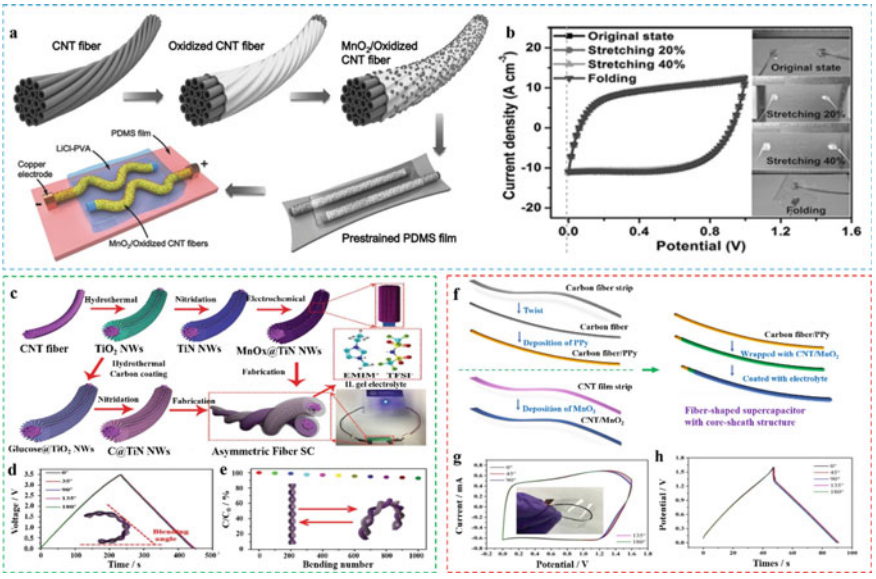

Fig. 4 **a** Schematic illustration of the fabrication process of a stretchable FSC. **b** CV curves of the FSC obtained at a scan rate of 50 mV s^{-1} under stretching and folding, respectively. Adapted with permission [35], Copyright (2017), Wiley–VCH. **c** Schematic illustration of the fabrication processes of an all-solid-state AFSC with an ionic liquid incorporated gel-polymer electrolyte. **d** GCD curves of the AFSC measured at 0.5 A cm^{-3} under different bending angles. **e** Normalized capacitance of the AFSC after bending at 90° for 1000 cycles. Adapted with permission [41], Copyright (2019), Wiley–VCH. **f** Schematic demonstration of a FSS with a core-sheath structure. **g–h** CV and GCD curves of the FSS under different bending angles. Adapted with permission [39], Copyright (2021), American Chemical Society

Constructed by twisting two fiber electrodes together along with an electrolyte in between, a twisted 1D fiber-shaped FSC can form a uniform electric field between its two electrodes. With this design, Pan et al. [41] twisted a MnOx@Titanium Nitride nanowires/CNT (MnOx@TiN NWs@CNT) fiber cathode and a carbon@TiN NWs/CNT (C@TiN NWs@CNT) fiber anode with an ionic liquid (IL) gel polymer electrolyte to assemble an asymmetric fiber-shaped SC (AFSC) (Fig. 4c). The resultant AFSC achieved a high working voltage up to 3.5 V and thus an ultrahigh energy density of 61.2 mWh cm^{-3}, comparable to those of commercially available planar lead-acid batteries (50 ~ 90 mWh cm^{-3}), and a high-power density of 10.1 W cm^{-3}. Furthermore, the well-maintained shape of the GCD curves under different bending angles (Fig. 4d) and the high capacitance retention of 92.7% after 1000 bending cycles (Fig. 4e) of this AFSC strongly indicate its exceptional flexibility.

The two fiber electrodes of a coaxial (or core–shell) 1D fiber-shaped FSC are well-arranged in a coaxial configuration, *i.e.*, an external electrode wrapping around an internal electrode with an electrolyte in between, making the electric field between the two electrodes uniform in both the axial and radial directions, maximizing the effective area for the electrodes, and lowering the internal resistance for the device [32]. This configuration is especially useful for fabricating stretchable FSCs. For example, Xu et al. [39] fabricated a fiber-shaped SC (FSS) by wrapping a MnO_2 deposited CNT film (MnO_2@CNT) electrode (as cathode) on a PPy deposited carbon fiber (PPy@CF) electrode (as anode) (Fig. 4f). The as-assembled FSS delivered a high capacitance of 66.27 mF cm^{-2} at 5 mV s^{-1} with a good rate performance retaining 67% of initial capacitance at 100 mV s^{-1}. Meanwhile, it displayed a high energy and power densities of 23.56 uWh cm^{-2} and 3.3 mW cm^{-2}, respectively, and exhibited a remarkable flexibility with a negligible change in capacitance under different bending angles (Fig. 4g, h) and a high capacitance retention of 90% after 200 bending cycles.

The active material loading of a 1D fiber-shaped FSC is relatively low (because of its use of small-sized fiber electrodes) and its internal resistance would increase upon the increase in length of its fiber electrodes [5]. Use of film electrodes would be capable of addressing these issues, resulting in two-dimensional film-shaped FSCs, to be discussed below.

3.2 Two-Dimensional Film-Shaped FSCs

2D FSCs have a film-shaped (or paper-like) appearance, in which two thin-film flexible electrodes sandwich an electrolyte [32]. In recent years, the substantial achievements in the research of pseudocapacitive materials have accelerated the development of 2D film-shaped FSCs with either a symmetric or asymmetric configuration [28, 42, 43].

In the symmetric configuration, for example, Li et al. [43] reported a bendable FSC by sandwiching two identical MX (Ti_3AlC_2)/α-Fe_2O_3-C-MoS_2-PEDOT:PSS/MX (Ti_3AlC_2) (M/FMP/M) film electrodes with a PVA/H_2SO_4 gel electrolyte in a

CC framework (Fig. 5a, b). In the electrode design, while PEDOT:PSS can provide active sites and lower resistance for α-Fe_2O_3 and C-MoS_2 to efficiently utilize their capacitances, the resultant FMP composite can suppress the restacking of the Ti_3AlC_2 sheets. At the device level, the CC framework can provide flexibility for the FSC. As a result, the as-assembled symmetric FSC delivered a high energy and power densities of 371 uWh cm^{-2} and 50 mW cm^{-2}, respectively, and showed a superior bendability retaining its capacitance up to 98.6% under a bending angle of 180° (Fig. 5c).

Constructed from two different electrodes, an asymmetric (hybrid) FSC has an enlarged operating voltage and hence an enhanced energy output. In an example by Patil et al. [44], a CC supported porous $Co_3(PO_4)_2$ transparent stacked micropetals (TSMs) decorated with $Co_2Mo_3O_8$ nanosheets ($Co_3(PO_4)_2$@$Co_2Mo_3O_8$) composite and a CC supported 2D CNT/MX (CNT-$Ti_3C_2T_X$) composite were employed as the positive electrode and negative electrode, respectively, to sandwich a PVA/KOH gel electrolyte (Fig. 5d). The resultant flexible hybrid solid-state SC (FHSC) realized an enlarged working voltage up to 1.5 V and thus delivered an exceptional energy and power as high as 2.47 mWh cm^{-3} and 225 mW cm^{-3}, respectively, along with

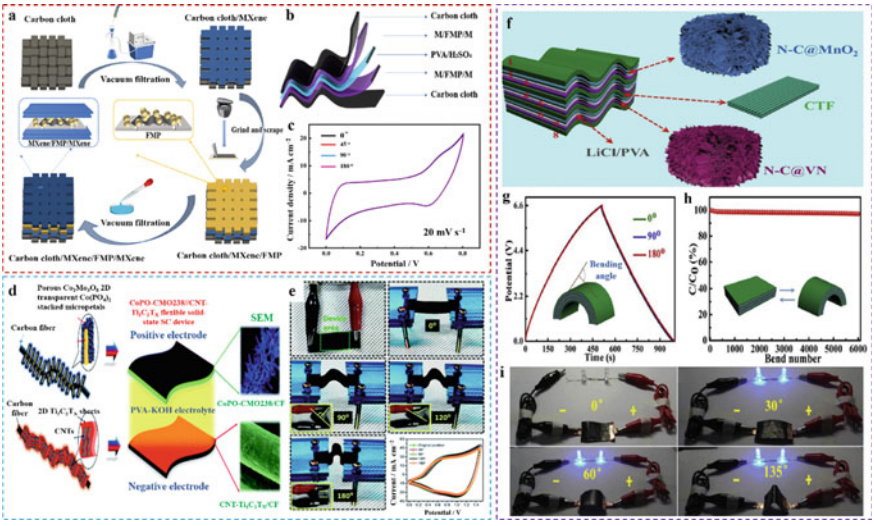

Fig. 5 **a** Illustration of the preparation of a M/FMP/M film on a carbon cloth. **b** Structure of a device assembled from two M/FMP/M-20% film electrodes. **c** Capacitance retention of the device tested at 20 mV s^{-1} in different bending states. Adapted with permission [43], Copyright (2022), American Chemical Society. **d** Schematic representation of the designing of a FHSC device by employing CoPO-CMO238 as the positive electrode and CNT–$Ti_3C_2T_X$/CC as the negative electrode with a PVA–KOH gel electrolyte. **e** Photos of the device in its initial position and at various bending angles of 90°, 120°, and 180°, and the corresponding CV curves at 100 mV s^{-1}. Adapted with permission [44], Copyright (2021), The Royal Society of Chemistry. **f** Schematic of an internal asymmetric tandem all-in-one FSC. **g** GCD curves of the FSC measured at 4 mA cm^{-2} under different bending angles. **h** Normalized capacitance of the FSC upon cycling with a bending angle of 90° for 6000 cycles. **i** Two blue-light LEDs powered by the FSC (bending angle from 0 to 135°). Adapted with permission [45], Copyright (2020), Elsevier

an outstanding cycling stability retaining its capacitance at 93.2% after charging/discharging for 5000 cycles. Under various bending angles (Fig. 5e), this FHSC was able to maintain its initial capacitance with negligible decay.

Moreover, by integrating multiple asymmetric cells into a tandem structure, the working voltage and hence energy density of the resultant FSCs can be further boosted. In this regard, Zhou et al. [45] built an asymmetric FSC by incorporating a CNT film supported MnO_2@N-doped carbon skeleton (CNTF/MnO_2@N–C) cathode, a CNTF/N–C@vanadium nitrogen (CTF/N–C@VN) anode, and a LiCl/PVA gel electrolyte in a tandem configuration (Fig. 5f). This tandem design enabled the as-assembled FSC to have a maximum working voltage up to 6.6 V (versus that of 2.2 V for a single cell), thereby a high energy and power of 118.2 mWh cm^{-3} and 3821.9 mW cm^{-3}, respectively. Furthermore, it retained 95.1% of its initial capacitance after charging/discharging for 15,000 cycles. More importantly, this FSC exhibited impressive mechanical deformabilities, maintaining its GCD curves almost unchanged upon the increase of bending angle from 0° to 180° (Fig. 5g), presenting a high capacitance retention of 97.2% after 6000 bending cycles (Fig. 5h), and holding a stable energy output under various bending angles (Fig. 5i). The above results clearly demonstrate the effectiveness of the asymmetric configuration and the tandem structure design in boosting the energy output for 2D film-shaped FSCs.

As can be seen, fruitful progress has been achieved for pseudocapacitive material-incorporated 1D fiber- and 2D film-shaped FSCs. For practical applications, moreover, the active material loading of these devices needs to be efficiently increased (without a decay in specific capacitance [46]) and their deformabilities need to be significantly improved. These have, in fact, triggered the efforts on the research of higher-dimensional, *i.e.*, 3D structural, FSCs [33].

3.3 Three-Dimensional Structural FSCs

A 3D structural FSC is constructed in a 3D configuration by integrating low-dimensional (1D or 2D) FSCs as the building units. Compared to their low-dimensional counterparts, 3D structural FSCs incorporate more active materials into the device and can omni-directionally accommodate mechanical deformations [32], more suitable for practical applications.

In this context, for example, Lv et al. [47] utilized a 2D film-shaped SC as the building unit to develop a 3D stretchable FSC in a configuration mimicking a honeycomb lantern. With a honeycomb lantern structure (Fig. 6a), the proposed 3D stretchable FSC was constructed by incorporating a symmetric capacitor composed of a PPy/black-phosphorous oxide electrodeposited on CNT film (PPy/BPO/CNT) composite electrode and a PVA/H_2SO_4 gel electrolyte as the building unit. Consequently, the unique expandable architecture of the honeycomb lantern enabled the FSC with device-thickness-independent ion-transport path and stretchability that allowed the fabrication of FSCs into customizable device thickness for enhancing the energy output and adjusting the integrability for fitting with various wearable

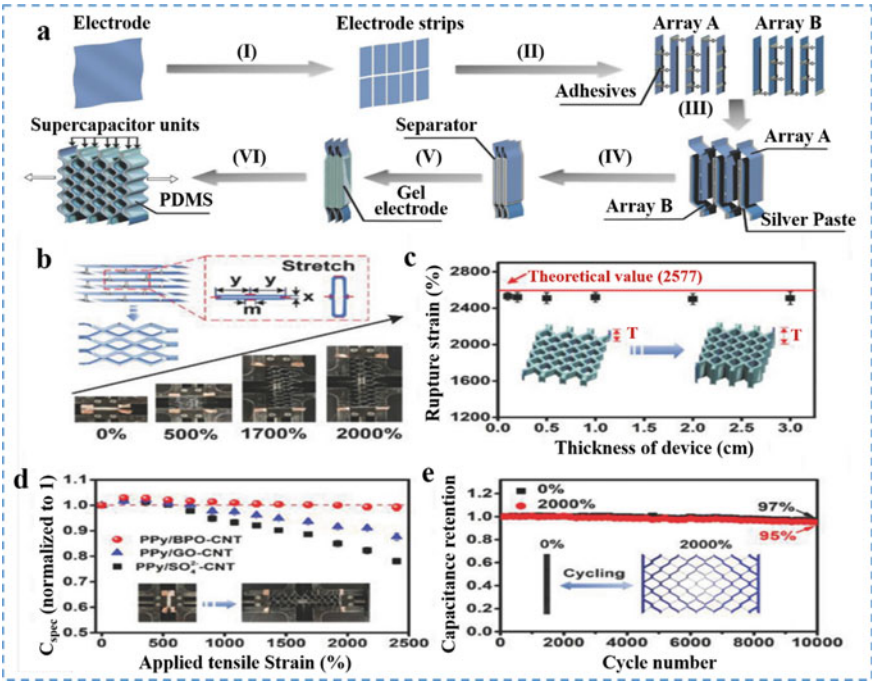

Fig. 6 **a** Schematic representation showing the fabrication procedure of a 3D rectangular-shaped stretchable FSC. **b** Digital images of the FSC under varied strains. Inset is a scheme presenting the expandable honeycomb structure and hexagonal unit cells of the FSC before and after stretching. **c** Effect of device thickness on the rupture strain of the FSC. **d** Normalized capacitances of FSCs from different PPy-based electrodes tested at 7.8 mA cm^{-2} with varied strains. **e** Capacitance retention of the FSC from PPy/BPO/CNT electrodes tested at 7.8 mA cm^{-2} under stretch cycling with a tensile strain of 2000%. Adapted with permission [47], Copyright (2018), Wiley–VCH

devices. Remarkably, a 1.0 cm-thick FSC thus fabricated displayed a boosted capacitance of 7.34 F cm^{-2}, 60 times that of its original 2D SC unit (120 mF cm^{-2}). Mechanically, this 3D FSC could be stretched up to 2400% (Fig. 6b) and exhibited a device-thickness/shape-independent stretchability (Fig. 6c). It maintained its electrochemical performance unchanged under 2400% stretching (Fig. 6d) and retained its capacitance at 95% even upon stretch-release cycling under 2000% strain for 10,000 cycles (Fig. 6e). These results clearly demonstrate the practical application superiorities of 3D structural FSCs over their low-dimensional counterparts.

To this end, remarkable progress has been achieved in the research of pseudocapacitive materials and the development of their FSCs. This has facilitated the practical application exploration of FSCs for flexible and wearable electronics as briefly elaborated as follows.

4 Practical Applications of Pseudocapacitive Material Incorporated FSCs

Pseudocapacitive material incorporated FSCs have shown great potentials for practical applications because of their excellent safety, electrochemical performances, and mechanical deformabilities [1, 48]. While 1D FSCs are promising for wearable applications, 2D and 3D FSCs have better suitability for large-scale flexible electronics, and 3D FSCs are especially useful for multi-direction-deformation applications. Pseudocapacitive material-incorporated FSCs have been incorporated into many application concepts and even prototypes, such as flexible and transparent electronics [49], healthcare monitoring systems [16, 42, 50], skin-attachable wearables and sensors [51], wearable digital electronics [38], and self-powered wearable devices [52]. In some specific scenarios, furthermore, the special functionalities, such as transparency or self-power, are needed, resulting in multifunctional FSCs.

For the emerging electronics of flexible and transparent devices [53], for instance, many attempts have been made to fabricate FSCs that are flexible and also transparent. In this regard, a multifunctional wearable electrochromic patch device powered by an all-transparent stretchable electrochromic SC (all-TSES) was developed (Fig. 7a) [54]. Attributed to the pseudocapacitive/coloration dual characteristics of the PEDOT:PSS/WO_3 electrodes, this patch device delivered a maximum energy and power densities of 52.6 Wh kg^{-1} and 19.1 kW kg^{-1}, respectively, and showed reversible coloration at –1.5 V and bleaching at –0.1 V (Fig. 7b, c). It demonstrated stable electrochromic and electrochemical properties by holding 95.0% and 97.6% of its normalized transmittance change and normalized specific capacitance, respectively, even after being exposed to the ambient conditions for 2 weeks (Fig. 7d). Mechanically, it was stable upon stretch-bend cycling and exhibited a high capacitance retention of 98.6% even under a tensile strain up to 20% (Fig. 7e, f). These results highlight the importance of fabricating FSCs with unique features such as transparency in providing power for emerging flexible electronics such as skin-attachable wearables and bioelectronics.

For self-powered wearable devices, on the other hand, a FSC is used to store the energy harvested from sunlight, body motion or even human biofluids rather than provided by conventional external power supplies. For example, Lv et al. [52] developed a screen-printed textile-based hybrid SC-biofuel cell (SC-BFC) system for on-body testing (Fig. 7g–m). In this self-powered system, an epidermal BFC (Fig. 7j) was used to harvest the biochemical energy generated from the wearer's sweat and a CNT/MnO_2/PEDOT:PSS composite based FSC (Fig. 7g, i) to store the energy thus harvested. Owing to the remarkable electrochemical stability and high energy density (17.5 mWh cm^{-2}) of the FSC, this self-powered hybrid system can deliver a stable energy output over long charging periods, boost the voltage output of the BFC, and exhibit excellent stability under a variety of mechanical deformations (Fig. 7k–m). These results clearly reveal the great potential of such unique FSC-based hybrid power systems as next-generation self-powered flexible power supplies for wearable electronics and smart textiles.

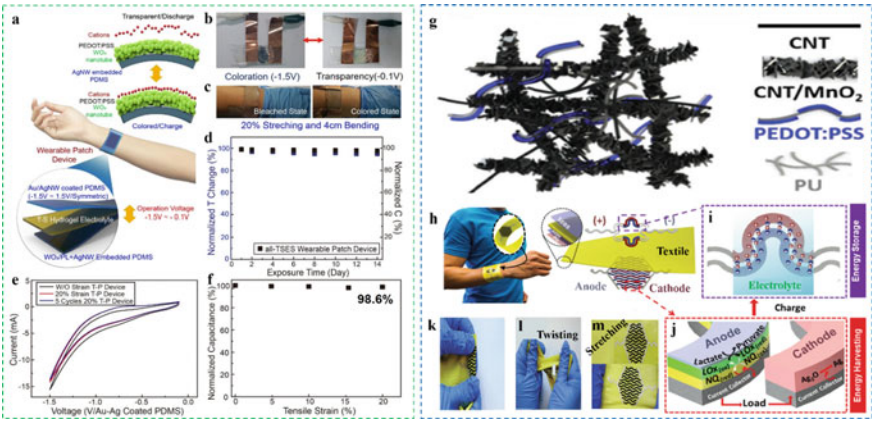

Fig. 7 **a** Schematic illustration of an all-TSES wearable patch device. **b** Real images of the bleached and colored states of the patch device. **c** Demonstration of the patch device. **d** Normalized transmittance change and capacitance change of the patch device after exposure in ambient conditions for 14 days. **e** CV results of the patch device under different stretching conditions. **f** Normalized capacitance change of the patch device under a tensile strain to 20%. Adapted with permission [54], Copyright (2019), American Chemical Society. **g** Illustration of the composition of a MnO_2–CNT/CNT/PEDOT:PSS composite. **h**–**j** Schematic illustration of a self-powered textile composed of a BFC and a FSC. The energy generated by the BFC from the lactate in sweat charges the FSC. **k**–**m** Photographs of the textile under different deformations of bending, twisting, and 20% stretching, respectively. Adapted with permission [52], Copyright (2018), The Royal Society of Chemistry

5 Summary and Outlooks

The research and development of FSCs as a group of flexible power sources for flexible and wearable electronic devices have gained significant progresses. In order for FSCs to be practically useful, they should have both superior electrochemical performances and excellent mechanical deformabilities. This has triggered substantial research on the electrode materials of FSCs and the development of their device configurations.

Largely owing to their high capacitances, pseudocapacitive materials (including MOs, CPs, and MXs) are promising electrode materials for FSCs. While the direct processing of pseudocapacitive materials into electrodes possesses shortcomings, the incorporation of varied pseudocapacitive materials together and the compositing of pseudocapacitive materials with carbon nanomaterials are efficient to fabricate flexible composite electrodes with both well-defined electrochemical and mechanical properties for FSCs. This also indicates a future direction to continue the research on synthesis method, composition optimization, and morphology design of such pseudocapacitive material-based composite electrodes for practically useful FSCs.

Pseudocapacitive material-incorporated FSCs have been realized in a range of configurations from 1D fiber-shaped to 2D film-shaped and 3D structural, providing them with tremendous opportunities for varied mechanical deformation

scenarios. Specifically, they have been integrated into prototype products with 1D FSCs promising for wearable, 2D and 3D FSCs for large-scale flexible, and 3D FSCs for multi-direction-deformation applications. Furthermore, with the incorporation of special features (such as transparency or self-power), the FSCs become multifunctional, significantly enhancing their practical application capabilities.

Therefore, with the remarkable progresses accomplished in the past and the extensive research in the future on pseudocapacitive materials and their FSCs, practically useful flexible power sources with both superior electrochemical performances and excellent mechanical deformabilities would be anticipated into the market for flexible and wearable electronic devices.

Acknowledgements This work was supported by The Special Significant Science and Technology Program of Yunnan Province (grant number: 2016HE001-2016HE002).

References

1. C. Wang, K. Xia, H. Wang, X. Liang, Z. Yin, Y. Zhang, Advanced carbon for flexible and wearable electronics. Adv. Mater. **31**, e1801072 (2019)
2. Y. Liu, M. Pharr, G.A. Salvatore, Lab-on-skin: a review of flexible and stretchable electronics for wearable health monitoring. ACS Nano **11**, 9614–9635 (2017)
3. L. Lyu, W. Hooch Antink, Y. S. Kim, C. W. Kim, T. Hyeon, Y. Piao, Recent development of flexible and stretchable supercapacitors using transition metal compounds as electrode materials. Small **17**, e2101974 (2021)
4. Y. Zhou, C.H. Wang, W. Lu, L. Dai, Recent advances in fiber-shaped supercapacitors and lithium-ion batteries. Adv. Mater. **32**, e1902779 (2020)
5. P. Xie, W. Yuan, X. Liu, Y. Peng, Y. Yin, Y. Li, Z. Wu, Advanced carbon nanomaterials for state-of-the-art flexible supercapacitors. Ene. Stor. Mater **36**, 56–76 (2021)
6. G. Shao, R. Yu, N. Chen, M. Ye, X.Y. Liu, Stretchable supercapacitors: From materials and structures to devices. Small Methods **5**, 2000853 (2021)
7. Y. Han, L. Dai, Conducting polymers for flexible supercapacitors. Macromol. Chem. Phys. **220**, 1800355 (2019)
8. S. A. Delbari, L. S. Ghadimi, R. Hadi, S. Farhoudian, M. Nedaei, A. Babapoor, A. Sabahi Namini, Q. V. Le, M. Shokouhimehr, M. Shahedi Asl, M. Mohammadi, Transition metal oxide-based electrode materials for flexible supercapacitors: a review. J. Alloys Compd. **857**, 158281 (2021)
9. S. Nam, J.-N. Kim, S. Oh, J. Kim, C.W. Ahn, I.-K. Oh, $Ti_3C_2T_x$ MXene for wearable energy devices: supercapacitors and triboelectric nanogenerators. APL Mater. **8**, 110701 (2020)
10. T. An, W. Cheng, Recent progress in stretchable supercapacitors. J. Mater. Chem. A **6**, 15478–15494 (2018)
11. S. Sahoo, R. Kumar, E. Joanni, R.K. Singh, J.-J. Shim, Advances in pseudocapacitive and battery-like electrode materials for high performance supercapacitors. J. Mater. Chem. A **10**, 13190–13240 (2022)
12. Y. Shao, M.F. El-Kady, J. Sun, Y. Li, Q. Zhang, M. Zhu, H. Wang, B. Dunn, R.B. Kaner, Design and mechanisms of asymmetric supercapacitors. Chem. Rev. **118**, 9233–9280 (2018)
13. Y. Wang, Y. Ding, X. Guo, G. Yu, Conductive polymers for stretchable supercapacitors. Nano Res. **12**, 1978–1987 (2019)
14. C. Zhao, X. Jia, K. Shu, C. Yu, G.G. Wallace, C. Wang, Conducting polymer composites for unconventional solid-state supercapacitors. J Mater Chem A **8**, 4677–4699 (2020)

15. L. Huang, D. Santiago, P. Loyselle, L. Dai, Graphene-based nanomaterials for flexible and wearable supercapacitors. Small **14**, e1800879 (2018)
16. Z. Lv, Y. Luo, Y. Tang, J. Wei, Z. Zhu, X. Zhou, W. Li, Y. Zeng, W. Zhang, Y. Zhang, D. Qi, S. Pan, X.J. Loh, X. Chen, Editable supercapacitors with customizable stretchability based on mechanically strengthened ultralong MnO_2 nanowire composite. Adv. Mater. **30**, 1704531 (2018)
17. Q. Zhuang, W. Li, Z. Zhu, H. Yu, W. Chen, J. Yang, M. Fu, Facile growth of hierarchical SnO_2@PPy composites on carbon cloth as all-solid-state flexible supercapacitors. J. Alloy. Compd. **906**, 164275 (2022)
18. X. Li, R. Liu, C. Xu, Y. Bai, X. Zhou, Y. Wang, G. Yuan, High-performance Polypyrrole/Graphene/$SnCl_2$ modified polyester textile electrodes and yarn electrodes for wearable energy storage. Adv. Funct. Mater. **28**, 1800064 (2018)
19. H. Du, M. Zhang, K. Liu, M. Parit, Z. Jiang, X. Zhang, B. Li, C. Si, Conductive PEDOT:PSS/cellulose nanofibril paper electrodes for flexible supercapacitors with superior areal capacitance and cycling stability. Chem. Eng. J. **428**, 131994 (2022)
20. J. Wang, L. Dong, C. Xu, D. Ren, X. Ma, F. Kang, Polymorphous supercapacitors constructed from flexible three-dimensional carbon network/polyaniline/MnO_2 composite textiles. ACS Appl. Mater. Inter. **10**, 10851–10859 (2018)
21. H.U. Lee, C. Park, J.-H. Jin, S.W. Kim, A stretchable vertically stacked microsupercapacitor with kirigami-bridged island structure: MnO_2/graphene/Poly(3,4-ethylenedioxythiophene) nanocomposite electrode through pen lithography. J. Power. Sources **453**, 227898 (2020)
22. C. Zhang, Y. Ma, X. Zhang, S. Abdolhosseinzadeh, H. Sheng, W. Lan, A. Pakdel, J. Heier, F. Nüesch, Two dimensional transition metal carbides and nitrides (MXenes): synthesis properties, and electrochemical energy storage applications. Energ. Environ. Mater **3**, 29–55 (2020)
23. M.R. Lukatskaya, S. Kota, Z. Lin, M.-Q. Zhao, N. Shpigel, M.D. Levi, J. Halim, P.-L. Taberna, M.W. Barsoum, P. Simon, Y. Gogotsi, Ultra-high-rate pseudocapacitive energy storage in two-dimensional transition metal carbides. Nat. Energy **2**, 17105 (2017)
24. H. Li, R. Chen, M. Ali, H. Lee, M.J. Ko, In Situ grown MWCNTs/MXenes nanocomposites on carbon cloth for high-performance flexible supercapacitors. Adv. Funct. Mater. **30**, 2002739 (2020)
25. C. Yu, Y. Gong, R. Chen, M. Zhang, J. Zhou, J. An, F. Lv, S. Guo, G. Sun, A solid-state fibriform supercapacitor boosted by host-guest hybridization between the carbon nanotube scaffold and MXene nanosheets. Small, e1801203 (2018)
26. Y.-L. Huang, S.-W. Bian, Vacuum-filtration assisted layer-by-layer strategy to design MXene/carbon nanotube@MnO_2 all-in-one supercapacitors. J. Mater. Chem. A. **9**, 21347–21356 (2021)
27. A. Salman, S. Padmajan Sasikala, I. H. Kim, J. T. Kim, G. S. Lee, J. G. Kim, S. O. Kim, Tungsten nitride-coated graphene fibers for high-performance wearable supercapacitors. Nanoscale, **12,** 20239–20249 (2020)
28. Y. Zhou, K. Maleski, B. Anasori, J.O. Thostenson, Y. Pang, Y. Feng, K. Zeng, C.B. Parker, S. Zauscher, Y. Gogotsi, J.T. Glass, C. Cao, $Ti_3C_2T_x$ MXene-reduced graphene oxide composite electrodes for stretchable supercapacitors. ACS Nano **14**, 3576–3586 (2020)
29. W. Chen, D. Zhang, K. Yang, M. Luo, P. Yang, X. Zhou, Mxene ($Ti_3C_2T_x$)/cellulose nanofiber/porous carbon film as free-standing electrode for ultrathin and flexible supercapacitors. Chem. Eng. J. **413**, 127524 (2020)
30. M. Zhu, Y. Huang, Q. Deng, J. Zhou, Z. Pei, Q. Xue, Y. Huang, Z. Wang, H. Li, Q. Huang, C. Zhi, Highly flexible freestanding supercapacitor electrode with enhanced performance obtained by hybridizing Polypyrrole chains with MXene. Adv. Energy Mater. **6**, 1600969 (2016)
31. Q. Zhu, J. Li, P. Simon, B. Xu, Two-dimensional MXenes for electrochemical capacitor applications: progress, challenges and perspectives. Energy Stor. Mater **35**, 630–660 (2021)
32. X. Chen, N.S. Villa, Y. Zhuang, L. Chen, T. Wang, Z. Li, T. Kong, Stretchable supercapacitors as emergent energy storage units for health monitoring bioelectronics. Adv. Energy Mater. **10**, 1902769 (2019)

33. J. Liang, C. Jiang, W. Wu, Toward fiber-, paper-, and foam-based flexible solid-state supercapacitors: electrode materials and device designs. Nanoscale **11**, 7041–7061 (2019)
34. Q. Zhou, X. Chen, F. Su, X. Lyu, M. Miao, Sandwich-structured transition metal oxide/graphene/carbon nanotube composite Yarn electrodes for flexible two-ply yarn supercapacitors. Ind. Eng. Chem. Res. **59**, 5752–5759 (2020)
35. M. Li, M. Zu, J. Yu, H. Cheng, Q. Li, Stretchable fiber supercapacitors with high volumetric performance based on buckled MnO_2/oxidized carbon nanotube fiber electrodes. Small **13**, 1602994 (2017)
36. S. Wang, N. Liu, J. Su, L. Li, F. Long, Z. Zou, X. Jiang, Y. Gao, Highly stretchable and self-healable supercapacitor with reduced graphene oxide based fiber springs. ACS Nano **11**, 2066–2074 (2017)
37. J. Sun, Y. Huang, C. Fu, Z. Wang, Y. Huang, M. Zhu, C. Zhi, H. Hu, High-performance stretchable yarn supercapacitor based on PPy@CNTs@urethane elastic fiber core spun yarn. Nano Energy **27**, 230–237 (2016)
38. Z. Wang, S. Qin, S. Seyedin, J. Zhang, J. Wang, A. Levitt, N. Li, C. Haines, R. Ovalle-Robles, W. Lei, Y. Gogotsi, R.H. Baughman, J.M. Razal, High-performance Biscrolled MXene/carbon nanotube Yarn supercapacitors. Small **14**, e1802225 (2018)
39. Y. Xu, Y. Yan, W. Lu, S. Yarlagadda, G. Xu, High-performance flexible asymmetric fiber-shaped supercapacitor based on CF/PPy and CNT/MnO_2 composite electrodes. ACS Appl. Energy Mater **4**, 10639–10645 (2021)
40. Z. Pan, J. Yang, L. Li, X. Gao, L. Kang, Y. Zhang, Q. Zhang, Z. Kou, T. Zhang, L. Wei, Y. Yao, J. Wang, All-in-one stretchable coaxial-fiber strain sensor integrated with high-performing supercapacitor. Ene. Stor. Mater **25**, 124–130 (2020)
41. Z. Pan, J. Yang, Q. Zhang, M. Liu, Y. Hu, Z. Kou, N. Liu, X. Yang, X. Ding, H. Chen, J. Li, K. Zhang, Y. Qiu, Q. Li, J. Wang, Y. Zhang, All-solid-state fiber supercapacitors with ultrahigh volumetric energy density and outstanding flexibility. Adv. Energy Mater. **9**, 1802753 (2019)
42. G. Lee, J.W. Kim, H. Park, J.Y. Lee, H. Lee, C. Song, S.W. Jin, K. Keum, C.H. Lee, J.S. Ha, Skin-Like, dynamically stretchable, planar supercapacitors with buckled carbon nanotube/Mn-Mo mixed oxide electrodes and air-stable organic electrolyte. ACS Nano **13**, 855–866 (2019)
43. C. Li, S. Wang, Y. Cui, X. Wang, Z. Yong, D. Liang, Y. Chi, Z. Wang, Sandwich-like MXene/alpha-Fe_2O_3-C-MoS_2-PEDOT:PSS/MXene Film electrodes with ultrahigh area capacitance for flexible supercapacitors. ACS Appl Mater Inter **14**, 9172–9182 (2022)
44. A.M. Patil, N.R. Chodankar, E. Jung, S. Roy, D.P. Dubal, G. Guan, Y.-K. Han, S.C. Jun, 2D-on-2D core-shell $Co_3(PO_4)_2$ stacked micropetals@$Co_2Mo_3O_8$ nanosheets and binder-free 2D CNT-$Ti_3C_2T_X$-MXene electrodes for high-energy solid-state flexible supercapacitors. J Mater Chem A **9**, 26135–26148 (2021)
45. Z. Zhou, Q. Li, L. Yuan, L. Tang, X. Wang, B. He, P. Man, C. Li, L. Xie, W. Lu, L. Wei, Q. Zhang, Y. Yao, Achieving ultrahigh-energy-density in flexible and lightweight all-solid-state internal asymmetric tandem 6.6 V all-in-one supercapacitors. Ener. Stor. Mater, **25**, 893–902 (2020)
46. N. Swain, A. Tripathy, A. Thirumurugan, B. Saravanakumar, L. Schmidt-Mende, A. Ramadoss, A brief review on stretchable, compressible, and deformable supercapacitor for smart devices. Chem. Eng. J. **446**, 136876 (2022)
47. Z. Lv, Y. Tang, Z. Zhu, J. Wei, W. Li, H. Xia, Y. Jiang, Z. Liu, Y. Luo, X. Ge, Y. Zhang, R. Wang, W. Zhang, X.J. Loh, X. Chen, Honeycomb-lantern-inspired 3D stretchable supercapacitors with enhanced specific areal capacitance. Adv. Mater. **30**, 1805468 (2018)
48. J. Wen, B. Xu, Y. Gao, M. Li, H. Fu, Wearable technologies enable high-performance textile supercapacitors with flexible, breathable and wearable characteristics for future energy storage. Energy Stor. Mater **37**, 94–122 (2021)
49. J. Yun, H. Lee, C. Song, Y.R. Jeong, J.W. Park, J.H. Lee, D.S. Kim, K. Keum, M.S. Kim, S.W. Jin, Y.H. Lee, J.W. Kim, G. Zi, J.S. Ha, A Fractal-designed stretchable and transparent microsupercapacitor as a Skin-attachable energy storage device. Chem. Eng. J. **387**, 124076 (2020)

50. H. Park, J.W. Kim, S.Y. Hong, G. Lee, H. Lee, C. Song, K. Keum, Y.R. Jeong, S.W. Jin, D.S. Kim, J.S. Ha, Dynamically stretchable supercapacitor for powering an integrated biosensor in an all-in-one textile system. ACS Nano **13**, 10469–10480 (2019)
51. H. Park, J. W. Kim, S. Y. Hong, G. Lee, D. S. Kim, J. H. Oh, S. W. Jin, Y. R. Jeong, S. Y. Oh, J. Y. Yun, J. S. Ha, Microporous polypyrrole-coated graphene foam for high-performance multifunctional sensors and flexible supercapacitors. Adv. Funct. Mater, **28** 1707013 (2018)
52. J. Lv, I. Jeerapan, F. Tehrani, L. Yin, C.A. Silva-Lopez, J.-H. Jang, D. Joshuia, R. Shah, Y. Liang, L. Xie, F. Soto, C. Chen, E. Karshalev, C. Kong, Z. Yang, J. Wang, Sweat-based wearable energy harvesting-storage hybrid textile devices. Energ. Environ. Sci. **11**, 3431–3442 (2018)
53. C. Zhang, V. Nicolosi, Graphene and MXene-based transparent conductive electrodes and supercapacitors. Energy Stor. Mater **16**, 102–125 (2019)
54. T.G. Yun, M. Park, D.H. Kim, D. Kim, J.Y. Cheong, J.G. Bae, S.M. Han, I.D. Kim, All-transparent stretchable electrochromic supercapacitor wearable patch device. ACS Nano **13**, 3141–3150 (2019)

Redox-Active Polymers for Batteries

Aswathy Vijayakumar Kumar, Treesa Karangattuserriyil James, and Suresh Mathew

Abstract Electrochemical energy storage is critical in accelerating the transition to a low-carbon future for grid storage and transportation. While most research on electrochemical energy storage devices has focused on improving performance (energy density and power density), little attention has been paid to designing devices that can be recycled at a low cost with minimal environmental impact. Renewable organic batteries are an excellent option for storing sustainably generated energy and can help to phase out current carbon-based energy production. Over the past 80 years, several strategies have been developed that use organic redox materials as active elements in batteries. Polymers have piqued the interest of numerous research groups due to their (1) fast redox chemistry in comparison to conventional active materials, (2) simple syntheses, and (3) tuneable solubility, all of which are desirable properties for a variety of electronic devices. Notably, the beginning of redox-active polymers is linked to the discovery of conductive polymers by Heeger, Mac Diarmid, and Shirakawa in 1977. RAPs have progressed from an intriguing phenomenon to a family of promising, tailor-made battery materials that have also reached commercialization. Redox-active Polymers (RAPs) are macromolecules with chemical groups that can reversibly modify their electrochemical state by losing (oxidation) or gaining (reduction). The conventional polymerization stages of initiation, propagation, and termination are used in the creation of redox polymers. This chapter focuses on redox-active polymers, their classification, the concept of electron transfer in RAPs, and redox-active polymer-based electrochemical energy storage devices and their application in energy storage devices i.e., batteries.

Keywords Redox-active polymers · Redox-flow battery · Electrochemistry · Electron transfer · Energy storage

A. Vijayakumar Kumar · T. K. James · S. Mathew (✉)
School of Chemical Sciences, Mahatma Gandhi University, Kottayam, Kerala 686560, India
e-mail: sureshmathewmgu@gmail.com

© The Author(s), under exclusive license to Springer Nature Switzerland AG 2024

R. K. Gupta (ed.), *Pseudocapacitors*, Engineering Materials,
https://doi.org/10.1007/978-3-031-45430-1_15

1 Introduction

The global battery market has expanded dramatically over the last decade [1]. Electric vehicles, wearable devices, the Internet of Things (IoT), and smart grids all necessitate more precisely tailored energy storage systems. Nowadays, the dominant technique is based on lithium-ion batteries (LIB) and conveniences with low costs, high voltages, and increasing power densities. The LIBs have become widely established, resulting in the displacement of many other systems, and their discovery was recently honoured with the Nobel Prize in 2019. However, inorganic lithium technology has limitations. Because the batteries are stiff, bending would result in leaks and serious hazards [2]. Furthermore, the frequently required cobalt raw materials are toxic and extracted under unsustainable mining conditions, including the use of child laborers; as a result, global cobalt market prices have risen over the last decade [3]. Larger battery packs also necessitate temperature control systems to keep them in safe conditions; otherwise, serious dangers, such as explosions, can occur. As a result of these drawbacks, inorganic lithium electrodes are unsuitable for small and flexible devices in smart clothing, smart packing, or other IoT devices, as well as resource-intensive applications like battery systems for grid stabilization and on-site storage. Based on organic raw materials, redox polymers represent a promising alternative approach for battery-active materials in these applications. They enable the production of flexible devices that are largely independent of rare metal commodity prices and employ a variety of scaffolding options, making additional tailoring much easier.

The concept of redox-active chains originates from early studies using ion exchange polymers. Lauth applied the concept of reversibly exchanging charged ions to exchanging electrons in 1944 when he synthesized his poly (resorcinol-trihydroxy benzene-formaldehyde) redox polymers for water deoxygenation. Nonetheless, he was not the first to synthesize electroactive polymers; poly(aniline) can be traced back to 1862 [4]. The second era of redox polymers (Fig. 1) began in 1977 when Heeger, MacDiarmid, and Shirakawa demonstrated the high electric conductivity of oxidized polyacetylene. Overall, the second era was defined by the fact that conjugated polymers, due to their novel redox properties, opened a new dynamic field of research called organic electronics. The concept of an organic radical battery (ORB) was developed in the early twenty-first century by Nakahara and Nishide, bringing the third era of redox polymers (Fig. 1), shows the timeline with the most net worthy inventions and scientific milestones in the field of redox-active polymers [5]. The most promising organic battery materials are polymers with stable radical side groups. Metal ion batteries with Li [6–8], Na [9, 10], K [11], Mg [12], Ca [13], Zn [13], or Al [13] as well as metal-free all-organic batteries and even redox flow batteries (RFBs) use redox-polymers [14, 15].

To achieve simple and effective cathode and anode material extraction, the redox-active materials should ideally function as single-phase electrode materials, avoiding additional separation steps of additives and binders during the recycling process [16]. Furthermore, the materials must be highly soluble in solvents used for recycling,

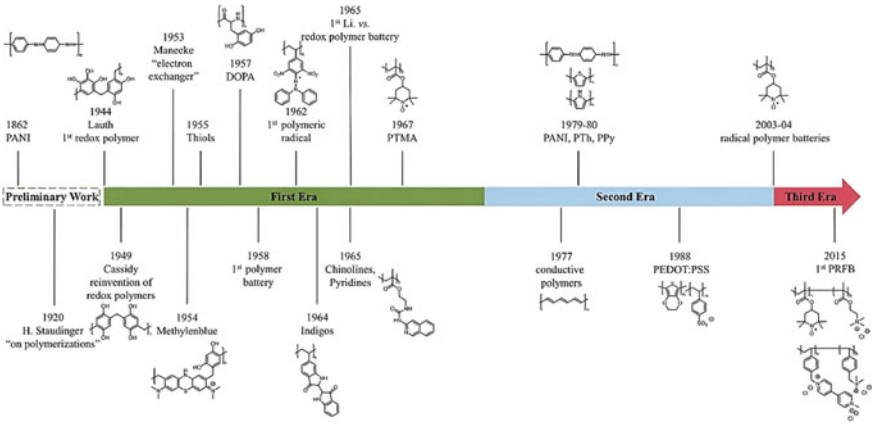

Fig. 1 Timeline with the most net-worthy inventions and scientific milestones in the field of redox-active polymers. Adapted with permission [5], Copyright (2021), Elsevier

while remaining insoluble in the operating electrolyte. Redox-active conjugated polymers are one type of material that is compatible with the proposed method. Recent advancements in their design have allowed for the creation of solution-processable redox-active polymers with balanced electronic/ionic transport properties. The functionalization of conjugated polymers with ion-transporting side chains has led to novel applications as cathode and anode materials in energy storage devices that operate in organic or aqueous electrolytes [17]. Furthermore, the design of polymer side chains allows for solubility in organic solvents, facilitating solution processing during device fabrication.

The current chapter primarily focuses on the redox-active polymers and their classification or the concept of charge transfer in redox-active polymers in batteries and what function redox polymeric materials can serve within these batteries.

2 Redox-Active Polymers

RAPs are macromolecules that contain chemical groups that can change their electrochemical state reversibly by losing (oxidation) or gaining (reduction). They enable the co-immobilization of enzymes and redox mediators on the electrode surface. To that end, redox-active polymers oversee managing the transfer of ions and electrons generated when their redox-active units interact with substrates. They are softer than inorganic electrode materials and do not require ions to intercalate into the solid-state structure [18].

2.1 Classification of Redox-Active Polymers

RAPs are classified into two types based on their chemical structures: (1) redox-active group-embedded polymers, which include conjugated polymers (i.e., conductive polymers), and (2) redox-active pendant-bearing polymers. Polymers with redox-active groups embedded in them have an electrochemically active backbone made up of redox-active monomers. Redox-active pendant-bearing polymers, on the other hand, have redox-active groups on their non-conductive polymer backbones, like a grafted polymer structure. They have different chemical and physical properties, redox reactions, and performances due to their different chemical structures.

2.1.1 Redox-Active Group-Embedded Polymers

Except for sulfur polymers, conjugated polymers are typical of redox-active group-embedded polymers. Dopant ions on the conjugated polymer backbone can provide good electrical conductivity in conjugated polymers with an alternative bonding structure of single and double bonds [19]. Particularly well-known redox-active conductive polymers with high electrical conductivity are polyaniline (PANI), poly (3,4-methylenedioxy thiophene) (PEDOT), polythiophene (PT), poly (3,4-propylenedioxy thiophene) (PProDOT), PEDOT: poly (4-styrene sulfonate) (PEDOT: PSS), and polypyrrole (PPy). Furthermore, polyacetylene (PA), poly(indole) (PI), and poly(p-phenylene) (P-p-P) are conjugated redox-active polymers. Doping and undoping cause redox reactions and the dopant ion depends on the polymer species. In contrast to other heterocyclic conductive polymers that are redox-active due to anionic dopants, PANI can be doped and undoped by cationic dopants [20]. The voltage of the resulting ESSs is not constant because the degree of doping varies during charging/discharging, which is a major issue for ESS applications. Sulfur polymer ESS applications have recently received a lot of attention due to their simple synthesis, low cost, suitability for large-scale production, and high capacitance. Sulfur polymers have sulfur-sulfur bonds (-S-Sn-S-) embedded on a non-conjugated polymer backbone, such as poly (sulfur-random-(1,3-di isopropenyl benzene)) (poly(S-r-DIB)), and they are highly redox-active and can be used for lithium- and sodium-sulfur batteries with high energy storage capability [21].

2.1.2 Redox-Active Pendant-Bearing Polymers

The majority of redox-active group-embedded polymers have good electrical conductivity, and many of their derivatives can be used for ESSs. Their doping level can be changed during redox reactions (i.e., by doping or dedoping); however, some well-known conjugated polymers are insoluble, limiting processing options. As a result, the redox-active group-embedded polymers have drawbacks in some applications. More information on redox-active pendant-bearing polymer derivatives and

their energy storage capabilities can be found in the literature [22–24]. Like grafted structures, these polymers have redox-active functional groups on non-conjugated polymer backbones. To make the redox-active pendant-bearing polymers, first, introduce polymerizable functional groups into the redox-active pendant groups. The prepared monomers are then polymerized using a variety of polymerization methods, including polycondensation, oxidative polymerization, free-radical polymerization, and so on. Because these polymerization methods limit fine control of molecular weight with narrow dispersity of the redox-active pendant-bearing polymers, detailed studies on the effects of molecular weight and their precise electrochemical characterization have been rarely reported [25].

3 Effects of Polymer Architecture on Cell Properties

The term "back-bone RAP" will be used to further justify polymers that contain the redox-active moiety in the backbone. Like this, the term "side chain RAP" will be used to describe polymers that contain a redox-active moiety as a side chain. Aside from the incorporation of active material into the polymer, the architecture of the polymer itself is critical. The architecture, on the other hand, is primarily determined by how and how frequently branching points are integrated into the polymer. Another important factor influencing polymer properties is their composition and whether they are made up of one or more monomers. This can but does not have to have an impact on the structural architecture. Overall, the trend is towards simple structures that can be easily synthesized using well-established techniques. The improved performance of complex structures frequently outperforms their costs, which could stymie future potential commercialization. Conjugated polymers have been heralded as the active material for the next environmentally friendly battery generation since the groundbreaking work of Heeger, MacDiamid, and Shirakawa [26]. Their most notable feature is the conjugated nature of their polymeric backbone, which is made up of -conjugated repeating units. Although the intrinsic conductivity is low, charging increases it by several orders of magnitude due to the introduction of delocalized charges along the main chain (i.e., doping) [20]. This is possible due to the polymer backbone's widely expanded system; however, the introduction of de-localized charges is also a significant disadvantage. The redox moieties are electrostatically influenced by each other due to the conjugated linkage. This produces a redox potential that is strongly dependent on the doping level, which varies with the state-of-charge (SOC) of the battery, resulting in a slope-like cell voltage (Fig. 2) [5].

Furthermore, the practically achievable doping levels (per monomeric unit) deviate significantly from unity, with real values ranging from 0.3 to 0.5, resulting in significantly lower capacities than would be theoretically possible for 100% doped materials [27]. Even though the doping is incomplete, the respective polymers represent highly charged species, resulting in a destabilized polymeric matrix that could cause unfavorable chain interactions or even chain destruction reactions, which is

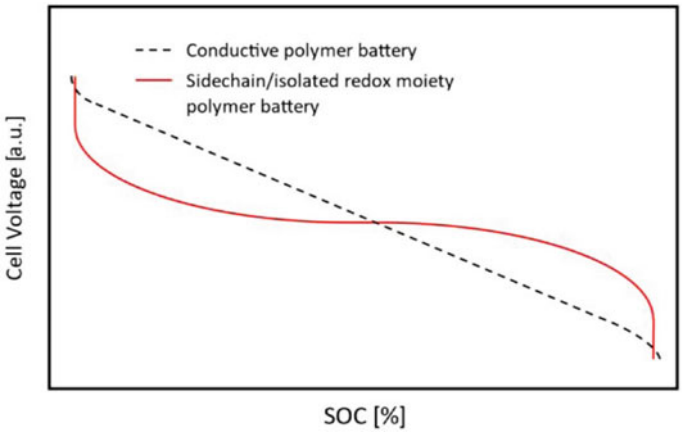

Fig. 2 The discharging behavior of batteries is compared schematically using conductive polymers (dashed line) and polymers with separated and isolated redox moieties (red solid line). Adapted with permission [5], Copyright (2021), Elsevier [5]

one disadvantage they share with most redox polymers that contain the active moiety in the backbone [28]. Higher charging levels are possible, and the typically desired plateau-like cell voltage is obtained over a wide SOC range (Fig. 2) if no interactions between the side chain moieties exist. Although sidechain polymers are preferred due to their superior electrochemical performance, the synthetic routes are frequently more difficult or economically unfavorable. Furthermore, due to the lack of intrinsic conductivity, conductive additives are required in the battery to form a composite electrode.

4 Concepts of Electron Transfer in RAPs

The dynamics of polymer solutions were first presented in pioneering publications by Flory and Huggins, among others, in the 1940s [29]. These theories would serve as the foundation for a whole class of macromolecular chemistries. The voltammetry of low molecular weight (<16 $K D_a$) poly (vinyl ferrocene) in solution was presented for the first time by Bard and Anson, who discovered that this system behaved similarly to its constituent monomer. This RAP exhibited a single oxidation wave with intensity proportional to an *n*-ferrocene center system. Because the ferrocene units were linked by an electronically insulating backbone, a single redox process was observed. Each pendant functioned as a separate ferrocene. Conjugated systems, on the other hand, exhibit electronic interactions that alter their redox potentials [26]. These pioneering studies opened the way for RAPs, but until 2012, there was little understanding of the role of polymer molecular weight and electrolyte dependencies on the electrochemical responses of soluble RAPs. Charge transport within RAPs

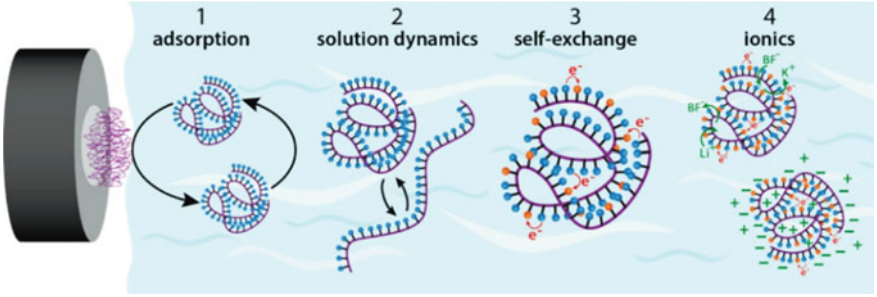

Fig. 3 Possible contributions of polymer dynamics to RAP electrochemical response. During all electrochemical measurements, there is an adsorbed polymer layer (1) that will mediate charge transfer to solution phase RAPs. Polyelectrolyte solution dynamics (2) of RAPs can change the conformation and orientation of the coil depending on the state of charge. Self-exchange of charges (3) and ionic interactions (4) modulate electrolysis rates of the particles. Adapted with permission [27], Copyright (2016), American Chemical Society

and at the electrode/electrolyte interface is influenced by polymer dynamics that do not exist in monomer solutions or are less important in small polymers. Some of the most common high polymer characteristics of RAPs are depicted in (Fig. 3) [27]. Small redox shuttles, such as ferrocene, undergo simple outer sphere electron transfer reactions via electron tunneling at an electrode. With larger RAPs, however, electron transfer at the polymer/electrode interface is replaced by intraparticle charge transport. When an insulating backbone is used, the charge propagates pendant-to-pendant via a charge diffusion process mediated by self-exchange reactions, i.e., charge hopping between neighboring redox species [27].

As illustrated in Fig. 3, charge transport via self-exchange becomes increasingly important for larger RAP structures. The DahmsRuff formalism is a widely used model for describing charge diffusion, D_E, in a system of mixed redox centers shown in Eq. 1. In this case, the diffusion of charges within a RAP is related to the rate constant for self-exchange, K_{EX}, and a distance parameter, δ, which describes the separation of redox centers. This equation has been particularly useful for describing electron hopping rates in small molecule dimer systems and redox-active polymer films.

$$D_E = \frac{K_{EX}\delta^2}{6} \tag{1}$$

However, when more degrees of structural freedom are introduced, as in the case of large RAPs, it is unclear whether this simple mathematical relationship is adequate to accurately describe charge hopping. The radius of gyration is well known to describe polymer size, but the distance between any two redox centers varies greatly depending on which chain segments are chosen. As a result, assigning the pendant separation distance parameter δ is ambiguous [30].

Synthetic control and systematic RAP studies are assisting in closing the knowledge gap in the cut-off boundary that distinguishes small and large redox systems. This is significant because the redox properties of monomers do not always scale linearly in polymer form. The redox mediator N, N, N′, N′-tetramethyl-p-phenylenediamine (TMPD), for example, is highly inaccessible to charge transfer in polymer form [31].

5 Redox- Active Polymers for Batteries

One of the most promising systems for large-scale electrochemical energy storage applications is the RFB. The creation of redox-active materials is a critical component of RFB research. Commercial RFBs use redox-active inorganic ions, which have various drawbacks, including expensive and hazardous active materials, redox species crossover, and the high expense of the ion exchange membrane. Incorporating redox-active polymeric materials is an intriguing solution because low-cost polymeric redox-active materials and size-exclusion porous membranes formed by commodity polymers could be used to replace expensive inorganic redox-active materials and ion exchange membranes. Polymer-based redox-active materials in RFB applications (PRFB) have improved considerably in recent years [32].

5.1 Development of Polymer-Based Aqueous RFB

During the investigation of electrically conducting polymers, the first concept of a water-soluble redox-active polymer was published. Heeger synthesized and studied a thiophene-based polymer with a sulfonate functional group in 1987. This polymer is soluble in concentrated sulfuric acid and has a bulky conductivity of 10^{-7} to 10^{-2} S/cm [33].

Using classical radical polymerization, the Schubert group developed and synthesized a 2,2,6,6-tetramethylpiperidiny-1-oxyl (TEMPO)-based copolymer for catholyte and a viologen-based copolymer for anolyte (Fig. 4) Because TEMPO is insoluble in water, the polymer was created by copolymerizing 2,2,6,6-tetramethylpiperidin-4-yl-methacrylate with the water-soluble monomer [2-(methacryloyloxy)- ethyl] trimethylammonium chloride. To convert the 2,2,6,6-tetramethylpiperidin group to TEMPO, the polymer (poly- (TEMPO-*co*-METAC)s) was treated with an oxidant. Because of the nonconjugated structure, the resultant polymer (Mw = 33,700 g/mol, polydispersity (PDI) = 1.7) is water soluble and has a similar redox potential as TEMPO monomer (0.64 vs Ag/AgCl) [34]. The viologen copolymer was created by copolymerizing styrene-based monomers and then quaternizing them with N-methyl-4,4-bipyridinium chloride (Fig. 4). The pendant group of the viologen copolymer (Mw = 73,400 g/mol, PDI = 2.4) is similar to that of methyl viologen (MV), which is very water-soluble. It is worth noting that the electrolytes

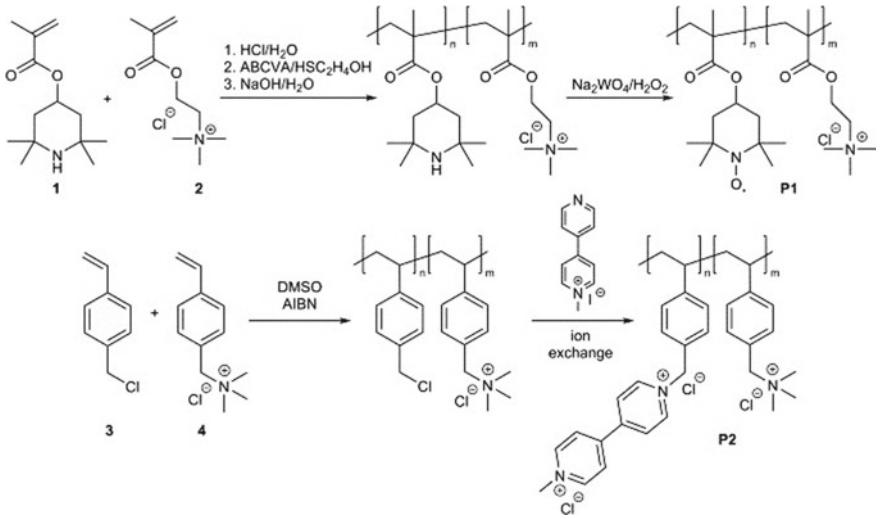

Fig. 4 Synthesis of poly (TEMPO-co-METAC) (P1) and poly (viologen) (P2) copolymers. Adapted with permission [34], Copyright (2015), Springer Nature

generated by both polymers exhibit Newtonian behavior, with viscosities of around 17 and 5 mPa.s, respectively (at the specific capacity of 10 Ah/L). In those electrolytes, no shear thickening behavior was seen, which would increase the expense of flow cell maintenance.

To test the battery cyclability and membrane permeability, a PRFB cell made of poly (TEMPO-co-METAC) and poly(viologen) was developed. The cell was manufactured in the same way as all organic- RFBs, except that the ion exchange membrane was replaced by a size-exclusion membrane with an MWCO of 6000 g/mol (Fig. 5a and b). This first aqueous PRFB system was run in neutral (pH ~ 7) settings with sodium chloride solution as the supporting electrolyte. The PRFB's capacity may be 8.2 Ah/L with 82% material utilization at a current density of 40 mA/cm^2, equivalent to an energy density of 8 Wh/l. After 100 cycles, the long-term cycling test demonstrated a 75% capacity retention, which is equivalent to the results of small molecule cells with ion exchange membranes. By using an anion exchange membrane, poly (TEMPO-co-METAC) was coupled with small molecule MV to construct a semi-PRFB system (Fig. 5c and d) The battery was stable for the first 100 cycles but declined dramatically after that. The conclusion is that the capacity loss was caused by osmotic pressure between the catholyte and anolyte.

Water molecules were found to migrate from polymer-based catholyte to MV-based anolyte, resulting in polymer material precipitation after approximately 100 cycles [35].

Another semi-PRFB study used poly (TEMPO-co-METAC) as the catholyte and zinc salt as the anolyte. The anode was zinc foil, and the electrolyte was a mixed electrolyte of 0.71 M NaCl, 0.08 M $ZnCl_2$, and 0.08 M NH_4Cl which served as

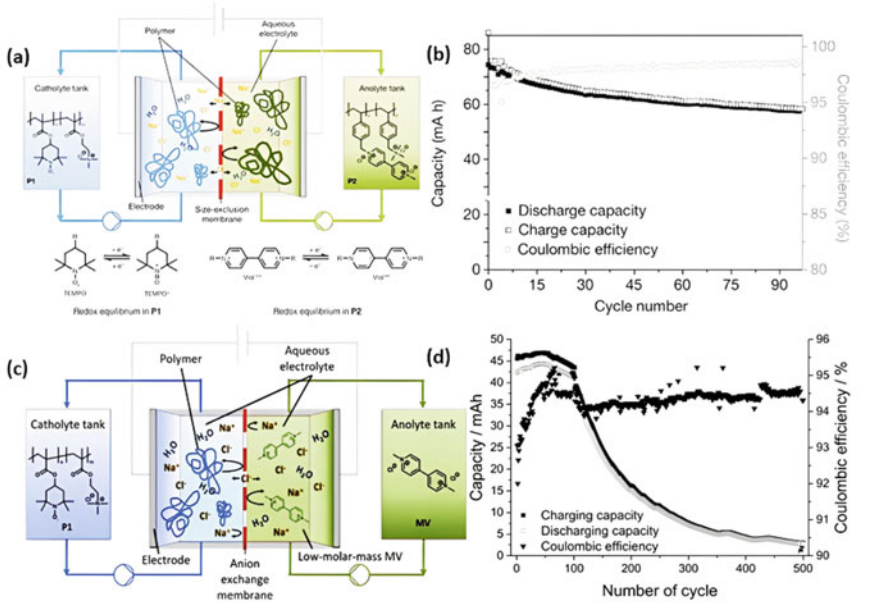

Fig. 5 **a** Schematic representation of all-polymer redox flow battery based on poly (TEMPO-co-METAC) and poly(viologen). **b** Cycle test of an all-polymer redox flow battery. **c** Schematic representation of poly (TEMPO-co-METAC)/MV redox flow battery. **d** Cycle test of poly (TEMPO-co-METAC)/MV redox flow battery. Figure a, b; Adapted with permission [34], Copyright (2015) Springer Nature. Figure c, d; Adapted with permission [38], Copyright (2017), Elsevier. Distributed under a Creative Commons Attribution License 4.0 (CC BY 4.0)

both an anolyte and supporting electrolyte. The cell voltage might reach 1.69 V due to the high potential of zinc chloride. Long-term cycling (1000 cycles) in a static cell was demonstrated, with relatively constant capacity retention (78.6%). The current densities in those trials, however, were quite low (between 220 mA/cm^2) [36]. The low current density was caused by the electrolyte's poor ionic conductivity (60 mS/cm), which is approximately one order of magnitude lower than that of 1 M H_2SO_4 (390 mS/cm). The scientists also created a new TEMPO copolymer (poly (TEMPO-co-PEGMA)s) by substituting an amphiphilic polyethylene glycol comonomer for the cationic comonomer. The poly (TEMPO-co-PEGMA)s/Zn flow cell (electrolyte and anolyte: 1.0 M $ZnCl_2$ and 1.0 M NH_4Cl) performed similarly to the poly(TEMPO-co-METAC)s/Zn cell but with a slightly higher energy density of 4.1 Wh/L.

A recent study described a novel method for increasing the solubility and ionic conductivity of polymeric redox-active compounds [37]. Because the zwitterionic group has both positive and negative charge centers on one unit, it has an extremely high solubility in an aqueous solution. The zwitterionic poly (TEMPO) copolymer has a solubility of more than 20 Ah/L, which is the highest value reported for all-polymeric redox-active materials in an aqueous medium. The materials' oxidation

degree is >98%, which is among the highest values reported in aqueous polymeric redox-active materials. Furthermore, the zwitterionic poly (TEMPO) copolymer had a viscosity of 4.59 mPas. and a specific capacity of 10 Ah/L at 20 °C, which was much lower than the cationic poly (TEMPO-co-METAC) copolymer. The cell comprising zwitterionic poly- (TEMPO) and MV was tested and found to be stable in the first 100 cycles [38].

5.2 Development of Polymer-Based Nonaqueous RFB

The non-aqueous method has been researched to improve the energy density of flow batteries with organic active species because it provides for a large electrochemical window. Since the initial publication of a nonaqueous RFB system with ruthenium bipyridine in 1988, various metal complexes have been shown to be redox-active species in nonaqueous electrolytes. However, due to the low ionic conductivity of IEMs in nonaqueous RFB systems, the power density of nonaqueous RFBs is often lower than that of aquatic RFBs [39]. The majority of reported nonaqueous RFBs utilized anion exchange membranes with ionic conductivities in the supporting electrolyte ranging between 0.2 and 0.5 mS/cm, which is nearly an order of magnitude lower than the ionic conductivity of Nafion in an aqueous system.

In nonaqueous RFBs, where a porous membrane paired with a liquid-supporting electrolyte could give increased ionic conductivity, macromolecule-based redox-active materials take advantage of their huge molecular size [40]. Computer simulation reveals that polymer/oligomer-based redox-active materials and size-exclusion porous membranes can minimize the crossover to less than 3 μmol/cm^2/day, which meets the battery industry's crossover standards. Many polymers were explored in nonaqueous RFB, including TEMPO-based polymer, viologen-based polymer, ferrocene-based polymer, and poly (ionic liquid).

5.2.1 TEMPO-Based Polymers

Organic radical polymers have been extensively studied in polymer batteries throughout the last few decades. TEMPO was also examined for nonaqueous PRFB as a stable radical. Poly(norbornene)-g-poly(4-methacryloyloxy-2,2,6,6-tetramethylpiperidin-1-oxyl) (PNB-g-PTMA) was initially synthesized and tested in a nonaqueous flow battery in 2014. Figure 6a and b depict the synthesis of PNB-g-PTMA: first, the branch chains containing TEMPO units were polymerized via live anionic polymerization, and then the main chain was polymerized by ring-opening metathesis polymerization (ROMP). PNB-g-PTMA produced a high yield (over 94% for anionic polymerization and over 98% for ROMP), and the polymer had a high molecular weight (Mn = 2.2 105 g/mol) and narrow PDI (1.2) [42]. Furthermore, the polymer can have a high radical concentration (95% for each unit) using this "grafting through" process. At 0.80 V (versus Ag/AgCl), a steady redox reaction

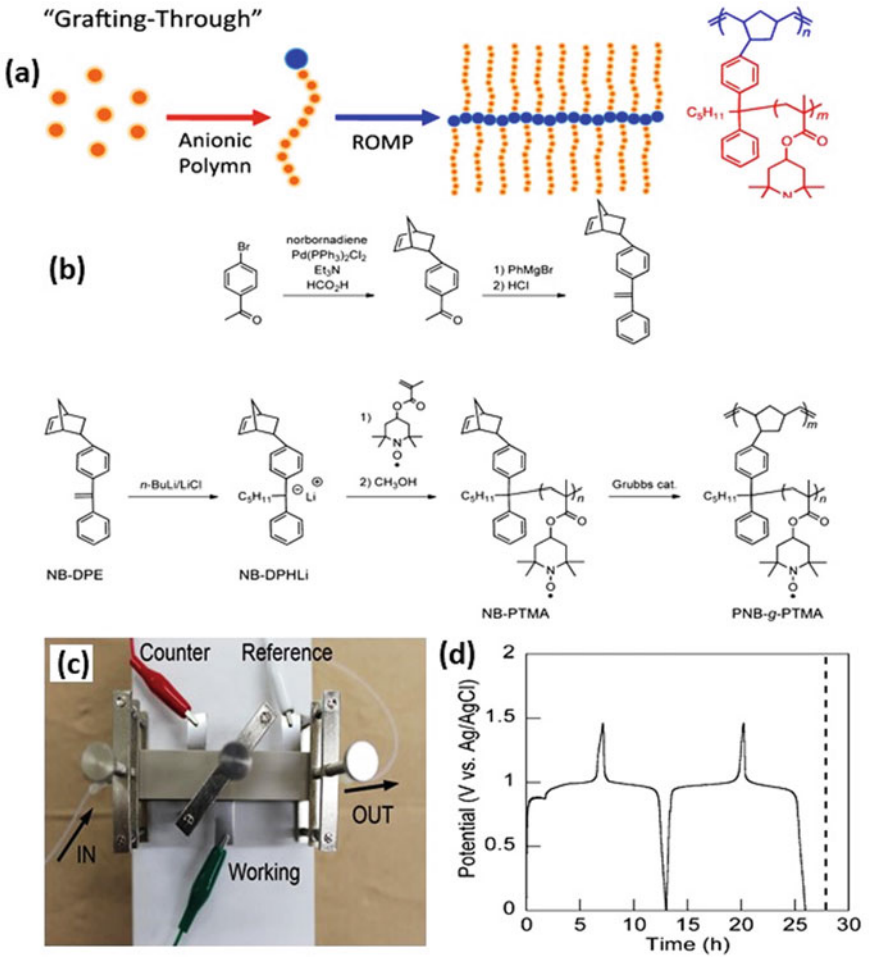

Fig. 6 **a**, **b** Synthesis scheme of PNB-g-PTMA. **c** Half-cell flow cell architecture for testing PNB-g-PTMA. **d** Charge/discharge profiles of PNB-g-PTMA half-cell. Adapted with permission [42], Copyright (2014), American Chemical Society

of TEMPO/TEMPO$^+$ was observed in 0.1 M $(n\text{-}C_4H_9)_4NClO_4/CH_3CN$ supporting electrolyte. The authors demonstrated a half-cell flow cell with 0.1 M PNB-g-PTMA in 0.1 M $(n\text{-}C_4H_9)_4NClO_4$ in ethylene carbonate/diethyl carbonate (1/1 in v/v) that supplied 95% of theoretical capacity (Fig. 6c and d) [41].

5.2.2 Viologen and Ferrocene-Based Polymers

The groups of Moore and Rodriguez-Lopez explored the viologen-based redox-active polymer in nonaqueous RFB. Poly-(vinylbenzylethyl viologen) with regulated molecular weights ranging from 21 to 318 KD_a was synthesized to investigate the effect of molecular weight on electrochemical characteristics and transport behavior over porous membranes. The viologen-based polymers were created by synthesizing the precursor polymer poly (vinylbenzyl chloride) with a certain molecular weight. To achieve ammonium hexafluorophosphate salt form, post-polymerization quaternization, and ion exchange processes were utilized. The polymer has good solubility in aprotic solvents such as acetonitrile and propylene carbonate, as well as a quick redox reaction at 0.7 V (versus Ag/Ag^+) [43].

Furthermore, in controlled potential bulk electrolysis studies, poly-(vinylbenzylethyl viologen) with varied molecular weights all showed high charge accessibility (9499%). To assess the separation effectiveness of polymers with varying molecular weights, commercially available porous separators (Celgard 2400 and Celgard 2325) were utilized. The results showed a significant relationship between molecular weight and rejection rate across the membrane. The crossover rate of polymers with high molecular weight was 70 times lower than that of charge-balancing ions ($Li^+BF_4^-$). It is concluded that porous membranes may effectively block the viologen-based polymer with a high molecular weight [44]. In subsequent work, the same group created polymers with two viologen groups on each styrene unit in ortho or meta orientations. Although the new polymers increased the density of redox-active centers in the polymer, only the polymer with two viologen groups on the meta position demonstrated faster redox kinetics than poly (vinylbenzylethyl viologen). Other research groups have reported viologen-based nonaqueous polymers; however, no flow cell studies were included in the publication.

The first ferrocene-based soluble polymer was synthesized in the 1950s.Poly(vinylferrocene) is commercially available but has a low solubility. Polymer-based RFB research recently disclosed a new ferrocene-based polymer poly (vinylbenzyl aminomethyl) ferrocene (PAF). By quaternization and ion exchange processes, PAF was synthesized from commercial poly- (vinylbenzyl chloride). The polymer was soluble in organic electrolytes such as 0.1 M $LiBF_4$ in acetonitrile and had a molecular weight of 271 kDa (Mn). To confirm the size-exclusion efficacy of nonaqueous RFBs, the viologen-based polymer was combined with a ferrocene-based polymer The separators in the testing were an ion-exchange membrane (Fumasep) and two distinct porous membranes (Celgard 2325 and Daramic 175) [45]. To produce reference cells with IEM or porous membranes, monomers of benzyl-ethyl viologen and benzyl(ferrocenylmethyl)-dimethylammonium were utilized. The battery with the porous membrane demonstrated greater conductivity and energy efficiency for polymer-based RFBs, with Coulombic efficiency exceeding 98% and capacity utilization over 80%. When the size-exclusion membrane was applied on viologen and ferrocene monomer-based cells, the crossover of redox-active components was severe [36]. Furthermore,

self-discharge studies demonstrated that polymer-based RFBs were stable, whereas monomer-based cells showed a large voltage loss, indicating a quick self-discharge. The study found that combining a size-exclusion barrier with polymeric redox-active materials could give a low-cost solution for nonaqueous RFBs.

5.2.3 Other Polymeric Materials for Nonaqueous RFB

Other RAPs have been reported as redox-active materials in nonaqueous RFB, including dicyanoanthraquinone diamine-containing polymer (poly(DCAQI)),phthalimide-containing polymer, cyclopropenium-containing polymer, poly(para-nitrostyrene), and boron-dipyrromethene (BODIPY)-based polymers, BODIPY derivatives in those polymers demonstrated a unique characteristic with two reversible redox reactions on one molecule.108 Poly(BODIPY-co-TEGSt) and poly(BODIPY-co-TASt) revealed two reversible redox peaks at 1.5 and 0.7 V versus Ag/Ag^+, respectively. (TEMPO-co-PEGMA) with a size-exclusion membrane (MWCO = 1000 g/mol) [46]. The cell demonstrated a high discharge voltage of 1.82 V as well as a high Coulombic efficiency of 99%. After 100 cycles, the capacity fading was 70%. BODIPY derivatives can be utilized as both a catholyte and an anolyte due to the presence of two redox peaks. The all-BODIPY static cell was built and tested with a size-exclusion membrane and a supporting electrolyte of 0.5 M Bu_4NClO_4 in propylene carbonate. The cell had a charging plateau at 2.06 V but no discernible discharging plateau. The first 10 cycles showed a significant drop in capacity, while the following 90 cycles were very steady [47].

5.2.4 Oligomer-Based Nonaqueous RFB

The size exclusion technique is applicable to both macromolecules and oligomers with significant molecular sizes. Recently, oligomer-based RFBs with porous membranes were reported (Fig. 7a). In research published in 2018, a series of tris(dialkylamino)cyclopropenium-based (CP-based) oligomeric catholyte with acetonitrile solubility of 0.1- 0.3 M was synthesized. The investigation concentrated on the effect of chain length between two CP groups on electrochemical stability and redox potential [48]. It was determined that a four-carbon linker length was required to sustain the reversible and steady redox behavior at 0.87 V (versus Fc/Fc^+). After 6 days of cycling, no crossover of CP tetramers was identified during the charging and discharging test for a proof-of-concept battery utilizing the tetramer and PIM (polymers of intrinsic microporosity) membrane. The cell with tetramers performed better than the cell with monomers (Fig. 7b). These tests demonstrated that the oligomers could be used in RFBs with size-exclusion membranes. The creation of oligomer-based materials has the potential to improve redox-active materials' solubility and electrochemical stability [49].

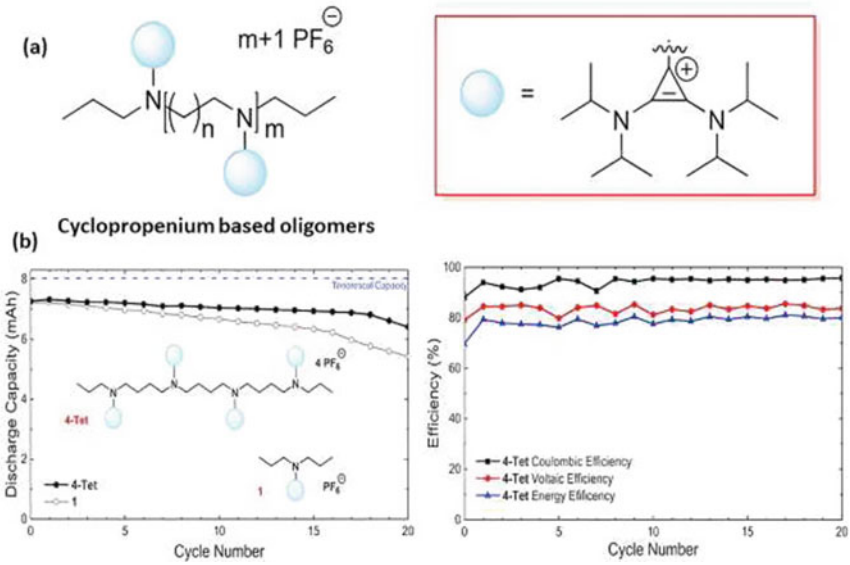

Fig. 7 **a** Oligomer structures reported for nonaqueous organic RFB. Adapted with permission [48], Copyright (2018), American Chemical Society. **b** RFB cycle results with cyclopropenium-based tetramer and monomer. Adapted with permission [49], Copyright (2018), American Chemical Society

5.3 Polymer Suspension-Based RFB

Polymer-based electrolytes enable the use of porous membranes in RFBs, which has the potential for cost savings and increased ionic conductivity. However, because polymeric molecules are often less soluble than their equivalent monomers, the PRFB has a low specific capacity and energy density. While highly soluble polymeric redox-active materials manufacture remains difficult, polymer-based RFBs based on redox-active colloids or suspensions have appeared in recent years [50]. A flow cell was constructed using polythiophene microparticles as both anolyte and catholyte. The supporting electrolyte was 1 M $TEABF_4$ (tetraethylammonium tetrafluoroborate) in propylene carbonate, and carbon black was suspended in the electrolyte as a conductivity-enhancing powder. The separator in the cell was an anion-exchange membrane. At a current density of 0.5 mA/cm^2, the cell used 34.5% of its potential capacity, according to testing data. The poor conductivity of neutral polythiophene, which is around 10^{-10} and 10^{-5} S/cm, which is substantially lower than that of doped polythiophene (1 to 10^4 S/cm), could be one cause for the low utilization of redox-active materials.

In a nonaqueous RFB system, Schubert's group examined polymer colloidal-based redox-active materials. In organic solvent, the block copolymer generated core-corona micelle structures. DLS measurements revealed that the polymer particles' hydrodynamic radius was roughly 40 nm. The polymer particles were utilized as

a catholyte with 0.5 M Zn $(ClO_4)_2.6H_2O$ as an anolyte and supporting electrolyte in EC/DMC/DEC (v:v:v = 1:1:1) [39]. The catholyte solubility was 13 mg/mL, which corresponded to 1.2 Ah/L. The RFB cell with a size-exclusion membrane demonstrated good nonflow stability (capacity retention of 95% after 1000 cycles). Under low current (0.2 mA/cm^2), materials utilization was 93%, but capacity declined quickly with higher current.

6 Conclusions

The current state of research, particularly in the field of secondary batteries, places the commercialization of new environmentally friendly and potentially metal-free batteries within reach. RAPs play an important role in these concepts because they represent a smart way of addressing many consumers' environmental concerns (e.g., material sources or recycling) while still combining cheap and easy synthetic pathways for industrial-scale production. However, some critical issues, such as the intrinsic stability of active materials or the ability to retain the applied charge over time, frequently go unaddressed. The use of solid additives in electrolytes promises significantly increased energy densities in the near future, exceeding the known benchmarks for these systems and boosting their competitiveness among known battery technologies. When it comes to the use of polymeric materials in energy storage, they are currently almost exclusively the pure carrier of redox moieties. Polymers have gained particular interest in the context of stimuli-responsive materials / smart materials in recent years, enabling a wide range of potential applications, such as soft robotics or sensors. As a result, we anticipate that other polymer properties/functionalities and stimuli-responsive behavior will find their way into the field of polymers for electrical energy storage.

References

1. J. Figgener, P. Stenzel, K. P. Kairies, J. Linßen, D. Haberschusz, O. Wessels, ... D. U. Sauer, The development of stationary battery storage systems in Germany–A market review. J. Ener. Stor. **29**, 101153 (2020)
2. K. Liu, Y. Liu, D. Lin, A. Pei, Y. Cui, Materials for lithium-ion battery safety. Sci. Adv. **4**(6), eaas9820 (2018)
3. C. Banza Lubaba Nkulu, L. Casas, V. Haufroid, T. De Putter, N. D. Saenen, T. Kayembe-Kitenge, ... B. Nemery, Sustainability of artisanal mining of cobalt in DR Congo. Nat. Sustain. **1**(9), 495-504 (2018)
4. H. Letheby, XXIX.—On the production of a blue substance by the electrolysis of sulphate of aniline. J. Chem. Soc. **15**, 161–163 (1862)
5. P. Rohland, E. Schröter, O. Nolte, G.R. Newkome, M.D. Hager, U.S. Schubert, Redox-active polymers: the magic key towards energy storage–a polymer design guideline progress in polymer science. Prog. Polym. Sci. **125**, 101474 (2022)

6. S. Muench, A. Wild, C. Friebe, B. Haupler, T. Janoschka, U.S. Schubert, Polymer-based organic batteries. Chem. Rev. **116**(16), 9438–9484 (2016)
7. R. Chen, D. Bresser, M. Saraf, P. Gerlach, A. Balducci, S. Kunz, ... J. Chen, A comparative review of electrolytes for organic-material-based energy-storage devices employing solid electrodes and redox fluids. Chem. Sus. Chem. **13**(9), 2205-2219 (2020)
8. Y. Liang, Z. Tao, J. Chen, Organic electrode materials for rechargeable lithium batteries. Adv. Energy Mater. **2**(7), 742–769 (2012)
9. Q. Zhao, Lu., Yong, J. Chen, Advanced organic electrode materials for rechargeable sodium-ion batteries. Adv. Energy Mater. **7**(8), 1601792 (2017)
10. Y. Lu, Q. Zhang, L. Li, Z. Niu, J. Chen, Design strategies toward enhancing the performance of organic electrode materials in metal-ion batteries. Chem **4**(12), 2786–2813 (2018)
11. J.C. Pramudita, D. Sehrawat, D. Goonetilleke, N. Sharma, An initial review of the status of electrode materials for potassium-ion batteries. Adv. Energy Mater. **7**(24), 1602911 (2017)
12. L. Chen, J.L. Bao, X. Dong, D.G. Truhlar, Y. Wang, C. Wang, Y. Xia, Aqueous Mg-ion battery based on polyimide anode and prussian blue cathode. ACS Energy Lett. **2**(5), 1115–1121 (2017)
13. J. Xie, Q. Zhang, Recent progress in multivalent metal (Mg, Zn, Ca, and Al) and metal-ion rechargeable batteries with organic materials as promising electrodes. Small **15**(15), 1805061 (2019)
14. K. Koshika, N. Chikushi, N. Sano, K. Oyaizu, H. Nishide, A TEMPO-substituted polyacrylamide as a new cathode material: an organic rechargeable device composed of polymer electrodes and aqueous electrolyte. Green Chem. **12**(9), 1573–1575 (2010)
15. S. Behzadi, M. Gallei, J. Elbert, M. Appold, G. Glasser, K. Landfester, D. Crespy, A triblock terpolymer vs. blends of diblock copolymers for nanocapsules addressed by three independent stimuli. Poly. Chem. **7**(20), 3434–3443 (2016)
16. D.H.S. Tan, Xu., Panpan, Z. Chen, Enabling sustainable critical materials for battery storage through efficient recycling and improved design: a perspective. MRS Ener. Sustain. **7**, E27 (2020)
17. D. Moia, A. Giovannitti, A. A. Szumska, I. P. Maria, E. Rezasoltani, .M. Sachs, ... & J. Nelson, Design and evaluation of conjugated polymers with polar side chains as electrode materials for electrochemical energy storage in aqueous electrolytes. Ener. Environm. Sci. **12**(4), 1349-1357 (2019)
18. A. Ruff, Redox polymers in bioelectrochemistry: Common playgrounds and novel concepts. Curr. Opin. Electrochem. **5**(1), 66–73 (2017)
19. J. Kim, J. You, E. Kim, Flexible conductive polymer patterns from vapor polymerizable and photo-cross-linkable EDOT. Macromolecules **43**(5), 2322–2327 (2010)
20. S. Bhadra, D. Khastgir, N.K. Singha, J.H. Lee, Progress in preparation, processing and applications of polyaniline. Prog. Polym. Sci. **34**(8), 783–810 (2009)
21. J.J. Griebel, R.S. Glass, K. Char, J. Pyun, Polymerizations with elemental sulfur: a novel route to high sulfur content polymers for sustainability, energy and defense. Prog. Polym. Sci. **58**, 90–125 (2016)
22. T.B. Schon, B.T. McAllister, P.F. Li, D.S. Seferos, The rise of organic electrode materials for energy storage. Chem. Soc. Rev. **45**(22), 6345–6404 (2016)
23. M. Miroshnikov, K.P. Divya, G. Babu, A. Meiyazhagan, L.M.R. Arava, P.M. Ajayan, G. John, Power from nature: designing green battery materials from electroactive quinone derivatives and organic polymers. J. Mater. Chem. A **4**(32), 12370–12386 (2016)
24. R. Gracia, D. Mecerreyes, Polymers with redox properties: materials for batteries, biosensors and more. Polym. Chem. **4**(7), 2206–2214 (2013)
25. Di Lena, Fabio, Krzysztof Matyjaszewski, Transition metal catalysts for controlled radical polymerization. Progr. Polym. Sci. **35.8**, 959-1021 (2010)
26. H. Shirakawa, E.J. Louis, A.G. MacDiarmid, C.K. Chiang, A.J. Heeger, Synthesis of electrically conducting organic polymers: halogen derivatives of polyacetylene, (CH) x. J. Chem. Soc. Chem. Commun. **16**, 578–580 (1977)
27. M. Burgess, J.S. Moore, J. Rodríguez-López, Redox active polymers as soluble nanomaterials for energy storage. Acc. Chem. Res. **49**(11), 2649–2657 (2016)

28. J. Flory, Paul, Thermodynamics of high polymer solutions. J. Chem. Phys. **9.8**, 660–660 (1941)
29. C. LeVanda, K. Bechgaard, D.O. Cowan, M.D. Rausch, Intervalence transfer in substituted biferrocene cations. J. Am. Chem. Soc. **99**(9), 2964–2968 (1977)
30. A.J. Bard, A life in electrochemistry. Annu. Rev. Anal. Chem. **7**, 1–21 (2014)
31. S. Conte, G.G. Rodríguez-Calero, S.E. Burkhardt, M.A. Lowe, H.D. Abruña, Designing conducting polymer films for electrochemical energy storage technologies. RSC Adv. **3**(6), 1957–1964 (2013)
32. Y.Y. Lai, X. Li, Y. Zhu, Polymeric active materials for redox flow battery application. ACS Appl. Poly. Mater. **2**(2), 113–128 (2020)
33. Z.J. Liu, L.B. Kong, Y.H. Zhou, C.M. Zhan, Polyanthra [1, 9, 8-b, c, d, e] [4, 10, 5-b, c, d, e] bis- [1, 6, 6a (6a-S) trithia] pentalene-active material for cathode of lithium secondary battery with unusually high specific capacity. J. Power. Sources **161**(2), 1302–1306 (2006)
34. T. Janoschka, N. Martin, M.D. Hager, U.S. Schubert, An aqueous redox-flow battery with high capacity and power: the TEMPTMA/MV system. Angew. Chem. Int. Ed. **55**(46), 14427–14430 (2016)
35. T. Liu, X. Wei, Z. Nie, V. Sprenkle, W. Wang, A total organic aqueous redox flow battery employing a low cost and sustainable methyl viologen anolyte and 4-HO-TEMPO catholyte. Adv. Energy Mater. **6**(3), 1501449 (2016)
36. Y. Ding, C. Zhang, L. Zhang, Y. Zhou, G. Yu, Molecular engineering of organic electroactive materials for redox flow batteries. Chem. Soc. Rev. **47**(1), 69–103 (2018)
37. J. Winsberg, T. Janoschka, S. Morgenstern, T. Hagemann, S. Muench, G. Hauffman, J.-F. Gohy, M.D. Hager, U.S. Schubert, Poly (TEMPO)/zinc hybrid-flow battery: a novel, "green", high voltage, and safe energy storage system. Adv. Mater. **28**(11), 2238–2243 (2016)
38. T. Hagemann, J. Winsberg, M. Grube, I. Nischang, T. Janoschka, N. Martin, M.D. Hager, U.S. Schubert, An aqueous all-organic redox-flow battery employing a (2, 2, 6, 6-tetramethylpiperidin-1-yl) oxyl-containing polymer as catholyte and dimethyl viologen dichloride as anolyte. J. Power. Sources **378**, 546–554 (2018)
39. P.J. Cappillino, H.D. Pratt III., N.S. Hudak, N.C. Tomson, T.M. Anderson, M.R. Anstey, Application of redox non-innocent ligands to non-aqueous flow battery electrolytes. Adv. Energy Mater. **4**(1), 1300566 (2014)
40. S.E. Doris, A.L. Ward, A. Baskin, P.D. Frischmann, N. Gavvalapalli, E. Chénard, C.S. Sevov, D. Prendergast, J.S. Moore, B.A. Helms, Macromolecular design strategies for preventing active-material crossover in non-aqueous all-organic redox-flow batteries. Angew. Chem. **129**(6), 1617–1621 (2017)
41. E.C. Montoto, G. Nagarjuna, J.S. Moore, J. Rodríguez-López, Redox active polymers for non-aqueous redox flow batteries: validation of the size-exclusion approach. J. Electrochem. Soc. **164**(7), A1688 (2017)
42. T. Sukegawa, I. Masuko, K. Oyaizu, H. Nishide, Expanding the dimensionality of polymers populated with organic robust radicals toward flow cell application: synthesis of TEMPO-crowded bottlebrush polymers using anionic polymerization and ROMP. Macromolecules **47**(24), 8611–8617 (2014)
43. G. Nagarjuna, J. Hui, K.J. Cheng, T. Lichtenstein, M. Shen, J.S. Moore, J. Rodríguez-López, Impact of redox-active polymer molecular weight on the electrochemical properties and transport across porous separators in nonaqueous solvents. J. Am. Chem. Soc. **136**(46), 16309–16316 (2014)
44. M. Burgess, E. Chénard, K. Hernández-Burgos, G. Nagarjuna, R.S. Assary, J. Hui, J.S. Moore, J. Rodríguez-López, Impact of backbone tether length and structure on the electrochemical performance of viologen redox active polymers. Chem. Mater. **28**(20), 7362–7374 (2016)
45. Y. H., Chen, M. Fernandez-Refojo, H. G. Cassidy, Electron exchange polymers. XII. Potentiometric titration of dicyclopentadienyliron ("ferrocene") and some derivatives. J. Poly. Sci. **40**(137), 433–441 (1959)
46. J. Winsberg, S. Benndorf, A. Wild, M.D. Hager, U.S. Schubert, Synthesis and characterization of a phthalimide-containing redox-active polymer for high-voltage polymer-based redox-flow batteries. Macromol. Chem. Phys. **219**(4), 1700267 (2018)

47. J. Winsberg, T. Hagemann, S. Muench, C. Friebe, B. Häupler, T. Janoschka, S. Morgenstern, M.D. Hager, U.S. Schubert, Poly (boron-dipyrromethene) A redox-active polymer class for polymer redox-flow batteries. Chem. Mater. **28**(10), 3401–3405 (2016)
48. K.H. Hendriks, S.G. Robinson, M.N. Braten, C.S. Sevov, B.A. Helms, M.S. Sigman, S.D. Minteer, M.S. Sanford, High-performance oligomeric catholytes for effective macromolecular separation in nonaqueous redox flow batteries. ACS Cent. Sci. **4**(2), 189–196 (2018)
49. M.J. Baran, M.N. Braten, E.C. Montoto, Z.T. Gossage, L. Ma, E. Chénard, J.S. Moore, J. Rodríguez-López, B.A. Helms, Designing redox-active oligomers for crossover-free, nonaqueous redox-flow batteries with high volumetric energy density. Chem. Mater. **30**(11), 3861–3866 (2018)
50. C. Montoto, Elena, Gavvalapalli Nagarjuna, Jingshu Hui, Mark Burgess, M. Nina Sekerak, Kenneth Hernández-Burgos, Teng-Sing Wei, Redox active colloids as discrete energy storage carriers. J. Am. Chem. Soc. **138**(40), 13230–13237 (2016)

Carbon-Based Pseudocapacitive Materials for Next Generation Batteries

B. Jeevanantham and M. K. Shobana

Abstract Sodium and potassium-ion batteries have been hampered by their low rates and capacities, making them less desirable as electrical energy storage devices at low prices. Lithium-ion batteries (LIBs) are the preferred electrochemical energy storage technology for portable devices, electric vehicles, and grid storage. Despite this, LIBs are not being developed further due to their lack of fast charging technology, low energy density, and safety concerns. Utilizing carbon substrates as composite electrodes is one of the most widely used strategies for improving their electrochemical performance. Metal oxides and metal sulfide materials also possess a low working potential and the highest practical reversible capacity compared with commercialized graphite. Thus, combining a carbon-based material with a metal oxide/sulfide-based material will result in excellent electrical conductivity and reactivity, high theoretical capacity, flexibility, and remarkable tensile strength. In this chapter, carbon materials with metal oxides/sulfides are discussed in detail based on their structure–property interactions and the different electrochemical mechanisms driving their behavior to discuss the possibilities and challenges of post-battery technologies.

Keywords Lithium-ion batteries · Carbon-based materials · Metal oxides/sulfides · Carbon–metal oxide/sulfide composites

1 Introduction

Our global energy consumption has been dramatically increased by the rapidly growing economy and population. The sustainability of energy supplies has been gaining attention worldwide due to the rapid depletion of fossil fuels. Modern society also requires mature energy storage systems because of hybrid electric vehicles and portable electronics. Batteries, supercapacitors, and fuel cells are gradually being investigated as initial energy storage devices [1, 2]. Lithium-ion batteries (LIBs)

B. Jeevanantham · M. K. Shobana (✉)
Department of Physics, School of Advanced Sciences, Vellore Institute of Technology, Vellore 632014, Tamil Nadu, India
e-mail: shobana.mk@vit.ac.in

© The Author(s), under exclusive license to Springer Nature Switzerland AG 2024

R. K. Gupta (ed.), *Pseudocapacitors*, Engineering Materials,
https://doi.org/10.1007/978-3-031-45430-1_16

have received rapid development in renewable energy sources and electric vehicles. Despite this progress, electric vehicles face several technical obstacles, such as mileage anxiety, low charging efficiency, time-consuming charging, safety concerns, and low energy density. To address these challenges, several efforts have been made, including the development of high-power cathodes and anodes, advanced separators, and safe electrolytes. Moreover, many efforts have been made to develop cathodes that are thermally stable and have long cycle lives, such as polyanion-based compounds and layered transition metal oxides [3]. But the anode materials are still challenging. Therefore, finding a feasible anode material could enable a significant breakthrough for rechargeable batteries.

Graphite and non-graphite carbon are carbon-based materials that have the advantages of widespread raw materials, chemical stability, low cost, and thermal stability. They can act not only as anodes for LIBs but also as additives for other anodes. Carbon materials play a crucial role in electrode material fabrication owing to their large surface area, high electrical conductivity, and natural ability to self-expand. Nanostructures with diverse morphologies and numerous pores have been designed for LIBs to enhance their electrochemical properties using carbon-based electrodes [4]. In most current commercial LIBs, they are the most traditional electrode materials. Similarly, metal oxides/sulfide-based materials also possess low working potential, the highest practical reversible capacity, and relatively efficient power capabilities. In general, graphite has a much lower capacity than metal oxides/sulfides. The most promising approach appears to be combining carbon with metal oxides/sulfides. A carbon-based material is excellent in electrical conductivity, flexible, and remarkable in tensile strength, while metal oxides/sulfides are excellent in reactivity and theoretical capacity. Also, customer convenience can be improved highly by reducing charging time without sacrificing mileage [5]. A composite design may consist of a core–shell, tube-in-tube or void-spaces, egg yolk to allow for expansion in volume. This review examines the underlying materials of composites, including carbon-based materials (carbon nanotubes, carbon nanofibers, graphite, and graphene), metal oxides, and metal sulfides. Finally, the electrochemical mechanisms and properties of carbon-based materials with metal oxides/sulfides are discussed.

2 Carbon-Based Materials

In this chapter, carbon nanofibers, carbon nanotubes, graphene, and graphite are discussed extensively. It inhibits dendrite growth with carbon-based electrolyte additives with unique physical and chemical properties. Carbon-based materials also accommodate volume changes due to their various structures, flexibility, and high surface area.

2.1 Carbon Nanotubes (CNTs)

CNTs are widely used as attractive candidates for energy storage technologies. These materials are ideal reinforcements for a wide range of materials, including polymers, metals, alloys, and ceramics, due to their high electrical and mechanical properties. Benzene molecules combine to form a crystalline CNT structure, and their large porosity and high electrolyte accessibility make them an ideal candidate for high-power electrode materials, flexible and stretchable electronic applications, and implantable microchips [6]. CNTs are categorized into single-walled CNT (graphene sheets rolled into a cylindrical tube with a nanometer diameter) and multi-walled CNTs (MWCNTs) (multiple nanotubes with high levels of impurities and defects), respectively. According to the microstructure of agglomerates, the agglomerates in CNTs are divided into entangled CNTs and CNT arrays. Entangled CNTs have twisted CNTs, while CNT arrays have parallel CNTs, as shown in Fig. 1a and b. These CNT arrays have a regular pore structure that influences their electrochemical properties and energy storage applications. Also, the CNT array is fabricated in two dominant ways: direct growing of CNT arrays and transfer techniques. CNT arrays are first grown directly over silicon or silica substrates by chemical vapor deposition (CVD). Second, the transfer techniques, in which the CNT array is detached from the original substrates by cutting and then placing it over the metal (Ni, Cu, and Al) foil and other current collectors with binders and solders to fabricate the CNT array electrode. Compared with these techniques, the growing array of current collectors is more attractive and powerful. This technique is a one-step procedure with robust CNT growth on metal contacts and low electrical resistance between the array and substrate [7].

2.2 Carbon Nanofibers (CNFs)

CNFs consist of curls of graphite sheets arranged in one-dimensional fibrous structures with diameters ranging from 100 to 500 nm and a length of about 1 nm. CNF has many advantages, including a large surface area, high mechanical stability, good electrical conductivity, and low density. These properties enable the CNFs to deliver excellent electrochemical properties, enhanced capacity, good cycle performance, and outstanding low-temperature performance. Since CNFs possess unique thermal, mechanical, and electrical properties, they possess great potential as large-scale energy storage, sensors, and nanocomposites. Figure 1c–e illustrates the shapes of carbon nanofibers based on the angles between graphene layers. Electrospinning, melt-blowing, bicomponent fiber spinning, chemical vapor deposition, and wet chemical synthesis are methods used to produce these nanofibers [8]. Although the CNFs are electrochemically good, some modification is needed to improve their performance. Because of CNF, the production cost is high, which inhibits widespread applications.

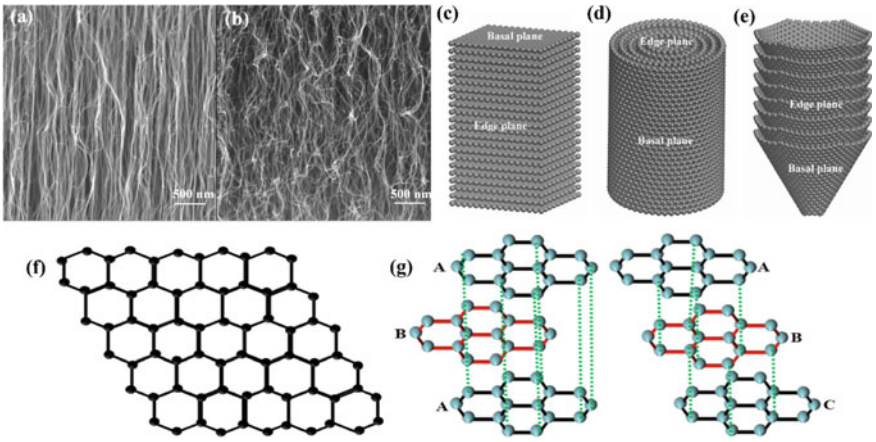

Fig. 1 Scanning electron microscope (SEM) images of **a** aligned CNTs and **b** entangled or waved CNTs. Adapted with permission [14], Copyright (2021), Springer Nature. **c**–**e** Represents the platelet-type, tubular-type, and fishbone-type CNFs. Adapted with permission [15], Copyright (2012), Elsevier. **f**, **g** Schematic illustrations of graphene and graphite. Adapted with permission [5], Copyright (2021), Elsevier

2.3 Graphene

Energy storage devices can greatly benefit from graphene's superior electronic, thermal, and mechanical characteristics, as well as its strong van der Waals force between sheets. Like charcoal, fullerenes, graphite, and carbon nanotubes, it consists of a single layer of carbon atoms. Some of the key features, like a large surface area, microporosity, and good electrical conductivity, make them an ideal candidate for energy storage applications [9]. A graphene molecule is composed of two-dimensional (2D) honeycombs of carbon atoms with a sp^2 hybrid, as shown in Fig. 1f [10]. It can increase the storage capacity of LIBs by adsorbing lithium (Li) ions on both sides of the anode. Also, they act as additives to construct the three-dimensional conducting framework and enhance the interfacial interaction, which is beneficial for full electrolyte infiltration. Graphene with perfect crystallinity can be produced by CVD and some mechanical methods. Here, the reduced graphene oxide (rGO) aids in feasible mass production and has layered graphene properties. It also exhibits enhanced performance due to its large specific surface area [11]. Graphene flakes buffer the volume impact when metals or metal oxides are used as anodes. Despite this, ionic-steric effects and low stability make graphene unsuitable to use in LIBs directly as an anode active material. Moreover, the development of graphene-based composites will show significant paths to LIBs [12].

2.4 Graphite

LIBs have been commercially designed with graphite because of its superior cycle life and low cost, with a theoretical capacity of 372 mAh g^{-1}. As graphite consists of crystalline carbon, it has a perfect c-axis crystal structure, as shown in Fig. 1g. In the plane, carbon atoms are delocalized, which results in exceptional electronic conductivity [5]. Graphite's layers are connected by van der Waals forces, allowing ions to diffuse between the layers, resulting in intercalation compounds [9]. Changes in the intrinsic properties of graphite, such as enlarging the gap between graphite layers, do not increase the capacity based on the insertion mechanism. Thus, lithium-graphite intercalation compounds are to be fabricated that show higher lithiation than LiC_6. It obtains nearly 1000 mAh g^{-1} with an enhanced microporous structure [13]. Anodes made from graphite experience superior cycling stability and high tap density, but their progress is slowed by low capacitances and sluggish kinetics. If graphite's lithium storage capabilities are further enhanced, it will make a promising component for electric vehicle power storage and grid-scale energy storage systems [4].

3 Metal-Based Materials

3.1 Metal Oxides

The excellent electrochemical performance of inorganic battery materials has enticed researchers for decades. As anode materials, metal oxides are widely used due to their simple preparation, low cost, and high specific capacity. It shows superior performance compared to commercialized graphite. Materials are generally classified into three types: intercalation, conversion, and alloying (Al, Sn, Mg, etc.) [16]. Some metal oxides like TiO_2, SiO_2, and V_3O_5 are intercalated with Li and de-intercalate to form Li_xMO_y. Metals like Co, Mn, Mo, etc. can react with Li but do not form alloys because of their poor metallic activity. In the interlayer reaction, Li^+ is only embedded in the material's interlayer structure during charging and discharging. The conversion is a redox reaction where, in the first charge–discharge process, metal oxides and Li^+ undergo oxidation–reduction reactions, generating metal and Li_2O. During the alloying process, metal oxides are converted into metallic elements by reacting with Li and forming Li_zM. Further, these oxides have a better effect than graphite anodes because they demonstrate high capacity, good stability, widespread availability, and are environmentally friendly. For example, SnO_2 has a theoretical storage capacity of 790 mAh g^{-1}, twice that of a graphite anode, while TiO_2 has low capacity but achieves low volume expansion and good stability [17].

Yang et al. synthesized titanium dioxide flakes via a simple spreading method. Flakes with a larger surface area provide a larger electrode/electrolyte contact area, which results in shorter solid-state paths and higher rates for Li-ions and electrons

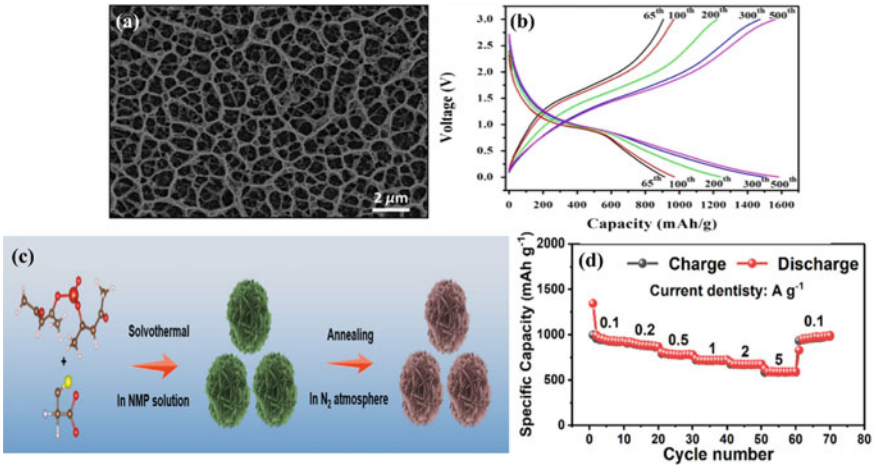

Fig. 2 SEM images of an (**a**) annealed Fe_2O_3 sample; (**b**) at 1C, the Fe_2O_3/Li half cells undergo charge/discharge cycles between 0.005 and 3.0 V using a 1000 mAh g^{-1} current density. Adapted with permission [20], Copyright (2014), Elsevier. (**c**) V_3S_4 synthesis process; (**d**) rate performance of V_3S_4 at 10 Ag^{-1} current density. Adapted with permission [25], Copyright (2022), Elsevier

[18]. Courtel et al. fabricated an AMn_2O_4 (A = Zn, Co, and Ni) anode using a co-precipitation technique. A $ZnMn_2O_4$ anode sintered at 800 °C provides a good performance of about 690 mAh g^{-1} at a C/10 rate and retains 88.5% [19]. Likewise, Jiang et al. prepared an amorphous Fe_2O_3 anode, and their SEM image is shown in Fig. 2a. As shown in Fig. 2b, the anode delivers 1600 mAh g^{-1} of reversible charge–discharge capacity over 500 cycles at 1000 mA g^{-1}. In this case, the anode yields good electrochemical behavior and unique capacitive storage [20]. However, the Li^+ penetration in the anode material causes volume expansion, which leads to poor cyclic performance. Some electrochemical mechanisms contribute to these performance issues. Since oxygen has a low atomic weight, lithium can react with a small amount of oxygen to form lithium oxide, which deposits on the surface of metals and alloy materials. Anodes made of alloys exhibit low Li^+ diffusion rates, thus trapping and preventing lithiation/de-lithiation from being reversible. During cycling, the current collector and the active material become electrically insulated due to their dramatic volume changes. This case more often occurs in the electrode material when Li^+ ions are de-lithiated [21]. Studying composites of metal oxides, such as those doped with carbon, improves electrical conductivity and reduces volume expansion [22].

3.2 Metal Sulfides

Recent research has focused on metal sulfides as anodes for LIBs with high specific capacities, a long life, and low redox potential. During charge/discharge reactions,

sulfide compounds have higher electrochemical reversibility than oxide materials. Its dazzling superiority in high theoretical specific capacity and easily controlled morphology have attracted great attention. Compared to metal oxides, metal sulfides have better conductivity; the bond between M and S in sulfides is weaker than the bond between M and O in oxides, which may favor conversion [23]. Like metal oxides, metal sulfides are also classified into three types: (a) intercalation, (b) conversion, and (c) alloying [16]. A combination of intercalation and conversion is generally attributed to metal sulfide lithiation/de-lithiation. Anodes made from transition metal sulfides usually accommodate lithium ions by conversion reactions lower than 1.5 V versus Li/Li^+, in contrast to intercalation electrodes in graphite. Compared to an intercalation mechanism-based compound, conversion reactions may deliver a greater energy density. Metal sulfides are also safer than graphite anodes because their voltage platform is usually well above 1 V, which prevents lithium dendrite formation. In addition to accommodating volumetric expansion upon lithium storage, the layered metal sulfides will also mitigate strain experienced during conversion or alloy reactions, improving cycling stability.

Nguyen et al. enhanced the performance of LIBs by decorating MoS_2 with B_2O_3 nanoparticles via a sintering technique, and the decorated material exhibits a stable capacity of 500 mAh g^{-1} after the first cycle [24]. Similarly, Zhang et al. synthesized self-assembled V_3S_4 nanosheets, as shown in Fig. 2c. Here, the nanosheets accelerate ion and electron migration while alleviating the volume changes. Further, at 0.1 A g^{-1}, it exhibits the remarkable performance of 1099.3 mAh g^{-1} and at 5 A g^{-1}, it attains the superior rate capability of 588.8 mAh g^{-1}, as shown in Fig. 2d [25]. Anodes containing $Fe_{1-x}S$ were synthesized by Xiao et al. and have high theoretical capacity, low cost, and excellent electrochemical conversion mechanisms. Here, the carbon-free anode shows long cycle life and high tap density. Building blocks and nanosheets are assembled in intertexture, which results in excellent performance, according to scientists. During the first cycle of discharge/charge, electrode materials expand significantly. Moreover, side reactions with electrolytes and the loss of active materials can result in poor performance. Further, these lead to cracking, disconnection from the current collectors, and fracture, which pave the way for capacity fading [26]. In this context, a combination of three strategies is often used to overcome these disadvantages: compositing, mitigating crystallite size, and nano-structuring.

4 Metal–Carbon Composites

4.1 Metal Oxide/Sulfide with CNT Composites

Metal oxides or sulfides were anchored on CNT surfaces to make 1D CNT-metal oxide/sulfide composites. High-rate capability is achieved by transferring ions or electrons between the metals and CNTs. Additionally, the spacing between the networks may prevent aggregation by buffering volume variations of metal oxides/

sulfides. Synthesis methods like coprecipitation, sol–gel, thermal decomposition, hydrothermal methods, etc. aid in the fabrication of CNTs. Consequently, metal oxides like SnO_2 [27], Fe_2O_3 [28], TiO_2 [29], NiO [30], and some ferrite materials, and metal sulfides like CoS_2 [31], SnS_2 [32], and MoS_3 [33] have been successfully anchored on CNT surfaces.

Among the metal oxides reported, SnO_2 is among the most popular for combining with CNTs. SnO_2, with a theoretical capacity of 781 mAh g^{-1} is being developed as a potential replacement for graphite. But high-volume changes due to continuous charge–discharge cause electrical contact loss and mechanical failure. Thus, many researchers have been focusing on overcoming this stress from volume change by using carbon support in SnO_2. Using ethylene glycol as a solvent, Ren et al. developed a SnO_2-CNT electrode. Here, the glycol, with a boiling point of 197.3 °C, acts as a stabilizer, an agglomeration prohibitor, and a limiter of particle growth. As shown in Fig. 3a, b, the SnO_2 was deposited over the MWCNTs. With a capacity of 500 mAh g^{-1}, it provides superior cycling stability for 300 cycles. It was attributed to the strong adhesion of SnO_2 nanocrystals on CNT, which has high electronic conductivity and flexibility [27]. Furthermore, Ban et al. fabricated a flexible meso-Fe_2O_3 layer on a conductive CNT-supporting skeleton using PI (meso-Fe_2O_3/PI/CNT). The ternary nanocomposite materials were designed by sequentially assembling the materials and dehydrating them at high temperatures. At 0.1 C, it attains a specific capacity of 708.9 mAh g^{-1}, and at 1 Ag^{-1}, it retains 95.6 mAh g^{-1} over 3000 cycles [28]. Likewise, Yuan et al. in 2022 investigated Cu–ZrO_2–TiO_2/CNTs as anode materials. Here, the presence of Zn^{4+}, Ti^{3+}, metal copper, and oxygen vacancies enhances the electrical conductivity and improves the porous structure of the material, which has a discharge capacity of 351 mAh g^{-1} at 100 mAg^{-1} and retains 92% after 200 cycles [29]. Similarly, Zhang et al. synthesized biochar-CNT-NiO electrodes via a simple air oxidation method for LIBs. Compared with biochar-NiO, the biochar-CNT-NiO composite attains 674.6 mAh g^{-1} and remains stable even after 100 cycles, as shown in Fig. 3c, d. Biochar-NiO-CNT, with its unique structure and CNT presence, make an electrode that attains this high capacity. This composite enhances the conductivity, promotes secondary electrolyte interface (SEI) formation, and mitigates the volume expansion [30].

Metal sulfides have attracted more attention due to their excellent specific capacities, but their poor cyclability due to Li^+ insertion and extraction has hindered their advancement and application in Li rechargeable batteries. Thus, combining metal sulfides with CNT will rectify these problems. Xu et al. assembled an interwoven CoS_2/CNT/graphene composite via a facile hydrothermal reaction. The well-designed architecture of 2D graphene creates a highly porous, flexible, and highly conductive network that prevents CoS_2 nanoparticles from aggregation and enhances the contact area between the electrolyte and composite anode. Additionally, for electron transfer and ionic diffusion, CoS_2 in the composite undergoes volume expansion during charge/discharge, which is accommodated by sufficient channels. Furthermore, at 100 mA g^{-1}, it delivers a discharge capacity of 993 mAh g^{-1} and a rate performance of 212 mAh g^{-1} under 2000 mA g^{-1} [31]. Likewise, a SnS_2/CNT composite with SnS_2 nanosheets growing along the CNTs via in-situ sulfuration in

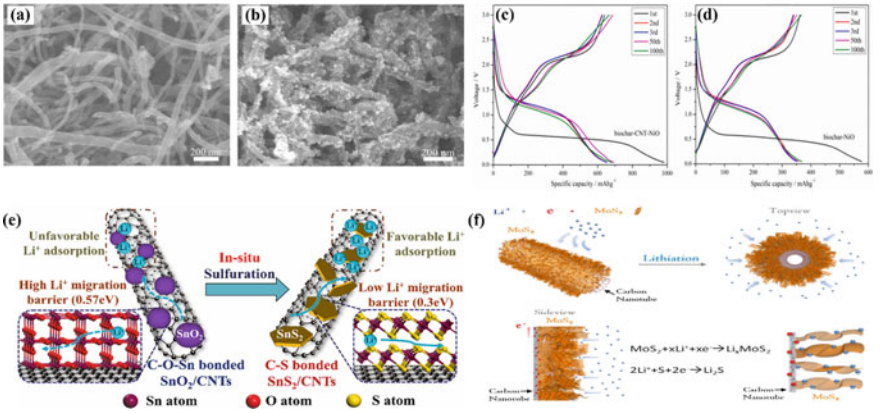

Fig. 3 SEM images of **a** MWCNTs and **b** SnO_2-CNT composite. Adapted with permission [27], Copyright (2011), Elsevier. Galvanostatic charge–discharge curves of **c** biochar-CNT-NiO and **d** biochar-NiO electrodes. Adapted with permission [30], Copyright (2021), Elsevier. **e** Advantage comparison of SnS_2/CNTs with SnO_2/CNTs in lithium storage. Adapted with permission [32], Copyright (2021), Elsevier. **f** Schematic representation of electron and lithium-ion diffusion with less resistance. Adapted with permission [33], Copyright (2013), Springer Nature

a liquid environment with excellent cycling and rate performances was fabricated by Cheng et al. According to density functional theory (DFT), hexagonal SnS_2 has a lower Li^+ migration barrier and adsorption energies when compared with tetragonal SnO_2, thus suggesting Li^+ transfer and storage in the SnS_2/CNT electrodes are much easier, as shown in Fig. 3e [32]. At 200 °C, Shi et al. synthesized a MoS_x/CNT ($2 < x > 3$) via a high-throughput solvent thermal method. In this case, MoS_2 layers have weak van der Waals interactions, so Li^+ ions diffuse (Fig. 3f) without much volume expansion, preventing the pulverization of active materials due to repeated lithiation and de-lithiation. Moreover, the designed hierarchical structure with increased layer distance and maximum surface has resulted in less strain and a low intercalation barrier of Li ions, ensuring high lithium storage capacities in reversible configurations, stable cycling lifetimes, and excellent rates [33].

4.2 Metal Oxide/Sulfide with CNF Composites

Composite anodes based on CNF have been extensively used in recent decades. Even though CNTs and CNFs provide continuous conducting paths for electrons and Li^+. A CNF matrix differs from a CNT matrix in that CNFs are typically encapsulated with active materials, which buffer their volume changes during cycling. Active materials like SnO_2, CoO, MoO_2, Fe_2O_3, WO_x, MnO_x, WS_2, and MoS_2 have been encapsulated into CNFs. The composites (metal oxide or sulfide/CNF) are generally synthesized by electrospinning with subsequent carbonization. Shen et al. developed

a Sn–SnO_2-CNF@C electrode via carbonization and low-temperature hydrothermal treatment. Composites have been used directly as anodes without polymer binders or electrical conductors being added. The carbon coating prevents the electrode from side reactions with the electrolyte, improves the electrical conductivity, and reduces volume changes. This material shows improved rate capability and enhanced cycling stability in the composite electrodes. Due to the protective carbon coating and the 3D CNF membrane, the Sn-SnO_2 particles exhibit improved electrochemical properties [34]. Chen et al. designed 2D CoO/Co/C nanosheets by adopting CNF precursors. At 10 Ag^{-1}, it delivers a good performance of 500 mAh g^{-1} and an outstanding cyclic performance of 800 cycles at 2 Ag^{-1} [35]. Also, the transition molybdate metals have been studied as LIB anodes. Wang et al. reported a low-cost lithium molybdate composited with CNFs via a sol–gel technique. Here, the lithium molybdate ($LiMoO_4$) is a shot-rod nanoparticle that gets tightly wound in the CNFs. At 100 mA g^{-1}, it attains a discharge capacity of 830 mAh g^{-1} and maintains 760 mAh g^{-1} over 100 cycles. Lithiation of $LiMoO_4$@CNF transforms it into $Li_{2+x}MoO_4$, followed by a phase transition into $Li_{0.98}MoO_2$ at low potentials. At last, the $Li_{0.98}MoO_2$ is further transformed into Li_2O and MO. Here, the CNFs bind the broken $LiMoO_4$ microcrystals during cycling, which enhances the composite's electrochemical performance [36]. Similarly, Guo et al. confined MXene nanofibers/CNF with MnO_x via electrospinning and subsequent carbonization. During charging and discharging, the MnO_x nanoparticles with fiber confinement effects embedded internally ensure structural stability and enables cyclic fluctuation through dual stabilization strategies. An electrospinning method prevents the MXene flakes from self-restacking by bonding the surface-anchored MnO_x nanoparticles with the nanofibers, which leads to a large surface area and anode-accessible sites [37].

Likewise, Yang et al. synthesized a WO_3@N-doped CNFs electrode by hydrothermal combined with electrospinning, as shown in Fig. 4a, and their SEM images are in Fig. 4b, c. A double 1D structure formed by the embedded WO_3 nanowires and N-CNFs improves the structural stability of the composite significantly. Further, by using this method, nanofibers can provide many active sites for the penetration of lithium ions due to their large surface-to-volume ratio. Here, the poorly conductive WO_3 combined with CNFs improves cyclic performance. At 0.2 Ag^{-1}, it exhibits a discharge capacity of 960 mAh g^{-1} over 300 cycles, and after 1300 cycles, it attains 550 mAh g^{-1} at 2 Ag^{-1}, as shown in Fig. 4d. Because of the synergistic effects of WO_3 nanorods and nitrogen doping in 1D carbon nanofibers, the electrochemical properties are excellent compared to those of most WO_3-based carbon composite materials [38]. Additionally, Chen et al. synthesized MoS_2 nanoflowers that got encapsulated into CNFs containing amorphous SnO_2. Here, the encapsulation is done by facile solvothermal and electrospinning methods, as shown in Fig. 4e and their transmission electron microscope (TEM) images in Fig. 4f, g. After 100 cycles and at 200 mAh g^{-1}, it yields a specific capacity of 983 mAh g^{-1}, and at 2000 mA g^{-1}, it obtains 710 mAh g^{-1} over 800 cycles, as shown in Fig. 4h. SnO_2 and MoS_2 nanoflowers that are present over the conductive CNFs not only enhance electron transfer but also show direct current pathways. Further, the p-n

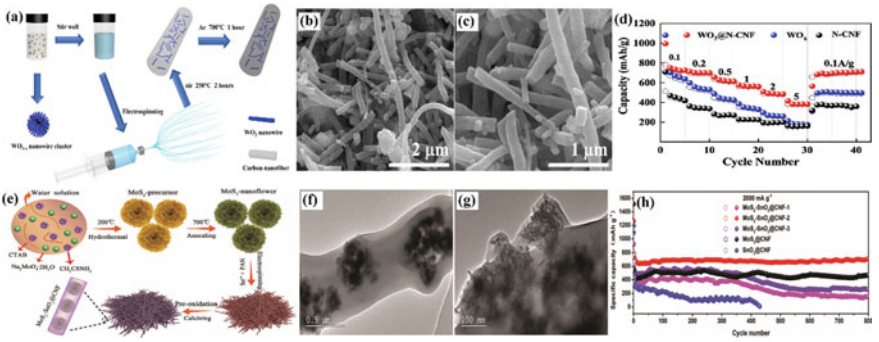

Fig. 4 **a** Synthesis of a double one-dimensional WO_3@CNFs composite; **b**, **c** SEM images of WO_3@CNFs; **d** rate performance of WO_x, N-CNF, and WO_3@N-CNFs electrodes at a different current density. Adapted with permission [38], Copyright (2022), John Wiley and Sons. **e** preparation of MoS_2–SnO_2@CNF composites; **f**, **g** TEM images of MoS_2–SnO_2@CNF composite; **h** cyclic performance of MoS_2–SnO_2@CNF composite at 2000 mA g^{-1} current density. Adapted with permission [39], Copyright (2009), Royal Society of Chemistry

heterogeneous interfaces with 3D interconnected conductive networks could facilitate ion diffusion, enhance mass transfer, and reduce diffusion distances [39]. Wu et al. developed a flexible WS_2@CNFs via a hydrothermal method with an electrospinning process. During extended cycling, WS_2 nanosheets transform into WS_2/W nanoparticles due to kinetic analysis. The capacitive mechanism dominates the Li-ion storage process. In addition to the three-dimensional porous architecture of CNFs and the good conductivity of CNFs, WS_2 nanosheets equiaxed structure during cycling induced an extrinsic capacitive effect, which could explain the superior cycling and rate properties. These nanoparticles also enhance electrochemical conductivity and reversibility, resulting in increased capacity and better cycles [40].

4.3 Metal Oxide/Sulfide with Graphene/Graphite Composites

LIBs with graphene anodes achieve relatively high specific capacities with some drawbacks, including voltage hysteresis, low initial coulomb efficiency, and a lack of plateau potential. The combination of metal oxides/sulfides with graphene offers several advantages, including excellent electrical conductivity, large surface areas, and the prevention of agglomeration of active materials. Lian et al. designed a nano-sized porous SnO_2@C/graphene composite where the carbon reduces nanoparticle aggregation and undesirable reactions. Further, the porous structure facilitates excellent electrolyte diffusion. At 100 mA g^{-1}, the nano-sized electrode exhibits a reversible capacity of 1115 mAh g^{-1} and stabilizes 1015 mAh g^{-1} over 100

cycles. These excellent performances are due to: (a) composites are highly reactive and have a short path for electronic and ionic transport; (b) nanoparticle aggregation is suppressed by carbon shells; and (c) graphene sheets and carbon shells guarantee good electrical conductivity [41]. In Fig. 5a, Liu et al. presented a novel carbon microspheres@SnO_2/reduced graphene electrode composite produced by a facile hydrothermal method and their SEM images in Fig. 5b and c. Here, the SnO_2 surrounds carbon microspheres, while the reduced graphene is shuttled through the outer layers. Due to its high flexibility and abundance of free space at the nanoscale, this composite was less affected by volume variation. In this case, graphene improves the poor electronic conductivity and acts as SnO_2's double protective layer. Here, the low-cost preparation methods also facilitate the practical preparation of SnO_2-based anodes and exhibit a reversibility of 789.5 mAh g^{-1}; over 350 cycles, it retains 68.6% at 200 mA g^{-1}, as shown in Fig. 5d [42]. Xu et al. prepared Fe_2O_3 nanoparticles anchored with multilayer graphene (obtained by ultrasonic exfoliation, which reduces the application cost due to the facile synthesis). Also, the chemical deposition method aids in anchoring Fe_2O_3 nanoparticles on multilayer graphene. On the multilayer graphene surface, dense Fe_2O_3 nanoparticle films are coated uniformly, which can entirely resist the stacking of multilayer graphene grains. As shown in Fig. 5e, this group also worked with anchoring Fe_2O_3 over the graphene oxide and reduced graphene oxide. At 0.1C, the Fe_2O_3/multilayer graphene electrode results in a discharge capacity of 1050 mAh g^{-1} over 100 cycles [43].

Wei et al. synthesized SnO_2@TiO_2 by a facile micro-arc oxidation technique to enhance electrochemical performance. SnO_2 and TiO_2 have a symbiotic structure

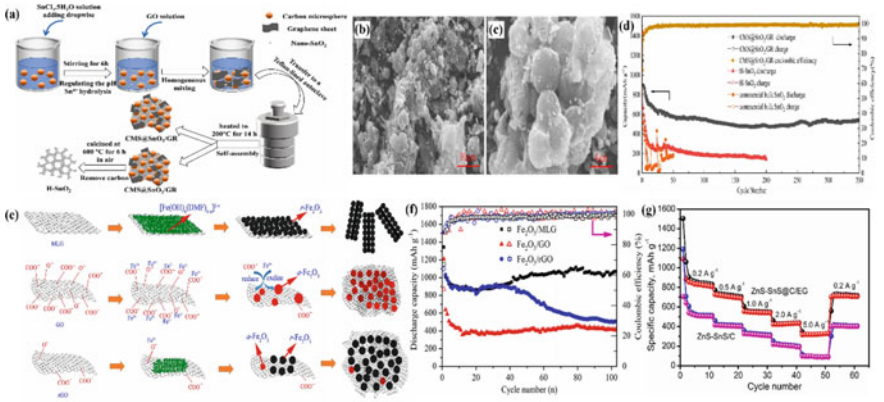

Fig. 5 **a** Preparation method of CMS@SnO_2/GR and H-SnO_2, **b**, **c** SEM images of CMS@SnO_2/GR, and **d** cyclic performance of CMS@SnO_2/GR, H-SnO_2, and commercial bulk SnO_2 at 200 mA g^{-1}. Adapted with permission [42], Copyright (2022), Elsevier. **e** Growth process of multilayer graphene (MLG), graphene oxide (GO), and reduced graphene oxide (rGO) over Fe_2O_3 nanoparticles; **f** Cyclic performance of MLG, Go, and rGO over the Fe_2O_3 composite. Adapted with permission [43], Copyright (2022), Elsevier. **g** Rate capability of ZnS@C/EG and ZnS-SnS/C composite. Adapted with permission [50], Copyright (2021), Elsevier

that allows them to function as active substances and current collectors. During lithiation and de-lithiation, TiO_2 rectifies the volume variation of SnO_2, resulting in a high specific capacity. This composite not only helps to alleviate the vertical directional volume variation but also enhances electron transportation. Also, the composite preparation method demonstrates an economic and facial strategy to synthesize the anode materials [44]. Yang et al. developed a biomass-derived porous carbon/MoO_2@TiO_2 anode for LIBs via the hydrothermal method. Because biomass-derived carbon materials are renewable, abundant, cheap, and environmentally friendly, they have attracted significant attention as LIB anode materials. Further, they display a large surface area, excellent conductivity, and a uniform pore structure. In addition to buffering volume changes during lithiation and de-lithiation, porous carbon anchored MoO_2 and TiO_2 nanoparticles provide a greater active surface area and a more convenient and effective means of transporting and storing lithium ions. Due to the MoO_2 and TiO_2 nanoparticles synergistic effect, the significant volume expansion can be reduced, which provides more active surface area, and lithium-ion storage and transport channels are more convenient and efficient [45]. Rao et al. fabricated a WS_2/MoS_2@carbon microsphere and anchored it to the graphene composite via solvothermal and hydrothermal methods. A conductive carbon structure based on graphene and carbon layers can mitigate electrode pulverization and volume variation. Additionally, the graphene introduction leads to abundant active sites and excellent mechanical stability, with an increase in capacity and cyclic performance. Similarly, these composites in sodium-ion batteries improve cyclic durability [46].

In the same way, graphite has proven to be an outstanding intercalation electrode material in commercial LIBs with a sloping voltage profile and large polarization during intercalation and de-intercalation. Thus, compositing with metal oxides/sulfides delivers a beneficial effect compared with pristine. Xu et al. obtained a MoO_2/graphite oxide anode using a simple solvothermal technique. As the graphite oxide precursor content increases, MoO_3 rods turn into MoO_2 nanorods. These nanorods are gradually distributed on graphite oxide sheets. This group studied the composite with different weight percents of graphite oxide, in which the 10 wt% graphite oxide exhibits good electrochemical properties. At 100 mA g^{-1}, it offers a specific capacity of 726 mAh g^{-1} after 30 cycles. Further, the composite demonstrates high performance, outstanding capacity retention, excellent capacity, and high-rate capability when compared to MoO_2. 2D graphite oxide sheets and MoO_2 nanoparticles in the composite interact strongly, preventing volume expansion and contraction as well as aggregation during charge/discharge [47]. Wang et al. synthesized a Fe_2O_3 and graphite composite via a facile and effective ball milling method. Here, Fe_2O_3 is poor (high volume variation) and leads to an insufficiency in redox reactions. Thus, nanostructured Fe_2O_3 with a large surface-to-volume ratio and carbon material (i.e., graphite) with good electrical conductivity exhibit enhanced performance. Further, due to the close contact between nanocrystalline Fe_2O_3 and graphite, the Fe_2O_3-graphite composites have improved electronic conductivity and minimized volume variation during cycling [48]. Furthermore, Liu et al. prepared a monodisperse MoS_2/graphitic anode with varying compositions. This anode is prepared by mechanical ball-milling and low-temperature annealing. Here, MoS_2 has many advantages, like

low cost, high theoretical capacity, and a unique layered structure. Graphite sheets in this composite reduce particle agglomeration and improve electrical conductivity. In this case, the MoS_2:graphite ratio of 80%:20% shows a discharge capacity of 832.70 mAh g^{-1} [49]. Liang et al. developed hetero-structured SnS-ZnS@C nanoparticles that act as an LIB anode and were embedded over the graphite via a facile and scalable method. In this case, the ZnS-SnS structure not only restricts the nanoparticle agglomeration but also mitigates the charge transfer resistance. In addition to increasing the conductivity of electrodes, expanded graphite buffers ZnS–SnS volume expansion and maintains electrode integrity during cycling. Thus, at 1 A g^{-1}, the nanoparticle composite exhibits a discharge capacity of 517 mAh g^{-1} after 600 cycles and attains a rate capability of 319 mAh g^{-1} at 5 A g^{-1}, as shown in Fig. 5g [50].

5 Conclusion and Perspective

In this featured chapter, we summarize the progress made in research on different anode materials used in LIBs. Each anode and its composition deliver high specific capacity and excellent cyclability. Specifically, combining nanostructured metal oxides/sulfides with carbonaceous matrices can help complement with each other's positive attributes. In general, carbon-based materials that are composited with metal oxides/sulfides have the advantages of charge storage, shorter diffusion paths for ion transport, alleviating volume changes, good electronic and ionic conduction, and mitigating nanoparticle agglomeration. Embedded active materials (e.g., carbon nanotubes, carbon nanofibers, and porous carbon) exhibit various advantages and disadvantages. In this case, graphene composites with metal oxides/sulfides enhance structural stability by preventing the active materials exfoliation and aggregation. As well as three-dimensional CNTs exhibit good mechanical integrity, electrical conductivity, and porosity to accommodate volume changes. Some of the challenges with carbon-composite metal oxides/sulfides include: (a) For LIB applications, understanding the working mechanism of metal oxides/sulfides is crucial; (b) during the first discharge, a SEI forms, resulting in a large irreversible capacity; (c) carbon-based materials focus on specific capacity, capability, and cyclability but do not focus on coulombic efficiency and volumetric energy density. Thus, more attention should be paid to the consideration of fast kinetics. As production scales up, complex, and time-consuming design strategies may also face escalating challenges. Simplified synthesis routes that are customized for industrial needs are necessary for their commercialization. Long-term use of expensive metals is not recommended. Also, it is essential to balance electrochemical performance with structural design when designing a rational carbon-based composite. Research should focus more on structural design and the electrochemical performance of composite structures. As a result, next-generation electrode designs will be optimized, and nanocomposites of carbon and metal oxides/sulfides for energy storage will be vigorously developed. It is essential to develop experimental and theoretical research so that advanced LIBs

with long cycling stability and high rate-capable electrode materials can be made commercially available.

References

1. B. Jeevanantham, Y. Song, H. Choe, M.K. Shobana, Structural and optical characteristics of cobalt ferrite nanoparticles. Mater. Lett.: X **12**, 100105 (2021)
2. B. Jeevanantham, M.K. Shobana, T. Pazhanivel, H. Choe, Pseudocapacitive behaviors of strontium-doped cobalt ferrite nanoparticles for supercapacitor applications. J. Alloy. Compd. **960**, 170651 (2023)
3. B. Jeevanantham, P. Sarathkumar, S. Kavita, M.K. Shobana, Magnesium doped LiNixMnyCozO$_2$ cathode-structural properties. Appl. Surf. Sci. Adv. **12**, 100350 (2022)
4. Y. Yuan, Z. Chen, H. Yu, X. Zhang, T. Liu, M. Xia, R. Zheng, M. Shui, J. Shu, Heteroatom-doped carbon-based materials for lithium and sodium ion batteries. Energy Storage Mater. **32**, 65–90 (2020)
5. L. Li, D. Zhang, J. Deng, Y. Gou, J. Fang, H. Cui, Y. Zhao, M. Cao, Carbon-based materials for fast charging lithium-ion batteries. Carbon **183**, 721–734 (2021)
6. R.N.A.R. Seman, M.A. Azam, A.A. Mohamad, Systematic gap analysis of carbon nanotube-based lithium-ion batteries and electrochemical capacitors. Renew. Sustain. Energy Rev. **75**, 644–659 (2017)
7. H. Zhang, G. Cao, Y. Yang, Carbon nanotube arrays and their composites for electrochemical capacitors and lithium-ion batteries. Energy Environ. Sci. **2**(9), 932–943 (2009)
8. V.A. Agubra, L. Zuniga, D. Flores, J. Villareal, M. Alcoutlabi, Composite nanofibers as advanced materials for Li-ion, Li-O$_2$ and Li-S batteries. Electrochim. Acta **192**, 529–550 (2016)
9. S. Iqbal, H. Khatoon, A.H. Pandit, S. Ahmad, Recent development of carbon based materials for energy storage devices. Mater. Sci. Energy Technol. **2**(3), 417–428 (2019)
10. W. Gao, L.B. Alemany, L. Ci, P.M. Ajayan, New insights into the structure and reduction of graphite oxide. Nat. Chem. **1**(5), 403–408 (2009)
11. X. Lu, X. Jin, J. Sun, Advances of graphene application in electrode materials for lithium ion batteries. Sci. China Technol. Sci. **58**, 1829–1840 (2015)
12. H. Zhang, Y. Yang, D. Ren, L. Wang, X. He, Graphite as anode materials: fundamental mechanism, recent progress and advances. Energy Storage Mater. **36**, 147–170 (2021)
13. B.M. Khan, W.C. Oh, P. Nuengmatch, K. Ullah, Role of graphene-based nanocomposites as anode material for Lithium-ion batteries. Mater. Sci. Eng., B **287**, 116141 (2023)
14. T. Hajilounezhad, R. Bao, K. Palaniappan, F. Bunyak, P. Calyam, & M.R. Maschmann, Predicting carbon nanotube forest attributes and mechanical properties using simulated images and deep learning. npj Comput. Mater. **7**(1), 134 (2021)
15. H.Y. Cheng, Y.A. Zhu, Z.J. Sui, X.G. Zhou, D. Chen, Modeling of fishbone-type carbon nanofibers with cone-helix structures. Carbon **50**(12), 4359–4372 (2012)
16. L. Zhang, H. Wang, X. Zhang, Y. Tang, A review of emerging dual-ion batteries: fundamentals and recent advances. Adv. Func. Mater. **31**(20), 2010958 (2021)
17. H.B. Wu, J.S. Chen, H.H. Hng, X.W.D. Lou, Nanostructured metal oxide-based materials as advanced anodes for lithium-ion batteries. Nanoscale **4**(8), 2526–2542 (2012)
18. M.C. Yang, Y.Y. Lee, B. Xu, K. Powers, Y.S. Meng, TiO$_2$ flakes as anode materials for Li-ion-batteries. J. Power Sources **207**, 166–172 (2012)
19. F.M. Courtel, H. Duncan, Y. Abu-Lebdeh, I.J. Davidson, High capacity anode materials for Li-ion batteries based on spinel metal oxides AMn$_2$O$_4$ (A= Co, Ni, and Zn). J. Mater. Chem. **21**(27), 10206–10218 (2011)
20. Y. Jiang, D. Zhang, Y. Li, T. Yuan, N. Bahlawane, C. Liang, W. Sun, Y. Lu, M. Yan, Amorphous Fe$_2$O$_3$ as a high-capacity, high-rate and long-life anode material for lithium ion batteries. Nano Energy **4**, 23–30 (2014)

21. P.U. Nzereogu, A.D. Omah, F.I. Ezema, E.I. Iwuoha, A.C. Nwanya, Anode materials for lithium-ion batteries: a review. Appl. Surf. Sci. Adv. **9**, 100233 (2022)
22. B. Jeevanantham, M.K. Shobana, Enhanced cathode materials for advanced lithium-ion batteries using nickel-rich and lithium/manganese-rich LiNixMnyCozO$_2$. J. Energy Storage **54**, 105353 (2022)
23. Y. Xiao, S.H. Lee, Y.K. Sun, The application of metal sulfides in sodium ion batteries. Adv. Energy Mater. **7**(3), 1601329 (2017)
24. T.P. Nguyen, I.T. Kim, Boron oxide enhancing stability of MoS_2 anode materials for lithium-ion batteries. Materials **15**(6), 2034 (2022)
25. Y. Zhang, J. Li, H. Li, H. Shi, Z. Gong, T. Lu, L. Pan, Facile self-assembly of carbon-free vanadium sulfide nanosheet for stable and high-rate lithium-ion storage. J. Coll. Interface Sci. **607**, 145–152 (2022)
26. X. Xu, W. Liu, Y. Kim, J. Cho, Nanostructured transition metal sulfides for lithium ion batteries: progress and challenges. Nano Today **9**(5), 604–630 (2014)
27. J. Ren, J. Yang, A. Abouimrane, D. Wang, K. Amine, SnO_2 nanocrystals deposited on multi-walled carbon nanotubes with superior stability as anode material for Li-ion batteries. J. Power Sourc. **196**(20), 8701–8705 (2011)
28. Q. Ban, Y. Liu, P. Liu, Y. Li, Y. Qin, Y. Zheng, Hierarchically nanostructured carbon nanotube/polyimide/mesoporous Fe_2O_3 nanocomposite for organic-inorganic lithium-ion battery anode. Microporous Mesoporous Mater. **335**, 111803 (2022)
29. Y. Yuan, Y. Shao, X. Zhou, An investigation of Cu–ZrO_2–TiO_2/CNTs anode material for lithium-ion batteries. Int. J. Energy Res. **46**(8), 11092–11108 (2022)
30. J. Zhang, A. Tahmasebi, J.E. Omoriyekomwan, J. Yu, Microwave-assisted synthesis of biochar-carbon-nanotube-NiO composite as high-performance anode materials for lithium-ion batteries. Fuel Process. Technol. **213**, 106714 (2021)
31. C. Xu, Y. Jing, J. He, K. Zhou, Y. Chen, Q. Li, J. Lin, W. Zhang, Self-assembled inter-woven CoS_2/CNTs/graphene architecture as anode for high-performance lithium ion batteries. J. Alloy. Compd. **708**, 1178–1183 (2017)
32. Y. Cheng, H. Xie, L. Zhou, B. Shi, L. Guo, J. Huang, In-situ liquid-phase transformation of SnS_2/CNTs composite from SnO_2/CNTs for high performance lithium-ion battery anode. Appl. Surf. Sci. **566**, 150645 (2021)
33. Y. Shi, Y. Wang, J.I. Wong, A.Y.S. Tan, C.L. Hsu, L.J. Li, Y.C. Lu, H.Y. Yang, Self-assembly of hierarchical MoSx/CNT nanocomposites ($2< x< 3$): towards high performance anode materials for lithium ion batteries. Sci. Rep. **3**(1), 1–8 (2013)
34. Z. Shen, Y. Hu, Y. Chen, R. Chen, X. He, X. Zhang, H. Shao, Y. Zhang, Controllable synthesis of carbon-coated Sn SnO_2 carbon-nanofiber membrane as advanced binder-free anode for lithium-ion batteries. Electrochim. Acta **188**, 661–670 (2016)
35. H. Chen, S. Zhang, S. Wu, K. Wang, C. Chen, Y. Chen, W. Chu, Z. Chen, H. Li, H. Liu, Design and synthesis of cellulose nanofiber-derived CoO/Co/C two-dimensional nanosheet toward enhanced and stable lithium storage. J. Colloid Interface Sci. **625**, 915–924 (2022)
36. J. Wang, J. Yao, W. Li, W. Zhu, J. Yang, J. Zhao, L. Gao, Lithium molybdate composited with carbon nanofibers as a high-capacity and stable anode material for lithium-ion batteries. Energy Mater **2**, 200026 (2022)
37. Y. Guo, D. Zhang, Z. Bai, Y. Yang, Y. Wang, J. Cheng, P.K. Chu, Y. Luo, MXene nanofibers confining MnOx nanoparticles: a flexible anode for high-speed lithium ion storage networks. Dalton Trans. **51**(4), 1423–1433 (2022)
38. J. Yang, S. Du, L. Ao, J. Zhang, C. Jin, M. Han, K. Jiang, L. Shang, Y. Li, J. Zhang, L. Zhu, Embedded double one-dimensional composites of WO_3@ N-doped carbon nanofibers for superior and stabilized lithium storage. ChemElectroChem. **9**(2), e202101477 (2022)
39. H. Chen, J. He, G. Ke, L. Sun, J. Chen, Y. Li, X. Ren, L. Deng, P. Zhang, MoS_2 nanoflowers encapsulated into carbon nanofibers containing amorphous SnO_2 as an anode for lithium-ion batteries. Nanoscale **11**(35), 16253–16261 (2019)
40. L. Zhang, W. Fan, T. Liu, Flexible hierarchical membranes of WS_2 nanosheets grown on graphene-wrapped electrospun carbon nanofibers as advanced anodes for highly reversible lithium storage. Nanoscale **8**(36), 16387–16394 (2016)

41. P. Lian, J. Wang, D. Cai, L. Ding, Q. Jia, H. Wang, Porous SnO_2@ C/graphene nanocomposite with 3D carbon conductive network as a superior anode material for lithium-ion batteries. Electrochim. Acta **116**, 103–110 (2014)
42. Y. Liu, X. Liu, X. Zhang, X. Miao, Y. Wang, P. Wang, A novel carbon microspheres@ SnO_2/reduced graphene composite as anode for lithium-ion batteries with superior cycle stability. Ceram. Int. **48**(13), 18625–18634 (2022)
43. J. Xu, D. Xu, J. Wu, J. Wu, J. Zhou, T. Zhou, X. Wang, J.P. Cheng, Ultra-small Fe_2O_3 nanoparticles anchored on ultrasonically exfoliated multilayer graphene for LIB anode application. Ceram. Int. **48**(21), 32524–32531 (2022)
44. B. Wei, S. Yan, D. Jia, C. Feng, J. Yin, Z. Wang, Preparation of SnO_2@ TiO_2/Graphene by micro-arc oxidation as an anode material for lithium ion batteries. Inorg. Chem. Commun. **145**, 110048 (2022)
45. L. Yang, Z. Niu, C. Wang, Z. Liu, X. Feng, Preparation and electrochemical performance of biomass-derived porous carbon/MoO_2@ TiO_2 composite as anode materials for lithium-ion batteries. Solid State Ionics **389**, 116110 (2023)
46. Y. Rao, J. Wang, P. Liang, H. Zheng, M. Wu, J. Chen, F. Shi, K. Yan, J. Liu, K. Bian, C. Zhang, Heterostructured WS_2/MoS_2@ carbon hollow microspheres anchored on graphene for high-performance Li/Na storage. Chem. Eng. J. **443**, 136080 (2022)
47. Y. Xu, R. Yi, B. Yuan, X. Wu, M. Dunwell, L. Fei, S. Deng, P. Andersen, D. Wang, H. Luo, High capacity MoO_2/graphite oxide composite anode for lithium-ion batteries. J. Phys. Chem. Lett. **3**(3), 309–314 (2012)
48. Y. Wang, L. Yang, R. Hu, L. Ouyang, M. Zhu, Facile synthesis of Fe_2O_3-graphite composite with stable electrochemical performance as anode material for lithium ion batteries. Electrochim. Acta **125**, 421–426 (2014)
49. B. Liu, F. Li, H. Li, S. Zhang, J. Liu, X. He, Z. Sun, Z. Yu, Y. Zhang, X. Huang, F. Guo, Monodisperse MoS_2/graphite composite anode materials for advanced lithium ion batteries. Molecules **28**(6), 2775 (2023)
50. Q. Liang, L. Zhang, M. Zhang, Q. Pan, L. Wang, G. Yang, F. Zheng, Y. Huang, H. Wang, Q. Li, Heterostructured SnS-ZnS@ C nanoparticles embedded in expanded graphite as advanced anode materials for lithium ion batteries. Chem. Phys. Lett. **775**, 138662 (2021)

Surfactant-Assisted Pseudocapacitive Materials for Li-Ion Batteries

Wan Mohd Abd Kalam, Hong Ngee Lim, Izwaharyanie Ibrahim, and Chuan Yi Foo

Abstract Lithium-ion batteries (LIBs) are broadly accustomed in many electrical devices, such as electric vehicles (EVs) and hybrid electric vehicles (HEVs). The selection of Li-based pseudocapacitive materials in LIBs has become the main focus of numerous research efforts to commercialize LIBs with great features, including good environmental compatibility, low-cost consumption, and most importantly, great electrochemical properties (capacity, open-circuit voltage, rate capability, life cycle, energy density, and power density). Unfortunately, the pseudocapacitive materials are not capable of standing alone without any external supportive materials due to their downsides, which are low electronic conductivity, low Li ion diffusivity, and poor cycling stability. Therefore, surfactants, also known as surface-active agents, are introduced in the active materials of LIBs to develop excellent electrochemical performance, as successfully presented in many reported articles. The properties of surfactants can promote a strong interaction between the particles with the advantages of physical captivity and chemical encapsulation, which enable adjusting the performance stability of Li-based pseudocapacitive materials. Herein, we disclose in detail the synthesis methods and structural morphology involved in achieving the high electrochemical performance of LIBs based on surfactant-assisted pseudocapacitive materials perspectives.

Keywords Lithium-ion battery · Surfactant · Pseudocapacitive materials · Li-based · Cathode

W. M. A. Kalam · H. N. Lim (✉) · I. Ibrahim
Functional Nanotechnology Devices Laboratory, Institute of Nanoscience and Nanotechnology, Universiti Putra Malaysia (UPM), 43400 Serdang, Selangor, Malaysia
e-mail: hongngee@upm.edu.my

H. N. Lim
Department of Chemistry, Faculty of Science, Universiti Putra Malaysia (UPM), 43400 Serdang, Selangor, Malaysia

C. Y. Foo
School of Energy and Chemical Engineering, Xiamen University Malaysia, 43900 Sepang, Selangor Darul Ehsan, Malaysia

College of Chemistry and Chemical Engineering, Xiamen University, Xiamen 361005, China

© The Author(s), under exclusive license to Springer Nature Switzerland AG 2024

R. K. Gupta (ed.), *Pseudocapacitors*, Engineering Materials,
https://doi.org/10.1007/978-3-031-45430-1_17

1 Introduction

Lithium-ion batteries (LIBs) are now the most sought-after power source for energy storage systems due to their exceptional qualities, including their high energy density, high power density, longevity, and environmental friendliness. In comparison to lead-acid (Pb-acid), nickel–cadmium (Ni–Cd) and nickel-metal hydride (Ni-MH) batteries, LIBs are another form of secondary battery that has been modified with qualified properties. The extensive use of LIBs in a variety of electrical equipment, including electric vehicles (EVs) and hybrid electric vehicles (HEVs), is entirely due to the conductivity of electrode materials. Typically, LIBs are built with positive electrodes (cathode) and negative electrodes (anode), which are separated by the electrolyte solution through a selective membrane. The ions are moved from the anode to the cathode during the charging process, whereas the ions are moved from the cathode to the anode during the discharging process. In a rechargeable energy storage system, these processes are actively repeated.

Pseudocapacitive materials like transition metal oxides, metal hydroxide, metal nitride metal sulfides and conducting polymer are among the active materials that have received the most attention in recent research because of their ability to conduct faster ion diffusion and good rate capability, providing higher energy density and higher power density to the battery [1]. Li-based pseudocapacitive materials and LIBs have worked together to establish a notable strategy to enhance battery performance by employing the active materials as cathodes. To mention a few, layered lithiated transition metal oxide, manganese spinel and olivine materials are the most dominant materials in the development of current LIBs. The layered lithiated transition metal oxide materials such as $LiCoO_2$ have been used on a large scale of manufacture despite of their potential high toxicity due to the cobalt (Co) element residues [2]. The manganese spinel materials are produced for commercial purposes with more affordable production, but the low durability and inadequate storage system have shown to be the unfavorable characteristics for long-term usage. The Olivine-structured materials such as $LiFePO_4$ are reliable materials, owing to their great theoretical capacity, high open-circuit voltage, excellent chemical and thermal stability, great environmental compatibility, and low cost of production [3]. However, these materials have significant drawbacks, including low electronic conductivity and slow Li ion diffusivity, which prevent efficient charging/discharging processes [3]. As a result, Li-based pseudocapacitive materials cannot totally solve the degradation of battery capacity, which has become a critical problem for LIBs.

The researchers have made numerous remarkable contributions to the improvement of electrochemical performance, promoting better pseudocapacitive materials of LIBs. One of the noteworthy works is combining the Li-based pseudocapacitive materials with surfactants, which introduces a strong physical and chemical interaction between the particles to control the stability of electrochemical performance [4]. Surfactants are also referred to as surface-active agents that are formed by the chemically self-arranging molecules to create aggregates, which are able to minimize the

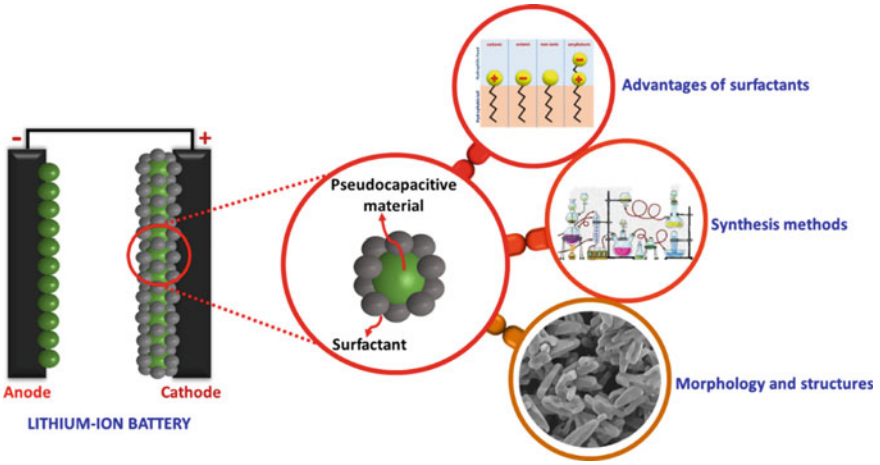

Fig. 1 Illustration of surfactant-assisted pseudocapacitive materials in LIBs

interfacial tension between two immiscible phases, such as oil and water. Accordingly, the formation of particles yields a different type of structures that has affected the electrochemical performance of batteries, depending on the methods used for material preparation. This chapter will present the studies of Li-based pseudocapacitive materials with the assistance of surfactants for performance enhancement of LIBs, as illustrated in Fig. 1. The advantages of surfactants in energy storage devices are further discussed to comprehend the importance of surfactant-assisted pseudocapacitive materials in LIBs. Besides, the synthesis methods for surfactant-assisted materials are demonstrated, including solvothermal, hydrothermal, sol–gel and solid-state methods, to reveal the outcomes obtained based on an overview of many type of structures, such as rod-like, plate-like and spherical-like structures.

2 Properties and Advantages of Surfactants in Active Materials of LIBs

Surfactants are formulated in many daily supplies such as cleaning products and detergents, as well as cosmetics and pharmaceutical products. The presence of surfactants in the formulation mobilised and integrated the molecular properties of materials with diverse phases (water, oil, solvents, and fats) in order to break down the chemical barriers, molecular weight and surface tension [5]. The positive characteristics of surfactants have opened up a huge possibility to collaborate on the development of pseudocapacitive materials for battery application. Due to the ability to combine the molecular characteristics, the aggregation between the surfactants and materials would result in better protected structures of the active components.

Surfactants are composed by molecules with a lower surface tension, possessing a hydrophobic tail (non-polar group) and a hydrophilic head (polar group). The properties of common non-polar group hydrophobicity are decreasing based on the following order of hydrocarbon groups [6]:

alkyl > alkylene > aryl radical with alkyl chain > aryl radical > $-CH_2-CH_2-CH_2O-$

Interestingly, surfactants are able to alter the particle–surface interaction forces that involved van der Waals force, electrostatic force and hydrophobic force, depending on the type of molecules. Besides, surfactants are the self-assembled molecular clusters that adsorbed to the interface between a solution, which enabled to insist and direct the formation of structural molecules with other particles, including pseudocapacitive materials. The electrochemical performance of LIBs is significantly impacted by morphological structures of battery materials.

There are four classification of surfactants: cationic, anionic, non-ionic and amphoteric surfactant, as shown in Fig. 2a. The charges of hydrophilic head are corresponded to the functional group of molecules, where the cationic surfactant has a positive charge, the anionic surfactant has a negative charge, the non-ionic surfactant has no charge, and the amphoteric surfactant has both positive and negative charges. Cetyltrimethylammonium bromide (CTAB) are the most popular example of cationic surfactants that consist a quaternary ammonium compound and a different alkyl group, as their polar and non-polar groups, respectively. To attract the negatively charged group, these surfactants are widely used in industrial production, including fabric softeners, hair conditioners, corrosion inhibitors, and emulsifiers. Instead, anionic surfactants, which are mostly suitable for high cleansing applications like detergent and shampoo, are linked to the positively charged particles in the presence of water. The examples of anionic surfactants are sodium dodecylsulfonate (SDS), and sodium dodecylbenzenesulfonate (SDBS), which are typically applied for industrial dispersion. In addition, non-ionic surfactants are long chain polymers that are distinctly not coupled with any charged functional groups, even if there is water present. The non-ionic surfactants are commercially available with low toxicity and biodegradable features, such as poly (alkylene-oxide) block copolymers, sorbitan esters and oleic acid. Amphoteric surfactants are also known as zwitterionic surfactants because they have a positive charge and a negative charge, which uniquely can change according to the pH of the surrounding solution, transforming the surfactants into anionic in an alkaline solution and cationic in an acidic solution. Betaine surfactants are the most famous amphoteric surfactants, but they are rarely applied in energy storage application. Generally, different types of surfactants are used for different objectives, such as emulsification, dispersion, foaming and defoaming, corrosion inhibition and many more.

In battery applications, surfactants are introduced with cathode active materials to increase the rate of ions diffusivity by encouraging the formation of surfactant micelles, which amplifies the electrochemical activity [7]. A surfactant micelle is produced from colloidal particles by the self-assembled aggregation of hydrophilic head segments and hydrophobic tail segments, as displayed in Fig. 2b. At a critical

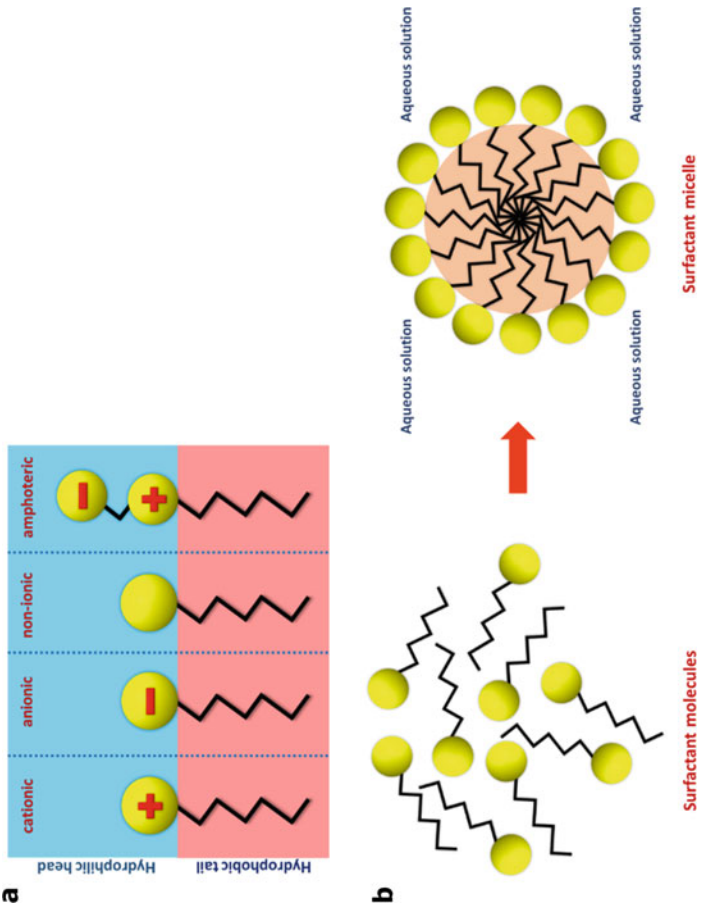

Fig. 2 **a** Classification of surfactants. **b** Formation of a surfactant micelle

micelle concentration (CMC), surfactant micelles form and maintain physical and chemical stability, depending on the factors involved, such as synthesis methods, solvent types, analytical methodologies, and more [8]. The utilisation of surfactant enables to facilitate the interfacial interaction between the particles, assisting the surface modification to increase the surface area of molecules, which in turn enhances the rate of ion diffusion of materials [9]. Surfactants can also be associated with silicon-based composites to develop a selective assembly method for LIBs. The cationic surfactants, such as CTAB, are able to selectively assemble the molecules due to their hydrophobic properties, which resulted in a homogeneous dispersion of silicon (Si) through electrostatic interaction [10]. Besides, the use of non-ionic surfactant, such as Triton-X100, with Si-based composites has demonstrated that Si particles are evenly distributed and encapsulated, improving the surface area of active materials and maintaining their structural stability [11]. These approaches have successfully increased the molecule sizes based on surface modification that has facilitated the Li ion transportation in LIBs [11]. Furthermore, surfactants can be acted as additive agents, for an instance, to stop the active materials of LIBs from combining with citric acid [12]. As a result, by linking citric acid and CTAB surfactant, an appropriate space has been created for lithiation/delithiation process to take place between the electrodes [12]. The surfactants as additive agents are capable to adjust the phase composition, morphological uniformity and particles crystallinity, depending on the quantity of surfactants employed in the system [12]. Therefore, the presence of surfactants helps to explain the interactive behaviour among the particles in the active materials of LIBs, which exhibited excellent electrochemical performance.

3 Synthesis Methods of Surfactant-Assisted Pseudocapacitive Materials

Li-based pseudocapacitive materials can be produced using a variety of surfactant-assisted synthesis techniques, such as solvothermal, hydrothermal, sol–gel, and solid-state methods, but these processes must be carried out under the right conditions because they may lead to different types of particle structures. The preparation methods enable the components to respond appropriately in response to variables like temperature, time, pressure and so on. Surfactants must also be introduced in the proper circumstances and directed to the necessary structures for batteries to perform more effectively based on the structures engineering. Some of the notable studies of surfactant assisted Li-based pseudocapacitive materials of LIBs based on the synthesis methods are summarised in Table 1.

Table 1 Surfactant assisted Li-based pseudocapacitive materials of LIBs based on the synthesis methods

Li-based pseudocapacitive materials	Type of surfactants	Synthesis methods	Solvents	Specific capacity (mAh g^{-1})	Capacity retention	References
$LiFePO_4$/C	CTAB (cationic)	Solvothermal 180 °C 6 h	Ethylene glycol	163 at 0.1C	99.2% after 200 cycles	[13]
$LiMnPO_4$/C	CTAB (cationic)	Solvothermal 190 °C 24 h	Water-DEG	148.6 at 0.1C	92.7% after 500 cycles	[14]
$Li_3V_2(PO_4)_3$/C	CTAB (cationic)/ Pluronic® P123 (non-ionic)/Tween® 20 (non-ionic)	Solvothermal 120 °C 24 h and 180 °C 24 h	Water–ethanol	112 at 2C	97.1% after 1000 cycles	[15]
$LiFePO_4$	SDS (anionic)	Hydrothermal 200 °C 6 h	Water	165 at 0.1C	–	[16]
$LiNi_{1/3}Co_{1/3}Mn_{1/3}O_2$-$V_2O_5$	SDBS (anionic)	Hydrothermal 170 °C 12 h	Water	101.7 at 10C	89.12% after 100 cycles at 0.5C	[17]
$Li[Li_{0.2}Ni_{0.2}Mn_{0.6}]O_2$	CTAB (cationic)/PVP (non-ionic)/SDBS (anionic)	Hydrothermal 160 °C 12 h	Water	270 at 0.1C	89.5% after 200 cycles at 1C	[18]
C-$Li1_{.05}FePO_4$	Oleic acid (non-ionic)	Sol–gel 160 °C 5 h	Ethanol	155 at C/3	–	[19]
LFP/C	Block copolymer (non-ionic)	Sol gel 70 °C 24 h	Tetrahydrofuran (THF)	160 at 0.1C	92% after 1000 cycles at 1C	[20]
$Li_4Ti_5O_{12}$-LTO	CTAB (cationic)	Sol–gel 70 °C 24 h	Ethanol-acetic acid	176 at C/15	92% after 30 cycles	[21]

(continued)

Table 1 (continued)

Li-based pseudocapacitive materials	Type of surfactants	Synthesis methods	Solvents	Specific capacity (mAh g^{-1})	Capacity retention	References
$LiFe_{0.5}Mn_{0.5}PO_4/C$	Oleic acid (non-ionic)	Solid-state 400 RPM 4 h	Ethanol	155 at 0.1C	94.8% after 500 cycles at 1C	[22]
$LiMnPO_4/C$	Oleic acid (non-ionic)	Solid-state	Paraffin	117 at 1C	–	[23]

PVP Polyvinylpyrrolidone

3.1 Solvothermal Methods

The adaptive process of solvothermal synthesis is frequently used to precisely regulate the well-defined morphological structures based on their size distribution, shape, and crystalline phases [24]. This kind of synthesis is carried out in sealed containers, like Teflon-lined stainless steel autoclaves, where the chemical reactions are conducted in a solvent at temperatures above the boiling point and pressures above 1 bar, which are able to promote the solubility and reactivity of the reagents [24]. Numerous non-water based solvents, such as ethanol, methanol, ammonia, hydrochloric acid, hydrofluoric acid are commonly employed in the process. Solvothermal process is one of the most efficient ways to prepare pseudocapacitive materials, which involves fine-tuning the structures with surfactant adsoption by using the selected solvents and inducing the high crystallinity diffraction patterns [25].

The methods can also be used for synthesis of pseudocapacitive materials and surfactants to stimulate the crystallisation process through the self-assembly mechanism. The addition of surfactants to a $LiFePO_4$ precursor solution with ethylene glycol solvent has shown high crystallinity of $LiFePO_4$ composites, accelerating the rate of capability and stabilising the cycling performance [13]. The aid of surfactant like CTAB has served to control the particles growth and inhibit an agglomeration of molecules, enlarging the specific surface area of Li-based pseudocapacitive materials, such as $LiMnPO_4$ composites [13, 14]. Besides, the solvothermal routes has played the roles to regulate the crystal orientation, control the particle sizes, and promote the carbon-coating, thus benefiting the electrochemical performance of LIBs [14]. Some of the studies has compared the significant effects of surfactants in electrochemical performance of LIBs based on pseudocapacitive composites by using solvothemal methods. The presence of cationic surfactants in the composites has generated a superior charge/discharge capacity with an improved cycling stability to the battery performance [14]. Moreover, the tailoring technique of surfactants has demonstrated well-defined cluster of microstructures through the formation of micelles, presenting better electrons pathway for ions migration for higher rate capability of LIBs [15, 26]. Surfactants also can be applied as structure-directing agents to create the core and shell regions, contributing larger particle sizes for ions conductivity [27]. In addition, the reaction of anionic surfactant and solvent under a high temperature of heating has developed the growth of Li-based materials that avoids the agglomeration of particles, which has exhibited high crystallinity of nanocomposite [28].

3.2 Hydrothermal Methods

Hydrothermal synthesis is analogous to solvothermal synthesis that must be carried out in a sealed container at high temperatures (100–250 °C) and high vapour pressures. The term of ‘hydrothermal’ clarifies water or aqueous solution is employed

as the solvent, which distinguishes it from a solvothermal process. This simple technique is another way to generate composites with controlled and maintained size, shape, porosity and composition. It also offers advantages, such as environmental friendliness, cost effectiveness, and improved the performance due to better solution dispersion [29].

Additionally, hydrothermal methods are commonly used to synthesize olivine composites, which also enable to produce well-crystallized compounds with high surface areas, similar as solvothermal methods. The large surface areas are important properties of psuedocapacitive materials to give high probability of electrons transportation and ions diffusion through the infiltration area of Li-based composites, making the hydrothermal is essential way for the synthesis [30]. The synthesis process also has achieved the desired morphologies that adjusted in the system. The assistance of SDS surfactant in a two-step hydrothermal process has developed high surface area of rhombohedral olivine structures with crystalline appearance that presented high discharged capacity of battery [16]. Other than that, the hydrothermal route has created a homogenous precipitation with a surfactant as the additive agent, which allowed the formation of crystalline particles by modifying the structural patterns [31]. The uniformity of structures can also be controlled through the stable formation of surfactant micelles. In other research, the surfactant-assisted hydrothermal reaction has been utilized for in-situ coating with the purpose of ions doping and surface modification of Li-based pseudocapacitive materials, such as the vanadium pentoxide (V_2O_5) coating in $LiNi_{1/3}Co_{1/3}Mn_{1/3}O_2$ cathode materials [17]. The technique has provided good dispersibility and uniform structures that accelerated rate of Li ion diffusion, where the coating effect had successfully reduce the electrolyte side reaction in the LIBs system [17]. Hydrothermal methods has also resulted different morphological structures, depending on the types of surfactant added in the solution, cationic, anionic, or non-ionic surfactants. The cationic surfactants have contributed small particle sizes with the most defined distribution that had shorten the pathway of Li ion transportation to generate the largest Li^+ diffusion coefficient and the smallest charge transfer resistance, producing excellent electrochemical performance of LIBs [18].

3.3 Sol–gel Methods

Sol–gel methods are another approach that managed effective routes to synthesize nanoparticles with high stability and high surface areas through the formation of a colloidal particle suspension in a solvent. The word ‘sol’ is referred to the dispersion of colloidal solid particles at maximum stability, whereas the word ‘gel’ is referred to three-dimensional (3D) network of solid particles in hydrolysis and condensation processes that has interlinked between solid phase and liquid phase. Sol–gel methods are common methods that used in a large scale manufacture due to the competency of controlling the materials composition at low temperatures with high purity level, making them suitable for surfactant-assisted synthesis [32].

Sol–gel routes are specified in many studies for carbon-coating process, which are collaborated to intensify electric and ionic conductivity of nanocomposites by controlling the uniform distribution of particles and modifying the nanoparticles proportion [33]. The non-ionic surfactants, like long chain polymers (i.e. oleic acid and PVP) are mostly applied in sol–gel methods to act as a carbon source, covering the active materials and minimizing the average particle sizes to reduce the Li ions path for a rapid ions diffusion [19]. Besides, the non-ionic surfactants has prevented the aggregation between the colloid particles and carbon by forming hydrogen bonds to obtain uniform small grains porous structure that had enhanced the electronic conductivity of pseudocapacitive nanomaterials [34]. The formation of non-ionic surfactant micelles has polymeric components with high molecular weight, operating as the surface-directing agents to yield a self-assembled aggregation to produce carbon-coated nanocomposites [20]. The other type of surfactants, such as anionic and cationic surfactants are also applied for the pseudocapacitive materials preparation with different purposes. The anionic surfactant, like lauric acid has served as blocking agents in sol–gel methods to inhibit the colloid agglomeration because the gel formation has produced a large amount of free hydroxyls that expanded the particle size distribution, resulting inhomogeneity of solution [35]. The surfactants has also managed the high dispersibility of solution, promoting better element doping process to Li-based materials without structure alteration, giving a good protection of active materials to maintain the cycling stability of LIBs [35]. A subsequent evaluation is also studied on cationic surfactant, like CTAB based on sol–gel synthesis, which provides well-dispersed particles orientation through the formation of phase pure, boosting high Li storage capacity for LIBs [21].

3.4 Solid-State Methods

Solid-state methods are utilized occasionally in preparation of Li-based cathode active materials, involving the chemical decomposition reactions of solid reactants through annealing and milling steps at high temperatures that depend on reactants properties, reaction conditions, and thermodynamic free energy. These methods are relatively inexpensive and facile approaches for nanomaterials preparation, including Li-based pseudocapacitive materials. The chain size of surfactants has influenced the surfactant-assisted synthesis in solid-state reaction. The alkyl C–C chain length in surfactants able to initiate the space steric effect, reducing the particle sizes of active materials as the chain length increases [36]. The smaller particles of composites has established a uniform distribution with stronger space steric effects that had ensured the high surface energy and kinetic reaction, contributing well-maintained Li-based molecules with shorter pathway of Li ion diffusion [36]. The surfactants in solid-state reaction are also supported the element substitution by decreasing the particle sizes as well, in which the synthesized Li-based materials have efficiently taken place the Li insertion and extraction that exhibited high specific capacity and high conductivity with excellent rate performance [22]. Besides, the alkyl chain length of surfactants

has generated a better surface capping to form a dictated nanocrystal pattern, which has also performed a surface-coating to avoid excessive agglomeration of particles, upgrading the electrochemical behaviour of the particles [23].

4 Structural Morphologies of Surfactant-Assisted Psedocapacitive Materials

The structures of pseudocapacitive materials are extensively explored due to their excellent characteristic and properties for use in electronics. The above-mentioned approaches have led to a number of different morphologies and structures of Li-based pseudocapacitive composites, which have potentially enhanced the electrochemical performance of LIBs. The most well-known structural morphologies will be discussed, including rod-like, plate-like and spherical-like structures, to study the importance of surfactants in fabrication of the achieved structures of LIBs cathode materials. The reported works of surfactant-aided pseudocapacitive composites synthesis are presented in Table 2, based on their structures.

4.1 Rod-Like Structures

Rod-like structures are one-dimensional (1D) structures that are applicable for many uses, including functional carriers, polymer composites, colloidal agents, and adsorbents due to their physical characteristics. Rod-like structures have a large surface area to facilitate the ions transportation and exhibit high stability of rate capability of LIBs [37]. The presence of surfactants has regulated the development rod-like structures and controlled the particles orientation of active materials.

The addition of surfactants in carbon-coated Li-based nanorods has promoted a better cycle performance of LIBs. The nanorods are developed by self-assembling properties of surfactants that displayed a better monodipersibility and good particle sizes distribution [42]. The surfactants have also stimulated the crystallization process of nanorods to favour the Li ion diffusion for high rate performance [42]. Moreover, the structures are able to withstand the electrolytes corrosion during charging/discharging process has become another alternative to overcome one of the downsides of Li-based pseudocapacitive materials, assisting the fast Li ions transportation of LIBs [37]. The external parameters of surfactant, like concentrations, temperatures and time have also influenced the thickness of rod-shaped Li-based materials. Increasing the surfactant concentrations has slightly stretched the particle shapes and lowering the concentrations has produced thinner rod-shaped structure, in which the thinner rod structures generated excellent yields of active materials that has improved the electrochemical performance [43]. Higher temperature (about 240–270 °C) and longer reaction time have developed the most compatible and the best condition of

Table 2 Surfactant assisted Li-based pseudocapacitive materials of LIBs based on their structural morphologies

Li-based pseudocapacitive materials	Type of surfactants	Type of structures	Type of synthesis methods	Specific capacity ($mAh\ g^{-1}$)	Capacity retention	References
LiV_3O_8	Pluronic-F127 (non-ionic)	Rod-shaped 0.5–1.0 μm (ø) 4–6 μm (length)	Sol–gel	292.0 at 1C	80.5% after 500 cycles	[37, 24]
$LiFePO_4$	SDBS (anionic)	Nanorods ~200 nm (ø) 1–2 μm (length)	Solvothermal	150 at 1C	88% after 50 cycles	[38]
$LiMnPO_4{\cdot}Li_3V_2(PO_4)_3/C$	Oleic acid (non-ionic)	Nanorods 40–100 nm (ø) 300–500 nm (length)	Solid-state	101.3 at 16C	79.39% after 4000 cycles at 4C	[39]
$LiNi_{1/3}Co_{1/3}Mn_{1/3}O_2$	Span 85 (non-ionic)	Nanoplates ~50 nm (length) ~3 nm (thickness)	Sol–gel	165 at 2C	98.2% after 200 cycles	[40]
$LiMnPO_4/C$	Oleic acid (non-ionic)	Plate-like 1–2 μm (length) ~50 nm (thickness)	Solid-state	117 at 1C	–	[23]
$LiMnPO_4/C$	CTAB (cationic)	Nanoplates 13 nm (thickness)	Solvothermal	148.6 at 0.1C	92.7% after 500 cycles	[14]
$LiFePO_4/C$	CTAB (cationic)	Hollow micro-spheres 1.2 μm (ø)	Solvothermal	163 at 0.1C	99.2% after 200 cycles	[13]
$Li(Li_{0.167}Mn_{0.5}\text{-}Co_{0.167}Ni_{0.167})O_2$	PEG-600 (non-ionic)	Spheres 200–250 nm (ø)	Hydrothermal	142 at 10C	–	[41]

PEG-600 Polyethylene glycol-600

nanorod structures, which have generated higher surface areas of active materials to manage higher discharged capacity and higher rate capability of LIBs [43]. The excellent yields of rod-shaped structures are also created with spaces between the neighbouring particles, supplying more open areas to penetrate the electrolyte for electron transportation of great LIBs performance [39]. Thus, longer rod-shaped morphologies of Li-based pseudocapacitive materials provide higher surface areas for better electrical performance of LIBs.

4.2 Plate-Like Structures

Plate-like structures are classified as notable structures that can be produced using a variety of synthesis techniques and environmental factors, modifying the structural morphologies in accordance. These structures are widely used in a wide range of application, including energy generators, sensors, solar cells, and detectors. The self-assembling structures using surfactant-assisted synthesis are suitable techniques to yield Li-based plate structures for improvement of high electrochemical performance in LIBs.

During the formation of plate-like structures, the surfactant micelles has surrounded the active material ions based on their charges to inhibit the growth of molecules and prevent the agglomeration that produced conductive particle sheets [18]. Then, the particle sheet planes are broaden and widen by strong electrostatic repulsion under heat treatment to form plate-like structures, making the designed surfactants and temperatures have played the important roles in generating plate-like structures [18]. Surfactant-aided pseudocapacitive materials, such as $LiMnPO_4$ composites require high heating and sintering temperatures (about 300–400 °C) to form a very stable and maintained plate structures during ions transportation [23]. The surfactant-capped active materials have oriented into plate-shaped structures by self-assembling process without particles agglomeration under very high temperatures [23]. The morphology modification of plate-like structures has expanded the contact areas of pseudocapacitive composites, accommodating the Li ion transportation between the electrodes to enhance the specific capacity of LIBs [40]. Besides, the thickness of plate structures has impacted the distance of Li ion pathways, in which lowering the thickness of plate structures has shorten the distance that benefitted the electrochemical performance [14]. The thickness of these structures are also effected by the temperatures or heating rates, where the higher temperature has created lower thickness of plates structure as it has widen the surface areas and structures are sustained in the presence of surfactants [44]. Hence, the plate-like structures with broader surface area and lower thickness are favourable structures for Li-based pseudocapacitive materials, which are capable to decrease Li ion transportation paths and facilitate the ions diffusion that led to high specific capacity and rate capability of LIBs.

4.3 Spherical-Like Structures

Spherical-like structures are fabricated with typical sizes between 10 and 200 nm in diameter, however they can be occasionally developed depending on the properties and conditions applied to the particles, such as stability, homogeneity of solution, and compatible active materials. The sphericals are capable to efficiently sustain the interaction between active materials and electrolyte by reducing the Li ion pathway due to the formation of porosity that are influenced by particle sizes and synthesis process [45]. The properties of sphericals are consequently has induced the conductivity of active composites. The surfactant-assisted approaches are also effectively established the spherical-like structures in preparation of Li-based pseudocapacitive materials.

The surfactants have acted as structure-directing agents to prepare hollow and porous interior of Li-based composites, producing a uniform distribution of spherical particles that are controlled by the surfactants [13]. The spherical structures are normally hollowed sphere structures with a vacant space inside, which created the porosity properties of sphericals that increased the specific area of active materials and led to faster ions diffusion [24]. The porous structure of sphericals have contributed well-dispersed of high crystallized particles with reduced particle sizes that improved the distribution consistency of Li-based spherical structures, comparing to the particles with non-presence of surfactant [13]. The good dispersion effect provides stability of molecules that has successfully prevented the irregular accumulation and agglomeration during growth of crystalline spherical structures [46]. The spherical morphologies are mostly formed by electrostatic interaction of surfactant micellar shells to protect the active materials from agglomeration [46]. Other than that, the surfactant-assisted synthesis, such as hydrothermal methods has positively affected the development of spherical structures that are proficient to narrow the particle sizes distribution [41]. The association of surfactant in precursor solution has increased the solution viscosity to give a homogeneous solution with better dispersion of particles. The surfactant-associated solution has underwent a high temperature (about 180 °C) for self-assembling of Li-based spheres by maintaining the structures and providing the best composition of spherical structure [41]. The bigger particle size distributions (200 nm–1 μm) are oppositely obtained without hydrothermal process, depleting the electrochemical performance of LIBs [13, 41]. Hence, the smaller particle size distributions of spherical-like structures are highly proposed to employ as Li-based pseudocapacitive cathode materials, resulting higher specific areas for Li ions diffusion, shorter distance for ions transportation, and faster Li ions diffusion that led to excellent electrochemical performance of LIBs.

5 Conclusion

In conclusion, the studied based on surfactant-assistant Li-based pseudocapacitive materials have a wide range of applications in diverse synthesis methods and structural morphologies to achieve excellent electrochemical performance of LIBs. The surfactants are mostly adaptable to Li-based cathode active materials because of their physical and chemical properties. The compatibility of surfactants and pseudocapacitive materials has significantly intensified the reversible cycling stability of LIBs, depending on the required parameters, including surfactant concentrations, designed temperatures, and operation time.

Acknowledgements The authors acknowledge the financial support from the Fundamental Research Grant Scheme (FRGS) FRGS/1/2021/STG05/UPM/01/1 awarded by the Ministry of Higher Education of Malaysia (MOHE).

References

1. M. Goswami, S. Kumar, H. Siddiqui, V. Chauhan, N. Singh, N. Sathish, M. Ashiq, S. Kumar, Hybrid energy storage devices: Li-ion and Na-ion capacitors, in *Emerging Trends in Energy Storage Systems and Industrial Applications* (Elsevier, 2023), pp. 223–258
2. Y. Nancharaiah, S.V. Mohan, P. Lens, Biological and bioelectrochemical recovery of critical and scarce metals. Trends Biotechnol. **34**, 137–155 (2016)
3. M. Mastali, M. Farkhondeh, S. Farhad, R.A. Fraser, M. Fowler, Electrochemical modeling of commercial $LiFePO_4$ and graphite electrodes: kinetic and transport properties and their temperature dependence. J. Electrochem. Soc. **163**, A2803 (2016)
4. F. Sun, Y. Zhang, J. Zhang, X. Yan, X. Liu, L. Wang, Preparation of ultrafine iron phosphate micro-powder from phosphate slag, in *MATEC Web of Conferences*, *EDP Sciences* (2018), p. 02002
5. M. Chen, S. Jiang, S. Cai, X. Wang, K. Xiang, Z. Ma, P. Song, A.C. Fisher, Hierarchical porous carbon modified with ionic surfactants as efficient sulfur hosts for the high-performance lithium-sulfur batteries. Chem. Eng. J. **313**, 404–414 (2017)
6. M. Miyake, Y. Yamashita, Molecular structure and phase behavior of surfactants. Cosmet. Sci. Technol. 389–414 (2017)
7. K. Naoi, Y. Oura, M. Maeda, S. Nakamura, Electrochemistry of surfactant-doped polypyrrole film (I): formation of columnar structure by electropolymerization. J. Electrochem. Soc. **142**, 417 (1995)
8. M. Joseph, H.M. Trinh, A.K. Mitra, Peptide and protein-based therapeutic agents, in *Emerging Nanotechnologies for Diagnostics, Drug Delivery and Medical Devices* (Elsevier, 2017), pp. 145–167
9. X. Liu, J. Lu, J. Jiang, Y. Jiang, Y. Gao, W. Li, B. Zhao, J. Zhang, Enhancing lithium storage performance by strongly binding silicon nanoparticles sandwiching between spherical graphene. Appl. Surf. Sci. **539**, 148191 (2021)
10. J. Jang, H. Kim, H. Lim, K. jae Kim, H.-G. Jung, S.O. Kim, W. Choi, Surfactant-based selective assembly approach for Si-embedded silicon oxycarbide composite materials in lithium-ion batteries. Chem. Eng. J. **401**, 126091 (2020)
11. T.K. Pham, J.H. Shin, N.C. Karima, Y.S. Jun, S.K. Jeong, N. Cho, Y.W. Lee, Y. Cho, S.N. Lim, W. Ahn, Application of recycled Si from industrial waste towards Si/rGO composite material for long lifetime lithium-ion battery. J. Power. Sources **506**, 230244 (2021)

12. H. Torkashvand, M. Bagheri-Mohagheghi, Synthesis of Si/rGO nano-composites as anode electrode for lithium-ion battery by CTAB and citrate: physical properties and voltage–capacity cyclic characterizations. J. Mater. Sci. Mater. Electron. **32**, 16456–16466 (2021)
13. Y. Liu, J. Zhang, Y. Li, Y. Hu, W. Li, M. Zhu, P. Hu, S. Chou, G. Wang, Solvothermal synthesis of a hollow micro-sphere $LiFePO_4$/C composite with a porous interior structure as a cathode material for lithium ion batteries. Nanomaterials **7**, 368 (2017)
14. W. Zhang, Z. Shan, K. Zhu, S. Liu, X. Liu, J. Tian, $LiMnPO_4$ nanoplates grown via a facile surfactant-mediated solvothermal reaction for high-performance Li-ion batteries. Electrochim. Acta **153**, 385–392 (2015)
15. S. Yu, A. Mertens, H. Kungl, R. Schierholz, H. Tempel, R.A. Eichel, Morphology dependency of $Li_3V_2(PO_4)_3$/C cathode material regarding to rate capability and cycle life in lithium-ion batteries. Electrochim. Acta **232**, 310–322 (2017)
16. S. Bolloju, R. Rohan, S.-T. Wu, H.X. Yen, G.D. Dwivedi, Y.A. Lin, J.T. Lee, A green and facile approach for hydrothermal synthesis of $LiFePO_4$ using iron metal directly. Electrochim. Acta **220**, 164–168 (2016)
17. M. Yuan, Y. Li, Q. Chen, C. Chen, X. Liu, W. Zeng, R. Wang, S. Xiao, Surfactant-assisted hydrothermal synthesis of V_2O_5 coated $LiNi_{1/3}Co_{1/3}Mn_{1/3}O_2$ with ideal electrochemical performance. Electrochim. Acta **323**, 134822 (2019)
18. H. Zhou, Z. Yang, C. Yin, S. Yang, J. Li, Fabrication of nanoplate Li-rich cathode material via surfactant-assisted hydrothermal method for lithium-ion batteries. Ceram. Int. **44**, 20514–20523 (2018)
19. K. Bazzi, M. Nazri, V. Naik, V. Garg, A. Oliveira, P. Vaishnava, G. Nazri, R. Naik, Enhancement of electrochemical behavior of nanostructured $LiFePO_4$/Carbon cathode material with excess Li. J. Power. Sources **306**, 17–23 (2016)
20. M.G. Fischer, X. Hua, B.D. Wilts, E. Castillo-Martínez, U. Steiner, Polymer-templated $LiFePO_4$/C nanonetworks as high-performance cathode materials for lithium-ion batteries. ACS Appl. Mater. Interfaces **10**, 1646–1653 (2018)
21. C. Sandhya, B. John, C. Gouri, Surfactant-assisted sol–gel route to lithium titanate and its electrochemical properties. J. Alloys Compd. **655**, 238–243 (2016)
22. X. Zhou, Y. Xie, Y. Deng, X. Qin, G. Chen, The enhanced rate performance of $LiFe_{0.5}Mn_{0.5}PO_4$/C cathode material via synergistic strategies of surfactant-assisted solid state method and carbon coating. J. Mater. Chem. A **3**, 996–1004 (2015)
23. D. Choi, D. Wang, I.-T. Bae, J. Xiao, Z. Nie, W. Wang, V.V. Viswanathan, Y.J. Lee, J.-G. Zhang, G.L. Graff, $LiMnPO_4$ nanoplate grown via solid-state reaction in molten hydrocarbon for Li-ion battery cathode. Nano Lett. **10**, 2799–2805 (2010)
24. R.S. Mane, V. Jadhav, *Spinel Ferrite Nanostructures for Energy Storage Devices* (Elsevier, 2020)
25. H. Yang, X.-L. Wu, M.-H. Cao, Y.G. Guo, Solvothermal synthesis of $LiFePO_4$ hierarchically dumbbell-like microstructures by nanoplate self-assembly and their application as a cathode material in lithium-ion batteries. J. Phys. Chem. C **113**, 3345–3351 (2009)
26. Y. Yao, X. Huang, D. Zhou, B. Yang, W. Ma, F. Liang, Surfactant assisted synthesis of rod-like $LiFePO_4$/C composite with cluster texture as cathode material for lithium ion batteries. Int. J. Electrochem. Sci. **14**, 2442–2451 (2019)
27. M.-Y. Cho, Y.S. Lim, S.-M. Park, K.-B. Kim, K.C. Roh, Size-tunable tavorite $LiFe(PO_4)(OH)$ microspheres with a core–shell structure. CrystEngComm **17**, 6149–6154 (2015)
28. J. Wang, Y. Niu, Y. Fu, Y. Yang, M. Hojamberdiev, Urea and ethylene glycol-assisted solvothermal synthesis of spheroidal $LiFePO_4$/C nanoparticles as a cathode material for lithium-ion batteries. ChemistrySelect **3**, 5471–5479 (2018)
29. A.K. da Silva, T.G. Ricci, A.L. de Toffoli, E.V.S. Maciel, C.E.D. Nazario, F.M. Lanças, The role of magnetic nanomaterials in miniaturized sample preparation techniques, in *Handbook on Miniaturization in Analytical Chemistry* (Elsevier, 2020), pp. 77–98
30. G. Du, Y. Xi, X. Tian, Y. Zhu, Y. Zhou, C. Deng, H. Zhu, A. Natarajan, One-step hydrothermal synthesis of 3D porous microspherical $LiFePO_4$/graphene aerogel composite for lithium-ion batteries. Ceram. Int. **45**, 18247–18254 (2019)

31. J. Wang, S. Zheng, H. Yan, H. Zhang, M. Hojamberdiev, B. Ren, Y. Xu, Na2EDTA-assisted hydrothermal synthesis and electrochemical performance of $LiFePO_4$ powders with rod-like and block-like morphologies. Mater. Chem. Phys. **160**, 398–405 (2015)
32. S. Prasad, V. Kumar, S. Kirubanandam, A. Barhoum, *Engineered nanomaterials: nanofabrication and surface functionalization, emerging applications of nanoparticles and architecture nanostructures* (Elsevier, 2018), pp.305–340
33. Y. Zhang, P. Xin, Q. Yao, Electrochemical performance of $LiFePO_4$/C synthesized by sol-gel method as cathode for aqueous lithium ion batteries. J. Alloys Compd. **741**, 404–408 (2018)
34. C. Fan, Q. Li, S. Chen, J. Fan, Z. Wen, T. Zeng, X. Zhang, S. Han, Poly (vinylpylrrolidone) as surfactant in the sol-gel preparation of lithium iron phospate/carbon cathodes for lithium-ion batteries. Energ. Technol. **4**, 973–979 (2016)
35. Y. Gao, L. Li, H. Peng, Z. Wei, Surfactant-assisted sol–gel synthesis of nanostructured ruthenium-doped lithium iron phosphate as a cathode for lithium-ion batteries. ChemElectroChem **1**, 2146–2152 (2014)
36. Q. Li, F. Zheng, Y. Huang, X. Zhang, Q. Wu, D. Fu, J. Zhang, J. Yin, H. Wang, Surfactants assisted synthesis of nano-$LiFePO^4$/C composite as cathode materials for lithium-ion batteries. J. Mater. Chem. A **3**, 2025–2035 (2015)
37. Z. Chen, F. Xu, S. Cao, Z. Li, H. Yang, X. Ai, Y. Cao, High rate, long lifespan LiV_3O_8 nanorods as a cathode material for lithium-ion batteries. Small **13**, 1603148 (2017)
38. F. Teng, M. Chen, G. Li, Y. Teng, T. Xu, S.-I. Mho, X. Hua, Synergism of ionic liquid and surfactant molecules in the growth of $LiFePO_4$ nanorods and the electrochemical performances. J. Power. Sources **202**, 384–388 (2012)
39. X. Cao, A. Pan, Y. Zhang, J. Li, Z. Luo, X. Yang, S. Liang, G. Cao, Nanorod-nanoflake interconnected $LiMnPO_4{\cdot}Li_3V_2(PO_4)_3$/C composite for high-rate and long-life lithium-ion batteries. ACS Appl. Mater. Interfaces **8**, 27632–27641 (2016)
40. W. Pi, T. Mei, Z. Zhang, X. Li, J. Wang, J. Li, X. Wang, Synthesis of disk-like $LiNi_{1/3}Co_{1/3}Mn_{1/3}O_2$ nanoplates with exposed (001) planes and their enhanced rate performance in a lithium ion battery. CrystEngComm **19**, 442–446 (2017)
41. J. Fan, G. Li, D. Luo, C. Fu, Q. Li, J. Zheng, L. Li, Hydrothermal-assisted synthesis of Li-rich layered oxide microspheres with high capacity and superior rate-capability as a cathode for lithium-ion batteries. Electrochim. Acta **173**, 7–16 (2015)
42. L. Bao, G. Xu, X. Sun, H. Zeng, R. Zhao, X. Yang, G. Shen, G. Han, S. Zhou, Mono-dispersed $LiFePO_4$@C core-shell [001] nanorods for a high power Li-ion battery cathode. J. Alloys Compd. **708**, 685–693 (2017)
43. N.H. Kwon, K.M. Fromm, Enhanced electrochemical performance of <30 nm thin $LiMnPO_4$ nanorods with a reduced amount of carbon as a cathode for lithium ion batteries. Electrochim. Acta **69**, 38–44 (2012)
44. C. Min, X. Ou, Z. Shi, G. Liang, L. Wang, Effects of heating rate on morphology and performance of lithium iron phosphate synthesized by hydrothermal route in organic-free solution. Ionics **24**, 1285–1292 (2018)
45. Y. He, A. Li, C. Dong, C. Li, L. Xu, Mesoporous tin-based oxide nanospheres/reduced graphene composites as advanced anodes for lithium-ion half/full cells and sodium-ion batteries. Chem. A Eur. J. **23**, 13724–13733 (2017)
46. J. Guo, M. Yu, F. Wu, Preparation of high purity iron phosphate based on the advanced liquid-phase precipitation method and its enhanced properties. J. Solid State Chem. **287**, 121346 (2020)

Pseudocapacitive Materials for Metal-Sulfur Batteries

Yogita Dahiya, Shivani Agarwal, Manoj Kumar, Debasish Sarkar, and Ankur Jain

Abstract Alkali metal-sulfur batteries have developed profound interest among researchers due to their high theoretical energy density (>2500 Wh kg^{-1}). However, their commercial exploitation potential is hindered due to the lower electronic conductivity of sulfur and other discharging products, deteriorating polysulfide shuttling, and substantial volume variations during discharging. Pseudocapacitive materials can address these issues. Their superior intrinsic properties, such as higher electronic conductivity, better ionic conduction, and abundant functional groups that, trap polysulfides and make them suitable candidates for batteries. Pseudocapacitive materials such as layered transition metal oxides (TMOs), phosphides (TMPs), chalcogenides (TMCs), MXenes, etc. have the metal center acting as Lewis's entity to attract polysulfide anions. In contrast, the anionic species, such as oxides/phosphides and chalcogens, react with metal ions (Li, Na, and K) to provide the synergetic effect. This chapter discusses the benefits of using these materials for metal-sulfur batteries and associated challenges in a detailed manner.

Keywords Pseudocapacitive materials · Metal-sulfur batteries · Shuttling effect · Hierarchical composites · MXenes

Y. Dahiya · M. Kumar · D. Sarkar
Department of Physics, Malaviya National Institute of Technology Jaipur, Jaipur, Rajasthan 302017, India

S. Agarwal
Department of Physics, JECRC University, Jaipur, India

A. Jain (✉)
Centre for Renewable Energy and Storage, Suresh Gyan Vihar University, Jaipur, Rajasthan 302017, India
e-mail: ankur.j.ankur@gmail.com

Natural Science Centre for Basic Research and Development, Hiroshima University, Higashi-Hiroshima, Japan

© The Author(s), under exclusive license to Springer Nature Switzerland AG 2024

R. K. Gupta (ed.), *Pseudocapacitors*, Engineering Materials,
https://doi.org/10.1007/978-3-031-45430-1_18

1 Introduction

In modern society, electrochemical energy storage (EES) systems such as batteries, fuel cells, and supercapacitors have been vastly employed in now-ubiquitous portable electrical devices and electrified transport. Pursuing sustainable energy storage technologies and renewable alternatives is a global research target to cater to growing energy demands. Among the batteries, group IA alkali metal-sulfur batteries (M-S batteries, M = Li, Na, K) hold enormous potential towards electrified transport to succeed conventional lithium-ion batteries because of their ability to provide appealing energy density and power density at a comparatively lower cost [1, 2]. In metal-sulfur batteries (Li–S and Na–S), the cathode comprises sulfur incorporated in the host matrix/framework coupled with the metal anode. Sulfur is an encouraging candidate as cathode material for next-generation metal-batteries owing to its environmental friendliness, abundance, high theoretical capacity (1673 mAh g^{-1}), and remarkable specific energy density (2500 Wh kg^{-1}, 2.15 V) [3]. In these batteries, sulfur follows a two-electron redox reaction and possesses much higher theoretical capacity than conventional intercalation cathodes in lithium-ion batteries due to the involvement of sulfur [4, 5]. While opportunities for metal-sulfur batteries abound, their performance is limited due to low sulfur utilization, lower rate performance, and inferior cyclic performance because of slow redox kinetics associated with metal polysulfides and the shuttling of these entities through the electrolyte. To resolve these problems, efficient sulfur hosts are required that may capture polysulfides and facilitate faster reaction kinetics. Traditionally, carbon-based sulfur composite electrodes include carbon nanotubes (CNTs) [6], graphene [7], fullerene [8] and porous carbon [9]. However, due to the non-polar nature of the carbon matrix, its binding energy with lithium polysulfides (LIPSs) is low, which eases the desorption of LiPSs. In addition, the conversion of polysulfides over carbon is sluggish. In such circumstances, pseudocapacitive materials have turned out to be the best performers to boost the performance of metal sulfur batteries and tap the energy density potential. Various categories of pseudocapacitive materials include layered transition metal oxides (TMOs) [9], phosphides (TMPs) [10], chalcogenides (TMCs) [11], conducting polymers [12], MXenes [13] and compounds derived from various metal-organic frameworks (MOFs) [14]. These materials inherently possess sufficient internal spaces that help in capturing polysulfides. The metal centers in such compounds act as Lewis's entities to attract polysulfide anions. In contrast, the anionic species, such as oxides/phosphides and chalcogens, act with metal ions (Li, Na, and K) to provide the synergetic effect [15]. Their properties, such as good electronic conductivity, favorable porous/layered structure, high specific area, and richer redox active sites, boost the reduction of long-chain polysulfides. Further, the porous framework of compounds such as TMCs and MOF-based materials can accommodate strains, produced during cycling [16].

In this chapter, we have comprehensively covered the fundamentals of the charge–discharge mechanism in alkali metal-sulfur batteries, their inherent limitations, followed by a discussion on critical progress in designing robust cathodes using pseudocapacitive materials. The mechanism underlying the preferential absorption of polysulfides due to polar interactions is systematically discussed. We have summarised strategies to tune the physiochemical properties of pseudocapacitive materials using defect engineering, heteroatom doping, composites/heterostructure designing, and phase engineering in respective sections. The further mechanisms underlying the anchoring of sulfides and catalyzing due to Lewis's acid–base pairs depend upon specific coordination environments concerning a probable structure–property relationship is highlighted.

2 Metal-Sulfur Batteries

Metal-sulfur batteries use elemental sulfur as a cathode coupled with metallic anodes (Li, Na, and K), as shown in Fig. 1a. Generally, sulfur is combined with diverse host materials such as carbon, TMOs, TMCs, conducting polymers (CPs), MOFs, their derivatives, etc., due to its insulating nature and absence of crystal or cage-like structure of sulfur that can accommodate ions. This section mainly focus on mechanisms related to Li–S batteries. Various other categories of existing M-S batteries using alkalis or other high-valent metals follow similar chemistry as Li–S batteries. Electrochemically, the reactions of S cathodes involve multi-step conversion reactions accompanying complex phase transfer of LIPSs during discharging [17]. In general, Sulfur (S_8) dissociates to bind with lithium ions from electrolytes and catches electrons from external circuits, and subsequently reduces into intermediate poly sulfides (Li_2S_n, $3 < n < 8$). Further, these intermediate polysulfides ultimately transform into Li_2S (Overall reaction: $16\,Li^+ + S_8 + 16\,e^- \rightarrow 8\,Li_2S$), providing a high theoretical capacity of 1672 mAh g^{-1}, energy density of 2600 Wh kg^{-1} and volumetric energy density of 3600 Wh L^{-1}. Figure 1b shows the general charge–discharge profile of a standard metal-sulfur battery. During discharging, at the first discharge plateau (potential range 2.15–2.4 V), intermediate lithium polysulfide (LiPSs) chains are formed, including Li_2S_8 to Li_2S_6. Then the intermediate polysulfides transform to Li_2S_4 involving 0.5 electron transfer per sulfur atom in the potential range 2.15–2.4 V with theoretical capacity 418 mAh g^{-1} [18, 19]. At lower potential (2.1 V), Li_2S_4 transforms into Li_2S_2/Li_2S featuring 1.5 electron transfer and providing a theoretical capacity of 1255 mAh g^{-1}. High-order polysulfides (Li_2S_n, $3 < n < 8$) which are highly soluble in nature, diffuse towards the anode to get reduced at the Li-metal surface, where they get reduced into low-order sulfides (Li_2S_2 and Li_2S). During charging, short-order sulfides, predominantly insoluble in nature, return to the cathode to oxidize in long-chain sulfides [20]. This process degrades the active material, leading to serious repercussions such as capacity fading, excessive consumption of electrolytes, and decay in coulombic efficiency. Thus, boosting the conversion reactions kinetics of long-chain polysulfides into short-chain during discharging

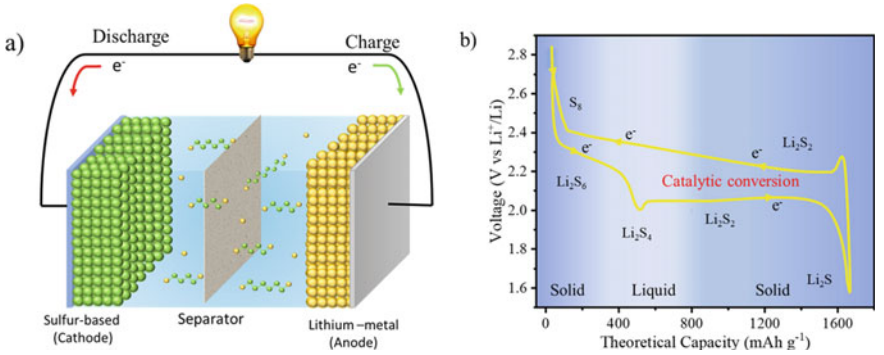

Fig. 1 **a** Schematics showing the configuration of Li–S battery composed of a sulfur-based cathode, lithium anode; **b** Typical charge–discharge profile for Li–S batteries

would inhibit the dissolution and improve the battery's performance. Unlike intrinsically intercalation-based cathode hosts, sulfur being a conversion-based cathode, needs an additional host to store and immobilize the mobile redox polysulfides. Despite having high surface area and good conductivity, conversion reactions with non-polar carbon nanomaterials are slow and partial due to the physical confinement of LiPSs, poor catalytic performance, and sluggish diffusion. Therefore, introducing catalysts in electrode material is suggested to boost the conversion kinetic of long-chain LiPSs into Li_2S_2/Li_2S. Catalytic conversion on conducting and polar entities are faster and complete due to faster diffusion and high catalytic performance [18].

Na–S and K–S batteries are also in trend with Li–S batteries as they are cost-effective, and a high abundance of sodium and potassium makes them suitable for large-scale practical applications. However, theoretical capacities for Na and K are 1166 and 664 mAh g^{-1}, respectively, much less than Lithium (3860 mAh g^{-1}) Na–S and K–S batteries have similar chemistry as Li–S; challenges exist, such as poor ionic transport and sluggish reaction kinetics due to the larger ions and less reducing behavior than Li^+ ions [21, 22].

All the drawbacks associated with Li–S batteries are listed as follows:

1. M-S batteries undergo a conversion reaction of Sulfur (S) to form Li_2S as a discharge product. The redox intermediates, metal polysulfides (Li_2S_x), migrate through the electrolyte, causing a notorious shuttling effect between the cathode and anode. This phenomenon leads to capacity fading and hinders the actual potential of metal-sulfur batteries [23, 24].
2. Both elemental S and polysulfides with electrical insulation behavior have intrinsically sluggish kinetics leading to enormous polarisation during cycling and deteriorating electrode rechargeability. Therefore, they require the incorporation of conducting materials, leading to low utilization of active materials [25, 26].
3. The conversion reaction between S and Li_2S is accompanied by extensive volume alterations as high as 80% during cycling, predominantly arising from different densities of S and the reduced metal sulfides [27].

The solution to the first problem is primarily rooted in the rationale of designing innovative cathode materials to tailor physiochemical interactions between sulfur and polysulfides [7, 28]. Nevertheless, the central problem of bettered storage and suppression of mobilization of metal polysulfides to safeguard coulombic efficiency and avoid self-discharging to design M-S batteries with long cyclability is still a challenge. In this regard, pseudocapacitive materials provide a promising solution.

3 Pseudocapacitive Materials

3.1 Transition Metal Oxides/Hydroxides

TMOs have been vastly employed in energy generation and storage applications owing to their favourable features such as eco-friendliness, economic viability, and excellent catalytic behavior. They exhibit more substantial adsorption capability due to ionic bonds associated with higher chemical polarisation. Various 2D metal oxides such as Iron oxide [7], Cobalt oxide [7], Silicon Oxide [29], Vanadium Oxide [30], manganese oxide [31], titanium oxide [32], etc., are explored by researchers in metal-sulfur batteries [33]. However, due to low electronic conductivity, TMOs can't be employed in pristine form and thus require conjunction with carbon-based entities to ensure smooth electronic and ionic transfer. The lithiated products Li_2S_2/Li_2S etc., should be in the conductive environment rather than on oxide to promise sufficient conversion efficiency [34]. Sun et al. reported the performance of hierarchical spinal sulfur-doped $ZnCo_2O_4$ particles anchored on graphene nanosheets synthesized via the hydrothermal method. Subsequently, they are doped with sulfur via a melt-diffusion process. The final composite could perform as a quirky cathode scaffold to suppress the shuttling effect efficiently by confining polysulfides chemically. On the other hand, graphene sheets provided for high surface area. They reported the electrochemical performance of three distinct configurations as depicted in Fig. 2. As revealed in Fig. 2b–d, cycling capability $ZnCo_2O_4$@N-RGO(I)/S71 (S loading—71%) was found to best among three samples due to lesser oxide content which have led to relatively inferior conductivity in other samples [35].

Xiaobo et al. reported NiO-carbon nanotubes/sulfur (NiO-CNT@S) composite. The composite revealed hierarchical features involving high conductivity of CNTs and synergetic physiochemical adsorption by both NiO and CNTs, boosting the electrochemical performance of Li–S batteries. NiO-CNT@S composite provided a high initial discharge capacity of 1072 mAh g^{-1} and could retain 609 mAh g^{-1} after completing 160 cycles at the current rate of 0.1 C [36].

Despite being most discussed and exploited profoundly, transition metal oxides could not be commercialized because of low electronic conductivity. Transition metal chalcogenides are great performers due to their better cyclic performance, enhanced redox activity, added catalytic activity, finer electronic conductivity, and worthier structural aspects such as high surface area, flexibility, and denser active sites.

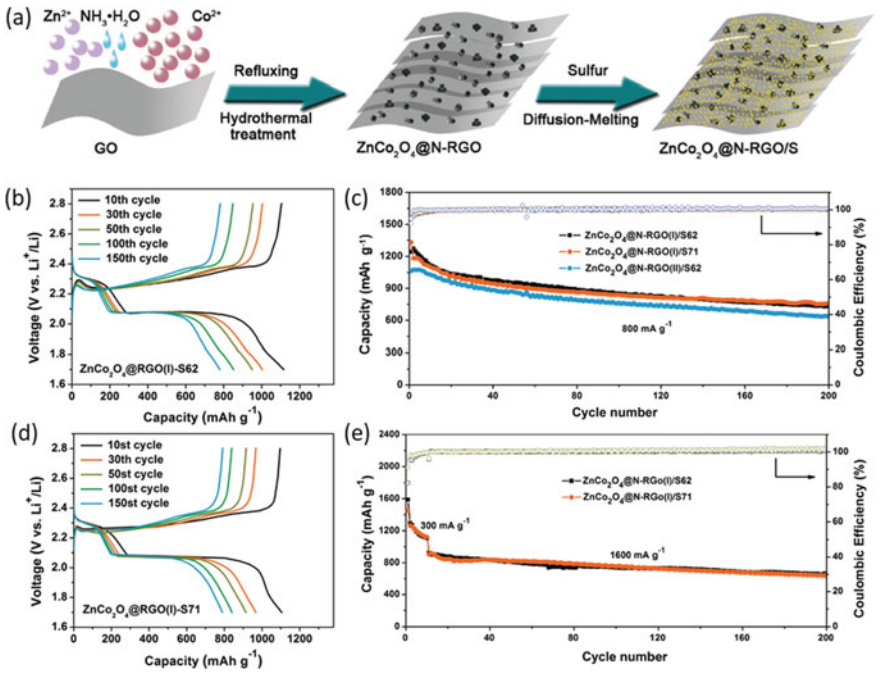

Fig. 2 **a** Scheme illustrating synthesis procedure for $ZnCo_2O_4$@N-RGo composites; **b** GCD curves for $ZnCo_2O_4$@N-RGo (I)-S62; **c** long-term cycling performance of various cathodes at 0.8 A g^{-1}; **d** GCD profiles for $ZnCo_2O_4$@N-RGo (I)-S71; (**e**) cyclic performance at current density 1.6 A g^{-1}. Adapted with permission [35], Copyright (2018), John Wiley & Sons

3.2 Transition Metal Chalcogenides (TMCs)

TMCs are anisotropic crystalline compounds with stoichiometry M_aX_b (M—elements from group 3 to group 12, X—chalcogens i.e., group 16 elements mainly S, Se, Te) [14]. Transition metal sulfides [37], selenides [38], and tellurides exhibit variable band gaps, tuneable structures, and distinct materials, making them attractive for various energy storage/conversion-based applications. TMCs are highly investigated materials for Li–S batteries because of their ability to trap LiPSs effectively chemically and boosting the kinetics of conversion of sulfides due to electro catalytic behavior [39, 40]. Qin et al. rationally designed multi-shelled hollows spheres of Mn_3O_4–MnS by controlled sulfurization of manganese oxide spheres and employed these as sulfur host to fabricate cathode for Li–S batteries. This structure provided ample active sites and strong adsorption and fast conversion are facilitated by Mn_3O_4 and MnS, respectively, which lead to a synergetic effect. As assembled battery delivered decent rate performance and prominent cyclic stability (00.016% decay per cycle at rate 2 C) up to 100 cycles [41]. Liu et al. reported various chalcogenides of manganese (including MnO, MnS, MnSe) implanted in carbon nanofibers synthesized by electrospinning method and by thermal treatment. It was observed that

MnO@CNF being polar in nature show best adsorption behavior while MnSe@CNF showed best catalytic performance leading to better rate performance and cyclability. Figure 3 shows electrochemical performance of all three cathodes in lithium-sulfur batteries. Figure 3a reveals highest capacity of 1056 mAh g^{-1} at 0.2 C for MnSe@CNF and exhibited superior rate performance in current range of 0.2 to 4 C. Long term cyclic measurements also reveals superiority of MnSe@CNF over other two electrodes [42].

Single step in-situ sulfidation strategy was employed to create a CoS_2-N-doped MXene heterostructure (N-MX-CoS_2) as a perspective sulfur host by X. Fan and co-workers to cultivate the desirable properties of MXene and CoS_2. Synergistic N-dopant sites and polar CoS_2 nanoparticles ensured efficient adsorption of LiPSs. In addition, the layered structure and high conductivity of MXene paved the way for faster redox reactions. This structure effectively immobilized LiPSs and enhanced their conversion reaction. An initial capacity of 1031 mAh g^{-1} at 1 C was observed, along with excellent rate performance and outstanding cyclability with a decay rate of 0.052% per cycle at 1 C [43].

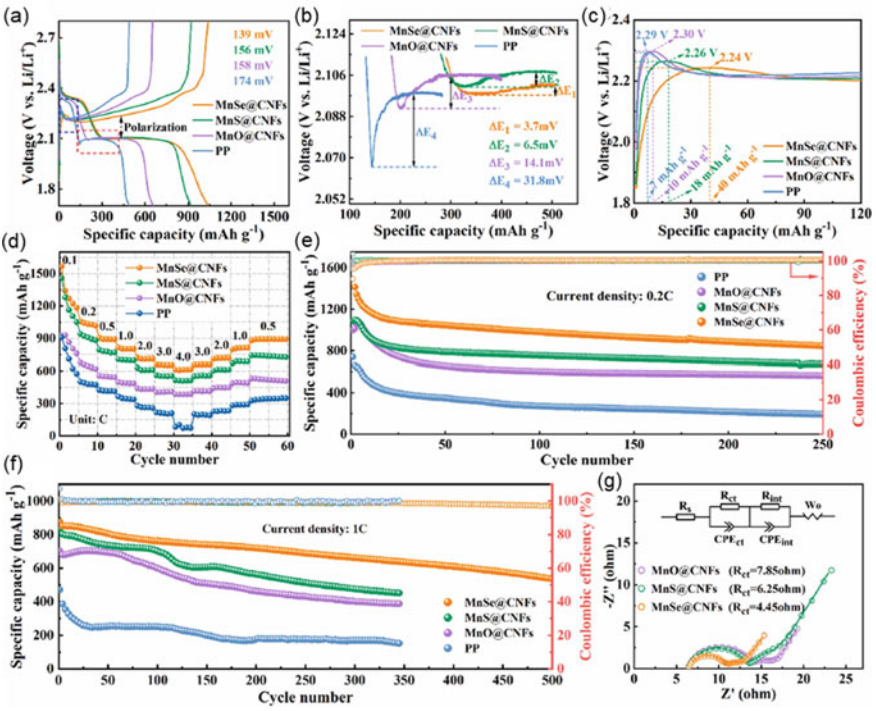

Fig. 3 Electrochemical performance of Li–S coin cells, **a** GCD profiles for various cathodes at 0.2 C; enlarged profiles corresponding to **b** discharge profile; **c** charge profile; **d** rate performance of various cathodes; **e** long-term cycling performance of coin cells; **f** Nyquist plots of cell post-cycling (0.2 C). Adapted with permission [42], Copyright (2022), Elsevier

To exploit the advantages of TMCs, various TMC heterostructures have been created with carbon-based materials [42], TMOs [41], Mxenes [43], and conducting polymers (CPs) [44] for their applications in metal-sulfur batteries. In these heterostructures, TMCs provided noticeable electrocatalytic capabilities for the conversion of LIPS; while TMOs, MXenes, or metal oxides exhibited superior trapping behavior towards polysulfides. Thus, hybrid structures synergistically boosted the trapping and conversion of LiPSs, suppressing the shuttle effect. For instance, a heterostructure composed of WS_2 nanosheets-WO_3 nanoparticles synthesized via vapor sulfurization of tungsten oxide provided abundant active sites at the interface, which leads to performance enhancement [45].

3.3 Transition Metal Phosphides/Borides

Transition metal Phosphides (TMPs) and Borides (TMBs) consist of metal-metalloid bonds (M-P or M-B) and metalloid-metalloid (P–P or B–B) bonds, respectively. Due to this peculiar bonding, they are endowed with abundant compositions, diverse crystal structures, exposed electronic states, strong electronegativity, and electronic conductivity [46, 47]. They are superior to TMOs and TMCs as sulfur hosts concerning their electrocatalytic behavior and LiPSs adsorption abilities. Thus, sulfur-based composites of TMPs/TMBs with carbon nanomaterials as conductive backbone possessing high catalytic response offer ultimate possibilities as a cathode in Li–S batteries [48]. However, these compounds must be dispersed on porous conductive surfaces to avoid their accumulation.

Cheng et al. prepared novel yolk-shell hollow nanospheres of Ni_2P to encapsulate sulfur in the interiors of spheres to capture the synergy from excellent adsorption and abundant electroactive sites. As-prepared S@Ni_2P cathode delivered an ultra-high capacity of 1409 mAh g^{-1} at 0.2 C rate and superior rate capability up to 10 C [49]. Chen's team reported Fe–Co–P Nanocubes with porous architecture, high conductivity, abundant adsorptive sites, and strong polarity. S@Co–Fe–P showed the reversible capacity of 1245 mAh g^{-1} at 0.1 C rate and better cyclic performance at 1 C for 500 cycles, as shown in Fig. 4. The areal capacity observed for this cathode was 4.6 mAh cm^{-2} with a sulfur content of 5.5 mg cm^{-2} [50].

Pang et al. reported superconductor MgB_2 that can fulfill the need for electron conduction and polysulfides immobilization and enhancing redox kinetics of LiPSs. They used a sandwiched structure of MgB_2 and graphene to provide a large surface area and prevent aggregation [51]. The graphene-MgB_2 electrode showed superior cyclic capacity retaining 92% capacity over 200 cycles at 0.5 C with a minimal fade rate of 0.04% per cycle. With the development of advanced futuristic materials, new strategies can be further incorporated into metal phosphides/borides as catalytic hosts for Li–S batteries. For instance, using high-entropy oxides and alloys in composite form with phosphides, etc., as catalytic hosts for sulfur cathodes in Li–S batteries.

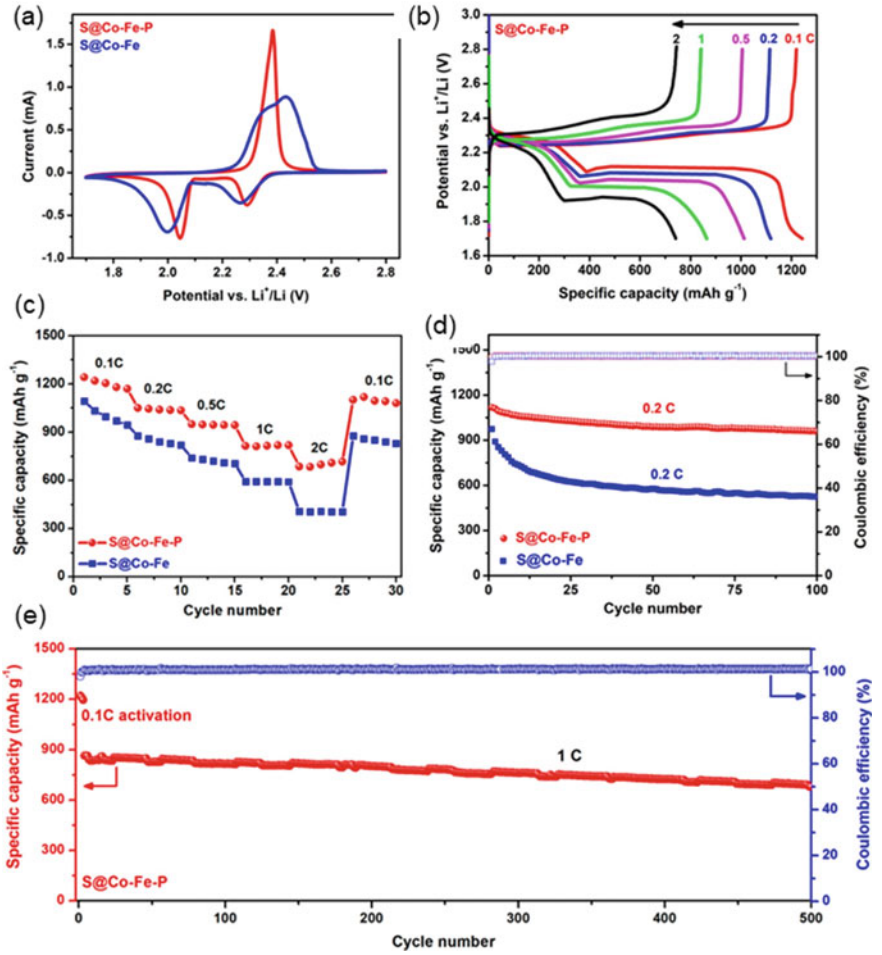

Fig. 4 **a** CV profiles for 2nd cycles for S@Co–Fe and S@Co–Fe–P; **b** GCD profiles for S@Co–Fe–Pat various scan rates from 0.1 to 2 C; **c** Rate performance; **d** Long-term cycling performance at 0.2 C for S@Co–Fe and S@Co–Fe–P; **e** cycling for S@Co–Fe–P cathode at 1 C. Adapted with permission [50], Copyright (2019), American Chemical Society

3.4 Conducting Polymers

Conducting polymers are organic materials whose structure consist of π-conjugated double bonds with high electrical conductivity and mechanical flexibility. Further, their favorable features including easy fabrication, cost-friendliness, lighter weight, tuneable physical properties, structural diversity, and redox reversible nature, make them attractive materials for M-S batteries. Conducting polymers can be incorporated with polar compounds (TMOs and MOFs) or carbon to make composite structures. Sometimes they contain functionalities such as S, N, and O that could interact

with LiPSs. Polyaniline (PANI) [44], polythiophene (PTh) [44], Polypyrrole (PPy) [52] and their derivatives are mainly employed in Li–S battery and energy storage research nowadays. They can be used as sulfur hosting materials, interlayers, redox mediators, or in coating layers of cathodes, separators or binders to eliminate volumetric changes during cycling. It plays a key role as an adsorbing material, active material, and a conductive agent [53].

Polyaniline has a theoretical capacity of 294 mAh g^{-1}, and it tends to capture migrating LiPSs via interaction between quinonoid imine linkages (–N=) with sulfur-containing entities to immobilize them. Dai et al. fabricated an S-rich copolymer containing PANI and S-composite, i.e., S-g-PANI/S (SPAS). As synthesized, copolymer S-based composite with a high S copolymerization degree of 52 at.% provided capacity rates of 1227 mAh g^{-1} at 0.1 C, 950 mAh g^{-1} at 1 C, and a retention of up to 54.2% of initial capacity was observed after 800 cycles, where a decay rate of only 0.06% per cycle is reported [53].

Polypyrrole (PPy) has a conjugated structure with alternate single and double bonds between carbon atoms. Zhao's group reported a core–shell composite of S/PPy by direct polymerization of monomeric pyrrole on nanospheres of sulfur. Polypyrrole could avoid aggregation of sulfur particles, LiPSs dissolution, and their shuttling while simultaneously providing efficient pathways for electronic and ionic conduction. As-fabricated cathode with sulfur loading of 80% could achieve the initial capacity of 1142 mAh g^{-1} and retained capacity of 65% after 100 cycles at 0.5 C [54]. In similar instances, a 3D porous cathode of sulfur and carbon nanotubes (CNT) composite (S/PSKC) encapsulated by a Polypyrrole layer (formed by vapor-phase polymerization) was reported. Figure 5 represents the schematic illustration of the synthesis process of the hybrid structure. The S/PSKC@PPy electrode with 72.8% sulfur loading provided the reversible capacity of 1109.2 mAh g^{-1}, and after 100 cycles, remarkable retention of the capacity of 93.1% was observed, as shown in Fig. 5b–d. As synthesized cathodes provided for superior cyclic performance and improved coulombic efficiency [55].

Chen's group used polythiophene in Li–S batteries in core–shell structure prepared by in-situ chemical oxidation polymerization method. The hybrid structure provided stable cyclability because of conductive PTh surrounding sulfur particles that prevented agglomeration of S particles, and the porous structure adsorbed LiPSs efficiently, boosting the battery's performance. The initial discharge capacity observed was 1119.3 mAh g^{-1}, and the capacity retained after 80 cycles was 830.2 mAh g^{-1} [56]. A facile strategy was employed to synthesize porous tin oxide nanoparticles-decorated tubular PPy (S/PPy@SnO_2) as a host for sulfur to integrate advantageous properties while tackling shortcomings. As synthesized material exhibit high specific surface area, highly conducting pathways, and large spaces to accommodate LiPSs and Li ions. Consequently, the cathode with sulfur loading of 65% exhibited excellent cycling stability with a minimal capacity decay rate of 0.05% per cycle till 500 cycles at 1 C is observed along with remarkable rate capability at 5 C (coulombic efficiency > 90%) [57].

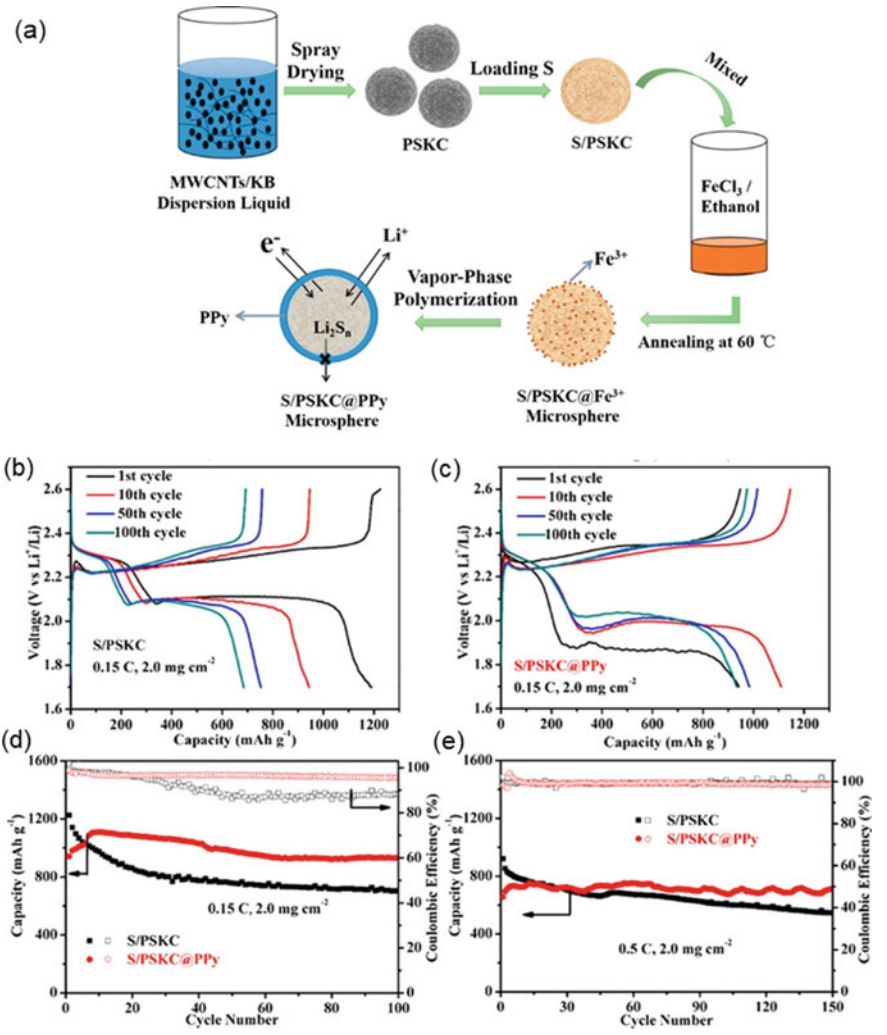

Fig. 5 **a** Schematics depicting the synthesis approach for S/PSKC@PPy composite; Charge–discharge profiles showing cycling performance for cathodes at 0.15 C up to 100 cycles for cell with; **b** S/PSKC cathode and **c** S/PSKC@PPy cathode; long term cycling performance of cathodes at **d** 0.15 C; **e** 0.5 C. Adapted with permission [55], Copyright (2019), American Chemical Society

Given the advantages and challenges mentioned above, it is suggested to look for the solution of existing problems of this system such as poor cyclic performance and low heat resistance which limits their potential of being used directly in commercial applications. Further, their conductivity is still unsatisfactory, which may be significantly improved by doping (chemical, electrochemical, or light excitation doping). In addition, functional groups may be attached via physical or chemical approaches to enhance the adsorption phenomenon. Further, to get deeper insight

regarding the mechanism of adsorption of polysulfide by CPs, operando IR, XPS or XAS techniques may be used to study the evolution of changes happening during the process.

3.5 MXenes (Nitrides and Carbides)

MXenes are a newly emerged class of 2D materials (nitrides and carbonitrides); first introduced in 2011. They have been extensively employed in energy storage applications because of their very high conductivity, low diffusion barrier, and hydrophilic surface [58]. Two-dimensional MXenes can realize efficient trapping-diffusion-conversion of LiPSs because of their inherent structural properties, such as rich active sites, better conductivity, surface functional groups, and structural maneuverability. Due to their unique porous 2D structure, they can act as suitable sulfur hosts in Li–S batteries [15, 59]. Zhang et al. reported a sulfur cathode based on a 3D composite of N-doped porous carbon and MXene (Ti_3C_2) synthesized via a sacrificial-template-assisted approach with 80% sulfur loading (Fig. 6). The composite could provide high specific area, conductive pathways, and ensured stronger physical and chemical interactions with LiPSs [60].

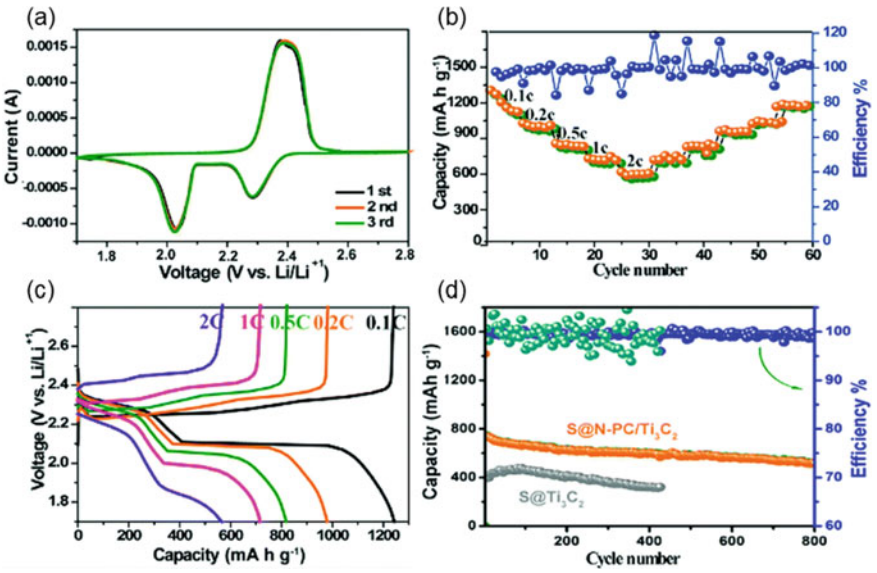

Fig. 6 Electrochemical behavior of S@N-PC/MXene-based cathode: **a** CV profiles for 1st, 2nd, and 3rd cycles; **b** Rate performance; **c** Initial GCD profiles at various scan rates; **d** cyclic performance at 1 C for pure S@MXene and S@N-PC/MXene. Adapted with permission [60], Copyright (2019), Royal Society of Chemistry

In the same way, the performance of an interlinked composite of MXenes and carbon nanotubes (CNTs) is unveiled by Liang et al., whereby they reported excellent cycling performance of composite along with negligible capacity fading of 0.043% per cycle till 1200 cycles [61]. The superior performance of the composite is ascribed to the interaction between metallic MXene and LiPSs by cleavage of Ti–OH bonds by the formation of thiosulfates (stronger Ti–S bonds). Meanwhile, interlinked CNT provided for a porous framework with conductive network pathways and enhanced LiPSs adsorption.

3.6 MOF-Derived Materials

MOFs serve as perspective sulfur hosts with a high specific surface area and large pore volume, leading to a long life span and enhanced capacity. Metal-organic frameworks (MOFs) are materials with well-defined crystallinity and high permanent porosity consisting of metal entities inter-connected by organic linkers. They can be rationally designed to get desirable structure and tuneable porosity [62].

The pioneering work based upon using a MOF-based template incorporating sulfur was demonstrated by Zhou et al. in which smaller MOFs are better for higher sulfur utilization. They suggested that functional groups attached in MOFs' apertures interact with polysulfide anions in Lewis's acid–base manner to provide stable and long cyclic performance by mitigating their movement through electrolytes. ZIF-8 particles with 30 wt% sulfur loading with size <20 nm could provide a higher specific capacity of ~950 mAh g^{-1} at 0.5 C, while the larger one with size ~200 nm could provide better capacity retention (75% after 250 cycles at 0.5 C) in metal-sulfur storage systems. They also revealed the electrochemical performance of other Al-based MOFs, MIL-53, NH_2-MIL-53, and HKUST-1, in a comparative manner. Rationally designed small sizes and smaller apertures are favorable for achieving high capacity and superior life span [63]. Chen et al. revealed the electrochemical performance of the micropores-rich structure of MIL-101(Cr) as a host for sulfur impregnation. They synthesized MIL-101(Cr)/S nanocomposite enfolded by graphene nanosheets to generate a conducting backbone that dramatically enhanced the cathode's cyclic stability and rate performance [64].

Besides, pristine MOFs as host matrix, MOF-derived carbon, and other compounds have also been investigated by researchers. Cheetham et al. revealed the performance of four different sulfur-loaded carbon materials derived from the ZIF-8, RT-MOF-5, Solvo-MOF-5, and Zinc furmate synthesized by pyrolysis in inert ambient. It was observed that specimens containing higher micropores content than mesopores provided enhanced initial capacity [65]. Wei et al. synthesized polyhedron-shaped porous Zn–Co oxide ($ZnCo_2O_4$) derived from their MOFs (ZIF-8@ZIF-67) anchored by MXene (Ti_3C_2) as an efficient sulfur immobilizer. As-synthesized $ZnCo_2O_4$@Ti_3C_2/S composite could provide a discharge capacity of 1283.9 mAh g^{-1} in its first cycle, along with coulombic efficiency of 98.7% at a current rate of 0.1 C. It exhibited outstanding cycling stability at 0.5 C up to 400

cycles and remarkable rate performance in diverse current density range varying from 0.1 to 2 C, as depicted in Fig. 7 [66]. The performance may be credited to a well-designed composite with an internal hollow structure that provides more space for sulfur storage sites, thus enhancing sulfur utilization. It also alleviates volume changes occurring during cycling. Meanwhile, $ZnCo_2O_4$ inhibited the dissolution and diffusion of polysulfides by providing enough polar sites which could strongly interact with LiPSs. Ti_3C_2 added to synergy by enhancing the composite's electronic conductivity, and the overall composite accounted for high reversible specific capacity and rate capability.

MOFs and MOF-derived carbon-based materials and their composites are perspective candidates for mitigating polysulfide shuttling between electrodes. All the advantages are listed as follows:

1. Abundant pores that can accommodate large amounts of sulfur to achieve high utilization of active material.
2. Tuneable pore size with desirable window apertures to absorb and capture polysulfide anions efficiently to prevent their electrolyte solubility.
3. Functionalities on inner surfaces of MOF structures endow them with a polarity that interacts with polysulfides and strengthens the immobilization ability.
4. Hierarchical carbonized structures and rigid scaffolds can effectively accommodate volume strains produced during cycling while simultaneously providing conducting pathways for electrons.

4 Conclusion and Future Perspective

Pseudocapacitive materials are opportune for metal-sulfur battery applications because of their distinctive structural, electrochemical, and electrical features. Advanced sulfur host matrices can be realized via precise size regulation from angstrom to the micron level. This chapter discussed metal-sulfur batteries, briefly introducing existing challenges with these systems. Minimizing polysulfides by reducing the shuttling and boosting reaction kinetics is a long-term research target towards realizing state-of-art metal-sulfur batteries. A perspective sulfur cathode should guarantee: (a) bettered electrical and ionic conductivity to compensate for the insulation behavior of the sulfur/sulfides family; (b) Smooth interfacial contacts and improved absorption and catalytic properties to mitigate shutting and poor kinetics; (c) enough spaces and suitable mechanical stability to accommodate volumetric strains produced during cycling.

In this regard, pseudocapacitive materials with a layered structure, adjustable morphology, and tuneable physical and chemical properties are promising. Lewis's acid centers in these metallic compounds provide high adsorption capabilities toward polysulfides, suggesting these configurations' importance. Furthermore, transition metal-based compounds' heterostructures/composites show rewarding catalytic abilities toward sulfur redox reactions by reducing the energy barrier. Enhanced reaction kinetics ensures the reversibility of metal-sulfur batteries. Predominantly in

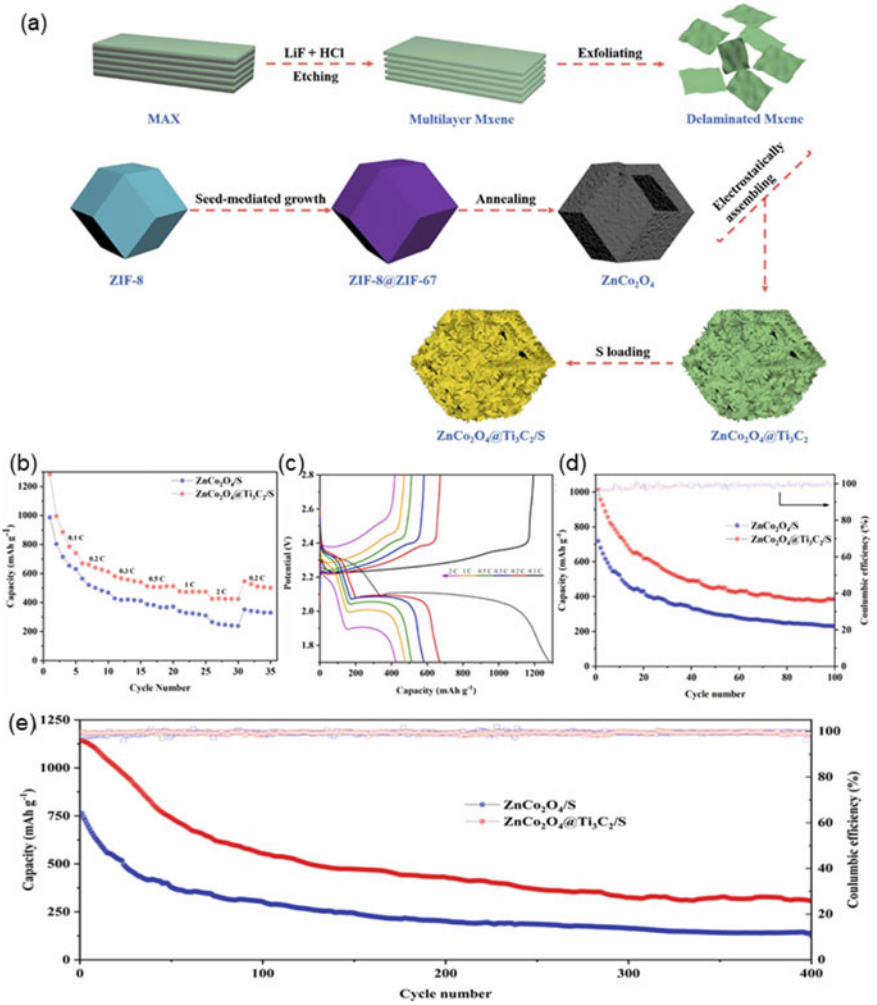

Fig. 7 **a** Schematic illustration for the synthesis of $ZnCo_2O_4$@Ti_3C_2/S composite; **b** Rate performance of $ZnCo_2O_4$@Ti_3C_2/S and $ZnCo_2O_4$/S cathodes from current densities 0.1–2 C; **c** Initial charge–discharge profiles at various scan rates ranging from 0.1–2 C; Cyclic performance of cathodes; **d** At 0.2 C up to 100 cycles; **e** At 0.5 C up to 400 cycles. Adapted with permission [66], Copyright (2022), Elsevier

crucial steps, the inadequate transformation of high-order sulfides into low-order insoluble sulfides creates a concentration gradient, exacerbating the shuttling effect and capacity fading.

Although significant progress has been made in fabricating state-of-art metal-sulfur batteries, several existing challenges still need to be addressed. The approaches to circumvent these challenges would define outlook as discussed below:

(A) Despite extensive research to develop state-of-art sulfur cathodes and towards the inner structure–property relationship, proper rational foundations for sulfur cathodes are yet to be laid due to its highly complex conversion process.
(B) In the near future, significant breakthroughs towards establishing redox chemistry behind the conversion mechanism in Li–S batteries are highly anticipated.

References

1. X. Wang, H.M. Kim, Y. Xiao, Y.K. Sun, Nanostructured metal phosphide-based materials for electrochemical energy storage. J. Mater. Chem. A **4**, 14915–14931 (2016). https://doi.org/10.1039/c6ta06705k
2. K. Kisu, S. Kim, R. Yoshida, H. Oguchi, N. Toyama, S. Orimo, Microstructural analyses of all-solid-state Li–S batteries using $LiBH_4$-based solid electrolyte for prolonged cycle performance. J. Energy Chem. **50**, 424–429 (2020). https://doi.org/10.1016/j.jechem.2020.03.069
3. H. Fan, W. Luo, S. Dou, Z. Zheng, Advanced two-dimensional materials toward polysulfides regulation of metal–sulfur batteries. SmartMat 1–30 (2023). https://doi.org/10.1002/smm2.1186
4. M. Salama, A.R. Rosy, R. Yemini, Y. Gofer, D. Aurbach, M. Noked, Metal-sulfur batteries: overview and research methods. ACS Energy Lett. **4**, 436–446 (2019). https://doi.org/10.1021/acsenergylett.8b02212
5. K. Fu, Y. Gong, G.T. Hitz, D.W. McOwen, Y. Li, S. Xu, Y. Wen, L. Zhang, C. Wang, G. Pastel, J. Dai, B. Liu, H. Xie, Y. Yao, E.D. Wachsman, L. Hu, Three-dimensional bilayer garnet solid electrolyte based high energy density lithium metal-sulfur batteries. Energy Environ. Sci. **10**, 1568–1575 (2017). https://doi.org/10.1039/c7ee01004d
6. D. Sui, L. Si, C. Li, Y. Yang, Y. Zhang, W. Yan, A comprehensive review of graphene-based anode materials for lithium-ion capacitors. Chemistry (Easton) **3**, 1215–1246 (2021). https://doi.org/10.3390/chemistry3040089
7. Q. Liu, X. Han, Q. Dou, P. Xiong, Y. Kang, S.-W. Kang, B.-K. Kim, H.S. Park, Multiphase and multicomponent nickel-iron oxide heterostructure as an efficient separator modification layer for advanced lithium sulfur batteries. Batter. Supercaps **4**, 1843–1849 (2021). https://doi.org/10.1002/batt.202100156
8. R. Vishnoi, K. Sharma, Y.S. Yogita, R. Singhal, Investigation of sequential thermal annealing effect on Cu-C70 nanocomposite thin film. Thin Solid Films **680**, 75–80 (2019). https://doi.org/10.1016/j.tsf.2019.04.004
9. V. Marangon, E. Scaduti, V.F. Vinci, J. Hassoun, Scalable composites benefiting from transition-metal oxides as cathode materials for efficient lithium-sulfur batteries. ChemElectroChem **9**, e202200374 (2022). https://doi.org/10.1002/celc.202200374
10. J. Xie, X. Luo, L. Chen, X. Gong, L. Zhang, J. Tian, ZIF-8 derived boron, nitrogen co-doped porous carbon as metal-free peroxymonosulfate activator for tetracycline hydrochloride degradation: performance, mechanism and biotoxicity. Chem. Eng. J. **440**, 135760 (2022). https://doi.org/10.1016/j.cej.2022.135760
11. X. Kang, Z. Jin, H. Peng, Z. Cheng, L. Liu, X. Li, L. Xie, J. Zhang, Y. Dong, The role of selenium vacancies functionalized mediator of bimetal (Co, Fe) selenide for high-energy–density lithium-sulfur batteries. J. Colloid Interface Sci. **637**, 161–172 (2023). https://doi.org/10.1016/j.jcis.2023.01.090
12. P. Han, S.H. Chung, A. Manthiram, Designing a high-loading sulfur cathode with a mixed ionic-electronic conducting polymer for electrochemically stable lithium-sulfur batteries. Energy Storage Mater. **17**, 317–324 (2019). https://doi.org/10.1016/j.ensm.2018.11.002

13. J. Wen, L. Huang, Y. Huang, W. Luo, H. Huo, Z. Wang, X. Zheng, Z. Wen, Y. Huang, A lithium-MXene composite anode with high specific capacity and low interfacial resistance for solid-state batteries. Energy Storage Mater. **45**, 934–940 (2022). https://doi.org/10.1016/j.ensm.2021.12.033
14. Y. Dahiya, M. Hariram, M. Kumar, A. Jain, D. Sarkar, Modified transition metal chalcogenides for high performance supercapacitors: current trends and emerging opportunities. Coord. Chem. Rev. **451**, 214265 (2022). https://doi.org/10.1016/j.ccr.2021.214265
15. Y.H. Liu, C.Y. Wang, S.L. Yang, F.F. Cao, H. Ye, 3D MXene architectures as sulfur hosts for high-performance lithium-sulfur batteries. J. Energy Chem. **66**, 429–439 (2022). https://doi.org/10.1016/j.jechem.2021.08.040
16. Y. Xu, L. Wang, Q. Xu, L. Liu, X. Fang, C. Shi, B. Ye, L. Chen, W. Peng, Z. Liu, W. Chen, 3D hybrids based on WS_2/N, S co-doped reduced graphene oxide: facile fabrication and superior performance in supercapacitors. Appl. Surf. Sci. **480**, 1126–1135 (2019). https://doi.org/10.1016/j.apsusc.2019.02.217
17. C. Ye, J. Shan, H. Li, C.-C. Kao, Q. Gu, S.-Z. Qiao, Reducing overpotential of solid-state sulfide conversion in potassium-sulfur batteries. Angew Chem. Int. Ed. **62**, e202301681 (2023). https://doi.org/10.1002/anie.202301681
18. R. Gao, Z. Wang, S. Liu, G. Shao, X. Gao, Metal phosphides and borides as the catalytic host of sulfur cathode for lithium–sulfur batteries. Int. J. Miner. Metall. Mater. **29**, 990–1002 (2022). https://doi.org/10.1007/s12613-022-2451-2
19. Z. Yang, C. Xu, M. Xia, X. Zhang, H. Yan, H. Yu, T. Sun, L. Zhang, F. Hu, J. Shu, Thermodynamic analysis and perspective of aqueous metal-sulfur batteries. Mater. Today **49**, 184–200 (2021). https://doi.org/10.1016/j.mattod.2021.01.012
20. G. Liu, Q. Sun, Q. Li, J. Zhang, J. Ming, Electrolyte issues in lithium-sulfur batteries: development, prospect, and challenges. Energy Fuels **35**, 10405–10427 (2021). https://doi.org/10.1021/acs.energyfuels.1c00990
21. M.K. Aslam, I.D. Seymour, N. Katyal, S. Li, T. Yang, S. Bao, G. Henkelman, M. Xu, Metal chalcogenide hollow polar bipyramid prisms as efficient sulfur hosts for Na-S batteries. Nat. Commun. 1–11. https://doi.org/10.1038/s41467-020-19078-0
22. H. Yang, B. Zhang, Y.X. Wang, K. Konstantinov, H.K. Liu, S.X. Dou, Alkali-metal sulfide as cathodes toward safe and high-capacity metal (M = Li, Na, K) sulfur batteries. Adv. Energy Mater. **10**, 1–24 (2020). https://doi.org/10.1002/aenm.202001764
23. S. Risse, S. Angioletti-Uberti, J. Dzubiella, M. Ballauff, Capacity fading in lithium/sulfur batteries: a linear four-state model. J. Power. Sources **267**, 648–654 (2014). https://doi.org/10.1016/j.jpowsour.2014.05.076
24. S. Bai, X. Liu, K. Zhu, S. Wu, H. Zhou, Metal–organic framework-based separator for lithium–sulfur batteries. Nat. Energy **1**, 16094 (2016). https://doi.org/10.1038/nenergy.2016.94
25. M.J. Klein, A. Dolocan, C. Zu, A. Manthiram, An effective lithium sulfide encapsulation strategy for stable lithium-sulfur batteries. Adv. Energy Mater. **7**, 1–9 (2017). https://doi.org/10.1002/aenm.201701122
26. H. Chu, H. Noh, Y.J. Kim, S. Yuk, J.H. Lee, J. Lee, H. Kwack, Y.K. Kim, D.K. Yang, H.T. Kim, Achieving three-dimensional lithium sulfide growth in lithium-sulfur batteries using high-donor-number anions. Nat. Commun. **10**, 1–12 (2019). https://doi.org/10.1038/s41467-018-07975-4
27. M. Zhu, S. Li, J. Liu, B. Li, Applied Surface Science Promoting polysulfide conversion by V_2O_3 hollow sphere for enhanced lithium-sulfur battery. Appl. Surf. Sci. **473**, 1002–1008 (2019). https://doi.org/10.1016/j.apsusc.2018.12.189
28. Z. Xu, M. Wu, Z. Chen, C. Chen, J. Yang, T. Feng, E. Paek, D. Mitlin, Direct structure-performance comparison of all-carbon potassium and sodium ion capacitors. Adv. Sci. **6**, 1802272 (2019). https://doi.org/10.1002/advs.201802272
29. P. Rajkumar, K. Diwakar, G. Radhika, K. Krishnaveni, R. Subadevi, M. Sivakumar, Effect of silicon dioxide in sulfur/carbon black composite as a cathode material for lithium sulfur batteries. Vacuum **161**, 37–48 (2019). https://doi.org/10.1016/j.vacuum.2018.12.016

30. Y. Zhang, X. Ge, Q. Kang, Z. Kong, Y. Wang, L. Zhan, Vanadium oxide nanorods embed in porous graphene aerogel as high-efficiency polysulfide-trapping-conversion mediator for high performance lithium-sulfur batteries. Chem. Eng. J. **393**, 124570 (2020). https://doi.org/10.1016/j.cej.2020.124570
31. Y. Li, B. Su, Manganese dioxide nanosheet functionalized sulfur@ PEDOT core–shell nanospheres for advanced lithium–sulfur batteries. J. Mater. Chem. A **4**, 9403–9412 (2016). https://doi.org/10.1039/c6ta03211g
32. Y. Wang, R. Zhang, J. Chen, H. Wu, S. Lu, K. Wang, H. Li, C.J. Harris, K. Xi, R.V. Kumar, S. Ding, Enhancing catalytic activity of titanium oxide in lithium–sulfur batteries by band engineering. Adv. Energy Mater. **9**, 1900953 (2019). https://doi.org/10.1002/aenm.201900953
33. X. Song, T. Gao, S. Wang, Y. Bao, G. Chen, L.-X. Ding, H. Wang, Free-standing sulfur host based on titanium-dioxide-modified porous-carbon nanofibers for lithium-sulfur batteries. J. Power Sources **356**, 172–180 (2017). https://doi.org/10.1016/j.jpowsour.2017.04.093
34. X. Lang, X. Wang, Y. Liu, K. Cai, L. Li, Q. Zhang, Cobalt-based metal organic framework (Co-MOFs)/graphene oxide composites as high-performance anode active materials for lithium-ion batteries. Int. J. Energy Res. **45**, 4811–4820 (2021). https://doi.org/10.1002/er.6080
35. Q. Sun, B. Xi, J.Y. Li, H. Mao, X. Ma, J. Liang, J. Feng, S. Xiong, Nitrogen-doped graphene-supported mixed transition-metal oxide porous particles to confine polysulfides for lithium-sulfur batteries. Adv. Energy Mater. **8**, 1–10 (2018). https://doi.org/10.1002/aenm.201800595
36. X. Jia, B. Liu, J. Liu, S. Zhang, Z. Sun, X. He, H. Li, G. Wang, H. Chang, Fabrication of NiO-carbon nanotube/sulfur composites for lithium-sulfur battery application. RSC Adv. **11**, 10753–10759 (2021). https://doi.org/10.1039/d1ra00216c
37. X.Y. Yu, X.W. (David) Lou, Mixed metal sulfides for electrochemical energy storage and conversion. Adv. Energy Mater. **8**, 1–37 (2018). https://doi.org/10.1002/aenm.201701592
38. Z. Ali, T. Zhang, M. Asif, L. Zhao, Y. Yu, Y. Hou, Transition metal chalcogenide anodes for sodium storage. Mater. Today **35**, 131–167 (2020). https://doi.org/10.1016/j.mattod.2019.11.008
39. C. Wang, L. Sun, K. Li, Z. Wu, F. Zhang, L. Wang, Unravel the catalytic effect of two-dimensional metal sulfides on polysulfide conversions for lithium-sulfur batteries. ACS Appl. Mater. Interfaces **12**, 43560–43567 (2020). https://doi.org/10.1021/acsami.0c09567
40. P. Wang, B. Xi, M. Huang, W. Chen, J. Feng, S. Xiong, Emerging catalysts to promote kinetics of lithium–sulfur batteries. Adv. Energy Mater. **11**, 2002893 (2021). https://doi.org/10.1002/aenm.202002893
41. B. Qin, Q. Wang, W. Yao, Y. Cai, Y. Chen, P. Wang, Y. Zou, X. Zheng, J. Cao, J. Qi, W. Cai, Heterostructured Mn_3O_4-MnS multi-shelled hollow spheres for enhanced polysulfide regulation in lithium-sulfur batteries. Energy Environ. Mater. 1–9 (2022). https://doi.org/10.1002/eem2.12475
42. G. Liu, Q. Zeng, X. Sui, S. Tian, X. Li, Q. Wu, X. Wang, K. Tao, E. Xie, Z. Zhang, Modulating the d-p orbital coupling of manganese chalcogenides for efficient polysulfides conversion in lithium–sulfur batteries. J. Power. Sources **552**, 232244 (2022). https://doi.org/10.1016/j.jpowsour.2022.232244
43. C. Yang, Y. Li, W. Peng, F. Zhang, X. Fan, In situ N-doped CoS_2 anchored on MXene toward an efficient bifunctional catalyst for enhanced lithium-sulfur batteries. Chem. Eng. J. **427**, 131792 (2022). https://doi.org/10.1016/j.cej.2021.131792
44. H. Xiang, N. Deng, H. Zhao, X. Wang, L. Wei, M. Wang, B. Cheng, W. Kang, A review on electronically conducting polymers for lithium-sulfur battery and lithium-selenium battery: progress and prospects. J. Energy Chem. **58**, 523–556 (2021). https://doi.org/10.1016/j.jechem.2020.10.029
45. B. He, W.C. Li, Z.Y. Chen, L. Shi, Y. Zhang, J.L. Xia, A.H. Lu, Multilevel structured carbon film as cathode host for Li-S batteries with superhigh-areal-capacity. Nano Res. **14**, 1273–1279 (2021). https://doi.org/10.1007/s12274-020-3102-4
46. Y. Liu, X. Que, X. Wu, Q. Yuan, H. Wang, J. Wu, Y. Gui, W. Gan, ZIF-67 derived carbon wrapped discontinuous CoxP nanotube as anode material in high-performance Li-ion battery. Mater. Today Chem. **17**, 100284 (2020). https://doi.org/10.1016/j.mtchem.2020.100284

47. R. Reinhold, U. Stoeck, H.J. Grafe, D. Mikhailova, T. Jaumann, S. Oswald, S. Kaskel, L. Giebeler, Surface and electrochemical studies on silicon diphosphide as easy-to-handle anode material for lithium-based batteries—the phosphorus path. ACS Appl. Mater. Interfaces **10**, 7096–7106 (2018). https://doi.org/10.1021/acsami.7b18697
48. Z. Li, P. Li, X. Meng, Z. Lin, R. Wang, The interfacial electronic engineering in binary sulfiphilic cobalt boride heterostructure nanosheets for upgrading energy density and longevity of lithium-sulfur batteries. Adv. Mater. **33**, 2102338 (2021). https://doi.org/10.1002/adma.202102338
49. J. Cheng, D. Zhao, L. Fan, X. Wu, M. Wang, N. Zhang, K. Sun, Ultra-high rate Li-S batteries based on a novel conductive Ni2P yolk-shell material as the host for the S cathode. J. Mater. Chem. A **5**, 14519–14524 (2017). https://doi.org/10.1039/c7ta03236f
50. Y. Chen, W. Zhang, D. Zhou, H. Tian, D. Su, C. Wang, D. Stockdale, F. Kang, B. Li, G. Wang, Co-Fe mixed metal phosphide nanocubes with highly interconnected-pore architecture as an efficient polysulfide mediator for lithium-sulfur batteries. ACS Nano **13**, 4731–4741 (2019). https://doi.org/10.1021/acsnano.9b01079
51. Q. Pang, C.Y. Kwok, D. Kundu, X. Liang, L.F. Nazar, Lightweight metallic MgB_2 mediates polysulfide redox and promises high-energy-density lithium-sulfur batteries. Joule **3**, 136–148 (2019). https://doi.org/10.1016/j.joule.2018.09.024
52. Y. Gu, L.Q. Fan, J.L. Huang, C.L. Geng, J.M. Lin, M.L. Huang, Y.F. Huang, J.H. Wu, N-doped reduced graphene oxide decorated $NiSe_2$ nanoparticles for high-performance asymmetric supercapacitors. J. Power. Sources **425**, 60–68 (2019). https://doi.org/10.1016/j.jpowsour.2019.03.123
53. J. Shen, Y. Feng, P. Wang, G. Qiu, L. Zhang, L. Lu, H. Wang, R. Wang, V. Linkov, S. Ji, Conductive sulfur-rich copolymer composites as lithium-sulfur battery electrodes with fast kinetics and a high cycle stability. ACS Sustain. Chem. Eng. **8**, 10389–10401 (2020). https://doi.org/10.1021/acssuschemeng.0c01791
54. Y. Xie, H. Zhao, H. Cheng, C. Hu, W. Fang, J. Fang, J. Xu, Z. Chen, Facile large-scale synthesis of core–shell structured sulfur@polypyrrole composite and its application in lithium–sulfur batteries with high energy density. Appl. Energy **175**, 522–528 (2016). https://doi.org/10.1016/j.apenergy.2016.03.085
55. X. Wang, S. Zhang, H. Zhang, S. Gao, S. Han, Q. Xu, J. Xu, W. Lu, X. Wu, L. Chen, 3D porous spherical sulfur/carbon cathode materials with in situ vapor-phase polymerized polypyrrole coating layer for high-performance lithium-sulfur batteries. ACS Sustain. Chem. Eng. **7**, 17491–17499 (2019). https://doi.org/10.1021/acssuschemeng.9b04805
56. F. Wu, J. Chen, R. Chen, S. Wu, L. Li, S. Chen, T. Zhao, Sulfur/polythiophene with a core/shell structure: synthesis and electrochemical properties of the cathode for rechargeable lithium batteries. J. Phys. Chem. C **115**, 6057–6063 (2011). https://doi.org/10.1021/jp1114724
57. W. Wei, J. Li, Q. Wang, D. Liu, J. Niu, P. Liu, Hierarchically porous SnO_2 nanoparticle-anchored polypyrrole nanotubes as a high-efficient sulfur/polysulfide trap for high-performance lithium-sulfur batteries. ACS Appl. Mater. Interfaces **12**, 6362–6370 (2020). https://doi.org/10.1021/acsami.9b18426
58. T. Wang, D. Luo, Y. Zhang, Z. Zhang, J. Wang, G. Cui, X. Wang, A. Yu, Z. Chen, Hierarchically porous Ti_3C_2 MXene with tunable active edges and unsaturated coordination bonds for superior lithium-sulfur batteries. ACS Nano **15**, 19457–19467 (2021). https://doi.org/10.1021/acsnano.1c06213
59. N. Li, Z. Xu, P. Wang, Z. Zhang, B. Hong, J. Li, Y. Lai, High-rate lithium-sulfur batteries enabled via vanadium nitride nanoparticle/3D porous graphene through regulating the polysulfides transformation. **398**, 1–8 (2020). https://doi.org/10.1016/j.cej.2020.125432
60. Y. Zhang, W. Tang, R. Zhan, H. Liu, H. Chen, J. Yang, M. Xu, An N-doped porous carbon/MXene composite as a sulfur host for lithium-sulfur batteries. Inorg. Chem. Front. **6**, 2894–2899 (2019). https://doi.org/10.1039/c9qi00723g
61. X. Liang, Y. Rangom, C.Y. Kwok, Q. Pang, L.F. Nazar, Interwoven MXene nanosheet/carbon-nanotube composites as Li–S cathode hosts. Adv. Mater. **29**, 1–7 (2017). https://doi.org/10.1002/adma.201603040

62. H. Liu, H. Guo, N. Wu, W. Yao, R. Xue, M. Wang, W. Yang, Rational design of nickel-cobalt selenides derived from multivariate bimetal metal-organic frameworks for high-performance asymmetric supercapacitor. J. Alloys Compd. 156535 (2020). https://doi.org/10.1016/j.jallcom.2020.156535
63. J. Zhou, R. Li, X. Fan, Y. Chen, R. Han, W. Li, J. Zheng, B. Wang, X. Li, Environmental Science for sulfur storage in fast, long-cycle Li–S batteries. Energy Environ. Sci. **7**, 2715–2724 (2014). https://doi.org/10.1039/c4ee01382d
64. S. Li, Z. Zhao, S. Wang, R. Liang, Z. Li, G. Chen, Graphene-wrapped chromium-MOF (MIL-101)/sulfur composite for performance improvement of high-rate rechargeable Li–S batteries. J. Mater. Chem. A **2**, 13509–13512 (2014). https://doi.org/10.1039/c4ta01241k
65. K. Xi, S. Cao, X. Peng, C. Ducati, R.V. Kumar, A.K. Cheetham, Metal–organic frameworks for lithium sulphur batteries. **49**, 2192–94 (2013). https://doi.org/10.1039/c3cc38009b
66. A. Wei, L. Wang, Z. Li, Metal-organic framework derived binary-metal oxide/MXene composite as sulfur host for high-performance lithium-sulfur batteries. J. Alloys Compd. **899**, 163369 (2022)

Pseudocapacitive Materials for Metal-Air Batteries

Allen Davis and Ram K. Gupta

Abstract Clean energy storage is a problem faced by many nations around the world. These issues range from storing fluctuating energy from green energy storage to improving the battery life of smart devices. Additionally, the need for flexible electronics is rapidly rising in the medical and private fields of use. All these devices require storage sources with high energy density, long life, and reusability. Metal air batteries (MABs) exist as an up-and-coming device that can fit each of these needs handily. MABs boast an incredibly high potential energy density, environmental compatibility, and potential for reuse or recharge. Additionally, specific engineering methods allow for these devices to be engineered for high flexibility. To further improve the efficacy of these devices, pseudocapacitive integration has been explored. By imbuing a redox nature further energy storage is possible. Given these facts, the functionality of MABs is explored in brief, alongside the integration of different materials to improve their performance and flexibility.

Keywords Energy storage · Metal-air battery · Pseudocapacitance · Transition metal oxides · Flexible materials

1 Introduction

Efficient energy usage has been a hallmark of an advancing society since the dawn of the written word. In early history, the wheel and axle were developed to efficiently leverage mechanical energy. At first, wheels were used to transport heavy loads quicker than they could be on foot. As society developed, earthen wheels known as millstones became more common, converting the force of wind and water into a grinding force for food production. The simple design of both wind and water

A. Davis · R. K. Gupta (✉)
Department of Chemistry, Pittsburg State University, Pittsburg, KS 66762, USA
e-mail: ramguptamsu@gmail.com

National Institute for Materials Advancement, Pittsburg State University, Pittsburg, KS 66762, USA

© The Author(s), under exclusive license to Springer Nature Switzerland AG 2024

R. K. Gupta (ed.), *Pseudocapacitors*, Engineering Materials,
https://doi.org/10.1007/978-3-031-45430-1_19

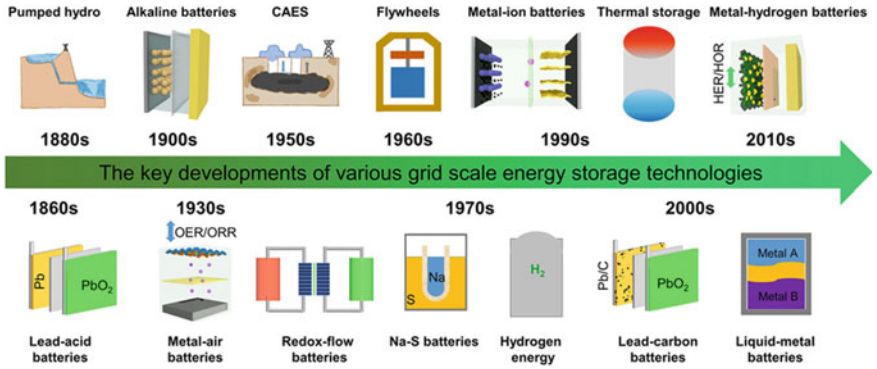

Fig. 1 The evolution of different grid-scale storage devices from 1860 to 2010. Adapted with permission [1]. Copyright © 2022, American Chemical Society

mills is replicated today in the construction of wind turbines and hydroelectric dams. Innovation, however, has brought humanity beyond its reliance on these two methods, with solar, nuclear, and a litany of other sources becoming ever more popular for clean and efficient energy generation. The excess of available energy has led to a new problem, however, the growing need for energy storage. When considering the scope of energy storage in society, grid storage, commercial storage, and personal storage are of top priority. Grid energy storage is the large-scale storage of energy for use in the electrical grid. Grid storage is done either to stabilize intermittent energy sources like wind and solar or to store the excess power of high-output energy emitters like oil and nuclear. Due to the scale involved, grid energy storage methods can be seen as atypical when compared to common sources, as seen in Fig. 1 [1].

Gravitational, compressed air, and water pump storage use potential energy as a physical form of energy storage, while flywheels store energy kinetically. Chemical energy storage is popular at this level as well, with a larger variety of batteries seeing use for this application. Commercial energy storage is significantly smaller in scale, existing at the building scale in lieu of the grid scale. At this level, chemical and thermal storage become more popular due to the scale limitations. Air conditioning units, for example, often make use of thermal energy storage to lower overall energy costs. Personal scale energy storage involves the capacitors and batteries used in everyday life. Capacitors physically store electrical charge on their surface and excel in applications where short bursts of energy are required. Meanwhile, batteries store their energy chemically, requiring a reaction of different reagents to create electricity. Batteries of all kinds are ubiquitous due to their portability and variety. While batteries have gotten more efficient, the overall designs have hardly changed. The first battery design was known as the voltaic pile, as seen in Fig. 2 [2].

This device consisted of a repeating pattern of zinc and copper electrodes separated by an electrolyte-soaked piece of cardboard. Each Zn–Cu set acted as an individual battery, combining additively to increase the overall voltage. Later, the first rechargeable batteries were created in the form of lead acid batteries. These batteries were

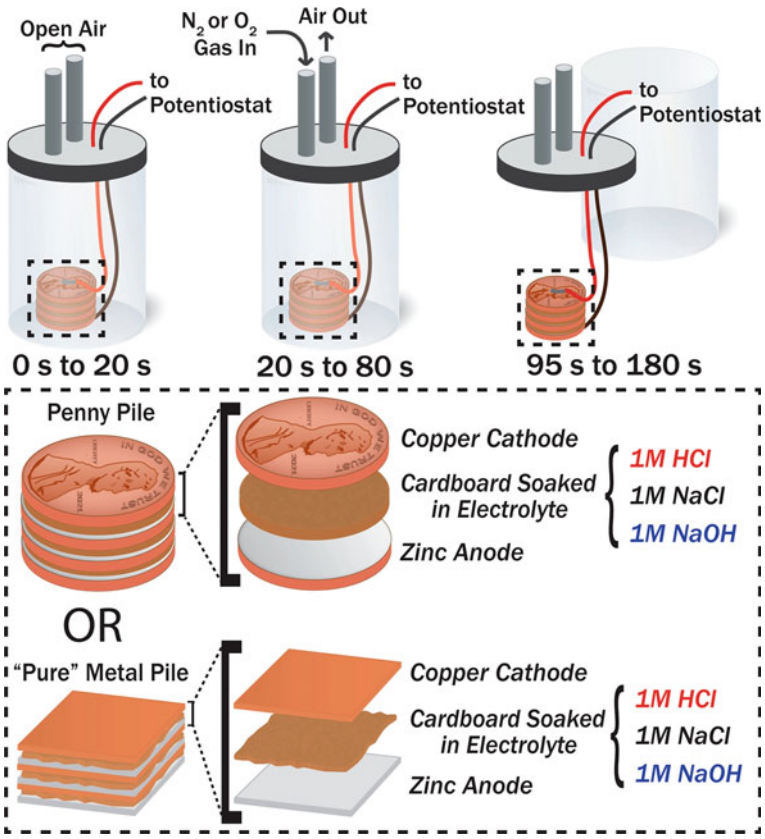

Fig. 2 Graphical example of a simple home-made metal air battery. Adapted with permission [2]. Copyright © 2021, American Chemical Society

much more efficient than the old voltaic piles, however, they were also large and unwieldy. Ni–Cd batteries were later developed, to fill the role of portable storage batteries. While these batteries were initially large, further technology reduced their size greatly. One of the greatest advancements in battery creation was the advent of alkaline batteries. These batteries could be made compact, with moderate energy density and low cost. These batteries often lack rechargeability and as such, must be disposed of after their power is drained. Lithium-ion (Li-ion) batteries were developed to counter this issue and are used globally for most portable consumer electronics. An additional benefit of Li-ion batteries is their high-power density, allowing them to be used for energy intensive devices. One important type of battery not discussed thus far is the metal air battery (MAB). MABs were discovered sometime after the voltaic pile but were not used commercially until the 1930s. Unlike the other batteries discussed here, MABs are designed to be partially open to air. This is because ambient oxygen is required to drive the electrochemical reaction. While this

process will be discussed in depth later, the general principle is that O_2 is reduced into hydroxide ions at the cathode. These hydroxide ions then go on to oxidize the metal anode, creating an electrical current in the process. This style of reaction has two major advantages for battery applications. The first advantage is that the reaction is reversible, meaning that the anode component of MABs can be recycled for further use. The second advantage is the material availability of certain metals versus other battery options. While lithium air batteries suffer the same scarcity issues that lithium-ion batteries have, other options are much more common. Aluminum, nickel, iron, and zinc are all exceedingly common metals that are accessible for battery use. Due to these facts, MABs are a hot topic in energy research, with many options being reviewed to enhance their performance. Pseudocapacitive materials are one of the larger areas of interest due to the supplemental storage they can offer. Pseudocapacitive materials store electrical energy both chemically and physically, improving overall energy storage in a material. Examples of such materials include metal oxides, metal sulfides, metal phosphides, conducting polymers, and composites. One other method to improve MABs is in the realm of flexibility. As the market for portable and wearable technology expands, flexible energy storage needs expand concurrently. Such devices require a flexible form of battery to operate ergonomically, a niche that is also explored with MABs.

2 Metal-Air Batteries: Fundamentals and Working

MABs, like all batteries, rely on electrochemical reactions to produce electrical energy. The unique requirement of free oxygen, however, makes MABs unique in design. MABs are composed of three distinct parts that contribute to energy generation. These parts are the anode, electrolyte, and cathode. The anode of a MAB is often made from a solid metal, of which its composition dictated the name and function of the battery. The electrolyte serves as a medium for ion transport and can be aqueous or nonaqueous depending on the reagents within the battery. Finally, the cathode of a MAB is designed to be extremely porous, allowing for the diffusion of oxygen through its structure. Each of these three components is vital for the electrochemical reaction to proceed and generate energy. For aqueous MABs, the reaction begins after oxygen diffuses into the system. At the anode, the metal species oxidizes into metal cations and electrons. Meanwhile, atmospheric oxygen reduces into hydroxide ions via the oxygen reduction reaction (ORR). Like other batteries, the flow of electrons generated from this process goes on to power the device of choice. However, this process results in the formation of metal oxide, with the content increasing as the battery depletes. For nonaqueous MABs, the process is slightly different, with the anode kicking off metal cations, followed by the formation of multioxidative metal oxide species. These reactions are demonstrated in Fig. 3 [3].

With the overall reaction in mind, research is performed to improve at least one of the core portions of the battery. In terms of the anode, different metals exhibit different electrochemical properties. These different properties influence the overall

Aqueous:	Nonaqueous:
Anode	**Anode**
$M \rightarrow M^{n+} + ne^-$	$M \leftrightharpoons M^+ + e^-$
$Mn^+ + 4OH^- \rightarrow M(OH)_4^{n-}$	
$M(OH)_4^{n-} \rightarrow MO + H_2O + 2OH^-$	
Cathode	**Cathode**
$O_2 + 2H_2O + 4e^- \rightarrow 4OH^-$	$xM^+ + O_2 + xe^- \leftrightharpoons MxO_2$

Fig. 3 Comparison of the electrochemical chemical half reactions that take place at the electrodes of both a aqueous and nonaqueous MAB

construction, and name, of the battery. Alkali and alkali-earth metals are known for their explosive reactivity with water, as such, they often require nonaqueous electrolytes. Meanwhile, transition metals such as zinc, cobalt, and iron oxidize readily in an aqueous solution. While the influence on the electrolyte is important, a more pressing concern is the metals theoretical energy density. The theoretical energy density of the battery is dependent on the metal selected for reaction, while the actual energy density is limited by kinetics, corrosion, and entropy. As seen in Fig. 4, lithium, aluminum, and magnesium have the highest theoretical energy density [3]. Even so, zinc-based batteries are one of the most popular items of MAB research around the world. This is due to two major limitations, material cost and electrode corrosion. While lithium air batteries may boast a high energy density, lithium itself is costly and competitive in other battery designs. Meanwhile, while corrosion is a consistent problem, it affects certain metals to different degrees. Aluminum for example, is heavily afflicted by corrosion when used as a battery limiting its use. As far as reducing an anode's corrosion, some work has been done to implement alloyed materials [4], apply surface modifications [5], or completely change the microstructure [6]. As with many problems, the design and function of the anode is but a portion of a complex system.

For a MAB to function correctly, efficient ion exchange must be observed. Thus, the selection of a proper electrolyte is an equally important consideration to the anode. As an example, lithium's volatility somewhat prohibits the selection of an aqueous electrolyte. While some examples of an aqueous Li-air battery do exist, they require extra components to prevent failure [7]. Due to this fact, aprotic, gel polymer, and solid-state electrolytes are preferred for battery construction [8–10]. Meanwhile, many of the less volatile transition metals are compatible with aqueous electrolytes. The advantage of aqueous based MABs is the higher availability and lower cost when compared to other costly solvents. Another concern in electrolyte selection is MAB's real life applications. Volatility, flexibility, and internal dynamic requirements can rapidly vary between applications. While these properties can be affected by the electrode material, electrolyte failure is liable to happen first. Nevertheless, the single most important property of the electrolyte is its capability for ion exchange. If hydroxide ions are unable to diffuse to the anode, the oxidation will fail to occur, and no energy will be generated.

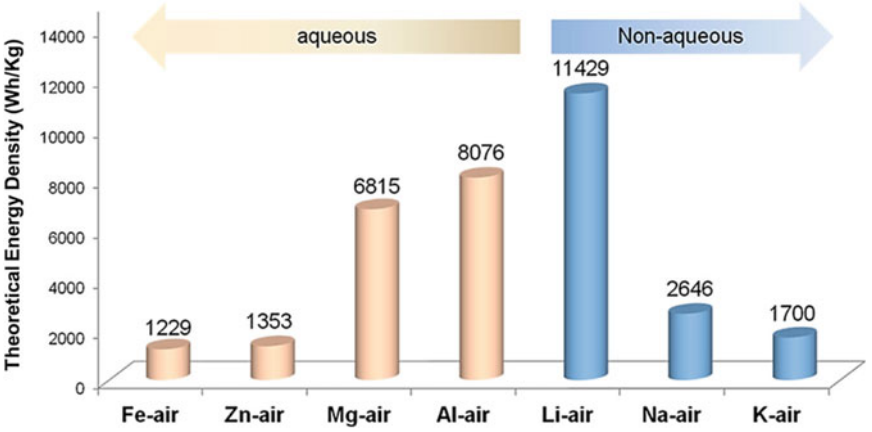

Fig. 4 Comparison of the theoretical energy density of different MABs. Adapted with permission [3]. Copyright © 2017, American Chemical Society

The third critical portion of a MAB is the oxygen reducing cathode. MAB cathodes are the limiting step of the overall reaction due to the sluggish kinetics involved in oxygen reduction. As such, they are also the most highly researched segment of MAB battery construction. Improving the kinetics of the ORR is an obvious point of investment, however, other improvements are also under review. Battery lifespan, for example, is important when considering the long-term use of MABs. One consideration for life extension is improving the electrode's electrocatalytic stability. This is often achieved by tuning the electrode's properties to reduce competitive reactions and electrochemical breakdown. One final zone of research is investigating bifunctional integration into the cathode end of the device to endow rechargeability. While generally non-rechargeable, engineering the cathode to participate in the oxygen evolution reaction (OER) when charged. This process allows for the batteries to be recharged and reused, further improving the functional lifespan of the battery.

With the different battery components, alongside their differing attributions to battery function, considered, the next step is observing their efficacy. There are a variety of different tests and measurements that can be performed to observe the real-world implementation of a MAB. The battery's lifespan, energy density, power density, and operating voltage are all important metrics of battery operation. Battery lifespan is a complex system reliant on many factors in battery construction. However, the generally accepted stability testing process for rechargeable batteries involves repeated charge/discharge of the battery, while measuring its change in the voltage polarization curve over time. Energy density and power density are similar terms that have vastly different meanings. Energy density refers to the total amount of energy stored in the battery per unit volume (J/m^3). Meanwhile, power density is the rate at which the battery delivers power per unit volume (W/m^3). While these methods are volumetric, areal measurements are also popular for battery specification. Operating voltage is related to the output of the battery when applied to the system. For example,

a 9 V battery can have an operating voltage ranging from ±0.5 V depending on its make. As the battery degrades the operating voltage shrinks until it fails to power the system. As such, operating voltage is an important characteristic to measure when considering battery function.

3 MAB Using Pseudocapacitive Materials

3.1 Transition Metal Oxides/Sulfides/Phosphide

The first category of pseudocapacitive materials under review are transition metal oxides (TMOs), sulfides (TMSs), and phosphides (TMPs). These three materials share many distinct similarities and differences that make them invaluable for electrochemical research. For starters, these compounds are of relatively low cost when compared to other battery materials [11]. Not only are they economically friendly, but environmentally friendly as well, with many options found directly in nature [12]. TMOs are renowned for their redox activity, finding extensive use as a pseudocapacitive supplement to more standard capacitor setups [13]. TMSs demonstrate further redox potential through their S–S bonds, allowing for rapid electron transfer [14, 15]. Finally, TMPs demonstrate improved electrochemical properties due to the high electronegativity of phosphorus [16]. While each of these materials are different, they confer similar electrochemical benefits. For example, improved conductivity, electron transport, and redox capability can be observed in each of these cases. With these prospects in mind there are plenty of examples where transition metal-based materials improve battery viability.

Zinc air batteries are a popular choice for development, this is in part due to the rechargeable nature achieved with some battery designs. To exhibit rechargeability, the battery must efficiently perform both the usual ORR observed in discharge, as well as an oxygen evolution reaction (OER) for recharging. Li et al. investigated the use of spinel structured metal oxide composites as a ORR/OER bifunctional electrocatalyst [17]. For this study, the team constructed different aluminum precursor alloys with a small amount of metal varying from iron, cobalt, manganese, or X (Ni, Cr, Nb, V). These alloys were prepared via pure melting under an argon atmosphere, followed by melt spinning to for the desired ribbon structure. The metallic ribbons were then chemically dealloyed and annealed to produce metal oxide nanocomposites. Finally, the nanocomposites were made into electrocatalytic ink via sonication alongside carbon nanotubes and Nafion in an isopropanol solution. The inks were then dropped onto a glassy carbon electrode and dried for electrochemical testing. To ensure elemental dispersion, scanning transmission electron microscopy and energy-dispersive X-ray spectrometry (STEM-EDS) microscopy was used. Herein, the expected distribution of the different elements was observed, barring the FeCoNi, FeCoV, and FeCo-based oxides, which had regions lacking manganese due to phase separation in the alloy, as seen in Fig. 5 [17].

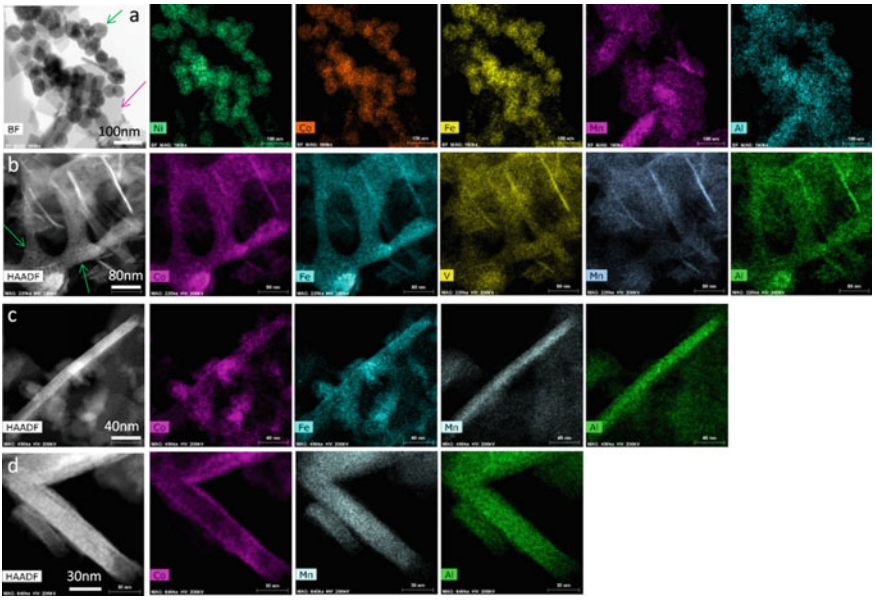

Fig. 5 STEM-EDS mapping of **a** dealloyed AlFeCoNiMn, **b** AlFeCoVMn, **c** AlFeCoMn, and **d** AlCoMnf. Adapted with permission [17]. Copyright © 2020, American Chemical Society

Furthermore, selective area electron diffraction (SAED) demonstrated the spinel type crystal structure. To measure the electrochemical ability of the materials, ORR, OER, and battery testing was performed. Overall testing demonstrated that Mn_3O_4 demonstrated improved ORR performance, with cobalt doping improving the effect and iron doping diminishing it. The best sample for OER proved to be the $(CoFe)_3O_4$-based oxides, with iron and manganese improving the ability. Additionally, it was observed that the addition of nickel, vanadium, or chromium further enhanced OER activity. The resulting $(FeCoNi)_3O_4/Mn_3O_4$-based Zn-air battery demonstrated a voltage gap of ~0.7 V, with good stability observed after 400 h of cycling at 2 mA/cm^2. Furthermore, a power density of ~136 mW/cm^2 was observed, indicating fantastic battery capability.

Meanwhile, metal sulfides have also been tested for zinc air battery construction. Shang et al. explored the construction of zinc air batteries containing core–shell-structured $NiO@Co_3S_4$ electrodes [18]. TMS materials often demonstrated better reversibility when compared to metal oxide materials. This is attributed to the lower electronegativity of sulfur as compared to oxygen. For this study Co_3S_4 was selected due to its desirable structure and electrochemical performance. To synthesize the $NiO@Co_3S_4$ electrodes, Co_3O_4 was grown on nickel foam and added to an autoclave. Next, an aqueous solution containing sodium sulfide nonahydrate was added to the autoclave which was then treated to hydrothermal synthesis. The resulting material was finally heat treated to create the $NiO@Co_3S_4$ electrodes. The nanostructure of the

electrode resembles nanowires of Co_3S_4 coated with a NiO_2 shell, hence the designation $NiO@Co_3S_4$. The confirmation of the material's structure and composition was observed using SEM, TEM, XRD, and XPS. Herein, wiry, hair like, prongs were observed with the SEM, while the encapsulated structure was observed with TEM. Furthermore, elemental mapping confirmed the expected elemental composition of the material as seen in Fig. 6. Battery testing revealed that the electrode can produce maximum power density of 26.2 mW/cm^2 at 49.4 mA/cm^2. Subsequently, the electrode demonstrates two operating voltage plateaus of 1.75 and 1.28 V at 1 mA/cm^2. These factors, alongside high stability, demonstrate the potential for metal sulfides for battery construction.

TMPs are an attractive option for electrocatalyst construction due to their complex crystalline nature and electronic interactions [19]. Wang et al. explored the construction of CoP nanoparticles embedded on (N,P) co-doped carbon for Zn-air batteries [20]. The nanoparticles themselves were synthesized through a metal organic framework (MOF) templating method. In this method, an equal mix zinc nitrate hexahydrate and cobalt nitrate hexahydrate were dissolved in water, after which 2-methylimidazole was added. The mixture was stirred at room temperature for 5 h to form the MOF. The resulting material was then separated, washed, and lyophilized to obtain the powdered product. To create the final product, the ZnCo-MOF precursor was phosphorized in a tube furnace using disodium hydrogen phosphate. This process simultaneously created the TMP, decomposed the MOF into a porous nitrogen doped carbon substrate, and further doped said substrate with phosphorus. As far as battery applications are concerned, the material demonstrated a heightened power density of 186 mW cm^{-2} alongside a minuscule charge–discharge potential gap of ~1 V.

3.2 Conducting Polymers

Intrinsically conducting polymers (ICPs) are a unique class of polymeric materials that are conducive to electron flow [21]. Examples of ICPs include polyaniline (PANi), polyvinylidene fluoride (PVDF), polypyrrole (PPy), and polyacetylene (PA) [22]. Traditional organic polymers are insulative in nature due to the sp^3 hybridization along the length of their chain. This is because the electrons responsible for binding are locked in place and are unable to flow. ICPs, however, are sp^2 hybridized, meaning that conjugated π bonds are present along the length of the chain. Conjugated bonds lend to a property known as resonance, in which the spare electrons are nonlocalized on the chain, allowing for electron flow. While maintaining a high conductivity is helpful for electrode construction, this is only half of the picture. For ICPs to demonstrate a pseudocapacitive nature, redox activity must be observed. Such redox activity is imbued to ICPs via doping. Doping is the process of purposely adding impurities to a material to enhance its electrochemical effects. This can occur either through the inclusion of electron doners (N-doping), or electron acceptors (P-doping). While both methods have opposing implementations, the result is a conductive polymer matrix capable of ionization. Despite these facts, research

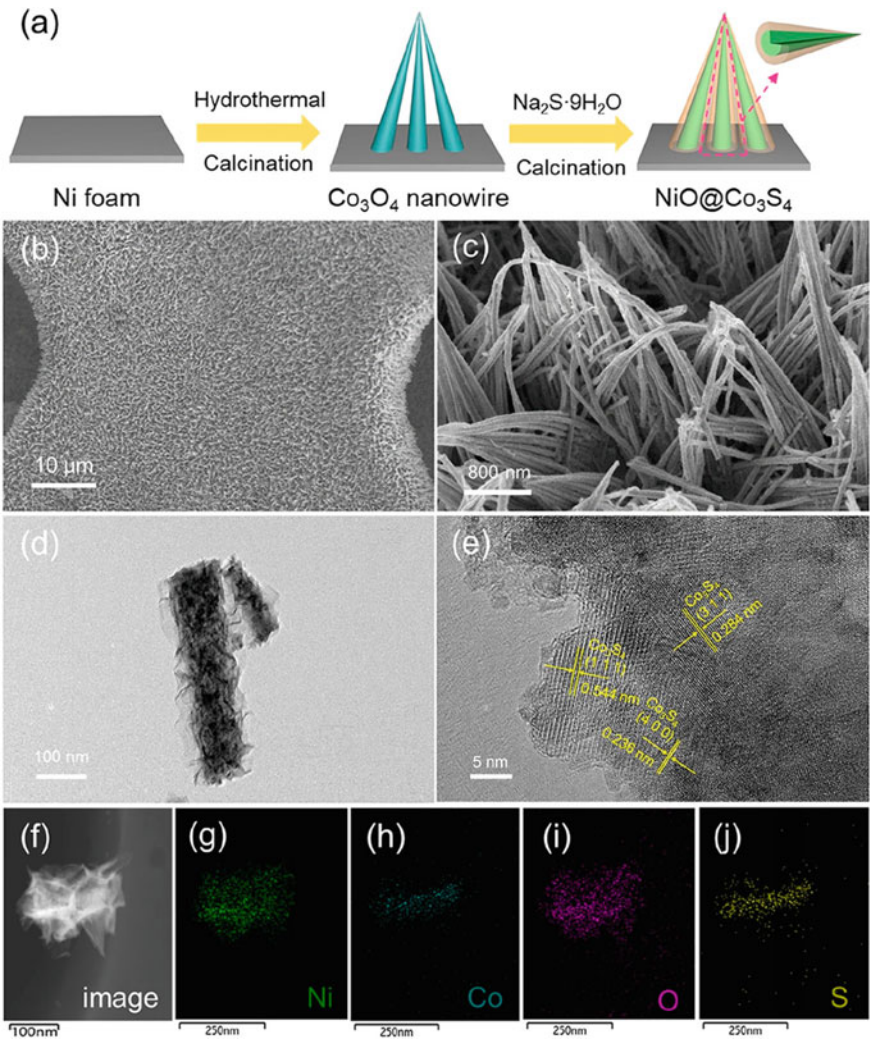

Fig. 6 **a** Synthesis diagram of $NiO@Co_3S_4$, **b**, **c** SEM images of $NiO@Co_3S_4$, **d** TEM image of $NiO@Co_3S_4$ of a single nanowire, **e** HRTEM image of $NiO@Co_3S_4$, and **f**–**j** TEM mapping of $NiO@Co_3S_4$. Adapted with permission [18]. Copyright © 2022, American Chemical Society

on pseudocapacitive conducting polymers for MABs is almost nonexistent beyond one specific application. Conducting polymers make for an excellent electrolyte/ion exchange material. This is due to the flexibility, conductivity, and compatibility of conducting polymers when implemented in this fashion. Due to the limitations on applicable data, stability and battery lifespan will be of greater focus as compared to voltage measurements.

The benefits of a compatible electrolyte when designing a MAB cannot be understated. At best an incompatible electrolyte will be inefficient or ineffective. At worst, the wrong electrolyte could lead to explosive results. One common issue faced by MABs is the process of dendritic growth. In this process, tree-like dendrites grow out from the electrodes, eventually these dendrites reach the opposing electrode and short circuit the battery or rupture the electrolyte [23]. Carbonate growth is another unintended side reaction that can prove harmful to MAB operation. While dendrite growth primarily affects the anode, carbonate accumulation occurs at the cathode. This process occurs when CO_2 enters the MAB. When CO_2 comes across the cathode, a competitive side reaction produces carbonate ions that interfere with battery processes [24]. To reduce the formation of these side products, Chen et al. designed a bipolar conducting polymer membrane to improve the stability of zinc-air batteries [25]. The membrane itself was designed to have a cationic layer and an anionic layer, with a catalytic layer in between. This setup allows for a pH difference across the membrane, which further enhances the unique electrocatalytic processes of the respective electrodes. To create the bipolar membranes, a Fumasep anion exchange membrane was prepared for a drop casting process. Next, a graphene oxide solution was drop cast onto the membrane, followed by a Nafion solution that was sprayed on the surface. For electrochemical testing, the bipolar membrane was compared to a standard nylon separator over different current densities. In testing, the nylon separated samples failed over so many cycles, meanwhile, the bipolar membrane demonstrated exceptional stability up to 300 h of cycling at 5 mA/cm^2. The stability comparison of the nylon separated battery and the bipolar separated battery is visible in Fig. 7 [25].

Ionic liquids are a powerful family of compounds that are under investigation for energy storage applications. Unlike salts which are solid at room temperature and must be dissolved, ionic liquids are capable of dissociating at lower temperatures, with some being liquid at room temperature. While ionic liquids can be used directly as an electrolyte, certain properties can be improved by including it in a conductive polymer gel. Unlike rigid solids and incompressible liquids, gel materials can

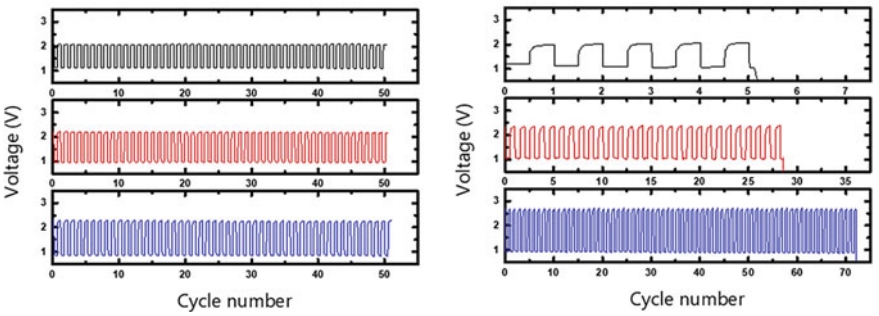

Fig. 7 Comparison of cycle life between the bipolar membrane batteries (left) and the nylon separated batteries (right). The black, red, and blue lines are 1, 5, 10 mA/cm^2, respectively. Adapted with permission [25]. Copyright © 2022, American Chemical Society

exhibit flexibility, compressibility, and mechanical stability. These properties are due to the unique interactions between the gel polymer network and the solvent within. While traditional materials dissolve in a compatible solvent, gels will swell. This fact alongside engineered chain flexibility allows a gel to be extremely flexible while still maintaining the electrolytic solvent. In one study, Shui et al. engineered two different ionic liquid-based gel polymer electrolyte membranes [26]. The two PVDF based membranes were labeled PVDF-[C_4mpyr]Cl, and PVDF-[BMIM]Cl. These gels were separated based on the ionic liquids they contained. PVDF-[C_4mpyr]Cl contained 1-butyl-1-methylpyrrolidinium chloride ([C_4mpyr]Cl), while PVDF-[BMIM]Cl contained 1-butyl-3-methylimidazolium chloride ([BMIM]Cl). These materials were created using the solution-casting method, wherein 30 wt% of PVDF-HFP, 60 wt% of the respective ionic liquid, and 10 wt% of $AgCl_3$ salt combined and stirred until viscous. Afterwards, the electrolyte was dried and stored for later device implementation. The finalized battery consisted of an aluminum anode, the designed gel electrolyte, and a commercially available air cathode. Initial testing demonstrated that PVDF-[C_4mpyr]Cl sample performed slightly better than the PVDF-[BMIM]Cl sample across the differing battery tests. This is especially visible in the open-circuit voltage spectra, where the samples exhibit a voltage of 1.16 and 1.09 V respectively. Further measurements showed a power density of 3.57 mW/cm^2, and a specific capacity of 532.7 mAh/g. To test the device's function under flex, the device was bent at 30°, 90°, and completely folded. During these flexural tests, galvanostatic discharge was measured over time, where it was observed that the PVDF-[C_4mpyr]Cl battery would lose some voltage when bent, as seen in Fig. 8 [26].

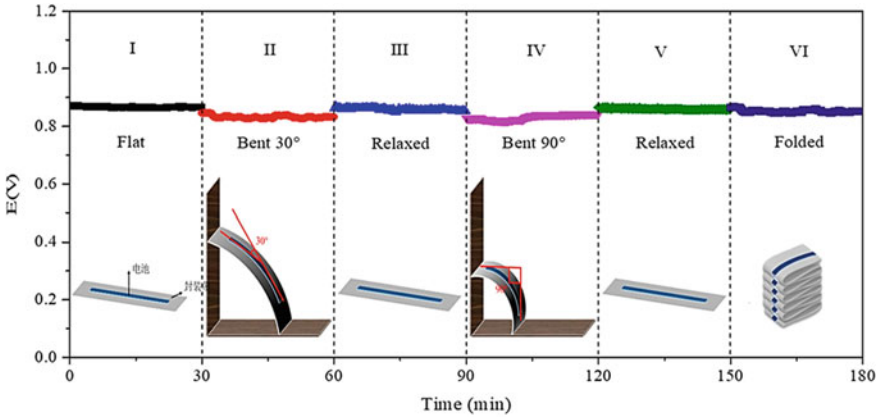

Fig. 8 Galvanostatic discharge of flexible aluminum-air battery with PVDF-[C_4mpyr]Cl in various configurations over time. Adapted with permission [26]. Copyright © 2022, American Chemical Society

3.3 Composites

The IUPAC gold book defines a composite as a "Multicomponent material comprising multiple, different (non-gaseous) phase domains in which at least one type of phase domain is a continuous phase" [27]. In simpler terms, a composite is the result of combining two or more separate materials to create something with properties unique to the sum of its parts. Examples of common composites include fiber reinforced plastics, particle board, and concrete. Taking fiber reinforced plastics as an example, fibrous materials have a high tensile strength, but completely lack rigidity. Meanwhile, plastics can demonstrate rigidity, but also suffer from when stretched. The resulting composite meanwhile exhibits a high degree of toughness because the weakness of one fraction is improved by the strengths of the other. As far as MABs are concerned, composite materials are the most common. In fact, almost every material discussed thus far can be considered a composite to a certain degree. For electrochemical devices, compositing is often performed to imbue pseudocapacitance into a purely conductive material, or vice versa. Further modifications could be sought to improve overall stability [28], reduce oxygen bubble accumulation [29], or introduce new physical properties into the material.

Graphene is a powerful material that is under scientific investigation for its variety of useful properties. Graphene has been explored for use as a conductor [30], mechanical enhancer [31], and filter [32]. These applications were selected due to graphene's high surface area and electronic structure. With a focus on improving graphene for energy storage, Ryu et al. explored the creation of a fluorinated graphene composite containing both silver nanoparticles and α phase NiO/$Ni(OH)_2$ [33]. $Ni(OH)_2$ was selected due to its low cost and environmental compatibility. Additionally, $Ni(OH)_2$ has two material phases, α-phase is randomly stacked along the c-axis of the crystalline plane, while β-phase $Ni(OH)_2$ is stacked in an ordered manner. For this study, α-phase $Ni(OH)_2$ was selected due to its improved electrochemical performance. To synthesize the α-NiO/$Ni(OH)_2$ material, nickel nitrate hexahydrate was dissolved alongside sodium dodecyl sulfate in a 50/50 ethanol-aqueous solution. Next, urea was added, and the solution was stirred until a green solution was obtained. The material was then separated, dried, and calcined to create $Ni(OH)_2$. Meanwhile, AgNP/F-graphene was synthesized from the photoirradiation of silver nitrate alongside F-graphene in an isopropanol solution. The final composite was synthesized from further photoirradiation of both the α-NiO/$Ni(OH)_2$ and AgNP/F-graphene materials, creating the α-NiO/$Ni(OH)_2$/AgNP/F-graphene composite. The microscopic structure of the material was gypsum rose-like in appearance under SEM due to the c-axis aligned crystals [33]. Electrochemical testing revealed that the material demonstrated a high affinity in terms of ORR-OER properties. As a Zn–Ni/Ag/air battery, a specific capacity of 1200 mAh/g was observed alongside a specific energy of 660 Wh/kg.

In a similar vein to graphene, carbon nanotubes (CNTs) are a novel material for conductive composites. Overall, CNTs can be considered the tubular cousin of the traditionally sheetlike graphene. One major benefit of this tubular structure

is the ability for CNTs to nestle other materials within. This fact, combined with their tunability, make CNTs an exceptional option for composite construction. For example, Kundu et al. experimented with MOF derived CNT encapsulated CoNi alloys for Zn-air battery electrocatalysts [34]. Like CNTs, some MOFs exhibit a high aspect ratio alongside their porosity. Furthermore, some of these MOFs can be reduced into carbon encapsulated metal composites, as seen in this report. To synthesize the sacrificial precursor MOF, trimesic acid, polyvinyl pyrrolidone, and a 3:1 mol ratio of nickel nitrate hexahydrate and cobalt nitrate hexahydrate was dissolved in a 1:1:1 ratio solution of dimethylformamide, ethanol, and water. The solution was then hydrothermally treated to produce the MOF, which was then separated, washed, and dried. To create the $Co_{0.25}Ni_{0.7}$ @NCNT composites, the MOF material was ground and mixed alongside dicyandiamide, then annealed first at 550 °C, and again at 750 °C. The purpose of the dicyandiamide was to dope the material with nitrogen, further improving the desired electrical properties. The battery itself demonstrated solid stability and a peak power density of 167 mW/cm^2.

One final class of materials that are popular for composite construction is the MXene family of materials. While generally similar in structure to graphene, MXenes have regular metallic inclusions that separate them as an entirely different material. One of the most unique traits that MXenes possess is their accordion-like structure [35]. This alternating atomic morphology changes the intermolecular stacking of the material, allowing for a greater variety of polymorphs. Another electrochemically active material that is of interest is the perovskite family of crystalline materials. Perovskites are in themselves a common crystal polymorph with desirable electrochemical properties. Taking advantage of this fac, Hui et al. developed a strontium titanate perovskite-Ti_3C_2 MXene composite (Ti_3C_2@$SrTiO_3$) for use as a zinc air battery electrocatalyst [36]. To create the perovskite composite, titanium carbide nanosheets were hydrothermally reacted with strontium hydroxide in extremely basic conditions. After 24 h of reaction, the material was washed and lyophilized to create the desired product. As seen in Fig. 9, the resulting material demonstrated perovskite crystal structures on the MXene sheets, with elemental analysis demonstrating elemental distribution. The Ti_3C_2@$SrTiO_3$ zinc air battery demonstrated powerful energy storage properties. A high open circuit potential of 1.44 V was observed alongside a power density of 122 mW/cm^2. The material also demonstrated excellent stability even after 1000 cycles.

4 Flexible Metal-Air Batteries

While improving the energetics of energy storage devices has always been a goal in research, recent technological developments have shed light on a new issue, flexibility. Wearable electronics are beginning to become a part of daily life, from medical devices to consumer electronics. One goal when designing such devices is the concept of ergonomics. The goal of ergonomics is to make a device or process more compatible with human interactions. In the case of wearable electronics, the

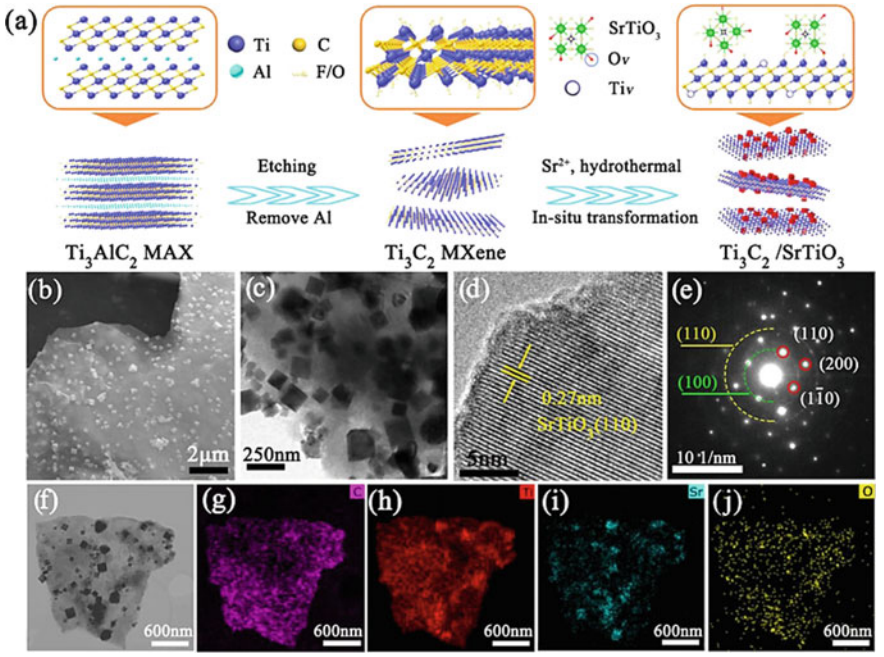

Fig. 9 Synthesis and morphological characterization of Ti_3C_2@$SrTiO_3$. **a** Schematic illustration for the preparation of the Ti_3C_2@$SrTiO_3$ composite; **b** SEM, **c** TEM, and **d** HRTEM images and **e** SAED pattern of Ti_3C_2@$SrTiO_3$; and **f**–**j**) TEM image and elements mappings of Ti_3C_2@$SrTiO_3$. Adapted with permission [35]. Copyright © 2022, American Chemical Society

electronic components themselves become the limiting factor. Solutions to some of these issues have been thoroughly explored, such as the creation of flexible logic devices [37], sensors [38], and displays [39]. Energy storage poses a unique problem however, in that traditional storage devices are bulky and inflexible. Thus, the goal is clear, to make effective, flexible, and ergonomic devices, a flexible energy storage system will be necessary. Such a solution has a major caveat, as the device will need to demonstrate the needed flexibility without sacrificing structural stability, energy storage efficiency, and safety. When constructing a flexible metal air battery, the electrolyte and the electrodes are the major bottleneck in design. Many solid and liquid state electrolytes risk rupture when flexed. Meanwhile, repeated flexing can physically wear down or snap the electrode depending on composition. As such, further characterization will take flexibility into account in addition to the standard measurements.

One attempt at creating a flexible MAB was pursued by Qu et al., who designed metal-coated polyurethane sponges as an electrode for a zinc-air battery [40]. Polyurethane foams can either be flexible or rigid depending on their design, however most polyurethanes are considered nonconductive. The opposite is true with metal electrodes, which are extremely conductive, but unable to naturally return to their

original state when bent. To get around this, Qu's team used both an electric and nonelectric plating method to coat a commercial polyurethane material. To achieve this, a clean polyurethane sample was soaked in a tin chloride solution for 30 min, then soaked in a palladium chloride solution. Afterwards, the material was added to a copper sulfate solution to copper plate the foam. Electroplating was then used to zinc plate the anode, and nickel plate the cathode. The resulting electrodes demonstrate extreme flexibility due to their polymeric nature. Furthermore, the strongest variant of the battery demonstrated an energy density of 23.6 W h L^{-1}, albeit with a slight reduction in flexibility. As with other samples, flexing leads to a slight reduction in electrochemical properties.

A similar study by Shui et al. designed a honeycomb shaped folding N/S codoped MnO_2 graphene composite material for flexible aluminum air batteries [41]. Metamaterial properties are an important aspect to consider when designing flexible materials. By designing material in a certain way, such as in the honeycomb pattern reported here, flexibility can be suffused to non-flexible materials. Such designs are often seen in the shipping industry, where cardboard spacers in a grid pattern gain anisotropic flexibility. To create the MnO_2-N/S graphene material, thiourea was slowly added to a graphene oxide solution. The N/S codoped graphene oxide was then mixed with manganese chloride tetrahydrate and potassium permanganate until a homogenous solution was formed. The solution was then reacted at an elevated temperature, cleaned, then lyophilized. To create the stretchy honeycomb metamaterial, layers of the battery were taped together in alternating spots. Battery testing demonstrated a variety of interesting properties, including an inbuilt battery activation feature, as seen in Fig. 10 [41]. Overall, the device demonstrated a specific capacity of 1203.2 mAh/g and an energy density of 1630.1 mWh/g. Additionally, the device maintained nominal output at up to 2500% elongation, and solid stability after 1000 stretch cycles.

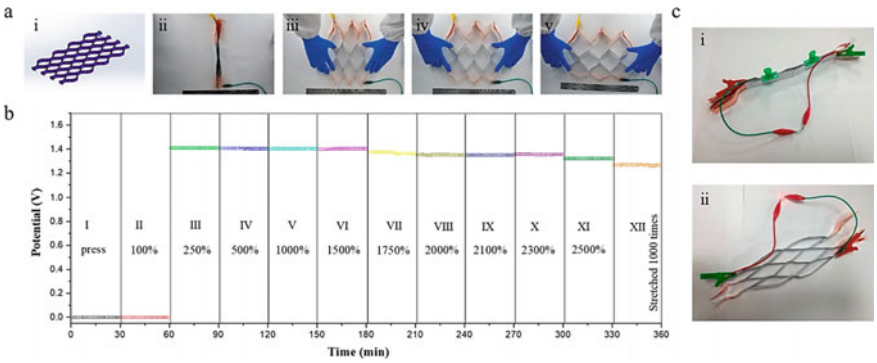

Fig. 10 **a** Demonstration of aluminum-air batteries' flexibility. **b** Galvanostatic discharge (1 mA/cm^{-2}) of the stretchable aluminum-air batteries at differing % elongations. **c** Demonstration of the batteries powering an LED. Adapted with permission [41]. Copyright © 2020, American Chemical Society

Extreme temperatures are a common concern when considering a device's operational conditions [42]. For a machine to be able to operate in arctic conditions, or at high altitudes, it must be resistant to cold temperatures. When considering batteries for low temperature applications, electrolyte swelling is a major concern. In aqueous electrolytes the fluid medium is likely to freeze, damaging the battery. Meanwhile, in gel electrolytes, trace bits of water can crystalize and damage the network. To counter these issues, Zhang et al. devised a flexible double-network electrolyte with extreme low temperature conditions [43]. To create the hydrogel electrolyte, a polyacrylamide hydrogel was made alongside a cellulose nanofiber hydrogel within the same vessel. The resulting PAM-CNF hydrogel was then soaked in an aqueous mixture of KOH and KI and allowed to swell. The final product demonstrated antifreezing properties alongside a fair bit of flexibility. The batteries made in this experiment demonstrated a narrow voltage gap of 0.43 V alongside a discharge voltage of 1.26 V and a charge voltage of 1.69 V at standard temperature. Meanwhile, the battery demonstrated a higher voltage gap of 0.74 V with a charge voltage of 1.75 V and discharge voltage of 1.03 V at −40 °C. While less efficient and flexible at these lower temperatures, most batteries fail well before −20 °C.

In addition to freezing temperatures, high humidity and rough conditions can cause extreme wear on a MAB. For many MABs, clipping, twisting, and full water immersion would cause rapid failure. However, Li et al. developed lithium air battery capable of activity in all of these scenarios [44]. The stalwart nature of this battery is attributed to its heavily integrated composite nature. The anode of the battery was made from lithium sheets rolled onto a copper mesh. The anode was then placed into a mold and suspended within a gel electrolyte precursor solution that was promptly cured. Finally, a cobalt oxide–carbon cloth cathode was used to sandwich the electrode. The assembled battery was then sealed and enclosed in a punched aluminum plastic film casing. Fortitude and flexibility were the main factors tested when observing battery operation. A high degree of cycling stability was observed at up to 180° of bending and lateral twisting. Furthermore, the battery was able to power an LED array under harsh bending, water submersion, partial cutting, and enclosure removal. The battery was also capable of extended operation at a relative humidity of ~50%, a trait which is uncommon amongst lithium air batteries.

While the prior battery was able to function when damaged, were it to be split it would cease to function. Such an issue is less so when considering regenerative materials. While not necessarily designed for MABs, Chen et al. developed a self-healing gel polymer electrolyte for lithium ion batteries [45]. Self-healing can be endowed to a material through ionic bonding, dynamic covalent interactions, and noncovalent interactions. In this materials case, self-healing is produced from noncovalent hydrogen bonding. The gel itself was formed from a complex polyvinylidene fluoride hexafluoropropylene copolymer with PEG-UPy side chains. To synthesize the gel electrolyte, UPyMA monomers were reacted with ethylene glycol using reversible addition-fragmentation chain transfer (RAFT) polymerization. The PEGMA-UPyMA copolymer was dispersed in dimethylformamide alongside PVDF-HFP and PEO. The solution was then spread across a glass plate to make the electrolyte film. A rough sketch of the synthesis, alongside the material's

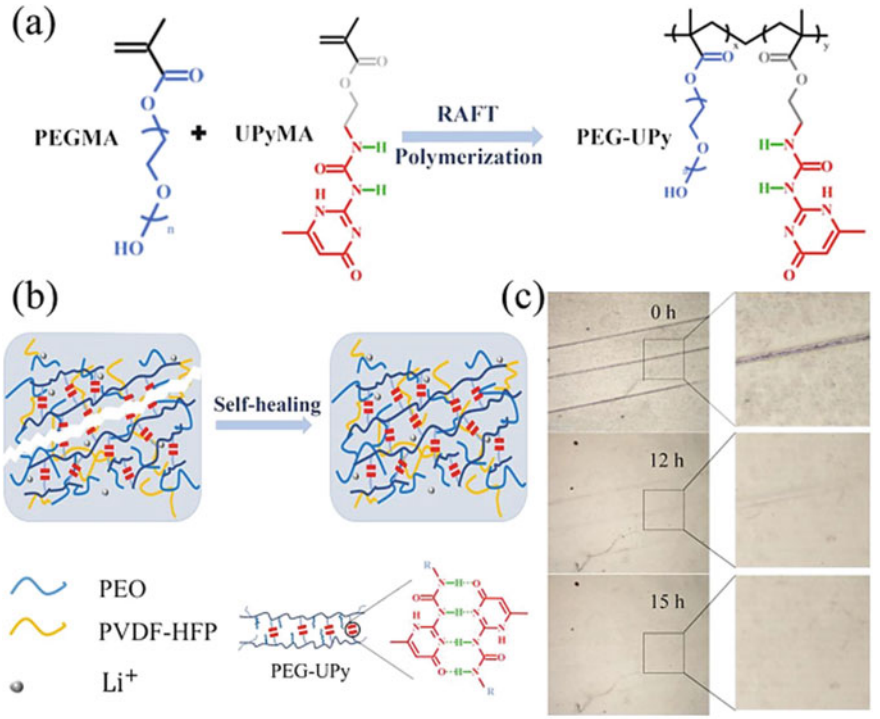

Fig. 11 **a** Schematic of the synthesis of brush-like copolymer PEG-UPy. **b** Graphic illustration of the formation of the PP-PU and the self-healing mechanism. **c** Images of the self-healing process of the gel electrolyte under standard conditions. Adapted with permission [45]. Copyright © 2022, American Chemical Society

self-healing properties, can be seen in Fig. 11. As shown in this figure, the material can heal so well that the original cut is invisible after 15 h of ambient self-repair. However, the initial repair can happen as quickly as 30 min after separation. The gel electrolyte also demonstrated excellent flexibility, with the material flexing up to 720° without structural failure.

5 Conclusion and Future Remark

With reliable energy storage becoming a major concern, renewable and reusable materials have grown in market value. This growth is particularly visible in the realm of consumer electronics, which generates great demand and even greater waste. The most popular source of power for these devices are lithium-ion batteries, which exhibit a long lifespan and a rechargeable nature. Lithium, however, is a volatile material that is prone to explosive failure if the batteries housing is breached and

exposed to water. Additionally, lithium is becoming increasingly expensive due to its intensive harvesting process and relative scarcity. To circumvent these issues, alternative sources are under investigation. MABs preside as one of the most popular alternatives that have been researched thus far. These batteries are popular due to their renewability, generally low cost, and environmental compatibility. Transition metals are abundant in nature and widely used in many fields. Subsequently, the metal oxides and hydroxides are low in cost and environmentally friendly when disposed of properly. Of even greater importance is the fact that the metal-based residue can be recycled back into their base metal, allowing them to be used for battery construction all over again. The greatest limitation of these batteries is their high rate of corrosion and overall lack of traditional rechargeability. One solution to these issues is the inclusion of pseudocapacitive materials into the device. Metal oxides, conducting polymers, and composites have all demonstrated their potential for improving the capabilities of MABs. This is due to the additional energy storage granted by their redox active behavior. Further electronic integration has been explored in the field of flexible batteries. Forward thinking designs all but ensure that metal air batteries will be a popular form of energy storage soon, barring any major discoveries in other fields. Prospects for the wider implementation of metal air batteries would be to unlock their maximum energy density. MABs have some of the highest potential energy densities reported, however, most implementations only scratch the surface of their potential. Regardless, due to their low cost, ease of swapping, and recyclable nature, MABs are at minimum a fantastic contender as the disposable battery of the future. With further tuning of these devices, MABs are likely to find purchase in other fields as well, such as in the medical field for use in integrated electronics, or in larger scale applications such as grid scale energy storage and as a power source for heavy machinery. While one might see a bleak future regarding humanities' rampant misuse of technology and the environment. Sustainable materials and devices like those seen in MABs echo calls of a bright future ahead.

References

1. Z. Zhu, T. Jiang, M. Ali, Y. Meng, Y. Jin, Y. Cui, W. Chen, Rechargeable batteries for grid scale energy storage. Chem. Rev. **122**, 16610–16751 (2022)
2. T.B. Clarke, M.W. Glasscott, J.E. Dick, The role of oxygen in the voltaic pile. J. Chem. Educ. **98**, 2927–2936 (2021)
3. Y. Li, J. Lu, Metal-air batteries: will they be the future electrochemical energy storage device of choice? ACS Energy Lett. **2**, 1370–1377 (2017)
4. P. Zhang, X. Liu, J. Xue, K. Jiang, The role of microstructural evolution in improving energy conversion of Al-based anodes for metal-air batteries. J. Power Sources **451**, 227806 (2020)
5. S.-M. Lee, Y.-J. Kim, S.-W. Eom, N.-S. Choi, K.-W. Kim, S.-B. Cho, Improvement in self-discharge of Zn anode by applying surface modification for Zn–air batteries with high energy density. J. Power Sources **227**, 177–184 (2013)
6. D. Huang, F. Cao, T. Ying, D. Zheng, G.-L. Song, High-energy-capacity metal-air battery based on a magnetron-sputtered Mg–Al anode. J. Power Sources **520**, 230874 (2022)
7. A. Manthiram, L. Li, Hybrid and aqueous lithium-air batteries. Adv. Energy Mater. **5**, 1401302 (2015)

8. Z. Jiang, A.M. Rappe, Mechanistic study of the Li–air battery with a Co3O4 cathode and dimethyl sulfoxide electrolyte. J. Phys. Chem. C **125**, 21873–21881 (2021)
9. J. Yi, X. Liu, S. Guo, K. Zhu, H. Xue, H. Zhou, Novel stable gel polymer electrolyte: toward a high safety and long life Li–air battery. ACS Appl. Mater. Interfaces **7**, 23798–23804 (2015)
10. Y. Liu, B. Li, H. Kitaura, X. Zhang, M. Han, P. He, H. Zhou, Fabrication and performance of all-solid-state Li–air battery with SWCNTs/LAGP cathode. ACS Appl. Mater. Interfaces **7**, 17307–17310 (2015)
11. P. Lang, N. Yuan, Q. Jiang, Y. Zhang, J. Tang, Recent advances and prospects of metal-based catalysts for oxygen reduction reaction. Energy Technol. **8**, 1900984 (2020)
12. A.A. Keller, H. Wang, D. Zhou, H.S. Lenihan, G. Cherr, B.J. Cardinale, R. Miller, Z. Ji, Stability and aggregation of metal oxide nanoparticles in natural aqueous matrices. Environ. Sci. Technol. **44**, 1962–1967 (2010)
13. W. Deng, X. Ji, Q. Chen, C.E. Banks, Electrochemical capacitors utilising transition metal oxides: an update of recent developments. RSC Adv. **1**, 1171–1178 (2011)
14. R. He, X. Huang, L. Feng, Recent progress in transition-metal sulfide catalyst regulation for improved oxygen evolution reaction. Energy Fuels **36**, 6675–6694 (2022)
15. J. Wu, T. Ye, Y. Wang, P. Yang, Q. Wang, W. Kuang, X. Chen, G. Duan, L. Yu, Z. Jin, J. Qin, Y. Lei, Understanding the catalytic kinetics of polysulfide redox reactions on transition metal compounds in Li–S batteries. ACS Nano **16**, 15734–15759 (2022)
16. J. Yang, Z. Wang, Z. Wang, J. Zhang, Q. Zhang, P.P. Shum, L. Wei, All-metal phosphide electrodes for high-performance quasi-solid-state fiber-shaped aqueous rechargeable Ni–Fe batteries. ACS Appl. Mater. Interfaces **12**, 12801–12808 (2020)
17. S. Li, X. Zhou, G. Fang, G. Xie, X. Liu, X. Lin, H.-J. Qiu, Multicomponent spinel metal oxide nanocomposites as high-performance bifunctional catalysts in Zn–Air batteries. ACS Appl. Energy Mater. **3**, 7710–7718 (2020)
18. W. Shang, W. Yu, X. Xiao, Y. Ma, Y. He, P. Tan, Free-standing electrode of core–shell-structured NiO@Co3S4 for high-performance hybrid Zn–Co/Air batteries. Energy Fuels **36**, 1121–1128 (2022)
19. C.A. Downes, K.M. Van Allsburg, S.A. Tacey, K.A. Unocic, F.G. Baddour, D.A. Ruddy, N.J. LiBretto, M.M. O'Connor, C.A. Farberow, J.A. Schaidle, S.E. Habas, Controlled synthesis of transition metal phosphide nanoparticles to establish composition-dependent trends in electrocatalytic activity. Chem. Mater. **34**, 6255–6267 (2022)
20. Y. Wang, M. Wu, J. Li, H. Huang, J. Qiao, In situ growth of CoP nanoparticles anchored on (N, P) co-doped porous carbon engineered by MOFs as advanced bifunctional oxygen catalyst for rechargeable Zn–air battery. J. Mater. Chem. A **8**, 19043–19049 (2020)
21. A.M. Bryan, L.M. Santino, Y. Lu, S. Acharya, J.M. D'Arcy, Conducting polymers for pseudocapacitive energy storage. Chem. Mater. **28**, 5989–5998 (2016)
22. C.I. Awuzie, Conducting polymers. Mater. Today Proc. **4**, 5721–5726 (2017)
23. M.K. Aslam, Y. Niu, T. Hussain, H. Tabassum, W. Tang, M. Xu, R. Ahuja, How to avoid dendrite formation in metal batteries: innovative strategies for dendrite suppression. Nano Energy **86**, 106142 (2021)
24. T. Wang, M. Kunimoto, T. Mori, M. Yanagisawa, J. Niikura, I. Takahashi, M. Morita, T. Abe, T. Homma, Carbonate formation on carbon electrode in rechargeable zinc-air battery revealed by in-situ Raman measurements. J. Power Sources **533**, 231237 (2022)
25. Y. Chen, W. Li, Y. Yao, P. Gogoi, X. Deng, Y. Xie, Z. Yang, Y. Wang, Y.C. Li, Enabling acidic oxygen reduction reaction in a zinc-air battery with bipolar membrane. ACS Appl. Mater. Interfaces **14**, 12257–12263 (2022)
26. Z. Shui, Y. Chen, W. Zhao, X. Chen, Flexible aluminum-air battery based on ionic liquid-gel polymer electrolyte. Langmuir **38**, 10791–10798 (2022)
27. J.V. Alemán, A.V. Chadwick, J. He, M. Hess, K. Horie, R.G. Jones, P. Kratochvíl, I. Meisel, I. Mita, G. Moad, S. Penczek, R.F.T. Stepto, Definitions of terms relating to the structure and processing of sols, gels, networks, and inorganic-organic hybrid materials (IUPAC Recommendations 2007). **79**, 1801–1829 (2007)

28. F. Daneshvar, S. Tagliaferri, H. Chen, T. Zhang, C. Liu, H.-J. Sue, Ultralong electrospun copper-carbon nanotube composite fibers for transparent conductive electrodes with high operational stability. ACS Appl. Electron. Mater. **2**, 2692–2698 (2020)
29. Y. Chen, J. Chen, K. Bai, Z. Xiao, S. Fan, A flow-through electrode for hydrogen production from water splitting by mitigating bubble induced overpotential. J. Power Sources **561**, 232733 (2023)
30. A.J. Samuels, J.D. Carey, Engineering graphene conductivity for flexible and high-frequency applications. ACS Appl. Mater. Interfaces **7**, 22246–22255 (2015)
31. F. Sarker, N. Karim, S. Afroj, V. Koncherry, K.S. Novoselov, P. Potluri, High-performance graphene-based natural fiber composites. ACS Appl. Mater. Interfaces **10**, 34502–34512 (2018)
32. U. Misra, N. Dixit, S.P. Singh, Effect of Laser parameters on Laser-induced graphene filter fabrication and its performance for desalination and water purification. ACS Appl. Mater. Interfaces **15**, 7899–7910 (2023)
33. S.Y. Ryu, M.R. Hoffmann, α-NiO/Ni(OH)2/AgNP/F-graphene composite for energy storage application. ACS Omega **8**, 10906–10918 (2023)
34. A. Kundu, A. Samanta, C.R. Raj, Hierarchical hollow MOF-derived bamboo-like N-doped carbon nanotube-encapsulated Co0.25Ni0.75 alloy: an efficient bifunctional oxygen electrocatalyst for zinc–air battery. ACS Appl. Mater. Interfaces. **13**, 30486–30496 (2021)
35. K.R.G. Lim, A.D. Handoko, S.K. Nemani, B. Wyatt, H.-Y. Jiang, J. Tang, B. Anasori, Z.W. Seh, Rational design of two-dimensional transition metal carbide/nitride (MXene) hybrids and nanocomposites for catalytic energy storage and conversion. ACS Nano **14**, 10834–10864 (2020)
36. X. Hui, P. Zhang, Z. Wang, D. Zhao, Z. Li, Z. Zhang, C. Wang, L. Yin, Vacancy defect-rich perovskite SrTiO3/Ti3C2 heterostructures in situ derived from Ti3C2 MXenes with exceptional oxygen catalytic activity for advanced Zn–air batteries. ACS Appl. Energy Mater. **5**, 6100–6109 (2022)
37. M. Li, C. Li, X. Xu, M. Wang, Z. Zhu, K. Meng, B. He, G. Yu, Y. Hu, L.-M. Peng, Y. Jiang, An ultrathin flexible programmable spin logic device based on spin–orbit torque. Nano Lett. (2023)
38. C. Li, H. Chen, S. Zhang, W. Yang, M. Gao, P. Huang, M. Wu, Z. Sun, J. Wang, X. Wei, Wearable and biocompatible blood oxygen sensor based on heterogeneously integrated lasers on a laser-induced graphene electrode. ACS Appl. Electron. Mater. **4**, 1583–1591 (2022)
39. B. Lim, J. Kim, M.S. Desai, W. Wu, I. Chae, S.-W. Lee, Elastic fluorescent protein-based down-converting optical films for flexible display. Biomacromolecules **24**, 118–131 (2023)
40. S. Qu, B. Liu, J. Wu, Z. Zhao, J. Liu, J. Ding, X. Han, Y. Deng, C. Zhong, W. Hu, Kirigami-inspired flexible and stretchable zinc-air battery based on metal-coated sponge electrodes. ACS Appl. Mater. Interfaces **12**, 54833–54841 (2020)
41. Z. Shui, X. Liao, Y. Lei, J. Ni, Y. Liu, Y. Dan, W. Zhao, X. Chen, MnO2 Synergized with N/S codoped graphene as a flexible cathode efficient electrocatalyst for advanced honeycomb-shaped stretchable aluminum-air batteries. Langmuir **36**, 12954–12962 (2020)
42. C. Aswin Karthik, P. Kalita, X. Cui, X. Peng, Thermal management for prevention of failures of lithium ion battery packs in electric vehicles: a review and critical future aspects. Energy Storage **2**, e137 (2020)
43. Y. Zhang, H. Qin, M. Alfred, H. Ke, Y. Cai, Q. Wang, F. Huang, B. Liu, P. Lv, Q. Wei, Reaction modifier system enable double-network hydrogel electrolyte for flexible zinc-air batteries with tolerance to extreme cold conditions. Energy Storage Mater. **42**, 88–96 (2021)
44. J. Li, Z. Wang, L. Yang, Y. Liu, Y. Xing, S. Zhang, H. Xu, A flexible Li–air battery workable under harsh conditions based on an integrated structure: a composite lithium anode encased in a gel electrolyte. ACS Appl. Mater. Interfaces **13**, 18627–18637 (2021)
45. X. Chen, L. Yi, C. Zou, J. Liu, J. Yu, Z. Zang, X. Tao, Z. Luo, X. Guo, G. Chen, B. Chang, Y. Shen, X. Wang, High-performance gel polymer electrolyte with self-healing capability for lithium-ion batteries. ACS Appl. Energy Mater. **5**, 5267–5276 (2022)

Pseudocapacitive Materials-Based Metal-Air Batteries

Sanjeev Verma, Vikas Kumar Pandey, Ram K. Gupta, Shivani Verma, and Bhawna Verma

Abstract Researchers' attraction has been sparked by the fabrication of green and renewable energy-storage innovations in view of the increasing hurdle around the needs of energy and environmental concerns. MABs (Metal-air batteries), mainly rechargeable MABs, are seen as a viable energy storage/conversion solution because of their high energy density and specific power, lower price, as well as its safety. Moreover, the fabrication of MABs is significantly hindered by their lower rate ability, corrosion, and dendrite formation between the electrochemical actions, less active material synthesis strategies expansion, slower oxygen reaction kinetics at cathode surface, electrolyte and electrode refinement, and a proper separator selection. This chapter goes into great detail to help readers understand many types of MABs, the fundamentals of electrode reactions and battery configurations, the function of electrode active materials, separators, and electrolytes, as well as future scenarios.

Keywords Pseudocapacitance · Metal-air batteries · Energy storage · Electrochemical · Energy density

1 Introduction

Through the processes of metal oxidation and oxygen reduction, MABs are an electrochemical cell type that can achieve high energy densities that are 3–30 times greater than those of commercially available Li–ion batteries. The three basic parts

S. Verma · V. K. Pandey · B. Verma (✉)
Department of Chemical Engineering and Technology, Indian Institute of Technology, Banaras Hindu University, Varanasi 221005, India
e-mail: bverma.che@itbhu.ac.in

R. K. Gupta
Department of Chemistry, National Institute for Materials Advancement, Pittsburg State University, Pittsburg, KS 66762, USA

S. Verma
Department of Chemistry, CBSH, G.B. Pant University of Agriculture and Technology, Pantnagar U.S. Nagar-263 145, Rudrapur, India

© The Author(s), under exclusive license to Springer Nature Switzerland AG 2024

R. K. Gupta (ed.), *Pseudocapacitors*, Engineering Materials,
https://doi.org/10.1007/978-3-031-45430-1_20

of this system; (i) a metal anode, (ii) an electrolyte separating the two electrodes, and (iii) a porous air cathode. Na, Li, Zn, Fe, K, Al, and more elements with strong electrochemical equivalency are used as anodes in MABs. Available electrolytes include solid-state, nonaqueous (aprotic), and aqueous (protic) electrolytes. With growing concern over the energy issue and environmental protection, considerable interest has been made in environmentally friendly, recyclable, and green energy storage technologies. Li-ion batteries are widely used in energy storage systems and electric cars due to their suitable ecological properties and huge energy density value. Li-ion batteries currently have an energy density in the range of 100 and 200 Wh/kg, that have inadequate to meet the endless design of EVs [1–5].

In MABs, the oxygen changes into OH^- at the cathode while the metal plate loses electrons and turns into metal ions that are dissolved into electrolytes at the anode during the discharge process. During the charging phase, all of these reactions are inverted. Additionally, this kind of operation is simply the opposite of the redox process that takes place in a traditional ionic battery, which is when metal ions go from the anode to the cathode. The gas diffusion layer in the MAB is where oxygen diffuses into the battery. According to Fig. 1, oxygen behaves differently in non-aqueous electrolytes than it does in aqueous media [6]. The following equation illustrates how the reactions at the electrodes in both of these media;

In aqueous electrolyte.

$M \leftrightarrow M^{n+} + ne^-$ (At anode).

$O_2 + 4e^- + 2H_2O \leftrightarrow 4OH^-$ (At cathode).

In non-aqueous electrolyte.

$M \leftrightarrow M^+ + e^-$ (At anode).

$xM^+ + O_2 + xe^- \leftrightarrow M_xO_2$ (x = 1, 2) (At cathode).

The absence of effective catalyst for the O_2 evolution reaction/O_2 reduction reactions (OER/ORR) at normal temperature, side reactions, and metal dendrite formation among other issues, remain major problems for metal-air batteries [7]. In addition, the volatility of the liquid electrolytes can be another challenging issue that metal-air batteries encounter in real-world settings. A lot of people have been worried recently about different MABs (Li, Na, Zn, etc.) [8–11]. In general terms, MABs are superior to traditional liquid metal-air batteries in the ways listed below: (1)

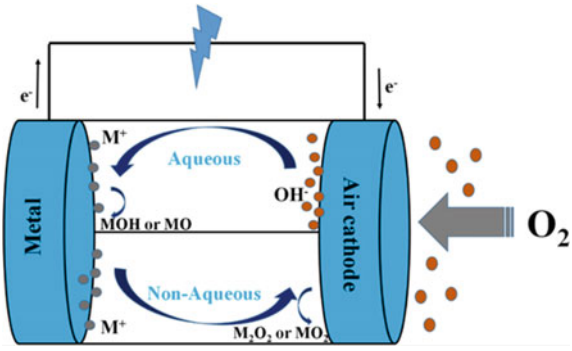

Fig. 1 Schematic diagram of MABs

increased safety. Liquid electrolytes are prone to a number of dangers, including as leakage concerns, thermal breakdown at huge thermal climate, and volatilization with its huge conductivity and robust electrodes wetting. Solid type electrolytes, having good ionic conductivity and better thermal stability at elevated temperatures, can successfully avoid the aforementioned problems. (2) cyclic life and higher energy density. A high-voltage platform can be used by the solid-state metal-air battery due to its greater chemical and mechanical stability [12, 13]. A longer cycle life can be achieved by successfully eliminating the undesired reactions in between H_2O/CO_2 and metal plate anodes. But solid-MABs are nevertheless in its roots and encounter several difficulties in practical use. First, the battery life may be greatly reduced by dendrite formation and side reactions brought on by very reactive metal plate anodes and intrinsic electrodeposition characteristic. Additionally, the metal anode's enormous volume variation lead to an unbalanced surface, which reduced the battery's cycle life [14–16]. Second, substantial interface resistance is typically caused by solid electrolytes' inadequate contact with the electrode. Finally, there are still a lot of unanswered questions regarding the multiple step catalytic type reactions, and additional study is still required to figure out how to create a high ability materials [17, 18].

In this chapter, we'll highlight the main developments and problems with several metal-air batteries, in particular Zn, Na, and Li batteries. In this study, we will concentrate on specific issues and difficulties associated with employing inorganic ceramic electrolytes (ICEs) for Li/Na-based MABs due to the abundance of materials on OPEs (organic polymer electrolytes). We will mostly rapidly cover the progression of OPEs based Zn-air batteries since fully developed ICEs are not yet available. The knowledge presented in this chapter will aid in the creation of MABs and point out the parts that require more study.

2 Metal Air Battery Working Mechanism

The reaction mechanism of metal-air batteries is affected differently by the metal anode and the electrolyte. In general, nonaqueous electrolytes are used in most alkali metal–air batteries. Because alkali metal anodes (such as Na, K and Li) usually react aggressively in aqueous electrolyte solutions, the majority of these type alkali MABs contain a nonaqueous type electrolyte solution and their corresponding reaction method is as below [19]:

$M \leftrightarrow e^- + M^+$ (At anode).

$aM^+ + O_2 + ae^- \leftrightarrow M_aO_2$ (a = 1, 2) (At cathode).

where x is the metal ion's oxidation number and M represents the alkali metal.

The ORR is now widely acknowledged to entail a first one-electron reduction, resulting in the formation of superoxide anion O^{2-}, which subsequently combines with a metal alkali cation to produce M_xO_2 peroxide (Fig. 2a). Later Li^+, a hard Lewis acid with a short ionic radius, is unable to pair with the soft Lewis base O^{2-}, which is very reactive, Li^+ prefers to generate Li_2O_2 as primary outlet product

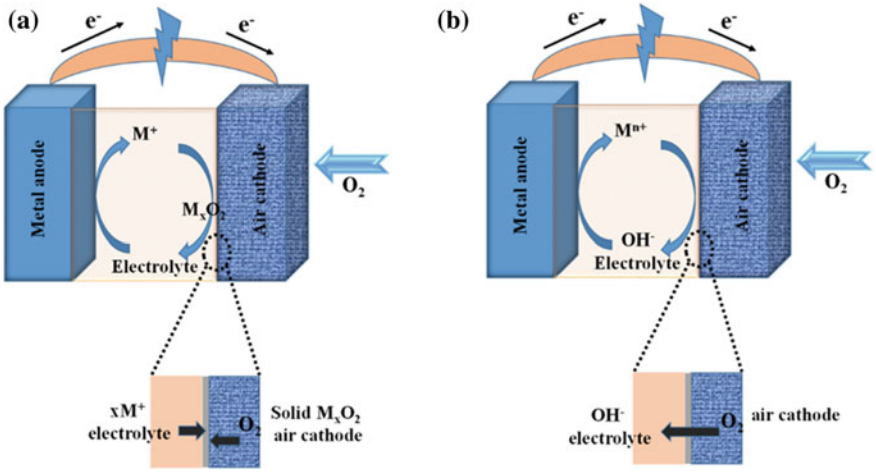

Fig. 2 Pictorial representation of metal air batteries mechanism **a** Nonaqueous metal air batteries, **b** Aqueous metal air batteries

for Li-based MABs [20]. In contrast, the principal outlet desired product of Na-based MABs is NaO_2, which is favored by the Na^+ with huge ionic radius. The thermodynamically and kinetically desired outlet product for K-air batteries at room temperature (>10 S/cm^2) is KO_2, which has good conductivity [21, 22]. Without a catalyst, a single electron transfer will cause the K-air battery to respond quickly. As a result, K-air batteries display great round-trip energy efficiency (over 90%) and minimal overpotential when compared to Na-air batteries and Li-air batteries [23].

A gradual blockage of the accessible cathode surface brought on by the buildup of peroxides and superoxides onto the air cathode always results in the battery shutting down. As a result, the behavior of the nonaqueous type MAB is always greatly influenced by the air cathode. For these batteries, it's also crucial to ensure that the cathode or catalyst has high activity and long-term stability in the air.

$M \leftrightarrow M^{n+} + ne^-$ (At anode).

$O_2 + 4e^- + 2H_2O \leftrightarrow 4OH^-$ (At cathode).

The electrode used in a battery is primarily dictated by the type of electrolyte used, which is mainly the thermodynamically stable field of the electrode/electrolyte. In contrast to nonaqueous systems, aqueous electrolytes are typically used in metal-air batteries for multivalent metal anodes (such as Zn, Fe, Al, and Mg). Although multivalent metals in aqueous environments have the same thermodynamic instability, their surfaces can be passivated by matching oxides or hydroxides to make them compatible with aqueous electrolytes. Typically, OH^- ions serve as the carriers in the electrolyte, whereas hydrates/salts (like $Zn(OH)_4^{-2}$) serve as the discharge products (Fig. 2b). These batteries operate differently than nonaqueous type MABs, which can see anions (OH^-) move from the air cathode towards metal plate anode [19].

3 Li-Air Batteries

As Li-O_2 batteries have one of the highest potential energy densities of any type of battery (3500 Wh/kg), they are considered highly promising for large-scale energy storage since Abraham and Jiang first reported on them in 1996 [24]. MABs in particular have drawn a lot of attention because they successfully prevent solvent volatilization and the side reactions between impurity gases (CO_2, H_2O etc.) and reactive metal anodes. Still, there are still many difficulties with Li-air, including high interfacial resistance, Li dendrite and a dearth of effective catalyst. Research continues to be conducted on the physical/chemical compatibility of the contact between solid electrolyte and Li metal anode. Historically, liquid electrolyte in a small amount has been added to lower the interfacial resistance between the electrolyte/Li-metal plate anode [25, 26]. Although, the continual use of liquid electrolytes during cycling is not completely sustainable. It is thought that even at greater current densities, the lithiophilic material's surface coating can effectively detain the Li metal infiltration. Higher Li-ion diffusion channel for ion transfer and the prevention of undesired reactions will arise from the creation of an uniform interface between metal anode and the coating substances (like metal oxides, metals, or sulfide) [27, 28].

Another popular method for preventing the growth of Li dendrites is the use of polymer interlayers. Due to the massive charges diffusion at interface with the huge volume variations in Li metal anode, the SEI (solid electrolyte interface) layer was instinctive unstable. Due to their favorable mechanical and chemical characteristics, polymer electrolytes can help. Gao et al. created an artificial SEI which was stable by an in-situ reaction using reactive polymer composites [29]. In order to safeguard the Li metal anode through prolonged cycling, Luo and coworkers suggested a gel–solid-state hybrid polymer based electrolyte [30]. The results shown that cycle stability greater than 140 times at 0.4 mA/cm^2 of current density.

Additionally, It has been demonstrated that a well-formed Li anode can prevent the inevitable volume shift of a Li anode during plating/stripping [31, 32]. By using carbon paper that has been co-doped with nitrogen and Sulphur and reacting with molten lithium, Li et al. created a novel hybrid anode [32]. With a host that has a layered structure, nitrogen and Sulphur co-doping can significantly improve the surface's lithophilicity capabilities to show strong wettability with liquid nitrogen. The distinctive hybrid anode's large number of holes could hold suficient Li in order to prevent change in electrode volume and reduce the local current density, which would otherwise encourage Li dendrite growth. The results showed that compared to the identical Li metal based batteries in atmospheric condition, the battery employing these anodes might have a greater cycling stability with less voltage polarisation.

In 1996, Abraham and Jiang presented a general reaction for a system of Li-air employing organic polymer electrolytes (OPEs), stating that during discharge, $2Li + O_2 \rightarrow Li_2O_2$ [24]. OPEs have a low ionic conductivity at normal temperatures, which affects the battery's performance. Since then, scientists have put in a lot of effort to improve OPEs' overall effectiveness, and one popular method has been to include inorganic particles in them [33]. It has been demonstrated that strong interactions

between organic molecules and inorganic particles could improve OPE durability, decrease electrolyte evaporation and increase ionic conductivity. However, because of their inferior air stability at room temperature and electrochemical stability at high potential, OPEs' utility is still constrained. Inorganic ceramic electrolytes (ICEs) are gaining popularity because of their increased ionic conductivity and chemical stability. garnet-type materials, LISICON (Li superionic conductors), perovskites and sulfides are among the ICEs for Li-based MABs that have received the most attention. The sulfide based electrolytes at ambient temperature, demonstrate a higher ionic conductivity of around 10^{-3} S/cm. Sulfide electrolytes are shown unstable nature in air, which significantly limits its use in Li-based MABs [34]. The perovskite type electrolyte's ability to mainly protect the Li anode and prevent O_2 crossing is made possible by its high density and ionic conductivity, but vastly hampered by the undesired reaction that arises when perovskites-Li metal contact happened.

Ultimately, it is critical to keep considering strategies to raise the electrolyte's relative density, ion conductivity, and air stability for Li-based MABs. Given this, electrolytes of LISICON or garnet could offer good future possibilities for Li-based MABs, but their electrolyte design must simultaneously accomplish high environmental adaptability and good electrochemical performance. Inorganic solid electrolytes are likewise severely limited in their applicability due to their rigid structure. It is challenging to produce a solid based electrolyte for solid Li-based MABs that satisfies the demands of exceptional electrochemical performance, high environmental adaptability, and excellent mechanical qualities.

In order for the air cathode to act as the domain for the dissolution/deposition of outlet, it must have high ORR and OER catalytic activity, good electron conductivity and a high degree of porosity. The discharge product (Li_2O_2) undergoes slow reaction kinetics during both its generation and decomposition in two-electron processes. In most cases, all-solid-state Li-air batteries have poor coulombic efficiency due to the limited electrochemical reversibility of Li_2O_2, which also causes high discharge over potentials. Additionally, the solid electrolyte's substantial interfacial resistance to the catalysts significantly limited the kinetics of the process. As a result, designing a high-efficiency catalyst for Li-based MABs is "a big challenge".

4 Na-Air Batteries

Due to its affordability, Na-based MABs have gained attention as a possible substitute for Li-based MABs. However, their safety method is much more complicated than that of the Li-based MABs due to the strong chemical reactivity of the anode's Na metal [35]. Because of the inadequate interaction between highly active Na and the solid electrolyte, it was shown that when ICE was utilized, the formation of Na dendrites was more severe. To extend the life of batteries, it is essential to protect the sodium anode. A frequent technique for improvement is the creation of extremely sodiophilic surfaces [36, 37].

Lu and coworkers selected 1 M fluoroethylene carbonate/ $NaClO_4$ to serve the sodium anode based on theoretical predictions, and resulting NaF 8 nm rich interlayer successfully promoted Na^+ transit and decreased interface resistance [36]. Additionally, it is important to employ a thick electrolyte to stop oxygen crossing since it can cause irreparable damage to the Na-air batteries if oxygen crosses from air to anode. Recent works [38, 39] demonstrated all solid-state NaO_2 battery with a proper-wettable intermediary phase (Na_xPb) between Na and electrolyte with high environmental compatibility and long cycle life. NaO_2 battery research by Peled et al. has rapidly increased since 2011 [40]. Since sodium and lithium share many traits, a number of NaO_2 battery management techniques can also be used with lithium-ion batteries. Because of their strong interface contact and machinability, solid-state polymer electrolytes (SPE) make up the majority of today's solid-state Na-air batteries. By including SiO_2 filler in the PVDF-HFP matrix, Wang et al. created a composited SPE. The SPE's ionic conductivity increased to about 1.0 mS/cm due to the presence of several fluorocarbon chains [11]. After 80 cycles and 1000 mAh/g discharge capacity, the created quasi-solid-state NaO2 battery can reach an average coulombic efficiency of 97%.

In hybrid NaO_2 batteries, the NASICON electrolyte has been used as a separation barrier due to its excellent chemical stability [41, 42]. It has been shown that when cycling Na-air hybrid batteries at room temperature, they functioned consistently. Kang and coworkers showed that in severely acidic circumstances, where Na and H went through ion exchange and oxide dissolution, the NASICON electrolyte stability was impaired [43]. Additionally, an interfacial layer could develop between the NASICON and organic electrolytes, raising the hybrid NaO_2 batteries' overall internal resistance. Solid-state NaO_2 batteries with a liquid electrolyte or gel electrolyte addition have also been reported to alleviate interface concerns. By minimizing bad contact and sluggish mass transfer kinetics across the electrode interface/NASICON and successfully avoiding O_2 crossing, this technique increased the battery's reversibility. The NASICON electrolyte, according to the most recent study, performs better than others in real-world applications because of its high ionic conductivity and good air stability [44, 45].

As previously mentioned, increasing the battery's specific energy density, it is essential to create a high activity based air cathode. Assuring the rapid transfer of cathode charge, desired product in all solid states is a further difficulty for Na-based MABs. Meanwhile, among all the MABs that have been described so far, it is very tough to be fully solid-state form. According to Chang et al. [45], a gel type cathode made of ionic liquid and SW-CNT could produce a quasi-solid Na-based MAB with a long cycling life of 125 cycles (528 h) at a current density of 0.1 mA/cm^2. It was demonstrated that during the working process, water from the surrounding ambient was moderately accumulated on the gel cathode's surface, and creation of soluble charge products of NaOH exhibited good reversibility. A recently developed all-solid-state NaO_2 battery by Sun et al. exhibited a high ionic conductivity of $2.39*10^{-3}$ S/cm with a NASICON type electrolyte [39]. It was demonstrated that the battery cycles steadily at 100 mA/g of current density and that humidity significantly affects the battery's performance.

5 Zn-Air Batteries

Due to the lack of appropriate inorganic zinc ion conductor electrolytes, OPEs now power the bulk of Zn-air batteries. Even though the primary Zn-air battery was available for a while, the secondary Zn-air battery remains in its infancy of development. The Zn dendrite of metal zinc during the deposition/dissolution process and volume deformation serve as the foundation for the creation of secondary zinc batteries. Solvent volatilization severely decreased the operational range of water-based Zn-air batteries' semi-open design.

One of the most extensively researched anodes has a high theoretical capacity of 820 mAh/g and a low potential (-0.762 V vs. SHE). This anode is zinc metal. However, the Zn metal anode frequently experiences dendrite formation due to hydrogen precipitation reactions and the difficulty of decomposing compound ZnO. Surface coating and structured design are typical strategies to increase the reversibility of the Zn metal anode [46–48]. A structured Zn metal anode's ability to efficiently suppress Zn dendrite growth and increase battery cycle life has been demonstrated. For instance, Chamoun and coworkers created a porous foam anode based on Zinc using in-situ electrochemistry, which may utilize up to 88% of the depth of discharge [49]. Even though zinc metal anodes are an ancient concept, achieving their reversible application is still a very difficult task. With more research being done on Zn-air or Zn-ion batteries in the future, we think that this aspect will gradually improve.

Nowadays, Zn-air batteries employ mostly aqueous OPEs-based electrolytes. It has been demonstrated that the converted zincate ions ($Zn(OH)_4^{2-}$) in the extremely alkaline solution can increase the Zn metal anode's reversibility [50]. The poly(vinyl alcohol)/poly(acrylic acid)/KOH solid polymer electrolyte had an ionic conductivity of 0.301 S/cm at room temperature [51]. Huang et al. absorbed and held 0.2 M $Zn(CH_3COO)_2 + 6$ M KOH solution to form a novel PANa hydrogel electrolyte [13]. The Zn dendrite growth was prevented by the quasi-SEI that was created on the PANa network, which also considerably facilitated ionic transport. Initiated polymerization was used by Zhao et al. to create the PAA-Na hydrogel electrolyte [52]. This material has excellent mechanical properties and interconnected mesh-type morphology that can hold and absorb significant volumes of electrolyte. The electrolyte will be quickly blocked by the newly produced ZnO, particularly at high current densities. As a result of the concentration gradient, $Zn(OH)_4^{2-}$ ions are forced to pass across the electrolyte membrane and directed towards cathode, where they might precipitate ZnO asymmetrically and shorten battery life. In order to solve the problem of generated ZnO block electrolytes accessing the cathode, it is imperative to manage the selective migration of ions in the solid electrolytes of these batteries. To address this issue, various academics have suggested separators that prevent zincate crossing. A novel design of electrospun nanofiber mat-reinforced elective composite membrane was created by Lee et al. [53]. It proved that the Zn $(OH)_4^{2-}$ crossovers may be successfully inhibited by electrospun nanofiber mat-reinforced perm-selective composite (ERC) membranes without compromising conductivity. The ERC film may significantly reduce the formation of ZnO after its seventh cycle, demonstrating better

discharge stability. Later, Kim et al. defined the separator of Zn-air batteries as a polymeric blend electrolyte (PBE) membrane composed of ion-conducting PAA/PVA and ion-repelling Nafion. By limiting zincate ion diffusion through the Donnan exclusion phenomenon, the Nafion phase can reduce the amount of ZnO that forms on the air electrode.

6 Alternative Metal Air Batteries

There are various types other metal-air battery being gradually investigated. Al-air batteries exhibited 8100 Wh/kg of theoretical specific energy, but their subpar rate capability made them very unreliable [54]. For fieldwork power supplies and portable power supplies, magnesium metal's small weight made it a great choice. Additionally, the magnesium hydroxide from the Mg-air battery's discharge process may be reutilized and transformed back into ingots [55]. These batteries, however, also had a number of glaring flaws, including catastrophic self-corrosion caused by the development of copious volumes of hydrogen gas. The Fe-air battery's low Coulombic efficiency raised numerous application-related issues, despite the fact that Fe metal was cheaper than most of other metal anode components used in conventional batteries [56, 57]. A revolutionary three-cell stack of carbon-air batteries with a specific energy of 3600 Wh/kg was reported by Yan et al., which was much higher than that of metal-air batteries that were at the cutting edge of technology [58]. Due to the large activation energy (190 kJ/mol) required for electrochemical carbon oxidation in this kind of battery, it is highly challenging to accomplish. The slow kinetics and consequently the electrochemical process need to be accelerated by high temperature, which severely constrained their development. Researchers were encouraged to continue their exploration of different kinds of metal-air batteries as they had potential in a variety of industries.

7 Summary and Vision

In the end, this research outlined several significant advancements and significant problems with solid-state metal-air batteries. Due to its great energy density and exceptional safety, solid-state metal-air batteries have numerous potential uses. However, there are still some issues with metal-air batteries like reasonable electrolyte development and interface side reactions because of metal dendrites. Future research should concentrate on the following aspects of solid-state metal-air batteries. First, interface instability, side reactions and dendrite development are the three main problems in the case of metal-air batteries of Li/Na type. Additionally, compared to liquid systems, the dendrite growth model for solid-state batteries is more complex due to the presence of a space charge layer with the weakened interface contact. There is currently no widely recognized model, hence a thorough investigation is required

going forward. Interfacial wettability can be increased and the interfacial specific resistance decreased using techniques like interfacial coatings and polymer interlayers. In order to achieve long-term stability of the interface, structured anodes have been shown to be successful in relieving volume variations and lowering deposition current density. Recent research has shown that lowering the electrical conductivity of electrolytes can also prevent dendritic development. Second, metal-air batteries function in an airy environment. It should be noted that metal anodes can sustain permanent harm if there is water or carbon dioxide in the air. The H_2O and CO_2 in the air have a tendency for interacting with discharge products, making the batteries more complex. Further, the voltage cutoff for charging for most metal-air batteries is typically set at around 4.5 V, the performance of the battery can be significantly impacted by the ease with which side reactions can be produced. The difference in the kinetics of the reaction between the original discharge products and impurity components from ambient air should be considered the cause of this occurrence. The battery's cycle life always rapidly decreases as a result of carbonate buildup. The effects of impurity gases on battery performance should be understood, as well as how to eliminate them. Also, from the past experience pertaining to fuel cells, we may learn how to efficiently minimize the cathode water content under the influence of air impurity molecules, for example, by designing the air diffusion layer. Additionally, novel materials like MOF or COF can be used to separate gas in an air cathode. MOF or COF materials have a lot of potential for use in gas separation since they can be experimentally tailored to modify their crystallinity, void regularity, and surface activity.

Additionally, solid electrolyte-based cathode catalysts still lack an adequate design and mechanism. The catalytic reaction on cathode for metal-air batteries differs from the conventional liquid system, and is comparable to the former, such as OER and ORR reaction, with apparent distinctions. A few liquid media can also work as induced catalysts, and the favourable wetting of the liquid solvent in the liquid system can facilitate intimate contact between the catalyst and metal ions. Although gas molecules can move through solid-state systems more efficiently, there are still a number of challenges, such as ensuring that air molecules, catalysts, and metal ions are able to interact. The widely used technique frequently involves intermediary media, like polymer electrolytes or ionic liquids. There are still many unknowns regarding these intermediates' long-term stability. Additionally, the limiting three-phase boundary can be successfully extended and the electrolyte/cathode interface resistance can be decreased by constructing an integrated structure of solid electrolyte and air cathode. High-performance metal-air batteries are predicted to be achieved with this innovative design. Finally, there is still much work to be done on the solid cathode's catalytic mechanism. In-situ online detection methods have advanced quickly in recent years. Examples include surface-enhanced Raman spectroscopy and in-situ differential electrochemical mass spectrometry. An important area of research for metal-air batteries is the investigation of more sophisticated in-situ characterization techniques. Additionally, theoretical simulation is a powerful tool, such as molecular dynamics simulation or first-principles calculations.

References

1. P.G. Bruce, S.A. Freunberger, L.J. Hardwick, J.-M. Tarascon, Li–O2 and Li–S batteries with high energy storage. Nat. Mater. **11**, 19–29 (2012)
2. J.B. Goodenough, K.-S. Park, The Li-Ion Rechargeable Battery: A Perspective. J. Am. Chem. Soc. **135**, 1167–1176 (2013)
3. M. Li, J. Lu, Z. Chen, K. Amine, 30 Years of Lithium-Ion Batteries. Adv. Mater. **30**, 1800561 (2018)
4. A. Cresce, K. Xu, Aqueous lithium-ion batteries, Carbon. Energy **3**, 721–751 (2021)
5. S. Verma, B. Verma, Graphene-Based Nanomaterial for Supercapacitor Application, in: 2022. pp. 221–244
6. A.G. Olabi, E.T. Sayed, T. Wilberforce, A. Jamal, A.H. Alami, K. Elsaid, S.M.A. Rahman, S.K. Shah, M.A. Abdelkareem, Metal-Air Batteries—A Review. Energies **14**, 7373 (2021)
7. C. Wang, Y. Yu, J. Niu, Y. Liu, D. Bridges, X. Liu, J. Pooran, Y. Zhang, A. Hu, Recent progress of Metal-Air Batteries—A mini review. Appl. Sci. **9**, 2787 (2019)
8. X. Zhao, N. Xu, X. Li, Y. Gong, K. Huang, Energy storage characteristics of a new rechargeable solid oxide iron–air battery. RSC Adv. **2**, 10163 (2012)
9. J. Park, M. Park, G. Nam, J. Lee, J. Cho, All-Solid-State Cable-Type Flexible Zinc-Air Battery. Adv. Mater. **27**, 1396–1401 (2015)
10. K. Liu, H. Sun, S. Dong, C. Lu, Y. Li, J. Cheng, J. Zhang, X. Wang, X. Chen, G. Cui, A rational design of High-Performance Sandwich-Structured quasisolid State Li-O 2 battery with redox mediator. Adv. Mater. Interfaces **4**, 1700693 (2017)
11. J. Wang, Y. Ni, J. Liu, Y. Lu, K. Zhang, Z. Niu, J. Chen, Room-Temperature flexible Quasi-Solid-State rechargeable Na–O 2 batteries. ACS Cent. Sci. **6**, 1955–1963 (2020)
12. J. Sun, N. Zhao, Y. Li, X. Guo, X. Feng, X. Liu, Z. Liu, G. Cui, H. Zheng, L. Gu, H. Li, A rechargeable Li-Air fuel cell battery based on garnet solid electrolytes. Sci. Rep. **7**, 41217 (2017)
13. Y. Huang, Z. Li, Z. Pei, Z. Liu, H. Li, M. Zhu, J. Fan, Q. Dai, M. Zhang, L. Dai, C. Zhi, Solid-State rechargeable Zn//NiCo and Zn-Air batteries with ultralong lifetime and high capacity: the role of a sodium polyacrylate hydrogel electrolyte. Adv. Energy Mater. **8**, 1802288 (2018)
14. X. Liu, X. Lei, Y.-G. Wang, Y. Ding, Prevention of na corrosion and dendrite growth for Long-Life Flexible Na–Air Batteries. ACS Cent. Sci. **7**, 335–344 (2021)
15. S. Verma, T. Das, V.K. Pandey, B. Verma, Nanoarchitectonics of GO/PANI/CoFe2O4 (Graphene Oxide/polyaniline/Cobalt Ferrite) based hybrid composite and its use in fabricating symmetric supercapacitor devices, J. Mol. Struct. (2022) 133515.
16. S. Verma, B. Verma, Synergistic interaction of bacteria with graphene oxide for high performance supercapacitor. Bioresour. Technol. Reports. **21**, 101354 (2023)
17. C. Zhao, J. Liang, X. Li, N. Holmes, C. Wang, J. Wang, F. Zhao, S. Li, Q. Sun, X. Yang, J. Liang, X. Lin, W. Li, R. Li, S. Zhao, H. Huang, L. Zhang, S. Lu, X. Sun, Halide-based solid-state electrolyte as an interfacial modifier for high performance solid-state Li–O2 batteries. Nano Energy **75**, 105036 (2020)
18. X. Chi, M. Li, J. Di, P. Bai, L. Song, X. Wang, F. Li, S. Liang, J. Xu, J. Yu, A highly stable and flexible zeolite electrolyte solid-state Li–air battery. Nature **592**, 551–557 (2021)
19. H.-F. Wang, Q. Xu, Materials Design for Rechargeable Metal-Air Batteries. Matter. **1**, 565–595 (2019)
20. J. Lu, L. Li, J.-B. Park, Y.-K. Sun, F. Wu, K. Amine, Aprotic and Aqueous Li–O 2 Batteries. Chem. Rev. **114**, 5611–5640 (2014)
21. S.K. Das, S. Lau, L.A. Archer, Sodium–oxygen batteries: a new class of metal–air batteries. J. Mater. Chem. A. **2**, 12623 (2014)
22. W. Wang, N.-C. Lai, Z. Liang, Y. Wang, Y.-C. Lu, Superoxide stabilization and a universal KO 2 growth mechanism in potassium-oxygen batteries, Angew. Chemie. **130**, 5136–5140 (2018)
23. Y. Sun, X. Liu, Y. Jiang, J. Li, J. Ding, W. Hu, C. Zhong, Recent advances and challenges in divalent and multivalent metal electrodes for metal–air batteries. J. Mater. Chem. A. **7**, 18183–18208 (2019)

24. K.M. Abraham, Z. Jiang, A polymer Electrolyte-Based rechargeable Lithium/Oxygen battery. J. Electrochem. Soc.Electrochem. Soc. **143**, 1–5 (1996)
25. B. Kumar, J. Kumar, R. Leese, J.P. Fellner, S.J. Rodrigues, K.M. Abraham, A. Solid-State, Rechargeable, long cycle life Lithium-Air Battery. J. Electrochem. Soc.Electrochem. Soc. **157**, A50 (2010)
26. Z. Guo, Q. Zhang, C. Wang, Y. Zhang, S. Dong, G. Cui, I-containing Polymer/Alloy Layer-Based Li Anode Mediating High-Performance Lithium-Air Batteries. Adv. Funct. Mater.Funct. Mater. **32**, 2108993 (2022)
27. T. Zhang, H. Zhou, A reversible long-life lithium–air battery in ambient air. Nat. Commun.Commun. **4**, 1817 (2013)
28. Y. He, C. Lu, S. Liu, W. Zheng, J. Luo, Interfacial Incompatibility and Internal Stresses in All-Solid-State Lithium Ion Batteries. Adv. Energy Mater. **9**, 1901810 (2019)
29. Y. Gao, Z. Yan, J.L. Gray, X. He, D. Wang, T. Chen, Q. Huang, Y.C. Li, H. Wang, S.H. Kim, T.E. Mallouk, D. Wang, Polymer–inorganic solid–electrolyte interphase for stable lithium metal batteries under lean electrolyte conditions. Nat. Mater. **18**, 384–389 (2019)
30. W.-B. Luo, S.-L. Chou, J.-Z. Wang, Y.-M. Kang, Y.-C. Zhai, H.-K. Liu, A hybrid gel–solid-state polymer electrolyte for long-life lithium oxygen batteries. Chem. Commun.Commun. **51**, 8269–8272 (2015)
31. Y. Chen, Y. Huang, H. Fu, Y. Wu, D. Zhang, J. Wen, L. Huang, Y. Dai, Y. Huang, W. Luo, TiO 2 Nanofiber-Modified lithium metal composite anode for Solid-State lithium batteries. ACS Appl. Mater. Interfaces **13**, 28398–28404 (2021)
32. D. Li, S. Zhang, Q. Zhang, P. Kaghazchi, H. Qi, J. Liu, Z. Guo, L. Wang, Y. Wang, Pencil-drawing on nitrogen and sulfur co-doped carbon paper: An effective and stable host to pre-store Li for high-performance lithium–air batteries. Energy Storage Mater. **26**, 593–603 (2020)
33. J. Yi, X. Liu, S. Guo, K. Zhu, H. Xue, H. Zhou, Novel stable gel polymer electrolyte: toward a high safety and long life Li–Air battery. ACS Appl. Mater. Interfaces **7**, 23798–23804 (2015)
34. F. Wu, W. Fitzhugh, L. Ye, J. Ning, X. Li, Advanced sulfide solid electrolyte by core-shell structural design. Nat. Commun.Commun. **9**, 4037 (2018)
35. E. Matios, H. Wang, C. Wang, W. Li, Enabling safe sodium metal batteries by solid electrolyte interphase engineering: a review. Ind. Eng. Chem. Res. **58**, 9758–9780 (2019)
36. Y. Lu, Y. Cai, Q. Zhang, L. Liu, Z. Niu, J. Chen, A compatible anode/succinonitrile-based electrolyte interface in all-solid-state Na–CO 2 batteries. Chem. Sci. **10**, 4306–4312 (2019)
37. W. Meng, J. Liu, L. Wang, L. Dai, S. Liu, In situ construction of a liquid film interface with fast ion transport for solid Sodium-Ion batteries. Nano Lett. **22**, 5214–5220 (2022)
38. S. Cai, H. Tian, J. Liu, S. Liu, L. Dai, J. Xu, L. Kong, L. Wang, Tuning Na 3 Hf 2 Si 2 PO 12 electrolyte surfaces by metal coating for high-rate and long cycle life solid-state sodium ion batteries. J. Mater. Chem. A. **10**, 1284–1289 (2022)
39. Q. Sun, L. Dai, Y. Tang, J. Sun, W. Meng, T. Luo, L. Wang, S. Liu, Designing a Novel Electrolyte Na 3.2 Hf 2 Si 2.2 P 0.8 O 11.85 F 0.3 for All-Solid-State Na-O 2 Batteries, Small Methods. 6 (2022) 2200345.
40. E. Peled, D. Golodnitsky, H. Mazor, M. Goor, S. Avshalomov, Parameter analysis of a practical lithium- and sodium-air electric vehicle battery. J. Power. Sources **196**, 6835–6840 (2011)
41. C. Xu, K. Zhang, D. Zhang, S. Chang, F. Liang, P. Yan, Y. Yao, T. Qu, J. Zhan, W. Ma, B. Yang, Y. Dai, X. Sun, Reversible hybrid sodium-CO2 batteries with low charging voltage and long-life. Nano Energy **68**, 104318 (2020)
42. J. Zhu, T. Qu, F. Su, Y. Wu, Y. Kang, K. Chen, Y. Yao, W. Ma, B. Yang, Y. Dai, F. Liang, D. Xue, Highly dispersed Co nanoparticles decorated on a N-doped defective carbon nano-framework for a hybrid Na–air battery. Dalt. Trans. **49**, 1811–1821 (2020)
43. Y. Kang, F. Su, Q. Zhang, F. Liang, K.R. Adair, K. Chen, D. Xue, K. Hayashi, S.C. Cao, H. Yadegari, X. Sun, Novel High-Energy-Density rechargeable hybrid Sodium-Air cell with acidic electrolyte. ACS Appl. Mater. Interfaces **10**, 23748–23756 (2018)
44. X. Lin, F. Sun, Q. Sun, S. Wang, J. Luo, C. Zhao, X. Yang, Y. Zhao, C. Wang, R. Li, X. Sun, O 2 /O 2 – Crossover- and Dendrite-Free Hybrid Solid-State Na–O 2 Batteries. Chem. Mater. **31**, 9024–9031 (2019)

45. S. Chang, M. Hou, B. Xu, F. Liang, X. Qiu, Y. Yao, T. Qu, W. Ma, B. Yang, Y. Dai, K. Chen, D. Xue, H. Zhao, X. Lin, F. Poon, Y. Lei, X. Sun, High-Performance Quasi-Solid-State Na-Air Battery via gel cathode by confining moisture. Adv. Funct. Mater.Funct. Mater. **31**, 2011151 (2021)
46. L. Kang, M. Cui, F. Jiang, Y. Gao, H. Luo, J. Liu, W. Liang, C. Zhi, Nanoporous CaCO 3 coatings enabled uniform Zn Stripping/Plating for Long-Life Zinc rechargeable aqueous batteries. Adv. Energy Mater. **8**, 1801090 (2018)
47. W. Yuan, G. Ma, X. Nie, Y. Wang, S. Di, L. Wang, J. Wang, S. Shen, N. Zhang, In-situ construction of a hydroxide-based solid electrolyte interphase for robust zinc anodes. Chem. Eng. J. **431**, 134076 (2022)
48. J.F. Parker, C.N. Chervin, I.R. Pala, M. Machler, M.F. Burz, J.W. Long, D.R. Rolison, Rechargeable nickel–3D zinc batteries: An energy-dense, safer alternative to lithium-ion, Science (80-.). 356 (2017) 415–418.
49. M. Chamoun, B.J. Hertzberg, T. Gupta, D. Davies, S. Bhadra, B. Van Tassell, C. Erdonmez, D.A. Steingart, Hyper-dendritic nanoporous zinc foam anodes. NPG Asia Mater. **7**, e178–e178 (2015)
50. T.N.T. Tran, D. Aasen, D. Zhalmuratova, M. Labbe, H. Chung, D.G. Ivey, Compositional effects of gel polymer electrolyte and battery design for Zinc-Air Batteries. Batter. Supercaps. **3**, 917–927 (2020)
51. G.M. Wu, S.J. Lin, C.C. Yang, Preparation and characterization of PVA/PAA membranes for solid polymer electrolytes. J. Memb. Sci. **275**, 127–133 (2006)
52. S. Zhao, K. Wang, S. Tang, X. Liu, K. Peng, Y. Xiao, Y. Chen, A New Solid-State Zinc-Air battery for fast charge. Energy Technol. **8**, 1901229 (2020)
53. H.-J. Lee, J.-M. Lim, H.-W. Kim, S.-H. Jeong, S.-W. Eom, Y.T. Hong, S.-Y. Lee, Electrospun polyetherimide nanofiber mat-reinforced, permselective polyvinyl alcohol composite separator membranes: A membrane-driven step closer toward rechargeable zinc–air batteries. J. Memb. Sci. **499**, 526–537 (2016)
54. Y. Wei, Y. Shi, Y. Chen, C. Xiao, S. Ding, Development of solid electrolytes in Zn–air and Al–air batteries: from material selection to performance improvement strategies. J. Mater. Chem. A. **9**, 4415–4453 (2021)
55. P. nam, B. J K, S. R C, A Review of Magnesium Air Battery Systems: From Design Aspects To Performance Characteristics, Int. J. Mater. Sci. Eng. 7 (2021) 18–28.
56. R.D. McKerracher, C. Ponce de Leon, R.G.A. Wills, A.A. Shah, F.C. Walsh, A Review of the Iron-Air secondary battery for energy storage. ChemPlusChem **80**, 323–335 (2015)
57. C. Zhang, K. Huang, A comprehensive review on the development of Solid-State Metal-Air batteries operated on Oxide-Ion chemistry. Adv. Energy Mater. **11**, 2000630 (2021)
58. X. Yan, M. Zhou, Y. Zhang, Q. Qiu, Q. Chen, W. Cai, Y. Tang, J. Liu, An all-solid-state carbon-air battery reaching an output power over 10 W and a specific energy of 3600 Wh kg−1. Chem. Eng. J. **404**, 127057 (2021)

Pseudocapacitive Materials for 3D Printed Batteries

Sagar Jariwala, Yash Desai, and Ram K. Gupta

Abstract Batteries are becoming more and more reliable energy storage devices and are promising information exchange platforms for real-time responses. They are getting more efficient in terms of performance and stability because of the use of advanced materials and their configurations. The ongoing demand for energy storage devices is being fulfilled by pseudocapacitive materials which lowers our dependence on single types of Li-ion batteries and other types that are being used in the market that are less abundant. For instance, the depletion of lithium reserves is a concerning issue. Pseudocapacitive materials are being explored for manufacturing batteries and supercapacitors with enhanced in terms of electrochemical and mechanical properties as alternatives to scarce materials. Furthermore, pseudocapacitive materials are being used with several other nanomaterials to improve the performance of the fabricated devices. Once the materials are found their manufacturing technique plays a vital role, where comes in the additive manufacturing technology. This technology provides fast and precise production of some complex miniature structures helping as a plus point in the electrochemical performance of the devices. 3D printing also enables the manufacturing of flexible and wearable energy storage devices which have been a hot area of research lately.

Keywords Pseudocapacitance · 3D printing · Flexible batteries · Polymeric composites · Transition metal oxide

S. Jariwala · Y. Desai · R. K. Gupta (✉)
Department of Chemistry, Pittsburg State University, Pittsburg, KS 66762, USA
e-mail: ramguptamsu@gmail.com

National Institute for Materials Advancement, Pittsburg State University, Pittsburg, KS 66762, USA

© The Author(s), under exclusive license to Springer Nature Switzerland AG 2024

R. K. Gupta (ed.), *Pseudocapacitors*, Engineering Materials,
https://doi.org/10.1007/978-3-031-45430-1_21

1 Introduction

Energy in the world is directly linked with the well-being and prosperity of mankind. It comes in from various sources and forms. Subsequently, energy is required to run most of the things in the world and outer space. Therefore, the surge in energy makes it a very important aspect; without energy, life seems impossible. Sun is the largest and eternal source of energy for the earth. However, in the present day, we are more reliant on fossil fuels for generating and supplying energy, which are non-renewable sources of energy. Due to the over-exploitation of these resources, severe adverse effects have been observed. Solar and tidal energy are good sources, but they aren't continuously supplying power, forcing the development of new and better energy storage systems. However, with the growing population and increasing consumption of energy, the development of new technologies becomes vital to support the functioning of the planet. Additionally, the development of new technologies to generate energy will need efficient storage methods. The world's progress toward decarbonization will escalate the growth of the energy storage industry. Decarbonization is the term used to denote the process of reducing the dependence on the energy sources such as fossil fuels which give out carbon dioxide gas while supplying energy and have adverse effects on the atmosphere such as global warming. So, this issue enables new opportunities and approaches for building different types of storage energy devices such as mechanical, thermal, electrochemical, and chemical.

Among many techniques, electrical and electrochemical storage devices have been widespread due to their easy operation and user-friendly operation. From the above categories, electrochemical and electrical comprise several devices such as batteries, flow batteries, supercapacitors, and superconducting magnetic energy storage which have gained popularity due to their performance [1–5]. Electrical energy storage devices also include a hybrid system of storage devices such as fuel cells which run on electricity as well as fuel to provide energy. These devices display good performance due to high energy density and long life span. Batteries and supercapacitors depend on electrochemical processes that determine the relative energy and power density. Many recent studies have prevailed that several materials demonstrate the high power density of the batteries as well as the long cycle life and short charging times of the supercapacitors which will be a breakthrough for manufacturing energy storage devices (ESD) [6, 7].

Furthermore, materials used to manufacture energy storage devices play a very important role as they make up the largest proportion of the system cost; materials also decide the performance and properties of the energy storage devices. Polymeric materials such as polyvinylidene fluoride (PVDF) have been a point of research for producing dielectric-based energy storage devices due to their good electrical resistance, mechanical strength, and high-volume resistivity. PVDF and PVDF copolymers are also being used as a host for gel polymer electrolytes, these electrolytes are a mixture of solid polymeric materials and liquid electrolytes [8]. Polymers have been in use for a few years to manufacture electrolytes moreover, other conventional materials were also used for energy storage devices but for two centuries the batteries

had been mainly dependent on liquid electrolytes due to their high ionic conductivity and excellent wetting properties of the electrodes, but they were vulnerable to corrosion and leakage. These issues were even more concerning due to the increasing demand for energy storage devices, so replacing liquid electrolytes with inorganic material-based solid-state electrolytes (SSE) is necessary and this SSE when incorporated with batteries made of lithium metal batteries, lithium-sulfur systems, and lithium-air batteries display exceptionally high power density and long durability and they are even better in terms of safety [9].

Apart from conductive polymers and inorganic metals, nanocomposites and nanomaterials are materials that have been great research electrochemical energy storage devices [10]. Nanomaterials have enabled electrically pseudocapacitive materials like transition metals oxides, to be used more efficiently in batteries and capacitors [11]. Nanomaterials in the form of natural biopolymers such as nano-cellulose, the most abundant biomaterials extracted from plants and other organisms obtained for use in several ESDs and on an industrial scale due to the unique and attractive mechanical and electrochemical properties that make nano cellulose highly suitable for manufacturing of several energy storage components such as electrolytes, separators, binder, and substrate materials [2, 12]. Apart from nanocellulose, researchers have also focused on building ESDs through several eco-friendly bionanomaterials such as lignin, cotton, and protein(silk) by incorporating electroactive nanomaterials for example carbon nanotubes (CNT), graphene, and metallic nanomaterials to make them electronically conductive [13].

Once we select the appropriate materials for manufacturing energy storage devices there arrive challenges for the process selection, here 3D printing comes into role. 3D printing has been a popular method in manufacturing quick prototypes of the product and parts which can be further tested to know if they comprise the desired properties or if they need improvement to enhance the overall performance [14]. Upon producing the prototypes 3D printing also enables us to produce innovative state-of-the-art products which are a leap ahead of the energy storage technologies [15].

2 Batteries: Fundamentals and Working

A battery is an electrochemical device that generates electrical energy by undergoing a chemical reaction. They are composed of two or more cells joined in series or parallel and transform chemical energy into electrical energy via electrochemical reactions that occur at the electrodes. Batteries comprise three active parts, including two conductive electrodes and an electrolyte and if the electrochemical reaction is irreversible, the battery is known as a primary battery. However, if the reaction is reversible, the battery can be charged again and classified as a secondary battery which is displayed through a schematic illustration in Fig. 1 where charge transfer is occurring through a semi-permeable membrane. A lot of research has been done over the past years and several aspects have been tackled such as low power density,

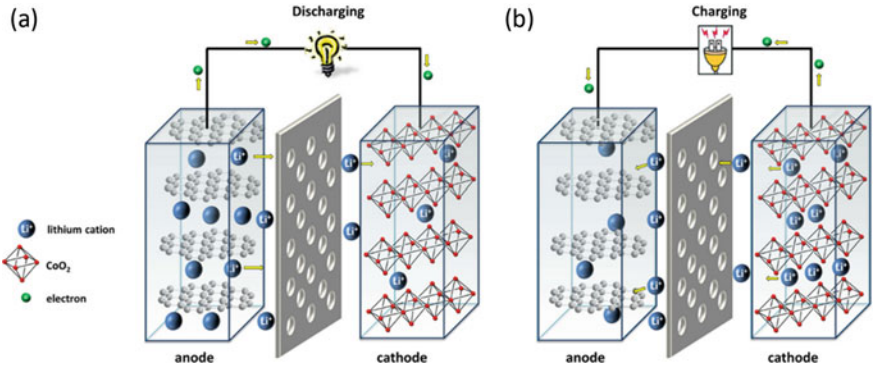

Fig. 1 Schematic illustration of **a** discharging and **b** charging of Li-ion battery. Adapted with permission [16]. Copyright © 2016, American Chemical Society

self-discharge, and cyclability. For this purpose, new materials have been explored for the manufacturing of the electrodes as well as the mechanism of the batteries has been manipulated which forces the battery to act in pseudocapacitive behavior, where it consists of higher power density with enhanced cyclic stability throughout time as compared to the conventional batteries.

Batteries are classified based on the materials used such as metal, Li-ion, organic batteries, and presently ample amount of research is being conducted on metal–organic batteries incorporating nanomaterials such as CNT, graphene, and nanofibers. Nanofibers are extensively researched as they provide a new dimension of flexibility to the batteries increasing the area of application batteries. Wherefore, metal-based secondary cells are made of metals such as copper, silver, etc. The materials are manufactured as electrodes and dipped into an electrolyte, which contains respective metal ions. Basically, the electrodes are separated into a semipermeable membrane which allows the transfer of ions through the electrolyte. The respective ion transfer plays a vital role in cell efficiency, which suggests that electrolyte with high ionic conductivity is required. Once the battery is discharged the cell is connected to power source where the anode is reduced and oxidizing the cathode and restoring its original state. Other than metal-based cells, Li-ion batteries have been in great use due to their high energy density and cyclic stability. However, the battery follows the same mechanism as described above for metal-based batteries. The anode in such batteries is composed of carbon-containing Li atom and Li-metal oxide materials such as lithium cobalt oxide as cathode materials. The anode gets oxidized and generates Li-ions moving towards the cathode through the cathode which eventually converts into $LiCoC_2$ as shown in Fig. 1.

Contradictory to Li-ion batteries, organic batteries offer better redox reactions and enhanced reaction rate. Like other batteries they have anode and cathode-based electrodes dipped into electrolytes and connected to an external circuit. However, organic materials are classified into three main categories based on their reaction pathway, such as p-type, n-type, and b-type. The n-type materials are reduced to

generate anions and are consumed at cathode; p-type materials oxidize at cathode and are applied to anode. Both oxidation and reduction reaction can be carried out with b-type materials. The reaction mechanism remains like metal batteries but due to the amorphous morphology of the electrodes they offer fast ionic movement during the reaction cycle providing good cyclic stability. The third type of battery configuration is obtained when metal electrode is used as the anode and an organic cathode such as p-type. The electrolyte in these batteries should contain cations of the corresponding metal electrodes. Firstly, Li possesses a bit of redox potential, which allows the organic cathode to utilize most of the potential. Secondly, in the case of n-type material, a small Li^+ radius helps in the fast migration of ions to the cathode. During the charging of p-type material, the cations are reduced and deposited at the metal anode. At the same time, the p-type material is oxidized. The discharge is the reverse of the process described above. When the n-type organic material is employed, the basic process remains the same. However, in this case, the battery stays charged after the fabrication, and the discharge takes place by reducing the cathode and oxidizing the anode.

Batteries are also classified based on the housing techniques used in the fabrication of the cell comprising of coin cell, Swagelok cell, pouch cell, and cylindrical cell are discussed below. A coin cell is a frequent form of test cell housing. It only necessitates a little amount of electrode materials. As indicated in Fig. 2a, a porous membrane is utilized between the electrodes, and the electrodes are pushed against each other by springs. This straightforward procedure allows for quick cell manufacture and testing. Next type of configuration is Swagelok cells, unlike coin cells, may be reused and are simple to disassemble. This capability enables scientists to conduct morphological research prior to and after charge/discharge cycles. Furthermore, reusability has both environmental and economic advantages. Swagelok cells, such as Swagelok T-cell, can be modified to provide additional testing benefits. Swagelok T-cells are three-electrode cells that are employed in more complicated experiments (Fig. 2b). In 1995, the basic pouch cell was created, offering 90% effective packing. In pouch cells, multiple layers of cathode and anode are sandwiched together with foils in between (Fig. 2c). To avoid direct electrode contact, foils are utilized. Each electrode's current is collected by attaching metal collectors, typically copper and aluminum for the anode and cathode, respectively. An aluminized plastic box contains heaps of electrodes. Because of its mechanical resilience, cylindrical cells are commonly employed in commercial applications. As shown in Fig. 2d, the electrodes are separated by a porous membrane, rounded, and packed in a cylinder.

3 3D Printed Batteries Using Pseudocapacitive Materials

Many pseudocapacitive materials are used for the fabrication of 3D printed batteries. Some of the most popular pseudocapacitive materials used for battery applications are discussed in the following sections.

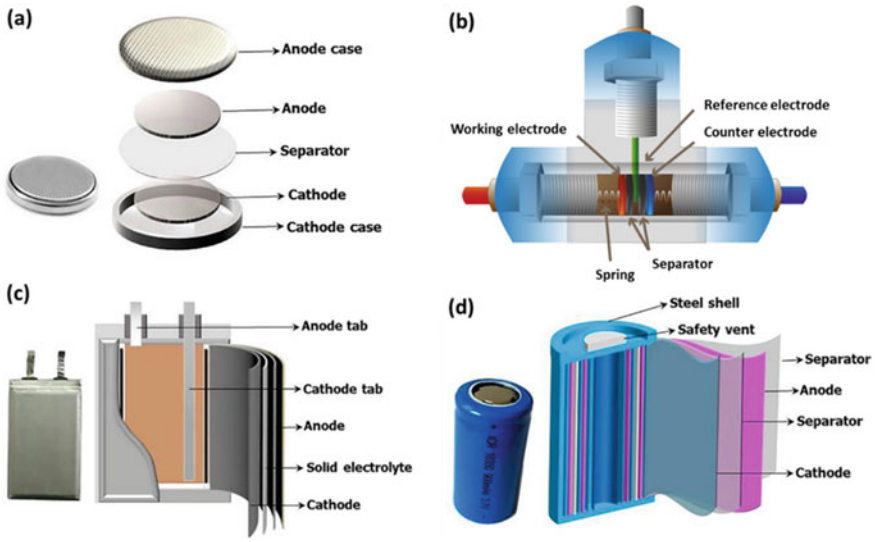

Fig. 2 Schematic illustration of **a** coin cell, **b** Swagelok cell, **c** pouch cell, and **d** cylindrical cell. Figure **a**–**d** are adapted from [17]. Copyright © 2019 The Authors. InfoMat published by John Wiley & Sons Australia, Ltd on behalf of UESTC. This is an open access article under the terms of the Creative Commons Attribution License. Figure b is adapted with permission [16]. Copyright © 2016, American Chemical Society

3.1 Transition Metal Oxides

Pseudocapacitive material-based energy devices are of great importance due to their balancing nature of high energy density and fast charging/discharging. Among many pseudocapacitive materials, transition metal oxides such as MnO_2, CuO, Fe_3O_4 have proven for their high theoretical specific capacitance, wide availability, and environmental friendliness [18]. Yoa et al. developed MnO_2 based current collector that simultaneously enabled efficient electron transport and ion diffusion by being a practical pseudocapacitive material for batteries. They addressed their research by direct ink method 3D printing graphene aerogels with rationally designed scaffolds for supporting pseudocapacitive MnO_2 as shown in Fig. 3. The scaffolds have lower surface area than the previously printed graphene aerogels, however, the large pores enabled uniform deposition of MnO_2 throughout the entire aerogel which possessed efficient ion diffusion during the charging and discharging even at high mass loading of the pseudocapacitive material. The material with mass loading of 45.2 mg/cm^2 of MnO_2 delivered excellent areal and volumetric capacitances of 11.55 and 115.5 F/cm^3, respectively and retained a high capability of 73.2% on increasing current density from 0.5 to 10 mA/cm^2. These results attest that charge transfer and ion diffusion in these 3D-printed electrodes are highly efficient.

Miniaturized and portable electronic devices have very compact designs and for such applications metal oxide-based 3D printed materials are being extensively used.

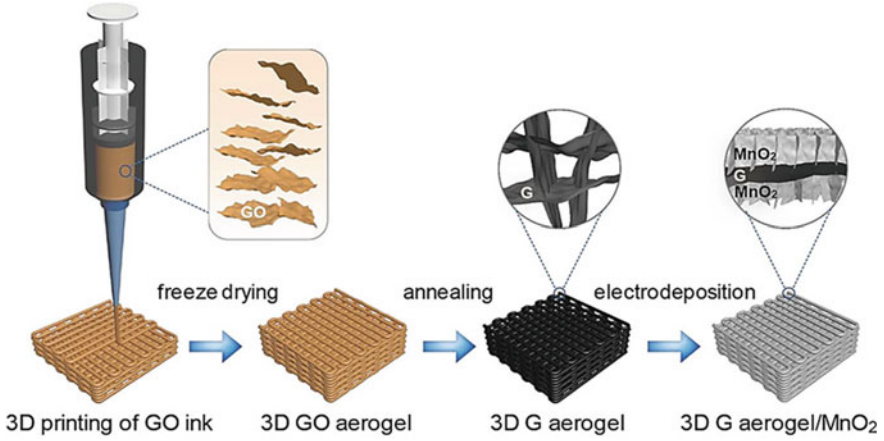

Fig. 3 Schematic illustration of fabrication of a 3D printed graphene aerogel/MnO_2 electrode. Reproduced with permission [19]. Copyright © 2019, Elsevier

One such research was carried out by Wang et al. [20]. Wherefore, they 3D printed cellular microelectrodes for micro-pseudocapacitive applications. The conventional microelectrodes struggled by offering unsatisfactory specific energy density due to surface or near-surface mechanisms. Towards this end, micro-supercapacitors constructed with additive manufacturing technology offered superior electrochemical performances supporting the urgent energy need for future applications. In this study two types of metal oxide-based pseudocapacitive materials Ni–Co–O nanosheets and MnO_2 were grown on 3D graphene oxide scaffolds where the scaffolds were pneumatically printed using a 3D extrusion system with the designed programmer (Fig. 4). The mass-loaded scaffolds exhibited superior electrochemical performance with a high specific capacity of up to 500 mC/cm^2 and high device capacitance, the energy density of 384.9 mF/cm^2 and 90 μWh/cm^2, respectively with a moderate voltage window of 1.3 V. The electrodes also provided device cycling stability during 10,000 charge–discharge cycles which opens a novel avenue to design and manufacture performance-oriented miniaturized electrochemical energy storage devices.

3.2 Transition Metal Sulfides

There is an inclining demand for electrochemical energy storage (EES) devices with high energy and power densities to meet the requirements for a sustainable future. For this reason, researchers have been working on transition metal sulfides due to their high theoretical capacity based on multi-electron reaction mechanisms and have been widely promising as pseudocapacitive anode materials for energy storage [21]. In addition to a handful of efforts on the innovation of electrode

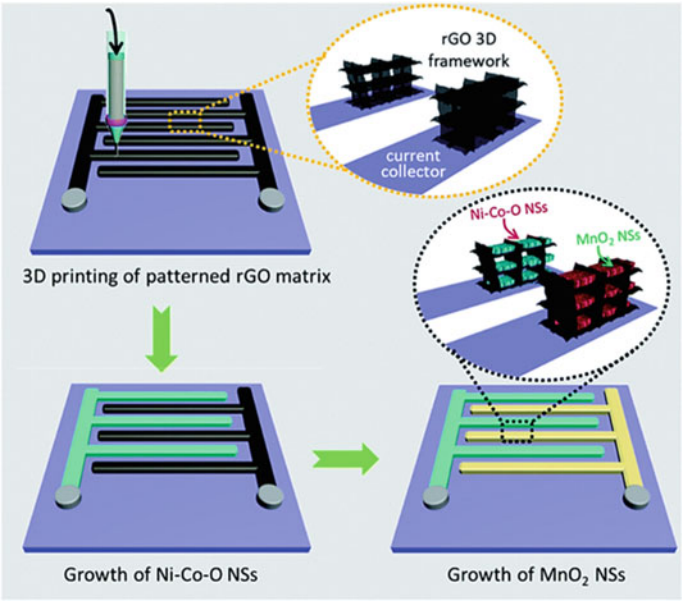

Fig. 4 Schematic representation of loading Ni–Co–O and MnO_2 nanosheet on the 3D printed reduced graphene oxide electrode scaffolds. Reproduced with permission [20]. Copyright © 2020, Royal Society of Chemistry

materials, lots of research has been focused on manufacturing 3D printed electrodes comprising state-of-the-art architectures and high performance. Therefore, Yu et al. designed and synthesized bimetallic sulfides/carbon composite [22]. The Cu_2S nanoplates were coated with MOFs-derived ZnS and an N-doped carbon layer composite (Cu_2S@ZnS/C) had been synthesized with a heterogeneous architecture having rich defects and homogeneous carbon coating layer offering multiple advantages for sodium ion storage with an ability to deliver high reversible capacity, excellent rate performance and high long term cyclic stability. At first, the 3D Cu_2S@ZnS/C inks were tested for printability, to guarantee that rheological properties were tested where the ink displayed a shear thinning behavior which was meant to be appropriate for 3D printing inks. While testing the ink as electrode materials for sodium storage with a high reversible capacity of 434 mAh/g, the durable cyclability of 94.7% after 1000 cycles. The electrodes were then assembled as active anode materials concerning Na^+ charge transfer constructing a sodium-ion battery (SIB) with a good power density of 203 W/k and stable cycle performance. The construction of the electrode material ink and SIB is displayed in Fig. 5.

Other than Cu_xS-based energy storage systems molybdenum sulfide (MoS_x) is a promising material for electrochemical storage devices. Therefore, Ghosh et al. researched free-standing electrochemically coated MoS_x-based 3D printed nanocarbon electrodes for solid-state supercapacitors [23]. The electrodes in this respective study were synthesized in three distinct shapes by depositing graphene/

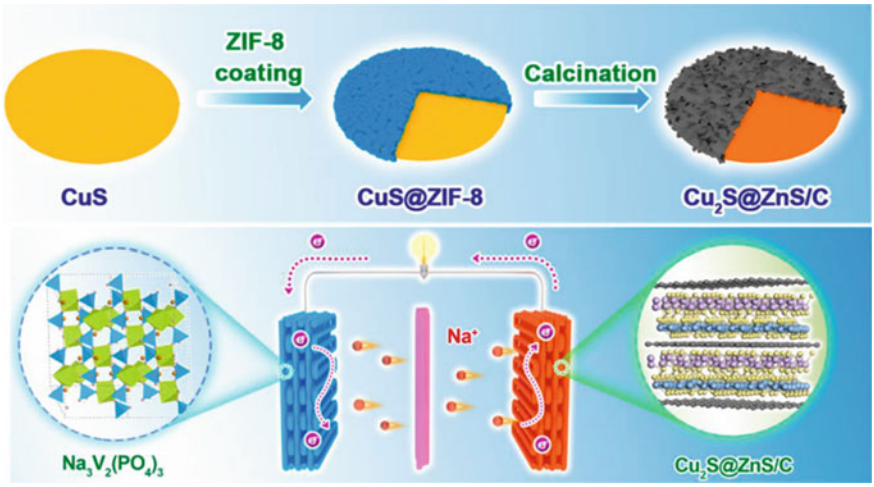

Fig. 5 Schematics displaying synthesis of 3D electrode ink and Na^+ charge transfer mechanism of SIB through the transition metal sulfide-based composite. Adapted with permission [22]. Copyright © 2022, Elsevier

PLA filament on the 3D printer and solvent treated by DMF taking out the PLA from the electrodes as shown in Fig. 6. The 3D printed filaments were then coated with MoS_x through an electrodeposition technique and free-standing 3D printed working electrode, Pt wire as a counter electrode, and Ag/AgCl as a reference electrode in ammonium tetra thiomolybdate electrolyte. The MoS_x coating displayed an intercalating and pseudocapacitive charge storage behavior giving out a capacitance of 27 mF/cm^2 at a scan rate of 10 mV/s, the current density of 0.13 mA/cm^2 and 90% of cyclic stability even after 10,000 cycles. Based on the above studies attests that the integration of 3D-printing and room temperature electrodeposition techniques allows high-performance transition metal sulfide-based pseudocapacitive materials, which leads to a better perspective for synthesizing novel materials for energy storage applications with better efficiency.

3.3 Transition Metal Phosphide

It has been a challenging task of designing high-performance electrodes via 3D printing for advanced energy storage. Generally, lightweight carbonaceous materials outperform excellent electrical conductivity, but they struggle with undermined areal and volumetric energy density, particularly for supercapacitors devices. Wherefore, researchers have been working on synthesizing better materials that show pseudocapacitive behavior and synthesized in-situ coupling of NiCoP bimetallic phosphide and Ti_3C_2 MXene to build up heavy NiCoP/MXene (NCPM) electrodes with tunable mass loading throughout 3D printing technology. In this study, $Ti_3C_2T_x$ nanosheets

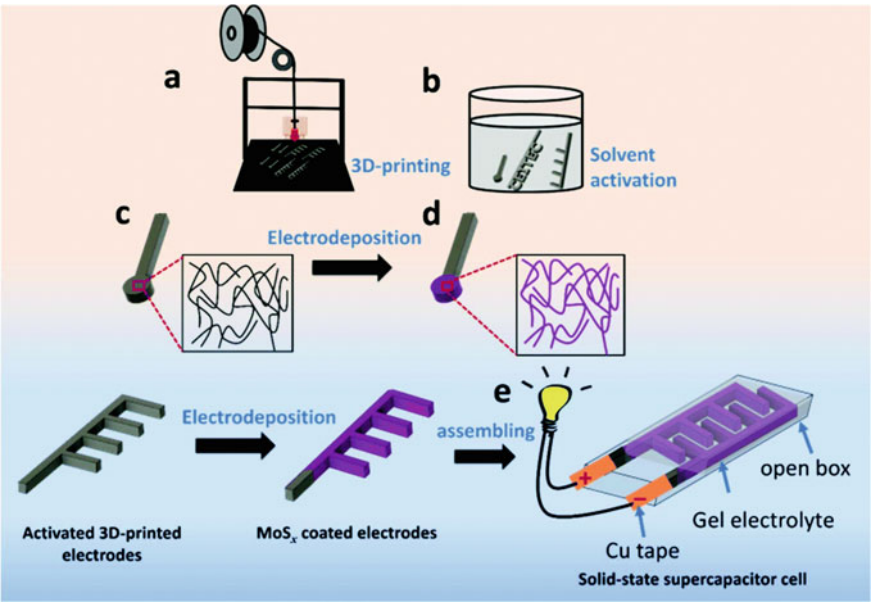

Fig. 6 Schematic representation of the synthesis of free-standing MoS_x electrodes and assembling them as pseudocapacitive energy storage devices. Reproduced with permission [23]. Copyright © 2021, Royal Society of Chemistry

were etched and obtained as an aqueous dispersion [24]. The bimetallic phosphide was electrodeposited on the MXene and mixed with CNT to obtain the 3D printing ink. Herein, it was observed that an 18 wt.% concentration of CNT in the suspension had the correct viscosity to manufacture self-standing electrodes. The same process from the material synthesis, ink formulation, and 3D printing of the electrodes is explained in Fig. 7. The 3D printed design of the NiCoP/MXene asymmetrical supercapacitor yields high volumetric energy density due to hierarchical pores and tunable mass loadings. These properties also enabled better charge transport and electrolyte penetration giving out outstanding rate capability and cyclic stability. Above all, the device delivered high areal and volumetric energy densities of 0.89 and 2.2 mWh/cm^3, respectively [24].

Other than bimetallic phosphides, mono phosphide-based materials for pseudocapacitive batteries have been a point of interest due to their advantages such as low cost, environmental friendliness, and excellent volumetric capacity with optimal power density. For this purpose, Xu et al. calcinated Cu_3P/N-CN composites through freeze drying as demonstrated in Fig. 8 [25]. The morphology suggested that the honeycomb-like structure of Cu_3P nanoparticles encapsulated in an N-CN composite had high crystallinity and were evenly distributed in the carbon network. Due to the above surface morphology, the composite displayed an excellent rate capability of 461.8 mAh/g at 2 A/g, and outstanding stability of 752.3 mAh/g at 0.1 A/g for over 100 cycles. The unique porous structure and noteworthy performance of the

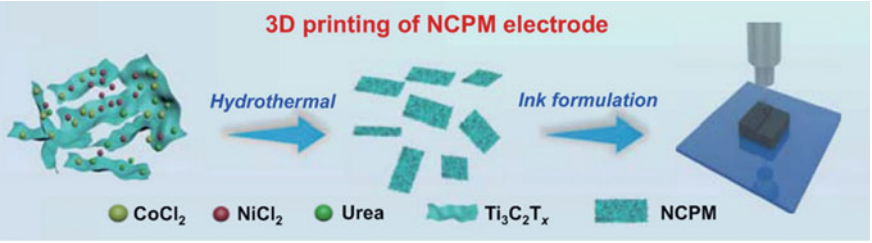

Fig. 7 Schematic representation for 3D printed transition metal phosphide-based pseudocapacitive electrodes. Adapted with permission [24]. Copyright © 2020 The authors, This article is licensed under a Creative Commons Attribution 4.0 International License

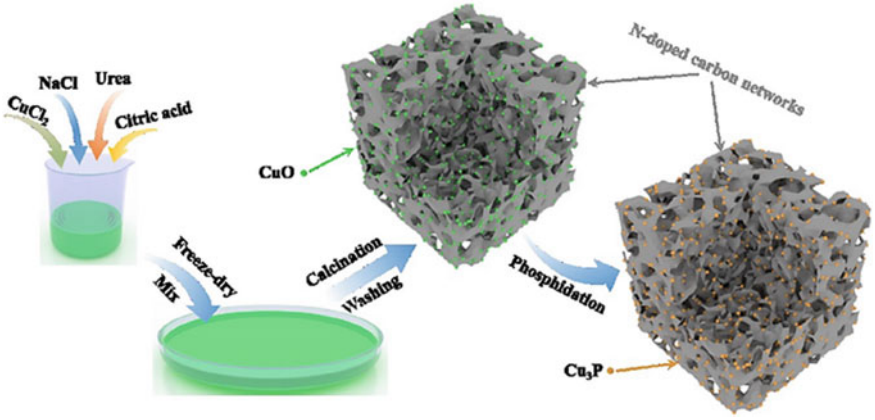

Fig. 8 Schematical synthesis route of 3D Cu_3P nanoparticle composite for pseudocapacitive lithium storage batteries. Reproduced with permission [25]. Copyright © 2020, Elsevier

material make the transition metal phosphides promising materials in providing high-performance 3D-printed electrodes for pseudocapacitive batteries.

3.4 Conducting Polymers

The development of hierarchically organized nanomaterial with modular structure has been a point of interest in diverse applications such as 3D printing and manufacturing of novel EES. Different combinations of pseudocapacitive materials, such as RuO_2, MnO_x, NiO, V_2O_5, polythiophenes, polypyrrole, and polyaniline have been explored for the development of hybrid SC materials. From the above-noted materials, MnO_x has been giving out the best outcome through high theoretical specific capacitance, natural abundance, and low cost [26]. To further improve the real-life properties of the materials several synthesis methods have been applied

such as solvothermal, hydrothermal, sonochemical, and sol–gel to the surface of the electrodes, these are generally combined with a conductive binder such as PVDF, PTFE, or Nafion in a paste [26]. Following the above steps, Rezaei et al. derived novel 3D pyrolytic carbon/Mn_3O_4 nanostructures for free-standing hybrid supercapacitor electrodes. Commercial photopolymers composed of acrylate monomers and methacrylate oligomers were incorporated to print complex 3D structures and identified as pyrolyzable materials. These 3D-printed photopolymers were directly used as substrates for the deposition of MnO_x nanoflakes and nanoflowers through the chemical reduction of manganese. The obtained material was then passed through a pyrolysis chamber to increase the uniformity of the thermal degradation and gas evolution [27]. The same process of synthesizing the 3D printed support-free printed scaffolds to pyrolysis of the electrode materials.

The electrochemical performance of the novel hybrid supercapacitor electrodes had good capacitance gravimetric and areal capacitance of 186 F/g and 968 mF/cm^2, respectively, rate capability, and excellent cyclic recovery loss of less than 8% up to 5000 cycles. The values in this research are comparable with the conventional material-based supercapacitor devices. Conducting polymer has also enabled the production of stretchable and flexible supercapacitors which give a huge leap in increasing the range of application of energy storage devices. One such study was conducted by Yang et al., which combined theoretical structural design and 3D printing giving out free-standing stretchable electrodes using poly(3,4-ethylene dioxythiophene): polystyrene sulfonate ink. First, they made polymer-based nanofibrils and integrated them with carbon nanotubes. The research showed that the incorporation of CNT improved the areal capacitance up to 99 mF/cm^2. The supercapacitor further exhibited a high energy density of 0.065 mWh/cm^2 and performed with excellent stability even after 14,000 cycles [28]. According to the research conducted above it is attested that 3D printed conducting polymers come out as potential materials for the manufacturing of pseudocapacitive electrochemical energy storage devices. It has also been observed that the electrode materials exhibited comparable electrochemical performance and were mechanically flexible to provide a better platform for application as flexible electrochemical storage devices.

3.5 Composites Based on Pseudocapacitive Materials

Supercapacitors are energy storage devices comprising higher energy density and lifetime than batteries on a wider span of temperature. There are several electrode materials but carbon-based organic materials such as CNT, CNFs, rGO, and carbon spheres have been a wide point of research [29]. These materials are incorporated with several metal oxides or conducting polymer forming composites which provide good mechanical properties such as flexibility up to 180° making them suitable for wearable devices. Such composite for pseudocapacitors was composed by Chen et al. using polyacrylonitrile (PAN) as a precursor polymer for the fabrication of CNFs

via electrospinning and carbonization [30]. Once the fibrils were synthesized particles of MnO were applied to the fibril structure through electrospinning, however, this reduced the electrical conductivity, in further study, they deposited copper onto the nanofibers to enhance the conductivity. Such kind of modification increased deeper electrolyte penetration which increased conductivity from 10 to 46 S/m from the MnO deposition to copper deposition respectively [30]. A similar study was conducted by Ren et al., constructing flexible zinc-ion batteries (ZIBs) [31]. Composites were constructed using carbon nanotubes and coated with MnO_2 to form flexible CNT@MnO_2 ink as cathode for flexible aqueous micro-ZIBs and zinc powder ink was used as an anode which gives out high flexibility and bendability. To fabricate the materials as the coin cell composition MnO_2 was mixed with PVDF as a binder and N-methyl-2-pyrrolidine (NMP) as a solvent to adjust the viscosity and the ink was coated on the carbon paper with an active material loading of 1.6 mg/cm^2 and glass fiber as a separator. Furthermore, they fabricated flexible batteries like coin cells and processed them as 3D-printed batteries including a substrate, current collector, electrodes, and an electrolyte. While discussing the electrochemical performance of the 3D printed flexible battery which showed a stable capacity of 63 μAh/cm^2 at 0.4 mA/cm^2. When the battery is bent in different states, the maximum capacity loss compared with the initial value is only 2.72%, indicating its stability [31]. Apart from transition metal-based composites for pseudocapacitive energy storage batteries, conducting polymer in association with carbon-based materials such as graphene oxide gives out high conductivity and pseudocapacitive behavior. Hong et al., conducted research with a combination of graphene with PANI composite for supercapacitor application [32]. The study was categorized into three sections, comprising flexible graphene/PANI composites, graphene framework-based composites, and printable graphene/PANI composites. The 3D printed composite was manufactured by first graphene templates were synthesized using the chemical vapor deposition method, which was then freeze-dried, and the electrochemical oxidative method was used to coat PANI on the templates which gave provided a fast fabrication of complicated shape electrodes, enhancing the material compatibility for the application of portable and wearable electronics. The electrodes performed outstandingly through the electrochemical performance test attesting to a specific capacitance of more than 800 F/g and capacitance retention over 10,000 cycles. Wherefore, the above-supplied data is sufficient to prove that printable inks synthesized from conductive polymers or transition metal-based composites and compatible printing techniques will promote the rapid growth of efficient energy storage microdevices and flexible wearable pseudocapacitor applications [32].

4 Flexible 3D Printed Batteries Using Pseudocapacitive Materials

Flexible batteries have been in growing demand due to their usage in wearable electronics, which proficiently cope with the power consumption of such wearable electronics [14, 33–35]. Concerning such devices pseudocapacitive materials have been extensively used due to their high energy density, large capacity, and outstanding mechanical flexibility [36]. To further enhance the electrochemical performance of the pseudocapacitive materials several strategies have been employed such as coating carbon-based substances upon the electrode materials which eventually improves the cyclic stability of the materials on which it has been lacking. Therefore, making electrode materials with the best performance in each aspect. Upon that advanced techniques in terms of additive manufacturing are used which provides ultra-high manufacturing capabilities with some miniature structures which further make the batteries minute in size but provide high electrochemical performance. As described above, Lu et al., developed fibrous electrodes using pseudocapacitive materials with a 3D printing technique [37]. The usage of fibrous materials improved the flexibility and electrochemical properties of the electrodes. Firstly, MnO_2 and MoS_2 nanosheets were synthesized and N-doped with porous carbon and graphene respectively. Once the base materials were synthesized, 3D printing ink was prepared with a predefined ratio of 1:0.2 for graphene and pseudocapacitive materials respectively. The mixture was dispersed into NMP and processed through ball milling and ultrasonication. Electrolyte inks were also synthesized through a mixture of PVA/LiCl. The ink was then 3D printed as a coaxial single fiber electrode and assembled as a flexible fibrous pseudocapacitive device. On successful printing of the device, it was tested to characterize its electrochemical properties wherefore, the device had excellent cyclic stability of which it had 98.63% of capacity retention rate after 12,000 cycles. The device displayed a specific capacitance of 318.82 mF/cm^2 and excellent bending capabilities showing no difference in performance with a bending angle of 90^o [37]. Other than carbon-based materials such as graphene oxide or carbon nanotubes, flexible pseudocapacitive batteries have also been manufactured using biomaterials such as gelatin and others. In the subsequent study, highly elastomeric, shear-thinning, 3D-printed hydrogels were constructed by incorporating defect-rich MoS_2 nanoscaffolds with thiolated gelatin. Further moving into the study, the defect density of the metal oxide materials was increased through engineering defects. These defects acted as crosslinking epicenters forming a mechanically robust, flexible polymeric network without the use of the crosslinker or UV exposure to join the thiolated gelatin as shown in Fig. 9 [38]. The hydrogel ink displayed compatible rheological characteristics which enabled 3D printing of complex patterns. The concentration of MoS_2 played a vital role in exhibiting hybrid conductivity and pseudocapacitive response due to the faradic and capacitive currents.

It was observed that nano assemblies were in vitro and in vivo biocompatible which suggested that such devices can be used in ingestible electronics, electroceuticals, and energy storage devices because of their hybrid conductivity, charge

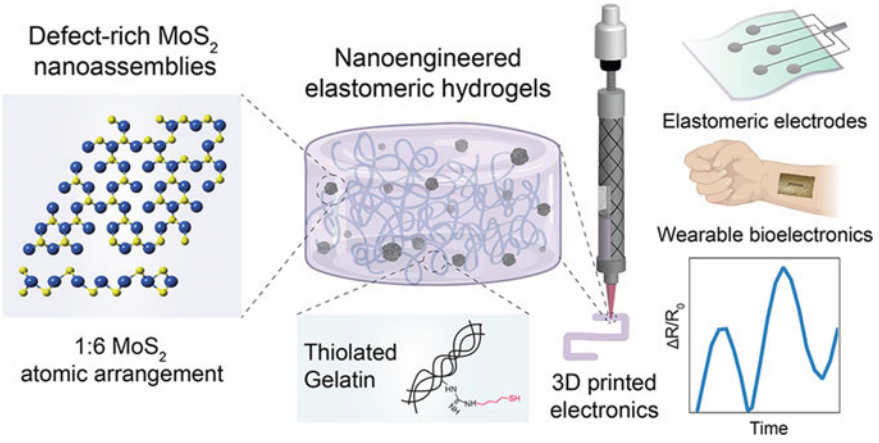

Fig. 9 Schematic representation of synthesis and fabrication of nanoengineered 3D hydrogel bio inks through defect-driven gelation between defect-rich MoS_2 nano-scaffolds and thiolated gelatin. Reproduced with permission [38]. Copyright © 2022, American Chemical Society

storage, and mechanical properties that correspond to human tissue [38]. Apart from conventional pseudocapacitive materials are compounded with biomaterials, and carbon-based materials to synthesize electrode materials. These materials are also used for manufacturing Lithium-ion batteries which are in popularity due to the electrochemical performance they offer. Researchers are also using 3D printing technology to fabricate Li-ion batteries with enhanced performance in comparison with conventional Li-ion batteries. Mwizerwa et al. synthesized 3D printed grid patterned $LiFePO_4$@MgO composite electrodes with a variable thickness [39]. Firstly, $LiFePO_4$@MgO composite was prepared through the freeze-drying method and used as cathode material. On the other side, $Li_4Ti_5O_{12}$ was employed as active anode electrode material. To make the active electrode materials they were mixed with carbon black and PVDF-co-HFP which were meant to be conductive agents and binders respectively once the appropriate rheological properties were obtained the material was 3D printed through conventional casting method. The ink preparation and electrode fabrication processes are displayed in Fig. 10.

Once the 3D printed electrodes were assembled as full battery it had an areal capacity of 3.01 mAh/cm^2 after 20 cycles at 0.1 C which was identical to previously reported Li-ion based electrode batteries. The electrodes displayed a high discharge capacity of 147.1 mAh/g at 0.1 C and maintained discharge capacity of 139.0 mAh/g after 400 cycles. Such enhanced electrochemical performance attests well-constructed 3D printed structures with porous structures with promising high capacity, stable cycling life and good flexibility. Such research paves way for the future development and widen the application of Li-ion batteries with high-energy density [39].

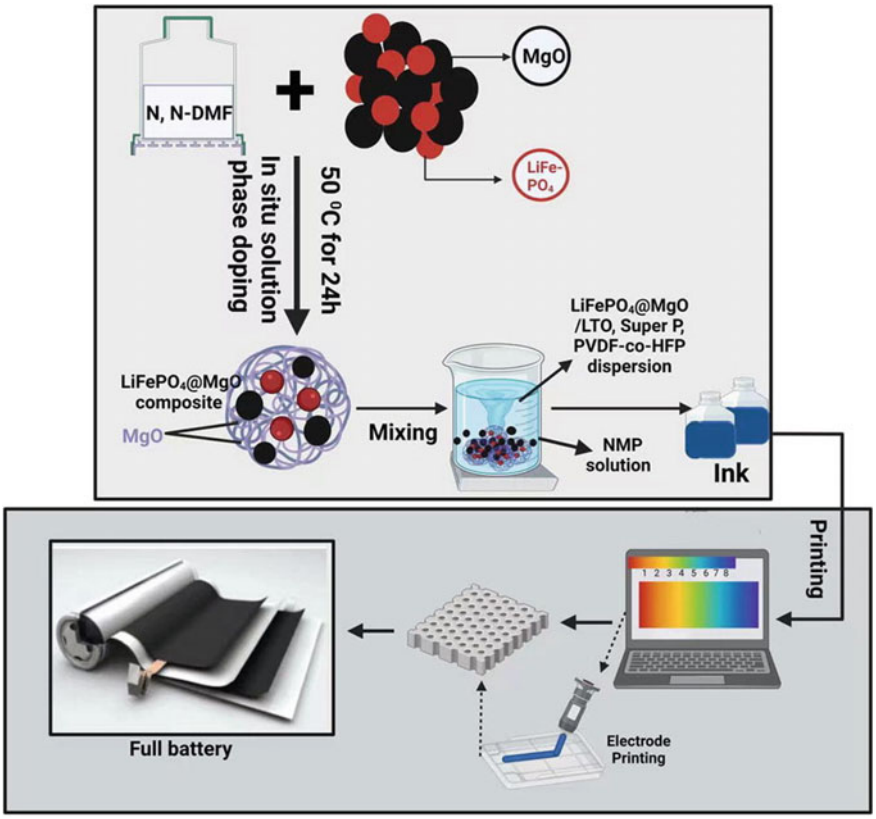

Fig. 10 Schematic of the synthesis of MgO-doped $LiFePO_4$ composite via solution phase method and 3D-printed electrodes with the structure of the full cell. Reproduced with permission [39]. Copyright © 2022, Elsevier

5 Conclusion and Future Remark

Pseudocapacitive materials, such as transition metal oxides, sulfides and phosphides have gained considerable attention recently to provide new alternatives of currently found electrochemical devices such as Li-ion batteries. This book chapter provided some recent research being conducted on pseudocapacitive materials for batteries. These materials were processed on the state of art technology of 3D printing providing a new dimension in terms of device performance and its physical properties. Battery fundamentals and different categories of batteries were also discussed which unwinds the basic working of the batteries. It was observed that these pseudocapacitive materials combined with the 3D printing technology gave out better electrochemical performance of the devices as compared to the conventionally available devices. The devices provided high power densities accompanied with long lasting cyclic stability being promising materials for commercial usage. We also discussed that polymers

and nanomaterials combined also enhanced the properties of the device. As a part of future remark, other materials and battery configurations can be explored such as sodium-ion batteries and metal air batteries respectively. Usage of polymeric materials should be maximized, and 3D printed electronic devices using biopolymers should be examined to provide cleaner and more sustainable energy storage devices.

References

1. R.K. Gupta, *Solid State Batteries: Emerging Materials and Applications* (American Chemical Society, Washington, DC, 2022)
2. R.K. Gupta, T.A. Nguyen, *Energy from Waste: Production and Storage*, 1st edn. (CRC Press, Boca Raton, FL, 2022)
3. R.K. Gupta, *Metal-Air Batteries: Principles, Progress, and Perspectives* (CRC Press, Boca Raton, FL, 2023)
4. R. Gupta, T.A. Nguyen, H. Song, G. Yasin, *Lithium-Sulfur Batteries: Materials, Challenges and Applications* (Elsevier, Cambridge, United States, 2022)
5. R.K. Gupta, *Solid State Batteries: Materials and Advanced Devices* (American Chemical Society, Washington, DC, 2022)
6. S. Thomas, A.B. Gueye, R.K. Gupta, *Nanostructured Materials for Supercapacitors* (Springer, Switzerland, 2022)
7. P. Simon, Y. Gogotsi, B. Dunn, Where do batteries end and supercapacitors begin? Science **343**(80-), 1210–1211 (2014)
8. S. Chen, A. Skordos, V.K. Thakur, Functional nanocomposites for energy storage: chemistry and new horizons. Mater. Today Chem. **17**, 100304 (2020)
9. W. Xia, Y. Zhao, F. Zhao, K. Adair, R. Zhao, S. Li, R. Zou, Y. Zhao, X. Sun, Antiperovskite electrolytes for solid-state batteries. Chem. Rev. **122**, 3763–3819 (2022)
10. R.K. Gupta, *Conducting Polymers for Advanced Energy Applications*, 1st edn. (CRC Press, Boca Raton, FL, 2021)
11. Y. Gogotsi, R.M. Penner, Energy storage in nanomaterials—capacitive, pseudocapacitive, or battery-like? ACS Nano **12**, 2081–2083 (2018)
12. C. Chen, L. Hu, Nanocellulose toward advanced energy storage devices: structure and electrochemistry. Acc. Chem. Res. **51**, 3154–3165 (2018)
13. O. Faruk, D. Hosen, A. Ahmed, M.M. Rahman, Functional bionanomaterials—embedded devices for sustainable energy storage, in *Biorenewable Nanocomposite Mater Vol 1 Electrocatal Energy Storage, Part 1—Funct Bionanomaterials—Embedded Devices Sustain Energy Storage 1*
14. J. Choi, T. Ingsel, R.K. Gupta, Printable and flexible solid-state batteries, in *Solid State Batteries Volume 2: Materials and Advanced Devices* (American Chemical Society, 2022), pp. 14–311
15. U. Gulzar, C. Glynn, C. O'Dwyer, Additive manufacturing for energy storage: Methods, designs and material selection for customizable 3D printed batteries and supercapacitors. Curr. Opin. Electrochem. **20**, 46–53 (2020)
16. S. Muench, A. Wild, C. Friebe, B. Häupler, T. Janoschka, U.S. Schubert, Polymer-based organic batteries. Chem. Rev. **116**, 9438–9484 (2016)
17. Y. Liang, C.-Z. Zhao, H. Yuan, Y. Chen, W. Zhang, J.-Q. Huang, D. Yu, Y. Liu, M.-M. Titirici, Y.-L. Chueh, H. Yu, Q. Zhang, A review of rechargeable batteries for portable electronic devices. InfoMat **1**, 6–32 (2019)
18. V. Augustyn, P. Simon, B. Dunn, Pseudocapacitive oxide materials for high-rate electrochemical energy storage. Energy Environ. Sci. **7**, 1597–1614 (2014)
19. B. Yao, S. Chandrasekaran, J. Zhang, W. Xiao, F. Qian, C. Zhu, E.B. Duoss, C.M. Spadaccini, M.A. Worsley, Y. Li, Efficient 3d printed pseudocapacitive electrodes with ultrahigh MnO_2 loading. Joule **3**, 459–470 (2019)

20. T. Wang, X. Tian, L. Li, L. Lu, S. Hou, G. Cao, H. Jin, 3D printing-based cellular microelectrodes for high-performance asymmetric quasi-solid-state micro-pseudocapacitors. J Mater Chem A **8**, 1749–1756 (2020)
21. J. Xu, E. Gu, Z. Zhang, Z. Xu, Y. Xu, Y. Du, X. Zhu, X. Zhou, Fabrication of porous Na3V2(PO4)3/reduced graphene oxide hollow spheres with enhanced sodium storage performance. J. Colloid Interface Sci. **567**, 84–91 (2020)
22. B. Yu, Y. Ji, X. Hu, Y. Liu, J. Yuan, S. Lei, G. Zhong, Z. Weng, H. Zhan, Z. Wen, Heterostructured Cu2S@ZnS/C composite with fast interfacial reaction kinetics for high-performance 3D-printed Sodium-Ion batteries. Chem. Eng. J. **430**, 132993 (2022)
23. K. Ghosh, M. Pumera, Free-standing electrochemically coated MoS: Xbased 3D-printed nanocarbon electrode for solid-state supercapacitor application. Nanoscale **13**, 5744–5756 (2021)
24. L. Yu, W. Li, C. Wei, Q. Yang, Y. Shao, J. Sun, 3D Printing of NiCoP/Ti_3C_2 MXene architectures for energy storage devices with high areal and volumetric energy density. Nano-Micro Lett. **12**, 1–13 (2020)
25. P. Xu, K. Dai, C. Yang, X. Wang, R. Zou, J. Shao, G. Zeng, M. Zhang, Q. Huang, Z. Su, Efficient synthesis of Cu3P nanoparticles confined in 3D nitrogen-doped carbon networks as high performance anode for lithium/sodium-ion batteries. J. Alloys Compd. **849**, 156436 (2020)
26. Y.C. Tsai, W.D. Yang, K.C. Lee, C.M. Huang, An effective electrodeposition mode for porous MnO_2/Ni foam composite for asymmetric supercapacitors. Materials (Basel) **9**, 246 (2016)
27. B. Rezaei, T.W. Hansen, S.S. Keller, Stereolithography-derived three-dimensional pyrolytic carbon/Mn_3O_4nanostructures for free-standing hybrid supercapacitor electrodes. ACS Appl. Nano Mater. **5**, 1808–1819 (2022)
28. J. Yang, Q. Cao, X. Tang, J. Du, T. Yu, X. Xu, D. Cai, C. Guan, W. Huang, 3D-Printed highly stretchable conducting polymer electrodes for flexible supercapacitors. J. Mater. Chem. A **9**, 19649–19658 (2021)
29. T.Y. Bin, J.M. Lee, Graphene for supercapacitor applications. J. Mater. Chem. A **1**, 14814–14843 (2013)
30. X. Chen, X. Liu, M. Ouyang, P. Childs, N. Brandon, B. Wu, Electrospun composite nanofibre supercapacitors enhanced with electrochemically 3D printed current collectors. J Energy Storage **26**, 100993 (2019)
31. Y. Ren, F. Meng, S. Zhang, B. Ping, H. Li, B. Yin, T. Ma, CNT@MnO2 composite ink toward a flexible 3D printed micro-zinc-ion battery. Carbon Energy **4**, 446–457 (2022)
32. X. Hong, J. Fu, Y. Liu, S. Li, X. Wang, W. Dong, S. Yang, Recent progress on graphene/polyaniline composites for high-performance supercapacitors. Materials (Basel) **12**, 1451 (2019)
33. R. Arukula, P.K. Kahol, R.K. Gupta, Electrodes for flexible-stretchable supercapacitors, in *Flexible Supercapacitor Nanoarchitectonics*, ed. by M.I. Ahamed, R. Boddula, T. Altalhi (Scrivener Publishing, Beverly, MA, 2021), pp. 485–531
34. T. Ingsel, R.K. Gupta, Smart and flexible energy devices: principles, advances, and opportunities, in *Smart and Flexible Energy Devices*. ed. by R.K. Gupta, T.A. Nguyen (CRC Press, Boca Raton, 2022), pp. 1–21
35. Q. Gui, L. Wu, Y. Li, J. Liu, Scalable wire-type asymmetric pseudocapacitor achieving high volumetric energy/power densities and ultralong cycling stability of 100 000 times. Adv. Sci. **6**, 1802067 (2019)
36. Y. Guo, X. Hong, Y. Wang, Q. Li, J. Meng, R. Dai, X. Liu, L. He, L. Mai, Multicomponent hierarchical Cu-Doped NiCo-LDH/CuO double arrays for ultralong-life hybrid fiber supercapacitor. Adv. Funct. Mater. **29**, 1–11 (2019)
37. H. Lu, Q. Peng, Z. Wang, J. Zhao, X. Zhang, L. Meng, J. Wu, Z. Lu, J. Peng, X. Li, 3D printing coaxial fiber electrodes towards boosting ultralong cycle life of fibrous supercapacitors. Electrochim. Acta **380**, 19–21 (2021)
38. K.A. Deo, M.K. Jaiswal, S. Abasi, G. Lokhande, S. Bhunia, T.U. Nguyen, M. Namkoong, K. Darvesh, A. Guiseppi-Elie, L. Tian, A.K. Gaharwar, Nanoengineered Ink for designing 3D printable flexible bioelectronics. ACS Nano **16**, 8798–8811 (2022)

39. J. Pierre Mwizerwa, C. Liu, K. Xu, N. Zhao, Y. Li, Z. Chen, J. Shen, Three-dimensional printed lithium iron phosphate coated with magnesium oxide cathode with improved areal capacity and ultralong cycling stability for high performance lithium-ion batteries. J. Colloid Interface Sci. **623**, 168–181 (2022)